

# Student Poster Book of Abstracts

*2014 IEEE Power and Energy Society General Meeting*

*National Harbor, MD (Washington, DC Metro Area), United States*

*July 27-31 2014*



## Welcome Message from the Chair

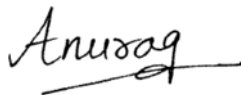
On behalf of the Student Activities Subcommittee, I would like to extend my welcome and thank all the students to participate in the Student Poster Contest at the 2014 IEEE Power and Energy Society General Meeting held in Washington, DC on July 29<sup>th</sup>, 2014, 7-9.30 AM.

At the time of printing the poster participation information, we had 224 extended abstracts from students from different parts of the world confirmed to participate in the 2014 IEEE PES GM student poster contest. This book of extended abstracts is aimed to showcase the outstanding research projects by students, and archive some of the activities of interest to our society at various educational institutions around the world presented at this meeting. The research topics of these posters fall into 17 categories:

1. Smart Sensors, Communication and Control in Energy Systems
2. Smart Grid Technology
3. Cyber and Physical Security of Smart Grid
4. Geometric Disturbance in Electric Power Systems
5. Advanced Computational Methods for Power System Planning, Operation, and Control
6. Emerging Software Needs for the Restructured Grid
7. System-Wide Events and Analysis Methods
8. Intelligent Monitoring and Outage Management
9. Integrating Renewable Energy into the Grid
10. Substation and Distribution Automation
11. Dynamic Performance and Control of Power Systems
12. Market Interactions in Power Systems
13. Asset Management
14. Flexible AC Transmission Systems
15. Power Electronics
16. Electric Machine and Drives
17. Power System Modeling and Simulation

All students are invited to attend the multiple events planned by student activities and local organizing committee, including the Student/Faculty/Industry (SFI) luncheon and job fair to be held on July 30<sup>th</sup>, 2014. Our luncheon speaker will be Don Niss, Deputy Coordinator, Power Africa and Trade Africa Initiative. The student poster contest winners will be also announced at the SFI Luncheon on July 30<sup>th</sup>, 2014.

Support from the Grainger Foundation, and the IEEE Power & Energy Society (PES) Power and Energy Education Committee (PEEC), for the student activities are gratefully acknowledged. The subcommittee acknowledges the services of all the judge volunteers and PESGM local organizing committee. Special thanks to Dr. Dennis Ray, University of Wisconsin; Dr. Jignesh Solanki, West Virginia University; and Dr. Aaron St. Leger, United States Military Academy for helping with the student activities.



Dr. Anurag K Srivastava  
Washington State University  
Pullman, WA



## **IEEE PES Student Activities Subcommittee**

### **Chair**

Dr. Anurag K Srivastava  
Assistant Professor  
School of Electrical Engineering and Computer Science  
Washington State University  
PO Box 642752  
EME 102  
Spokane St Pullman  
Washington 99164-2752, USA  
asrivast@eecs.wsu.edu

### **Vice-Chair**

Dr. Jignesh M. Solanki  
Assistant Research Professor  
Lane Department of Computer Science and Electrical Engineering  
West Virginia University  
395 Evansdale Drive,  
Morgantown, WV 26506-6109, USA  
jmsolanki@csee.wvu.edu

### **Secretary**

Dr. Aaron St. Leger  
Assistant Professor  
Department Electrical Engineering and of Computer Science  
United States Military Academy  
646 Swift Road  
West Point, NY 10996-1905, USA  
Aaron.StLeger@usma.edu

### **Webmaster**

Dr. Jignesh M. Solanki  
Assistant Research Professor  
Lane Department of Computer Science and Electrical Engineering  
West Virginia University  
395 Evansdale Drive,  
Morgantown, WV 26506-6109, USA  
jmsolanki@csee.wvu.edu

**Created By: Dr. Jignesh Solanki**

## Smart Sensors, Communication and Control in Energy Systems

No.	ID	Poster Title	Student Name
101	A01	Investigation of the Communication Delay and Its Impact on Wide-area Monitoring	Can Huang
102	A02	Adaptive frequency control application for a real autonomous islanded grid	Tofis Yiannis
103	A03	Smart Grid Distributed Energy Management under Packet Loss Environment	Yuan Zhang
104	A04	Parameter Identification of Doubly Fed Induction Generator (DFIG) Using Real-time Measurements	Shaotong Guo
105	A05	Distributed Automatic Generation Control	Wang Siqi
106	A06	A Partially Observable Markov Decision Process Approach to Customer Home Energy Management Systems	Timothy Hansen
107	A07	Conceptual Architecture of Building Energy Management Open Source Software (BEMOSS)	Avijit Saha

## Smart Grid Technology

No.	ID	Poster Title	Student Name
108	A08	A New Trading Framework for Demand Response Aggregators	Nadali Mahmoudi
109	A09	Aggregated Demand Response From Smart Loads	Diptargha Chakravorty
110	A10	Distributed Voltage and Frequency Control Using Electric Springs	Zohaib Akhtar
111	A11	Uncertainty of Measurement Error in Intelligent Electronic Devices	Po-Chen Chen
112	A12	Distributed Electric Vehicles Cooperative Charge Control with Wind Power	Chengcheng Shao
113	A13	Real-time energy management strategies for microgrids	Xiong Wu
114	A14	Distributed Electric Vehicles Cooperative Charge Control with Wind Power	Chengcheng Shao
115	A15	Economic Analysis of Plug-in Electric Vehicle Parking Deck with Dynamic Pricing	Yan Yu
116	A16	A Distributed Data Storage and Processing Framework for Next-Generation Residential Distribution Systems	Yan Yu
117	A17	Tie-Line Bias Control of a Power System with Variable Renewable Energy Generation	Iroshani
118	A18	Impact of Electric Vehicles on LV Feeder Voltages	LI YUN
120	A20	Testing and Implementation of the Linear State Estimator in a Real Power System	Zhang Lin
121	B01	Benefits of DC Microgrids: Economic Operation and Enhancing the Resilience by Hierarchical Control	Liang Che
122	B02	Aggregator based Economic Model for Residential Distribution Systems with DR and V2H	Long Zhao
123	B03	Scheduling of Flexi-load through Extended Second Price Auctions in Smart Distribution Grids	Saptarshi Bhattacharya
124	B04	A Multi-agent Simulation Platform for Incentive-based Demand Response in Smart Distribution Grid	Xinbo Geng
125	B05	Decision Tree Based Novel Control Techniques for Microgrid Stability Enhancement	Riyasat Azim

126	B06	Power System Real-time Event Detection and Associated Data Archival Reduction Based on Synchrophasors	Yinyin Ge
127	B07	A Comparative Study of Optimal PMU Placement Algorithms for Cost Minimization	Timothy Nugent
128	B08	Real-Time Tuning of Power System Stabilizer	P. Arunagirinathan
129	B09	Agent Arbitration Approach for Coordinated Control in Active Power Network Management System	Ayodeji Owonipa
130	B10	Economic Assessment of Demand Side Response in the Future GB Electricity System	Fei Teng
131	B11	Intelligent Power Conditioning and Monitoring Interface for Smart Grids Prosumers (Prosumer Interface)	Chmielowiec Krzysztof
132	B12	Stability Design Criteria for Distribution Systems with Solid State Transformers	Darshit Shah
133	B13	Modeless Reconstruction of Missing Synchrophasor Measurements	Pengzhi Gao
134	B14	An Approach for Control of Battery Energy Storage Management Systems Considering Multiple Functions	Sherif Abdelrazek
135	B15	Nash Equilibria with Energy Trading in PV-Equipped Microgrids	M.Nazif Faqiry
136	B16	A Power Factor-Based Estimator of Load Capability for Smart Distribution Systems	Nicholas Coleman
137	B17	CIM Standards Conformed Cloud Based Power System Applications and Data Management tools	Gelli Ravikumar

## Cyber and Physical Security of Smart Grid

No.	ID	Poster Title	Student Name
138	B18	Local cyber attacks in power systems and protection strategy	Xuan Liu
139	B19	Application of Game-theoretic approaches for cyber-physical security of Smart Grid	Aditya Ashok
140	B20	Secure Distributed Energy Management in the Presence of Misbehaving Generation Units	Ziang Zhang
141	C01	Cyber Attacks on AC State Estimation: Unobservability and Physical Consequences	Liang Jingwen
142	C02	Secure Distributed Energy Management in the Presence of Misbehaving Generation Units	Ziang Zhang
143	C03	Modeling and Monte Carlo Simulation of Markovian Switching in Power Grid	Yichen Zhang
144	C04	Latency Monitoring of PMU Packets for Detecting Packet-Drop Attacks	Seemita Pal
145	C05	Cyber Risk Modeling of Hidden Failures in Smart Grid Protection System	Pengyuan Wang
146	C06	Implications of Cyber Attacks on Distributed Power System Operations	Jiazi Zhang
147	C07	Cyber Attacks on AC State Estimation: Unobservability and Physical Consequences	Liang Jingwen
148	C08	Resilience of Power Grids against Random Failures	Deepjyoti Deka
Advanced Computational Methods for Power System Planning, Operation, and Control			

No.	ID	Poster Title	Student Name
149	C09	Reserve Response Sets for Security-Constrained Unit Commitment with Wind	Joshua Lyon
150	C10	Dimensionality Reduction of Synchrophasor Data for Power System Event Classification	Yang Chen
151	C11	Distributed Security-Constrained Unit Commitment for Large-Scale Power Systems	Amin Kargarian
152	C12	Co-Simulation Platform for Smart Grid OPF	Adnan Anwar
153	C13	Stochastic Look-ahead Dispatch with Intermittent Renewable Generation via Progressive Hedging and L-shaped Method	Yingzhong Gu
154	C14	Fast Algorithms for Two-stage Robust Security Constrained Unit Commitment Problem	Wei Yuan
155	C15	Voltage and Reactive Power Control by using PV Power Factor and Var Controllers for Large Scale PV Penetration	Takayuki Ito
156	C16	Study of Wind Power Curtailment Considering Transient Stability	Takato Otani
157	C17	A Power Flow Adjustment Technique for Large Scale Generation Outages	Yuta Mori
158	C18	A MIP Based Optimization Framework for Unit Commitment and Energy Pricing	Yu Xia
159	C19	On the Robust Solution to SCUC with Load and Wind Uncertain Intervals	Bingqian Hu
160	C20	Power Flow Analysis with GPU-based Chebyshev Preconditioner and Conjugate Gradient Method	Xue Li
161	D01	Constraint relaxation based on risk-based security constrained economic dispatch	Xian Guo
162	D02	Stochastic Optimization Formulations for Reliability Unit Commitment Runs	Kai Pan
163	D03	Min-Max Regret Bidding Strategy for Thermal Generator Considering Price Uncertainty	Fan Lei
164	D04	Reliability Evaluation of Composite Electric Power Systems under Different Weather Conditions	Yang Liu
165	D05	Optimal Power Flow with Primary and Secondary Frequency Constraint	Guangyuan Zhang
166	D06	Security Constrained Unit Commitment Considering Voltage Stability	Mojtaba K. Ghehi
167	D07	Stochastic Security Constrained Unit Commitment in Parallel Structure	Chunheng Wang
168	D08	Security-Constrained Co-optimization Planning of Electricity and Natural Gas Transportation Infrastructures	Xiaping Zhang
169	D09	Bi-level Linear Programming Based Interval Optimization for SCED in the Presence of Wind Power Uncertainty	Ding Tao
170	D10	A MIP Based Optimization Framework for Unit Commitment and Energy Pricing	Yu Xia
171	D11	A Voltage Sag Severity Index Considering the Power System and Consumer Equipment	Xiang Zhou
172	D12	A Study of Hardware Requirements on Implementations of Phasor Measurement Algorithms	Samarth Deo

173	D13	Neighborhood Electric Vehicle Charging Scheduling Using Particle Swarm Optimization	Jouni Peppanen
174	D14	Load Forecasting Methods for Demand Resource Planning	Jonathan Berardino
175	D15	Power System Severe Contingency Screening Considering Renewable Energy	Jiang Yazhou
176	D16	Multi-Agent-Based Information Collection Algorithm for Isolated Power Systems	Guanqun Wang
177	D17	An Investigation of Capacitor Control and Demand Response Actions for Voltage Spread Reduction in Distribution Systems	Nicole Segal
178	D18	Modeling Flexibility and Optionality in Grid Planning using Multistage Stochastic Programming: The Benefits of Additional Decision Stages	Bala G.S. Kasina
179	D19	Role of Communication on the Convergence Rate of Fully Distributed DC Optimal Power Flow	Javad Mohammadi
180	D20	MDP Methods for Operation and Valuation of Multi-Purpose Battery Energy Storage under Uncertainty	Jonathan Donadee
181	E01	Assessing the Influence of Climatic Variables on Electricity Demand	Dao Vu
182	E02	Comprehensive and Smarter Load Shedding Scheme	Kaiumuzzaman Mollah
183	E03	Application of a Resistive Superconducting Fault Current Limiter for Shunt Capacitor Bank Switching	Elizaveta O. Egorova

## Emerging Software Needs for the Restructured Grid

No.	ID	Poster Title	Student Name
184	E04	Transmission Expansion Planning Under Uncertainty: the Stochastic Transmission Expansion Planning (STEP) Model	Pearl Donohoo

## System-Wide Events and Analysis Methods

No.	ID	Poster Title	Student Name
185	E05	A Study on Fluctuations in Electromechanical Oscillation Frequencies of Power Systems	Bin Wang
186	E06	A Comparative Study of Measurement-Based Thevenin Equivalents Identification Methods	Haoyu Yuan
187	E07	An Adaptive Three-bus Power System Equivalent for Estimating Voltage Stability Margin from Synchronized Phasor Measurements	Fengkai Hu
188	E08	Detection of Fault Event and Location with A Support Vector Machine-based Approach	Li-Yuan Hsu
189	E09	Identification and Wide-area Visualization of the Centers of Oscillation for a Large-scale Power System	Leonardo Bernal
190	E10	Outages on the GB Transmission Network due to Adverse or Extreme Weather	Kirsty Murray

## Intelligent Monitoring and Outage Management

No.	ID	Poster Title	Student Name
-----	----	--------------	--------------

191	E11	Differential Partial Discharge Extraction Technique for Online Power Transformer Insulation Assessment	Seo Junhyuck
192	E12	Measurement System for Power Quality Analysis of Energy-Saving Lamps	Yi-Ying Chen
193	E13	Real time monitoring of area stress via the susceptance and angle across the area	Atena Darvishi
194	E14	A Two-Stage Hybrid State Estimator for Dynamic Monitoring of Power Systems	Asprou Markos
195	E15	Behavior of Power Cable Resonant Frequencies Under Fault Conditions	Youngdeug Kim
196	E16	Performance Evaluation of Relays and Auto-Reclosing Operations	Min Lwin
197	E17	Speed up of Data-Driven State Estimation Using Low-Complexity Indexing Method	Yang Weng
198	E18	Improved Method for Locating Faults Upstream from Distributed Generation	Kyung Woo Min

## Integrating Renewable Energy into the Grid

No.	ID	Poster Title	Student Name
199	E19	Reliability Evaluation of Wind Farms Considering Generation and Transmission Systems	Mehdi Mosadeghy
200	E20	A Battery Energy Storage System Dual-Layer Control Strategy for Mitigating Wind Farm Fluctuations	Yuzhong Gong
201	F01	Incorporating Wind Power Self-Reserve in Energy and Reserve Scheduling with Substantial Wind Generation	Mojgan Mehdiabadi
202	F02	An Analytical Approach to Assess Static Voltage Stability of Distribution System with Rooftop PV Units	Jalil Yaghoobi
203	F03	A Novel Renewable Energy Technology - Energy Harvesting from Distilled and Stationary Water	Chien-Chang K. Kung
204	F04	Do-not-exceed Limits for Renewable Resources with Robust Corrective Topology Control	Akshay Korad
205	F05	Reliability Study of Onshore and Offshore Wind Generation and Impact of Location	Shijia Zhao
206	F06	A Battery Energy Storage System Dual-Layer Control Strategy for Mitigating Wind Farm Fluctuations	Yuzhong Gong
207	F07	A Equal Incremental Rate Continuous Time- varying Optimal Power Distribution Method for the Power System Containing Microgrids	Xiaobo Zhang
208	F08	Analysing the PV output variability and its mitigation through aggregation in Queensland	Saeid Raygani
209	F09	Verification of Voltage Ride-Through Capability of Wind Turbines Using Reachability Analysis	Hugo Villegas
210	F10	An Operating Reserve Risk Map for Quantifiable Reliability Performances in Renewable Power Systems	Mohammad Modarresi
211	F11	Impact of Wind Variations on Power System Sub-Synchronous Oscillation	Meng Wu
212	F12	A New Point Estimate Method for Probabilistic Load Flow With Correlated Variables Including Wind Farms	Can Chen

213	F13	Multi-objective Robust Optimization Model for Microgrids Considering Tie-line Power Constraints and Wind Uncertainty	Bai Linqun
214	F14	Frequency Response with Significant Wind Power Penetration: Case Study of a Realistic Power System	Nahid-Al Masood
215	F15	Application of DSTATCOM for Surplus Power Circulation in MV and LV Distribution Networks with Single-phase Distributed Energy Resources	Ruwan Chandrasena
216	F16	Emission-based Optimal Dispatch Framework with DR and Volatile Wind Power	Hantao Cui
217	F17	Dynamic Voltage Stability Analysis of Sub-Transmission Networks with Large-Scale Photovoltaic Systems	Shahariar Kabir
218	F18	Determination of Design Parameters for Direct-Drive Wind Turbines	Yichuan Niu
219	F19	Valuation of the Deterministic and Stochastic Uncertainty Models in Unit Commitment Applications	Yishen Wang
220	F20	Available Transfer Capability of Photovoltaic Generation Incorporated System	Xin Fang
221	G01	Harmonic Emissions in Grid Connected PV Systems: A Case Study on a Large Scale Rooftop PV Site	Annapoorna Chidurala
222	G02	Long Term Energy Storage Capacity Optimization in Energy Buffer System	Ahmad Abuelrub
223	G03	Minimizing Wind Power Spillage Using an OPF With FACTS Devices	Amin Nasri
224	G04	Optimal Coordination of Q(P) Characteristics among PV Systems in Distribution Grids for Minimizing Reactive Power Consumption	Afshin Samadi
225	G05	Adaptive Real Power Capping Methods for Fair Overvoltage Regulation of Distribution Networks with High Penetration of PV Systems	Junhui Zhao
226	G06	Frequency-Based Load Control Schemes Through Voltage Reduction for Power Systems with Wind Penetration	Felipe Wilches-Bernal
227	G07	Automatically Gain Tuning Control Method for Automatic Generation Control with Effects of Wind Resources	Yao Xu
228	G08	Reducing Post Contingency Congestion Risk and Wind Curtailment using Dynamic Line Rating	Binayak Banerjee
229	G09	Analysis of Time-varying Harmonics of Wind Power Plants using Wavelet Transform	Choongman Lee
230	G10	Application of Computational Intelligence in Reliability Improvement of Active Distribution Systems Through Feeder Reconfiguration	Salem Elsaiah
231	G11	PV Interconnection Risk Analysis through Distribution System Impact Signatures and Feeder Zones	Matthew Reno
232	G12	Application of Computational Intelligence in Reliability Improvement of Active Distribution Systems Through Feeder Reconfiguration	Salem Elsaiah
233	G13	Optimal Bidding Strategy of a Strategic Wind Power Producer in the Short-Term Market	Ting Dai



234	G14	Holonic Architecture for Loss Minimization in Distribution Systems with High Rooftop PV Penetration	Ahmadreza Malekpour
235	G15	Value of Wind Diversity for Increased Integration of Wind Power into the Grid	Novacheck Josh
236	G16	Supplementary control on a DFIG to damp small disturbance oscillations in a power system	Parimal Saraf
237	G17	Consumption Shifting Methodology and Optimization Approach for Demand Response Programs	Pedro Faria
238	G18	Large Scale Energy Storage Sizing to Mitigate Challenges in High Wind Penetration Scenarios	Hamideh Bitaraf
239	G19	Peak Performance of a Microgrid with Optimal Sizing of Energy Storage and Intelligent Control	Afshin Ahmadi

## Substation and Distribution Automation

No.	ID	Poster Title	Student Name
240	G20	Dynamic Adjustment of OLTC Parameters using Voltage Sensitivity while utilizing DG for Volt/VAr Support	Dothinka Rallage
241	H01	Recloser and Sectionalizer Placement for Reliability Improvement Using Discrete Event Simulation	Qiu Qin
242	H02	A Novel Wave-head Identification Method based on PCA & WMA	Fei Xu
243	H03	Faulty Line Identification by Distance Relay in Series Compensated Parallel Transmission Line	Venkatesh Chakrapani
244	H04	Dynamic Adjustment of OLTC Parameters using Voltage Sensitivity while utilizing DG for Volt/VAr Support	Dothinka Rallage

## Dynamic Performance and Control of Power Systems

No.	ID	Poster Title	Student Name
245	H05	Investigation of Reactive Power Limit Induced Voltage Collapse	Hung-Ming Chou
246	H06	Power System Mode Estimation Using Stochastic Subspace Identification Methods	Seyed Arash Sarmadi
247	H07	Distribution Side Mitigation Strategy for Fault Induced Delayed Voltage Recovery	Yuan Liu
248	H08	Singular Value Sensitivity Based Optimal Control of Embedded VSC based HVDC for Enhancing System Voltage Stability	Omar Urquidez
249	H09	Design of a Nonlinear Excitation Controller Using Inverse Filtering for Transient Stability Enhancement	Reza Goldoost Soolot
250	H10	Subspace Algorithms for Power System Oscillation Monitoring	Tianying Wu
251	H11	Stability Improvement with Series compensation on Transmission network	Naik Prem
252	H12	Distributed Excitation Control for Future Power Systems	Meimanat Mahmoudi
253	H13	A Lyapunov Function Based Remedial Action Screening Tool Using Real-Time Data	Mohammed Ben-Idris
254	H14	Grid-Adaptive Equivalencing of Power System for Generator Tripping	Daham Min
255	H15	Decentralized Communication and Control Systems for Power System Operation	Yannan Wang
256	H16	Control of DC voltage in Multi-Terminal VSC-HVDC System using H-infinity method	Mohammad Nazari

257	H17	Load Modeling in a Reduced WECC Model for Studying Voltage Controls	Yidan Lu
258	H18	A New Approach to Optimization of Dynamic Reactive Power Sources Addressing FIDVR Issues	Weihong Huang
259	H19	Methodology for droop control dynamic analysis of multi-terminal VSC-HVDC grids for offshore wind farms	Eduardo Prieto-Araujo
260	H20	Flatness-Based Control of Doubly Fed Induction Generator	Maryam Variani
261	I01	Novel Load Frequency Control in a Multi-agent based Microgrid Power System in Presence of Cyber Intrusions	Hessam Keshkar
262	I02	Impact of Induction Motor Load Dynamics on Droop Controlled Inverter based Microgrid	Puspall Hazra
263	I03	Lyapunov Function Based Remedial Action Schemes	Mohammad E. Raoufat
264	I04	Wide Area Control of Multi-machine Power Systems using Online Coherency Analysis	Ke Tang
266	I05	Near Optimal Fuel Scheduling for Enhanced Real Time Dispatch (RTD) with Diverse Generation Technologies	Nipun Popli

## Market Interactions in Power Systems

No.	ID	Poster Title	Student Name
267	I06	Analyzing the Impacts of Constraint Relaxation Practices in Electric Energy Markets	Yousef Al-Abdullah
268	I07	Inventory Management of DSCC System via Improved	Yongquan Nie
269	I08	Analysis of Market Operator Adjustments within Day-Ahead Energy Markets	Mojdeh Abdi-Khorsani
270	I09	An Optimal Framework for Residential Load Aggregators	Qinran Hu
272	I10	Cost Allocation in Stochastic Market Clearing	Ting Qiu
273	I11	Optimizing demand response price and quantity in wholesale markets	Ahlmahz Negash
274	I12	Uncertainty Clearing Price in Real-time Market	Hongxing Ye
275	I13	Incentive Based Demand Response to Reduce Costs and Minimize Price Volatility	Ailin Asadinejad
276	I14	Piecewise Affine Dispatch Policies for Economic Dispatch under Uncertainty	Daniel Munoz-Alvarez
277	I15	Production Scheduling Considering Energy Consumption	Mostafa G.

## Asset Management

No.	ID	Poster Title	Student Name
278	I16	A Diffusion-Driven Model for Investigating Moisture Effects on Dielectric Response Measurement of Transformer Insulation	Yi Cui
279	I17	Investigating the Sensitivity of Frequency Response Analysis on Transformer Winding Structure	Mohd Fairouz Yousof
280	I18	Experimental Research of Vibration Characteristics of Shunt Reactor	Song Chen
281	I19	Distributed Flywheel Energy Storage Systems for Mitigating the Effects of Pulsed Loads	Ahmed Elsayed
282	I20	Optimal transformer rating in the presence of probabilistic electric vehicle charging	Sachin Argade

283	J01	Quantifying Battery State-of-Health in Microgrid Applications	Christopher Lashway
-----	-----	---	---------------------

## Flexible AC Transmission Systems

No.	ID	Poster Title	Student Name
284	J02	Hybrid Power Flow Controller Modeling and Operating Constraints for Power Flow Studies	Behnam Tamimi
285	J03	Combinatorial Weighting Method for Lightning Transformation Effect Evaluation of 500kV Transmission Lines	Ruochen Duan
286	J04	Operating Regions of Modular Multilevel Converter under Various Cell Capacitances	Heejin Kim
287	J05	Optimal branch numbering for UPFC benefit study	Niannian Cai

## Power Electronics

No.	ID	Poster Title	Student Name
288	J06	High performance FPGA-based digital real-time controller for electric power conversion applications	Dziwinski Tomasz
289	J07	Unlocking Energy from Limit Cycles	Aaron Rosenthal
290	J08	Performance of a DC Multi-Converter Power System due to Variations of Plant Parameters	Juan Jimenez
291	J09	Improving Performance of Single-Phase SOGI-FLL under DC-Offset Voltage Condition	Tuan Ngo
292	J10	Modeling Six-level MMC with PQ Control in Simulink	Yan Ma
293	J11	Modeling Six-level MMC with PQ Control in Simulink	Yin Li
294	J12	Medium Frequency Soft Switching DC/DC Converter Based HVDC Transmission System	Tao Li
295	J13	Circulating Current Control for Reducing Energy Storage Requirement in Modular Multilevel Converter	Sangmin Kim

## Electric Machine and Drives

No.	ID	Poster Title	Student Name
296	J14	Application of Multifractal Spectrum to the Vibration Analyses of Power Transformer under DC Bias	Pei Gao
297	J15	Estimation of Stator Resistance in Direct Torque Control Synchronous Motor Drives	Younes Sangsefidi
298	J16	Induction Motor Control Based on Approximate Stator Flux	Saleh Ziaeinejad

## Power System Modeling and Simulation

No.	ID	Poster Title	Student Name
299	J17	Detailed Modeling of a Photovoltaic System for Distribution Networks	Farhan Mahmood
300	J18	Reliability Modeling and Evaluation of VSC-HVDC Transmission Systems	Guo Jingli
301	J19	Performance Analysis of Flux-lock Type SFCL Influenced by Characteristics of Two Coils	YU Zhao
302	J20	Simulation Studies of Cascading Blackouts via Hidden Failure-Based Load Shedding Models	Lai Po Jen

303	K01	Transient Model of Air-Conditioner Compressor Single Phase Induction Motor	Yuan Liu
304	K02	Stability Synthesis of Power Hardware-in-the-Loop (PHIL) Simulation	Mahdi D
305	K03	Dynamic Modeling of Electric Vehicle Movable Loads based on Driving Pattern Analysis	Difei Tang
306	K04	A Multi-input Lead-Lag Power System Stabilizer with H-infinity Control Performance	Junnosuke Kobayashi
307	K05	Comparison of Scenario Reduction Techniques for the Stochastic Unit Commitment	Yury Dvorkin
308	K06	Unified Stochastic And Robust Unit Commitment	Chaoyue Zhao
309	K07	A Model Predictive Approach for Community Battery Energy Storage System Optimization	Houman Pezeshki
310	K08	Identification of power system stressed conditions	Georgios Anagnostou
311	K09	Generalized Sequence Impedances and Fault Types for Polyphase Power Systems	Brian Pierre
312	K10	Unbalanced Distribution System Three-Phase State Estimation	Ankur Majumdar
313	K11	Performance Characterization for Photovoltaic-Vanadium Redox Battery Microgrid Systems	Tu Nguyen
314	K12	Appearance of multiple stable load flow solutions under power flow reversal conditions	Hung Nguyen
315	K13	Addressing illiquidity for intra-day and real-time markets for short-term hydropower planning	Vardanyan Yelena
316	K14	Expediting the Optimization Process of Measurement-based Load Modeling by Parameter Sensitivities	Jae-Kyeong Kim
317	K15	Aggregation of Induction Motor Load Models using Coherency-Based Technique	Kyungsung An
318	K16	Challenges for Balancing Area Coordination Considering High Wind Penetration	Robin B. Hytowitz
319	K17	Sequential Quadratic Programming Based Optimal Power Flow Incorporated with Magnetic Amplifier	Xiaohu Zhang
320	K18	Increasing Distribution System Model Accuracy with Extensive Deployment of Smart Meters	Jouni Peppanen
322	K20	Reliability Evaluation of Distribution System using Modified Sequential Monte Carlo Simulation	Banajiger Avinash
323	L01	Application of Droop Control in a Hybrid MTDC System	Omar Kotb
324	L02	Impact of Demand Side Management on the Tap Operation of Primary Distribution Transformers	Suvagata Chakraborty
325	L03	Modeling of Water Tree Capacitance in Underground Cables	Qi Chen
326	L04	Grid Connected Building Load Operation	Mohammed Muthalib
327	L05	Frequency Dependent Network Equivalent Model for Simultaneous Electromechanical and Electromagnetic Transient Analysis	Xu Zhang
328	L06	Stochastic Process Based Harmonic Current Regeneration for Harmonic Assessment in Wind Power Plant	Youngho Cho
329	L07	Case Study on Korea-China Grid Interconnection from Perspective of South Korea	Hyun-Jae Lee

# Cyber Attacks on AC State Estimation: Unobservability and Physical Consequences

Jingwen Liang, Oliver Kosut and Lalitha Sankar

School of Electrical, Computer, and Energy Engineering, Arizona State University, Tempe, AZ 85287, USA

Email: jingwen.liang@asu.edu, okosut@asu.edu, lalitha.sankar@asu.edu

**Abstract**—This paper develops both DC and AC attack models for an attacker restricted to such a subgraph, having access only to local measurements and no direct state information. It is shown that unobservability of the attack, in the absence of noise, is guaranteed when the attacker exploits its local network knowledge to perform AC SE locally than the simpler DC SE. Then, the consequences of such an unobservable attack are highlighted via a scenario in which the physical system is changed due to false data injection. Specifically, we give examples in which an unobservable false data attack on AC state estimation can impact the physical system via the control center re-dispatching generation by using ACOPF from the (corrupted) state estimate.

**Index Terms**—State estimation, false data injection, consequence.

## I. KEY EQUATIONS AND DESCRIPTIONS

The non-linear AC power flow measurement  $z$  is given by:

$$z = h(x) + e \quad (1)$$

where  $h(\cdot)$  denotes a non-linear relationship between the states and measurements and  $e$  is assumed to be independent and Gaussian distributed with 0 mean and  $\sigma^2$  covariance.

The attack model changes the  $i$ -th measurement from  $z_i$  to  $z_i^{(a)}$  such that:

$$z_i^{(a)} = \begin{cases} z_i & \text{if } i \notin I_S \\ \tilde{z}_i & \text{if } i \in I_S \end{cases} \quad (2)$$

where  $\tilde{z}_i$  is chosen by attacker and  $I_S$  denotes measurement indices inside of attack subgraph  $S$ .

If the  $k$ -th state  $x_k$  is required to compute  $h_i(x)$  for any  $i \notin I_S$ , then for any unobservable attack the corresponding  $k$ -th entry in attack vector must satisfy  $c_k = 0$ . Therefore, for a feasible attack, the attack region  $S$  must be chosen such that  $c$  is a non-zero vector. The whole attack subgraph will be:

$$S_{sum} = \bigcup_{\text{injection bus } k : c_k \neq 0} S_k \quad (3)$$

For a simple DC attack model

$$z_i^{(attack)} = \begin{cases} z_i & \text{if } i \notin I_{SP} \\ z_i + H_{(i,:)}c & \text{if } i \in I_{SP} \end{cases} \quad (4)$$

where,  $z_i$  denotes the  $i$ th measurement  $I_P$  denotes the sets of indices of active power measurements,  $I_{SP} = I_S \cap I_P$  and  $H_{(i,:)}$  denotes the  $i$ -th row of  $H$

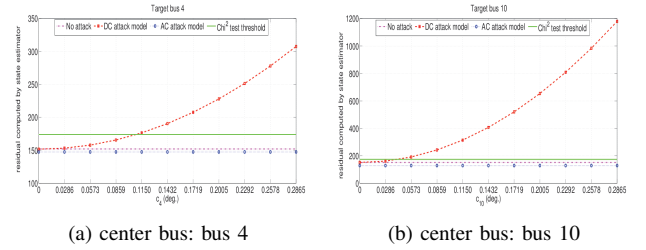
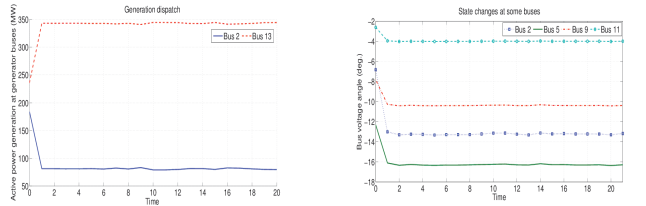


Figure 1: Residual for DC and AC attacks as the attacker increases the voltage angle of center bus



(a) For attack centered at bus 2, active power generation dispatch before and after attack. Attack starts at  $t = 1$  (b) For attack centered at bus 2, real state evolution at bus 2, 5, 9 and 11: Angle (degree)

Figure 2: Physical consequences

For a refined AC attack model

$$z_i^{(attack)} = \begin{cases} z_i & \text{if } i \notin I_S \\ h_i(\hat{x}_k + c) & \text{if } i \in I_S \end{cases} \quad (5)$$

where  $k \in K_S$  and  $\hat{x}_k$  is a state estimate found by the attacker using local AC state estimation from its available measurements in  $S$ .

## II. KEY RESULTS

### A. Unobservability

Fig.1 shows the residue of sample attacks. The attack with AC attack model passes through  $\chi^2$  bad data detector.

### B. Physical consequences

Fig.2 shows one scenario of continuous attack. The generation re-dispatch is triggered by line violation and decided by the output of ACOPF and the same attack vector  $c$  is applied during the time.

# Min-Max Regret Bidding Strategy for Thermal Generator Considering Price Uncertainty

Lei Fan, *Student Member, IEEE*; Jianhui Wang, *Senior Member, IEEE*; Ruiwei Jiang, *Member, IEEE*; Yongpei Guan, *Senior Member, IEEE*

**Abstract**—The electricity price volatility brings challenges to bidding strategies in the electricity markets. In this paper, we propose a minimax regret approach for a market participant to obtain an optimal bidding strategy and the corresponding self-scheduled generation plans. Motivated by recently proposed robust optimization approaches, our approach relies on the confidence intervals of price forecasts rather than point estimators. We reformulate the minimax regret model as a mixed-integer linear program (MILP), and solve it by the Benders' decomposition algorithm. Moreover, we design a bidding strategy based on the price forecast confidence intervals to generate the offer curve. Finally, we numerically test the minimax regret approach, in comparison with the robust optimization approach, on three types of thermal generators by using real electricity price data from PJM to verify the effectiveness of our proposed approach.

## I. KEY EQUATIONS

Under the minimax regret criterion, the objective function is to minimize the largest regret value  $\text{Reg}(x, y, z, p)$  over all possible scenarios of  $\lambda$  as follows:

$$(\text{MMRC}) \quad \min_{(x,y,z,p) \in \mathcal{S}} \max_{\lambda \in \Lambda} \text{Reg}(x, y, z, p). \quad (1)$$

The objective function (1) can be reformulated in the following way:

$$\begin{aligned} (\text{MMRC}) \quad & \min_{(x,y,z,p) \in \mathcal{S}} \max_{\lambda \in \Lambda} \text{Reg}(x, y, z, p) \\ & = \min_{(x,y,z,p) \in \mathcal{S}} \max_{\lambda \in \Lambda} \text{Prof}(\lambda) - \left\{ \lambda^\top p - c(x, y, z, p) \right\} \end{aligned} \quad (2)$$

$$\begin{aligned} & = \min_{(x,y,z,p) \in \mathcal{S}} \left\{ c(x, y, z, p) + \right. \\ & \quad \left. \max_{\lambda \in \Lambda, (\bar{x}, \bar{y}, \bar{z}, \bar{p}) \in \mathcal{S}} \left\{ \lambda^\top \bar{p} - c(\bar{x}, \bar{y}, \bar{z}, \bar{p}) - \lambda^\top p \right\} \right\}, \end{aligned} \quad (3)$$

The problem (MMRC) now becomes a two-stage optimization problem, in which the first stage decides the bidding amount and unit commitment decisions and the second stage discovers the worst-case price information.

$$\begin{aligned} (\text{MAP}) \quad & \min_{(x,y,z,p,\theta)} \left\{ c(x, y, z, p) + \theta \right\} \\ \text{s.t.} \quad & (x, y, z, p) \in \mathcal{S}, \\ & \theta \in \mathbb{R}. \end{aligned} \quad (4)$$

$$\begin{aligned} (\text{SUB}) \quad & \theta_s = \max_{\lambda, \bar{x}, \bar{y}, \bar{z}, \bar{p}} \left\{ \lambda^\top \bar{p} - c(\bar{x}, \bar{y}, \bar{z}, \bar{p}) - \lambda^\top p \right\} \\ \text{s.t.} \quad & (\bar{x}, \bar{y}, \bar{z}, \bar{p}) \in \mathcal{S}, \\ & \lambda \in \Lambda. \end{aligned} \quad (5)$$

## II. KEY FIGURES

Figure 1 shows the flowchart of the min-max regret algorithm.

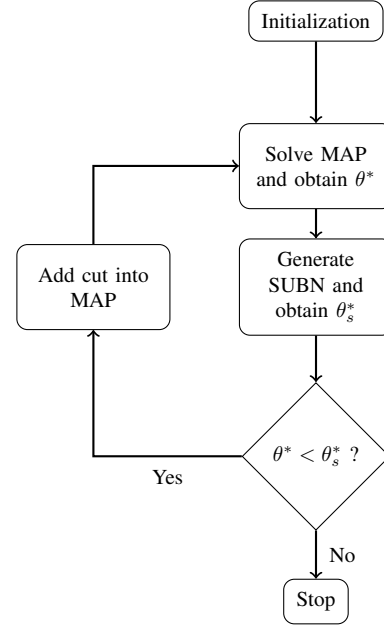


Fig. 1. Flowchart of the Min-max Regret Algorithm

## III. KEY RESULTS

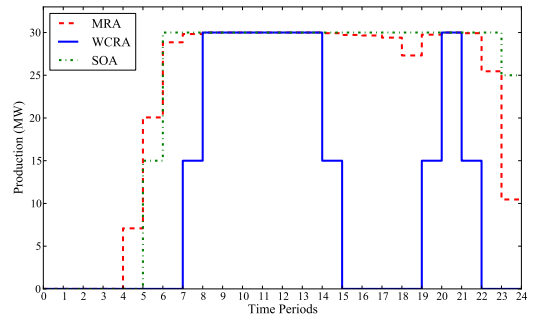


Fig. 2. G1 Generation Amounts for 24-hours in April

# Peak Performance of a Microgrid with Optimal Sizing of Energy Storage and Intelligent Control

A. Ahmadi, *Student Member, IEEE*

G. K. Venayagamoorthy, *Senior Member, IEEE*  
 Real-Time Power and Intelligent Systems Laboratory  
 Clemson University, Clemson, SC 29634, USA  
 aahmadi@clemson.edu and gkumar@ieee.org

R. Sharma, *Senior Member, IEEE*

NEC Laboratories America Inc., CA 95014, USA  
 ratnesh@nec-labs.com

**Abstract** — Advanced control systems for microgrids are critical to minimize the power outage to meet critical loads, and maximize the utilization of renewable sources of energy such as wind and solar. This paper presents a study on the impact of the size and state of charge (SOC) of a battery energy storage system for a given microgrid with a dynamic energy management system (DEMS). Results are presented to show the relative performance of the DEMS with different battery size and SOC.

**Index Terms**— battery, dynamic energy management system, micro-grids, renewable energy, state of charge.

## I. INTRODUCTION

Micro-grids integrate modular distributed energy sources, such as solar, wind, thermal generators, fuel cells, etc., with energy storage devices and both critical and noncritical loads to form low-voltage distribution systems. Traditional priority energy dispatch controllers dispatch energy based on power availability and the state of energy storage. The controller fulfills the entire critical and non-critical load without assigning priority, and will power up the battery only if more energy is available than load. If energy sources are not available, the battery fulfills full load demands until it discharges fully.

Intelligent DEMS controllers allow the renewable energy sources (RES) and energy storage devices to be utilized to their maximum in order to supply the critical load at all times. These controllers take into account state of charge (SOC) of battery storage to maximize its lifecycle and reduce O&M costs, while critical load is met. The size of battery storage plays a significant rule in the performance of microgrid as well.

To measure the impact of intelligent controllers on the performance of microgrid, a performance metric was developed (1). The maximum value of (1) is 1, which is obtained when all of the critical and controllable load requirements were met without the use of a diesel generator, grid import or a non-zero net battery discharge. The higher the value of the performance index (PI), the better the controller.

## II. KEY EQUATIONS

New Performance Index (PI-1) = (1)

$$\frac{\sum(P_{PV}(t) + P_W(t))}{\sum(P_{PV}(t) + P_W(t) + P_{DG}(t) + \alpha \cdot P_{B\_dischr}(t) + P_{G\_import}(t))} \cdot \frac{\sum(P_{NCL,D}(t))}{\sum(P_{NCL,S}(t))}$$

## III. KEY FIGURES

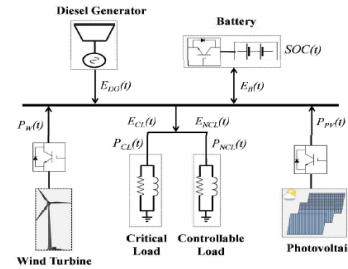


Fig. 1. Islanded micro-grid system.

## IV. KEY RESULTS

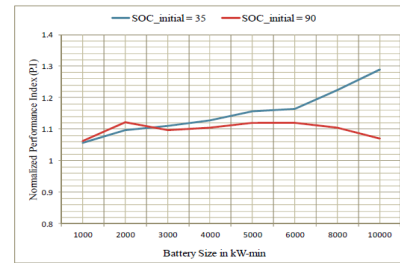


Fig. 2. Variation of normalized PI ( $\alpha = 1$  in (1)) with size of battery.

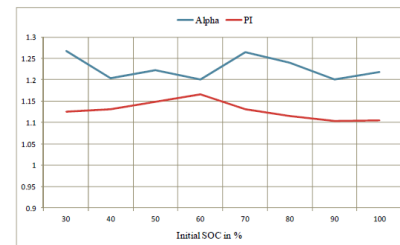


Fig. 3. Variation of  $\alpha$  and normalized PI with battery initial SOC for a 4000 kW-min battery capacity.

## REFERENCES

- [1] G. K. Venayagamoorthy, R. Sharma, and P. K. Gautam, "Dynamic Energy Management System for a Smart Micro-Grid", *submitted to IEEE Transactions on Neural Networks and Learning Systems*.
- [2] M.C. Bozchalui and R. Sharma, "Optimal operation of commercial building microgrids using multi-objective optimization to achieve emissions and efficiency targets," in *Proc. IEEE Power and Energy Society General Meeting*, pp. 1-8, July 22-26, 2012.
- [3] Luitel B, Venayagamoorthy G, "Decentralized Asynchronous Learning in Cellular Neural Networks," *IEEE Transactions on Neural Networks and Learning Systems*, November 2012, pp. 1755-1766, vol. 23. no. 11.

# On the Robust Solution to SCUC with Load and Wind Uncertain Intervals

Bingqian Hu, *Student Member, IEEE*, Lei Wu, *Senior Member, IEEE*, and Muhammad Marwali, *Senior Member, IEEE*

**Abstract**—This paper proposes an effective approach for deriving robust solutions to the security-constrained unit commitment (SCUC) problem, which considers load and wind uncertainties via interval numbers. Instead of exploring robust unit commitment (UC) solutions for immunizing against the worst economic scenario in terms of the highest minimum dispatch cost, the proposed robust SCUC model minimizes operation cost for the base case while guaranteeing that the robust UC and dispatch solutions could be adaptively and securely adjusted in response to uncertain intervals. The proposed robust SCUC model is solved by Benders decomposition, which decomposes the original problem into a master UC problem for the base case and subproblems for the base case network evaluation and the security checking for uncertain intervals. Feasibility cuts are generated and fed back to the master problem for further iterations when violations are identified in subproblems.

**Index Terms**—Benders decomposition, interval number, power system operation, robust SCUC, scenario-based approach.

## I. MODEL DESCRIPTION

$$\text{Min}_{P_{dt}^b \in D, P_{f,wt}^b \in W, P_{ik}^b, P_{it}^b, I_{it}^b, P_{wt}^b} \sum_t \sum_i \left[ \sum_k c_{ik} \cdot P_{ikt}^b + N_i \cdot I_{it}^b + SU_{it}^b + SD_{it}^b \right] \quad (1)$$

$$\sum_i P_{it}^b + \sum_w P_{wt}^b = \sum_d P_{dt}^b \quad (2)$$

$$P_i^{\min} \cdot I_{it}^b \leq P_{it}^b \leq P_i^{\max} \cdot I_{it}^b \quad (3)$$

$$0 \leq P_{ikt}^b \leq P_{ik}^{\max} \cdot I_{it}^b \quad (4)$$

$$P_{it}^b = \sum_k P_{ikt}^b \quad (5)$$

$$0 \leq P_{wt}^b \leq P_{f,wt}^b \quad (6)$$

$$\left[ X_{on,i(t-1)} - T_{on,i} \right] \cdot \left[ I_{i(t-1)}^b - I_{it}^b \right] \geq 0 \quad (7)$$

$$\left[ X_{off,i(t-1)} - T_{off,i} \right] \cdot \left[ I_{it}^b - I_{i(t-1)}^b \right] \geq 0 \quad (8)$$

$$SU_{it}^b \geq su_i \cdot \left( I_{it}^b - I_{i(t-1)}^b \right) \quad SU_{it}^b \geq 0 \quad (9)$$

$$SD_{it}^b \geq sd_i \cdot \left( I_{i(t-1)}^b - I_{it}^b \right) \quad SD_{it}^b \geq 0 \quad (10)$$

$$P_{it}^b - P_{i(t-1)}^b \leq UR_i \cdot I_{i(t-1)}^b + P_i^{\min} \cdot \left( I_{it}^b - I_{i(t-1)}^b \right) + P_i^{\max} \cdot \left( 1 - I_{it}^b \right) \quad (11)$$

$$P_{i(t-1)}^b - P_{it}^b \leq DR_i \cdot I_{it}^b + P_i^{\min} \cdot \left( I_{i(t-1)}^b - I_{it}^b \right) + P_i^{\max} \cdot \left( 1 - I_{i(t-1)}^b \right) \quad (12)$$

$$-PL_l^{\max} \leq \sum_m SF_{l,m} \cdot \left( \sum_{i \in U(m)} P_{it}^b + \sum_{w \in W(m)} P_{wt}^b - \sum_{d \in D(m)} P_{dt}^b \right) \leq PL_l^{\max} \quad (13)$$

$$\sum_i P_{it}^u \left( P_{dt}^u, P_{f,wt}^u \right) + \sum_w P_{wt}^u \left( P_{dt}^u, P_{f,wt}^u \right) = \sum_d P_{dt}^u \quad (19)$$

$$P_i^{\min} \cdot I_{it}^b \leq P_{it}^u \left( P_{dt}^u, P_{f,wt}^u \right) \leq P_i^{\max} \cdot I_{it}^b \quad (20)$$

$$0 \leq P_{wt}^u \left( P_{dt}^u, P_{f,wt}^u \right) \leq P_{f,wt}^u \quad (21)$$

$$-R_i^{\text{down}} \cdot I_{it}^b \leq P_{it}^u \left( P_{dt}^u, P_{f,wt}^u \right) - P_{it}^b \leq R_i^{\text{up}} \cdot I_{it}^b \quad (22)$$

$$P_{it}^u \left( P_{dt}^u, P_{f,wt}^u \right) - P_{i(t-1)}^u \left( P_{d(t-1)}^u, P_{f,w(t-1)}^u \right) \leq \quad (23)$$

$$UR_i \cdot I_{i(t-1)}^b + P_i^{\min} \cdot \left( I_{it}^b - I_{i(t-1)}^b \right) + P_i^{\max} \cdot \left( 1 - I_{it}^b \right)$$

$$P_{i(t-1)}^u \left( P_{d(t-1)}^u, P_{f,w(t-1)}^u \right) - P_{it}^u \left( P_{dt}^u, P_{f,wt}^u \right) \leq \quad (24)$$

$$DR_i \cdot I_{it}^b + P_i^{\min} \cdot \left( I_{i(t-1)}^b - I_{it}^b \right) + P_i^{\max} \cdot \left( 1 - I_{i(t-1)}^b \right)$$

$$-PL_l^{\max} \leq \left[ \sum_m SF_{l,m} \cdot \left( \sum_{i \in U(m)} P_{it}^u \left( P_{dt}^u, P_{f,wt}^u \right) + \sum_{w \in W(m)} P_{wt}^u \left( P_{dt}^u, P_{f,wt}^u \right) - \sum_{d \in D(m)} P_{dt}^u \right) \right] \leq PL_l^{\max} \quad (25)$$

$$D \left( P_{dt}^-, P_{dt}^+ \right) := \left\{ P_{dt}^u \in \left[ P_{dt}^-, P_{dt}^+ \right] \right\} \quad (26)$$

$$W \left( P_{f,wt}^-, P_{f,wt}^+ \right) := \left\{ P_{f,wt}^u \in \left[ P_{f,wt}^-, P_{f,wt}^+ \right] \right\}$$

## II. KEY FIGURES

*Step 1:* The master UC problem for the base case is solved, which minimizes the operation cost for the base case subject to constraints and all Benders cuts obtained so far.

*Step 2:* The base case hourly network evaluation subproblem checks possible network violations of the master UC solution for the base case.

*Step 3:* This step checks possible violations when wind and load vary within their uncertain intervals, which includes two substeps. The first substep solves for identifying the worst wind and load realizations that would lead to the largest minimum security violation. If the largest minimum violation is larger than the predefined threshold, the second substep solves the hourly security checking subproblem and generates the feasibility Benders cut.

*Step 4:* The iterative procedure stops when the master solution satisfies all security violation checks. That is, no more feasibility cuts are generated in Steps 2 and 3.

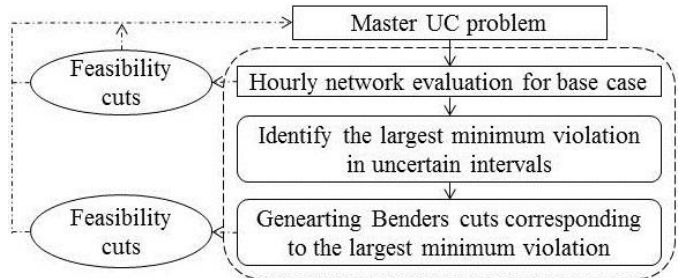


Fig. 1. Flowchart of the proposed solution methodology

## III. SOLUTION METHODOLOGY

We are working on the case study for this problem using the IEEE 6 bus system and 118 bus system. We will provided detailed results in the poster.

## References

- [1] B. Hu, L. Wu, and M. Marwali, "On the robust solution to SCUC with load and wind uncertainty correlations," *IEEE Trans. Power Syst.*, 2014 (to appear).



# A Distributed Data Storage and Processing Framework for Next-Generation Residential Distribution Systems

Ni Zhang, *Student Member, IEEE*, Yu Yan, *Student Member, IEEE*, and Wencong Su\*, *Member, IEEE*

Department of Electrical and Computer Engineering, University of Michigan-Dearborn, Dearborn, MI, USA

{niz, yuya, wencong}@umich.edu

**Abstract** - In the next-generation power system, the massive volume of real-time data will help the power system operators gain a better understanding of a large-scale and highly dynamic power grid. In order to maintain the reliability and stability of the grid, a large amount of data, which is collected by the local devices referred to as smart meters, are needed for monitoring and controlling the system as well as predicting the electricity price. Therefore, how to store and process the great amount of data becomes a critical issue. In conventional power systems, the system operation is performed using purely centralized data storage and processing approaches. As the number of smart meters increases to more than hundreds of thousands, and huge amount of data would be generated. It is rather intuitive that the state-of-the-art centralized information processing architecture will no longer be sustainable under such data-explosion. On the other hand, to protect the privacy and keep the fairness of market competition, some users do not wish to disclose their operational conditions to each other. A fully distributed scheme may not be practically possible either. This poster shows a radically different approach through a Hadoop-based high-availability and fault-tolerant distributed data management framework to handle a massive amount of Smart Grid data in a timely and reliable fashion. All the system operational information is executed into the distributed data storage and processing platform which consists of a cluster of low-cost commodity servers. This high-availability distributed file system and data processing framework can be easily tailored and extended to support data-intensive Smart Grid applications in a full-scale power system.

## I. KEY CONCEPT

Investigate a radically different approach through distributed software agents to process a massive amount of smart meter data in a timely and reliable fashion. Also, we substantiate the proposed distributed data storage and processing framework on a proof-of-concept testbed for the grid, in order to do so, a large amount of data, which is collected

by the local devices.

So far, we have four technical challenges:

**High-Volume:** smart meter data is expected to be in much larger quantities in the near future

**High-Velocity:** the high-speed data processing and storage is needed.

**High-Variety:** non-traditional data formats may exhibit a dizzying rate of change.

Need to move smart grid operations from being **data-intensive** to information-directed.

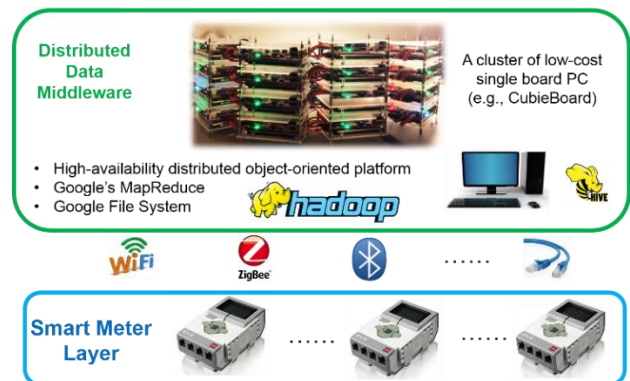


Fig. 1 Hadoop-based proof-of-concept demonstration

Fig. 1 shows the Hadoop-based proof-of-concept demonstration using a cluster of low-cost and credit-card-sized single-board computers.

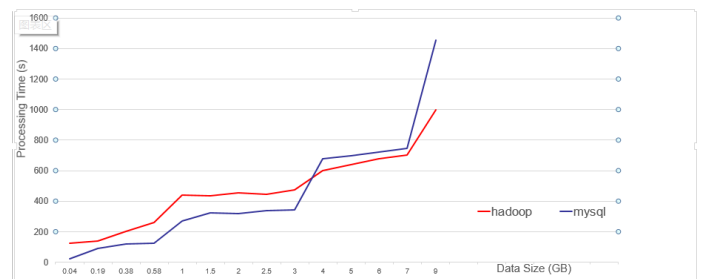


Fig. 2 Performance analysis

Fig. 2 shows the data processing performance on smart meter application using Apache Hadoop's Hive and conventional database (MySQL server).

# A New Point Estimate Method for Probabilistic Load Flow With Correlated Variables Including Wind Farms

<sup>1</sup>Can Chen, <sup>1</sup>Wenchuan Wu, <sup>1</sup>Boming Zhang, <sup>2</sup>Chanan Singh

1. Department of Electrical Engineering Tsinghua University  
Beijing 100084, P.R.China

2. Department of Electrical and Computer Engineering  
Texas A&M University  
College station, TX 77843 USA

**Abstract**—In this paper, a novel probabilistic load flow (PLF) method that combines Nataf transformation with Zhao’s point estimate method (PEM) is proposed. The new method can deal with correlated non-normal input random variables (RVs) in PLF evaluation with improved accuracy and less computation time than existing methods. The proposed method is applied to a modified IEEE 118-bus test system with wind farms. A comparison with Monte Carlo Simulation (MCS) using correlated variables is presented. In the end, the sensitivity analysis considering different correlation coefficients of wind speed is shown.

## I. KEY EQUATIONS

A. Get sample matrix  $\mathbf{S}_z$  in independent standard normal space

B. Get sample matrix  $\mathbf{S}_w$  in correlated standard normal space

Make Cholesky decomposition on correlation matrix  $\mathbf{C}_w$ ,  $\mathbf{C}_w = \mathbf{B}\mathbf{B}^T$ , where  $\mathbf{B}$  is a lower triangular matrix. Then,  $\mathbf{S}_w$  can be obtained using  $\mathbf{S}_w = \mathbf{S}_z\mathbf{B}$ .

C. Get sample matrix  $\mathbf{S}_y$  in desired space

$$w_k = \Phi^{-1}(F_k(y_k)), k = 1, 2, \dots, n \quad (1)$$

Where  $\Phi$  is the CDF of standard normal distribution and  $F_k$  is the CDF of input variable  $y_k$ .

D. Perform load flow calculation

E. Statistical analysis of output variables

The load flow equation can be approximated using the following expressions.

$$g(\mathbf{Y}) \approx \sum_{i=1}^n (g_i - g_\mu) + g_\mu \quad (2)$$

Where

$$g_i = g(N^{-1}(\mathbf{Z}_i)) \quad (3)$$

$$\mu_x = \sum_{i=1}^n (\mu_{x_i} - g_\mu) + g_\mu \quad (4)$$

The mean and  $k^{\text{th}}$  order statistical moments of the output variables

$$M_{kx} = \sum_{i=1}^n M_{kx_i}, k = 2, 3 \quad (5)$$

Where

$$\mu_{x_i} = \sum_{m=1}^3 p_m g(N^{-1}(\mathbf{Z}_{i-m})) \quad (6)$$

$$M_{kx_i} = \sum_{m=1}^3 p_m (g(N^{-1}(\mathbf{Z}_{i-m})) - \mu_{x_i})^k, k = 2, 3 \quad (7)$$

## II. KEY RESULTS

TABLE 1 AVERAGE RELATIVE ERRORS FOR BUS VOLTAGES USING TWO TRANSFORMATION METHODS

Transformation Method	Average relative error for bus voltages (%)	
	$\bar{\varepsilon}_\mu^V$	$\bar{\varepsilon}_\sigma^V$
Nataf	0.0237	2.4338
Orthogonal	0.0238	2.5921

TABLE 2 AVERAGE RELATIVE ERRORS FOR LINE POWER USING TWO TRANSFORMATION METHODS

Transformation Method	Average Relative Error For Active Power (%)	
	$\bar{\varepsilon}_\mu^P$	$\bar{\varepsilon}_\sigma^P$
Nataf	1.3709	2.4101
Orthogonal	1.3710	2.5527

TABLE 3 SIMULATION TIME COMPARISON

Method	PEM	CMCS
Time (s)	14.58	220.71

## III. CONCLUSIONS

The main features of the proposed method are as follows. Nataf transformation is more accurate in dealing with correlated non-normal RVs’ sampling, so the proposed method can achieve computation results with higher accuracy. Compared with the CMCS method with 5000 iterations, the computational time is significantly reduced. In conclusion, the method reported here is found to be effective for power system PLF calculations with correlated wind farms.

# Security-Constrained Co-optimization Planning of Electricity and Natural Gas Transportation Infrastructures

Xiaping Zhang, Student Member, IEEE, Mohammad Shahidehpour, Fellow, IEEE

Department of ECE, Illinois Institute of Technology, Chicago, IL, USA, Email: [xzhan126@hawk.iit.edu](mailto:xzhan126@hawk.iit.edu), [ms@iit.edu](mailto:ms@iit.edu)

**Abstract**— This paper presents a co-optimization planning model that considers the long-term interdependency of natural gas and electricity infrastructures. The model incorporates the natural gas transportation planning objective in the integrated planning of power generation and transmission systems. The co-optimization planning model is decomposed into a least-cost master planning problem for natural gas and electricity systems which interacts with feasibility (security) and optimality (economic) subproblems. In addition, the natural gas subproblem would check the feasibility of fuel supply transportation system as part of the power system integrated planning. Furthermore, the power system reliability subproblem would ensure that the co-optimization planning of electricity and natural gas infrastructures satisfies the desired power system reliability criterion. The iterative process will continue between the co-optimization planning and reliability subproblem until an economic, secure, reliable, and fuel-supply feasible planning for the two interdependent infrastructures is obtained.

## I. INTRODUCTION

North American electric power sector has transitioned from a small consuming sector of the natural gas industry to the largest consuming sector in the last decade. The majority of new power generating capacity projected for the next decade is expected to utilize natural gas as its primary fuel driven by low prices and increasingly stringent environmental regulations. This increased reliance on natural gas as the primary source of fuel for power generation could intensify the electric power system's exposure to shortcomings in natural gas supply and delivery systems and raise challenges to the long-term system planning in some regions of the country. Consequently, we incorporate the fuel supply associated with specifics of natural gas infrastructure in the power system expansion planning in this work.

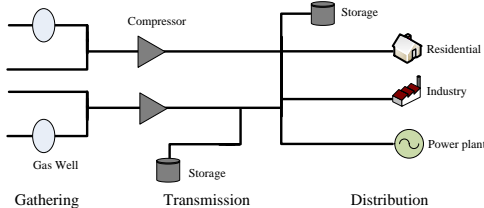


Fig. 1. Natural gas system architecture

## II. KEY EQUATIONS OF CO-OPTIMIZATION PLANNING

The co-optimization planning model is to minimize the total present value of the interdependent electricity and natural gas infrastructures in the planning horizon. The objective (1) includes the annual investment planning and operation costs associated with generating units ( $GC_{it}$ ), transmission lines ( $FC_{it}$ ), and natural gas pipelines ( $PC_{pt}$ ), in addition to the cost of unserved energy.

$$\begin{aligned} \text{Min} \quad & \sum_t \sum_{i \in CG} \frac{1}{(1+d)^{t-1}} GC_{it} + \sum_t \sum_{i \in CL} \frac{1}{(1+d)^{t-1}} FC_{it} + \sum_t \sum_{p \in CP} \frac{1}{(1+d)^{t-1}} PC_{pt} \\ & + \sum_t \frac{1}{(1+d)^{t-1}} VOLL \times EENS \end{aligned} \quad (1)$$

A decomposition strategy is applied to solve the problem as shown in Fig. 2. The planning candidates identified at the master planning problem would be checked for feasibility (security) and optimality (economic) by the corresponding subproblems.

The natural gas transportation feasibility subproblem is to minimize the nodal natural gas load imbalance with steady state natural gas flow constraints (2). The natural gas required by each gas-fired unit depends on its hourly dispatch, which represents as negative injection in gas network node. Natural gas suppliers including gas wells and storage facilities are modeled as positive gas injections in the natural gas network.

$$\text{Min} \quad w_{bht} = \mathbf{1}^T * w_1 + \mathbf{1}^T * w_2 \quad (2)$$

$$\sum_{sp=1}^{NGS} E_{jsp} v_{sp} - \sum_{l=1}^{NGL} D_{lg} L_g - \sum_{p \in G(j)} f_p + w_1 - w_2 = 0$$

The reliability subproblem is to minimize the power system load curtailment (3). EENS (expected energy not supplied) is adopted as index to measure the system reliability.

$$\text{Min} \quad W_{bht} = \mathbf{1}^T * S_1 + \mathbf{1}^T * S_2 \quad (3)$$

$$K * PL_{bht} + S_1 - S_2 = A * P_{bht} - B * PD_{bht}$$

$$EENS_t = \sum_h \sum_b DT_{bht} W_{bht}$$

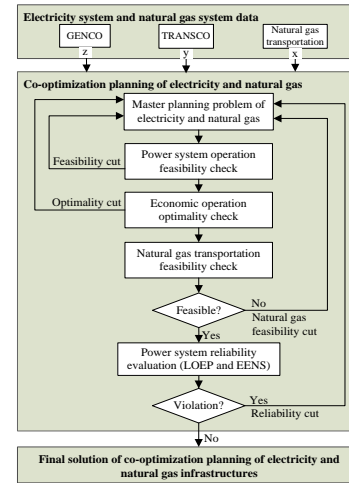


Fig. 2. Flowchart of security-based co-optimization planning

## III. KEY RESULTS

A 20-year planning horizon study of IEEE 118-bus system with 14-node natural gas system is reported in Table I. Results demonstrate that natural gas transportation constraints would impact the long-term planning schedule. The installation of new pipelines and fuel switch capabilities are effective strategies for alleviating intense fuel shortage constraints and further reducing the operation cost.

TABLE I COMPARISON OF CO-OPTIMIZATION PLANNING COSTS

Cost (\$Billion)		Case 1	Case 2	Case 3	Case 4
Investment cost	Generation unit	0.271	0.243	0.316	0.292
	Transmission line	0.039	0.046	0.052	0.039
	Natural gas pipeline	-	-	0.011	-
Operation cost		4.081	4.139	4.047	4.062
Unserved energy cost		.0007	.0010	.0008	.0009
Total planning cost		4.393	4.429	4.427	4.402

**Note:** **Case1:** Planning of only generating units and transmission lines.  
**Case2:** Natural gas transportation constraints are incorporated in Case1.  
**Case3:** Installing new natural gas pipelines are considered in Case2.  
**Case4:** Gas-fired units are assumed to have fuel switching capability.

# Reliability Study of Onshore and Offshore Wind Generation and Impact of Location

Shijia Zhao, *Student Member, IEEE*, Chanan Singh, *Fellow, IEEE*

Department of Electrical and Computer Engineering  
Texas A&M University, College Station, 77843, TX USA  
Email: zsjames@tamu.edu, singh@ece.tamu.edu

**Abstract**—In this poster, reliability study of potential wind generation in Texas has been conducted with the objective of providing some insights into issues that one faces in making various choices. Through comparison between potential onshore and offshore wind farm sites, offshore wind farms prove to have slightly lower reliability due to higher variation of wind patterns. The study also includes the impact of wind farm location, which could be of importance in making operational and planning decisions.

## I. KEY DATA SOURCES

### A. Onshore Wind Generation

In order to investigate the impact of location, 3 nearby sites and 3 faraway sites are chosen from Fig. 1.

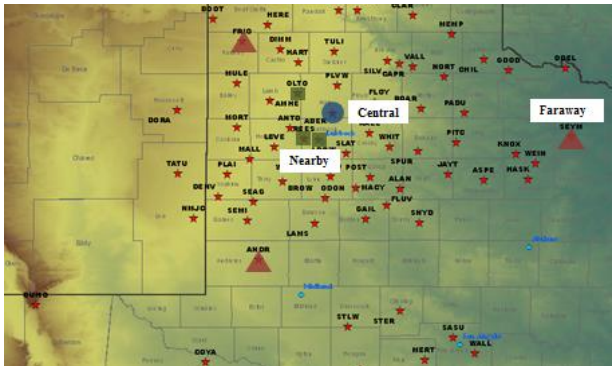


Figure 1 Map of onshore wind farm sites

### B. Offshore Wind Generation

In order to investigate the impact of location, 3 nearby wind farm sites and 3 faraway wind farm sites are chosen from Fig. 2.

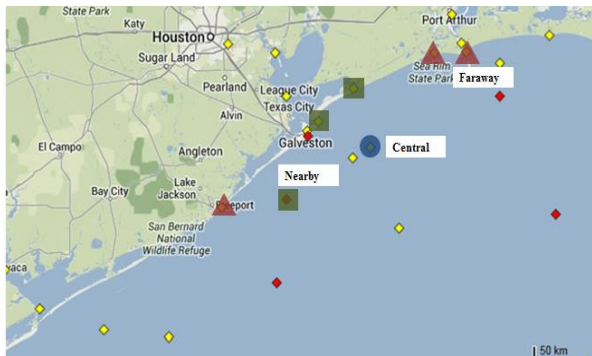


Figure 2 Map of offshore wind farm sites

## II. KEY CONSLUCIONS

Reliability study of onshore/offshore wind generation in Texas was conducted; impact of location was considered under different penetration levels. With insights analysis of the case study, the following observations can be made, two selected reliability indices are shown in Fig. 3.

1. Reliability of system with wind power generation results from a combination of impacts of both wind output average and wind output variance.
2. Reliability of system is reduced with increase of wind power penetration level because wind output average is much less than output average of reliable traditional generation.
3. Without considering impact of location, offshore wind farms appear to have slightly lower reliability than onshore wind farms due to high wind output variance.
4. Impact of location is a combination of impacts of both wind output average and variability, yet faraway clustering proves to have greater “smoothing” effect than nearby clustering due to the high geographic correlation between nearby farms.

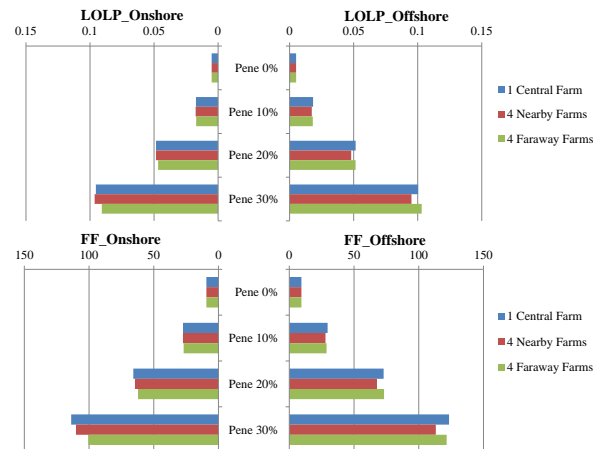


Figure 3 Selected case study results

# Fast Algorithms for Two-stage Robust Security Constrained Unit Commitment Problem

Wei Yuan, *Student Member, IEEE* and Bo Zeng, *Member, IEEE*, Tongxin Zheng, *Member, IEEE*, and Eugene Litvinov, *Fellow, IEEE*

**Abstract**—Unit Commitment problem plays a key role in power systems’ operations. Due to the capacity of robust optimization to deal with the uncertainties in power systems, including renewable generation, demand uncertainty, demand response, and contingencies, two-stage Unit Commitment problem has been developed and intensively studied both in academia and industry. However, this tri-level optimization problem is difficult to solve considering large-scale real power systems. In this research, we investigate the state-of-art strong formulations for basic Unit Commitment model, derive new valid inequalities considering network constraints and implement a novel cutting plane generation procedure. On a large-scale test system, our solution approach leads to a much better computational performance, compared to existing formulations or methods.

## I. INTRODUCTION

The unit commitment problem is a critical problem in the power industry. The unit commitment problem minimizes system-wide operational costs by providing an optimal power generation schedule for each generator so that the demand for electricity is met considering the constraints for generators and transmission network. To improve power generation efficiency and reduce greenhouse gas emissions, more and more renewable energy sources ( solar, wind, tidal etc.) are incorporated into power grid in addition to traditional coal and natural gas generation. However, uncertainty and intermittent generation pattern in renewable energy and the complexity of demand side management pose huge challenges.

Two-stage robust unit commitment problem [1] is thus formulated to deal with uncertainties in a power grid. However, the model complexity which ensures the reliability of the system cast heavy burden on solution algorithms. So far, most algorithms for two-stage robust unit commitment problem are not fast enough for real-time market operations.

## II. KEY EQUATION

An abstract formulation of the two-stage unit commitment model is formulated as the following.

$$\text{RUC} : \min_{\mathbf{y}, \mathbf{z}} (\mathbf{a}\mathbf{z} + \mathbf{r}\mathbf{y}) + \max_{\mathbf{v} \in \mathbb{V}} \min_{\mathbf{x}, \mathbf{s} \in \Omega(\mathbf{y}, \mathbf{z}, \mathbf{v})} (\mathbf{g}\mathbf{x} + \mathbf{q}\mathbf{s}) \quad (1)$$

$$\text{st. } \mathbf{D}\mathbf{y} + \mathbf{F}\mathbf{z} \geq \mathbf{f}; \mathbf{y}, \mathbf{z} \text{ binary} \quad (2)$$

$$\Omega(\mathbf{y}, \mathbf{z}, \mathbf{v}) = \{(\mathbf{x}, \mathbf{s}) : \mathbf{E}\mathbf{X} \leq \mathbf{e}, \quad (3)$$

$$\mathbf{A}\mathbf{X} \leq \mathbf{L} - \mathbf{G}\mathbf{y}, \mathbf{I}\mathbf{x} + \mathbf{H}\mathbf{s} = \mathbf{v}\} \quad (4)$$

where  $\mathbf{y}, \mathbf{z}$  are the first stage commitment decisions that take binary values,  $(\mathbf{x}, \mathbf{s})$  are the second stage economic dispatch and (market buy/sell) decisions that are continuous,  $\mathbf{v}$  represents some uncertain factor, e.g., the renewable energy generation, load uncertainty or contingencies, whose randomness is captured by the uncertainty set  $\mathbb{V}$ . Detailed formulation can be found in [1, 2].

## III. METHODOLOGY

The formulation of basic unit commitment is essential for the solution of robust unit commitment problem. We first investigate tight formulations for unit commitment based on [3] and validate the correctness and effectiveness of replacing traditional unit commitment problem constraints with tight constraints. We then incorporate strong formulations into robust Unit Commitment model and analyze their performance improvement.

Generally, transmission network is a large complex network which makes the unit commitment even harder to solve. We investigate and implement possible network reduction technique to reduce the complexity of transmission network by reducing buses and transmission lines without losing optimality of unit commitment.

In addition, a set of valid inequalities based on partitioning the power grid are developed and investigated, which leads to significant computational improvements.

## REFERENCES

- [1] L. Zhao and B. Zeng, “Robust unit commitment problem with demand response and wind energy,” in *Power and Energy Society General Meeting, 2012 IEEE*. IEEE, 2012, pp. 1–8.
- [2] D. Bertsimas, E. Litvinov, X. A. Sun, J. Zhao, and T. Zheng, “Adaptive robust optimization for the security constrained unit commitment problem,” *Power Systems, IEEE Transactions on*, vol. 28, no. 1, pp. 52–63, 2013.
- [3] J. Ostrowski, M. F. Anjos, and A. Vannelli, “Tight mixed integer linear programming formulations for the unit commitment problem,” *Power Systems, IEEE Transactions on*, vol. 27, no. 1, pp. 39–46, 2012.

W. Yuan and B. Zeng are with the Department of Industrial and Management Systems Engineering, University of South Florida, Tampa, FL, 33620 USA (e-mail: weiyuan@mail.usf.edu; bzeng@usf.edu)

T. Zheng and E. Litvinov are with ISO New England, Inc., Holyoke, MA 01040 USA (e-mail: tzheng@iso-ne.com; elitvinov@iso-ne.com).

# Benefits of DC Microgrids: Economic Operation and Enhancing the Resilience by Hierarchical Control

Liang Che, *Student Member*, Mohammad Shahidehpour, *Fellow, IEEE*

Electrical and Computer Engineering Department, Illinois Institute of Technology, Chicago, IL 60616, USA.

E-mail: [lche@hawk.iit.edu](mailto:lche@hawk.iit.edu), [ms@iit.edu](mailto:ms@iit.edu)

**Abstract**—The penetration of DC distributed energy resources (DERs) and the growth of DC loads have attracted attentions to the DC microgrids. DC microgrids can offer more straightforward interfaces to the DC generations, fewer stages of power conversions, less complicated control strategies and higher resilience. In this paper, the structure, components and the hierarchical control strategy of a DC microgrid, with natural-gas turbine, solar PV and wind generations and battery storages, are discussed and analyzed. The simulation results are compared with those of an AC microgrid and demonstrate that the proposed hierarchical coordinated DC strategy is an effective way of optimizing the economic operation at steady state and the resilience of DC microgrids in emergencies. Case studies are applied to an existing microgrid at Illinois Institute of Technology (IIT) to test the economic operation and the resilience of the IIT DC microgrid.

## I. KEY FIGURES

Fig. 1 shows the proposed DC configuration for an existing microgrid at IIT, where the natural-gas turbine, battery storage, and the PV and wind generations are connected into seven loops. A hierarchical coordinated control strategy including the primary, secondary and tertiary control is applied to the IIT DC microgrid.

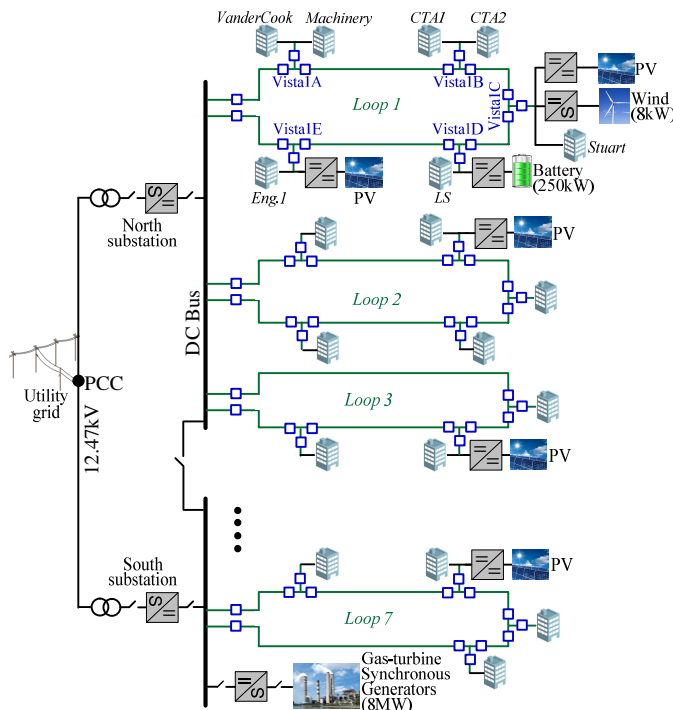


Fig. 1. Configuration of DC microgrid at IIT.

## II. KEY RESULTS

In this paper, we consider the same cases as in the AC version [1]-[2] and compare the results in this study with those in [1]. The simulation cases, with the results shown in Fig. 2, address the economic operation and short-time reliability of the IIT DC microgrid in both grid-connected and island mode. The simulation results verify the proposed hierarchical coordinated DC strategy is an effective way of optimizing the economic operation at steady state and the resilience in emergencies of DC microgrids.

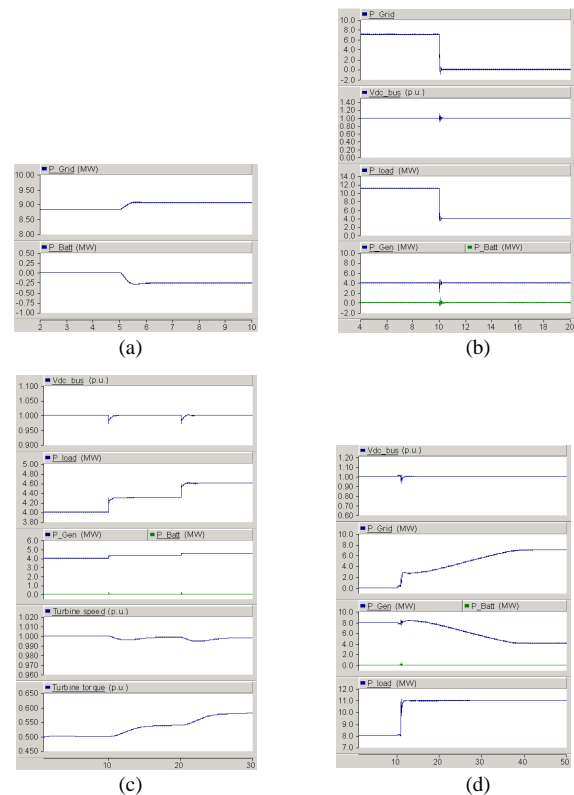


Fig. 2. Case studies for DC IIT microgrid: (a) economic dispatch of battery storage in grid-connected mode; (b) unplanned islanding due to external fault; (c) load restoration in island mode; and (d) resynchronization to the utility grid.

## REFERENCE

- [1] L. Che, M. Khodayar and M. Shahidehpour, "Only Connect: Microgrids for Distribution System Restoration," *IEEE Power Energy Mag.*, vol. 12, no. 1, pp. 70-81, Jan/Feb. 2014.
- [2] M. Shahidehpour and M.E. Khodayar, "Cutting Campus Energy Costs with Hierarchical Control: The Economical and Reliable Operation of a Microgrid," *IEEE Electric. Mag.*, vol. 1, no. 1, Sep. 2013.



# A Battery Energy Storage System Dual-Layer Control Strategy for Mitigating Wind Farm Fluctuations

Yuzhong Gong, Quanyuan Jiang, and Haijiao Wang

College of Electrical Engineering  
Zhejiang University  
Hangzhou, China

Email: [yzgong@zju.edu.cn](mailto:yzgong@zju.edu.cn), [jqy@zju.edu.cn](mailto:jqy@zju.edu.cn), [wanghaijiao@zju.edu.cn](mailto:wanghaijiao@zju.edu.cn)

**Abstract**— The intermittent power output of a wind farm is the main challenge behind increasing wind power penetration of power systems. This paper proposes a battery energy storage system (BESS) dual-layer control strategy—consisting of a fluctuation mitigation control layer and a power allocation control layer—to mitigate wind farm power output fluctuations. The fluctuation mitigation control layer calculates the power instructions for the BESS so that the combined wind farm and BESS power output meets fluctuation mitigation requirements (FMR). The layer implements a flexible first-order low-pass filter (FLF), updating the time constant of the FLF through use of a particle swarm optimization (PSO) algorithm. The power allocation control layer optimizes power instructions allocation among the battery energy storage units of the BESS. The layer’s energy management of the BESS uses a mixed-integer quadratic programming (MIQP) model, which improves reliability. Moreover, the paper compares two types of charge/discharge switching constraints to reduce the number of charge/discharge cycles, which can prolong the operational lifetime of the BESS. Finally, the effectiveness of the proposed dual-layer control strategy is verified through case studies.

## I. KEY EQUATIONS

The power instruction of BESS is obtained with the flexible first-order low-pass filter (FLF) as follow.

$$\begin{cases} P'_{O,exp} = \frac{T_f}{T_f + \Delta t} \cdot P'_{O,exp} + \frac{\Delta t}{T_f + \Delta t} \cdot P'_W \\ P'_{B,ord} = P'_{O,exp} - P'_W \end{cases} \quad (1)$$

Two types of charge/discharge switching constraints based on duration time and residual energy are proposed to reduce the number of charge/discharge cycles as follow.

$$\begin{cases} U'_{i+*} (D_{i-}^{\min} - C_{i-}^{t-1}) \leq 0 \\ U'_{i-*} (D_{i+}^{\min} - C_{i+}^{t-1}) \leq 0 \end{cases} \quad (2)$$

$$\begin{cases} U'_{i+*} (E_i^t - \delta_+) \geq 0 \\ U'_{i-*} (E_i^t - \delta_-) \leq 0 \end{cases} \quad (3)$$

The expended lifetime of batteries after  $N_C$  cycles is calculated as

$$Life_{\text{expended}} = \sum_{i=1}^{N_C} \frac{1}{\text{CycleLife}(DOD)} \times 100\% \quad (4)$$

## II. KEY FIGURES

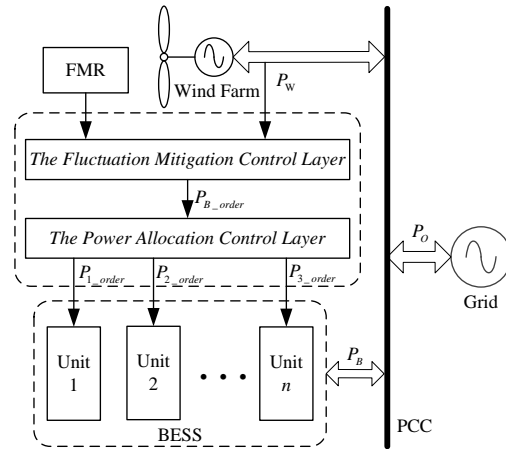


Fig. 1. Wind farm power fluctuations mitigation with BESS

## III. KEY RESULTS

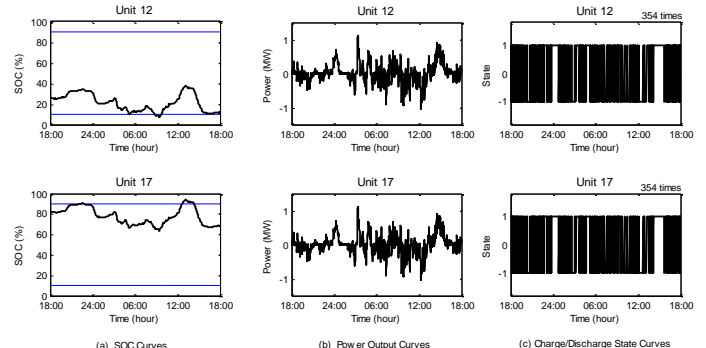


Fig. 2. Typical operating curve with average allocation strategies

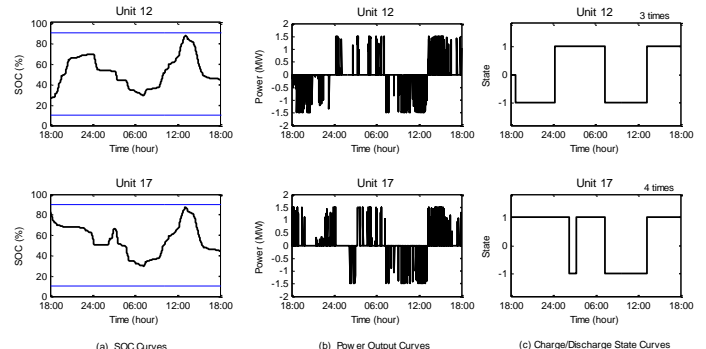


Fig. 3. Typical curves with residual capacity constrained model

# Analysing the PV output variability and its mitigation through aggregation in Queensland, Australia

Saeid Veysi Raygani, *Student Member, IEEE*, Rahul Sharma, *Member, IEEE*, Tapan K. Saha, *Senior Member IEEE*  
 The University of Queensland  
 Brisbane, Australia  
 s.veysiraygani@uq.edu.au, rahul.sharma@uq.edu.au, saha@itee.uq.edu.au

**Abstract**— Aggregation of photovoltaic (PV) plants has a potential to reduce the variability in power output to enhance large-scale integration of PV plants with power systems. Nevertheless, effectiveness of aggregation has to be evaluated on a case-by-case basis for various PV plants. This paper performs a quantitative analysis to investigate the reduction in PV output variability in Queensland, Australia by considering two utility scale PV plants. Based on some existing results, a PV output prediction model is developed, which explicitly takes into account the module temperature. This model is then used to predict the PV output of a modeled PV plant and aggregates it with the existing PV plant at The University of Queensland. Substantial reductions in ramp rate variability are observed through the aggregation for all the four seasons with most reductions obtained for the summer season.

## I. METHODOLOGY

To model the PV power output, global horizontal irradiance (GHI) and temperature are considered as inputs.



Figure 1. Block diagram to predict the PV plant output.

## II. KEY EQUATIONS

$$P_{out} = I_{sc} \times V_{oc} \times FF \quad (1)$$

$$I_{sc} = POAI \cdot N_S \cdot I_{sc0} \cdot [1 + \alpha(T_m - T_0)] / 1000 \quad (2)$$

$$V_{oc} = N \cdot V_{oc0} \cdot [1 + \beta(T_m - T_0)] [1 + \delta(POAI / 1000)] \quad (3)$$

$$FF = a + (b \times POAI + c) / \ln(POAI) + T_m(d + e \times POAI + f / POAI) \quad (4)$$

where, the  $POAI$  is the plane of arrays irradiance.

$$T_m = POAI(e^{a_1 + b_1 \cdot WS}) + T_a \quad (5)$$

## III. KEY RESULTS

TABLE I. STANDARD DEVIATION OF RAMP RATES FOR UQ (PU)

Site name	Winter	Spring	Summer	Fall
UQ Site A (%)	5.96	7.97	10.7	8.28
UQ Site B (%)	6.12	8.41	10.4	8.32
Aggregation (%)	4.53	6.28	7.7	6.06

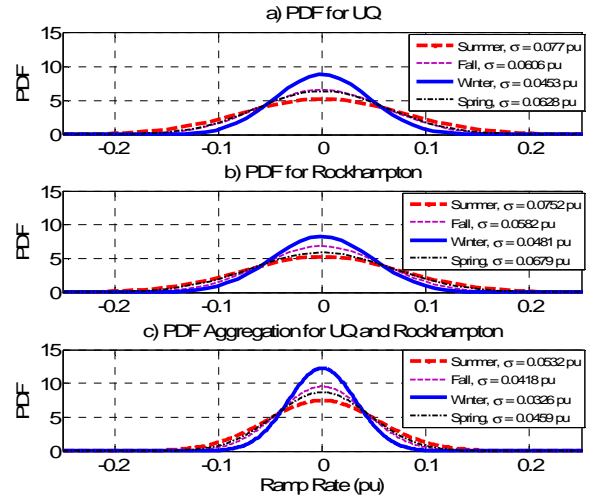


Figure 2. PDF for ramp rates of UQ, Rockhampton, and their aggregation.

TABLE II. CORRELATION COEFFICIENT OF OUTPUT POWER (%)

Season	Winter	Spring	Summer	Fall
Correlation	96.89	94.00	89.06	93.96
Coefficient ( $\rho$ )	87.73	79.64	66.34	80.52

## IV. KEY FINDINGS

- Aggregation results in reduction in variability. Decrease in variability through dispersion is more effective in summer.
- Correlation coefficients decrease with increasing distance, when the highest reduction is in summer (the most variable season) and the lowest is in winter, the clearest season.



# Performance Analysis of Flux-lock Type SFCL Influenced by Characteristics of Two Coils

Yu Zhao<sup>1</sup>, Olav Kraus<sup>1</sup>, Tapan Saha<sup>1</sup>, Yong Li<sup>2</sup>

<sup>1</sup>School of Information Technology and Electrical Engineering  
The University of Queensland, Brisbane, QLD, 4072, Australia

<sup>2</sup>College of Electrical & Information Engineering  
Hunan University, Changsha, China

Email: [y.zhao5@uq.edu.au](mailto:y.zhao5@uq.edu.au), [o.krause@uq.edu.au](mailto:o.krause@uq.edu.au), [saha@itee.uq.edu.au](mailto:saha@itee.uq.edu.au), [yongli@hnu.edu.cn](mailto:yongli@hnu.edu.cn)

**Abstract**—In this paper the fundamental working principle of the flux-lock type SFCL is analyzed, considering parameters such as the iron core structure, the coils and HTS material characteristics. Then by means of PSCAD/EMTDC, the time domain model of SFCL is presented based on the theoretical analysis. Finally, simulations focusing on the coils characteristics are developed to analyze their impacts on SFCL's current limiting performance.

## I. KEY EQUATIONS

Fig.1 depicts the basic configuration of a simplified flux-lock type SFCL.

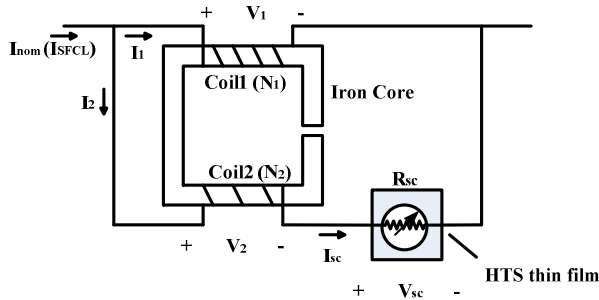


Fig.1. Basic configuration of Flux-lock type SFCL

According to the device structure, under nominal conditions, the voltages across the two windings are given as:

$$V_1 = V_2 = j\omega L_1 \frac{(1-k^2)p^2}{1+p^2 \pm 2kp} I_{nom} \quad (1)$$

where  $L_i$  is self-inductance of each coil,  $p$  is turn number ratio and  $k$  is the coupling coefficient. Sign “+” or “-” is determined by the directions of the coils on the core.

Under fault conditions, the increased current flowing through the HTS element will cause it to quench. In this case, the fault current limiting impedance ( $Z_{SFCL}$ ) of the SFCL is represented as follows:

$$Z_{SFCL} = \frac{j\omega L_1 R_{sc} - \omega^2(L_1 L_2 - M^2)}{j\omega(L_1 + L_2 \pm 2M) + R_{sc}} \quad (3)$$

where  $R_{sc}$  is the resistance of the HTS material during faults. This equation shows that the impedance of flux-lock type of SFCL can be adjusted by different groups of settings.

## II. KEY FIGURES

The model of flux-lock type of SFCL based on the equations is built in environment of PSCAD/EMTDC.

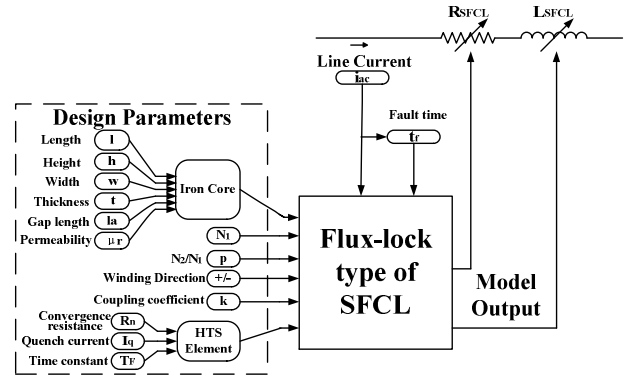


Fig. 2. PSCAD model of the Flux-lock type of SFCL

## III. KEY RESULTS

When achieving similar symmetrical fault current limitation features, the comparison among three different SFCLs installed in the test system are shown in Table I and Fig. 3.

TABLE I. SIMULATION RESULTS OF SFCL (75% FAULT CURRENT LIMITATION)

Parameters	Type A	Type B	Resistive
$R_{sc}$	11.6	8.35	10
<b>Results</b>			
$I_{sc\_0}$ (kA)	0.938	1.107	1.044
$I_{sc\_1}$ (kA)	5.116	6.035	5.973
$I_{sfcl}$ (kA)	5.955	5.957	5.973

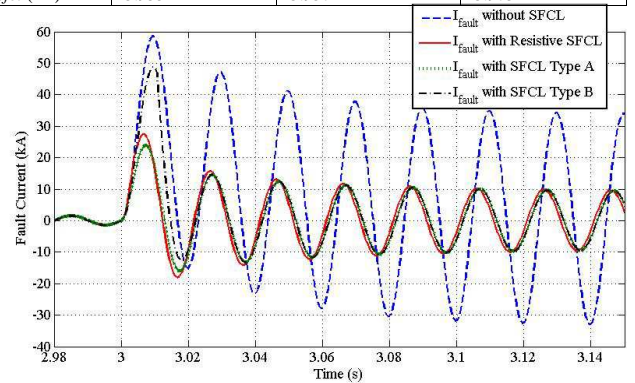


Fig. 1. Limited fault currents

# Frequency Response with Significant Wind Power Penetration: Case Study of a Realistic Power System

Nahid-Al-Masood, Student Member, IEEE, Ruifeng Yan, Member, IEEE and Tapan Kumar Saha, Senior Member, IEEE  
 School of Information Technology and Electrical Engineering  
 The University of Queensland  
 Brisbane, Australia  
 n.masood@uq.edu.au, ruifeng@itee.uq.edu.au, saha@itee.uq.edu.au

**Abstract**—Wind power penetration in power system is increasing rapidly in many countries due to its zero fuel cost and zero air pollution. Unlike the conventional synchronous generation, wind generation has different dynamic characteristics and hence influences the frequency response of a power system. This paper investigates the frequency response of a realistic power system with reasonable integration of wind power. The investigation is carried out on six different load scenarios, with three different wind power penetrations. The frequency sensitivity index and the rate of change of frequency (ROCOF) of the system are estimated. It is observed that the system may become more vulnerable in terms of frequency response as the penetration level of wind power increases. Based on different case studies, this paper also attempts to estimate the minimum synchronous generation requirement of the system after a synchronous generator trips to prevent possible under frequency load shedding (UFLS).

## I. KEY EQUATIONS

Dynamic simulation of the studied system is performed in PSS<sup>®</sup>E simulation platform. The equivalent system frequency, frequency nadir, frequency sensitivity index and the maximum ROCOF are calculated using (1)-(6).

$$f_{eq} = \frac{\sum_{i=1}^{i=n} MVA_i \times \omega_i}{\sum_{i=1}^{i=n} MVA_i} \quad (1)$$

$$FN_j = \min[f_{eq,j}(t_0), f_{eq,j}(t_1), \dots, f_{eq,j}(t_f)]_{t=t_0}^{t=t_f} \quad (2)$$

$$FN = (S_p \times P_o) + f_c \quad (3)$$

$$\beta = \frac{1}{|S_p|} \times 0.1 \quad (4)$$

$$\frac{df_j}{dt} = \frac{\Delta P_{me,j}}{2H_j} \times f_0 \quad (5)$$

$$ROCOF_{max} = \max(ROCOF_1, ROCOF_2, \dots, ROCOF_n) \quad (6)$$

## II. KEY TABLES

TABLE I. WIND PENETRATION LEVEL AND NON-SYNCHRONOUS TO SYNCHRONOUS GENERATION RATIO

Load scenario	WPL (%)			NSSR (%)		
	Case study-1	Case study-2	Case study-3	Case study-1	Case study-2	Case study-3
Summer high	7.75	18.15	35.75	8.45	22.15	55.60
Summer low	0.10	18.55	49.60	85.00	129.60	188.75
Winter high	4.65	12.80	27.00	4.90	14.65	37.00
Winter low	0.08	13.35	35.95	0.08	15.40	56.15
Spring high	1.75	13.25	33.20	1.80	15.30	49.70
Spring low	9.40	24.10	49.65	10.35	31.75	98.65

TABLE II. FREQUENCY SENSITIVITY INDEX, MAXIMUM ROCOF AND MAXIMUM FREQUENCY DEVIATION IN CASE STUDY-1

Load scenario	$\beta$ (MW/0.1 Hz)	$ROCOF_{max}$ (Hz/s)	$\Delta f_{max}$ (Hz)
Summer high	14.30	0.35	0.90
Summer low	6.00	0.69	2.27
Winter high	12.00	0.40	1.18
Winter low	9.60	0.70	1.54
Spring high	16.70	0.34	0.84
Spring low	9.25	0.65	1.44

## III. KEY FIGURES

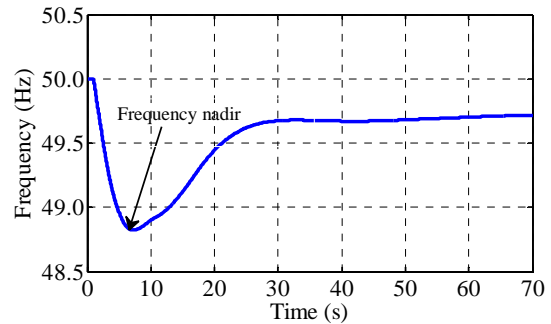


Figure 1. Frequency nadir due to 137 MW generation outage

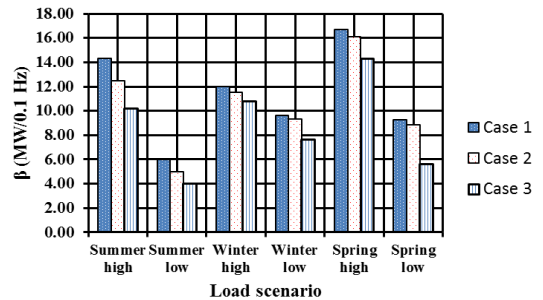


Figure 2. Comparison of frequency sensitivity indices

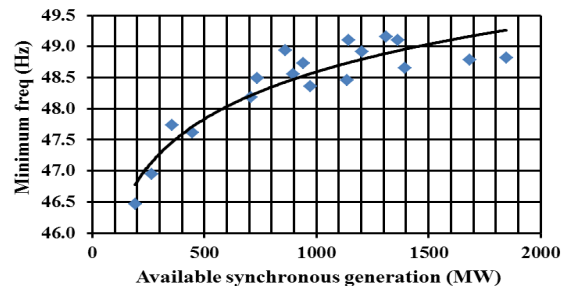


Figure 3. Minimum frequency vs. corresponding available synchronous generation

# A Trading Framework for Demand Response Aggregators

Nadali Mahmoudi, Tapan Kumar Saha, Mehdi Eghbal  
 School of Information Technology and Electrical Engineering  
 The University of Queensland, Brisbane, Australia  
[n.mahmoudi@uq.edu.au](mailto:n.mahmoudi@uq.edu.au), [saha@itee.uq.edu.au](mailto:saha@itee.uq.edu.au), [m.eghbal@uq.edu.au](mailto:m.eghbal@uq.edu.au)

**Abstract**— Demand Response aggregators are becoming a major player in electricity markets. They have an intermediary role through which they apply DR programs to small consumers and sell the outcome to DR buyers and/or electricity markets. This paper proposes a new trading framework for DR aggregators. New price and incentive-based DR programs are proposed through which the aggregators implement DR programs on consumers. On the other hand, new DR agreements are formulated, which allow the aggregator to sell DR to DR purchasers. The presented problem is formulated in stochastic programming and its feasibility is studied on a case of the Australian National Electricity Market (NEM).

## I. KEY EQUATIONS

$$\begin{aligned} \text{MAX} \quad & \sum_{t=1}^T [R^{FDR}(t) + R^{DRO}(t) - EC^{DR}(t)] \\ & + \rho \cdot \left( \xi - \frac{1}{1-\beta} \sum_w \eta_w \cdot \pi_w \right) \end{aligned} \quad (1)$$

**Subject to:**

$$-Profit(w) + \xi - \eta(w) \leq 0; \forall w \quad (2)$$

$$\eta(w) \geq 0; \forall w \quad (3)$$

$$\sum_{op=1}^{N_{op}} P_{op}(t) \cdot v_{op}(t) + \sum_{f=1}^{N_{FDR}} \sum_{b=1}^{N_{BDR}} P_{f,b}^{DR}(t) \cdot \lambda_{f,b}^{DR}(t) \cdot d(t) = p^{DR}(t) - p^{TOU}(t) \quad (4)$$

**Where,**

**Fixed DR revenue:**

$$R^{FDR}(t) = \sum_{t=1}^T \sum_{f=1}^{N_{FDR}} \sum_{b=1}^{N_{BDR}} P_{f,b}^{DR}(t) \cdot \lambda_{f,b}^{DR}(t) \cdot d(t) \quad (5)$$

$$P_{f,b}^{DR,MIN}(t) \leq P_{f,b}^{DR}(t) \leq P_{f,b}^{DR,MAX}(t) \quad (6)$$

**DR option revenue:**

$$\begin{aligned} R^{DRO}(t) = \sum_{t \in T} \sum_{op=1}^{N_{op}} [P_{op}(t) \cdot \lambda_{op}(t) \cdot v_{op}(t) \cdot d(t) \\ - (1 - v_{op}(t)) \cdot f_{op}^{pen}(t)] \end{aligned} \quad (7)$$

$$P_{op}^{MIN}(t) \leq P_{op}(t) \leq P_{op}^{MAX}(t) \quad \forall op = 1, 2, \dots, N_{op} \quad (8)$$

**Reward-based DR cost:**

$$\begin{aligned} EC^{DR}(t) \\ = \sum_{w \in \Omega_w} \pi(w) \cdot \sum_{t=1}^T \left( \sum_{j=1}^{N_j} PF(w, t) \cdot \bar{P}_j^{DR}(t) \cdot R_j^{DR}(t) \cdot d(t) \right) \end{aligned} \quad (9)$$

**TOU Formulation:**

$$p^{TOU}(t) = \sum_{c=1}^N D_0(c, t) \cdot \sum_{p=1}^P E(c, t, p) \cdot \left( \frac{\lambda(c, p) - \lambda_0(c, p)}{\lambda_0(c, p)} \right) \quad (10)$$

## II. KEY RESULTS

TABLE I. ELASTICITY MATRIX

		Peak	Off Peak
Residential	Peak	-0.15	0.05
	Off Peak	0.02	-0.03
Commercial	Peak	-0.16	0.06
	Off Peak	0.03	-0.04
Industrial	Peak	-0.2	0.1
	Off Peak	0.07	-0.08

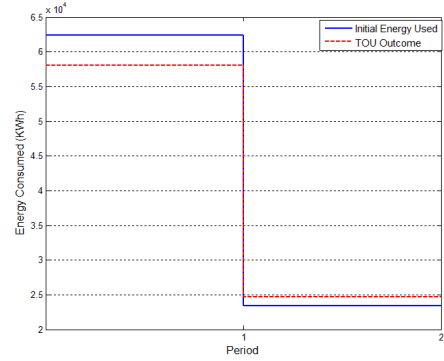


Figure 1. TOU Results

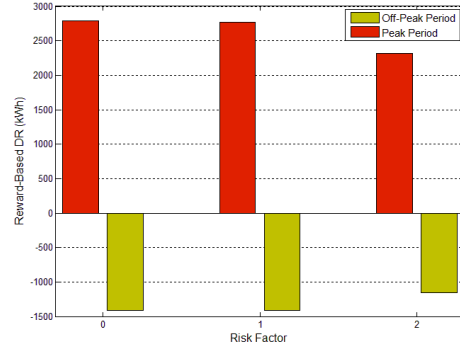


Figure 2. Reward-Based DR Results

TABLE II. FIXED DR ENERGY (kWh)

$\rho$	Peak	Off Peak
0	4559	-1004
1	4539	-1004
2	4735	-1074

TABLE III. DR OPTION EXERCISEMENT

$\rho$	Peak	Off Peak
0	All	All
1	All	All
2	OP2-OP4	OP1, OP2, OP4

# Reliability Evaluation of Wind Farms Considering Generation and Transmission Systems

Mehdi Mosadeghy, Student Member, IEEE, Tapan Kumar Saha, Senior Member, IEEE  
 Ruifeng Yan, Member, IEEE and Simon Bartlett, Member IEEE  
 School of Information Technology & Electrical Engineering  
 The University of Queensland, Brisbane, Australia

Email: [m.mosadeghy@uq.edu.au](mailto:m.mosadeghy@uq.edu.au), [saha@itee.uq.edu.au](mailto:saha@itee.uq.edu.au), [ruifeng@itee.uq.edu.au](mailto:ruifeng@itee.uq.edu.au), [simon.bartlett@uq.edu.au](mailto:simon.bartlett@uq.edu.au)

**Abstract**— This paper studies reliability contribution of wind farms for a typical power system in Australia. Reliability evaluation has been done in two different levels; generation system level and generation-transmission composite system. State Sampling Monte Carlo technique is utilized for reliability assessment and Fuzzy C-means clustering method is employed to create multistep models for load and wind power. Furthermore, different scenarios have been studied to evaluate the effect of tie-line power transfer modeling on the reliability benefit of wind farms. Results show that the capacity value of wind farms in a composite system assessment is lower than generation level and is related to transmission system limits, power flow constraints and tie lines power transfer model. Moreover, results of the composite system study can be utilized in transmission expansion planning in order to increase the reliability contribution of wind energy.

## I. KEY EQUATIONS

In this study Fuzzy C-means method is applied to classify load and wind power data:

$$J(U, V) = \sum_{m=1}^M \sum_{c=1}^C (\mu_c(i))^m \|X_i - V_c\|^2, \quad 1 \leq m < \infty \quad (1)$$

Demand not supplied, annualized loss of energy expectation and Expected Energy Not Supplied are computed by (2, 4):

$$DNS_s = \max \left\{ 0, D - \sum_{j=1}^g G_{js} \right\} \quad (2)$$

$$LOEE = \frac{\sum_{s=1}^N DNS_s \times 8760}{N} \quad (3)$$

$$EENS = \sum_{i \in S} C_i p_i \times 8760 \quad (4)$$

## II. KEY TABLE

TABLE I. WIND SPEED STATISTICAL DATA FOR BOTH WIND SITES

Site	Mean (m/s)	Standard Deviation (m/s)
Site A	9.73	4.94
Site B	6.80	3.65

This system has 165 high voltage buses (110kV-220kV), 67 transformers, and 3,650 circuit kilometers of transmission lines, 47 substations and nine switching stations.

## III. KEY RESULTS

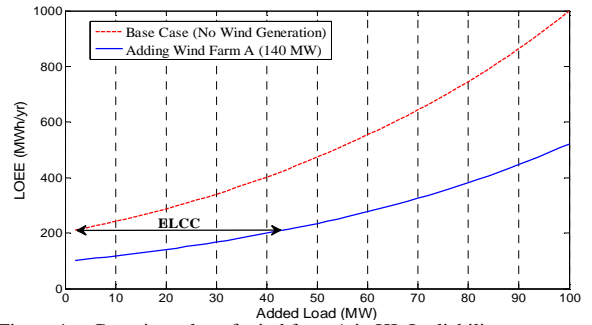


Figure 1. Capacity value of wind farm A in HL I reliability assessment

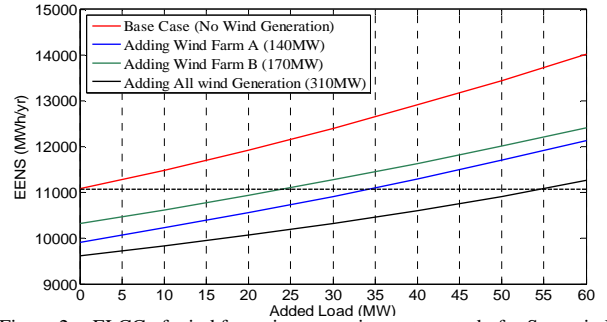


Figure 2. ELCC of wind farms in composite system study for Scenario I

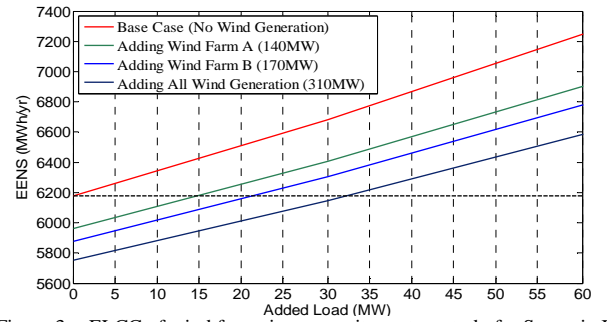


Figure 3. ELCC of wind farms in composite system study for Scenario II

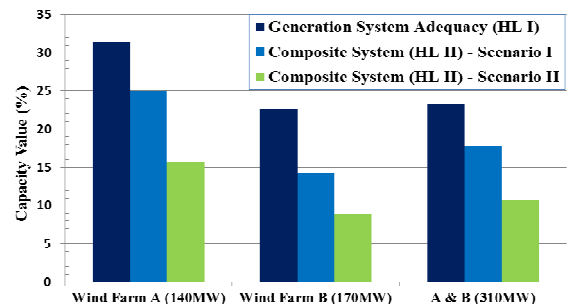


Figure 4. ELCC of wind farms in two reliability assessment levels

# Uncertainty Clearing Price in Real-time Market

Hongxing Ye, *Student Member, IEEE*, Zuyi Li, *Senior Member, IEEE*

Electrical and Computer Engineering Department, Illinois Institute of Technology, Chicago, IL, 60616  
[hxye@hawk.iit.edu](mailto:hxye@hawk.iit.edu), [lizu@iit.edu](mailto:lizu@iit.edu)

**Abstract**— The increasing penetration of renewable energy, price-sensitive demand response load, and potentially more electric vehicle charging stations in recent years have led to increasing uncertainties in power systems. In order to maintain system security, Independent System Operator (ISO)/Regional Transmission Organizations (RTO) has to consider these uncertainties in their SCUC/SCED problems. Recently, both stochastic and robust optimization approaches are successfully applied to Day-Ahead (DA) market and Real-time (RT) market. Although the stochastic and robust optimization methods are studied extensively, fewer researchers report the impacts on Market Clearing Price (MCP) based on robust methods when uncertain parameters are considered in the SCUC/SCED. It is widely accepted that total operation cost of the system will be raised due to the consideration of uncertainties. Then two new and critical issues are raised on how to define a fair price for the uncertainties and how to charge the deviation of generation/load. In this paper, a novel concept Locational Marginal Uncertainty Pricing (LMUP) is proposed to illustrate the price for those uncertainties in robust optimization framework. It consists of system ramp capacity component and transmission congestion component. The derivation of two components is made under the affine adjustable robust framework. The prices for the uncertainties vary with the location and time. A mechanism to charge and credit the uncertainties based on LMUP and its revenue adequacy is also studied. Based on LMUP, a new market regarding energy uncertainty can be built. A 3-Bus illustrative example is presented to illustrate the concept of LMUP and the possibility of creating an uncertainty market.

## I. KEY EQUATIONS

In order to analyze the marginal pricing for the uncertainties, we consider the problem below

$$\begin{aligned}
 UP(\varepsilon) \quad & \min_{P_0, G} z(\varepsilon) = P_0^T Q P_0 + B \cdot P_o + Tr \left[ G^T Q G \cdot E(uu^T) \right] \\
 \text{s.t.} \quad & -v + AP^0 + \pi^T h(\varepsilon) \leq 0, \\
 & M G + C - \pi^T s = 0, \\
 & \pi \geq 0,
 \end{aligned}$$

where  $h(\varepsilon) = h + \varepsilon \cdot \tilde{h}$ ,  $\tilde{h} \in R^K$ . The specified element(s) in perturbation vector  $\tilde{h}$  is (are) 1. And the polyhedron set of uncertainty vector is  $su \leq h$ .

Consider a perturbation  $\tilde{h}$  to the right hand side of uncertainty set  $h$  and assume modified problem is still feasible and bounded, and then the derivative of production cost  $z$  with respect to  $\tilde{h}$  at  $\varepsilon=0$  is

$$\begin{aligned}
 z'(0) &= \lim_{\varepsilon \rightarrow 0^+} \frac{z(\varepsilon) - z(0)}{\varepsilon} \\
 &= \lambda^* \cdot \pi^{*T} \cdot \tilde{h}
 \end{aligned}$$

The *LMUP* consists of two components, one is derived from system ramping capability limits and the other is derived from transmission line congestion. It is rewritten into the following format

$$\begin{aligned}
 LMUP &= LMUP^R + LMUP^C \\
 &= \lambda_{ramp}^* \cdot \pi_{ramp}^{*T} + \lambda_{FL}^* \cdot \pi_{FL}^{*T}.
 \end{aligned}$$

Market participants with uncertainty are required to fulfill the obligation to purchase the reserve. On the other side, the reserve providers including generators/adjustable loads and FTR holders receive credit in each constrained hour.

The payment obligation for  $k$ th constraints in uncertainty polyhedron set is defined as

$$Ch_k = LMUP_k \cdot h_k.$$

Generators with large ramping rate and adjustable loads receive the credit according to

$$Cr_{i,t} = \sum_m \left( G_{i,t,m} \cdot \sum_{k \in \Omega(t)} Ch_{k,m} \right).$$

The holder of FTR between points  $m-n$  is entitled a credit  $Cr_{m-n,t}$  at each time interval as

$$Cr_{m-n,t} = \sum_{l \in \Theta(t)} \left( -LMP_{m,t} + LMP_{n,t} \right) \cdot \Delta FL_{m-n}^l$$

## II. KEY RESULTS

LUMP RESULTS FOR 3-BUS SYSTEM (\$/MWH)

Time	Bus 2				Bus 3			
	Ramp.	Trans.	LMUP	Pay(\$)	Ramp.	Trans.	LMUP	Pay(\$)
1	0	0	0	0	0	0	0	0
2	0	22.5	22.5	22.5*7.5	1.125	12.375	13.5	13.5*3
3	7.5	0	7.5	7.5*8	4.5	0	4.5	4.5*3



# A Distributed Data Storage and Processing Framework for Next-Generation Residential Distribution Systems

Ni Zhang, *Student Member, IEEE*, Yu Yan, *Student Member, IEEE*, and Wencong Su\*, *Member, IEEE*

Department of Electrical and Computer Engineering, University of Michigan-Dearborn, Dearborn, MI, USA

{niz, yuya, wencong}@umich.edu

**Abstract** - In the next-generation power system, the massive volume of real-time data will help the power system operators gain a better understanding of a large-scale and highly dynamic power grid. In order to maintain the reliability and stability of the grid, a large amount of data, which is collected by the local devices referred to as smart meters, are needed for monitoring and controlling the system as well as predicting the electricity price. Therefore, how to store and process the great amount of data becomes a critical issue. In conventional power systems, the system operation is performed using purely centralized data storage and processing approaches. As the number of smart meters increases to more than hundreds of thousands, and huge amount of data would be generated. It is rather intuitive that the state-of-the-art centralized information processing architecture will no longer be sustainable under such data-explosion. On the other hand, to protect the privacy and keep the fairness of market competition, some users do not wish to disclose their operational conditions to each other. A fully distributed scheme may not be practically possible either. This poster shows a radically different approach through a Hadoop-based high-availability and fault-tolerant distributed data management framework to handle a massive amount of Smart Grid data in a timely and reliable fashion. All the system operational information is executed into the distributed data storage and processing platform which consists of a cluster of low-cost commodity servers. This high-availability distributed file system and data processing framework can be easily tailored and extended to support data-intensive Smart Grid applications in a full-scale power system.

## I. KEY CONCEPT

Investigate a radically different approach through distributed software agents to process a massive amount of smart meter data in a timely and reliable fashion. Also, we substantiate the proposed distributed data storage and processing framework on a proof-of-concept testbed for the grid, in order to do so, a large amount of data, which is collected

by the local devices.

So far, we have four technical challenges:

**High-Volume:** smart meter data is expected to be in much larger quantities in the near future

**High-Velocity:** the high-speed data processing and storage is needed.

**High-Variety:** non-traditional data formats may exhibit a dizzying rate of change.

Need to move smart grid operations from being **data-intensive** to information-directed.

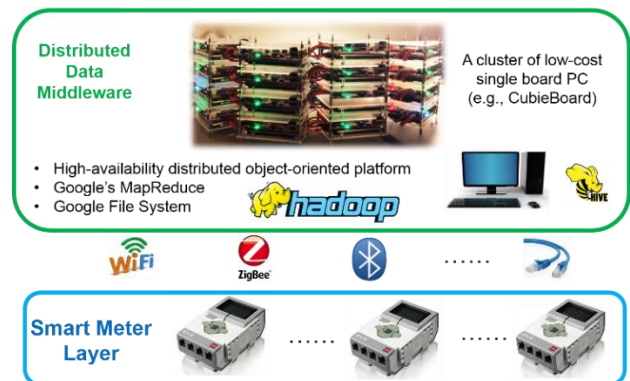


Fig. 1 Hadoop-based proof-of-concept demonstration

Fig. 1 shows the Hadoop-based proof-of-concept demonstration using a cluster of low-cost and credit-card-sized single-board computers.

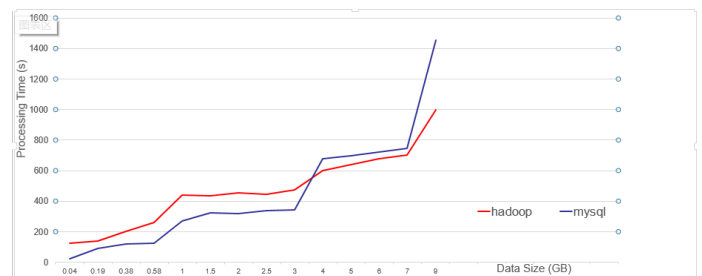


Fig. 2 Performance analysis

Fig. 2 shows the data processing performance on smart meter application using Apache Hadoop's Hive and conventional database (MySQL server).

# Harmonic Emissions in Grid Connected PV Systems: A Case Study on a Large Scale Rooftop PV Site

Annapoorna Chidurala, *Student Member, IEEE*, Tapan Kumar Saha, *Senior Member, IEEE*, N. Mithulananthan, *Senior Member, IEEE* and Ramesh C. Bansal, *Senior Member, IEEE*

**Abstract**— With rapid increase in installation of rooftop Solar Photovoltaic (PV) systems in low voltage (LV) distribution networks, power quality becomes a key area of interest. Among various poor power quality problems in LV networks, harmonic distortions, which could come from several sources, have become a major concern. The solar PV systems can generate harmonics itself. Besides this, the increasing use of power electronics based nonlinear loads and PV system penetrations in the network inducing harmonics lead to poor power quality resulting in overheating of equipment and malfunction of controls. In this paper, harmonic distortion issues accompanied with solar PV inverter due to variations in solar irradiance has been thoroughly analyzed. Simulations have been performed in IEEE-13 bus distribution system with nonlinear loads to examine the harmonic emissions from conventional PV system for varying solar condition. To verify the simulation results and capture the trends harmonic measurements were made at the University of Queensland 1.2 MW PV site. The paper has also proposed a control algorithm for the harmonic compensation. Simulation results confirm that the proposed controller has effectively eliminated the harmonic issues for varying solar conditions.

## I. KEY FIGURES

Harmonic emissions associated with the grid-tied three phase PV inverter system due to variation in solar irradiation.

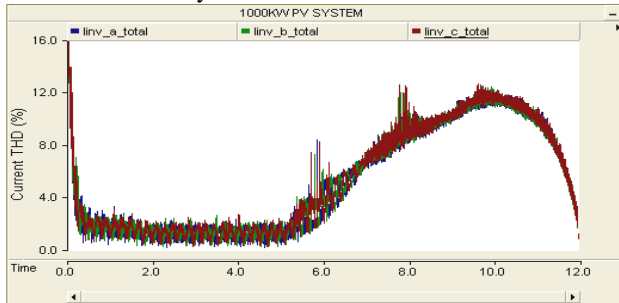


Figure 1. Percentage of THDs of PV inverter output currents.

## A. Harmonic Measurement at the UQ PV Site - Analysis of Data

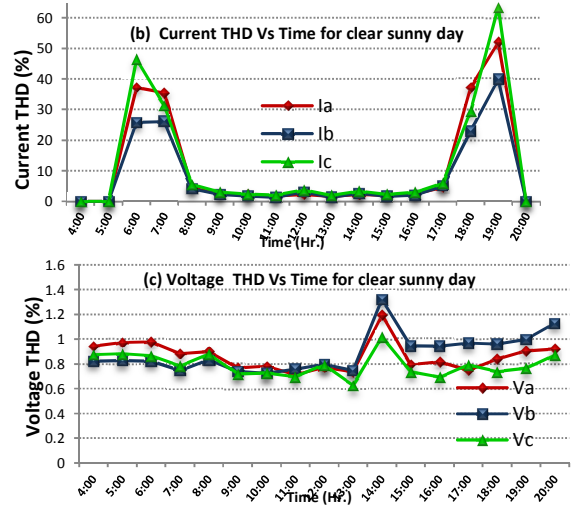
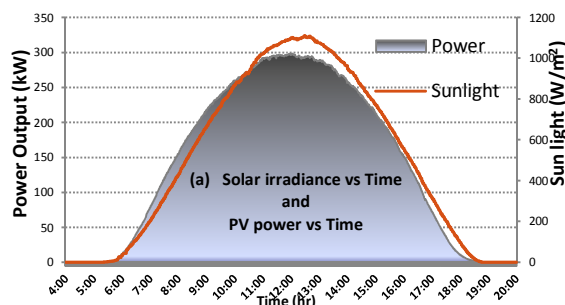


Figure 2. Measured data for clear sunny day.

## II. SOLAR-DSTATCOM CONTROL APPROACH

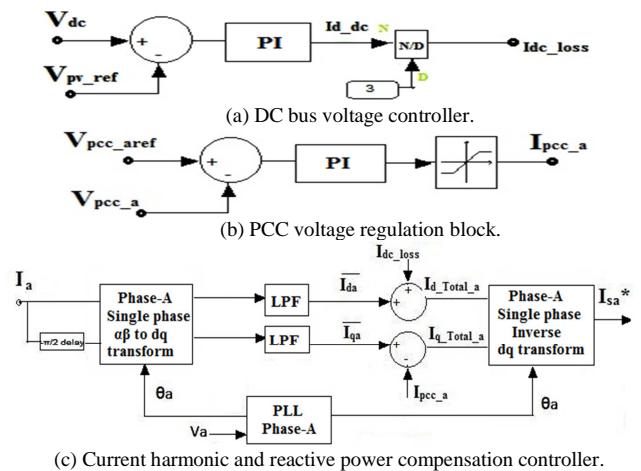


Figure 3. Block diagram of control scheme.

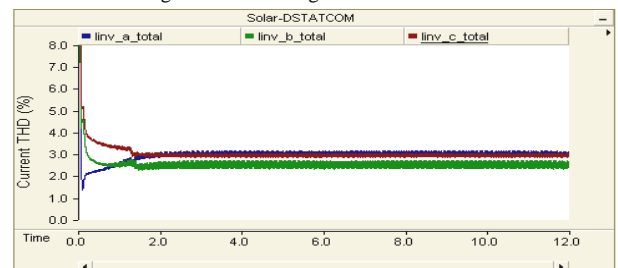


Figure 4. Percentage of THDs of Solar-DSTATCOM output currents.

# A Diffusion-Driven Model for Investigating Moisture Effects on Dielectric Response Measurement of Transformer Insulation

Yi Cui, Hui Ma, Tapan Saha, Chandima Ekanayake

School of Information Technology and Electrical Engineering  
The University of Queensland, Brisbane, QLD, 4072, Australia

Email: [y.cui3@uq.edu.au](mailto:y.cui3@uq.edu.au), [huima@itee.uq.edu.au](mailto:huima@itee.uq.edu.au), [saha@itee.uq.edu.au](mailto:saha@itee.uq.edu.au), [chandima@itee.uq.edu.au](mailto:chandima@itee.uq.edu.au)

**Abstract**— This paper proposes a diffusion-driven dielectric response model, which aims to reveal the effect of moisture diffusion on the dielectric response measurement of transformer insulation. In the proposed diffusion-driven model, the oil-impregnated pressboards are modeled as multiple layers and it is assumed moisture diffuses from one side of the pressboard. Then the dependency between the moisture concentration and dielectric losses and permittivity of the pressboard is studied. Subsequently, the dielectric response of the pressboard is calculated to model the dielectric relaxation behavior driven by the moisture migration between oil and pressboard. The proposed model is verified by laboratory experimental results.

## I. KEY EQUATIONS

During diffusion process, the moisture distribution inside the pressboard is calculated by solving the Fick's second law.

$$\frac{\partial C(x,t)}{\partial t} = \frac{\partial}{\partial x} \left( D \frac{\partial C(x,t)}{\partial x} \right) \quad (1)$$

The impedance  $Z(\omega)$  of the pressboard in frequency domain can be written as (2)

$$Z^*(\omega) = \frac{1}{S} \left[ \int_0^l \frac{\sigma_x}{\sigma_x^2 + (\omega \varepsilon_0 \varepsilon'_x)^2} dx - j \int_0^l \frac{\omega \varepsilon_0 \varepsilon'_x}{\sigma_x^2 + (\omega \varepsilon_0 \varepsilon'_x)^2} dx \right] \quad (2)$$

Admittance and capacitance can be written as (3) and (4)

$$G_i^*(\omega) = (\sigma_i + j\omega \varepsilon_0 \varepsilon'_i) \frac{S}{\Delta x} \quad (3)$$

$$C_i^*(\omega) = \varepsilon_i^*(\omega) C_0 = \varepsilon_0 \frac{S}{\Delta x} (\varepsilon'_i + j\varepsilon''_i) \quad (4)$$

Complex capacitance (4) can be expressed as (5)

$$C_i^*(\omega) = \frac{G_i^*(\omega)}{j\omega} = (\varepsilon_0 \varepsilon'_i - j \frac{\sigma_i}{\omega}) \frac{S}{\Delta x} \quad (5)$$

By comparing (4) and (5), it can be obtained

$$\varepsilon'_x = \varepsilon'_i, \quad \sigma_x = \sigma_i = \varepsilon_0 \omega \varepsilon''_i \quad (6)$$

## II. KEY FIGURES

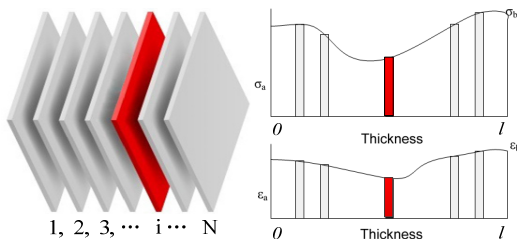


Fig. 1. Diffusion-driven model of pressboard in transformer

## III. KEY RESULTS

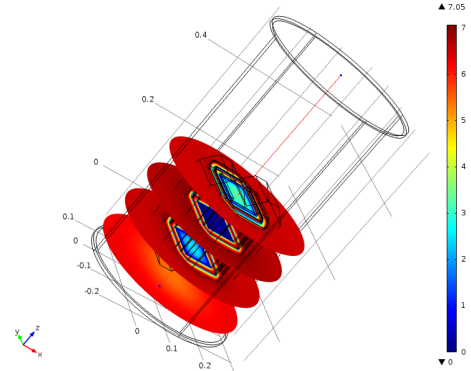


Fig. 2. FEM modelled moisture distribution in transformer during diffusion process

An exponential function is used for describing the dependency between the loss and the position before uniform moisture distribution has reached

$$\sigma = e^{\alpha + \beta \cdot x} \quad (7)$$

TABLE I. FITTING PARAMETERS FOR DIELECTRIC LOSS WITH RESPECT TO DIFFUSION POSITION (AFTER 18 HOURS DIFFUSION)

Freq	$\alpha$	$\beta$	Mse.	Freq	$\alpha$	$\beta$	Mse.
1000	-20.58	0.04	$5.20 \times 10^{-13}$	$4.6 \times 10^{-2}$	-24.94	-0.80	$7.86 \times 10^{-14}$
10	-23.31	-1.03	$4.53 \times 10^{-13}$	$2.2 \times 10^{-2}$	-25.31	-0.64	$4.76 \times 10^{-14}$
1	-23.77	-1.36	$3.21 \times 10^{-13}$	$10^{-2}$	-25.80	-0.89	$3.52 \times 10^{-14}$
0.46	-23.97	-1.30	$2.61 \times 10^{-13}$	$4.6 \times 10^{-3}$	-25.92	-0.36	$1.76 \times 10^{-14}$
0.22	-24.23	-1.14	$1.90 \times 10^{-13}$	$2.2 \times 10^{-3}$	-26.09	-0.23	$1.02 \times 10^{-14}$
$10^{-1}$	-24.57	-0.97	$1.25 \times 10^{-13}$	$10^{-3}$	-26.20	-0.15	$6.31 \times 10^{-15}$

Freq: frequency in Hz. MSE: mean square error.

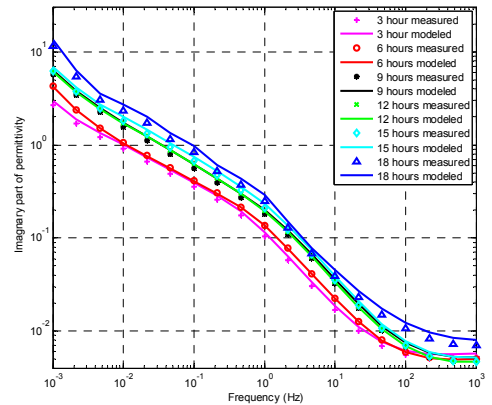


Fig. 3. Comparison between measured and modelled imaginary part (dielectric dissipation) of complex permittivity



# Power System Real-time Event Detection and Associated Data Archival Reduction Based on Synchrophasors

Yinyin Ge, *Student Member, IEEE*, Alexander J. Flueck, *Senior Member, IEEE*

Department of Electrical and Computer Engineering, Illinois Institute of Technology, Chicago, IL 60616 USA  
[yge9@hawk.iit.edu](mailto:yge9@hawk.iit.edu), [flueck@hawk.iit.edu](mailto:flueck@hawk.iit.edu)

**Abstract**— The aim of this paper is to present methods on real-time event detection and data archival reduction based on synchrophasor data produced by a phasor measurement unit (PMU) for wide-area measurement systems (WAMS). Event detection is performed with Principal Component Analysis (PCA) and a second order difference method with a hierarchical framework used for the event notification strategy based on a small-scale Microgrid. The type of a certain event can also be determined through event decision rules. Compared with the existing methods, the proposed method is more practical and efficient in the combined use of event detection and data archival reduction. The proposed method on data reduction, which is an “Event oriented auto-adjustable sliding window method”, implements a curve fitting algorithm applied with the weighted exponential function based variable sliding window according to different event types. The simulation results indicate they work efficiently with minimal information loss especially around detected events. The performance is shown through the results of analysis on actual PMU data based on the IIT Campus Microgrid, thus successfully improving the situational awareness (SA) over the campus power system network.

- Auto-adjustable sliding window based on event types:

$$L_n = l_0 \alpha_i e^{-\beta_i V_k}$$

$$K = \min(L_{n-2} + L_{n-1}, l_0)$$

## II. RESULTS FROM CASE STUDIES

### I. METHODS DESCRIPTION

#### 1. Real-time Event Detection

The event detection methods are developed to detect the real-time voltage/ real power events.

- Principal Component Analysis (PCA) for abnormal data detection.
  - Measure the trend of a data set and detect abnormal data.
  - Identify the start of an event.
- Second Order Difference for “event complete” check:
 
$$D_L(i) = (L(i) - L(i+1)) - (L(i+1) - L(i+2))$$
- Event type determination through the decision rules (voltage sag/swell, interruption, undervoltage, overvoltage and real power drop/surge).
- Hierarchical framework based event notification scheme.
  - Administrator informed by email of important events.
  - Hierarchical framework created for the event notifications.

#### 2. Real-time Data Archival Reduction

“Event Oriented Auto-adjustable Sliding Window Method”:

- Curve fitting by ordinary least square method.
  - Quadratic curve fitting done upon sliding window.
  - 3 points on the quadratic curve archived.

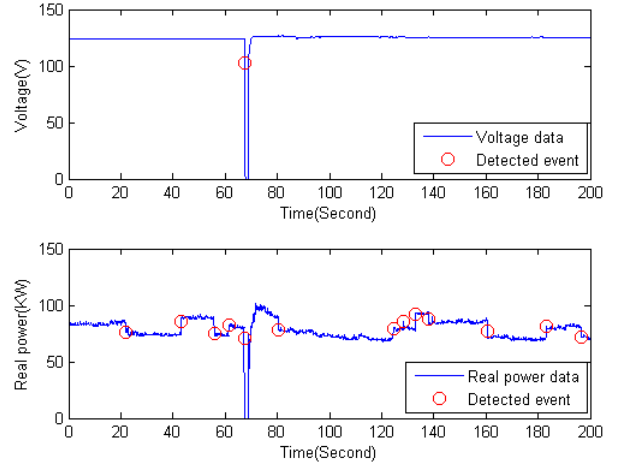


Fig. 1. Detected Events on Life Science Building

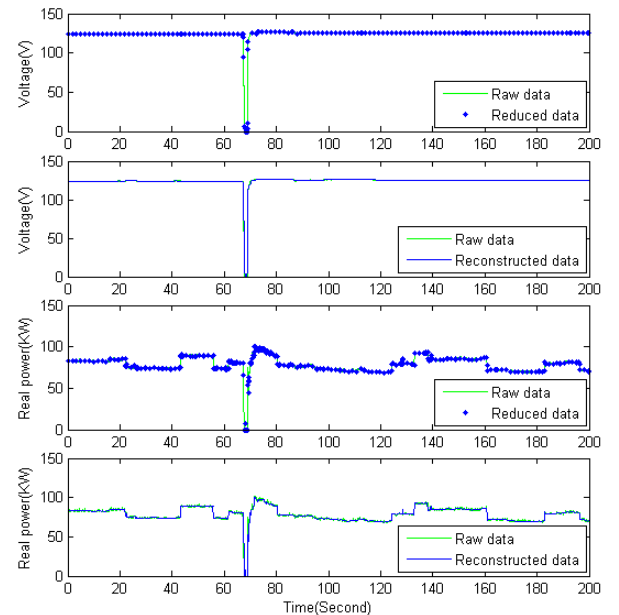


Fig. 2. Reduced and Reconstructed Data on Life Science Building

# Novel Load Frequency Control in a Multi-agent based Microgrid Power System in Presence of Cyber Intrusions

Hessam Keshtkar, *Graduate Student Member, IEEE*, Jignesh Solanki, *Member, IEEE*

Lane Department of Computer Science and Electrical Engineering, West Virginia University Morgantown, WV 26505, USA

[hkeshtka@mix.wvu.edu](mailto:hkeshtka@mix.wvu.edu) and [Jignesh.Solanki@mail.wvu.edu](mailto:Jignesh.Solanki@mail.wvu.edu)

**Abstract**— In this paper an isolated smart microgrid comprising both controllable and uncontrollable sources, such as solar, wind as Renewable Energy Sources (RES), diesel generator, fuel cell as Distributed Generation (DG) units, aqua-electrolyser, hydrogen storage, and Superconducting Magnetic Energy Storage (SMES) as storage unit in a multi-agent based infrastructure is modeled. This microgrid network is subjected to a large load with rapid changes, which results in system frequency to be severely deteriorated and become oscillatory. In addition, the stability issues grow with wide penetration of wind generation into microgrid. After discussing the modeling of the multi-agent based power system and different generating units, different kinds of frequency control approaches, including Adaptive Dynamic Programming (ADP) which is based on the neural networks and belongs to the family of Adaptive Critic Design (ACD), have been used and the results have been compared to each other. The Particle Swarm Optimization (PSO) technique has been applied to come up with the best control parameters such that the frequency oscillation due to a disturbance in the microgrid is minimized. The proposed control approaches are tested in presence of different frequency changes in the system including cyber attack effects. Implementation of new attack detection and learning method is also examined in the simulations. The results show improvement in frequency response of the microgrid system using the proposed control method and defense strategy against cyber attacks.

## I. KEY EQUATIONS

A Recurrent Neural Network (RNN) Dual Heuristic dynamic Programming (DHP) critic network is trained online to approximate  $\lambda(k+1)$ , the partial derivative of  $J(k+1)$  with respect to  $y(k+1)$ , by minimizing the following error:

$$E_c(k) = \|e_c(k)\|^2 \quad (1)$$

$$e_c(k) = \hat{\lambda}(k) - \left\{ \frac{\partial U(k)}{\partial y(k)} + \left[ \frac{\partial u(k)}{\partial y(k)} \right] \frac{\partial U(k)}{\partial u(k)} \right.$$

$$\left. + \gamma \left[ \frac{\partial \hat{y}(k+1)}{\partial y(k)} + \frac{\partial \hat{y}(k+1)}{\partial u(k)} \frac{\partial u(k)}{\partial y(k)} \right] \hat{\lambda}(k+1) \right\}$$

Assuming a linear output activation function for the critic network, the DHP critic network output at time  $k$  is obtained by

$$\hat{\lambda}(k+1) = W_{oc} S_c(k) = W_{oc} f_c [W_{ic} \hat{y}(k+1) + W_{sc} S_c(k-1)] \quad (2)$$

## II. KEY FIGURES

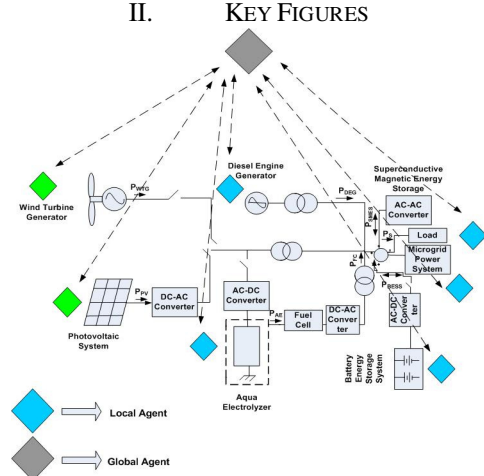


Fig. 1. Multi agent microgrid system for LFC.

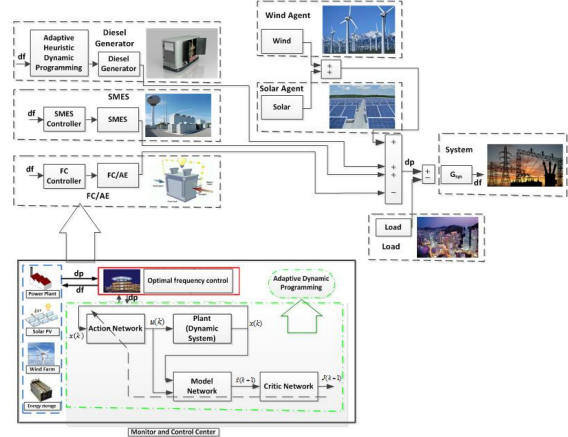


Fig. 2. Simulation model of the studied Microgrid

## III. KEY RESULTS

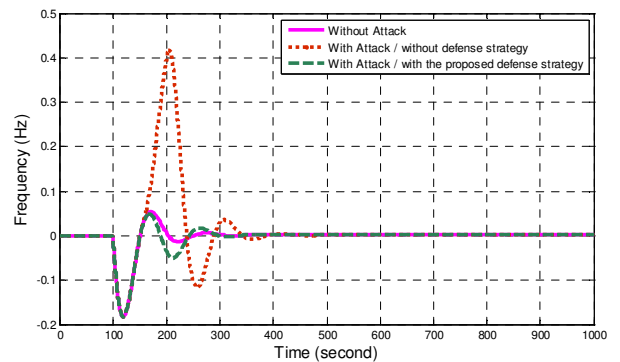


Fig. 3. Frequency response with/without control, detection and learning (defense) algorithm

# CIM Standards Conformed Cloud Based Power System Applications and Data Management tools

Gelli Ravikumar, *Student Member, IEEE*, Shrikrishna A. Khaparde *Senior Member, IEEE*.

**Abstract**—Although the standard CIM brings an integration for proprietary software applications of a utility, managing a sheer volume of data exchanges among software application systems is still challenging for utility operators due to lack of seamlessness across them. Furthermore, distributed processing and real-time computation are the requirements for analyzing large interconnected power networks at control centers and thereby ensure a secure power system operation. In response to these challenges, this paper presents a cloud based service oriented architecture for executing and analyzing power system domain applications. The proposed architecture draws advantage of cloud computing features such as distributed real-time processing, seamless information retrieval and dissemination, and ubiquitous access. A usage of simple object access protocol for communication between web services in the proposed architecture is explained. As a case study, this paper demonstrates few applications such as CIM profile creation, visualizing power grid networks and online network topology processing.

**Index Terms**—CIM, Cloud Computing, Data Management, Power Networks, Service Oriented Architecture, and XML.

## I. KEY CONCEPT

COMMON information model (CIM) standard provides a basis for semantical understanding of messages correspond to power system applications. In power system domain or smart grid domain, the CIM plays a significant role for clear understanding of message payloads and thereby it will be center for various power system or smart grid information standards. For enhancing the use of CIM, a software web service in cloud computing paradigm under software as a service (SAAS) is presented. On similar lines, a model for managing smart grid data in cloud computing has been presented [1].

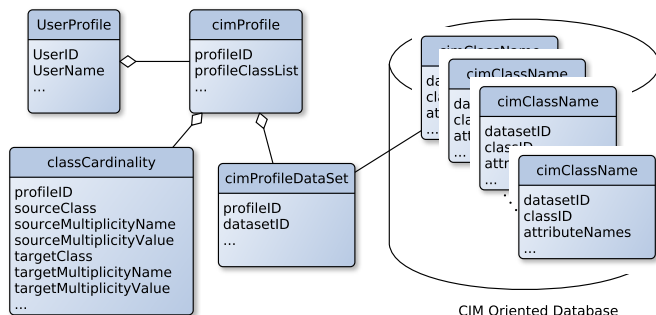


Fig. 1. Schema for User and Application Database linked to CIMODB

In addition to cloud protocols such as simple object access protocol (SOAP), the implementation of proposed architecture

Gelli Ravikumar (gravikumar@iitb.ac.in) and S. A. Khaparde (sak@ee.iitb.ac.in) are with IIT Bombay, India.

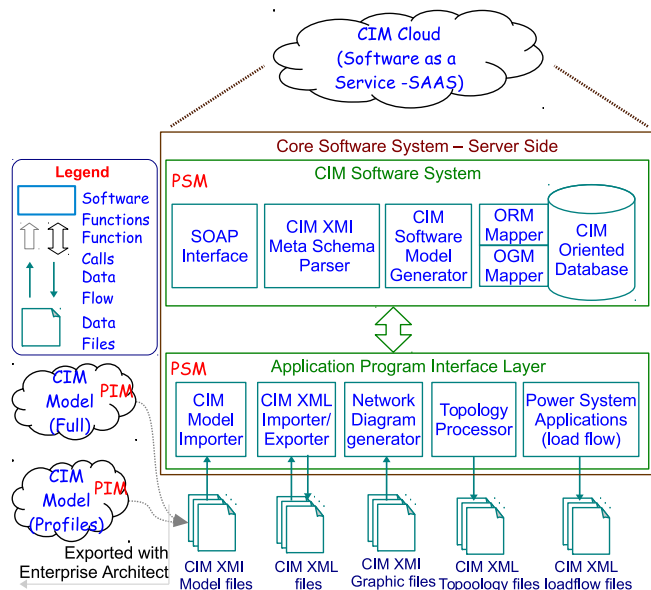


Fig. 2. Core Software System Architecture for CIM Cloud (SAAS)

is carried out via a coordinated use of various standards and open source technologies such as CIM, Unified Modeling Language (UML), eXtensible Markup Language (XML), Scalable Vector Graphics (SVG), Relational Databases, graph databases, object and graph relational mappers, Python and Django web development framework. These are supported by consortia such as IEC TC 57, W3C, OMG and the open source community. A high level view of proposed database schema is shown in Fig. 1. Proposed architecture emphasizing core software system components in a cloud computing paradigm is shown in Fig. 2. One of the significant feature of the architecture is use of graph database design, which is an extension of earlier proposed CIM oriented database schema [2].

## II. CONCLUSION

This paper has introduced a cloud based environment for executing applications pertaining to CIM. The developed system is helpful for utilities and academia for interacting power system applications through CIM.

## REFERENCES

- [1] S. Rusitschka, K. Eger, and C. Gerdes, "Smart grid data cloud: A model for utilizing cloud computing in the smart grid domain," in *Smart Grid Communications (SmartGridComm), 2010 First IEEE International Conference on*, Oct 2010, pp. 483–488.
- [2] G. Ravikumar, S. Khaparde, and Y. Pradeep, "Cim oriented database for topology processing and integration of power system applications," in *Power and Energy Society General Meeting (PES), 2013 IEEE*, July 2013.

# Reliability Evaluation of Composite Electric Power Systems under Different Weather Conditions

Yang Liu, *Student Member, IEEE*, Jin Zhong, *Senior Member, IEEE*

Department of Electrical and Electronic Engineering, the University of Hong Kong, Hong Kong

Email: [yangliu@eee.hku.hk](mailto:yangliu@eee.hku.hk)

**Abstract**--The multi-concurrent failure in the composite electric power system is a severe accident, which might result in the power failure in a large area, or even the crashing of the entire system. Usually, the possibility of the multi-concurrent failure in a stable power system is very low, but it increases dramatically when interfered by severe weather. As a result, the system operator hopes to evaluate the possibility of the cascading failure considering the future weathers, as well as the consequences and expectations caused by the outage.

This paper develops an approach to evaluate the risk of multi-concurrent failures for complex power system, which simulates the transmission lines' outages and associates the occurrence probability of multi-concurrent failures with their consequences under different weather conditions, then a quantitative risk index is proposed based on failure probability and the shedding load. On this basis, the software for risk assessment of multi-concurrent failures in power system is developed based on Matlab and BPA software. Taking the real large-scale power system of Guangdong Province for example, the simulation result shows the feasibility of the proposed method.

## I. KEY EQUATIONS

The index of reliability evaluation is defined as:

$$E(f) = \sum_{x \in X} P(x) \cdot f(x) \quad (1)$$

where  $P(x)$  is power systems' failure probability, and  $f(x)$  is the consequence of it, which can be regarded as the shedding load of outage.

**Probability of Failure:** The probability of outage can be expressed by equation (2) with only the transmission lines' failures considered.

$$P(x) = \prod_{i=1}^n F_i(L) \quad (2)$$

A hyperbolic function model is used to calculate the probability of transmission lines' failures:

$$F_l(L) = \frac{1}{2} [1 + \tanh(a_l L + b_l)] \quad (L \geq 0) \quad (3)$$

where  $L$  is the apparent power of transmission line  $l$ , and both  $a_l$  and  $b_l$  are the parameters of model, which can be determined by substituting equations (4) and (5) into (2).

$$\frac{1}{L_{normal}} \int_0^{L_{normal}} F_l(L) dL = \bar{F}_l \quad (4)$$

$$F_l(L_{max}) = \bar{1} \quad (5)$$

Considering the main reasons of transmission failures under severe weather are no longer overload and overprotection, the probability of chain outage which is conjectured from historical data depends on the severity of weather.

**Consequence of Failure:** The shedding load of outage is defined as the rated power of nodes split from the original system, which can be determined by measuring their electrical distances to the swing bus.

## II. KEY FIGURES

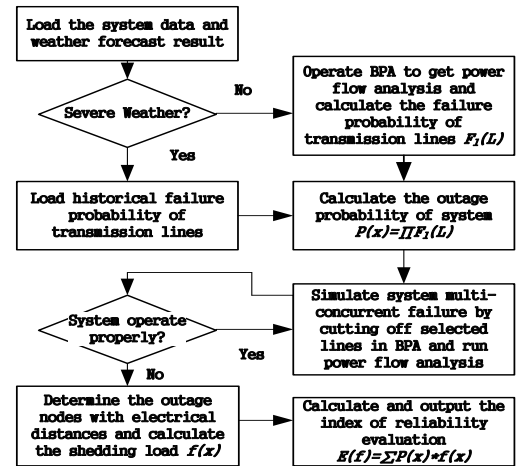


Figure 1. Flow chart for reliability evaluation

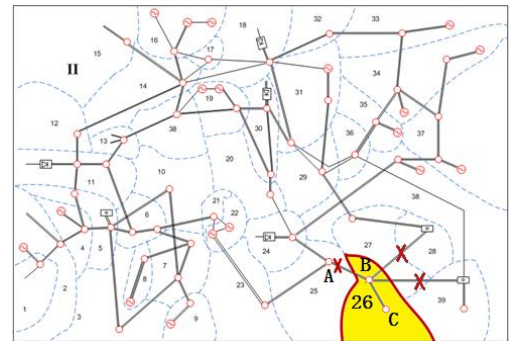


Figure 2. A simulated multi-concurrent system failure in Guangdong

## III. KEY RESULTS

TABLE I: Risk index of a multi-concurrent failure in Guangdong under different weathers

	Outage Probability	Outage Nodes	Load Shedding	Index
Normal Weather	0.21%	Station B	+115.8MW	0.486 (Low Risk)
	0.17%	Station C	+162.6MW	
	0.049%			
Severe Weather	2.1%	Station B	+115.8MW	1627.6 (High Risk)
	3.2%	Station C	+162.6MW	
	0.87%			

The results for this evaluation above show the risk level of a multi-concurrent failure under different weather conditions, and provide a reference to system operators to prepare preventive actions to future outages.

# Role of Communication on the Convergence Rate of Fully Distributed DC Optimal Power Flow

Javad Mohammadi, Gabriela Hug, Soumya Kar

Department of Electrical and Computer Engineering, Carnegie Mellon University  
 Email: jmohamma@ece.cmu.edu, ghug@ece.cmu.edu, soumyak@andrew.cmu.edu

**Abstract**—In a grid with highly distributed resources, an effective distributed algorithm for solving Optimal Power Flow (OPF) will result in efficient resource allocation across the system. This paper investigates the impact of communication on the performance of a fully distributed DC OPF algorithm, which solves the first order optimality conditions through an iterative process. In this distributed algorithm, at each iteration, every bus exchanges information with its physically connected neighboring buses and updates the local variables by evaluating a simple function. This paper suggests that sharing additional information between buses without physical connections across the system can speed up the convergence of the algorithm. A key aspect is the constrained selection of these additional communication links and the effective integration of this information in the update of the local variables which is the focus of this paper. A proof of concept is given using the IEEE-118 bus test system as a test case.

## I. KEY FORMULATION

In order to solve the DC Optimal Power Flow problem, our distributed solution distributes the computations among the buses. Each bus  $i$  is responsible for updating and finding the optimal value for the variables associated with it, namely  $x_i$ . The updates are formulated according to the following general format

$$x_i(k+1) = x_i(k) + \Phi_i g_i(x(k)), \quad (1)$$

where  $g_i(\cdot)$  correspond to the equality constraints in the first order optimality conditions associated with bus  $i$  and depends on its local and neighboring variables only;  $\Phi_i$  is a vector of tuning parameters. Addition of new communication links modifies the  $\Phi_i$  such that the convergence rate of the algorithm improves. Given that adding communication links can be expensive, the choice of which buses should be connected by additional communication links is critical and influences the level of convergence rate improvement. In the following, we present some general guidelines which may be employed while selecting additional communication links. These criteria determine the merit of a specific bus to become part of an additional communication link.

**Generation Capacity and Cost Parameters:** Since generators are responsible for supplying the demand of the system, the sooner large and low cost generators detect the supply/demand imbalance the fewer iterations are needed for them to respond and counterbalance the imbalance.

**Demand:** Major load buses have a notable influence on the supply/demand equality. Thus, the communication of the power imbalance at buses to which large consumers are connected with other influential players such as low cost

generators, can have a significant impact on the required number of iterations to solve the problem.

**Distance:** The distance between two buses, i.e. the shortest path between two buses, is another important criteria when choosing additional communication links. The higher the distance, the more effective (in general) the communication link in improving convergence speed.

Performance improvement based on these selection criteria is demonstrated for the IEEE 118-bus test system in the following section.

## II. KEY RESULTS

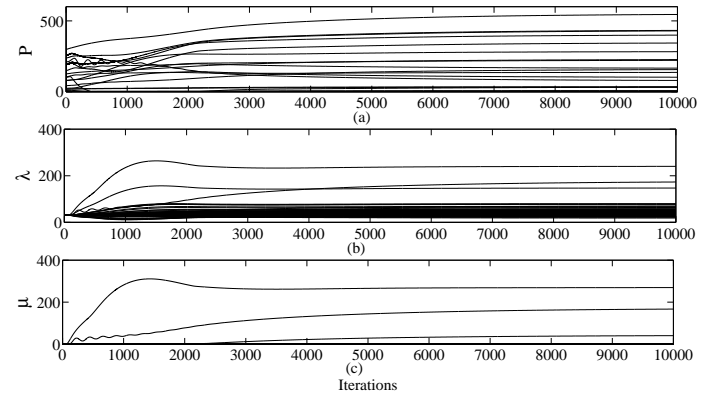


Fig. 1. (a) Generation output (b) Lagrangian multiplier  $\lambda$  (c) Lagrangian multiplier  $\mu$  without additional communication links.

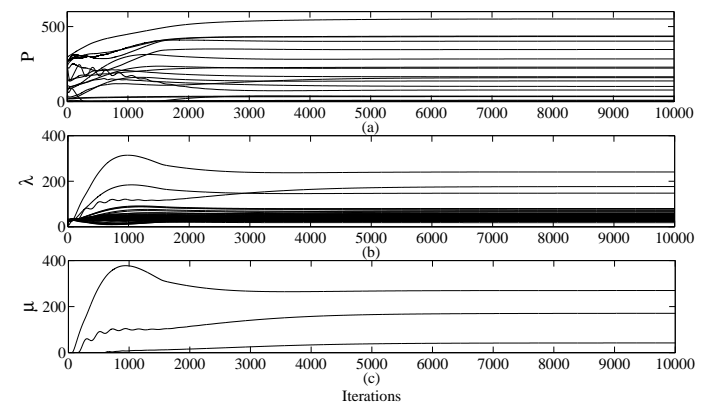


Fig. 2. (a) Generation output (b) Lagrangian multiplier  $\lambda$  (c) Lagrangian multiplier  $\mu$  with four additional communication links.



# Uncertainty of Measurement Error in Intelligent Electronic Devices

Po-Chen Chen, *Student Member, IEEE*, Yimai Dong, *Member, IEEE*, Vuk Malbasa, *Member, IEEE*, and Mladen Kezunovic, *Fellow, IEEE*

**Abstract**—In this paper we attempt to quantify uncertainty in measurements obtained from Intelligent Electronic Devices (IED). IEDs have emerged in distribution systems as a prevalent source of measurements in monitoring and protection, as well as for different kinds of higher order applications beyond their intended purpose. These measurement devices are installed across the system, from substations down to the customer locations, and provide measurements for a wide array of quantities. We study how IEDs respond to external disturbances in order to account the possible implications in various applications.

## I. KEY FIGURES

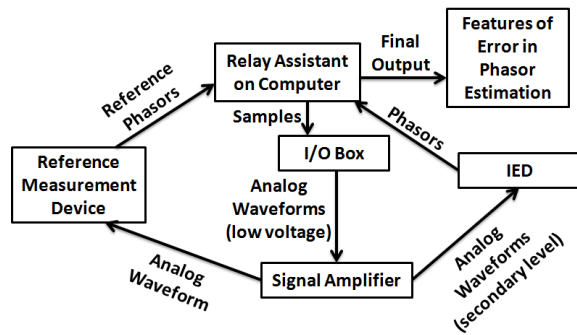


Figure 1: Hardware setup.

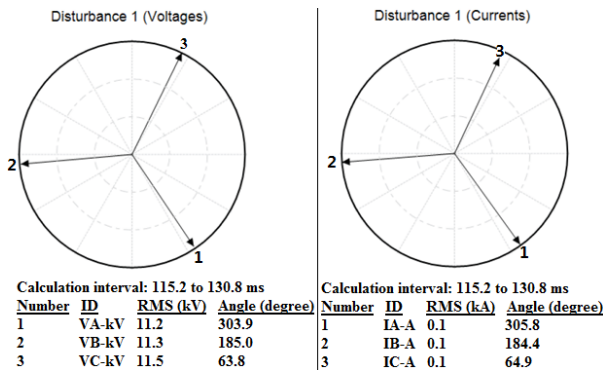


Figure 2: Phasor information from disturbance report.

## II. KEY RESULTS

1. Both voltage and current amplitude measurements produce very stable outputs during repeated tests, with very low variances.

- Offsets in both voltage and current amplitude measurements show a negative correlation with the amplitude of test signals. The errors show a linear pattern, suggesting that with proper settings of the amplitude correction factors, most of the error can be eliminated.
- No obvious impact of frequency and harmonics has been observed during tests of amplitude measurements.
- Errors in angle measurements are not as stable as those in amplitude measurements, but the mean error in phase angle differences never exceeded  $\pm 5^\circ$ ; the largest absolute error detected is  $8.6^\circ$ .
- No clear pattern in the angle difference errors, frequency or harmonics in the test waveforms has been observed. The errors in angle differences may be related to the calculated phase angles, the inception angles of the phasor calculation process when disturbance reports are generated.

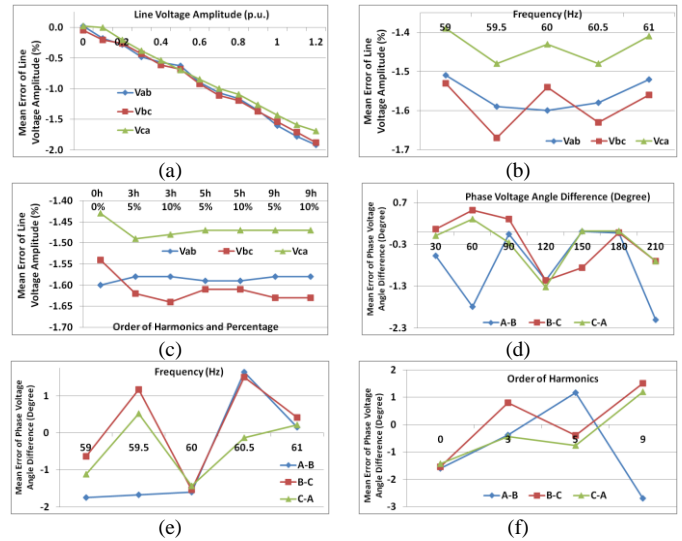


Figure 3: All the quantities are referred to the test signal, and the quantities of y-axis are referred to mean errors in the sub-figure descriptions; (a) line voltage amplitude vs. line voltage amplitude; (b) line voltage amplitude vs. frequency; (c) line voltage amplitude vs. harmonic level; (d) phase voltage angle difference vs. phase voltage angle difference; (e) phase voltage angle differences vs. frequency; (f) phase voltage angle difference vs. harmonic level.

# Reserve Response Sets for Security-Constrained Unit Commitment with Wind

Joshua Lyon<sup>1</sup>, *Student Member, IEEE*, Muhong Zhang<sup>1</sup>, and Kory W. Hedman<sup>2</sup>, *Member, IEEE*

<sup>1</sup>Department of Industrial Engineering, Arizona State University, Tempe, AZ 85287, USA

<sup>2</sup>School of Electrical, Computer, and Energy Engineering, Arizona State University, Tempe, AZ 85287, USA

Email: [joshua.lyon@asu.edu](mailto:joshua.lyon@asu.edu); [muhong.zhang@asu.edu](mailto:muhong.zhang@asu.edu); [kory.hedman@asu.edu](mailto:kory.hedman@asu.edu)

**Abstract**— Power system scheduling faces growing uncertainty from intermittent renewable resources. Conventional unit commitment models may overlook economical solutions if uncertainty is not properly handled. This paper modifies capacity requirements in unit commitment to anticipate the cost of dispatching backup capacity if and when it is needed. The model distinguishes capacity that is suitable for different scenarios by using response sets. The response sets identify capacity that may be dispatched for individual scenarios. Response sets are updated in an iterative manner to reassess the value of backup capacity from different generators. The approach is shown to be faster than stochastic unit commitment. The approach is not only fast but intuitive and more economical than deterministic models that are used today.

## I. KEY EQUATIONS

Stochastic unit commitment is often formulated to determine the commitment status of “slow” generators. All other decisions are auxiliary because they can be deferred until a later time. An efficient deterministic formulation may use a proxy requirement like (1) to help ensure that the commitment decisions are efficient.

$$\sum_{g \in G} C_{gt}^s u_{gt}^0 + \sum_{g \in G^{\text{fast}}} U_{gt}^s (1 - u_{gt}^0) \geq \sum_{n \in N} D_{nt}^s, \quad \forall s \in S, t \in T \quad (1)$$

Constraint set (1) specifies that capacity must meet the total demand for every period  $t$  of each scenario  $s$ . Additional capacity may be required to create an operating margin: rather than increasing the right-hand-side of (1), we reduce the left-hand-side by specifying that capacity can only come from within a pre-defined response set.  $C_{gt}^s$  is the subset of capacity from committed generator  $g$  that belongs to the response set for scenario  $s$  in period  $t$ . Likewise,  $U_{gt}^s$  is the capacity from an uncommitted “fast” generator that belongs to the respective response set. Parameter  $U$  accounts for fast generators that are off in the UC solution but may be turned on during scenario response. The proposed algorithm iteratively prunes  $C$  and  $U$  to remove unsuitable (expensive) capacity from the response set.

## II. KEY FIGURES



Fig. 1. Stylized response set for a particular scenario-period ( $s, t$ ). This figure shows a birds-eye-view of what a response set could look for a single scenario  $s$  during a particular period  $t$ . Lighter shades indicate capacity that has been removed from the response set because it is too expensive, slow ramping, or undeliverable.

## III. METHODOLOGY

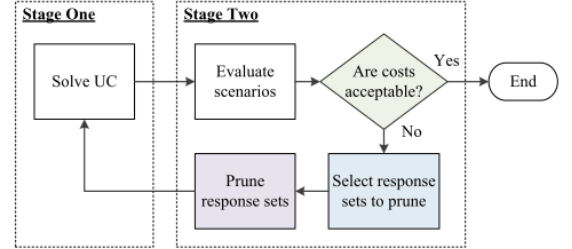


Fig. 2. Decomposition algorithm for day-ahead unit commitment (UC). The key contribution of this research comes through pruning the response sets in order to update constraint (1).

## IV. KEY RESULTS

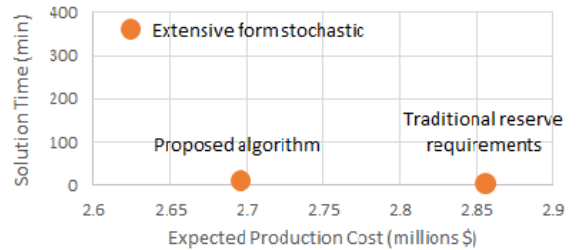


Fig. 3. Preliminary testing results on a modified RTS-96 test case.

## V. REFERENCES

- [1] J. D. Lyon, M. Zhang, and K. W. Hedman, “Reserve response sets for unit commitment with wind,” *IEEE Trans. Power Syst.*, in preparation, Apr. 2013.
- [1] J. D. Lyon, M. Zhang, and K. W. Hedman, “Dynamic reserve zones for distinct scenarios,” *IEEE Trans. Power Syst.*, submitted, Mar. 2014.

# Analyzing the Impacts of Constraint Relaxation Practices in Electric Energy Markets

Yousef M. Al-Abdullah, *Student Member, IEEE*, and Kory W. Hedman, *Member, IEEE*  
 School of Electrical, Computer, and Energy Engineering, Arizona State University, Tempe, AZ 85287, USA  
 Email: [yousef.al-abdullah@asu.edu](mailto:yousef.al-abdullah@asu.edu) and [kory.hedman@asu.edu](mailto:kory.hedman@asu.edu)

**Abstract**—Electric power grids are among the most complex engineered systems today. Operators must ensure a continuous supply of electric power all while trying to operate their system in the most efficient manner possible. This includes responsibilities such as managing hundreds to thousands of generators with complex operating requirements, maintaining system synchronism, and monitoring and managing thousands of transmission assets that could span thousands of miles across multiple states, regions, and possibly even countries. Operators must also cope with stringent reliability standards, increasing presence of variable generation (e.g. photovoltaic solar and wind power), and limited economical energy storage capability. Market models today, which attempt to optimize the dispatch of the generation, can only approximate some of these complex operating, reliability, and transmission requirements. The approximations incorporated in the market models impact the solution. Therefore, instead of forcing market models to abide by strict constraints that are approximates, market designers choose to relax a selection of these constraints. However, to discourage the market solution from readily choosing to relax these constraints, the system must pay a penalty price, which is pre-determined. System operators can potentially receive several benefits from employing constraint relaxations practices in the market models. First, constraint relaxations allow operators to manage prices. Previously, market were designed only using a bid cap, which limited the price independent power producers (IPPs) could bid in the market, and was used in an attempt to cap the locational marginal price (LMP). However, the LMP, which is used to determine different system settlements (e.g. payments to generators), is not limited by imposing a bid cap. Instead, only through the use of relaxing the node/energy balance constraint and imposing a penalty price on that relaxation, is the LMP actually capped. This penalty price then becomes the cap on the LMP, which will be presented in this poster. Another benefit that could be achieved by employing constraint relaxations practices includes the potential to obtain substantial gains in market surplus, even with small relaxations. In order to analyze the impacts of constraint relaxations, a day-ahead security constrained unit commitment (SCUC) model is solved with and without constraint relaxations. After the SCUC solutions are obtained, dispatch solutions are then corrected, using PSS-E along with its preventive security optimal power flow (PSC-OPF) tool, such that the dispatch solutions become not only AC feasible, but also N-1 reliable. A comparison between these corrected dispatch schedules and the original SCUC solutions with and without constraint relaxations will be displayed.

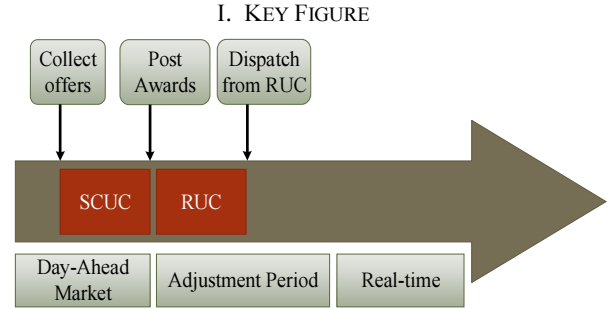


Figure 1 – Day-Scheduling Process

## II. KEY EQUATIONS

Primal Problem with Constraint Relaxations

$$\text{minimize: } c_1x_1 + c_2x_2 + P_1s_1 + P_2s_2 \quad (1)$$

$$a_{11}x_1 + a_{12}x_2 \geq b_1 - s_1 (\lambda_1) \quad (2)$$

$$a_{21}x_1 + a_{22}x_2 \geq b_2 - s_2 (\lambda_2) \quad (3)$$

$$x_1, x_2 \geq 0 \quad (4)$$

$$s_1, s_2 \geq 0 \quad (5)$$

Corresponding Dual Problem

$$\text{maximize: } b_1\lambda_1 + b_2\lambda_2 \quad (6)$$

$$a_{11}\lambda_1 + a_{21}\lambda_2 \leq c_1 (x_1) \quad (7)$$

$$a_{12}\lambda_1 + a_{22}\lambda_2 \leq c_2 (x_2) \quad (8)$$

$$\lambda_1 \leq P_1 (s_1) \quad (9)$$

$$\lambda_2 \leq P_2 (s_2) \quad (10)$$

$$\lambda_1, \lambda_2 \geq 0 \quad (11)$$

## III. KEY RESULTS

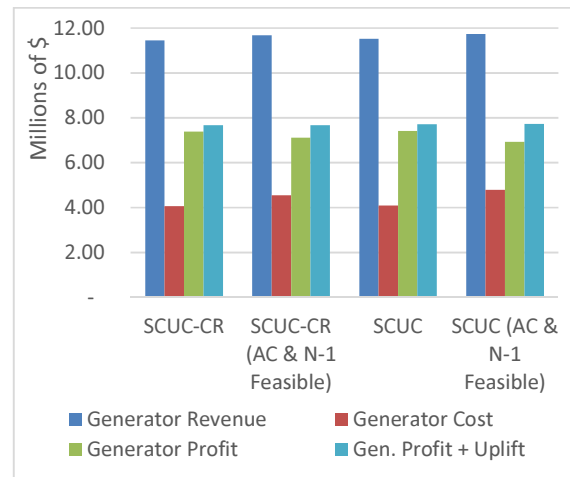


Figure 2 – System Settlements with (SCUC-CR) and without (SCUC) constraint relaxations



# Incorporating Wind Power Self-Reserve in Energy and Reserve Scheduling with Substantial Wind Generation

Mojgan Hedayati, *Student Member, IEEE*, Kory W. Hedman, *Member, IEEE*, and Junshan Zhang, *Fellow, IEEE*  
 School of Electrical, Computer, and Energy Engineering, Arizona State University, Tempe, AZ85287, USA  
 Email: [mhedayat@asu.edu](mailto:mhedayat@asu.edu), [khedman@asu.edu](mailto:khedman@asu.edu), [Junshan.Zhang@asu.edu](mailto:Junshan.Zhang@asu.edu)

**Abstract**—With the significant growth in the integrated capacity of wind power generation, the variability of wind energy production poses new challenges to power system operations. In particular, more rapid reserve is required, which may result in a scarcity of balancing services. With the increasing share of renewable generation, it is expected that, at some point, these renewable sources will have to take part in the electricity system balancing tasks. In this paper, a combined energy and reserve scheduling policy is proposed by introducing wind self-reserve into the reserve structure. In order to provide self-reserve, wind generators under-schedule in the hour-ahead energy market so as to hold some expected output for reserves. Excess expected wind is then available for mitigating forecast errors and other system uncertainties. This paper focuses on developing a framework to find the optimum scheduling policy for incorporating wind self-reserve into the hour-ahead market. To come up with an affine policy for scheduling energy and reserve from the wind generation resources, the cost-reliability tradeoff should be addressed properly. The more energy the operator schedules from the wind farm generation, the more uncertainty the system is exposed to and the more reserve is needed accordingly to account for the uncertainty. In order to address this tradeoff, one should consider the operational costs of the scheduled energy and reserve as well as the risk costs associated with the uncertainty in the wind generation. A finite-state Markov chain wind power forecast model, based on spatio-temporal analysis, has been utilized for studying the hour-ahead energy and reserve scheduling process. In this method, the conditional probability distribution of the wind farm generation for each step is calculated according to the most recent state of the wind farm output. Based on this conditional distribution, a two-stage scenario-based optimization framework is used to find the appropriate level of wind self-reserve. The proposed structure minimizes the aggregate operating costs and risk costs relative to the modeled scenarios. The decision is then tested against a larger set of scenarios to ensure the adequacy of scheduled energy and reserve. The proposed optimization approach is applied to a test system using the Markov chain forecast method of wind generation applied to extensive measurement data collected from a large wind farm where multiple classes of wind turbines are installed. The actual and forecasted wind generation data are used to analyze the effectiveness of the presented model in coping with the forecast errors and achieving a more secure system operation.

## I. PROBLEM FORMULATION

The objective function is formulated as a standard two-stage stochastic problem. The total cost is given in (1), in which the first line is the cost of energy production and scheduling spinning reserve from conventional generators as well as the wind generators. The next term is the expected cost of providing security in scenarios. This includes the cost of deploying spinning reserve, supplied either through the scheduled reserve or by the excess generation from the wind farm (wind self-reserve), the penalty cost associated with the wind generator not being able to provide the scheduled energy, and the cost of involuntary load curtailment.

## II. KEY EQUATIONS

$$\text{Min} \sum_{g,t} (c_w^e P_{wt} + c_w^r r_{wt}) + \sum_{g,t} (c_g^e P_{gt} + c_g^r r_{gt})$$

$$+ \sum_{s,t} \text{prob}_s \left( \sum_g (c_g^e r_{gst}) + \sum_w (c_w^e r_{wst}) + \sum_w (c_w^r \Delta_{w,s,t}) + \sum_w (c_p + c_w^e) P_{wst}^{\text{penalty}} + \sum_n c_c^n (LS_{nt}^+ + LS_{nt}^-) \right)$$

*Subject to:*

**Base case constraints:**

$$\sum_{g \in g(n)} P_{g,t} + \sum_{k \in \delta^+(n)} P_{k,t} - \sum_{k \in \delta^-(n)} P_{k,t} + \sum_{w \in w(n)} P_{w,t} = d_{n,t}, \forall n, t \quad (1)$$

$$P_g^{\min} u_{g,t} \leq P_{g,t}, \forall g, t \quad (2)$$

$$P_{gt} + r_{gt} \leq P_g^{\max} u_{g,t}, \forall g, t \quad (3)$$

$$0 \leq r_{gt} \leq R_g^{10} u_{g,t}, \forall g, t \quad (4)$$

$$\sum_{q \in G} r_{qt} \geq P_{gt} + r_{gt} + \sum_w \xi_{wt}, \forall g, t \quad (5)$$

$$\xi_{wt} \geq P_{wt} - (P_{wt}^f - \alpha \sigma_{wt}), \forall w, t \quad (6)$$

$$P_{gt} - P_{g,t-1} \leq R_g^{10}, \forall g, t, u_{gt} = 1, u_{g,t-1} = 1 \quad (7)$$

$$P_{g,t-1} - P_{gt} \leq R_g^{10}, \forall g, t, u_{g,t-1} = 1, u_{gt} = 1 \quad (8)$$

$$P_{wt} + r_{wt} \leq P_{wt}^f, \forall w, t \quad (9)$$

$$P_{kt} - b_k(\theta_{nt} - \theta_{mt}) = 0, \forall k, t \quad (10)$$

$$-P_k^{\max} \leq P_{kt} \leq P_k^{\max}, \forall k, t \quad (11)$$

**Second Stage constraints (for scenarios):**

$$\sum_{g \in g(n)} (P_{g,t} + r_{gst}) + \sum_{k \in \delta^+(n)} P_{k,s,t} - \sum_{k \in \delta^-(n)} P_{k,s,t} + \sum_{w \in w(n)} (P_{w,t} + r_{w,s,t}) + LS_{nt}^+ - LS_{nt}^- = d_{n,t}, \forall n, t \quad (12)$$

$$r_{g,s,t} \leq r_{gt}, \forall g, s, t \quad (13)$$

$$-r_{g,s,t} \leq r_{gt}, \forall g, s, t \quad (14)$$

$$P_g^{\min} \leq P_{g,t} + r_{gst} \leq P_g^{\max}, \forall g, s, t \quad (15)$$

$$RR_{g,s,t} = r_{g,t} - r_{g,s,t} \quad (16)$$

$$-r_{w,s,t} \leq r_{wt} + P_{wts}^{\text{penalty}}, \forall w, s, t \quad (17)$$

$$0 \leq P_{wt} + r_{w,s,t}, \forall w, s, t \quad (18)$$

$$P_{wt} + r_{w,s,t} + RR_{w,s,t} \leq W_{w,s,t}, \forall w, s, t \quad (19)$$

$$\Delta_{w,s,t} \geq r_{wst} + RR_{w,s,t} - r_{wt} \quad (20)$$

$$\Delta_{w,s,t} \geq 0 \quad (21)$$

$$\sum_{g \in g(n)} RR_{g,s,t} + \sum_{w \in w(n)} RR_{w,s,t} \geq P_{gt} + r_{gt}, \forall g, s, t \quad (22)$$

## References

- [1] Miao He, L. Yang, J. Zhang, V. Vittal, "A Spatio-Temporal Analysis Approach for Short-Term Forecast of Wind Farm Generation," *IEEE Trans. Power Syst.*, vol. pp, no. 99, Jan. 2014.

# An Analytical Approach to Assess Static Voltage Stability of Distribution System with Rooftop PV Units

Jalil Yaghoobi, *Student Member, IEEE*,  
 Nadarajah Mithulananthan, *Senior Member, IEEE*,  
 Tapan Kumar Saha, *Senior Member, IEEE*  
 School of Information Technology & Electrical Engineering  
 The University of Queensland  
 Brisbane, Australia  
 Emails: j.yaghoobi@uq.edu.au, mithulan@itee.uq.edu.au,  
 saha@itee.uq.edu.au

Ramesh C. Bansal, *Senior Member, IEEE*  
 Dept. of Electrical, Electronic & Computer Engineering,  
 University of Pretoria  
 Pretoria, South Africa  
 Email: rc Bansal@ieee.org

**Abstract**— This paper presents analytical expressions to examine the effect of power injection from rooftop PV units on the static voltage stability of distribution system with theoretical and practical limits. Using an equivalent two-bus system, change in the loadability of the system as a direct measure of static voltage stability by PV power is obtained analytically for various limits. The analytical results then are simulated and compared. To validate the methodology, IEEE 37 bus distribution test system is implemented in PSCAD software and simulation results are presented.

## I. KEY EQUATIONS

In this paper, for an equivalent two-bus system, the loadability in  $V_{col}$ ,  $I_{max}$ , and  $V_{min}$  are calculated as given in (1) to (3).

$$P_{mC} = E^2 \cos \theta_L / (2Z_S(1 + \cos \Delta \theta)) \quad (1)$$

$$P_{mI} = \left( \sqrt{E^2 - Z_S^2 I_{max}^2 \sin^2 \Delta \theta} - Z_S I_{max} \cos \Delta \theta \right) I_{max} \cos \theta_L \quad (2)$$

$$P_{mV} = \left( \sqrt{E^2 - V_{min}^2 \sin^2 \Delta \theta} - V_{min} \cos \Delta \theta \right) \frac{V_{min}}{Z_S} \cos \theta_L \quad (3)$$

For  $V_{col}$ ,  $I_{max}$ , and  $V_{min}$ , change in loadability ( $\Delta P$ ) is as given in (4) – (6) and  $\theta_{imax}$ , in which the maximum increase in loadability happens, is as given in (7) – (9) respectively.

$$\Delta P_{mC} = (S_{m1} - S_{m2} + S_i \cos(\theta_i - \theta_S)) \cos \theta_L / \cos \Delta \theta \quad (4)$$

$$\Delta P_{mI} = \left( \left( \sqrt{E^2 - (Z_S I_{max} \sin \Delta \theta - S_i \sin(\theta_i - \theta_L) / I_{max})^2} - \sqrt{E^2 - Z_S^2 I_{max}^2 \sin^2 \Delta \theta} \right) I_{max} + S_i \cos(\theta_i - \theta_L) \right) \cos \theta_L \quad (5)$$

$$\Delta P_{mV} = \left( \left( \sqrt{E^2 - (V_{min} \sin \Delta \theta - Z_S S_i \sin(\theta_i - \theta_L) / V_{min})^2} - \sqrt{E^2 - V_{min}^2 \sin^2 \Delta \theta} \right) V_{min} / Z_S + S_i \cos(\theta_i - \theta_L) \right) \cos \theta_L \quad (6)$$

$$\theta_{imaxC} \cong (\theta_S + \theta_L) / 2 \quad (7)$$

$$\theta_{imaxI} = \theta_L + \arcsin(Z_S I_{max}^2 \sin \Delta \theta / (S_i + E I_{max})) \quad (8)$$

$$\theta_{imaxV} = \theta_L + \arcsin(V_{min}^2 \sin \Delta \theta / (Z_S S_i + E V_{min})) \quad (9)$$

## II. KEY SIMULATION RESULTS

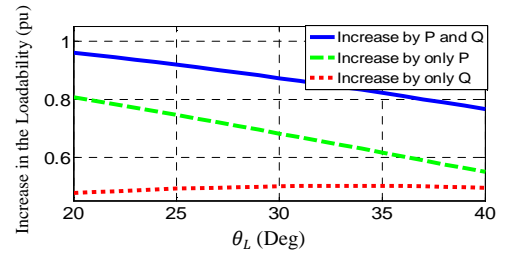


Fig. 1. Increase in the Loadability for  $S_i = 1$  pu with different  $\theta_L$ , and  $\theta_S = 45^\circ$ : (a)  $V_{col}$ ; (b)  $I_{max}$ ; (c)  $V_{min}$ .

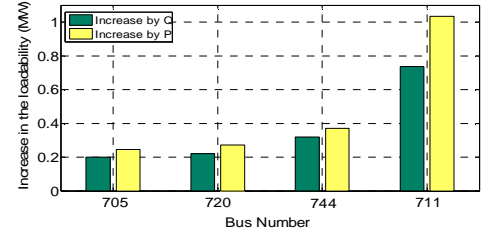


Fig. 2. Increase in the loadability by  $P=1$  MW and  $Q=1$  MVar injections to four buses of IEEE-37 system: (a)  $V_{col}$ ; (b)  $I_{max}$ ; (c)  $V_{min}$ .

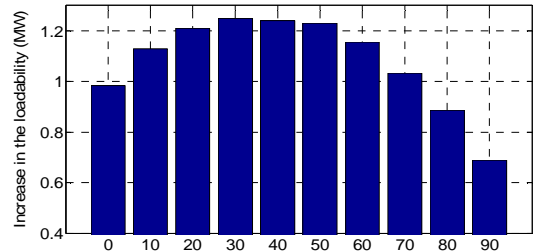


Fig. 3. Increase in the loadability with different  $\theta_i$  and  $S_i = 1$  MVA to bus 711: (a)  $V_{col}$ ; (b)  $I_{max}$ ; (c)  $V_{min}$ .

# Dynamic Voltage Stability Analysis of Sub-Transmission Networks with Large-Scale Photovoltaic Systems

Shahariar Kabir, Olav Krause, Ramesh Bansal  
 School of Information Technology and Electrical  
 Engineering  
 University of Queensland  
 Brisbane, Australia  
 m.kabir2, o.krause@uq.edu.au

Jayashri Ravishanker  
 School of Electrical Engineering and  
 Telecommunications  
 University of New South Wales  
 Sydney, Australia  
 jayashri.ravishanker@unsw.edu.au

**Abstract**—This research paper presents analyses of the impact of large-scale PV on dynamic voltage stability with respect to short and long term state variables for the 14 bus system. Preliminary findings suggest that the influence of large-scale PV depends on PV controller type and setting. It is also noted that the integration of large-scale PV has implications on dynamic behavior that are not adequately captured by static analysis.

## I. INTRODUCTION

It can be observed from literature review that voltage stability studies in terms of short and long term state variables are common, but usually excluding large-scale PV. Therefore, the key objective of this research paper is to illustrate the effects of large-scale PV on voltage with respect to short and long term state variables for the IEEE 14 bus network.

## II. ANALYSIS OF SHORT TERM VOLTAGE STABILITY

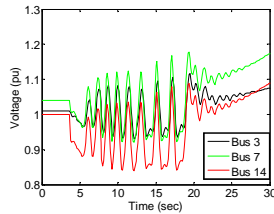


Figure 1. Voltage profile of IEEE 14 bus system due to load increase with PV in active power generation (PQ) mode.

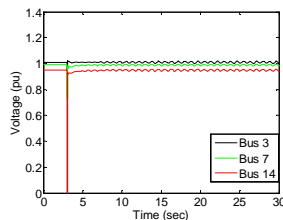


Figure 2. Voltage profile during fault study with PV in active and reactive power generation (PV) mode.

Thus, with the presence of PV in both operational modes, it can be concluded that short term instability can mainly occur due to oscillatory instability of equilibrium or loss of stable equilibrium related to fast dynamics after disturbance.

## III. ANALYSIS OF LONG TERM VOLTAGE STABILITY

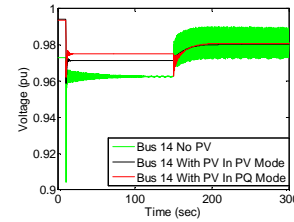


Figure 3. Voltage profile for long term voltage stability analysis.

It can be observed from Fig. 3 that the integration result depends on the inverter controller settings as well as the time constant, step size, reference voltage and dead band of OLTC.

## IV. IMPORTANCE OF DYNAMIC STABILITY ANALYSIS

After the considered contingencies of losing transmission line and consequently losing generator, with PV at active and reactive power generation (PV) mode, the minimum singular value decreases from 0.51 to 0.29 while the eigenvalue decreases from 2.59 to 2.34. However, while considering the dynamics, the following voltages are obtained symbolizing unstable system under the considered controller parameters.

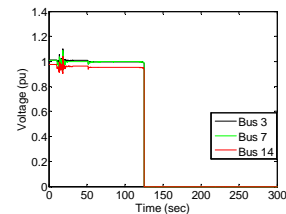


Figure 4. Dynamic voltage profile of studied network with PV.

# Do-not-exceed Limits for Renewable Resources with Robust Corrective Topology Control

Akshay S. Korad and Kory W. Hedman

School of Electrical, Computer, and Energy Engineering, Arizona State University, Tempe, AZ 85287, USA  
Email: [korad@asu.edu](mailto:korad@asu.edu) and [Kory.Hedman@asu.edu](mailto:Kory.Hedman@asu.edu)

**Abstract**— In recent years, the penetration of renewable resources, such as wind and solar generation, in electrical power systems has increased. These renewable resources add more complexities to power system operations, due to their intermittent and unpredictable nature. As a result, operators must acquire additional reserves in order to maintain a balanced system. However, one persistent challenge is determining the optimal location of the reserves and this challenge is exacerbated by the inability to predict key transmission bottlenecks due to this added uncertainty. The presented research utilizes robust corrective topology control as a congestion management tool to manage power flows and the associated renewable uncertainty. The proposed day-ahead method determines the maximum amount of uncertainty in renewable resources in terms of do-not-exceed (DNE) limits combined with corrective topology control actions. The day-ahead topology control formulation is based on the direct current optimal power flow; therefore, switching solutions obtained from these algorithms are tested for AC feasibility and system stability. The numerical results presented are based on the IEEE-118 bus test case with 20% wind penetration.

## I. KEY EQUATIONS

The robust corrective topology control algorithm to determine DNE limits is a three stage optimization problem; however, it can be reduced to a two stage optimization problem. The generic form of two stage robust topology control formulation is given in (1)-(3).

$$\min_{x \in X} (c^T x + \max_{w \in W} b^T y(w)) \quad (1)$$

$$\text{s.t.} \quad Fx \leq f, Hy(w) \leq h, Ax + By(w) \leq g, \quad (2)$$

$$Ey(w) = d, x \in \{0,1\}. \quad (3)$$

## II. KEY FIGURES

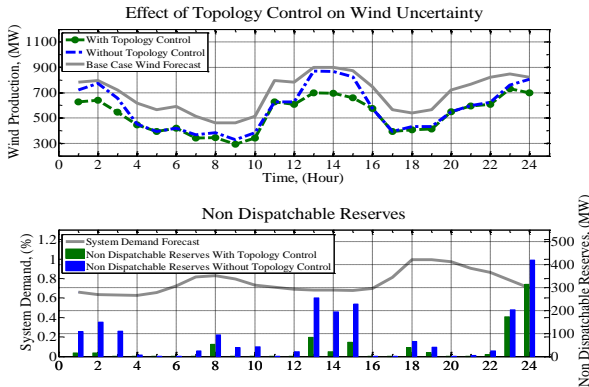


Figure 1. Lower bound of do-not-exceed limits with and without topology control actions.

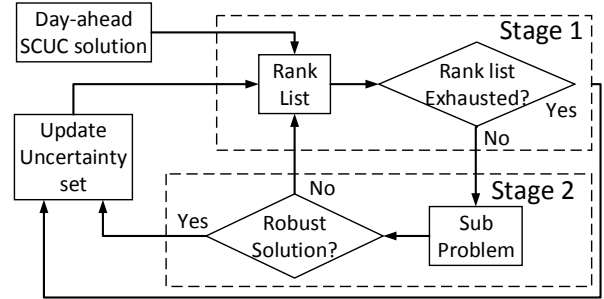


Figure 2. Solution method for robust corrective topology control.

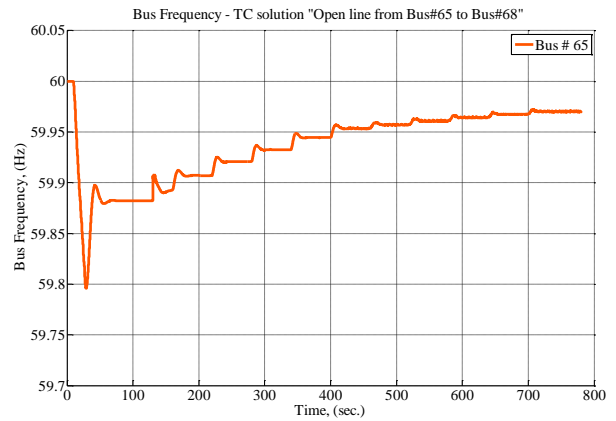


Figure 3. Effect of sudden drop of wind and associated corrective topology control action on system frequency.

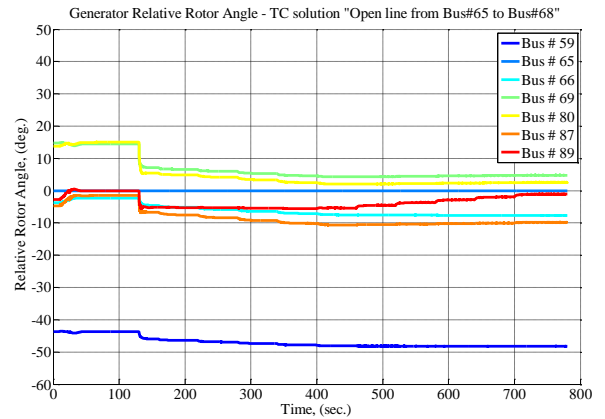


Figure 4. Effect of sudden drop of wind and associated corrective topology control action on generator relative rotor angles.

# A Model Predictive Approach for Community Battery Energy Storage System Optimization

H. Pezeshki<sup>1</sup>, Member, IEEE, P. Wolfs<sup>2</sup>, Senior Member, IEEE and G. Ledwich<sup>1</sup> Senior Member, IEEE

<sup>1</sup>School of Engineering and Computer Science, Queensland University of Technology, Brisbane, Australia

<sup>2</sup>Central Queensland University, Rockhampton, Australia

**Abstract**—This paper presents an efficient algorithm for optimizing the operation of battery storage in a low voltage distribution network with a high penetration of PV generation. A predictive control solution is presented that uses wavelet neural networks to predict the load and PV generation at hourly intervals for twelve hours into the future. The load and generation forecast, and the previous twelve hours of load and generation history, is used to assemble load profile. A diurnal charging profile can be compactly represented by a vector of Fourier coefficients allowing a direct search optimization algorithm to be applied. The optimal profile is updated hourly allowing the state of charge profile to respond to changing forecasts in load.

## I. METHODOLOGY

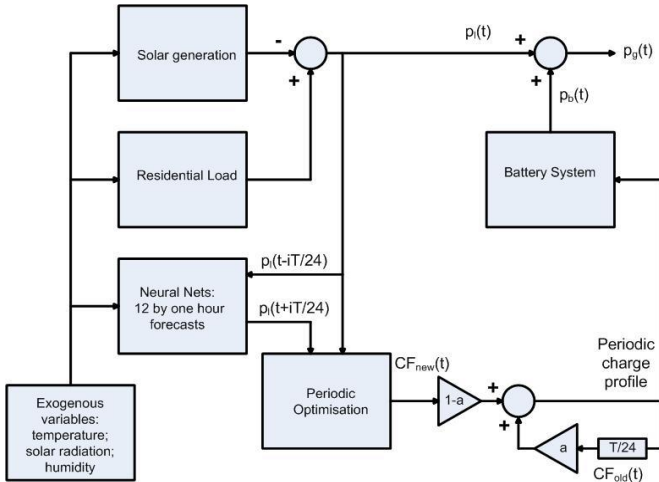


Fig. 1. Receding Horizon Periodic Control

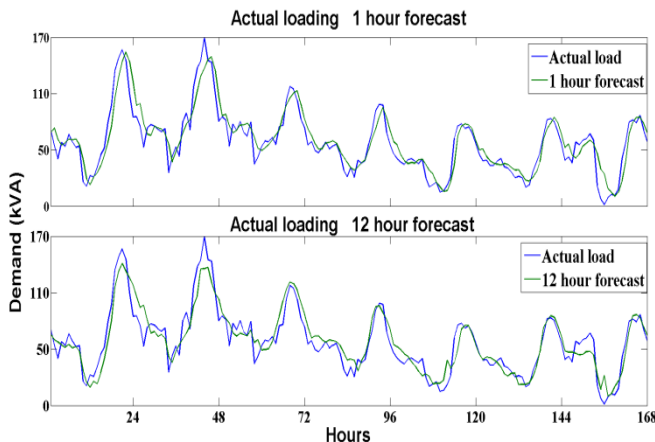


Fig. 2. WNN based one and twelve hour load forecast

## II. KEY RESULTS

Table I Daily MAE and MAPE of forecast windows

Forecast (hours)	MAE (kW)	MAPE	Forecast (hours)	MAE (kW)	MAPE
1	4.8	2.82%	8	9.2	5.41%
4	6.9	4.06%	12	9.7	5.54%

### Scenario I: Peak Shaving

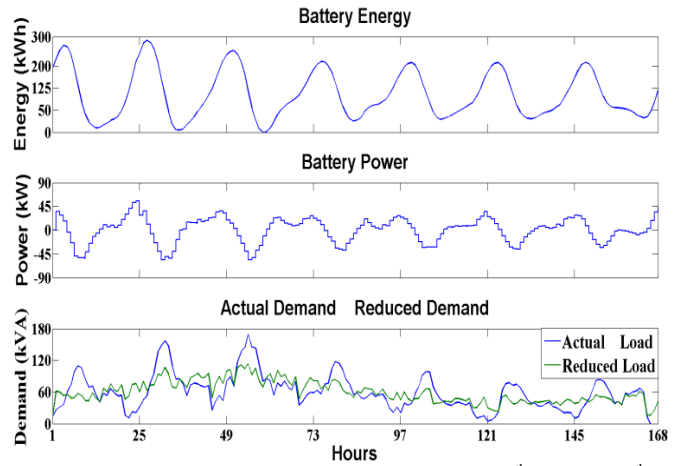


Fig. 3. LV Receding Horizon Control Response - 30<sup>th</sup> January to 6<sup>th</sup> February

### Scenario II: Smooth load

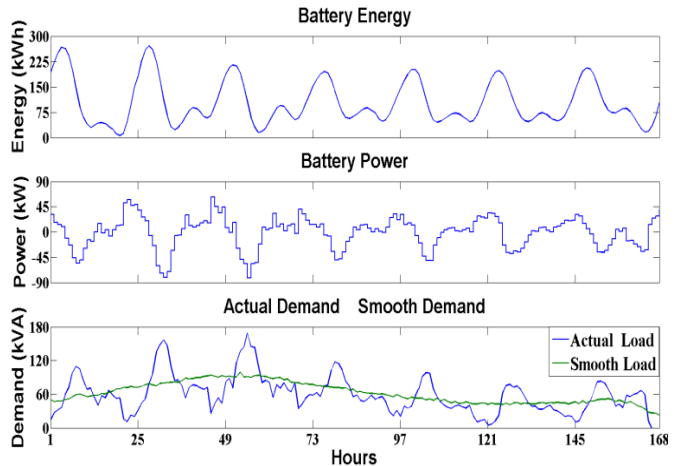


Fig. 4. Smooth LV grid power with receding horizon response



# Design of a Nonlinear Excitation Controller Using Inverse Filtering for Transient Stability Enhancement

R. Goldoost-Soloot, Graduate Student Member, IEEE, Y. Mishra, Member, IEEE, G. Ledwich, Senior Member, IEEE  
 School of Electrical Engineering and Computer Science, Queensland University of Technology (QUT), Brisbane, Australia  
 Email: r.goldoostsoloot@qut.edu.au, yateendra.mishra@qut.edu.au, g.ledwich@qut.edu.au

**Abstract**—In this paper a new nonlinear excitation controller is proposed which improves transient stability of power system and damps power system oscillations while maintaining voltage regulation. The concept of energy functions and prediction of the required future states of the system are used to achieve the desired flux for the next time step of the system. The obtained desired flux enhances the stability of power system. From this, an inverse filtering method is applied to obtain a supplementary control input for the excitation system. The inverse filtering technique enables the system to provide an additional input for the excitation system which forces the system to track the desired flux. An autoregressive model (AR) is derived from inverse filtering and generates the supplementary control input by using future values of desired flux. The acquired auxiliary control input increases the damping of power system oscillations and transient stability of the system. The proposed nonlinear control method is implemented on single machine infinite bus (SMIB) test system while generator flux saturation is considered and transient stability is assessed by using time-domain simulations.

**Index Terms**—excitation controller; transient stability; inverse filtering; power system oscillations; autoregressive model.

## I. KEY EQUATIONS

To determine derivative of kinetic energy, the classic model of the swing equation is used:

$$\dot{V}_{KE} = (T_m - \frac{E'_q V_\infty}{X} \sin \delta - D(\omega - \omega_s)) \dot{\delta}_i \quad (1)$$

The desired flux for minimizing the kinetic energy of the system is achieved by differentiating from (1) with respect to  $E'_q$ :

$$\frac{\partial \dot{V}_{KE}}{\partial E'_q} = -\frac{V_\infty}{X} \sin \delta \dot{\delta}_i = K \sin \delta \dot{\delta}_i \quad (2)$$

The obtained value is used as the desired flux for the system which will be produced by injecting a supplementary control input to the excitation system.

Inverse filtering technique is used for finding a unique input based on knowledge of required future outputs. The purpose of inverse filtering is calculating a suitable supplementary control input ( $V_s$ ) which produces the desired flux for power system.

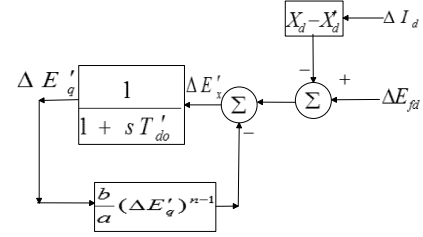


Fig. 1. Block diagram of generator dynamics

$$\Delta E'_{fd} = \Delta I_d (X'_d - X'_d) + \frac{b}{a} (\Delta E'_q)^n + \Delta E'_x \quad (3)$$

$$\frac{\Delta E'_q}{\Delta E'_x} = \frac{1}{1 + sT'_{do}} \quad (4)$$

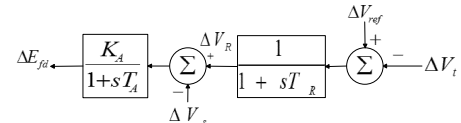


Fig. 2. Block diagram of exciter dynamics

$$\frac{\Delta E'_{fd}}{\Delta V_R - \Delta V_S} = \frac{K_A}{1 + sT'_A} \quad (5)$$

AR model through inverse filtering is constructed to secure the desired flux for the system by generating supplementary control input.

$$\Delta E'_{x_k} = K_1 \Delta E'_{q_k} + K_2 \Delta E'_{q_{k+1}} + \dots \quad (6)$$

$$\Delta E'_{fd_k} = \Delta E'_{x_k} + \frac{b}{a} (\Delta E'_{q_k})^n + (X'_d - X'_d) \Delta I_{d_k} \quad (7)$$

$$\Delta V_{S_k} = c_0 \Delta E'_{fd_k} + c_1 \Delta E'_{fd_{k+1}} + c_2 \Delta E'_{fd_{k+2}} + \dots \quad (8)$$

## II. SAMPLE RESULTS

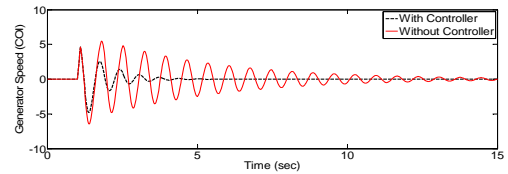


Fig. 3. Generator rotor speed for 150ms short-circuit fault

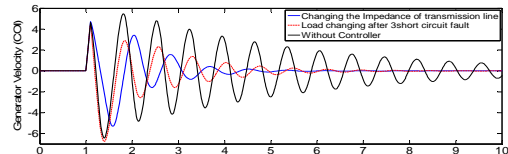


Fig. 4. Controller performance under 2 different conditions

# An Adaptive Three-bus Power System Equivalent for Estimating Voltage Stability Margin from Synchronized Phasor Measurements

Fengkai Hu, Kai Sun  
University of Tennessee  
Knoxville, TN, USA  
[fengkaihu@utk.edu](mailto:fengkaihu@utk.edu)  
[kaisun@utk.edu](mailto:kaisun@utk.edu)

Alberto Del Rosso, Evangelos Farantatos,  
Navin Bhatt  
Electric Power Research Institute  
Knoxville, TN, USA

**Abstract**—This paper utilizes an adaptive three-bus power system equivalent for measurement-based voltage stability analysis. With that equivalent identified online, a measurement-based approach is developed to estimate real-time voltage stability margin for a load-rich area supported by remote generation via multiple tie lines. Compared with traditional Thevenin equivalent based approach, this new approach is able to provide more accurate voltage stability margin for each individual tie line. This approach is validated on a three-bus system and the IEEE 39-bus system.

## I. STRATEGIES FOR THREE-BUS EQUIVALENCING

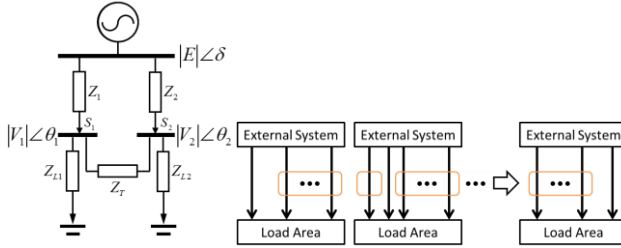


Figure 1. Strategies for three-bus equivalencing – N equivalents

## II. APPROACH FOR VOLTAGE STABILITY MARGIN CALCULATION

### A. External System Parameters Estimation

$$\begin{bmatrix} E_r & E_i & R_1 & X_1 & R_2 & X_2 \end{bmatrix} = (H^T H)^{-1} H^T Z \quad (1)$$

### B. Load Area Parameters Estimation

$$\begin{aligned} |V_{1a}|^2 Y_{11a} + (|V_{1a}|^2 - V_{1a}^* V_{2a}) Y_{12} &= S_{1a}^* \\ |V_{1b}|^2 Y_{11b} + (|V_{1b}|^2 - V_{1b}^* V_{2b}) Y_{12} &= S_{1b}^* \\ |V_{2a}|^2 Y_{22a} + (|V_{2a}|^2 - V_{2a}^* V_{1a}) Y_{12} &= S_{2a}^* \\ |V_{2b}|^2 Y_{22b} + (|V_{2b}|^2 - V_{2b}^* V_{1b}) Y_{12} &= S_{2b}^* \end{aligned} \quad (2)$$

### C. Finding the Power Transfer Limits

The maximum limits of the active power transferred to two load buses are solved by an exhaustive searching method.

## III. CASE STUDIES

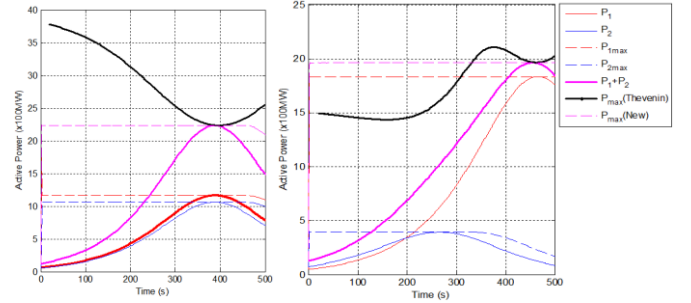


Figure 2. Line flow limits for tight (a) and weak (b) interconnections (3-bus system)

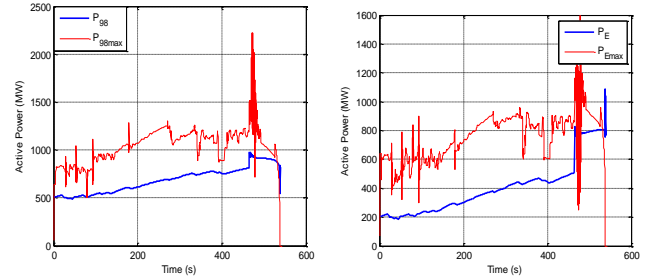


Figure 3. Active powers of two lines and their voltage stability limits (IEEE 39-bus system)

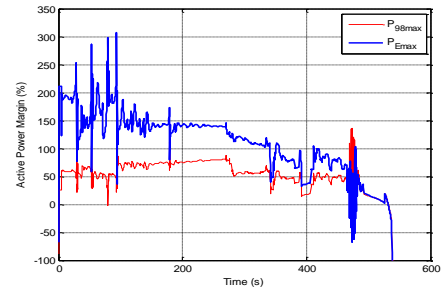


Figure 4. Comparison of the percentage active power margins of two lines (IEEE 39-bus system)

# A Study on Fluctuations in Electromechanical Oscillation Frequencies of Power Systems

Bin Wang, Kai Sun  
University of Tennessee  
Knoxville, TN USA  
[bwang13@utk.edu](mailto:bwang13@utk.edu)  
[kaisun@utk.edu](mailto:kaisun@utk.edu)

Alberto Del Rosso, Evangelos Farantatos, Navin Bhatt  
Electric Power Research Institute  
Palo Alto, CA, USA

**Abstract**—This poster introduces the fluctuation phenomenon in the electromechanical oscillation frequency of a power system. Analysis on the power system swing equation explains that the oscillation frequency fluctuates around a central frequency due to the nonlinear system nature of a power system. A Phase-Plane Trajectory based method is used to track the real-time frequency fluctuation, based on which a real-time angular stability margin index is proposed for early warning of angular stability issues. That index is tested by case studies on a two-generator system and a 179-bus power system.

**Index Terms**—oscillation frequency; phase-plane trajectory method; prony analysis; stability margin; phasor measurement unit; synchrophasor

## I. THE FLUCTUATION PHENOMENON IN THE ELECTROMECHANICAL OSCILLATION FREQUENCY

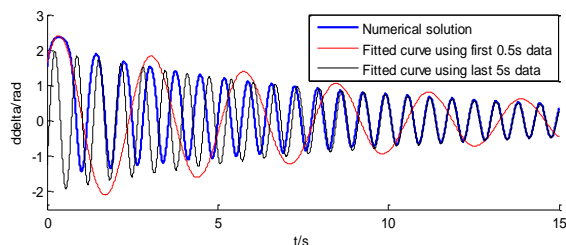


Figure.1. Numerical solution of rotor angle and its fitting curves

It can be seen from Fig. 1 that after 1 second, the optimal fitted curve using the first 0.5 second data has a slower oscillation than the numerical solution, while the curve from the last 5 seconds seems to have a faster oscillation in the beginning of the whole time window. Thus, the constant oscillation frequency (OF) assumption does not hold for the solution to the nonlinear swing equation. Furthermore, a simple conclusion could be drawn that in this stable case, the OF will start from a relatively small value and gradually increase as the angle difference is damped gradually.

## II. ESTIMATION OF INSTANTANEOUS OF AND THE ANALYSIS OF STABILITY MARGIN

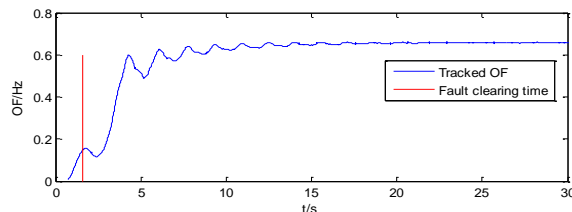


Figure.2. Tracked oscillation frequency after a disturbance

The OF may change within a certain range over a post-disturbance period. Note that right after the disturbance, the system gets closest to the stability boundary and the OF has the largest fluctuations. In the later time, the system approaches a stable equilibrium point and the OF fluctuation also decreases. Thus, the range of fluctuation may represent the criticality to instability.

## III. SYSTEM STABILITY ENHANCEMENT

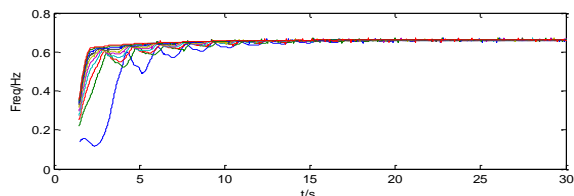


Figure.3. Tracked OF under different operating conditions

## IV. CONCLUSIONS

This poster presents the fluctuation phenomenon of the oscillation frequency in power systems. Case studies have demonstrated that real-time monitoring the fluctuating OF can help estimate the angular stability margin and even suggest preventive control actions.

## REFERENCES

- [1] K. Sun, K. Hur, P. Zhang, "A New Unified Scheme for Controlled Power System Separation Using Synchronized Phasor Measurements", *IEEE Trans. Power Systems*, vol. 26, No. 3, pp. 1544-1554, Aug. 2011
- [2] K. Sun, et al, "An adaptive power system equivalent for real-time estimation of stability margin using phase-plane trajectories," *IEEE Trans. Power Systems*, vol. 26, No.2, pp. 915-923, May. 2011.



# Dimensionality Reduction of Synchrophasor Data for Power System Event Classification

Yang Chen, Le Xie, and P. R. Kumar  
 Department of Electrical and Computer Engineering  
 Texas A&M University, College Station, Texas 77843  
 Email: hebe.cheny@tamu.edu

**Abstract**—Given the strong capability of synchrophasor measurements for wide-area monitoring, protection and control, our research focuses on the analysis of the fundamental dimensionality of the data from the increasingly deployed synchrophasors.

This work proposes an online data-driven tool to classify power system events using synchrophasor measurements. A scatter-plot-based event classification (SPEC) algorithm is proposed with the dimensionality reduction of the emerging ambient phasor measurement unit (PMU) data. In contrast with model-based analysis, the SPEC algorithm does not require a system model. It projects real-time PMU data onto the core subspace constructed from pre-event data, and then utilizes their scatter plots to detect and classify the system events. Projections lying outside the core subspace indicate the occurrence of an event, and the topological shapes of these projections classify the events.

Numerical examples using synthetic and realworld PMU data are conducted to demonstrate the efficacy of the proposed approach.

## I. SPEC ALGORITHM

The SPEC algorithm, consisting of two parts, is shown in Fig. 1.

Define the measurement matrix  $Y_{n \times N} := [y^{(1)}, \dots, y^{(N)}]$  with  $N$  measurements of ambient PMU data. Each measurement has  $n$  samples constituting a time history, i.e.,  $y^{(i)} := [y_1^{(i)}, \dots, y_n^{(i)}]^T, i = 1, \dots, N$ .

1) *Dimensionality Reduction based Adaptive Training*: The adaptiveness refers to the update of measurement matrix  $Y$  after an event is detected and classified.

The threshold is in the form of

$$\Gamma^1 = [PC_2^{min}, PC_2^{max}]. \quad (1)$$

2) *Scatter Plot based Event Detection and Classification*:

The pre-event space and the threshold from training will be utilized as prerequisites for the online detection and classification using the PCA-based scatter plot.

If the transient projection lies inside the threshold, i.e.,  $\bar{y}(t)^{(i)} \in \Gamma$ ,  $y(t)^{(i)}$  is classified as an ambient data, and the next measurement will be taken into the algorithm; otherwise, if  $\bar{y}(t)^{(i)} \notin \Gamma$ , an event detection alert will be issued to trigger the event classification.

<sup>1</sup>In this case, the first principal component (PC) reflects the system-wide frequency synchronism, and the second PC ( $PC_2$ ) is shown to dominate in the decision of the threshold.

Once receiving an event alert, start matching the scatter topology<sup>2</sup>. Whenever the current scatter topology is matched to an existing one, the event can be classified.

After the event classification and the system operating at a new condition, update the measurement matrix  $Y$  with a new set of ambient data, and repeat training steps.

## II. KEY RESULTS

### SPEC Algorithm

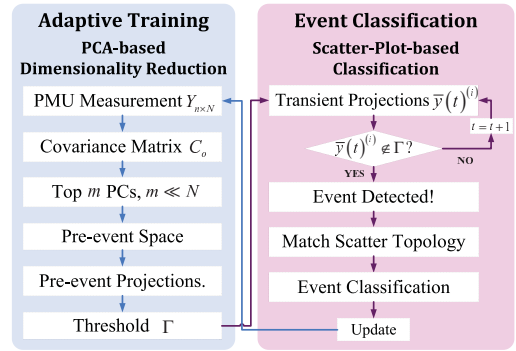


Fig. 1. Implementation of SPEC algorithm.

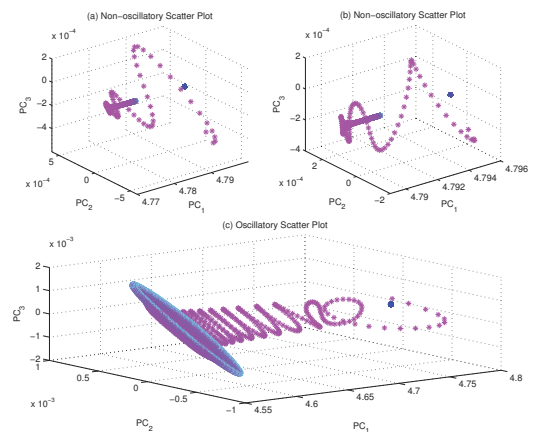


Fig. 2. Scatter plots for events.

<sup>2</sup>The scatter topology is a group of scatter plots for various system events.

# Reducing Post Contingency Congestion Risk and Wind Curtailment using Dynamic Line Rating

Binayak Banerjee, Dilan Jayaweera and Syed M. Islam  
Electrical and Computer Engineering, Curtin University, Perth, Australia

**Abstract**— Large-scale integration of wind power can be deterred by post contingency congestion that results in constrained network capacity. Post contingency congestion can be mitigated by the application of event control strategies, however they may not always benefit large wind farms. This poster investigates this problem in detail and proposes an advanced mathematical framework to capture post contingency risk of network congestion resulting through the constrained network capacity that limits high penetration of wind. The approach models network congestion as functions of stochastic limits of network assets and assesses the risk of congestion through the proposed mathematical framework. The uniqueness of the approach is that it can limit the generation to be curtailed or re-dispatch by dynamically enhancing the network latent capacity in the events of contingencies or as per the need. The case study results with large and small network models suggest that the wind utilization can be considerably increased if the networks are operated around 15% less than the nominal rating of the assets and incorporated dynamic asset ratings.

**Index Terms**— dynamic line ratings, risk of congestion, wind power generation,

## I. KEY EQUATIONS

. Cost of DLR in the objective function is given by (1)

$$C_{DLR} = \sum_{p=1}^{N_p} \sum_{q=1}^{N_q} \left[ c_{OLP} \left( \sum_{k=1}^{N_k} h_{pq,k} a_{pq,k} \right)^2 \right] \quad (1)$$

. The constraints in (3) complement the expression for  $C_{DLR}$  in (1).

$$a_{pq,k} \geq s_{max,pq,k} - S_{sch,pq} \quad (2)$$

$$P_{local,n} \leq P_{D,n}, a_{pq,k} \geq 0, P_{local,n} \geq 0,$$

$(h_{pq,k}, s_{max,pq,k})$  is the  $k^{th}$  ordered pair (probability, value) representing line capacity probability distribution. The term  $a_{pq,k}$  (with per unit cost  $c_{OLP}$ ) represents the amount by which the actual line flow exceeds the discrete line capacity in the  $k^{th}$  ordered pair and it corrects any violation in the constraint  $S_{sch,pq} > s_{max,pq,k}$ . Network congestion is measured by the term  $LMP_V$  defined by (3).

$$LMP_V = \sqrt{\frac{1}{\sum_{i=1} P_{D,i}} \left( \sum_{i=1} P_{D,i} \left( \frac{LMP_i - LMP_{i,base}}{LMP_{i,base}} \right)^2 \right)} \quad (3)$$

## II. KEY RESULTS

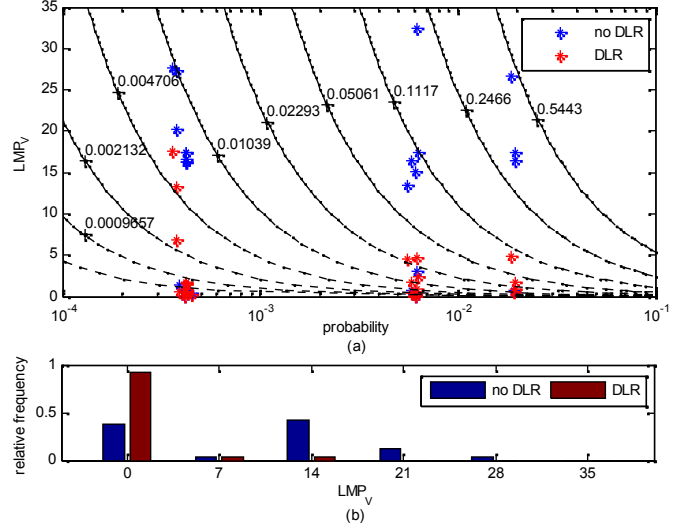


Fig. 1 Comparison of post contingency congestion risk profile of 118 bus system with and without dynamic line rating (a) contingencies against risk contours (b) histogram of  $LMP_V$

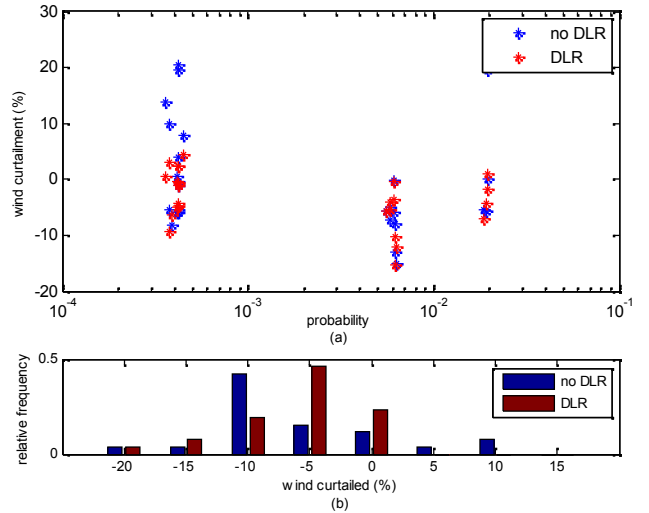


Fig.26 (a) Post contingency wind curtailment profile for 118 bus system (b) Histogram of wind curtailment

# Cyber Attacks on AC State Estimation: Unobservability and Physical Consequences

Jingwen Liang, Oliver Kosut and Lalitha Sankar

School of Electrical, Computer, and Energy Engineering, Arizona State University, Tempe, AZ 85287, USA

Email: jingwen.liang@asu.edu, okosut@asu.edu, lalitha.sankar@asu.edu

**Abstract**—An algorithm is developed to construct unobservable attacks for an AC state estimator (SE). It is shown that unobservability of the attack, in the absence of noise, is guaranteed when the attacker exploits its local network knowledge to perform AC SE locally than the simpler DC SE often assumed in the literature. Finally, the consequences of such an unobservable attack are highlighted via a scenario in which the physical system is changed due to false data injection.

**Index Terms**—State estimation, false data injection, consequence.

## I. KEY EQUATIONS AND DESCRIPTIONS

The AC measurement model is given by  $z = h(x) + e$  where  $h(\cdot)$  denotes a non-linear relationship between the states and measurements and  $e$  is assumed to be independent and Gaussian distributed with 0 mean and  $\sigma^2$  covariance.

Suppose the  $i$ -th measurement prior to attack is  $z_i = h_i(x) + e_i$ , the attack model changes the  $i$ -th measurement  $z_i$  to  $z_i^{(a)}$  such that:

$$z_i^{(a)} = \begin{cases} z_i & \text{if } i \notin I_S \\ \tilde{z}_i & \text{if } i \in I_S \end{cases} \quad (1)$$

where  $\tilde{z}_i$  is chosen by attacker and  $I_S$  denotes measurement indices inside of attack subgraph  $S$ .

Given a target injection bus  $k$ , the corresponding *attack subgraph*  $S_k$  is the set of buses consisting of the target bus and its adjacent buses. When the attacker controls an attack subgraph, it may arbitrarily change the phase at the target bus without detection at the control center.

**Definition 1.** We say an attack is *unobservable* for a measurement model  $h(\cdot)$  if, in the absence of measurement noise, there exists a  $c \neq 0$  such that  $z_i^{(a)} = h_i(x + c)$  for all  $i$ .

Therefore, (1) becomes:

$$z_i^{(a)} = \begin{cases} z_i & \text{if } i \notin I_S \\ h_i(x + c) & \text{if } i \in I_S \end{cases} \quad (2)$$

Contrary to the DC attack, the attacker must know all entries of  $x$  that appear in  $h_i$ , for all  $i \in I_S$ , to construct  $z_i$  precisely. However, this information is not available to the attacker. Thus, attacker uses the following model instead:

$$z_i^{(a)} = \begin{cases} z_i & \text{if } i \notin I_S \\ h_i(\hat{x}_k + c) & \text{if } i \in I_S \end{cases} \quad (3)$$

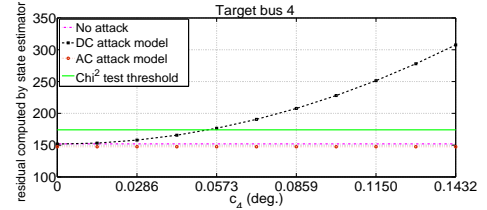


Figure 1. Residual for DC and AC attacks as the attacker increases the voltage angle of center bus 4.

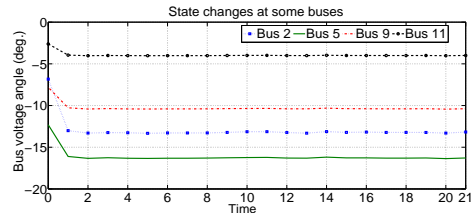


Figure 2. Physical consequences for attack centered at bus 7. Voltage angle evolution at bus 2, 5, 9 and 11 (degree).

where  $k \in K_S$  and  $\hat{x}_k$  is a state estimate found by the attacker using local AC state estimation from its available measurements in  $S$ .

## II. KEY RESULTS

We use the IEEE RTS 24 bus system as a test system. We assume that both active and reactive power flows are measured at two ends of each line and both active and reactive injection are measured at each injection bus, which makes 192 measurements in total. All measurements are assumed to have an error  $e_i \sim N(0, 10^{-4})$  and the  $\chi^2$  detector threshold is set to be 174.1 with 95% confidence of detection.

For an attack targeted at bus 4 we plot the residual as a function of  $c$  in Fig. 1. As expected, the residuals resulting from the AC attack model are always below the  $\chi^2$  threshold irrespective of the value of  $c_k$ . Moreover, Fig. 1 shows the result of a DC attack on the AC model, which crosses the  $\chi^2$  threshold for fairly small attack size.

Fig. 2 illustrates an attack with physical consequences. In particular, the attacker targets bus 7, which causes a false state estimate at the control center. This false state estimate is run through ACOPF, which leads to a re-dispatch, decreasing the generation at bus 7 and increasing it at bus 13. Fig. 2 shows the time evolution of several real states during the attack.

# Detection of Fault Event and Location with A Support Vector Machine-based Approach

Li-Yuan Hsu (Advisor: Gary W. Chang)

Department of Electrical Engineering, National Chung Cheng University, Chia-Yi, Taiwan

e-mails: afriend0911@hotmail.com, wchang@ee.ccu.edu.tw

**Abstract**—This poster presents an application of the support vector machine (SVM) classification technique to identify the power system fault event and the fault location. The proposed new feature selection can reduce the SVM training time. Also, this feature selection distinguishes the characteristics of each fault event. Thus, it improves the SVM classification accuracy. Finally, an actual 34-bus transmission system is simulated by using EMTP/ATP to produces data of fault events for testing and validating the proposed method.

## I. KEY EQUATIONS

SVM problem can be summarized by the following equations:

$$\begin{cases} \min_{w,b} & \frac{1}{2} w^T w \\ \text{subject to} & y_i(w^T x_i + b) \geq +1 \end{cases} \quad (1)$$

This optimization problem can be expressed by (2) and is then solved.

$$\begin{cases} \max & L_D = \sum_{i=1} \alpha_i - \frac{1}{2} \sum_{ij} \alpha_i \alpha_j y_i y_j x_i^T x_j \\ \text{subject to} & \sum_i \alpha_i y_i = 0, \alpha_i \geq 0 \forall i \end{cases} \quad (2)$$

The hyper-plane of decision is dependent on  $w$  and  $b$ , and it can be expressed by

$$f(x) = \sum_i \alpha_i y_i x_i^T x + b \quad (3)$$

In the case of having non-linear separable data set, the kernel function  $\phi$  is used to map the input data onto a higher dimensional space. Then, the decision function can be rewritten as

$$f(x) = \sum_i \alpha_i y_i \phi(x, x_i) + b \quad (4)$$

The SVM-based algorithm is proposed for identifying the fault location based on the changing rate of apparent power,  $\Delta S$ . It is associated with RMS voltage and current. The  $\Delta S$  is defined as follows.

$$\Delta S = (S_{di} - S_i) / S_b, \quad i = a, b, c \quad (5)$$

## II. KEY FIGURES

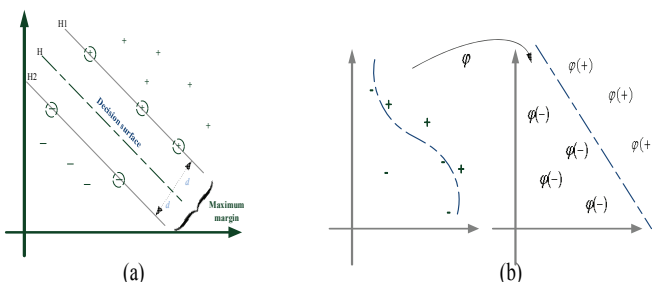


Fig. 1. (a) SVM concept, (b) mapping input data onto feature space.

In the study, an actual 34-bus transmission system is used for testing the proposed method, as shown in Fig. 2.

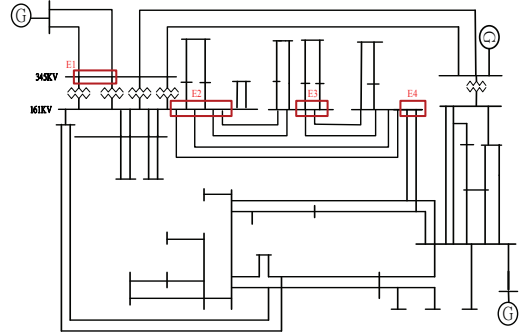


Fig. 2. Actual 34-bus test system.

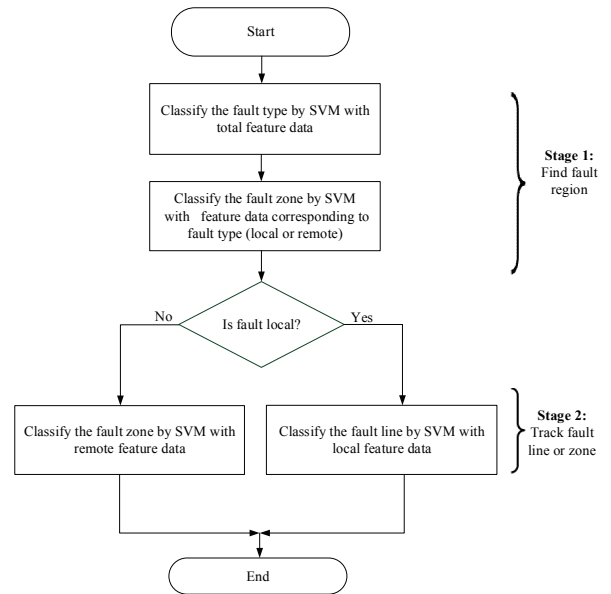


Fig. 3. Flowchart of the proposed method.

## III. KEY RESULTS

The proposed algorithm has been implemented with a LabVIEW-based platform to detect different power system faults. Figure 4 depicts the user interface to show the detection results when a fault occurs in the 34-bus system.

	FEATURE VALUE	ZONE	EVENT	OPEN CIRCUIT
E1	E1-1			
	-0.524789	0.025744	-0.092356	A B C
	E1-2			
	17.1478	0.739674	16.9609	A B C
	FEATURE VALUE	ZONE	EVENT	OPEN CIRCUIT
E2	E2-1			
	0.0035295	-0.074461	-0.018847	A B C
	E2-2			
	0.0040486	-0.075092	-0.019065	A B C

Fig. 4. Example test results (a double-line fault occurred at line E1-2).

# Distributed Electric Vehicles Cooperative Charge Control with Wind Power

Chengcheng Shao and Xifan Wang

Department of Electrical Engineering, Xi'an Jiaotong University

**Abstract**—Load dispatch such as electric vehicles (EVs) is considered as a promising approach to promote the integration of wind power. In this paper, a distributed framework is proposed to coordinate a large number of EVs with wind power based on stochastic dual programming theory. Lagrangian Relaxation (LR) and Auxiliary Problem principle are adopted in the problem decomposition. Compared with existing distributed methods, the proposed method gains an advantage in minimizing generation cost and is proper for masses of EVs. In addition, it can depose of non-convex problems with coupling constraints and it is with larger applications. The method is verified feasible and valid by the case study on IEEE-RTS.

## I. KEY EQUATIONS

### A. Model of a Single EV

$$0 \leq pch_{ei,t} \leq pch_{ei,max} u_{ei,t} \quad (1)$$

$$0 \leq disp_{ei,t} \leq disp_{ei,max} u_{ei,t} \quad (2)$$

$$E_{ei,min} \leq E_{ei,t} \leq E_{ei,max} \quad (3)$$

$$E_{ei,t} = E_{ei,t-1} + pch_{ei,t} \eta_{ei,c} \Delta t - disp_{ei,t} \eta_{ei,dc} \Delta t - Econs_{ei,t} \quad (4)$$

$$rpch_{ei,t} = pch_{ei,t} - disp_{ei,t} \quad (5)$$

### B. Model of Wind Power

Stochastic wind power is described by a multi-scenario model.

$$RW_{wi,t,s} \leq W_{wi,t,s}, \quad (6)$$

### C. Charge Control Model

$$\min F = \sum_{t=1}^T \sum_{gi} [s_{gi} u_{gi,t} (1 - u_{gi,t-1}) + \sum_s f_{gi}(p_{gi,t,s}) prob_s], \quad (7)$$

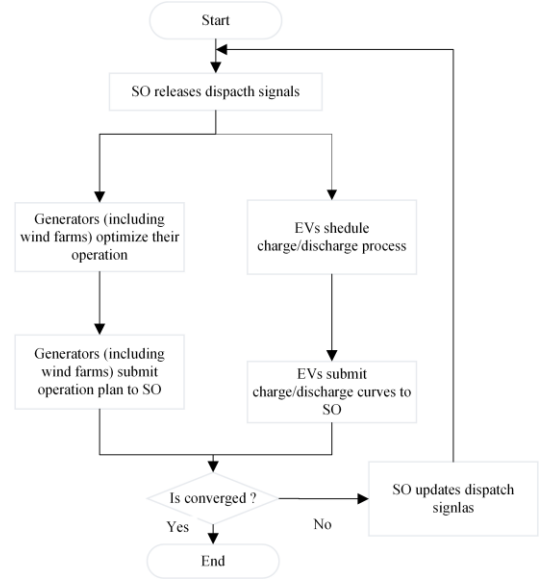
$$P_{gi,t,s_1} - P_{gi,t,s_2} \leq \Delta_{gi}, \quad (8)$$

$$\sum_{gi} P_{gi,t,s} + \sum_{wi} RW_{wi,t,s} - P_{L,t} - \sum_{ei} rpch_{ei,t} = 0 \quad (9)$$

$$\sum_{gi} pdr_{gi,t,s} - DR_t \geq 0 \quad (10)$$

$$\sum_{gi} pur_{gi,t,s} - UR_t \geq 0 \quad (11)$$

## II. ALGORITHMS



## III. CASE STUDY

TABLE I. GENERATION COST OF DIFFERNET METHODS (\$)

Modes	Cost	Centralized	Existing	Proposed
Pure Charge Control	Fuel	615647.26	616 625.53	616 373.55
	Start/Shut	1 940	1 940	2 060
	Sum	617 587.26	618 565.53	618 393.55
V2G Control	Fuel	609 215.04	612 530.043	609 721.62
	Start/Shut	1 700	1 900	1 860
	Sum	610 915.04	614 430.043	611 581.62

TABLE II. PRODUCTION INDEXES IN DIFFERENT CASES (\$)

Indexes	No-control	Charge	V2G
Fuel cost(\$)	631 790.10	616 09 9.23	611 480.32
Startup/Shutdown cost(\$)	1 900	1 860	1860
Total cost(\$)	633 690.10	617 959.23	613 340.32
Deserted wind (MWh)	114.58	27.30	49.55
Thermal unit cost(\$/MWh)	10.99	10.82	10.63

# Reliability Modeling and Evaluation of VSC-HVDC Transmission Systems

Jingli Guo, Xiuli Wang, Zhaohong Bie, Yushen Hou

Department of Electrical Engineering

Xi'an Jiaotong University

Xi'an, China

guojingli.xjtu@gmail.com

**Abstract**—This paper presents an improved reliability modeling and an analytical reliability evaluation of Voltage Source Converter based High Voltage Direct Current (VSC-HVDC) transmission systems. First, two VSC topologies, namely Modular Multilevel Converter (MMC) and Cascaded Two-level (CTL), are thoroughly studied. Then detailed reliability models of converters in different topologies are established based on the k-out-of-n model. Furthermore, a reliability assessment procedure for transmission systems is developed. The presented method has been employed into an assumed VSC-HVDC bipolar transmission system. Converters in two topologies as well as corresponding transmission systems are compared with respect to reliability. Moreover, impacts of redundant modules on converter reliability and system reliability are examined. The numerical results show that the CTL converter is more reliable but need more IGBT cells than the MMC do. When the redundancy rate increases, the reliability of a MMC-based system improves more significantly than that of a CTL-based one.

**Index Terms**—Cascaded two-level Converter; k-out-of-n model; Modular Multilevel Converter; reliability assessment; VSC-HVDC

## I. KEY FIGURES

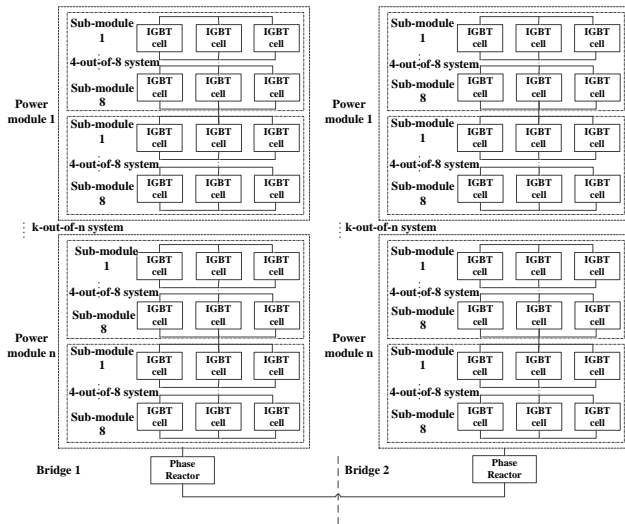


Figure 1. Reliability diagrams of the CTL converter

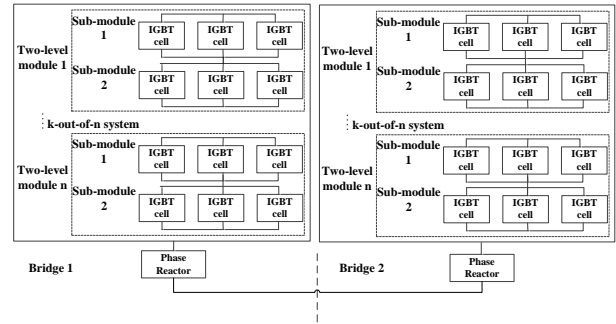


Figure 2. Reliability diagrams of the MMC

## II. KEY RESULTS

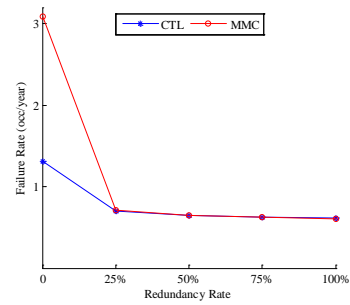


Figure 3. Converter failure rates at various redundancy rates

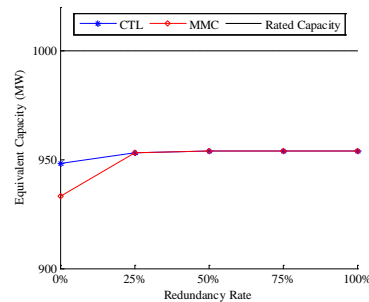


Figure 4. System equivalent capacity when redundancy rate changes



# Measurement System for Power Quality Analysis of Energy-Saving Lamps

Yi-Ying Chen (Advisor: Gary W. Chang)

Department of Electrical Engineering, National Chung Cheng University, Chia-Yi, Taiwan  
e-mails: minijo7978@gmail.com, wchang@ee.ccu.edu.tw

**Abstract**—With the wide-spread use of energy-saving lighting devices in recent years, the associated power quality (PQ) disturbances have attracted much attention. This poster presents the implementation of a system for power quality analysis of energy-saving lamps. The measuring system includes a hardware circuit design, the LabVIEW-based PQ analysis algorithm and graphical user interface, and database implementation for PQ data management. In the PQ analysis algorithm, a frequency-domain method is firstly adopted for determining the system fundamental frequency. Then the fast Fourier transform (FFT) is used to analyze the measured electric waveforms. The developed measuring system has been tested and shows its effectiveness in understanding the PQ disturbances associated with modern energy-saving lamps.

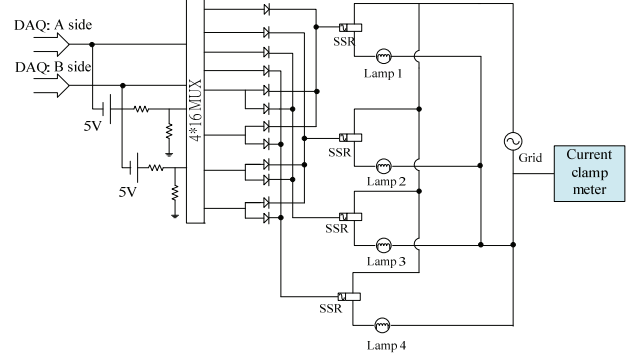


Fig. 2. Measuring circuit for lamps

## I. KEY EQUATIONS

In the system, the measured lamp voltage and current can be retrieved from the data acquisition (DAQ) card. Six electric quantities and power quality indices including rms voltage, rms current, total harmonic voltage distortion, total harmonic current distortion, fundamental and harmonic active power, and total power factor, as listed in (1)-(4).

$$V_{rms} = \sqrt{\sum_{h=1}^{\infty} V_h^2} \quad \text{and} \quad I_{rms} = \sqrt{\sum_{h=1}^{\infty} I_h^2} \quad (1)$$

$$THD_V = \sqrt{\sum_{h=2}^{\infty} V_h^2} / V_1 \quad \text{and} \quad THD_I = \sqrt{\sum_{h=2}^{\infty} I_h^2} / I_1 \quad (2)$$

$$P = \sum_{h=1}^{\infty} V_h I_h \cos(\theta_h - \delta_h) = \sum_{h=1}^{\infty} P_h = P_1 + P_H \quad (3)$$

$$P_F = \frac{[1 + (P_H / P)] P_1}{V_1 I_1 \sqrt{1 + (THD_V)^2} \sqrt{1 + (THD_I)^2}} \quad (4)$$

## II. KEY FIGURES



Fig. 1. Measuring System for Lamps

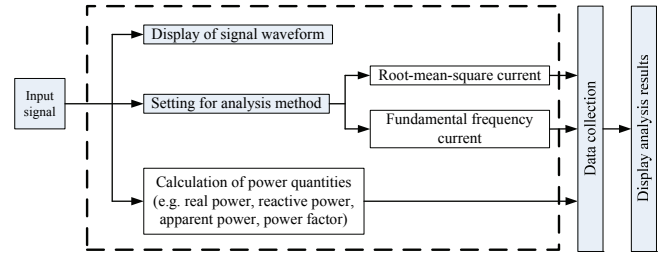


Fig. 3. Functional blocks of measurement and PQ analysis

## III. KEY RESULTS

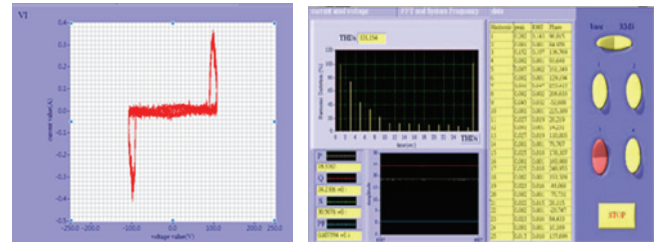


Fig. 4. Graphical user's interface to show measurement results

TABLE I: MEASUREMENT RESULTS OF DIFFERENT LAMPS

brand	shape	wattage (W)	Power Factor(%)	Current (A)	Voltage (V)	RMS current measurement data					THDi (%)	
						Sument (A)	Voltage (V)	R(W)	Q(var)	S(VA)		PF(%)
A	Spherical	20	62	0.1667	120	0.260	107.630	18.450	21.128	28.050	65.5	92
A	3U	20	57	0.1667	120	0.275	108.250	18.100	23.295	29.500	59	104
A	Spiral	20	58	0.1667	120	0.270	107.500	16.400	23.309	28.500	58	105
A	Bright spiral	20	58	0.1667	120	0.268	108.450	16.010	24.120	28.950	59.95	98
B	Spherical	17	50	0.1478	115	0.225	106.000	14.500	18.506	23.510	62.5	106
C	Spherical	17	60	0.1417	120	0.215	106.000	16.500	15.297	22.500	73.5	91
D	Spherical	17	50	0.1417	120	0.190	107.000	12.510	14.234	18.950	61	127
A	Spiral	23	61	0.1045	220	0.165	107.700	13.020	12.138	17.800	73	104
C	Spiral	23	60	0.1917	120	0.290	107.500	20.000	24.526	31.500	64	82
E	Spiral	23	57	0.1917	120	0.270	106.500	17.010	22.867	28.500	61.5	97
F	Spiral	23	55	0.1917	120	0.255	107.000	15.980	23.114	28.100	60	99
G	Spiral	23	60	0.1917	120	0.235	106.500	16.010	19.848	25.500	67	91
H	Spiral	23	>60	0.1917	120	0.255	106.000	18.480	19.949	27.200	68	93
A	Incandescence	100	100	0.8333	120	0.820	105.500	87.000	0.000	87.000	99.6	1.7
B	Incandescence	25	100	0.2174	115	0.210	106.000	22.500	0.000	22.500	99	4
B	Fluorescent lamp	13	90	0.1130	115	0.200	108.000	9.510	19.282	21.500	48	12

# Detailed Modeling of a Photovoltaic System for Distribution Networks

Farhan Mahmood<sup>1</sup>, Luigi Vanfretti<sup>1,2</sup>, and Hossein Hooshyar<sup>1</sup>

<sup>1</sup>Electric Power Systems Department, KTH Royal Institute of Technology, Stockholm, Sweden

<sup>2</sup>Research & Development Division, Statnett SF, Oslo, Norway

farhanm@ee.kth.se, luigiv@kth.se, luigi.vanfretti@statnett.no, hossein.hooshyar@ee.kth.se

**Abstract--** This article presents a detailed three-phase grid connected PV model which includes important control systems required for EMT-type simulation. A one diode model for the PV array is used to simulate environmental constraints such as solar irradiation. A detailed control system including dc voltage control, inner current control, Maximum Power Point Tracking and PWM control are implemented in order to simulate the model during steady state and dynamic conditions. The main objective of this type of control is that both active and reactive power can be independently controlled. The (MPPT) control is applied in order to ensure maximum output power. The PV model is merged with a simple distribution network including static and dynamic loads to investigate the PV's interaction with the AC grid. Several simulation scenarios are presented in order to validate the performance of the model.

$$L \frac{di_d}{dt} = -R i_d + L \omega i_q + \frac{V_{dc}}{2} m_d - v_{sd} \quad (6)$$

$$L \frac{di_q}{dt} = -R i_q + L \omega i_d + \frac{V_{dc}}{2} m_q - v_{sq} \quad (7)$$

$$m_d = \frac{2}{V_{dc}} (u_d - L \omega i_q + v_{sd}) \quad (8)$$

$$m_q = \frac{2}{V_{dc}} (u_q - L \omega i_d + v_{sq}) \quad (9)$$

## III. KEY SIMULATION RESULTS

### I. KEY FIGURES

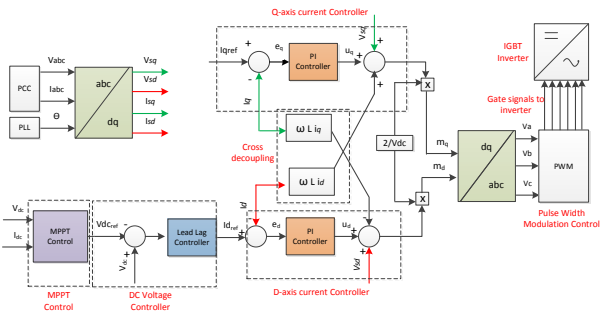


Fig. 1. Control Systems

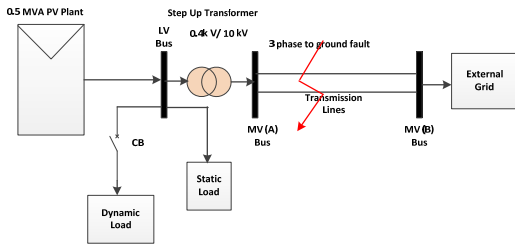


Fig. 2. Simulation Setup

### II. KEY EQUATIONS

$$I = I_{ph} - I_D = I_{ph} - I_0 \exp\left(\frac{V + I R_s}{V_t}\right) \quad (1)$$

$$I_{ph} = I_{sc} \quad (2)$$

$$I_0 = \frac{I_{sc}}{\exp\left(\frac{V_{oc}}{V_t}\right)} \quad (3)$$

$$P = \frac{3}{2} v_{sd} i_d \quad (4) \quad Q = -\frac{3}{2} v_{sd} i_q \quad (5)$$

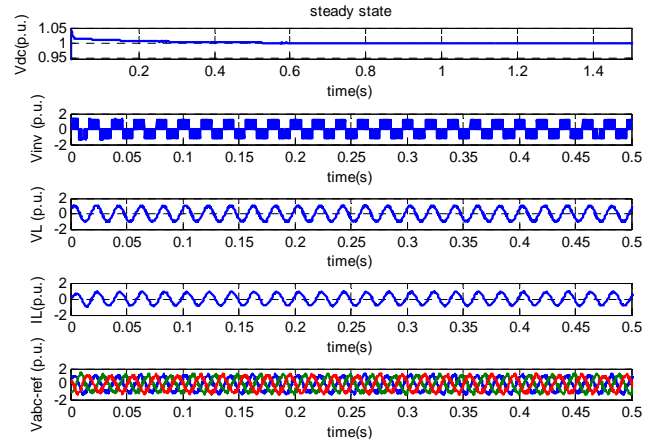


Fig. 3. Steady State operation of PV Model

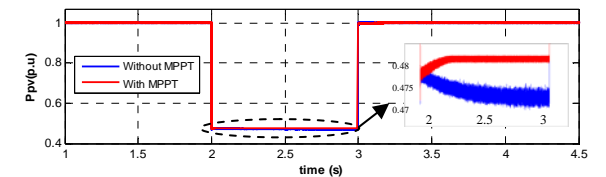
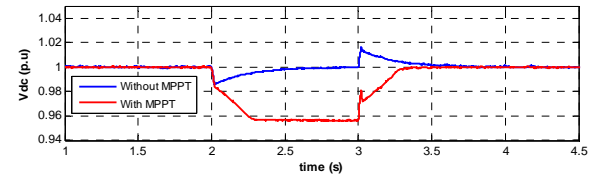
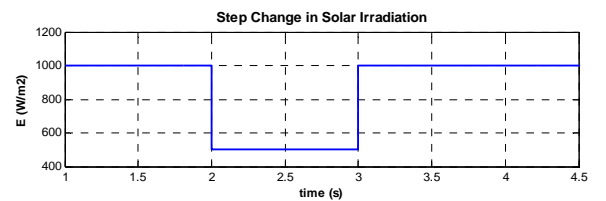


Fig. 4. Step Change in Solar Irradiation



# Hybrid Power Flow Controller Modeling and Operating Constraints for Power Flow Studies

Behnam Tamimi, *Student Member, IEEE*, and Claudio Cañizares, *Fellow, IEEE*

Electrical & Computer Engineering Department  
University of Waterloo  
Waterloo, ON, Canada

**Abstract**—Steady state models of the Hybrid Power Flow Controller (HPFC) for power flow studies are discussed in this presentation, considering multiple control modes. A strategy for control limit handling in power flow calculations is proposed while considering a discrete shunt capacitor bank within the structure of the device. A cost-benefit analysis is used to determine the optimal ratings of the device. The proposed model is tested using a benchmark test system and several loadability studies, examining the device’s performance and the effectiveness of the proposed limit handling strategy under stressed conditions.

## I. HPFC MODELING

The HPFC, a cost effective FACTS controller, is introduced in [1]. This device yields operating characteristics similar to those of a unified power flow controller (UPFC), but requires a lower capital investment. Compared to the UPFC, the aforementioned savings stem from a few structural differences between the two devices, including using passive elements for supplying the bulk of the required reactive power as well as half-sized converters. Benefits from an HPFC installation are constrained by its limits and operating constraints; therefore, the impact of the device internal limits on its performance must be considered during design and planning stages.

The transitions between the four control modes are shown in Fig. 1. The device by default starts operating in the PVV mode; if the device reaches its limits on at least one of the main variables, the controller switches to PQQ mode to resolve the limit violation. The HPFC continues operating in the PQQ mode until the limit violations cannot be resolved by the modification of the active and reactive powers set-points, at which point the device switches to V mode, which is a voltage regulation mode. Voltage control is not always possible because of the limited shunt device capability, which forces the device to switch to Z mode and behave as a fixed shunt impedance.

## II. MAIN RESULTS

A benchmark two-area test system is used for the studies. The areas are connected by a tie-line with two corridors, which provides for a potential application for the HPFC.

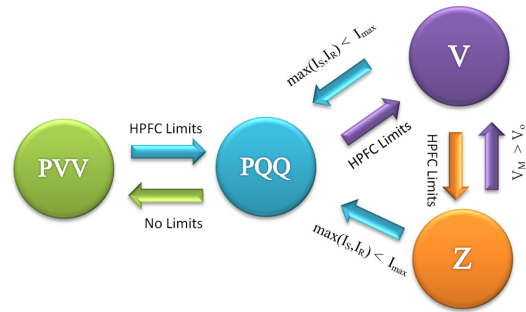


Figure 1. Transitions between the four HPFC control modes.

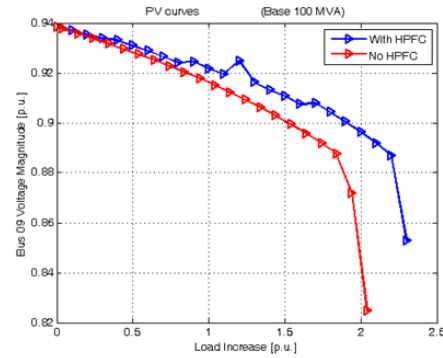


Figure 2. PV curves at the sink bus with and without the HPFC.

The HPFC is assumed to be installed on one of the corridors and the system transfer capability is examined using loadability studies. The analysis is performed assuming two buses across the tie-line as power sink and source. Thus, the power transfer between these two nodes is increased until the system collapses and the power flow cannot be solved. The voltage profile at the sink bus is depicted in Fig. 2, with and without the HPFC. Observe that the HPFC improves the loadability and voltage profile at the main power sink.

## REFERENCES

- [1] J. Z. Bebic, P. W. Lehn, M. R. Iravani, “The hybrid power flow controller - a new concept for flexible ac transmission,” in *Proc. IEEE PES General Meeting*, pp. 1-7, October 2006.

# Real-time energy management strategies for microgrids

Xiong Wu, Xiuli Wang, Zhaohong Bie  
 School of Electrical Engineering  
 Xi'an Jiaotong University  
 Xi'an, China  
 Wuxiong432@126.com

Pingliang Zeng  
 China Electric Power Research Institute  
 Beijing, China  
 plzeng@hotmail.com

**Abstract**—This paper proposes two real-time energy management strategies from both the perspectives of economy and stability, which could be categorized as optimization method and heuristic method. The optimization method constructs an optimization model, aiming at minimizing the total operational cost in least violation of the schedule, to yield a real-time power dispatch scheme for distributed generators (DGs). The heuristic method dispatches the deviated power from schedule based on economy and feasibility. Both methods are applicable to microgrids in different scenarios. Case studies were conducted to verify the effectiveness of the proposed strategies. The results indicate that the optimization method is efficient to handle complicated situation considering various constraints while the heuristic method can provides a good real-time scheme with low time consumption.

## I. KEY EQUATIONS

### A. Optimization Method

$$\min \sum_{i \in G} f_{dg,i}(x_t) + \sum_{i \in B} f_{es,i}(x_t) + f_{grid}(x_t) + f_p(x_t) \quad (1)$$

where:

$$f_{dg,i}(x_t) = C_i(P_{dg,i,t}) + \rho_{mai,i} \cdot P_{dg,i,t} \quad (2)$$

$$f_{es,i}(x_t) = \rho_{es,i} \cdot |P_{es,i,t}| \quad (3)$$

$$f_{grid}(x_t) = \rho_{buy,t} \cdot P_{grid+,t} - \rho_{sell,t} \cdot P_{grid-,t} \quad (4)$$

$$f_p(x_t) = \rho_p \cdot \sum_{i \in G} |P_{dg,i,t} - P_{dg,i,t}^*| + \quad (5)$$

$$\rho_p \cdot \sum_{i \in B} |P_{es,i,t} - P_{es,i,t}^*|$$

### B. Heuristic Method

$$\Delta P_t = (P_{ld,t} - \sum_{i \in R} P_{rg,i,t}) - (P_{ld,t}^* - \sum_{i \in R} P_{rg,i,t}^*) \quad (6)$$

$$P_{i,t} = P_{i,t}^* + K_e \cdot \min(\bar{P}_i - P_{i,t}^*, \Delta P_t) + K_p \cdot \frac{\bar{P}_i}{\sum_i \bar{P}_i} \Delta P_t \quad (7)$$

$$K_e + K_p = 1$$

$$\Delta P_t = \Delta P_t - \min(\bar{P}_i - P_{i,t}^*, \Delta P_t) \quad (8)$$

## II. KEY FIGURES

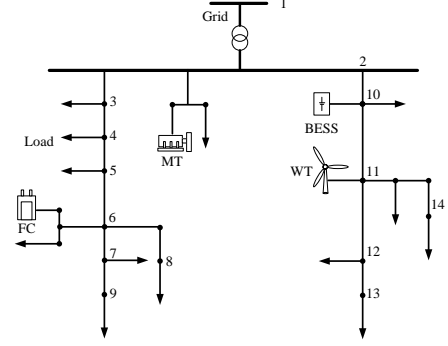


Figure. 1 Configuration of the microgrid system

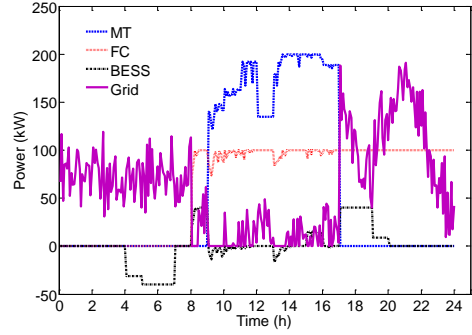


Figure. 2 Real-time operation using optimization method

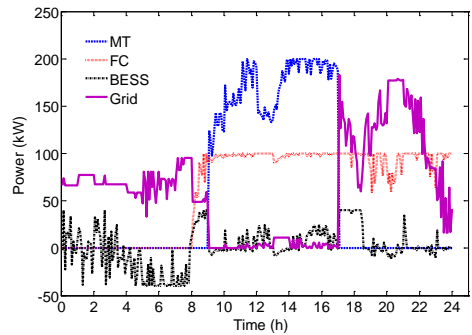


Figure. 3 Real-time operation using heuristic method when  $K_e=0.5$ ,  $K_p=0.5$

# Aggregated Demand Response From Smart Loads

D. Chakravorty, *Student Member, IEEE* and B. Chaudhuri, *Senior Member, IEEE*, S.Y.R Hui, *Senior Fellow, IEEE*

**Abstract**—This work focuses on extracting demand response from non-critical loads (e.g. heaters etc.) while tightly regulating the voltage across the critical loads. A controlled voltage source is used in series with non-critical loads to turn those into ‘smart loads’. The voltage source works in input voltage control mode allowing the voltage across the non-critical load and hence their active power consumption to vary and thus contribute to demand response. The objective of this study is to demonstrate the aggregated impact of several (potentially millions) such smart loads on stabilization of the grid frequency.

**Keywords**—demand side response; smart load; distributed frequency control

## I. BACKGROUND

Balancing the supply and demand on an instantaneous basis is a major challenge with high penetration of intermittent renewable (e.g. photovoltaic, wind etc.) energy resources. A paradigm shift from the traditional approach of generation following demand is required where the demand would follow the available generation. Demand response could be achieved in several ways and is exercised without properly considering the requirement of tight voltage regulation for the sensitive or critical loads.

## II. CONCEPT OF SMART LOAD

The concept of smart load was proposed in [1] as an effective means of achieving demand response and voltage regulation in a unified framework. A smart load comprises a controlled voltage source in series with the non-critical load as shown in Fig. 1.

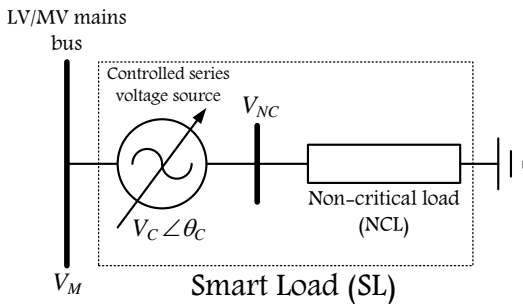


Fig. 1: Smart Load configuration

The injected series voltage ( $V_C \angle \theta_C$ ) is controlled to tightly regulate the LV/MV mains voltage ( $V_M$ ) while allowing the voltage across the non-critical load ( $V_{NC}$ ) and consequently its active power consumption to vary. The non-critical loads are assumed to be predominantly constant impedance type which is reasonably true for water heaters. Thus voltage regulation for

the critical loads (connected elsewhere to the mains) is ensured while demand response from non-critical loads is achieved in a unified framework.

## III. SCOPE OF STUDY

The smart loads would be deployed at the LV/MV distribution level. The collective action of these smart loads would help achieve the supply-demand balance at the bulk power transmission network level and thus stabilize the grid frequency. The objective here is to investigate appropriate control of smart loads and perform simulation studies to demonstrate the effectiveness of the smart loads at the system level. The study was conducted at the bulk power transmission network level by aggregating the effect of the smart loads within the LV/MV networks as shown in Fig. 2.

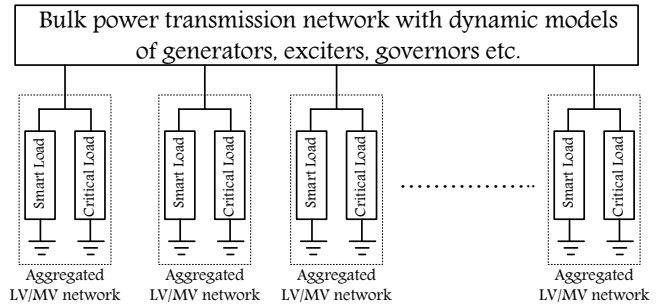


Fig. 2: Aggregated smart load representation at bulk power transmission level

The standard dynamic models for generators, exciters and governors were used while the aggregated loads were split into a parallel combination of smart loads and critical loads as shown in Fig. 2.

The smart loads can be configured to control only the magnitude of the series injected voltage while keeping the phase angle fixed at  $90^\circ$  and thus exchanging only reactive power. To introduce more flexibility, the phase angle should be allowed to change at the expense of some finite energy storage requirement. Limitations of the former option and effectiveness and storage requirement of the latter version would be demonstrated through this study.

## REFERENCES

- [1] S. Tan, C. K. Lee, and S. Y. R. Hui, “General Steady-State Analysis and Control Principle of Electric Springs With Active and Reactive Power Compensations,” *IEEE Transactions on Power Electronics*, vol. 28, no. 8, pp. 3958–3969, 2013

# Distributed Voltage and Frequency Control Using Electric Springs

Z. Akhtar, *Student Member, IEEE*, B. Chaudhuri, *Senior Member, IEEE*, and S.Y.R. Hui, *Fellow, IEEE*

Department of Electrical and Electronics Engineering, Imperial College London

**Abstract**—An integrated approach to voltage and frequency control in distribution networks is presented in this poster. This is achieved through distributed voltage compensation and demand response in an autonomous fashion without any need for communication. The idea is based on dividing the loads into critical loads requiring constant voltage and non-critical loads which can tolerate a degree of voltage variations. Smart loads are created by adding a controlled voltage source (known as electric spring) in series with the non-critical loads. At times of generation shortfall or network constraint, the series voltage source can reduce the voltage of the non-critical loads which reduces their power consumption while keeping the critical load voltages constant. The objective of this study is to analyze the role of distributed smart loads on local voltage control while contributing to demand response at the same time. The effectiveness is demonstrated through case studies on an IEEE standard feeder network.

**Index Terms**—electric spring, demand side response; distributed voltage control; distributed frequency control; smart load

## I. ELECTRIC SPRING

The concept of ‘Electric Spring (ES)’ has been proposed as an effective means of distributed voltage and frequency control [1]. The basic idea is to tightly regulate the voltage  $V_C$  across the critical load (load which is sensitive to voltage change) while allowing the voltage  $V_{NC}$  across the non-critical load (load which is not sensitive to voltage change) to vary as shown in Fig. 1.

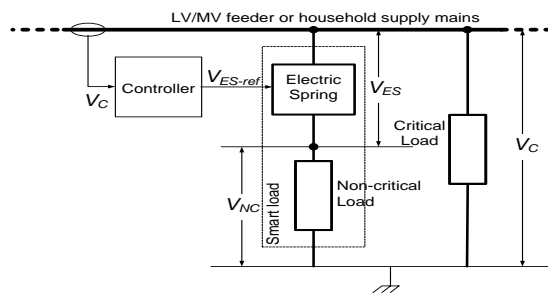


Figure 1: Electric Spring set-up for a Smart Load

A controllable voltage source (electric spring) is connected in series with the non-critical load. The voltage injected by the ES  $V_{ES}$  is controlled to regulate the voltage  $V_C$  across the critical load.

Depending on the injected voltage magnitude and phase angle, the smart load is capable of providing inductive, capacitive, positive real power or negative real power compensation. Reducing the non-critical load voltage reduces its power consumption as it is assumed to be a constant impedance load (e.g. water heaters).

The ES will only provide reactive power compensation if the injected voltage is forced to be in quadrature with the current. However, better controllability is achieved with a variable phase angle but it will result in a battery storage requirement as ES will provide both active and reactive compensation.

## II. OBJECTIVES

In this study, distributed voltage control and frequency regulation using demand response is investigated in a MV/LV distribution networks. The effectiveness of this approach is analyzed by considering different degrees of distributed deployment of electric spring at the LV network (household appliances e.g. fridge, washing machine) and MV network (large commercial complexes). The total power ratings of these devices are calculated and are compared against shunt voltage compensation devices like a D-STATCOM.

For demand response a combination of active and reactive compensation is more effective. The energy storage requirement in such cases is evaluated. The study involves modeling, control design and simulation of MV/LV distribution networks with different load types, load compositions and varying degrees of distributed deployment of ES in order to ascertain the potential and identify the required ratings of the compensators and associated energy storage.

## III. TEST CASE

We are using IEEE 13 distribution test feeder as a test case. The loads on the MV side of the test feeder are divided into critical and non-critical loads. LV side of the network is extended. Effects of distributed ESs on voltage and frequency regulation are analyzed under different operating conditions.

## REFERENCES

- [1] H. Shu Yuen, L. Chi Kwan, and F. F. Wu, "Electric Springs - A New Smart Grid Technology," *Smart Grid, IEEE Transactions on*, vol. 3, pp. 1552-1561, 2012.

# Differential Partial Discharge Extraction Technique for Online Power Transformer Insulation Assessment

Junhyuck Seo, *Student Member, IEEE*, Hui Ma, *Member, IEEE*, Tapan K. Saha, *Senior Member, IEEE*

The University of Queensland  
Brisbane, Australia

j.seo@uqconnect.edu.au, huima@itee.uq.edu.au, saha@itee.uq.edu.au

**Abstract**—Partial discharge (PD) measurement by using high frequency current transducer (HFCT) provides a means for online monitoring of power transformers. However, extensive interferences and noise can cause difficulties in PD signals interpretation and consequently lead to ambiguity in transformer insulation condition assessment. Therefore, necessary signal processing techniques need to be adopted for PD signals extraction. Wavelet transform is one of such techniques. However, wavelet transform has some limitations when applied to online PD measurement of power transformer. This paper proposes a differential PD signal extraction technique for online PD measurement on transformers. The performance of the proposed technique will be verified through case studies on data obtained from PD measurements on experimental PD models and in-service transformers.

**Index Terms**—Differential, high frequency current transducer (HFCT), Partial Discharge (PD), power transformer, and wavelet transform (WT).

## I. KEY FEATURES

Differentiation and thresholding:

$$y'(n) = \frac{y(n+1) - y(n)}{t(n+1) - t(n)}$$

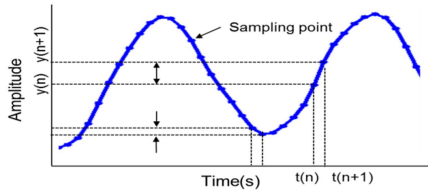


Figure 1. Signal changing rate determination

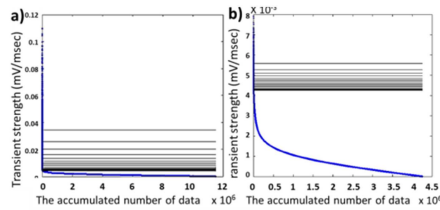


Figure 2. Thresholds based on transient strength (changing rate) of signals

$$\text{Thresholding ratio} \geq \frac{(\sum_{i=\text{quantile}(k2,N)}^{p=\text{quantile}(k3,N)} |x'_i|) / (n(p) - n(i) + 1)}{(\sum_{i=\text{quantile}(k1,N)}^{p=\text{quantile}(k2,N)} |x'_i|) / (n(p) - n(i) + 1)} \quad (2)$$

## II. KEY RESULTS

Single PD test model (Corona):

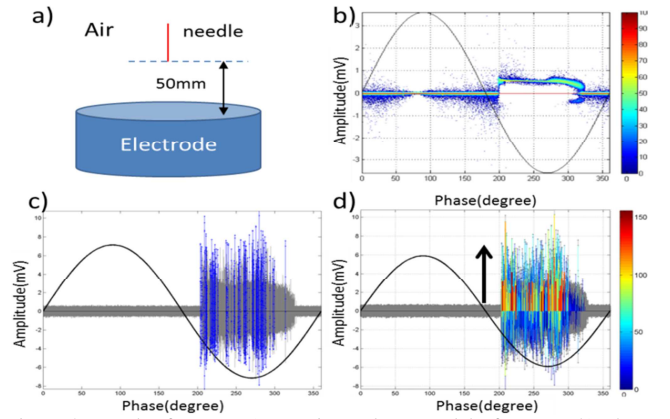


Figure 3. Result of corona a) experimental PD model of corona; b) Phase resolved PD distribution acquired by capacitive PD measurement; c) Extracted PD signals by wavelet transform from inductive (HFCT) PD measurement; d) Extracted PD signals by the proposed differential technique from inductive (HFCT) PD measurement

(1) Multiple PD test model:

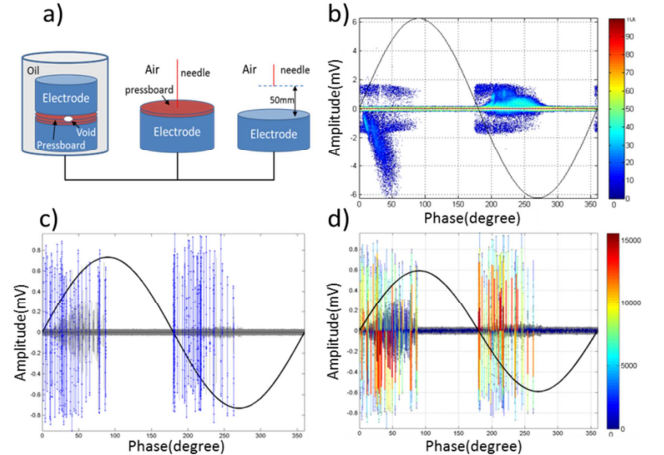


Figure 4. Result of multiple PD sources a) experimental PD model of multiple PD sources; b) Phase resolved PD distribution acquired by capacitive PD measurement; c) Extracted PD signals by wavelet transform from inductive (HFCT) PD measurement; d) Extracted PD signals by the proposed differential technique from inductive (HFCT) PD measurement

# A Equal Incremental Rate Continuous Time-varying Optimal Power Distribution Method for the Power System Containing Microgrids

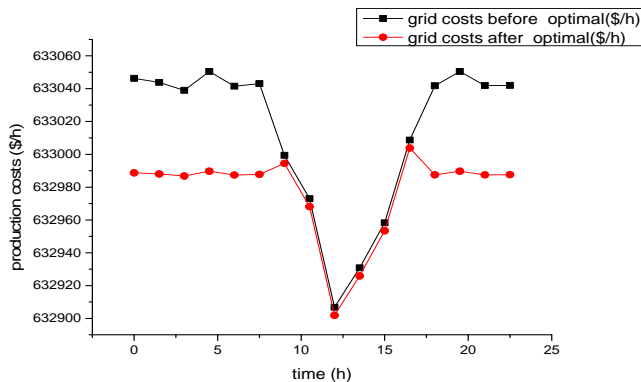
Zhang Xiaobo, Zhang Baohui, *Senior Member, IEEE*

**Abstract**—Many microgrids in the using process need to be accessed in external grid. As a part of the union power system, how to dispatching the devices in the microgrid and the external grid scheduling so as to make the entire system running more economically, saving operating costs and fuel costs, is an area worthy of study. The issue of dispatching the union power system of microgrids and external grid involved load forecasting, the basic principles of economical dispatching, the correction of transmission loss, security constraints and so on. Based on these analysis, the economical dispatching and optimal power flow calculation method based on equal incremental rate non-renewable fuels consumption theory was introduced.

Optimal power flow(OPF) is often about the issue of the optimal distribution of grid power at a certain moment, which cannot show the randomness of new energy, a continuous time-varying optimal power distribution method was advised for the power system containing microgrids. It was used in a simulation calculating example to show the advance of this method.

**Index Terms**—Equal incremental rate, microgrids, smart grids, power control, power generation dispatch, continuous time-varying optimal power distribution.

## I. RESULT OF OPTIMAL CALCULATING EXAMPLE



This work was supported in part by the Special Fund for Major State National Basic Research Program of China (973 Program) (2009CB219700).

Zhang Xiaobo is with the School of Electrical Engineering, Xi'an Jiaotong University Xi'an, 710049 China, (e-mail: dna19831983@163.com).

Zhang Baohui is with the School of Electrical Engineering, Xi'an Jiaotong University Xi'an, 710049 China, (e-mail: bhzhang@mail.xjtu.edu.cn).

Fig. 1. Total grid costs before/after optimal

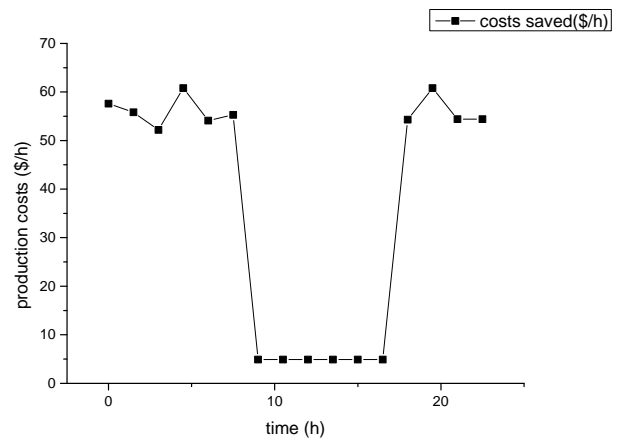


Fig. 2. Total production costs saved

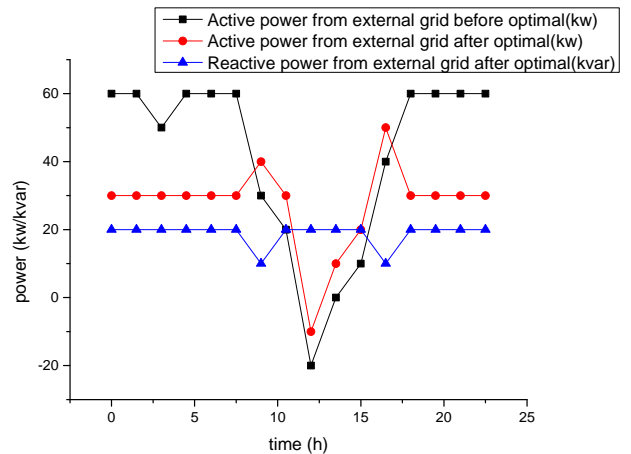


Fig. 3. Power injected from external grid before/after optimal

The using of continuous time-varying optimal power distribution method for the power system containing microgrids, combined with the existed power prediction algorithm of wind power and PV is scientific and reasonable. Which taking the randomness of the wind power, PV and other new energy into account, and not only improve the economics of grid operation, but also improve the security of grid at some aspects.



# Equal Incremental Rate Economic Dispatching and Optimal Power Flow for the Union System of Microgrid and External Grid

Zhang Xiaobo, Zhang Baohui, *Senior Member, IEEE*

**Abstract**—With the extensive use of renewable energy, the microgrid as an access and management structure of renewable energy has also been widely used. Many microgrids in the using process need to be accessed in external grid. As a part of the union power system, how to dispatching the devices in the microgrid and the external grid scheduling so as to make the entire system running more economically, saving operating costs and fuel costs, is an area worthy of study. The issue of dispatching the union power system of microgrids and external grid involved load forecasting, the basic principles of economical dispatching, the correction of transmission loss, security constraints and so on. Based on these analysis, the economical dispatching and optimal power flow calculation method based on equal incremental rate non-renewable fuels consumption theory was introduced here.

**Index Terms**—Equal incremental rate, load forecast, microgrids, smart grids, power control, power generation dispatch.

## I. INTRODUCTION

The structure of microgrids also changed from a single point of common coupling(PCC) accessed to multimicrogrids and internal ring accessed and other complex structure showing in fig.1.

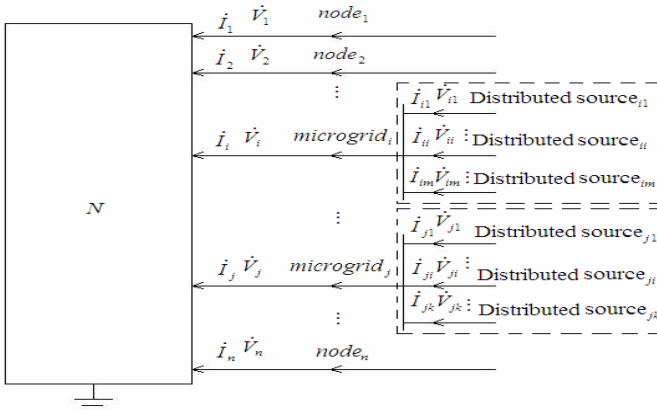


Fig. 1. the union system consisting of microgrids and external grid.

## II. KEY EQUATIONS

Objective function (total fuel consumption):

$$B = B_1(P_1) + B_2(P_2) + \dots + B_m(P_m) \quad (1)$$

The constraints (load power balance):

$$P_1 + P_2 + \dots + P_m - P_D = 0 \quad (2)$$

$$B^* = B_1(P_1) + B_2(P_2) + \dots + B_m(P_m) - \lambda(P_1 + P_2 + \dots + P_m - P_D) \quad (3)$$

$$\lambda_a \left( 1 - \frac{\partial P_{La}}{\partial P_{Ba}} \right) = \lambda_b \left( 1 - \frac{\partial P_{Lb}}{\partial P_{Eb}} \right) \quad (4)$$

$$\begin{pmatrix} \lambda_a \\ \lambda_b \end{pmatrix} = \begin{pmatrix} R_a \\ R_b \end{pmatrix} \lambda_a \quad (5)$$

1) Flywheel conditions:  $a(t)\Delta x(t)$

$$A_{\min} \leq a(t)\Delta x(t) \leq A_{\max} \quad (6)$$

$$-D_{A_{\max}} \leq \frac{d[a(t)\Delta x(t)]}{dt} \leq D_{A_{\max}} \quad (7)$$

2) Supercapacitors conditions:  $b(t)\Delta x(t)$

$$B_{\min} \leq b(t)\Delta x(t) \leq B_{\max} \quad (8)$$

$$-D_{B_{\max}} \leq \frac{d[b(t)\Delta x(t)]}{dt} \leq D_{B_{\max}} \quad (9)$$

3) Battery conditions:  $c(t)\Delta x(t)$

$$C_{\min} \leq c(t)\Delta x(t) \leq C_{\max} \quad (10)$$

$$-D_{C_{\max}} \leq \frac{d[c(t)\Delta x(t)]}{dt} \leq D_{C_{\max}} \quad (11)$$

4) diesel generator and microturbine conditions:  $d(t)\Delta x(t)$

$$0 \leq d(t)\Delta x(t) \leq D_{\max} \quad (12)$$

$$\begin{cases} d(t)\Delta x(t) = D(t), & 0 \leq t \leq t_{start} \\ d(t)\Delta x(t) = D_{\max}(t), & t \geq t_{start} \end{cases} \quad (13)$$

External grid conditions:  $e(t)\Delta x(t)$

$$e(t)\Delta x(t) = k_G E(t), \quad k_G = \begin{cases} 0 \\ 1 \end{cases} \quad (14)$$

5) Wind power conditions:  $f(t)\Delta x(t)$

$$f(t)\Delta x(t) = k_W F(t), \quad k_W = \begin{cases} 0 \\ 1 \end{cases} \quad (15)$$

6) Photovoltaic conditions:  $g(t)\Delta x(t)$

$$g(t)\Delta x(t) = k_P G(t), \quad k_P = \begin{cases} 0 \\ 1 \end{cases} \quad (16)$$

$$C(x) = F(x) + r^T g^2(x) + s^T h^2(x) \quad (17)$$

This work was supported in part by the Special Fund for Major State National Basic Research Program of China (973 Program) (2009CB219700).

Zhang Xiaobo is with the School of Electrical Engineering, Xi'an Jiaotong University Xi'an, 710049 China, (e-mail: dna19831983@163.com).

Zhang Baohui is with the School of Electrical Engineering, Xi'an Jiaotong University Xi'an, 710049 China, (e-mail: bhzhang@mail.xjtu.edu.cn).

# Investigation of Reactive Power Limit Induced Voltage Collapse

Hung-Ming Chou, *Student Member, IEEE*, Garng M. Huang, *Senior Member, IEEE*,  
Karen L. Butler-Purry, *Senior Member, IEEE*

**Abstract**—Voltage instability is caused by the inability of the system to meet reactive power demand. The problem of voltage instability is even more critical for an isolated microgrid, which only has generators with limited reactive power capacities. In this paper, we investigated what happens if all generators in the system hit their reactive power limit. To simplify the analysis, a simple two-bus example was used. Analytical power flow solutions was derived, and the corresponding physical interpretation was discussed. The physical constraints of the generator determined whether the power flow solution is feasible. It was found that when the reactive power limit of the generators is hit, even though there is a power flow solution, due to the physical limitation of the generator, no feasible solution exists. This causes the system to experience voltage collapse.

## I. KEY EQUATIONS

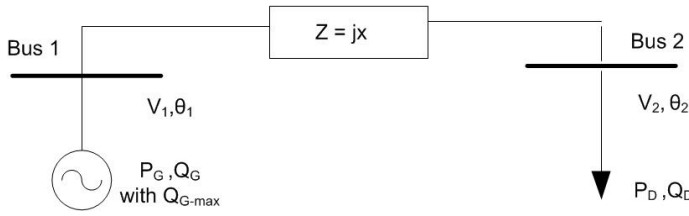


Fig. 1. Two bus example

When the reactive load at Bus 2  $Q_D$  is equal to  $Q_{D-crt}$ , the generator hits its reactive power limit and the generated reactive power  $Q_G$  is equal to  $Q_{G-max}$ .

$$Q_{D-crt} = \frac{-1 + \sqrt{1 - 4\left(\frac{x}{|V_{1sp}|^2\beta^2}\right)\left[\left(\frac{X}{|V_{1sp}|^2}\right)Q_{G-max}^2 - Q_{G-max}\right]}}{2\left(\frac{x}{|V_{1sp}|^2\beta^2}\right)} \quad (1)$$

where  $|V_{1sp}|$  is the specified voltage at Bus 1.

When  $Q_D \geq Q_{D-crt}$ , the generator hits its reactive power limit. The terminal voltage  $|V_1|$  is no longer regulated at  $|V_{1sp}|$ , and the generated reactive power  $Q_G = Q_{G-max}$ .

$$|V_1| = \sqrt{\frac{x(P_D^2 + Q_{G-max}^2)}{Q_{G-max} - Q_D}} \quad (2)$$

$$|V_2| = \frac{\sqrt{x(P_D^2 + Q_D^2)}}{\sqrt{Q_{G-max} - Q_D}} \quad (3)$$

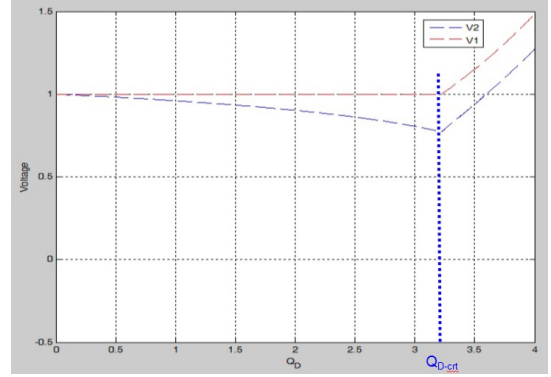


Fig. 2. Voltage collapse when load is increased to certain amount

However, if the generator constraints are considered, this solution is unfeasible and voltage instability will occur.

## II. PSCAD SIMULATION

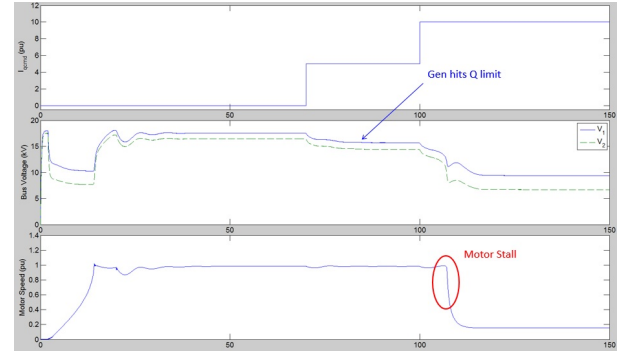


Fig. 3. Voltage collapse when load is increased to certain amount

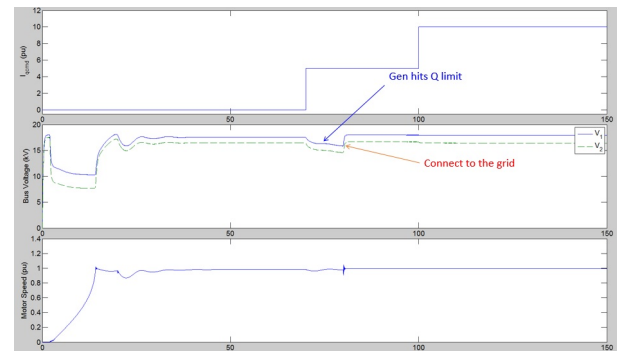


Fig. 4. Get reactive power support from external source



# Adaptive Real Power Capping Methods for Fair Overvoltage Regulation of Distribution Networks with High Penetration of PV Systems

<sup>1</sup>Junhui Zhao, <sup>1,2</sup>Yang Wang, <sup>1</sup>Caisheng Wang  
<sup>1</sup>Wayne State University, Detroit, MI 48202, USA  
<sup>2</sup>Chongqing University, Chongqing, China  
[junhui.zhao@wayne.edu](mailto:junhui.zhao@wayne.edu)

**Abstract-** For distribution networks with a high penetration of photovoltaic (PV) systems, overvoltage is a common and major issue that needs to be addressed to not only assure reliable and secure system operation, but also to fully utilize PV generation capacity. In order to prevent overvoltages by adaptively setting the power caps for PV inverters, two new real power capping methods are studied and compared. The methods try to fairly curtail the real power generation of PVs in a real-time or a long term operation. The voltage profiles can be maintained below a pre-set upper limit while maximizing the PV generation, and the real power curtailments among all the PV systems in the network can be fairly distributed. Each of the PV systems in the network has equal opportunity to generate electricity and shares the responsibility of voltage regulation.

**Index Terms** - Distribution network, distributed generation, active management, optimization, photovoltaic.

## I. KEY EQUATIONS

In this study, the objective is to minimize the total PV curtailments in a DN by minimizing  $f_{min}$  as following

$$f_{min} = w_1 * P_{1,cut} + \dots + w_n * P_{n,cut} \quad (1)$$

where  $P_{n,cut}$  is the curtailment of PV<sub>n</sub>.  $w_n$  is the weight of curtailment of PV<sub>n</sub>. If  $w_1 \dots w_n$  are all 1, the objective is to minimize the summation of real power curtailment.

Subject to the following constraints:

1) *Power balance equations:*

$$\begin{aligned} \sum P_{load} + \sum P_{loss} &= P_{trans} + \sum P_{n,PV} \\ \sum Q_{load} + \sum Q_{loss} &= Q_{trans} \end{aligned} \quad (2)$$

2) *PV generation constraints:*

$$P_{n,PV} + P_{n,cut} = P_{n,max} \quad (3)$$

3) *Power supply limits:*

$$\begin{aligned} P_{trans} &\leq P_{trans}^{max} \\ Q_{trans} &\leq Q_{trans}^{max} \end{aligned} \quad (4)$$

4) *Voltage security limits:*

$$V_{min} \leq V_k \leq V_{max} \quad (5)$$

The optimization weights are updated when the curtailment happens.

$$\begin{cases} w_{17} = 1 + \sum P_{17,curt}/a_1 \\ w_{32} = 1 + \sum P_{32,curt}/a_2 \\ w_{33} = 1 + \sum P_{33,curt}/a_3 \\ w_{34} = 1 + \sum P_{34,curt}/a_4 \end{cases} \quad (6)$$

## II. KEY FIGURES

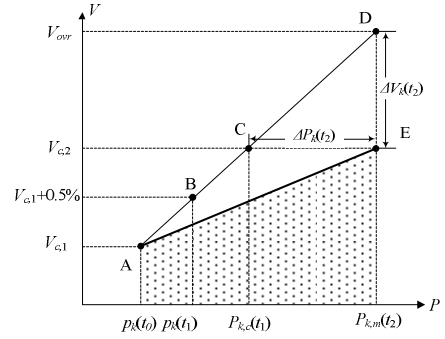


Fig. 1 PV power capping control for voltage regulation: At bus k.

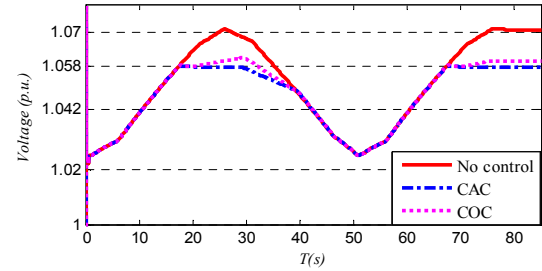


Fig. 2 Variations of voltage at weak bus under three conditions.

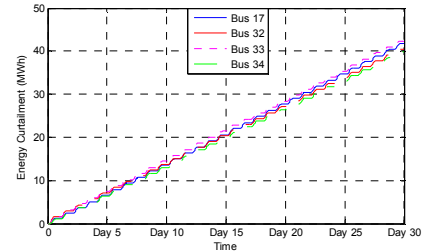


Fig. 3 Accumulated energy curtailment with adjustment of optimization weights.

# An Operating Reserve Risk Map for Quantifiable Reliability Performances in Renewable Power Systems

Mohammad Sadegh Modarresi

Electrical and Computer Engineering Department  
Texas A&M University  
College Station, TX, USA  
sadegh.modarresi@neo.tamu.edu

Le Xie

Electrical and Computer Engineering Department  
Texas A&M University  
College Station, TX, USA  
lxie@ece.tamu.edu

**Abstract**— This poster focuses on quantification of operating reserve requirement in power systems with high penetration of renewable resources. Built upon the recently introduced concept of dedicated operating reserve for renewable resources (termed as renewables reserve), we decompose the operating reserve into day-ahead portion and intra-day portion. The latter portion is determined and procured with closer-to-real-time forecast of renewable output after the closing of day-ahead market. Recognizing the inherent correlation between system reserve level and its reliability performances, we introduce a Risk Map as an intuitive tool for updating reserve levels with quantifiable reliability performances during the intra-day operation. The proposed procurement method prevents overly conservative deployment of operating reserves and uses less expensive units. It also provides evolving visualization of system reliability performances with updated information of renewable forecast each hour. Numerical simulation based on a modified IEEE Reliability Test System suggests the efficacy of the proposed method in providing cost-effective reserve levels in power systems with high levels of renewable resources.

**Index Terms**-- Operating reserve, Loss of Load Probability, Visualization, Wind power forecast, Renewable power.

## I. KEY TABLES, FIGURES AND RESULTS

The proposed procedure provides the amount of  $RnewR_{(t)}^h$  in equation (1), where  $R_{(t)}^h$  stands for the total operating reserve assigned for the " $h^{th}$ " hour of the day at time " $t$ ". " $h$ " is each of the 24 hours of day " $N$ ". It should be noted that RnewR is not going to be procured unless the risk of the system exceeds the predefined criteria, ( $LOLP_{max}$  in (2))

$$R_{(t)}^h = Contingency\ reserve^h + RnewR_{(t)}^h \quad (1)$$

$$LOLP \leq LOLP^{max} \quad (e.g. 0.02) \quad (2)$$

TABLE 1 DIFFERENT RENEWABLES RESERVE SETTINGS

R1*	R2	R3	R4	R5	R6	R7	R8	R9	R10	R11
0	12	24	36	48	60	80	100	120	140	190

TABLE 2 NET LOAD LEVELS CONSIDERED FOR THE TEST SYSTEM

L1*	L2	L3	L4	L5	L6	L7	L8	L9	L10
2400	2450	2500	2550	2600	2650	2700	2750	2800	2850

\* MW

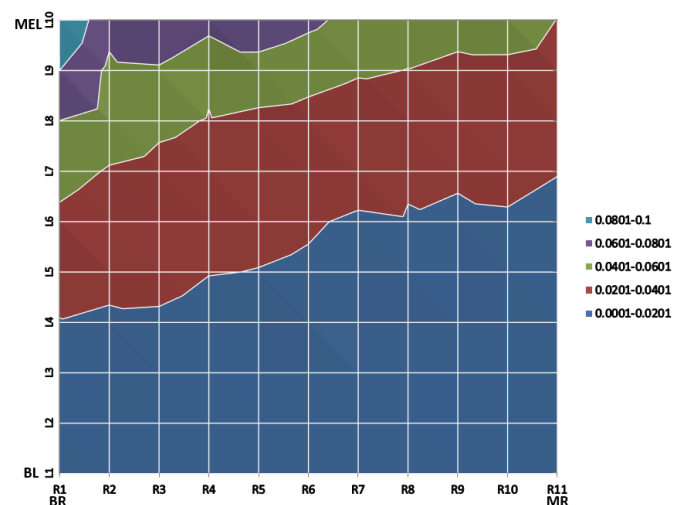


Figure 1. LOLP Contours in different loading and different renewables reserve settings. R1 represents base Reserve (BR), R11, Maximum Reserve (MR), L1, Base Load (BL), and L10, Maximum Expected Load (MEL).

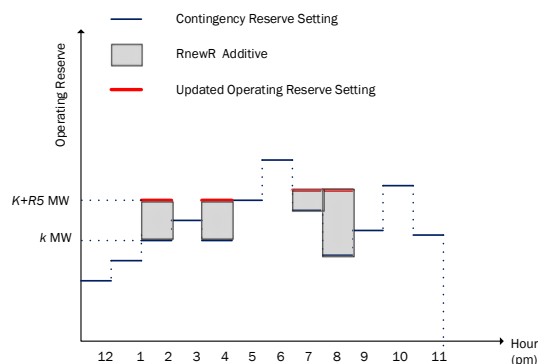


Figure 2. Illustration of hourly operating reserve after the closure of RnewR market.

# Impact of Electric Vehicles on LV feeder Voltages

Y. Li, *Graduate Student Member, IEEE*, P. Crossley, *Senior Member, IEEE*

**Abstract**— The impact of electric vehicles (EVs) on the voltage amplitude variation and voltage imbalance seen on a low voltage (LV) feeder are investigated in this paper. The Monte Carlo (MC) method was used to understand the impact of diversity of demand on LV feeders and especially the effect of uncontrolled human behavior. A statistical model of an EV was established to generate random high-resolution EV charging demand profiles, and it was combined with a distribution network model to establish a MC simulation platform. Moreover, both the balanced and unbalanced scenarios, with different EV charging locations, were investigated in a MC simulation study. The results were analyzed from a viewpoint of probability.

**Index Terms**—Voltage imbalance, electric vehicles, smart grids, low voltage networks, power system planning

## I. METHODOLOGY

The Monte Carlo (MC) method was adopted to tackle the diversity of demand seen on an LV feeder and especially the impact of uncontrolled human behavior and fig. 1 shows the adopted MC procedure. As shown in fig. 1, a pool of 10,000 one-minute daily demand profiles is firstly loaded, from which, each customer in the studied LV feeder is assigned with a residential demand profile. Then the EV model generates a random EV charging profile for each owner of an EV. Following this, the final demand profiles are imported into the distribution network model and the sequential power flow calculation for a one-day period is repeatedly executed until the convergence criteria is satisfied. Finally, numerous one-minute profiles of the investigated parameters are obtained.

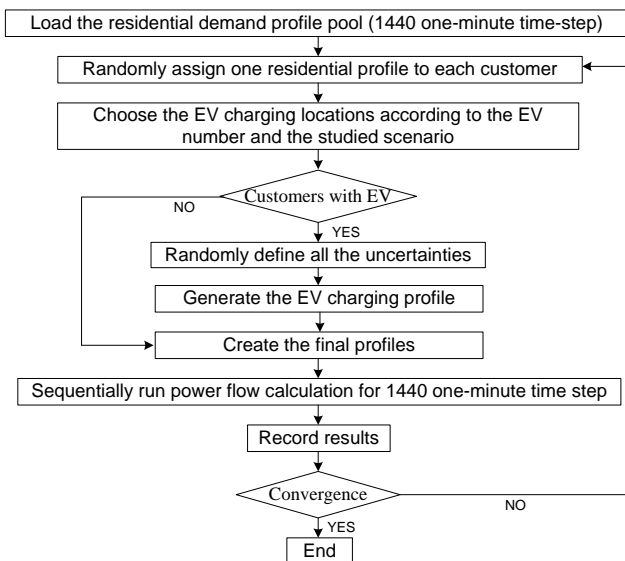


Fig. 1 The adopted MC procedure

A statistical load model capable of generating random high-resolution demand profiles was developed based on the characteristics of EVs in combination with traditional loads. Fig.2 shows the adopted distribution network model and the MC simulation study was carried out on the LV feeder F1. Moreover, to reflect the uncertainty of the results, both the mean and the corresponding 95<sup>th</sup> percentile profiles of each investigated parameter were analyzed.

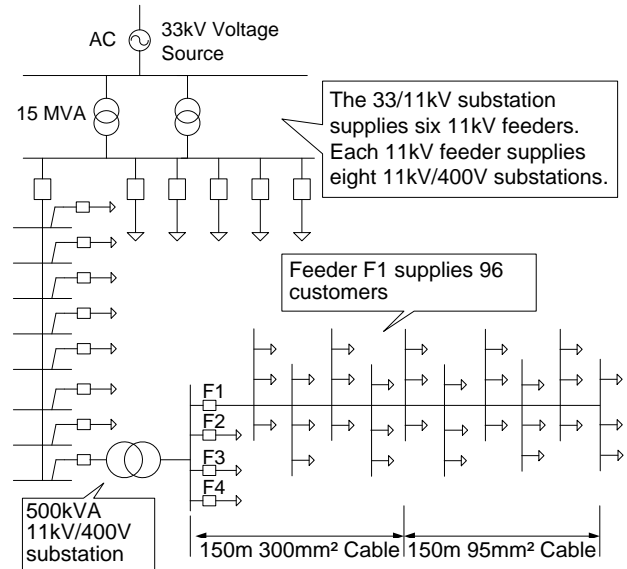


Fig. 2 The adopted distribution network

## II. KEY RESULTS

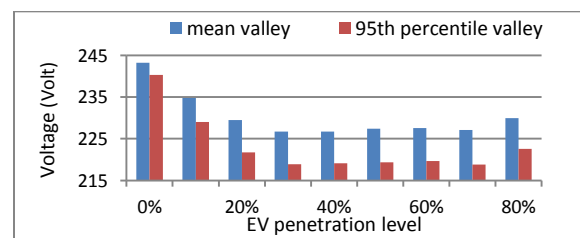


Fig. 3 Voltage amplitude in unbalanced scenario

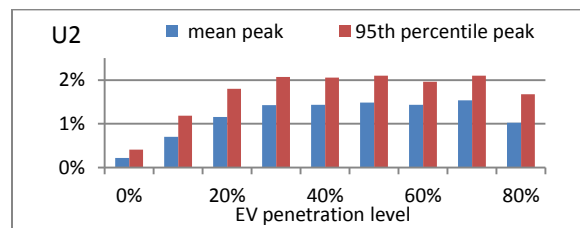


Fig. 4 U2 in unbalanced scenario

# Power System Mode Estimation Using Stochastic Subspace Identification Methods

S.A. Nezam Sarmadi and Mani V. Venkatasubramanian

School of Electrical Engineering and Computer Science  
Washington State University  
Pullman, WA 99163

Email: [snezamsa@eecs.wsu.edu](mailto:snezamsa@eecs.wsu.edu), [mani@eecs.wsu.edu](mailto:mani@eecs.wsu.edu)

*Abstract*— Accurate knowledge of modal properties of power system electromechanical modes is needed to avoid the small signal stability issues. Modal properties monitoring of a power system can be done by linearizing power system non-linear equations about an operating equilibrium point or by using measurement based estimation methods [1]. The latter is the only possible way of real-time oscillation monitoring which can help the system operator to choose appropriate actions when needed.

There are two different types of measurement data: ringdown data and ambient data. Ringdown data is the response of power system to a sudden disturbance such as a line tripping and clear oscillation can be seen on the PMU data like voltage magnitude or phase angle. On the other hand, the ambient data is the PMU data when power system is operating at its steady state condition and the system input is the continuous change of loads or other variations and the data looks like to be noisy. Since these ambient data is always available, the algorithms which can be applied on the ambient data are more attractive.

Several methods have been introduced so far for this modal estimation problem in power system and other fields like civil and mechanical engineering. Between these methods, an effective group of identification methods are Stochastic Subspace Identification (SSI) methods. They can simply be applied on a multi-channel data and estimate mode frequency and dampings as well as mode shapes. They have a relatively simple order selection technique and they are good choices for handling large data and system dynamic changes.

SSI can be applied on the system as a block processing or a recursive method. In the block processing, SSI estimates the modal properties of the system in a fixed time window say 4 minutes and the independent estimations will be done by moving this window after receiving new data. But in the recursive methods, estimated modes are updated with each new sample of data so the mode estimation updates based on the new sample and previous estimations. The advantage of recursive SSI is the speed which is a well known problem of block processing SSI due to SVD computation of a large matrix and the disadvantage is being slow in tracking the changes in modal properties due to using old estimations.

All Subspace methods start with assuming the state space model of system as [2]:

$$\begin{cases} x_{k+1} = Ax_k + w_k \\ y_k = Cx_k + v_k \end{cases}$$

where  $x_k$  is the state of system;  $y_k$  is the output or measurements;  $w_k$  is the process noise and  $v_k$  is the measurement noise. The modal properties of the given system can be obtained from state and output matrices A and C.

The first step in SSI is constructing the past and future output matrices as follows:

$$Y_p = \begin{bmatrix} y_0 & y_1 & \cdots & y_{J-1} \\ y_1 & y_2 & \cdots & y_J \\ \vdots & \vdots & \ddots & \vdots \\ y_{I-1} & y_I & \cdots & y_{I+J-2} \end{bmatrix} \quad Y_f = \begin{bmatrix} y_I & y_{I+1} & \cdots & y_{I+J-1} \\ y_{I+1} & y_{I+2} & \cdots & y_{I+J} \\ \vdots & \vdots & \ddots & \vdots \\ y_{2I-1} & y_{2I} & \cdots & y_{2I+J-2} \end{bmatrix}$$

Differing in implementation aspects, the block SSI can be developed in two different ways: the covariance-driven (SSI-COV) and the data-driven (SSI-data).

SSI-COV methods will extract A and C from the covariance matrix H:

$$H = Y_f Y_p^T$$

While SSI-data methods (such as N4SID) extract those matrices by calculating the projection of future data on the past data:

$$\rho_i = Y_f / Y_p = Y_f Y_p^T (Y_p Y_p^T)^{\dagger} Y_p$$

Recursive methods on the other hand, estimates the SVD of these matrices after the first initial calculation without a need to take a new SVD at each step.

This poster will explain these methods with examples of simulation data and real PMU data.

## REFERENCES

- [1] P. Kundur, *Power System Stability and Control*, New York: McGraw-Hill, Inc., 1994.
- [1] S. A. Nezam Sarmadi, and V. Venkatasubramanian, "Electromechanical mode estimation using recursive adaptive Stochastic Subspace Identification", *IEEE Trans. Power Syst.*, vol.29, no.1, pp. 349–358, Jan. 2014.

# Application of DSTATCOM for Surplus Power Circulation in MV and LV Distribution Networks with Single-phase Distributed Energy Resources

Farhad Shahnia, *Member, IEEE*, Ruwan P.S. Chandrasena, *Student Member, IEEE*, Arindam Ghosh, *Fellow, IEEE*  
Sumedha Rajakaruna, *Member, IEEE*

**Abstract**—Presence of large number of single-phase distributed energy resources (DER) in a particular phase can cause reverse power flow in that phase making the upstream network unbalanced. In this poster, the possibility of using a Distribution Static Compensator (DSTATCOM) to circulate the excess generation in one phase to the phases with higher load demand is presented. Two different topologies are proposed for DSTATCOM to be installed in low and medium voltage feeders. Accordingly, two different power circulation strategies are proposed for power circulation through the DSTATCOM. A suitable state feedback control scheme is developed and utilized for each topology. The proposals are validated via PSCAD/EMTDC simulation studies.  
**Index Terms**—DSTATCOM, DER, Power circulation

## I. INTRODUCTION

**I**n this poster, utilization of a DSTATCOM with different topologies and control algorithms are proposed for both LV and MV feeders to enable the power circulation. The DSTATCOM current and voltage output references are generated such that a set of balanced currents are drawn from the upstream. The proposals are validated through PSCAD simulation studies.

## II. DSTATCOM TOPOLOGIES

The schematic diagram of the selected topology for the DSTATCOM to be installed in LV and MV feeders are shown in Fig. 1 below.

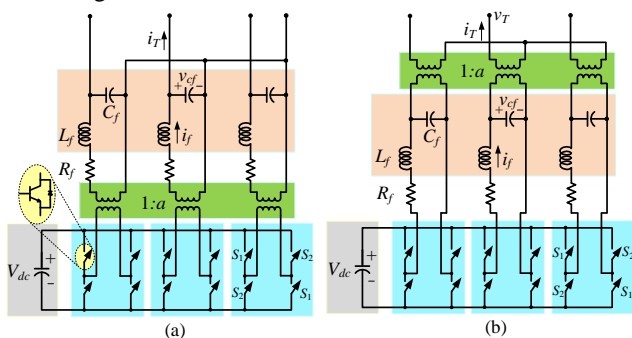


Fig. 1. DSTATCOM topology with power circulation capability to be installed in: (a) LV feeders, (b) MV feeders.

## III. POWER CIRCULATION STRATEGIES

Two different power circulating strategies are proposed for each topology of the DSTATCOM, introduced in Section II.

### A. Power Circulation Strategy for DSTATCOM in LV Feeder

The reference voltage across the three filter capacitors ( $C_f$ ) in PCC is

$$[V_{cf}]_{ABC}^{ref} = E_{DSTAT} \angle \delta_{cf,A}^{ref} \times [1 \quad \lambda^2 \quad \lambda]^T \quad (1)$$

where  $E_{DSTAT}$  is the desired phase voltage RMS

The angle of the voltage across the AC filter capacitor ( $\delta_{cf}$ ) must be varied with respect to the DC capacitor voltage variations as

$$\delta_{cf}^{ref} = \left( k_P + \frac{k_I}{s} \right) (V_{dc}^{ref} - V_{dc}) \quad (2)$$

### B. Power Circulation Strategy for DSTATCOM in MV Feeder

The reference currents for the DSTATCOM in MV feeders can be calculated as

$$[i_T]_{ABC}^{ref} = [i_L]_{ABC} - \frac{v_{A1}i_{LA} + v_{B1}i_{LB} + v_{C1}i_{LC}}{v_{A1}^2 + v_{B1}^2 + v_{C1}^2} [v_1]_{ABC} \quad (3)$$

where  $i_L$  is the current in the downstream of DSTATCOM.

## V. SIMULATION RESULTS

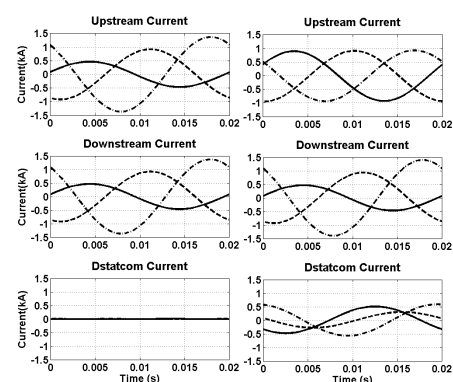


Fig. 2. Simulation results before (left column) & after DSTATCOM connection (right column)

F. Shahnia and A. Ghosh are with center of smart grid and sustainable power systems, Department of Electrical and Computer Engineering, Curtin University, Perth, Australia (farhad.shahnia@curtin.edu.au)

R.P.S. Chandrasena and S. Rajakaruna are with Department of Electrical and Computer Engineering, Curtin University, Perth, Australia.



# Identification and Wide-area Visualization of the Centers of Oscillation for a Large-scale Power System

Leonardo E. Bernal, Fengkai Hu, Kai Sun  
 University of Tennessee  
 Knoxville, TN, USA  
[leo.bernal@gatech.edu](mailto:leo.bernal@gatech.edu)  
[fengkaihu@utk.edu](mailto:fengkaihu@utk.edu)  
[kaisun@utk.edu](mailto:kaisun@utk.edu)

Evangelos Farantatos  
 Electric Power Research Institute  
 Palo Alto, CA, USA  
[efarantatos@epri.com](mailto:efarantatos@epri.com)

**Abstract--** A system wide disturbance event usually triggers inter-area oscillations at the system. Understanding the nature of those oscillations is important for taking necessary early mitigation actions. This work presents a novel scheme for analyzing inter-area oscillations by identification of the centers of oscillation (CoO) using two methods based on wide-area measurement data: one method directly calculate CoOs for transmission lines with synchrophasors on both ends and the other estimate CoOs based on contour visualization about frequency deviations extrapolated for the entire map. CoOs serve as pivots between oscillating parts under disturbances and hence indicate the grid interfaces involved in oscillation, so this scheme can provide the operator recommendations on where mitigation actions may be taken to prevent instability. The proposed scheme is tested using simulated synchrophasor data on a WECC 179-bus test system.

## I. EQUATIONS

$$f_{(x,y),t} = \sum_{i=1}^n \frac{K_{(x_i,y_i),t} \times f_{(x_i,y_i),t}}{(x-x_i)^2 + (y-y_i)^2} \bigg/ \left[ \sum_{i=1}^n \frac{K_{(x_i,y_i),t}}{(x-x_i)^2 + (y-y_i)^2} \right] \quad (1)$$

$$\Delta f_{1,avg} = \frac{\sum_{j=1}^m (f_{(x_i,y_i),t-j+1} - f_{(x_i,y_i),t-j})}{m} \quad (2)$$

$$dist_1 = \frac{|\Delta f_{1,avg}| \times dist_{1-2}}{|\Delta f_{1,avg}| + |\Delta f_{2,avg}|} \quad (3)$$

## II. KEY FIGURE

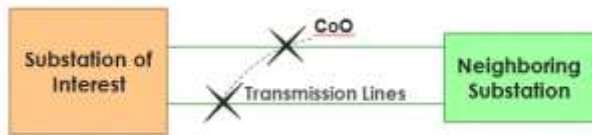


Fig. 1. Local center of oscillation located at points in the transmission lines some distance between neighboring substations.

## III. KEY RESULTS

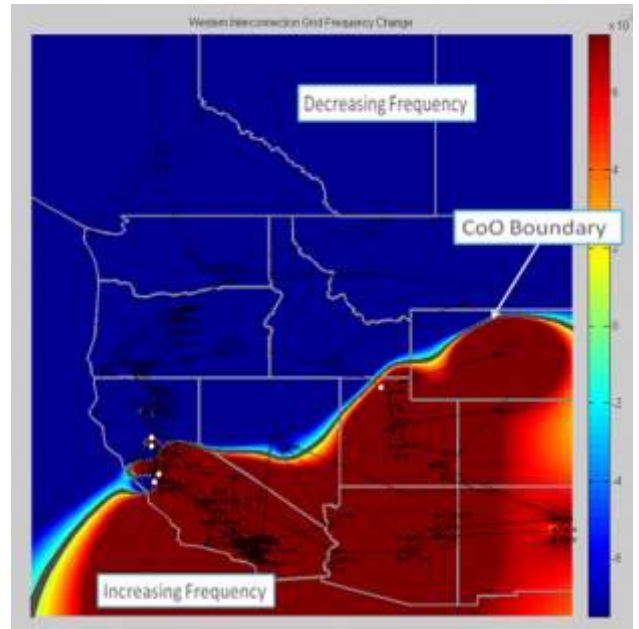
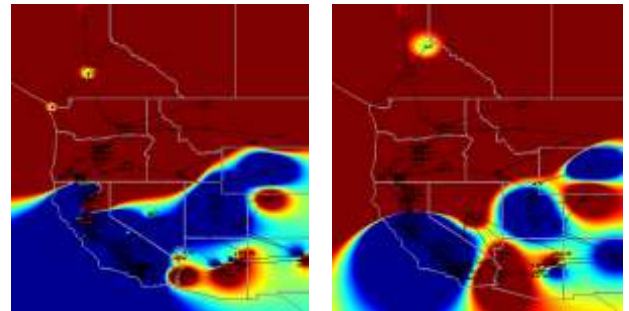


Fig. 9. CoO boundary between two islanded systems in oscillation



(a) PMUs at 50% buses  
 (b) PMUs at 29 generators  
 Fig. 10. Center of Oscillation boundary identified by the pixel method

# Quantifying Battery State-of-Health in Microgrid Applications

Christopher R. Lashway, *Student Member, IEEE*, Osama Mohammed, *Fellow, IEEE*  
 Department of Electrical and Computer Engineering, Florida International University,  
 Miami, FL 33174, USA  
 Email: clash006@fiu.edu, mohammed@fiu.edu

**Abstract** —The emerging microgrid concept relies heavily on batteries in cooperation with renewables to provide resilient support to the customer. Both solar and wind power generate DC power, either directly or through the means of a rectifier before it is passed through an inverter for connection to the grid. In order to ensure a high level of efficiency, electrochemical energy storage is installed on the DC link to provide backup when wind and PV are unavailable. The issue, however, lies in the sporadic nature of the current produced from these sources. Voltage transients in the PV panel voltage or WTG translate to a rapid increase in current on the DC grid. If the energy is not directly injected to the AC side, this current is passed to a battery array which is not designed to charge with nonlinear current pulses and transients. At the same time, this array would be required to source pulsed loads and transients during outage periods. The nonlinearity of the charging and discharging profiles take a serious toll on the state-of-health of the bank which varies with respect to different cell configurations, chemistries, and sizes. To investigate this problem, a battery testing bed has been to test a wide range of different battery cell chemistries (Fig. 1). The testbed features a controllable resistive load connected to a National Instruments data acquisition platform. Through a software front-end, the battery chemistry, number of cells, and capacity is input. The user can then designate the method of charging and discharging as constant or pulsed with a wide range of independent frequencies for each. As each cycle concludes, data is passed to a MATLAB script to evaluate the performance trend of the battery under test generating the state-of-health and input-output efficiency.

## I. KEY FEATURES

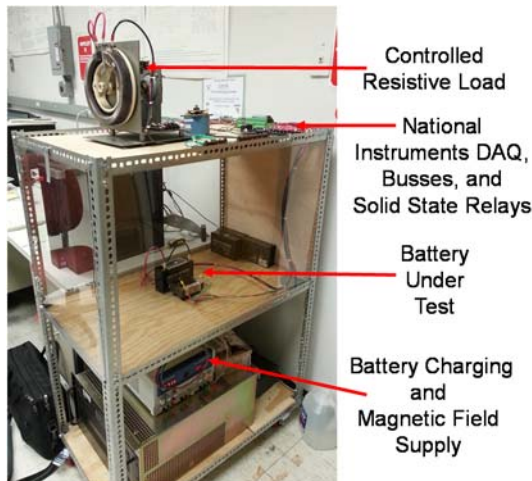


Fig.1 Battery Testing Hardware Platform.

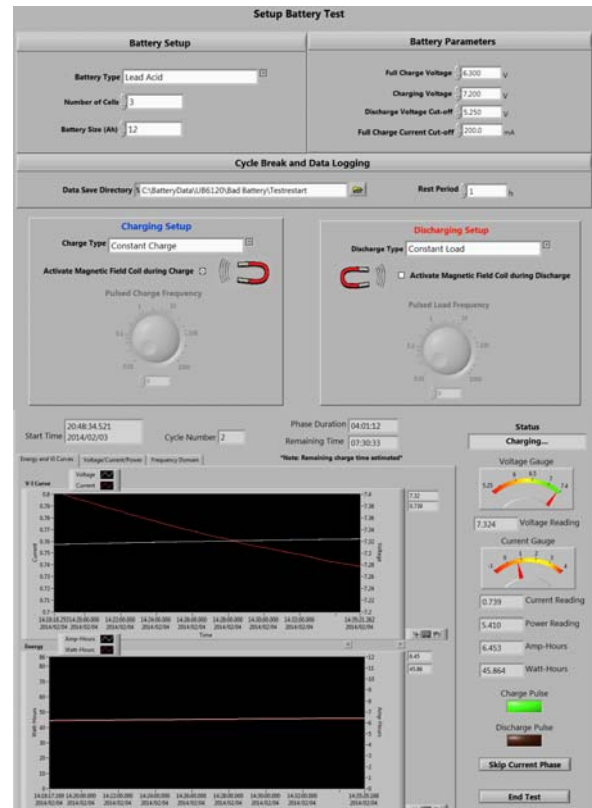


Fig.2 Battery Testing Software Suite: Setup (top) and Status (bottom).

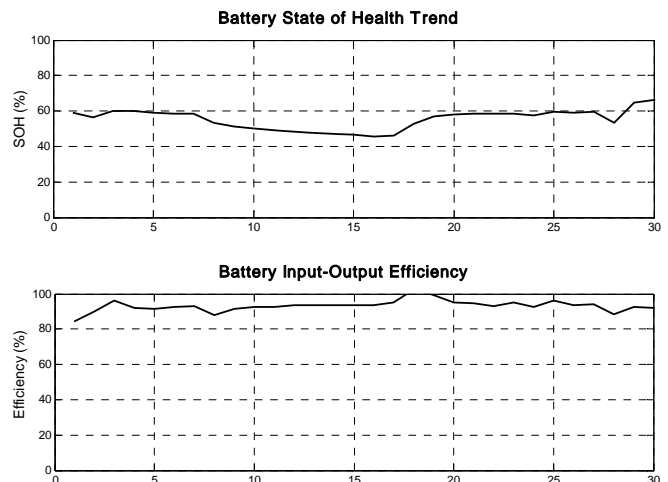


Fig.3 Battery State-of-Health Trend and Cyclic Efficiency.



# Performance Characterization for Photovoltaic-Vanadium Redox Battery Microgrid Systems

Tu A. Nguyen, Xin Qiu, Joe D. Guggenberger\*, M. L. Crow, *IEEE Fellow*, and A. C. Elmore\*

Department of Electrical and Computer Engineering

\*Department of Geological Engineering

Missouri University of Science and Technology, Rolla, MO 65401

**Abstract**—The integration of photovoltaics (PV) and vanadium redox batteries (VRB) in microgrid systems has proven to be a valuable, environmentally-friendly solution for reducing the dependency on conventional fossil fuel and decreasing emissions. The integrated microgrid system must be characterized to develop appropriate charging strategies specifically for VRBs, sizing microgrid systems to meet a given load, or comparing the VRB to other energy storage technologies in different applications. This paper provides a performance characterization analysis in a PV-VRB microgrid system for military installations under different conditions of load and weather.

**Index Terms**—microgrid, renewable energy, energy storage, vanadium redox battery, efficiency characterization

## I. INTRODUCTION

MICROGRIDS with integrated renewable resources are emerging as a solution for reducing the dependency on conventional fossil fuel and reducing emissions in distribution systems. The variability of renewable power sources requires quick response and highly efficient storage devices with larger power and energy density, which creates a challenge in developing renewable energy-based microgrids in large scale. To obtain the optimal performance from an integrated renewable energy, the round trip efficiency of the entire system must be characterized. Although many new energy storage technologies are reaching the consumer market, there is little field experience to support their adoption. Furthermore, most commercially available charging systems have been designed for lead acid batteries and when used with other energy storage technologies may adversely affect the round trip efficiency of the system. Thus the energy storage system may not reflect the manufacturer’s predicted performance. Therefore in this paper, we fully characterize the round trip efficiency of a photovoltaic (PV) system that uses a vanadium redox battery to provide increased confidence in their deployment.

The Vanadium Redox Battery (VRB) is a relatively new commercially available energy storage system. The vanadium redox battery energy storage system is an electrical energy storage system based on the vanadium-based redox regenerative fuel cell that converts chemical energy into electrical energy. The VRB differs from traditional battery storage in that the amount of energy it can store is independent of its power rating. The size of the stack determines the power rating whereas the amount of electrolyte determines the energy capacity. Thus

the energy rating of the VRB can be changed “on the fly” by increasing or decreasing the amount of electrolyte in the storage tanks. Furthermore, the VRB can be stored for long periods of time without charge degradation.

Due to its recent commercialization, the information available in the literature on VRB-based microgrids is limited. Most work has focused on electrochemical and electrical modeling of the VRB, [1], on electrode, electrolyte, and membrane materials characterization [2], or on optimal VRB pump operation [3]. Only recently has the VRB been considered for microgrid applications. In [4], the VRB-based microgrid performance was predicted based on geographic location, weather data and loading conditions; however, the effect of the charging/discharging voltage levels and VRB internal losses on system efficiency were neglected.

In this paper, a complete PV-VRB microgrid is characterized holistically. The analysis is based on a prototype system installation deployed at Fort Leonard Wood, Missouri, USA. Specifically, the following contributions are made in this paper:

- the characterization of the PV-VRB microgrid performance under different loading and weather conditions,
- the development of a two-stage charging strategy for the VRB, and
- a quantification of the component efficiencies and their relationships.

## REFERENCES

- [1] T. Nguyen, X. Qiu, T. Gamage, M. L. Crow, B. McMillin, and A. C. Elmore, “Microgrid application with computer models and power management integrated using PSCAD/EMTDC,” *Proc. North Amer. Power Symp.*, 2011.
- [2] M. Vijayakumar, L. Li, G. Graff, J. Liu, H. Zhang, Z. Yang, and J. Z. Hu, “Towards understanding the poor thermal stability of v5+ electrolyte solution in vanadium redox flow batteries,” *Journal of Power Sources*, vol. 196, no. 7, pp. 3669 – 3672, 2011.
- [3] X. Ma, H. Zhang, C. Sun, Y. Zou, and T. Zhang, “An optimal strategy of electrolyte flow rate for vanadium redox flow battery,” *Journal of Power Sources*, vol. 203, pp. 153 – 158, 2012.
- [4] J. Guggenberger, A. C. Elmore, J. Tichenor, and M. L. Crow, “Performance prediction of a vanadium redox battery for use in portable, scalable microgrids,” *IEEE Transactions on Smart Grid*, vol. 3, no. 4, 2012.

# Simulation Studies of Cascading Blackouts via Hidden Failure-Based Load Shedding Models

Po Jen Lai, *Student Member, IEEE*

Department of Electrical Engineering, National Tsing-Hua University, HsinChu, Taiwan, R.O.C.

Email: blazeinsky@gmail.com

**Abstract**—This paper presents a methodology to simulate cascading blackouts of bulk power systems on the basis of a computer program using Matpower. With the usage of the hidden failure model and importance sampling, DC OPF is utilized to investigate steady-state characteristics of bulk power grids encountering cascades. The core control method used to deal with cascading blackouts is load shedding because the purpose of this paper is to provide a worst case perspective. Statistic results of cascading blackouts are generated and analysed under variations of different factors including loading level and hidden failure probability. The simulation program has been tested on the IEEE 300-bus system and Taiwan power systems and the results indicate that they have self-organized criticality(SOC).

**Index Terms**—Hidden Failures, Importance Sampling, Optimal Power Flow, Load Shedding, Spinning Reserve, Self-Organized Criticality.

## I. INTRODUCTION

Hidden Failure (HF) is a kind of fault such that when a line in a power system trips due to initial accidents, other lines sharing a bus with that tripped line will have a probability to trip. The hidden-failure model can be seen as an analogy of the sand pile model from the study of complex networks because the historical blackouts data implies that the power grids possess a power law tail and hence are similar to complex networks having cascades [1].

## II. METHODOLOGY

To lower the simulation complexity, DC OPF is used to simplified the procedure. In addition, because the probability of HF is very small, importance sampling is incorporated to improve the results [2]. The estimated probability of the  $i$ -th distinct cascading path and the simulation procedure are shown below.

$$\hat{p}_i = \frac{N_{occur}}{N_{total}} \times \frac{p_i^{actual}}{p_i^{simulate}} \quad (1)$$

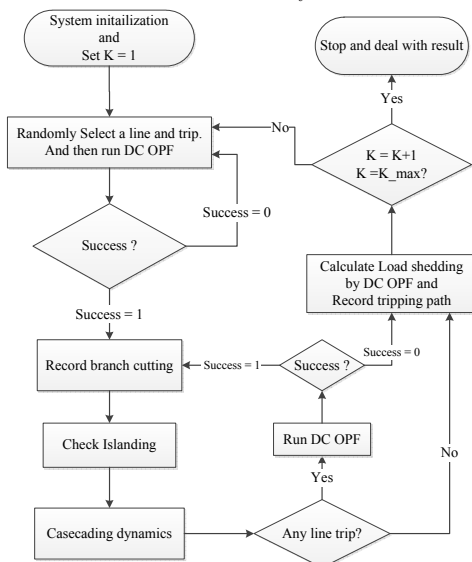


Fig. 1. Flow chart of the simulation procedure.

## III. KEY RESULTS

In Fig. 2, the pictures in the third row are under critical loading and embody a straight line which indicates SOC. In Fig. 3, it is obvious that the variations of HF probability can keep the systems from SOC and hence can mitigate larger blackouts.

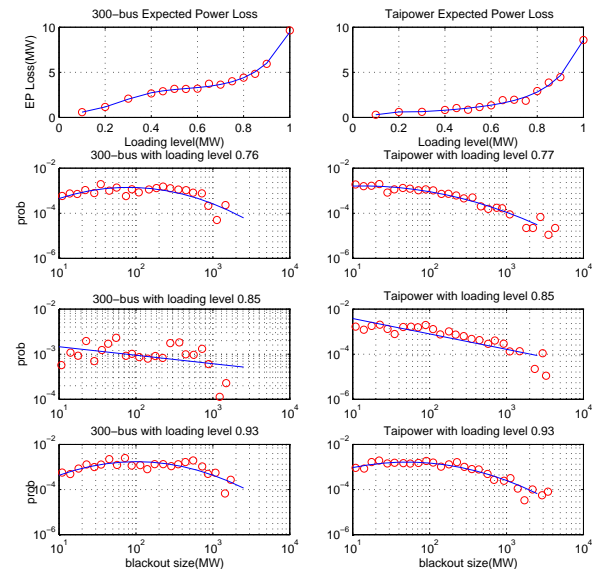


Fig. 2. Simulation results under different loading levels

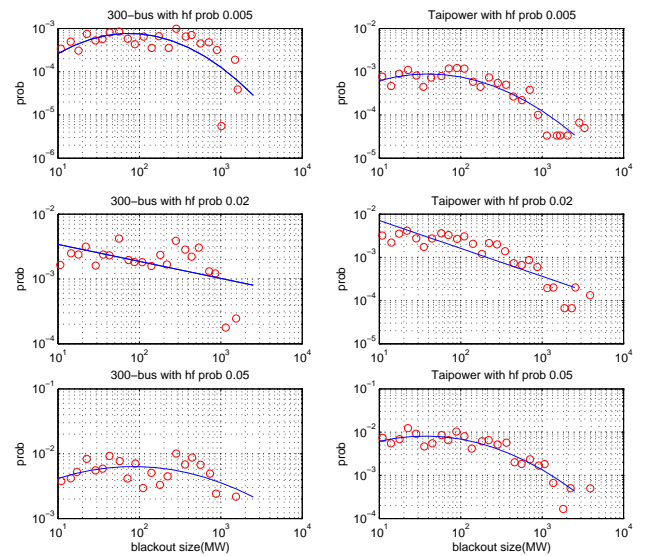


Fig. 3. Simulation results under different hidden failure probabilities.

## REFERENCES

- [1] S. Mei, et al, *Power Grid Complexity*. TsingHua University Press, 2011.
- [2] J. Bucklew, *Introduction to Rare Event Simulation*. Springer Series in Statistics, 2004, ch. 4, pp. 57–61.

# Inventory Management of DSCC System via Improved (s, S) Model

Yongquan Nie, C. Y. Chung, Senior Member, IEEE, Lidan Chen and Mingwen Qin

Department of Electrical Engineering, The Hong Kong Polytechnic University

Email: [nieyongquanv@gmail.com](mailto:nieyongquanv@gmail.com) and [c.y.chung@polyu.edu.hk](mailto:c.y.chung@polyu.edu.hk)

**Abstract**—Adequate battery charging facilities can be a major obstacle to the development of EV. Generally, battery charging and battery swapping are the two feasible methods for refilling depleted batteries. This paper focuses on the operation and logistics among stations by proposing the distributed swapping & centralized charging (DSCC) system. Firstly, the traffic conditions are formulated such that the swapping stations and other supporting facilities can be deployed. Secondly, the real-time available batteries and battery demand are investigated with the improved (s, S) inventory management to achieve adequate supply of recharged batteries.

**Index Terms**—Battery swapping, Battery reserves, Electric vehicle, Inventory management

## I. INTRODUCTION

(s, S) model is used to keep inventory in a safe level.  $s$  is assumed to be the trigger point for inventory replenishment while  $S$  is assumed to be the initial inventory level.

## II. MODEL FORMULATION

The  $SOC_{ini}$  when coming by follows uniform distribution in (1). For safety consideration, the SOC of batteries needs to be no less than 30% at any given time (2).

$$U(SOC_{min}, SOC_{max}) \quad (1)$$

$$SOC_{ini} \cdot E - \omega L < 0.3E \quad (2)$$

The vehicle flow rate  $\xi$  is assumed to follow poisson process.

$$f(h, \xi \cdot \Delta T) = P(N(\Delta T) = h) = e^{-\xi \cdot \Delta T} \frac{(\xi \cdot \Delta T)^h}{h!} \quad (3)$$

$$\lambda = \xi \cdot r \quad (4)$$

## III. BATTERY INVENTORY MANAGEMENT

### A. Operation of swapping stations

Inventory management protects the regular and planned inventory level against the random disturbance of redundant storage or running out of goods. Ordinary goods can be promptly replenished in traditional inventory management whereas batteries need long time to be recharged for recycling..

Referring Fig. 1, in order to prevent stockout, the trigger point  $s_t$  at time interval  $t$  for starting inventory replenishment shall be set as (5) taking anticipation stock into account.

$$s_t = F^{-1}(p', \lambda_{t+\Delta T} \cdot \frac{T_n}{\Delta T}) \quad (5)$$

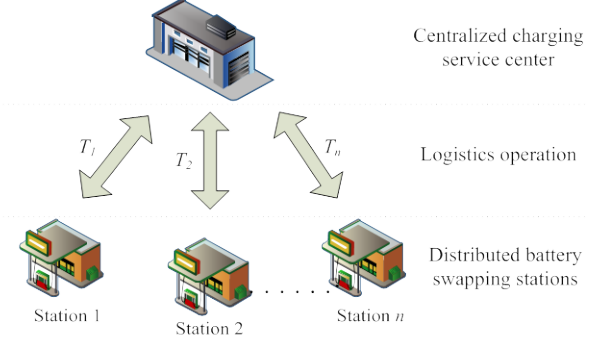


Fig. 1. Centralized battery charging & dispatching mode

Over-storage increases the cost, so the number of recharged batteries delivered back is denoted as in (6).

$$C_t = S - S_t + s_t \quad (6)$$

### B. Operation of centralized charging center

One centralized charging center is assigned to provide service to several nearby swapping stations, the charging duration  $T_c$  is calculated as (7). Total charging power in (8):

$$T_c = \frac{(1 - SOC_{mi}) \cdot E}{eP_c} \quad (7) \quad P_t = \sum_{k=1}^K P_c \cdot u_t^k \quad (8)$$

Recharged batteries can be delivered back to swapping stations for later use.

## IV. CONTROL SCHEME

For optimization control of this DSCC system, the charging load impact on the local power system and the inventory turnover should be specifically considered.

Objective:

$$\text{Min Obj} = \alpha_1 \cdot D(P) + \alpha_2 \cdot \frac{1}{I} \quad (9)$$

$$D(P) = \frac{1}{T} \sqrt{\sum_{t=1}^T (P_t - \mu_T)^2} \quad (10)$$

$$I = \frac{\sum_{t=1}^T \lambda_t \cdot \Delta T}{\sum_{n=1}^N S_n + S'} \quad (11)$$

Constraint:

$$S_n(t) > 0, S'(t) > 0, \forall t \quad (12)$$

$$0 < P_c < P_{c,max} \quad (13)$$

# Transient Model of Air-Conditioner Compressor Single Phase Induction Motor

Yuan Liu<sup>1</sup>, *Student Member, IEEE*, Vijay Vittal<sup>1</sup>, *Fellow, IEEE*, John Undrill<sup>1</sup>, *Fellow, IEEE*,  
and Joseph H. Eto<sup>2</sup>, *Member, IEEE*

<sup>1</sup>School of Electrical, Computer and Energy Engineering, Arizona State University, Tempe, AZ 85287, USA

<sup>2</sup>Lawrence Berkeley National Laboratory, Berkeley, CA 94720 USA

Email: [yliu250@asu.edu](mailto:yliu250@asu.edu)

**Abstract--** In some portion of the U.S. grid interconnection, fault induced delayed voltage recovery (FIDVR) phenomenon is found to be caused by the large-scale stalling of A/C compressor motors. This model is developed to analyze FIDVR and explain the cause of motor stalling. The abstract describes an air-conditioner (A/C) compressor single phase induction motor (SPIM) model for use in an electro-magnetic transients (EMTs) simulation. The system of differential equations representing the SPIM model is developed and formulated. The angular position of the rotor shaft is retained in the electrical and mechanical equations of the model so that position dependence of the driven-load torque can be explicitly recognized. The equivalent circuit of the proposed model is represented as an interface to the external electric network in the EMTs simulator. Motor dynamic response to voltage dip at different points on the voltage waveform has been studied. Simulation results reveal that the A/C compressor stalling is closely related to the instant at which voltage dip occurs rather than the depth of voltage dip. It is also found that the vulnerability of motor stalling is determined by the extent of negative electromagnetic torque rather than the magnitude of the mechanical torque. Multiple aggregate units of the proposed model have been implemented on a distribution feeder to test and verify the motor dynamics in an EMTs simulation.

## I. KEY EQUATIONS

Equations describing the equivalent circuits of the single phase induction motor model.

$$I_{as}(t) = \frac{V_{as}(t) - E_{thas}(t - \Delta t)}{Z_{aa}} = \frac{V_{as}(t)}{Z_{aa}} + I_{an}(t - \Delta t) \quad (1)$$

$$I_{bs}(t) = \frac{V_{bs}(t) - E_{thbs}(t - \Delta t)}{Z_{bb}} = \frac{V_{bs}(t)}{Z_{bb}} + I_{bn}(t - \Delta t) \quad (2)$$

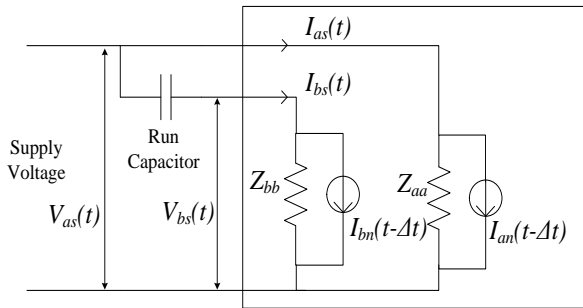


Fig. 1. Equivalent schematic of A/C compressor motor in EMTs simulator

## II. KEY RESULTS

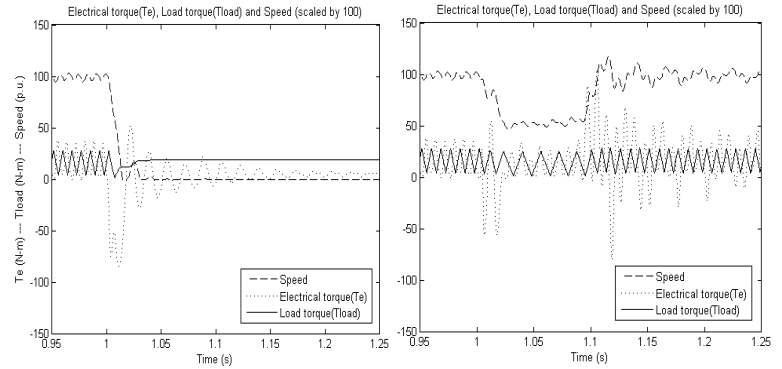


Fig. 2. Plot of electrical torque, load torque and motor speed (Left: steady state load torque is 16 N-m and voltage dip is applied at 0 degree. Right: steady state load torque is 16 N-m and voltage dip is applied at 90 degrees)

TABLE I  
RESULTS OF MOTOR STALLING

Point-on-wave (°)	$T_{load}$ (N-m)	$T_{av}$ (N-m)	Average load torque (N-m)	Stall or Not-stall
0	6	8	14	Stall
0	4	12	16	Stall
45	6	8	14	Not-stall
45	4	12	16	Stall
90	6	8	14	Not-stall
90	4	12	16	Not-stall

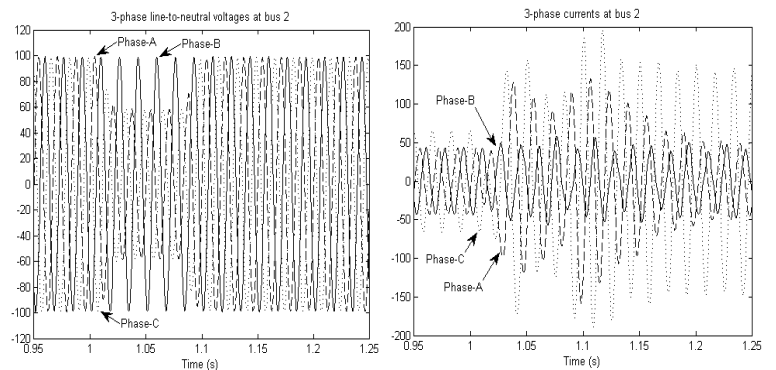


Fig. 3. Bus voltage (left, kV) and current (right, A) at the head of feeder subject to a two-phase (phase -A and -C ) voltage dip from rated to 59%

# Distribution Side Mitigation Strategy for Fault Induced Delayed Voltage Recovery

Yuan Liu, *Student Member, IEEE*, Vijay Vittal, *Fellow, IEEE*

School of Electrical, Computer and Energy Engineering, Arizona State University, Tempe, AZ 85287, USA

Email: [yliu250@asu.edu](mailto:yliu250@asu.edu)

**Abstract--** Fault induced delayed voltage recovery (FIDVR) is known to be caused by stalled air-conditioner compressor single phase induction motors (SPIMs). The traditional strategies to mitigate this phenomenon include tripping off the motors using thermal protection devices and installing voltage support devices to prevent voltage sag on the load side. This abstract presents investigations and outcomes of several mitigation methods implemented on the distribution system using a recently developed point-on-wave transient air-conditioner compressor motor model. The effects of the dynamic voltage regulator (DVR) on preventing voltage sag are studied. A classical single phase variable speed H-bridge converter is implemented to explore its capability and fast response in mitigating FIDVR problem induced by a short-duration transient fault. An enhanced H-bridge converter is proposed to mitigate the impact of the long-duration fault contingency.

## I. KEY FIGURES

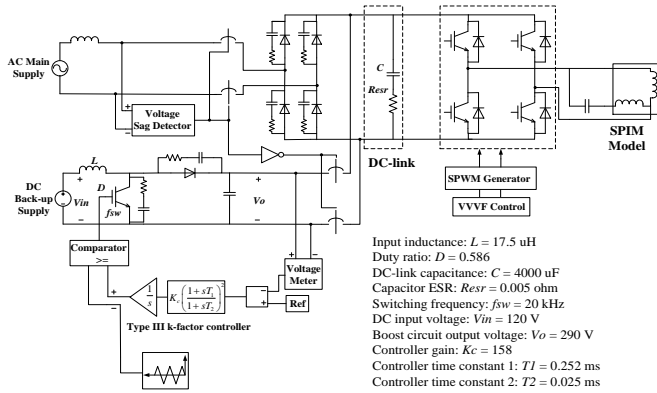


Fig. 1. Enhanced variable speed H-bridge converter

Voltage-fed controller for the back-up boost circuit:

$$G_c = \frac{\Delta d(s)}{\Delta v_e(s)} = \frac{K_c}{s} \left( \frac{1+T_1s}{1+T_2s} \right)^2 \quad (1)$$

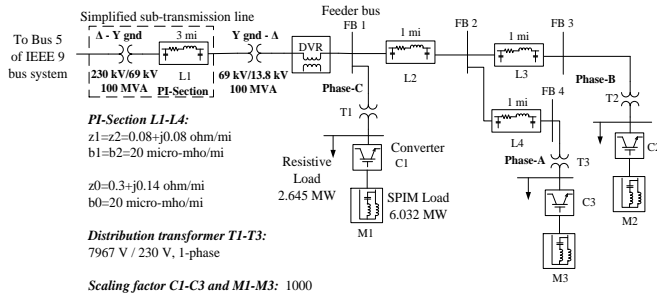


Fig. 2. Simplified feeder model (including sub-transmission line)

## II. KEY RESULTS

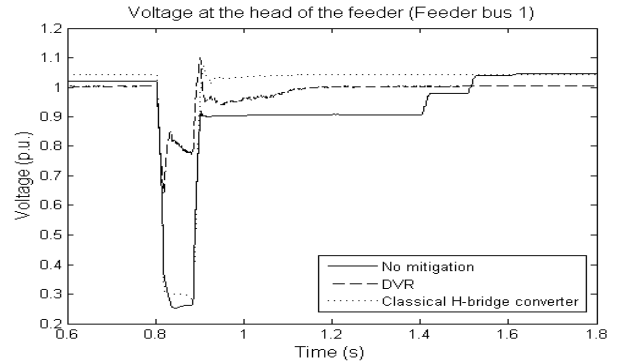


Fig. 3. RMS voltage at the head of feeder (4.8 cycles three phase fault)

TABLE I

Sensitivity of motor stalling (The stalled motors are recorded)

		Fault duration (cycles)		
		3	5	7
DC-link capacitance (mF)	5	M2	M2	M1, M2, M3
	10	0	0	M2, M3
	15	0	0	0

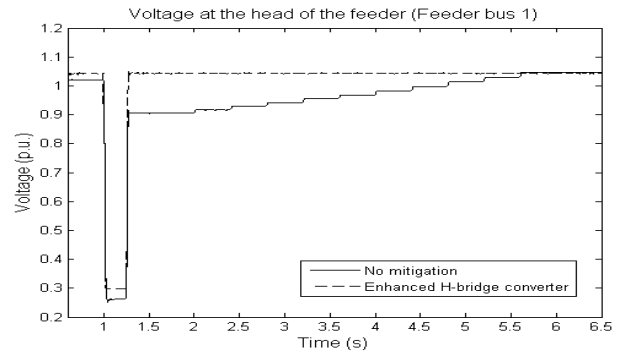


Fig. 4. RMS voltage at the head of feeder installed with enhanced H-bridge converter (15 cycles three phase fault)

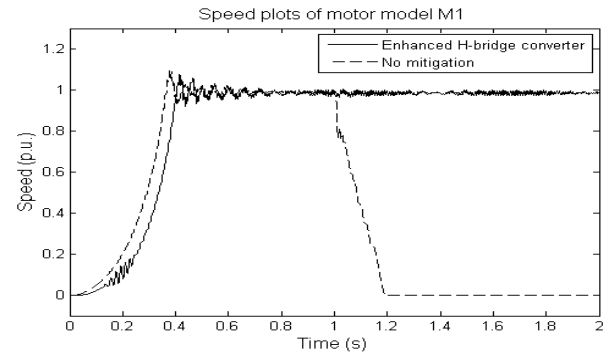


Fig. 5. Speed plots of motor model M1 (15 cycles fault)



# Analysis of Market Operator Adjustments within Day-Ahead Energy Markets

Mojdeh Abdi-Khorsand, *Student Member, IEEE*, Yousef Al-Abdullah, *Student Member, IEEE*,  
 Mostafa Sahraei-Ardakani, *Member, IEEE*, and Kory W. Hedman, *Member, IEEE*  
 School of Electrical, Computer, and Energy Engineering, Arizona State University, Tempe, AZ 85287, USA  
 Email: [mabdikho@asu.edu](mailto:mabdikho@asu.edu), [yousef.al-abdullah@asu.edu](mailto:yousef.al-abdullah@asu.edu), [msahraei@asu.edu](mailto:msahraei@asu.edu), and [kory.hedman@asu.edu](mailto:kory.hedman@asu.edu)

**Abstract**— The day-ahead scheduling process is generally very complex. In the USA, Independent System Operators (ISO) start by solving a security-constrained unit commitment (SCUC) market model, which maximizes the social welfare. SCUC is a Mixed-Integer Program (MIP), which aims at specifying the status and output of the units for the next day based on the demand forecast. Due to the complexities and assumptions involved in SCUC, market operators must adjust the SCUC solution in order to obtain a valid solution. Some of these modifications are handled within the market, while others must be handled outside the market. The inclusion of binary variables (to capture non-zero minimum operating levels, start-up and no-load costs, minimum up and down time constraints, as well as other requirements) makes the SCUC market model non-convex. The solution of the SCUC problem, along with using LMPs for settlements, does not possess the properties of a market equilibrium because of the non-convexities of the market. A generator may be scheduled to produce while it makes negative profits due to the existence of fixed costs (start-up, shut-down, and no-load costs), reliability requirements, and non-zero minimum operating levels, which are not reflected in market prices. Thus, ISOs make uplift payments to the generators to overcome these phenomena. In electricity markets today, SCUC is not solved to optimality. The algorithm stops after a certain amount of time, or if a specific optimality gap, is achieved. The number of the potential sub-optimal solutions that satisfy the stopping criteria is large. The potential solutions have relatively close total cost but other market outcomes may be drastically different. One of the outcomes, which is of particular interest, is the uplift payment. Uplift payments distort the price signal and, hence, are not preferred by the ISOs. Thus, ISOs may favor solutions with significantly lower uplifts. This work acknowledges an ISO practice to consider choosing different SCUC solutions based on their uplift payment. It is shown that very close SCUC solutions, in terms of the total cost, may result in very different market outcomes. Then, the implications for the market players are studied. SCUC is run on an industrial scale PJM model. Figure 1 shows the uplift payment and total cost for the obtained SCUC solutions [1].

The day-ahead scheduling procedure can involve a variety of additional steps as well, including a reliability unit commitment (RUC) model, a scheduling run and a pricing run, as well other stages that adjust the market solution in order to get the final day-ahead schedule. We refer to these additional changes that happen outside the market model as out-of-market corrections (OMCs). Performing an OMC changes the original solution, which is considered to be the most economical solution but is infeasible; it occurs when a dispatch solution must be corrected by the operator in order to satisfy a system requirement that was not implicitly or adequately

modeled within the dispatch optimization problem. Existing SCUC market models incorporate a linear approximation of the AC optimal power flow (ACOPF), which leads to the most common need for an OMC, to obtain an AC feasible solution. OMCs may also be needed because market models approximate the network model, i.e., only select transmission lines are monitored. OMCs may be necessary since proxy reserve requirement policies do not guarantee N-1 because the available reserve might not be deliverable in the post-contingency state. This work also analyzes the market implications and required out-of-market corrections for the day-ahead scheduling process [2]-[3]. Figure 2 shows the day-ahead scheduling process. The proposed OMC methods are tested on the IEEE 118-bus system.

## I. KEY EQUATIONS

$$UL_g^1 = \sum_{t \in T} \left( \lambda_{n(g)t} - c_g \right) (P_g^{max} - P_{gt}) \quad (1)$$

$$\Pi_g^1 = \sum_{t \in T} (\lambda_{n(g)t} P_{gt} - TC(P_{gt})) + UL_g^1 \quad (2)$$

$$UL_g^2 = \begin{cases} -\Pi_g^1 & \text{if } \Pi_g^1 < 0 \\ 0 & \text{otherwise} \end{cases} \quad (3)$$

$$UL_g = UL_g^1 + UL_g^2 \quad (4)$$

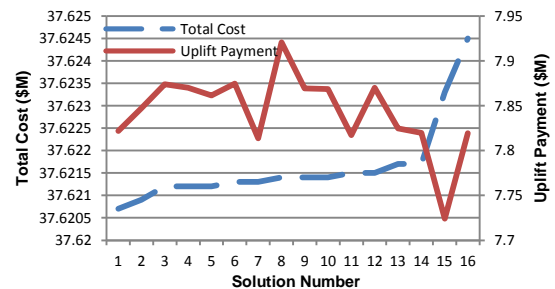


Figure 1. Total uplift payment versus total system cost

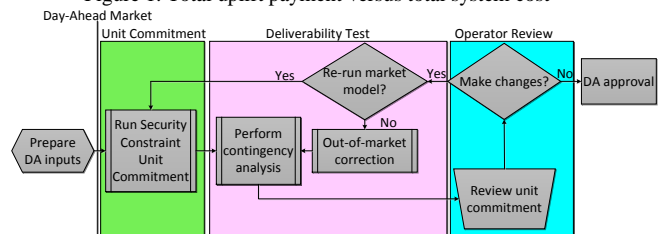


Figure 2. Day-ahead scheduling process

## References

- [1] M. Sahraei-Ardakani, M. Abdi-Khorsand, and K. W. Hedman, "The Economic Implications of Augmented Objectives in Non-Convex Electricity Markets: The Role of Uplift Payments," *Submitted to Journal of Regulatory Economics*.
- [2] Y. Al-Abdullah, M. Abdi-Khorsand, and K. W. Hedman, "The Role of Out-of-Market Corrections in Day-Ahead Scheduling," *Submitted to IEEE Transactions on Power Systems*.
- [3] Y. Al-Abdullah, M. Abdi-Khorsand, and K. W. Hedman, "Analyzing the Impacts of out-of-Market Corrections," *In Proc. of 2013 IREP Symposium-Bulk Power System Dynamics and Control-IX (IREP)*, Rethymnon, Greece, Aug. 2013.

# Real time monitoring of area stress via the susceptance and angle across the area

Atena Darvishi                      Ian Dobson  
 Electrical and Computer Engineering Department  
 Iowa State University, Ames IA USA  
 darvishi@iastate.edu, dobson@iastate.edu

**Abstract**—We apply the new concept of area angle to measure the stress caused by the single line outages inside the area. Area angle is a combination of voltage angles around the border of the area. Both simple and practical examples are given to show that the variation of the area angle for single line outages can be approximately related to changes in the overall susceptance of the area and the area stress caused by line outages.

## I. INTRODUCTION

The angle across an area of a power system is a weighted combination of synchrophasor measurements of voltage phasor angles around the border of the area [1].

We previously showed how area angle responded to single line outages inside the area in some simple Japanese test cases [2]. Here we want to show and explain how the area angle can track the severity of the outage inside the area and how it can be related to the changes in the overall susceptance of the area.

$$\theta_{\text{area}}^{(i)} \approx \frac{P_{\text{area}}}{b_{\text{area}}^{(i)}} \quad (1)$$

To better understand the relationship between the susceptance of the area and the area voltage angle we will first give a simple example.

## II. SIMPLE EXAMPLE

Consider a very simple case of 3 parallel lines connecting bus  $a$  to bus  $b$  with respective susceptances  $b_1$ ,  $b_2$ , and  $b_3$ . Power  $P_a$  is generated at bus  $a$  and consumed at bus  $b$ . In this simple case, the area susceptance  $b_{\text{area}} = b_1 + b_2 + b_3$  is the sum of the line susceptances and the area angle  $\theta_{\text{area}} = \theta_a - \theta_b$  is the angle difference between the voltages at bus  $a$  and  $b$ , and the equivalent power through the area  $P_{\text{area}} = P_a$ . In the base case,

$$\theta_{\text{area}} = \frac{P_{\text{area}}}{b_{\text{area}}} = \frac{P_a}{b_1 + b_2 + b_3} \quad (2)$$

If line 1 outages, the power flowing through the area  $P_{\text{area}} = P_a$  remains constant, the area susceptance decreases to  $b_{\text{area}}^{(1)} = b_2 + b_3$ , and the area angle increases to

$$\theta_{\text{area}}^{(1)} = \theta_{\text{area}}^{[1]} = \theta_a^{(1)} - \theta_b^{(1)} = \frac{P_{\text{area}}^{(1)}}{b_{\text{area}}^{(1)}} = \frac{P_a}{b_{\text{area}}^{(1)}} = \frac{P_a}{b_2 + b_3} \quad (3)$$

The voltage angle increase reflects the decreased susceptance in the network and the increased area stress. We also have  $\theta_{\text{area}}^{(2)} = P_a/b_{\text{area}}^{(2)}$  and  $\theta_{\text{area}}^{(3)} = P_a/b_{\text{area}}^{(3)}$ , and it can be seen that outaging the line with the largest susceptance gives the largest increase in area angle.

## III. RESULTS FOR ANGLE ACROSS AN AREA OF WECC

We illustrate the use of area angles and area susceptance to monitor single, non-islanding line outages inside a specific area of the WECC system. This area contains roughly Washington and Oregon. The northern border is near the borders of Canada-Washington, Washington-Montana and Oregon-Idaho, and the south border is near the Oregon-California border.

We are interested in monitoring the north-south area stress with the area angle when there are single non-islanding line outages, and relating changes in the area angle to the area susceptance and the outage severity. We take out each line in the system in turn and calculate the monitored area angle  $\theta_{\text{area}}^{(i)}$  and the area susceptance  $b_{\text{area}}^{(i)}$  in each case. We consider the maximum power coming to the area as a measure of the severity of the outage. Both the area angle and the area susceptance track the severity of the outage for each line outage in Figure 1. The similar patterns of changes in the area angles and the severity of the outage confirm the relationship between area angle and the severity of the outage.

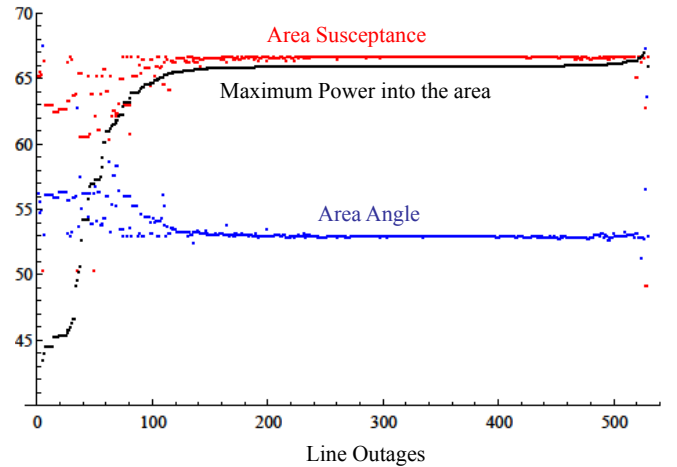


Fig. 1. Area angle  $\theta_{\text{area}}^{(i)}$ , area susceptance  $b_{\text{area}}^{(i)}$ , and max power into the area for each line outage in WECC area. Base case (the point at extreme right) is  $\theta_{\text{area}} = 52.9^\circ$ ,  $b_{\text{area}} = 66.7$  pu, max power = 66.0 pu.

## REFERENCES

- [1] I. Dobson, Voltages across an area of a network, *IEEE Transactions on Power Systems*, vol. 27, no. 2, May 2012, pp. 993-1002.
- [2] A. Darvishi, I. Dobson, A. Oi, C. Nakazawa, Area angles monitor area stress by responding to line outages, NAPS North American Power Symposium, Manhattan KS USA, September 2013.



# Co-Simulation Platform for Smart Grid OPF

Adnan Anwar, Abdun Naser Mahmood  
 School of Engineering and Information Technology  
 University of New South Wales, Canberra, Australia  
 Email: Adnan.Anwar@adfa.edu.au, Abdun.Mahmood@unsw.edu.au

**Abstract**—Distribution Management System (DMS), which is the brain of the future smart grid, needs to incorporate advanced planning and analysis functionalities for smooth and efficient operation of power distribution system. Optimal Power Flow (OPF), which is a powerful tool for solving numerous DMS applications, requires to address smart grid challenges and requirements. In this paper, an Unbalanced Multi-phase OPF (UM-OPF) technique based on a co-simulation platform is proposed for planning and extended real-time operation of a smart grid. During the formulation of the proposed algorithm, multi-phase power distribution system is considered which has unbalanced loadings, voltage control and reactive power compensation devices. For the optimization purpose, constriction factor particle swarm intelligence is used to achieve a global optimum solution of different smart grid OPF problems. The assessment of the proposed multi-phase OPF technique is performed based on the IEEE 123-bus test distribution system.

## I. KEY EQUATIONS

The problem of UM-OPF can be formulated as [1], [2]:

$$\min f_{obj}(\mathbf{x}, \mathbf{u}) \quad (1)$$

subject to

$$\mathbf{g}(\mathbf{x}, \mathbf{u}) = 0 \quad (2)$$

$$\mathbf{h}(\mathbf{x}, \mathbf{u}) \leq 0 \quad (3)$$

Here  $f_{obj}$  is the objective function which needs to be minimized,  $\mathbf{x}$  is the vector of dependent variables,  $\mathbf{u}$  is the vector of independent variables which are generally different power system parameters. In (2),  $\mathbf{g}$  is the set of equality constraints which are basically load-flow equations and  $\mathbf{h}$  represents the set of inequality constraints shown in (3).

## II. SOLUTION FRAMEWORK AND TEST SYSTEM

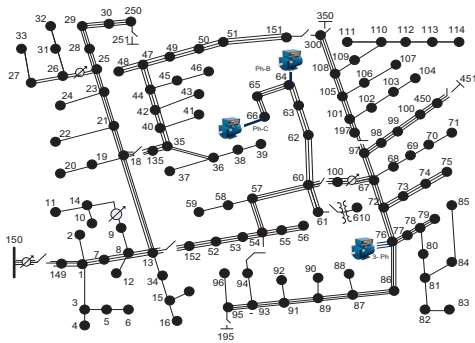


Fig. 1. 123 node test feeder with DG

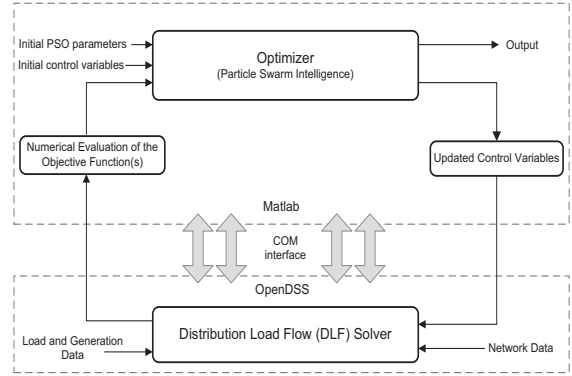


Fig. 2. Co-Simulation platform for UM-OPF

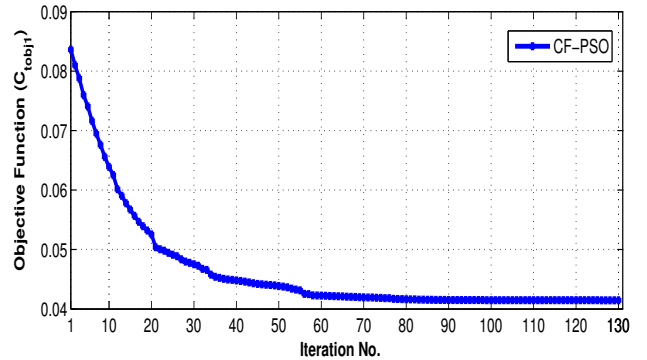


Fig. 3. Convergence behavior of the CF-PSO based UM-OPF

## III. RESULTS

TABLE I  
 COMPARISON OF THE OPTIMUM EMPLOYMENT OF DG WITH BASE CASE

Method	Loss (kW)	$I_a$ (A)	$I_b$ (A)	$I_c$ (A)
Base Case	155.38	804.00	523.88	643.69
Case with optimum DG	48.40	416.67	138.40	214.33

## REFERENCES

- [1] A. Anwar and H. Pota, "Optimum capacity allocation of DG units based on unbalanced three-phase optimal power flow," in *IEEE PES General Meeting*, Jul. 2012.
- [2] S. Bruno, S. Lamonaca, G. Rotondo, U. Stecchi, and M. La Scala, "Unbalanced three-phase optimal power flow for smart grids," *IEEE Transactions on Industrial Electronics*, vol. 58, no. 10, pp. 4504–4513, 2011.

# A Multi-input Lead-Lag Power System Stabilizer with $H_\infty$ Control Performance

Junnosuke Kobayashi, Keisuke Suzuki, and Shinichi Iwamoto  
 Power Systems Laboratory, Department of Electrical Engineering and Bioscience,  
 Waseda University, Tokyo, 169-8555, JAPAN  
 Email: iwamoto.lab.pwrs@gmail.com

**Abstract--** We propose a method of designing a low-dimensional multi-input power system stabilizer (PSS) that achieves  $H_\infty$  performance. In recent years, robust PSS designs that adopt an  $H_\infty$  controller have been investigated as a method to guarantee performance when the state of the system and power flow change. Although  $H_\infty$  controllers offer highly robust control, they have not been adopted in practice because of the complex theory and intricate structure involved. Thus, to obtain high robustness, we consider the  $H_\infty$  problem under the assumption that the PSS structure is fixed as a lead-lag compensator. To satisfy this assumption, we use an additional reactive power input to the PSS [1]. The parameter of the multi-input lead-lag PSS is optimized by particle swarm optimization, which provides an evaluation function that satisfies a closed-loop  $H_\infty$  norm to yield the desired response. The validity of the proposed PSS is demonstrated on a 3-machine 9-bus system model [2].

**Index Terms—**Dimensional reduction, H-infinity control theory, Lead-lag compensation, Multi-input PSS, Particle Swarm Optimization, PSS.

## I. KEY EQUATIONS

$$T_{ZW} = G_{11}(s) + \frac{G_{12}(s)G_{21}(s)K(s)}{1 - G_{22}(s)K(s)} \dots\dots\dots (1)$$

$$\|T_{ZW}\|_\infty = \sup \frac{\|z\|_2}{\|w\|_2} < g \dots\dots\dots (2)$$

## II. KEY FIGURES

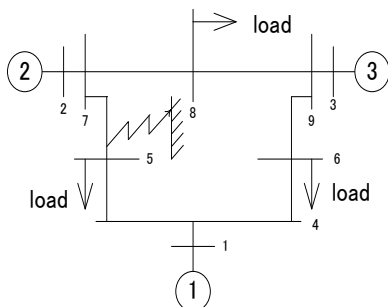


Fig. 1. 3-machine 9-bus system

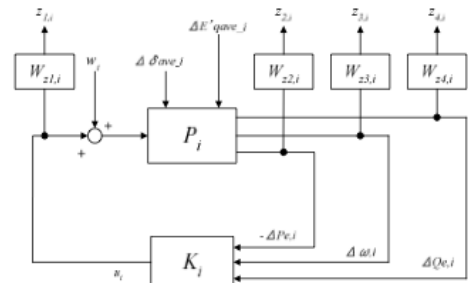


Fig. 2. Generator control system model of each subsystem

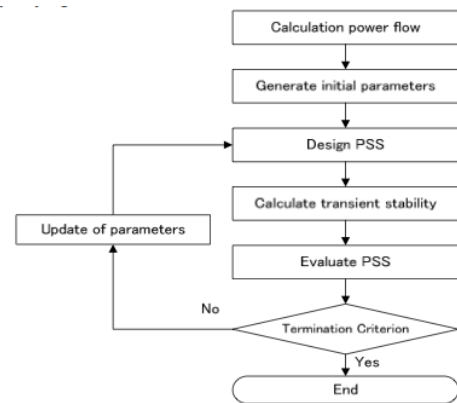


Fig. 3. Flowchart of the proposed PSS parameter tuning

## III. KEY RESULTS

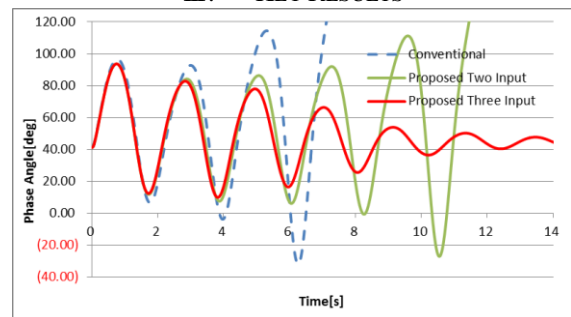


Fig. 4. Phase angle of generator 2 when a fault occurred (fault5-other7)

## IV. REFERENCES

- [1] Y. Kitauchi, H. Taniguchi, T. Shirasaki, Y. Ichikawa, M. Amano, and M. Banjo, "Experimental verification of multi-input PSS with reactive power input for damping low frequency power swing", *IEEE Trans.*
- [2] P.M. Anderson, and A.A. Fouad, "Power System Control and Stability", *The Iowa University Press* (1977).

# Voltage and Reactive Power Control by using PV Power Factor and Var Controllers for Large Scale PV Penetration

Takayuki Ito, Shunsuke Aida, Shinichi Iwamoto

Power Systems Laboratory, Department of Electrical Engineering and Bioscience, Waseda University, Tokyo, 169-8555, Japan

Email: [iwamoto.lab.pwrs@gmail.com](mailto:iwamoto.lab.pwrs@gmail.com)

**Abstract**—In Japan, introduction of a large capacity of photovoltaic (PV) power is planned to solve environmental problems. The Japanese government has set the target amount of PV penetration 53GW by 2030. However, a large penetration of PV will cause several problems in power systems. One of these problems is the increase in voltage from decreased load demands associated with the active power output of PV systems. Another problem is voltage fluctuation caused by PV system output variation. In this paper, voltage and reactive power control for large penetration of PV is investigated. First, a var controller (VC) control by using VMPI-i sensitivity is proposed, where VC is defined as a general term for both static capacitor and a shunt reactor. Second, a coordinating control for the power factor of PV system (PF) and VCs is proposed. In the proposed method, voltage fluctuation is controlled by PF regulation and voltage increase is controlled by VCs. Simulations are carried out with the Ward-Hale system to verify the validity of the proposed method.

**Index Terms**—Higher Voltage System, Photovoltaic Power, Voltage and Reactive Power Control, Var Controller, Power Factor

## I. KEY EQUATIONS

<Specified Vector>

$$y = \begin{bmatrix} e_{slack} & f_{slack} & P_{Gen} & V_{Gen} & P_{Load} & Q_{Load} \end{bmatrix}^T$$

<Objective Function>

minimize  $f = k$  (for calculating  $y_{upper}$ ) or  $-k$  (for calculating  $y_{lower}$ )

<Equality Constraint>

$$\begin{aligned} P_{Gen} &= k \cdot P_{Gen}, & V_{Gen} &= V_{Gen} & V_{min} &< V_{Load,i} < V_{max} \\ P_{Load} &= k \cdot P_{Load}, & Q_{Load} &= k \cdot Q_{Load} & P_{Gen,min} &< P_{Gen} < P_{Gen,max} \\ e_{Slack} &= e_{Slack}, & f_{Slack} &= f_{Slack} & Q_{Gen,min} &< Q_{Gen} < Q_{Gen,max} \end{aligned}$$

<VMPI-i & VMPI-i VC Sensitivity>

$$VMPI-i_{upper} = \begin{cases} \cos^{-1} \frac{y_s^T \cdot y_{upper}}{\|y_s\| \cdot \|y_{upper}\|} & (\|y_s\| > \|y_{upper}\|) \\ -\cos^{-1} \frac{y_s^T \cdot y_{upper}}{\|y_s\| \cdot \|y_{upper}\|} & (\|y_{upper}\| > \|y_s\|) \end{cases}$$

$$VMPI-i_{lower} = \begin{cases} \cos^{-1} \frac{y_s^T \cdot y_{lower}}{\|y_s\| \cdot \|y_{lower}\|} & (\|y_{lower}\| > \|y_s\|) \\ -\cos^{-1} \frac{y_s^T \cdot y_{lower}}{\|y_s\| \cdot \|y_{lower}\|} & (\|y_s\| > \|y_{lower}\|) \end{cases}$$

$$VMPI-i \text{ VC Sensitivity} = \begin{bmatrix} \frac{\Delta VMPI_i}{\Delta VC_1} & \dots & \frac{\Delta VMPI_i}{\Delta VC_j} & \dots & \frac{\Delta VMPI_i}{\Delta VC_n} \\ \vdots & \ddots & \vdots & \ddots & \vdots \\ \frac{\Delta VMPI_i}{\Delta VC_1} & \dots & \frac{\Delta VMPI_i}{\Delta VC_j} & \dots & \frac{\Delta VMPI_i}{\Delta VC_n} \\ \vdots & \ddots & \vdots & \ddots & \vdots \\ \frac{\Delta VMPI_m}{\Delta VC_1} & \dots & \frac{\Delta VMPI_m}{\Delta VC_j} & \dots & \frac{\Delta VMPI_m}{\Delta VC_n} \end{bmatrix}$$

## II. KEY FIGURE

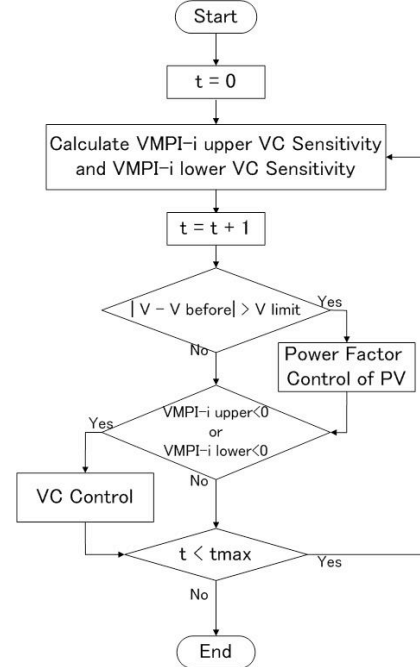


Figure 1 Flowchart of the Proposed Method

## III. KEY RESULTS

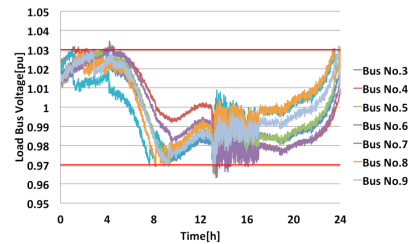


Figure 2 Load Bus Voltages with Only SC Control

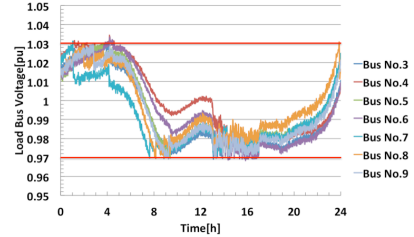


Figure 3 Load Bus Voltages with Both SC and PF of PV Control (Proposed Method)

## IV. REFERENCES

- [1] Y. Kataoka, M. Watanabe and S. Iwamoto, "A New Voltage Stability Index Considering Voltage Limits", 2006 IEEE PES PSCE '06, Nov. 1 2006, pp.1878 – 1883, Oct 2006.
- [2] A. Enomoto, S. Aida and S. Iwamoto, "Capacitor control considering voltage stability for large penetration of photovoltaic power", 2012 IEEE PES General Meeting, PESGM2012-001154.PDF

# Verification of Voltage Ride-Through Capability of Wind Turbines Using Reachability Analysis

Hugo N. Villegas Pico, *Student Member, IEEE* and Dionysios C. Aliprantis, *Senior Member, IEEE*

**Abstract**—Wind turbines are required to meet grid interconnection codes for voltage ride-through, which mandate that they should not disconnect during a specified range of grid disturbances. One of the tasks of a turbine’s design verification process is to ensure that it will be able to withstand any such event. In this poster, reachability theory is employed to find sets that enclose all possible trajectories of a Type-3 wind turbine caused by a given set of unknown-but-bounded disturbances. The proposed method can provide assurance as to whether the currents and voltages of a wind turbine will remain within acceptable bounds.

**Index Terms**—Converters, power system faults, reachability analysis, wind power generation.

## I. INTRODUCTION

INTEGRATION of wind energy sources presents various challenges at the system and device level. This poster focuses on a technical problem at the turbine level, namely, the dynamic response of wind turbines to grid disturbances, commonly referred to as voltage ride-through (VRT) capability.

Wind turbines are required to meet grid interconnection codes for VRT, which mandate that they should not disconnect during a specified range of grid disturbances. An example of a ‘no tripping zone’ for North America is shown in Fig. 1. Turbine’s engineers face the design verification task of ensuring that it will be capable of safely withstanding any conceivable terminal voltage disturbance that lies within the ‘no tripping zone’. This poster addresses this issue by using reachability theory to find sets that enclose all possible trajectories of the states of a system driven by given unknown-but-bounded voltage disturbances.

One of the most common examples is the Type-3 turbine that employs a doubly-fed induction generator as shown in Fig. 2. Reachable sets for uncertain faulted symmetric voltages at the terminals of a DFIG are presented in Fig. 3 which are computed following [1]. The proposed method can provide assurance with regards to whether the turbine’s currents and voltages will remain within acceptable bounds.

## REFERENCES

- [1] H. N. Villegas-Pico and D. C. Aliprantis, “Voltage ride-through capability verification of wind turbines with fully-rated converters using reachability analysis,” *IEEE Trans. Energy Convers.*, to appear 2014.

H. N. Villegas Pico and D. C. Aliprantis are with the School of Electrical and Computer Engineering, Purdue University, West Lafayette, IN 47907, USA (e-mail: {hvillega, dionysis}@purdue.edu).

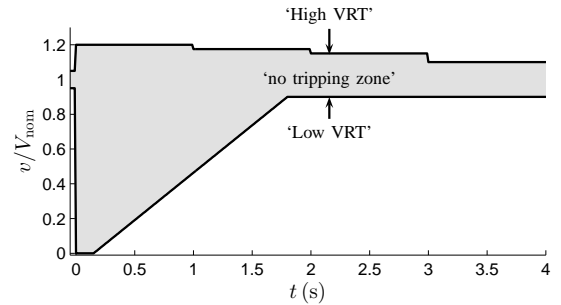


Fig. 1. Western Electricity Coordinating Council (WECC) VRT envelope standard. The voltage magnitude  $v$  is measured at the high-voltage side of the interconnection with the bulk electric system.  $V_{nom}$  is the nominal grid voltage.

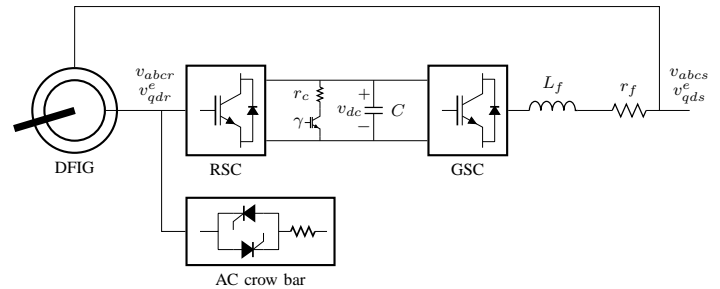


Fig. 2. DFIG turbine drive system.

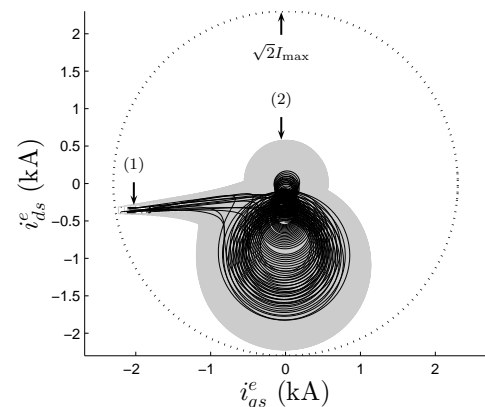


Fig. 3. Evolution of reachable sets of DFIG stator currents (gray) with deterministic trajectories (black). (1) Reachable set at  $t = 0$  s (uncertain initial condition). (2) Reachable sets for  $t \in [0, 0.15]$  s (encloses all possible trajectories).

# Subspace Algorithms for Power System Oscillation Monitoring

Tianying Wu, S. A. Nezam Sarmadi and Vaithianathan “Mani” Venkatasubramanian

The School of Electrical Engineering and Computer Science

Washington State University

Pullman, WA 99163, USA

Email: [tianying.wu@email.wsu.edu](mailto:tianying.wu@email.wsu.edu), [snezamsa@eecs.wsu.edu](mailto:snezamsa@eecs.wsu.edu) and [mani@eecs.wsu.edu](mailto:mani@eecs.wsu.edu)

**Abstract**—With synchrophasors getting installed widely across the power grid, measurement based oscillation monitoring algorithms are becoming increasingly useful in identifying the real-time oscillatory modal properties in power systems. They extract the critical electromechanical mode information, such as mode frequency, damping ratio and mode shapes from wide-area PMU data, and can detect presence of poorly damped or growing oscillations in their early stages. Appropriate control actions can then be initiated to damp out the oscillations before they become problematic. There are two types of measurement data available through PMUs: ring-down and ambient data. The first one is the response to a sudden disturbance such as outage of a generator or line tripping. The other one is the measurement data when the system is operating at its steady state. Fig. 1 shows an example of both types of data. Two ring-downs can be found in the time plots, and the ambient data are before and after the ring-downs. Different algorithms are applied for these two types of data. This study focuses on an ambient oscillation monitoring algorithm namely, Stochastic Subspace Identification (SSI) method. The simulation data of Kundur two-area system as shown in Fig. 2 are used to analyze the performance of SSI method. We also compare the estimation results with ring-down analysis algorithms such as Prony, Matrix Pencil, HTLS and ERA. Experimental results demonstrate that, the SSI method gives accurate estimations of the frequency and damping ratio and can therefore identify the oscillation modes successfully in the test system. This ambient data based SSI method is more attractive than the ring-down algorithms, because unlike the ring-down data which can only be obtained after disturbances, the ambient data are always available in power systems.

## I. KEY FIGURES

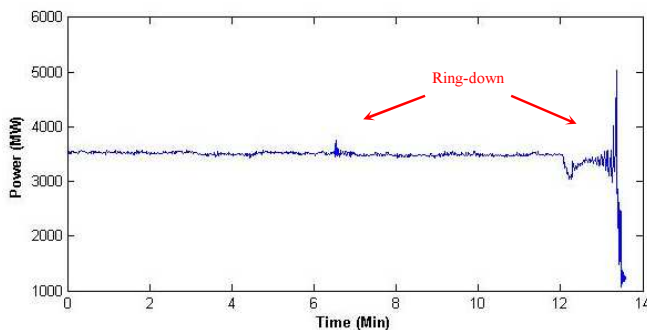


Fig. 1. Measurement data from PMUs.

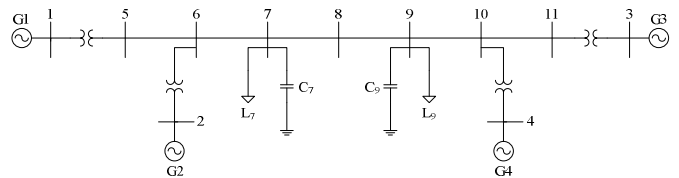


Fig. 2. Kundur two-area test system.

## II. KEY RESULTS

TABLE I  
ESTIMATION RESULTS OF TWO-AREA SYSTEM USING SSI

$l$	$2l$	Size of $H$	$f$ (Hz)		$\zeta$ (%)	
			Mean	Std	Mean	Std
3	6×30	270×270	0.624	0.007	4.609	0.844
	10×30	450×450	0.625	0.007	4.620	1.081
10	6×30	900×900	0.625	0.007	4.509	0.828
	10×30	1500×1500	0.624	0.009	4.490	1.037

## REFERENCES

- [1] H. Ghasemi, C. Canizares and A. Moshref, "Oscillatory Stability Limit Prediction Using Stochastic Subspace Identification," *IEEE Trans. on power syst.*, vol.21, no.2, pp. 736-745, May 2006.
- [2] N. Zhou, J. W. Pierre, and J. F. Hauer, "Initial results in power system identification from injected probing signals using a subspace method," *IEEE Trans. Power Syst.*, vol.21, no.3, pp. 1296-1302, Aug. 2006.
- [3] S. A. Nezam Sarmadi, and V. Venkatasubramanian, "Electromechanical mode estimation using recursive adaptive Stochastic Subspace Identification", *IEEE Trans. Power Syst.*, vol.29, no.1, pp. 349-358, Jan. 2014.

# Stochastic Look-ahead Dispatch with Intermittent Renewable Generation via Progressive Hedging and L-shaped Method

Yingzhong Gu, *Student Member, IEEE*, Le Xie, *Member, IEEE*  
Email: lxie@ece.tamu.edu

**Abstract**— Due to the continuous growth in renewable penetration, the increasing complexity in managing operational uncertainty in near-real-time may not be fulfilled by deterministic dispatch. Starting from our earlier work on look-ahead dispatch, we explore the benefits and implementation feasibility of stochastic real-time look-ahead dispatch. In order to implement a large scale stochastic programming for real-time operation, an innovative parallel computing algorithm is developed. The algorithm has hybrid architecture of progressive hedging and L-shaped method, which can reduce the original problem's size significantly and solve the problem efficiently. Theoretical studies on the computational complexity are performed. Numerical experiments of a modified IEEE RTS 24 bus system as well as a practical 5889 bus system are conducted to illustrate the effectiveness and efficiency of this proposed algorithm.

## I. KEY EQUATIONS

### A. Mathematical Formulation

A stochastic look-ahead dispatch model can be written as follows:

$$\min : f = \sum_{k \in T_1} \sum_{i \in G} C_{G_i, s_0} P_{i, s_0}^k + \sum_{s \in S} \rho_s \sum_{k \in T_1} \sum_{i \in G} C_{G_i, s} P_{i, s}^k + R_s^k$$

Subject to:

$$Ax = b, x \geq 0 \quad (2)$$

$$Tx + Wy_s = h, y \geq 0, \forall s \in S, \quad (3)$$

where  $s$  is the indicator of each scenario,  $P(s)$  is the occurrence probability of scenario  $s$ ,  $y_s$  is the vector of the second-stage decision variables of scenario  $s$ .

In order to solve the problem, the progressive hedging algorithm is applied. We formulate the initial sub-scenario problem in (4)-(6). By solving this problem for each scenario, a set of deterministic optimal solutions corresponding to each scenario is established.

$$\min : f = c^T x_s + q^T y_s \quad (4)$$

Subject to:

$$Ax_s = b, x_s \geq 0 \quad (5)$$

$$Tx_s + Wy_s = h, y \geq 0, \forall s \in S. \quad (6)$$

For each iteration, an auxiliary sub-scenario problem is

solved.

$$\min : f = c^T x_s + q^T y_s + w_s^{k-1} x_s + 0.5\rho \|x_s - \bar{x}^{k-1}\|^2$$

Subject to:

$$Ax = b, x \geq 0, \quad (7)$$

$$Tx + Wy_s = h, y \geq 0, \forall s \in S. \quad (8)$$

In the auxiliary sub-scenario problem, the multiplier term  $w_s^{k-1} x_s$  forces the scenario decision variables to change in the direction toward the mean solution while the penalty term  $0.5\rho \|x_s - \bar{x}^{k-1}\|^2$  keeps the optimal solution within a certain neighborhood of the mean solution for the sake of convergence stability.

## II. KEY FIGURES

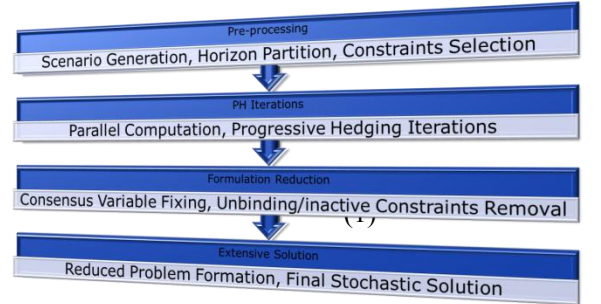


Fig. 1. ENHANCED PROGRESSIVE HEDGING ALGORITHM

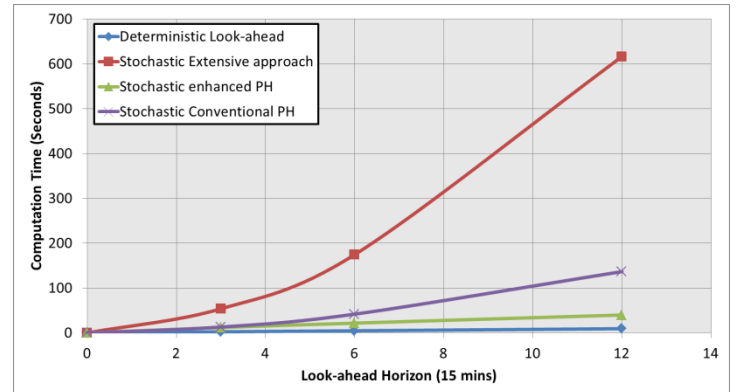


FIG. 2 COMPUTATION TIME FOR 1 DAY STOCHASTIC LOOK-AHEAD SCHEDULING SIMULATION (UNIT: SECONDS)



# Investigating the Sensitivity of Frequency Response Analysis on Transformer Winding Structure

M. F. M. Yousof<sup>1,2,\*</sup>, T. K. Saha<sup>1</sup> and C. Ekanayake<sup>1</sup>

<sup>1</sup>The School of Information Technology and Electrical Engineering, The University of Queensland, Brisbane, Australia

<sup>2</sup>Faculty of Electrical and Electronic Engineering, Universiti Tun Hussein Onn Malaysia, Batu Pahat, Malaysia

\*fairouz@ieee.org

**Abstract**—This paper investigates the sensitivity of frequency response analysis (FRA) on the structure of transformer winding. Frequency response of a winding is simulated using the multi-conductor transmission line (MTL) model based on the winding parameter. Subsequently, several responses of the same winding are also simulated with varying its original parameter. This is to observe the winding response sensitivity. This paper also studies the response sensitivity on mechanical deformation for three different windings. It is to determine whether a deformation will produce similar response changes of any winding. Additionally, three statistical indicators are employed to measure the sensitivity and assess the performance of each indicator.

## I. MECHANICAL DEFORMATION

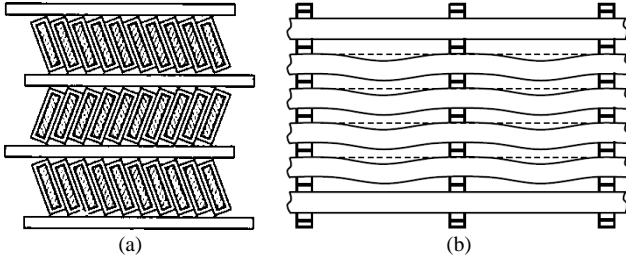


Fig. 1 Winding deformation. (a) The tilting of conductors. (b) The bending of conductors.

## II. METHODOLOGY

TABLE I  
PARAMETERS OF THREE DIFFERENT WINDINGS

Parameters	A	B	C
Arrangement	Interleaved	Continuous	Continuous
Number of disc	40	60	62
Number of turn per disc	14	9	6
Conductor height	5.6 mm	9 mm	6 mm
Conductor height with insulation	6 mm	10 mm	8.4 mm
Conductor width	1.2 mm	2.5 mm	3 mm
Conductor width with insulation	1.6 mm	3.5 mm	5.4 mm
Inter-winding insulation thickness	3 mm	4 mm	24.4 mm

$$C_t = \frac{2\pi d}{\ln(r_{2,inner}/r_{1,outer})} \quad (1)$$

$$C_d = \frac{\pi \epsilon (r_{outer}^2 - r_{inner}^2)}{d} \quad (2)$$

$$C_w = \frac{2\pi d}{\ln(r_{HV}/r_{LV})} \quad (3)$$

## III. SENSITIVITY ANALYSIS ON THE WINDING

### A. Winding Response Sensitivity: Winding Parameter

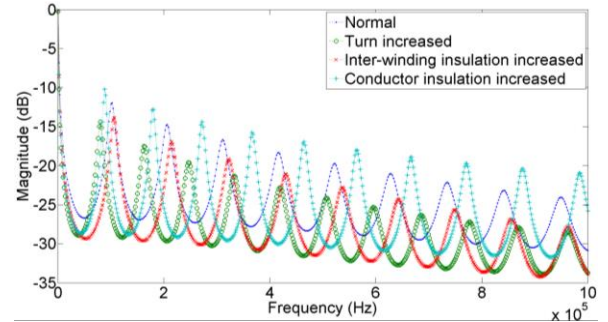


Fig. 2 Sensitivity of winding response on variation of parameters.

### B. Winding Response Sensitivity: The Tilting of Conductors

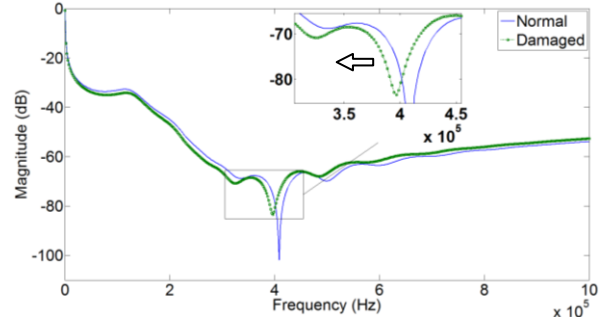


Fig. 3 Frequency response of normal and damaged winding A due to the tilting of conductors.

### C. Winding Response Sensitivity: The Axial Bending of Conductors

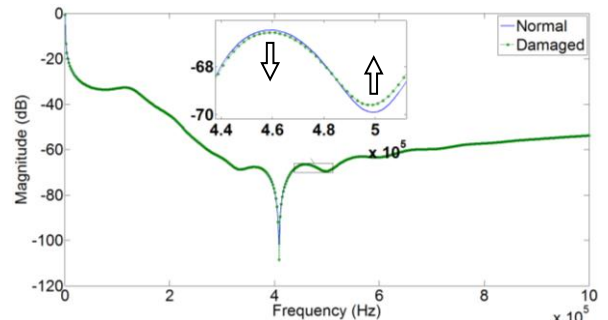


Fig. 4 Frequency response of normal and damaged winding A due to the bending of conductors.



# Piecewise Affine Dispatch Policies for Economic Dispatch under Uncertainty

Daniel Munoz-Alvarez, Eilyan Bitar and Lang Tong

Jianhui Wang

**Abstract**—As renewable energy resources increase their share of aggregate supply in electric power systems, the need for strategies capable of accommodating significant intermittency and uncertainty in supply becomes critical. From an operational perspective, a central challenge resides in designing resource procurement and dispatch policies that optimally trade-off the evolution of information against cost, while retaining computational tractability.

We deal with the problems of (i) characterizing socially optimal policies for economic dispatch within a class of admissible policies to compensate pervasive uncertainty in supply and demand, and (ii) the design of a two-settlement market that yields the said outcome as a market equilibrium between rational and price-taking participants.

## I. SUMMARY OF CONTRIBUTIONS

We extend the work in [10] by leveraging on decision rule techniques for stochastic optimization developed in [12] as follows: First, we compute continuous piecewise affine (CPWA) dispatch policies for the economic dispatch problem and show they outperform affine policies in [10]. Second, consider a two-settlement market based on derived ex-ante and ex-post nodal energy prices, where the derived policies and prices support a competitive equilibrium. Finally, the derived ex-post prices are showed to be CPWA functions of the system uncertainties.

## II. PROBLEM FORMULATION

1) *Notation*: We consider a set  $\mathcal{I} = \{1, \dots, I\}$  of market participants and a set  $\mathcal{B} = \{1, \dots, B\}$  of buses. The system uncertainties are denoted by  $\boldsymbol{\xi} \in \Xi \subset \mathbb{R}^k$ . The individual reserve ranges and dispatches are given by  $[\underline{r}_i, \bar{r}_i] \subset \mathbb{R}$  and  $u_i \in \mathbb{R}$ , respectively. Moreover,  $g_i(\mathbf{r}_i, u_i)$  denotes the quadratic cost/benefit functions of participants and  $\mathcal{U}_i(\mathbf{r}_i, \boldsymbol{\xi})$  denotes the individual polytopic dispatch constraints. Finally,  $\mathcal{S}^N$  and  $\mathcal{S}^B$  denote the polytope of transmission network capacity limits and the affine hyperplane corresponding to the power balance equation, respectively.

2) *Dispatch Policy as Solution Concept*: The presence of uncertainty requires a dispatch policy instead of a single dispatch. To that end, we restrict our search to the class of disturbance *feedback* dispatch policies that are CPWA over a predefined partition  $\mathcal{L}$  of  $\Xi$ , i.e.,

$$\mu_i \in \mathcal{U}^{\mathcal{L}} := \{\mu : \Xi \rightarrow \mathbb{R} \mid \mu \text{ is CPWA over } \mathcal{L}\}, \text{ and}$$

D. Munoz-Alvarez, E. Bitar, and L. Tong (dm634,eyb5,lt35@cornell.edu) are with the School of Electrical and Computer Engineering at Cornell University, Ithaca, New York, and J. Wang (jianhui.wang@anl.gov) is with the Division of Decision and Information Sciences at Argonne National Laboratory, Lombard, IL.

$$\pi \in \Pi^{\mathcal{L}} := \mathcal{U}^{\mathcal{L}} \times \dots \times \mathcal{U}^{\mathcal{L}}.$$

Among these, we are interested only in *feasible* policies, i.e.,

$$\mu_i \in \mathcal{U}_i^{\text{feas}} := \{\mu \in \mathcal{U}^{\mathcal{L}} \mid \mu(\boldsymbol{\xi}) \in \mathcal{U}_i(\mathbf{r}_i, \boldsymbol{\xi}) \text{ a.s.}\}, \text{ and}$$

$$\pi \in \Pi^{\text{feas}} := \{\pi \in \Pi^{\mathcal{L}} \mid \mu_i \in \mathcal{U}_i^{\text{feas}}, \pi(\boldsymbol{\xi}) \in \mathcal{S}^B \cap \mathcal{S}^N \text{ a.s.}\}.$$

3) *Two-Settlement Market*: We consider a mandatory two-settlement market with ex-ante and ex-post nodal prices  $\lambda_b^0 \in \mathbb{R}$  and  $\lambda_b : \Xi \rightarrow \mathbb{R}$  for each bus  $b \in \mathcal{B}$ . Each participant's profit is given by

$$P_i(\mathbf{r}_i, u_i; \mu_i^0, \lambda_{b(i)}(\boldsymbol{\xi}), \lambda_{b(i)}^0) := \mu_i^0 \lambda_{b(i)}^0 + (u_i - \mu_i^0) \lambda_{b(i)}(\boldsymbol{\xi}) - g_i(\mathbf{r}_i, u_i).$$

4) *Participant's Problem*: Assuming rational price-taking participants, each participant's problem becomes

$$\mathcal{P}_i : \max_{\mathbf{r}_i, \mu_i \in \mathcal{U}_i^{\text{feas}}} \mathbb{E} P_i(\mathbf{r}_i, \mu_i(\boldsymbol{\xi}); \mu_i^0, \lambda_{b(i)}(\boldsymbol{\xi}), \lambda_{b(i)}^0)$$

5) *Independent System Operator's Problem*: As a social planner, the ISO is interested in implementing a feasible policy that minimizes the expected cost of operating the system. That is, to solve

$$\mathcal{P}_{\text{so}} : \min_{\mathbf{r}, \pi \in \Pi^{\text{feas}}} \mathbb{E} \sum_{i \in \mathcal{I}} g_i(\mathbf{r}_i, \mu_i(\boldsymbol{\xi})).$$

To do that, the ISO can set ex-ante dispatches and prices  $(\mu^{0*}, \lambda^{0*})$  and ex-post prices  $\lambda^*$  such that these induce a socially optimal dispatch decision  $\mu_i^*$  and reserve range  $\mathbf{r}_i^*$  in each participant's problem  $\mathcal{P}_i$ .

6) *Main Results*:

- 1) An optimal solution to  $\mathcal{P}_{\text{so}}$  can found by solving a quadratic programming problem whose size is linear in the system data.
- 2) Such solution to  $\mathcal{P}_{\text{so}}$  produces dual multipliers that give closed form expressions to ex-ante prices  $\lambda_b^0 \in \mathbb{R}$  and ex-post CPWA prices  $\lambda_b : \Xi \rightarrow \mathbb{R}$  for each bus  $b \in \mathcal{B}$ .
- 3) These prices induce a socially optimal behavior in each participant, and thus they implement a socially optimal outcome.

## REFERENCES

- [1] J. Warrington, P. Goulart, S. Mariethoz, and M. Morari, "Policy-based reserves for power systems," *Power Systems, IEEE Tran. on*, vol. 28, no. 4, pp. 4427–4437, 2013.
- [2] A. Georghiou, W. Wiesemann, and D. Kuhn, "Generalized decision rule approximations for stochastic programming via liftings," *Optimization Online*, 2010.

# A Power Flow Adjustment Technique for Large Scale Generation Outages

Yuta Mori, Fumihito Nakatani, Shinichi Iwamoto

Power Systems Laboratory, Department of Electrical Engineering and Bioscience,  
Waseda University, 169-8555, Tokyo Japan

Email: [iwamoto.lab.pwrs@gmail.com](mailto:iwamoto.lab.pwrs@gmail.com)

**Abstract** — In some loop systems, considerable power flow differences between heavy and light loads may occur. Moreover, after the Great East Japan Earthquake, significant changes in the power system will likely result in even larger differences in existing loop systems. It is generally difficult to maintain or replace heavily loaded lines. For electric power facilities planning, it is thus necessary to solve such power flow problems. In this paper, we assume protracted loss of nuclear power plant generation capabilities, and examine the resulting load changes in the loop system<sup>[1][2]</sup>. We propose use of series capacitors on non-heavily loaded lines to alleviate load differences among transmission lines<sup>[3]</sup>. We also propose the concept of mitigation flow sensitivity (MFS). By installing series capacitors at effective locations and determining compensation amounts by prioritizing MFS, we solve the power flow problems. We carry out simulations for a modified IEEJ EAST 10-machine O/V system model to confirm the validity of the proposed method.

**Index Terms** — Power System, Transmission Planning, Series Capacitor, Line Flow Sensitivity

## I. KEY EQUATIONS

$$\Delta x_i = x_i \times \alpha_i$$

$$\Delta g_i = \operatorname{Re} \left( \frac{1}{r_i + j(x_i + \Delta x_i)} \right) - \operatorname{Re} \left( \frac{1}{r_i + jx_i} \right)$$

$$\Delta b_i = \operatorname{Im} \left( \frac{1}{r_i + j(x_i + \Delta x_i)} \right) - \operatorname{Im} \left( \frac{1}{r_i + jx_i} \right)$$

$$MFS = \sum (\Delta PL_{lighter}) - \sum (\Delta PL_{heavier})$$

## II. KEY FIGURES

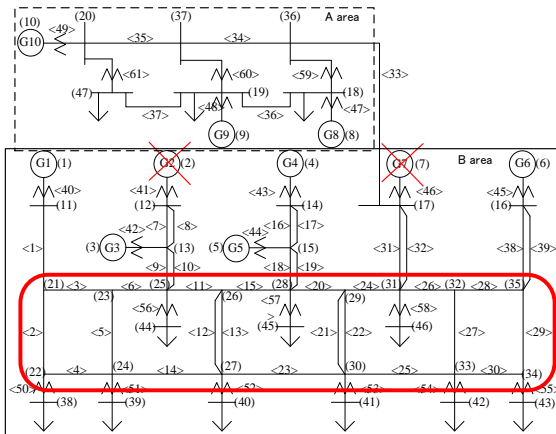


Fig.1 The modified IEEJ EAST 10-machine O/V system model

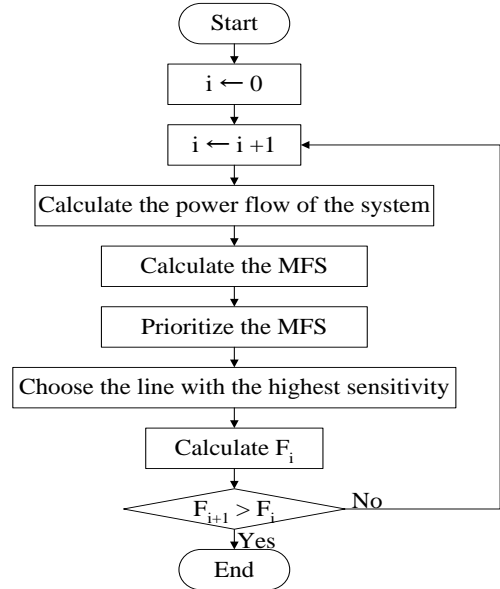


Fig.2 Flowchart of the proposed method

## III. KEY RESULTS

Table 1 Comparison of the difference the amount of active power flow

	Before generator outage	After generator outage	Proposed method
Max. power flow [pu] (line no.)	7.062 (29)	8.097 (15)	7.114 (15)
Min. power flow [pu] (line no.)	0.020 (26)	0.278 (24)	0.432 (24)
Difference between the amount of active power flow [pu]	7.042	7.819	6.682
Evaluation value F [pu]	-	15.897	13.981

## IV. REFERENCES

- [1] T. Jibiki, E. Sakakibara, S. Iwamoto, "Line Flow Sensitivities of Line Reactances for Congestion Management", IEEE PES General Meeting, 2007
- [2] Y. Takamizawa, F. Nakatani, S. Iwamoto, "A Novel Index on Transmission Renewal Planning Considering Transmission Loss and Voltage Quality", 2012 IEEE PES General Meeting, PESGM2012-001359.PDF
- [3] Sandoval N, Molina A, Petersson A, Stromberg G, Samuelsson J. : "Introduction of Series Capacitors in the Venezuelan EHV-grid", TDC '06. IEEE/PES (Transmission & Distribution Conference and Exposition), pp.1-6 (2006)

# Performance of a DC Multi-Converter Power System due to Variations of Plant Parameters

Juan C. Jimenez and Chika O. Nwankpa

Center for Electric Power Engineering, Department of Electrical and Computer Engineering, Drexel University  
Philadelphia, PA 19104, USA,  
{jcj26,con22}@drexel.edu

**Abstract**— Integration of multi-converter systems into power system infrastructures has been necessitated by the increasing popularity of microgrids, renewable energy systems and DC distribution systems. The understanding and quantification of system-level effects due to unforeseen complex dynamic interactions between power electronic converters and electromechanical equipment are dependent on a number of factors such as system architecture and parameters. In this work, the authors address the employment of a developed observability formulation applied to a DC multi-converter power system model and the effects of plant parameters such as converters' internal control gains. The observability of the system is developed through a jacobian matrix and its condition number used as a performance index.

## I. KEY EQUATIONS

The dynamics of interest in the buck-boost based multi-converter system in Fig. 1 with  $i$  source converters and  $j$  load converters are those of converters and main DC bus. Its DAE model is presented in (1) - (5).

$$\frac{dv_i}{dt} = \frac{1}{C_i} \left( i_{L_i} + k_1 i_{L_i}^2 + k_2 v_i i_{L_i} - V_{ref} i_{L_i} - \frac{P_i}{v_i} \right) \quad (1)$$

$$\frac{di_{L_i}}{dt} = \frac{1}{L_i} (V_{ref} v_i - k_2 v_i^2 - k_2 v_i v_i - k_1 i_{L_i} v_i - v_i + v_i V_{ref} - k_1 v_i i_{L_i}) \quad (2)$$

$$\frac{di_{L_j}}{dt} = \frac{1}{L_j} (V_{ref} v_j - k_2 v_j^2 - k_2 e_j v_j - k_1 i_{L_j} v_j - v_j + e_j V_{ref} - k_1 e_j i_{L_j}) \quad (3)$$

$$\frac{dv_{EXT}}{dt} = \frac{i_{C_T}}{C_T} = \frac{\sum i_j - \sum i_{L_j}}{C_{EXT}} \quad (4)$$

$$0 = \sum P_i - \sum P_j \quad (5)$$

The observability formulation is given in terms of the Jacobian:

$$J_O = \begin{bmatrix} G_x & G_x & G_w \\ H_x & H_x & H_w \end{bmatrix} \quad (6)$$

The condition number of the observability Jacobian is the metric used to measure how observable the system is and it is defined as:

$$\eta = \frac{\lambda_{\max}(J_O)}{\lambda_{\min}(J_O)} \quad (7)$$

Simulation results are shown for cases with different load converters' internal control gains as the system is loaded according to (9) and voltage regulation through the variation of external control variable  $V_{ref}$  for specific load converters.

$$\begin{bmatrix} P_2 \\ P_3 \end{bmatrix} = \begin{bmatrix} P_2^0 \\ P_3^0 \end{bmatrix} + \alpha \begin{bmatrix} \Delta P_2 \\ \Delta P_3 \end{bmatrix} \quad (8)$$

## II. KEY FIGURES

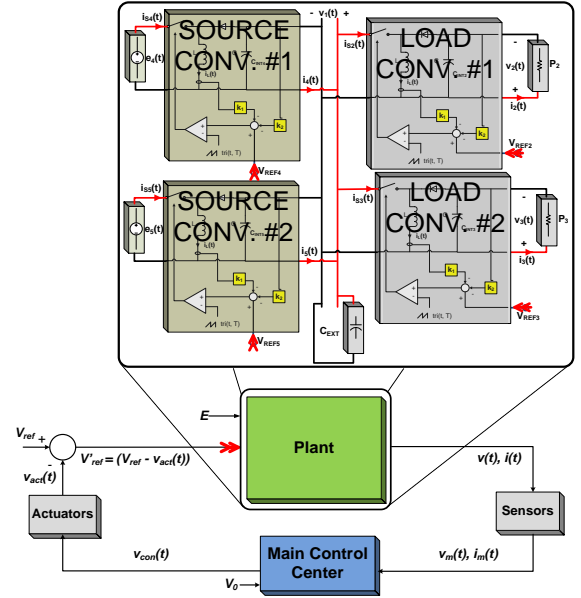


Figure 1. DC multi-converter based power system

## III. KEY RESULTS

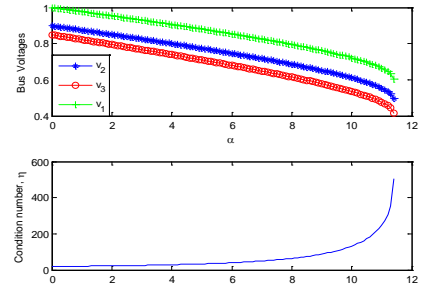


Figure 2.  $V$ - $\alpha$  and  $\eta$ - $\alpha$  curves

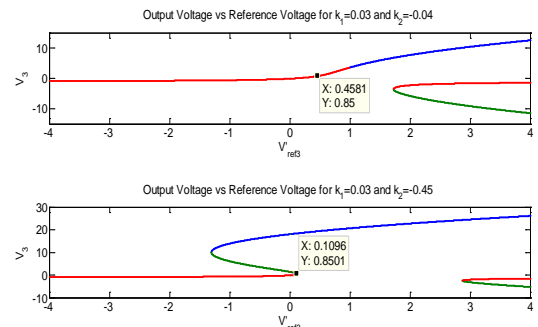


Figure 3.  $V$ - $V_{ref}$  curves for load converter #2

# Optimizing Demand Response Price and Quantity in Wholesale Markets

Ahlmahz I. Negash, Student Member, IEEE, Daniel S. Kirschen, Fellow, IEEE

**Abstract**—We propose a method to create a supply curve for demand response (DR) analogous to, but separate from, a generation supply curve. This demand side “supply curve” is used to offer DR into the wholesale market as a demand resource, not a competitive generation source and therefore, unable to set locational marginal price (LMP). This DR supply curve is based on the value of increased gross margin due to load modifications. While this supply curve is based on optimizing a load serving entity’s gross margin, the maximum level of DR allowed in the market is based on the amount of DR that brings the market balance to zero (i.e. wholesale revenue equals generator and DR expenses). The proposed method is compared to compensation according to FERC Order 745. We find that while Order 745 results in a negative balance (less revenue than expenses) and a need to allocate cost, the proposed method achieves a positive balance for low levels of DR, zero balance at an optimal DR level, and a negative balance only if too much DR is purchased.

## I. PROPOSED PRICING SCHEME

### A. Generation Supply Curve and Optimal Demand

The premise behind this method is that for a given generation supply curve for the day, there is a specific load that maximizes  $g$ , the gross margin for the LSEs:

$$g = \sum_h^H (r - w_h(L_h)) * L_h, \quad (\$) \quad (1)$$

Here,  $r$  is the average volumetric retail rate,  $w_h$  is the hourly wholesale price,  $h$  is the hour ( $h=1 \dots H$ ,  $H=8760$ ), and  $L_h$  is the hourly demand (1). For each (daily) generation supply curve the optimal demand,  $L^{opt}$ , is the  $L_d$  that maximizes gross margin (2), ( $d=1 \dots D$ ,  $D=365$ ). Taking the sum over the year, we find the daily “optimal daily loads” for the year.

$$\max_{L_d} \sum_h^{24} \sum_d^D (r - w_h(L_d)) * L_d \quad (2)$$

### B. Required Demand Response

Using historical or forecast demand, we can then estimate the demand response  $D_h^d$  required to achieve the optimal load,  $L^{opt}$ , where  $D_h^d$  is the demand required in hour,  $h$ , on day,  $d$  (3).

$$D_h^d = L_h^d - L_d, \quad (\text{MWh}) \quad (3)$$

### C. Demand Response Value (benefit in \$/MWh)

The value,  $V_h^d$ , of the demand response is then the difference in gross margin with and without demand response divided by the required load modification (4).

$$V_h^d = \frac{(r - w_h(L_h - D_h^d)) * (L_h - D_h^d) - (r - w_h(L_h)) * L_h}{D_h^d}, \quad (\frac{\$}{\text{MWh}}) \quad (4)$$

### D. Fitting of Demand Response Supply Curve

We calculate the value,  $V_h^d$ , in each period and plot  $V_h^d$  vs.  $D_h^d$  to form the desired supply curve, where the curve in each period is approximated by a suitable function,  $p_i$ , ( $i=1,2,3$ ).

$$p_i = f(D_h^d), \quad (\frac{\$}{\text{MWh}}) \quad (5)$$

## II. RESULTS

Figure 1 shows the “supply curve” for demand response based on historical price, and load data for the PJM region.

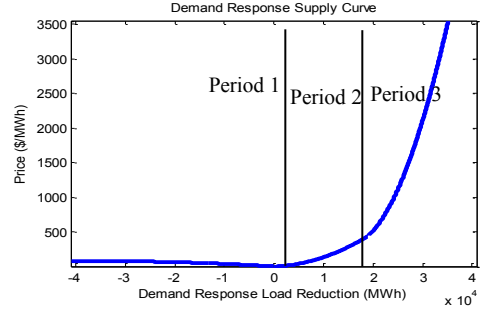


Figure 7. Piecewise curve: negative demand response (x-axis) implies load increase; positive demand response implies load decrease.

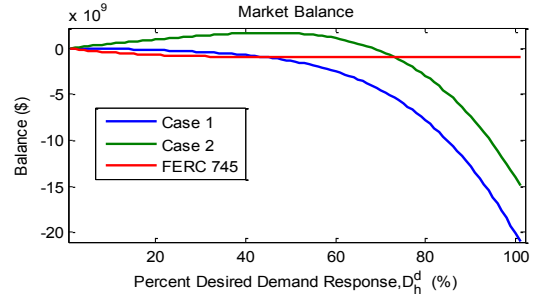


Figure 8. Market Balance Comparison

Figure 8 compares the market balance when demand response compensation is according to FERC Order 745 and for each of two cases using the proposed DR supply curve: Case 1, where DR reduces LMP and Case 2, where DR is not allowed to reduce LMP, but can only balance supply and demand. We observe that when demand response sets LMP (Case 1 and FERC method), the balance is always negative. However, when the proposed method is used, and DR is not allowed to set the LMP (Case 2), then for increasing purchases of DR, the market balance first grows increasingly positive, peaks, then drops as greater, (but less economic) payments go to DR. Eventually, at about 70% of the DR required to maximize the LSE gross margin, the balance becomes zero. This represents the point where the market is perfectly balanced. In other words, this point marks the maximum DR that the ISO should allow to be purchased, regardless of the LSE’s bid. From a market point of view, this quantity of DR is optimal. If more DR is purchased, then the balance becomes negative, and costs must be allocated.

# A Comparative Study of Measurement-Based Thevenin Equivalents Identification Methods

Haoyu Yuan and Fangxing Li

Department of Electrical Engineering and Computer Science  
The University of Tennessee, Knoxville  
Knoxville, TN 37996, USA  
{hyuan2, fli6}@utk.edu

**Abstract**— With the development of phasor measurement units, real-time voltage stability monitoring techniques using phasor measurements have been widely discussed in the past decade. For various measurement-based techniques, the fundamental idea behind them is to identify the Thevenin equivalents of the outer system seen from the nodes/areas of interests and then to assess the voltage stability margin based on the equivalent circuits. Therefore, fast and accurate identification of the Thevenin equivalents is crucial for such online monitoring applications. Though several identification methods have been proposed claiming to achieve good performance, they have not been explicitly compared with each other. This work presents such a comparative study of four different methods. After briefly introduced, the four methods are first compared in the aspect of time complexity and measurements needed through an algorithm analysis. Then they are tested on the measurements generated from time domain simulations of the NPCC 140-bus system. Detailed performance analysis is given following the case study and can serve as a general guidance on choosing the Thevenin equivalents identification methods and the corresponding parameters.

**Keywords**— *adaptive method, coupled single-port circuit, least square method, phasor measurement unit, Tellegen's theorem, Thevenin equivalent identification, voltage stability assessment.*

## I. KEY RESULTS AND FIGURES

In our study, the test results of four existing methods from [1-4] on the practical NPCC 140-bus system discover some new characteristics of these methods that are not mentioned in previous works.

Time complexity of the four methods is analyzed. Tellegen's Theorem (TT) and adaptive (AD) methods are both  $O(M)$  for calculating  $M$  load buses at one time step. The run time of least square (LS) and coupled (CP) methods depends on specific problems. However, for CP, an overhead of  $O(N^3)$  will potentially become a burden for a large system.

The results on Scenario 1 voltage collapsing are shown in Fig. 1 to Fig. 4 respectively. In this particular case, TT and AD methods indicate the collapsing point accurately while AD and CP methods are not performing as well. Scenario 2, another voltage collapsing, is also used to test the algorithms. It is found that CP performs better in that case. TT shows more distortion. AD measures the impedance smaller than actual value which may causes by the assumption it makes.

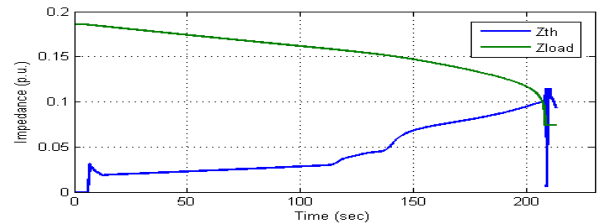


Fig. 1. Thevenin impedance of LS method for Scenario 1

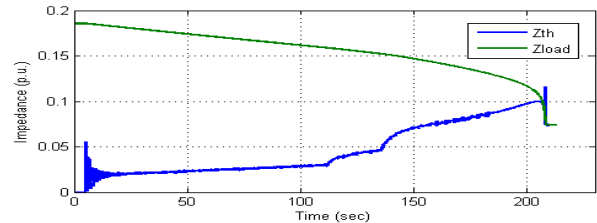


Fig. 2. Thevenin impedance of TT method for Scenario 1

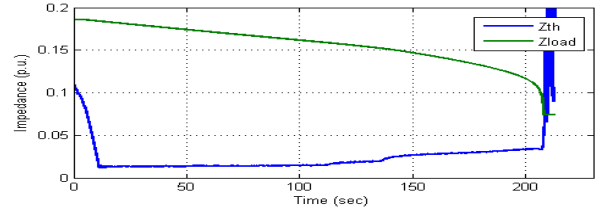


Fig. 3. Thevenin impedance of AD method for Scenario 1

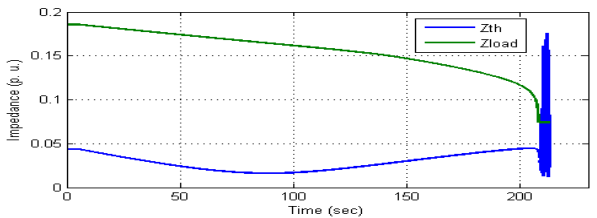


Fig. 4. Thevenin impedance of CP method for Scenario 1

## REFERENCES

- [1] K. Vu et al, "Use of local measurements to estimate voltage stability margin," IEEE Trans. Power Syst., vol. 14, no. 3, pp. 1029–1035, 1999.
- [2] I. Smon, G. Verbic, and F. Gubina, "Local voltage-stability index using tellegen's Theorem," IEEE Trans Power Syst., vol. 21, no. 3, pp. 1267–1275, Aug. 2006.
- [3] S. Corsi, and G. N. Taranto, "A Real-Time Voltage Instability Identification Algorithm Based on Local Phasor Measurements," IEEE Trans. Power Syst., vol.23, no.3, pp.1271-1279, Aug. 2008.
- [4] Y. F. Wang, I. R. Pordanjani, "Voltage stability monitoring based on the concept of coupled single-port circuit," IEEE Trans. Power Syst., vol. 26, no. 4, pp. 2154–2163, Nov. 2011..

# Recloser and Sectionalizer Placement for Reliability Improvement Using Discrete Event Simulation

Qiu Qin and N. Eva Wu

Department of Electrical and Computer Engineering, Binghamton University  
 Binghamton, New York 13902–6000 USA  
 qqin@binghamton.edu, evawu@binghamton.edu

**Abstract**—Existing works generally estimate the mean values for reliability index and used them for optimal placement of recloser and sectionalizers. This paper presents a cost-effective strategy to place automatic reclosers and sectionalizers into electric distribution systems for reliability improvement using simulation and probability. Evaluation of reliability indices in the placement process is carried out via discrete event simulation that takes advantage of high performance parallel computing cluster. The requirements on probabilities evaluated from the empirical distributions of two reliability indices (SAIFI and CAIDI) are imposed as placement constraints or objectives, rather than the annual sample means used in the conventional placement problems. As a result, our placement solution is robust against the variability in model predicted SAIFI and CAIDI. The proposed placement strategy is illustrated through a Roy Billinton Test System (RBTS).

## I. KEY EQUATIONS

### A. Reliability Indices [1]

$$\text{SAIFI} = \frac{\text{Total number of customers interrupted}}{\text{Total number of customers served}} \quad (1)$$

$$\text{CAIDI} = \frac{\sum \text{Customer Minutes of Interruption}}{\text{Total number of customers interrupted}} \quad (2)$$

### B. Problem Formulation

Minimize:  $k$

Subject to:  $\mathbf{P}(\text{Total Cost} < k) > p_k$

$$F_{\text{SAIFI}}(s) = \mathbf{P}(\text{SAIFI} < s) > p_s \quad (3)$$

$$F_{\text{CAIDI}}(c) = \mathbf{P}(\text{CAIDI} < c) > p_c \quad (4)$$

$$\text{Number of Reclosers} < N_R \quad (5)$$

$$\text{Number of Sectionalizers} < N_S \quad (6)$$

## II. KEY FIGURES

### A. Cost Function [2]

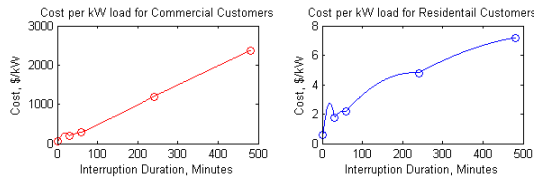


Fig. 1. Cost per kW average load for customers

### B. Simulation Results

TABLE I  
 VERIFICATION OF THE SIMULATION RESULTS

	Method	SAIFI	CAIDI	SAIDI
This paper	Simulation	0.247	14.64	3.59
Allen91 [3]	Analytical	0.248	14.55	3.61
Goel00 [4]	Simulation	0.249	14.54	3.62

TABLE II  
 STATISTICS OF SAIFI, CAIDI AND COST FOR BASE CASE (A)

	Mean	Std. Deviation	90 percentile
SAIFI	0.247	0.026	0.281
CAIDI	14.64	4.527	20.75
Cost	4.830	1.510	6.836

The distributions of SAIFI, CAIDI and cost are shown by the following histograms.

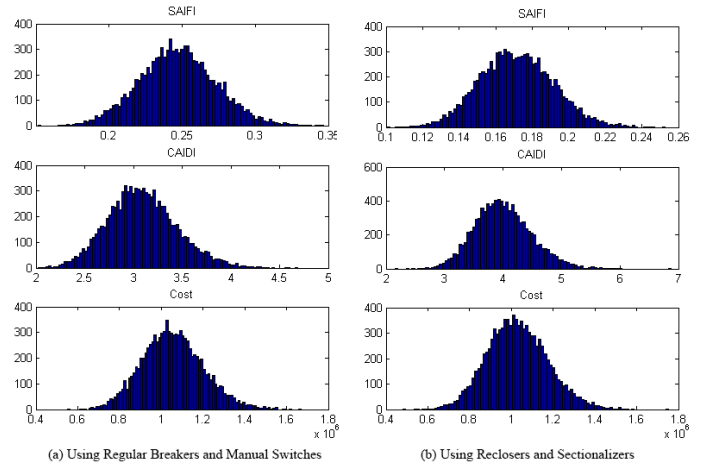


Fig. 2. Histogram of SAIFI, CAIDI and Cost

## REFERENCES

- [1] "IEEE Guide for Electric Power Distribution Reliability Indices," *IEEE Std 1366-2012 (Revision of IEEE Std 1366-2003)*, pp. 1–43, May 2012.
- [2] M. J. Sullivan, *Estimated Value of Service Reliability for Electric Utility Customers in the United States*, 2009.
- [3] R. Allan, R. Billinton, I. Sjarief, L. Goel, and K. S. So, "A reliability test system for educational purposes-basic distribution system data and results," *IEEE Trans. Power Syst.*, vol. 6, no. 2, pp. 813–820, 1991.
- [4] L. Goel, "Monte carlo simulation-based reliability studies of a distribution test system," *Electric Power Systems Research*, vol. 54, no. 1, pp. 55 – 65, 2000.



# Online Data-Driven State Estimation

Yang Weng, Christos Faloutsos\*, Marija D. Ilić, and Rohit Negi

Department of Elec. Comp. Eng., \*College of Computer Science, Carnegie Mellon University, Pittsburgh, Pennsylvania, 15213  
Email: yangweng@andrew.cmu.edu, christos@cs.cmu.edu, {milic, negi}@ece.cmu.edu

**Abstract**—Traditional power system state estimation methods lack the ability to track and manage increasing uncertainties inherent in the new technologies, such as recent and ongoing massive penetration of renewable energy, distribution intelligence, and plug-in electric vehicles. To deal with the inability, we propose to utilize the unused historical data for power system state estimation, thanks to the recent investment of huge amount of sensors, which create variant contexts for training examples. Specifically, kernel ridge regression is proposed in a Bayesian framework based on Nearest Neighbors search. This is based on the observation that similar states create similar measurement sets. Although able to achieve much higher accuracy, the new approach is slow due to the burden by sequential similarity check over large volumes of high dimensional historical measurements, making it unsuitable for online services. This calls for a general approach to preprocess the historical data. Therefore, we propose to speed up the data-driven state estimation with three steps. First, because the power systems are with periodic patterns, which create clustered measurement data, dimension reduction is proposed to remove redundancy, but still able to retrieve similar measurements. To further reduce the computational time, the  $k$ -dimensional tree indexing approach is employed in step two to group the clustered power system data into a tree structure, resulting in a log-reduction over searching time. Finally, we verify the obtained historical power system states via AC power system model and the current measurements to filter out bad historical data. Simulation results show that the new method can dramatically reduce the necessary computational time for the proposed online data-driven state estimation, while producing a highly accurate state estimate.

## I. KEY EQUATIONS

### A. Data Driven State Estimation

The data-driven state estimate  $\mathbf{x}$  is a result of mapping from the current measurements  $\mathbf{z}$ . The mapping matrix  $\mathbf{Q}^T$  is learned from historical similar measurements  $\mathbf{Z}_{mat}$  and the corresponding historical states  $\mathbf{X}_{mat}$  via ridge regression. The new approach is illustrated in Fig.1. Finally, kernel trick are used in such a process to deal with non-linearity.

$$\mathbf{x} = \mathbf{Q}^T \mathbf{z} \quad (1)$$

$$\hat{\mathbf{Q}} = (\mathbf{Z}_{mat} \mathbf{Z}_{mat}^T + 2\gamma \mathbf{I})^{-1} \mathbf{Z}_{mat} \mathbf{x}_{current} \quad (2)$$

### B. Speed Up

Notice that, to find historical similar measurements, exhaustive search is required, which is slow. Fig.2 shows the result of mapping the historical data onto some two dimensional features associated with significant singular values. As the data in the figure are highly clustered, dimension reduction is conducted to remove redundancy in Nearest Neighbor search.

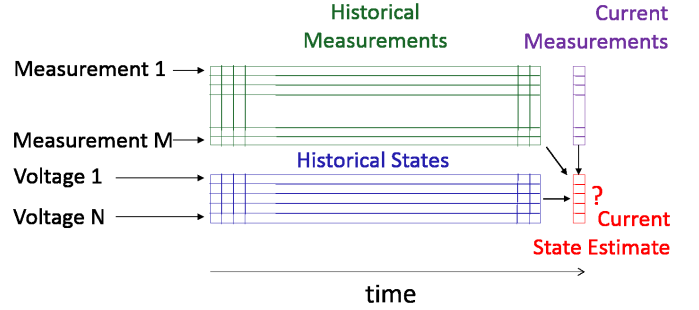


Fig. 1: The Scheme of Data-Driven State Estimation.

$K$ -Dimensional tree indexing method is subsequently used to further achieve log reduction of searching time.

## II. KEY RESULTS

Fig.2 shows the Singular Value Decomposition results with clustered points. In Fig.3, we illustrate that the new scheme can improve accuracy with 1000 times speed up.

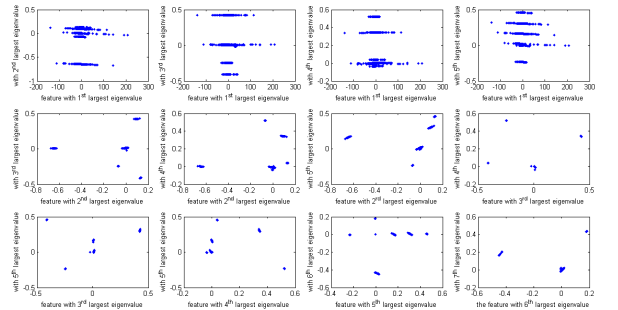
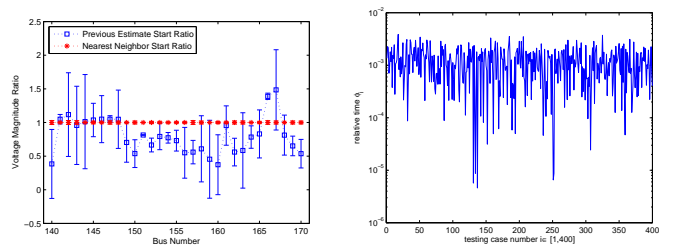


Fig. 2: Clustering of Power Systems Data for Speed Up.



(a) Improved Voltage Magnitude Est. (b) 1000 Times Speed Up

Fig. 3: Improved Accuracy and Speed Up.

# Stability Synthesis of Power Hardware-in-the-Loop (PHIL) Simulation

Mahdi Dargahi, *Student Member, IEEE*, Arindam Ghosh, *Fellow, IEEE*,  
and Gerard Ledwich, *Senior Member, IEEE*

*Abstract*--A virtual power system can be interfaced with a physical system to form a power hardware-in-the-loop (PHIL) simulation. In this scheme, the virtual system can be simulated in a fast parallel processor to provide near real-time outputs, which then can be interfaced to a physical hardware that is called the hardware under test (HuT). Stable operation of the entire system, while maintaining acceptable accuracy, is the main challenge of a PHIL simulation. In this paper, after an extended stability analysis for voltage and current type interfaces, some guidelines are provided to have a stable PHIL simulation. The presented analysis have been evaluated by performing several experimental tests using a Real Time Digital Simulator (RTDS™) and a voltage source converter (VSC). The practical test results are consistent with the proposed analysis.

## I. INTRODUCTION

There are two different stability aspects that need attention for PHIL simulation. One is the numerical stability associated with the splitting a system into two parts. The other is associated with the practical implementation, such as the power converter bandwidth, sensor noise, time delay, and ripple of the power amplifier. In addition to stability, accuracy of the results is another important issue. In this paper, stability and accuracy problems of PHIL simulations are analytically addressed and impacts of employing a low-pass filter (LPF) and changing its parameters are investigated. The presented studies have been tested experimentally using an RTDS.

## II. KEY FIGURES

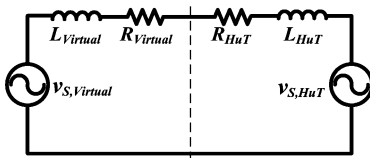


Fig. 1. The system under study.

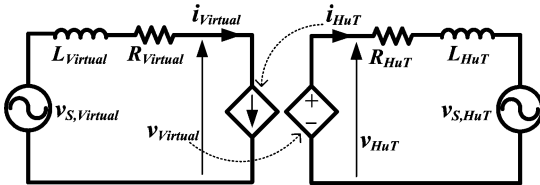


Fig. 2. System under study divided into two parts based on voltage type ITM.

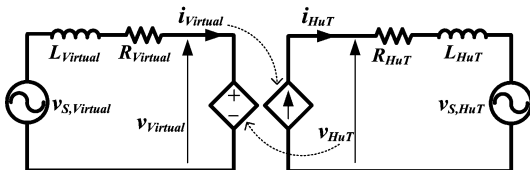


Fig. 3. System under study represented based on current type ITM.

## III. KEY EQUATIONS

For voltage type ITM:

$$T_{OL} = \frac{\alpha Z_{Virtual}}{Z_{HuT}(\alpha + s)} e^{-st_d}$$

For current type ITM:

$$T_{OL} = \frac{\alpha Z_{HuT}}{Z_{Virtual}(\alpha + s)} e^{-st_d}$$

## IV. KEY RESULTS

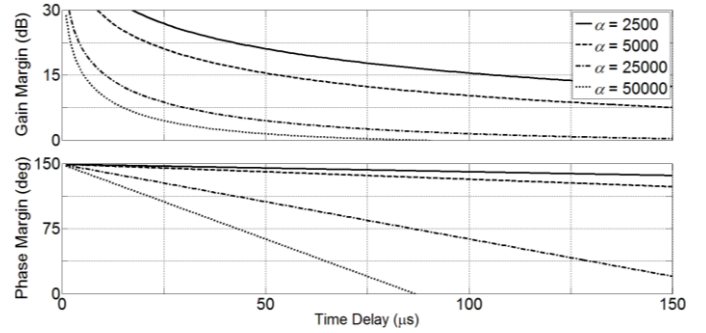


Fig. 4. Effect of delay and filter cut-off frequency on stability margins.

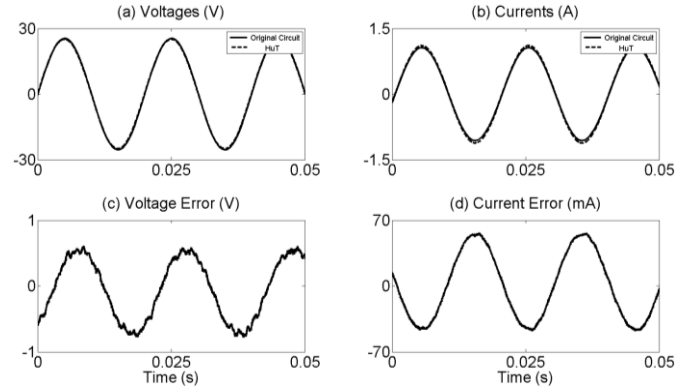


Fig. 5. Practical PHIL results for inherently stable voltage type interface.

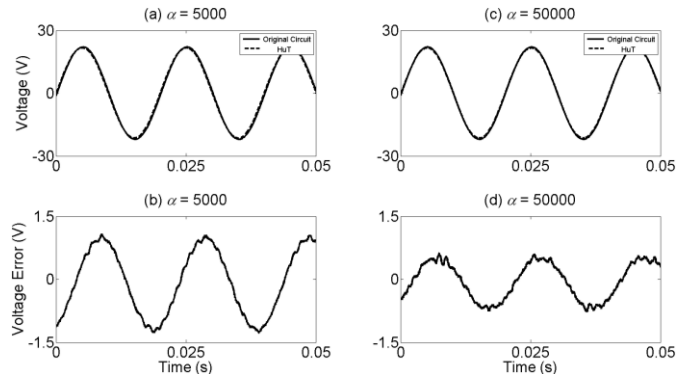


Fig. 6. Practical PHIL results for inherently unstable voltage type interface.

# A Novel Wave-head Identification Method based on PCA & WMA

Fei Xu, Student Member, IEEE, Xinzhou Dong, Senior Member, IEEE

**Abstract**—The most essential problem in Single-ended Travelling Wave Fault Location (STWFL) is the identification of the subsequent reflection on the fault line after the initial one. Reflected wave-head from the adjacent bus which has the same polarity as the real fault point reflection may cause the failure of STWFL. Wave-head Comparison Method (WCM) has been raised to solve this, yet did not consider the impact of the distributed capacitor of the bus and noises in the sample data. Given this, the inapplicability of the conventional WCM is analyzed in the paper, and a novel data process method is proposed using both the Principal Component Analysis (PCA) and Wavelet Multi-scale Analysis(WMA). Based on that, a modified WCM is proposed and abundant EMTP/ATP simulation results have shown the effectiveness and progress of the new method.

**Index Terms**—Single-ended fault location, travelling wave, principal component analysis, wavelet multi-scale analysis, wave-head comparison method .

## I. PROPOSED METHOD AND KEY EQUATIONS

### A. Data processing using WMA and PCA

**D**ATA processing flow chart is shown as Fig.1.  $L_X$  is the line that connected to the same bus as well as the fault line.  $T_x'$  is the principle component of the high frequency multi-scales data set from the wavelet transform of the original sample data..

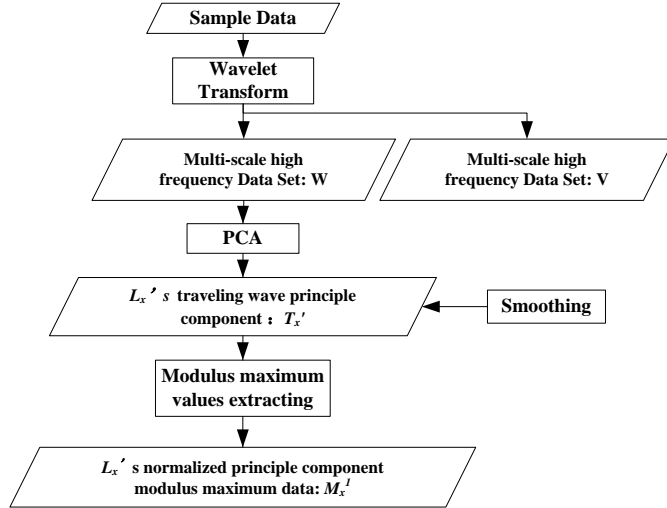


Fig.1 proposed method flow chart

### B. Key equations

$C$  is the original covariance matrix of the data set  $T$ ;  $A$  is the new covariance matrix in the new space,  $E^T$  is linear transformation of PCA.

$$E^T C E = \Lambda = \begin{pmatrix} \lambda_1 & & & \\ & \lambda_2 & & \\ & & \ddots & \\ & & & \lambda_n \end{pmatrix} \quad (1)$$

$$T' = E^T T = P T \quad (2)$$

Wavelet Multi-scale Analysis is shown as below:

$$\begin{cases} V_{2^j} f(n) = \sum_k h_k V_{2^{j-1}} f(n - 2^{j-1} k) \\ W_{2^j} f(n) = \sum_k g_k V_{2^{j-1}} f(n - 2^{j-1} k) \end{cases} \quad (3)$$

$$\begin{cases} h_k = \{0.125, 0.375, 0.375, 0.125\} (k = -1, 0, 1, 2) \\ g_k = \{-2, 2\} (k = 0, 1) \end{cases} \quad (4)$$

## II. SIMULATION RESULTS

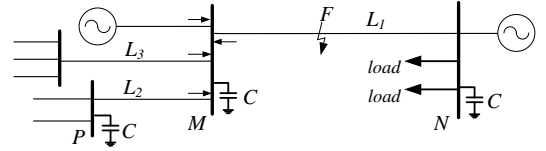


Fig.2 simulation model

$D_F=22km$ ,  $L_2=20km$ , Time gap between reflection of the fault point and the adjacent is  $7\mu s$ . Bus capacitor  $C=15nF$ .  $SNR=40dB$ .

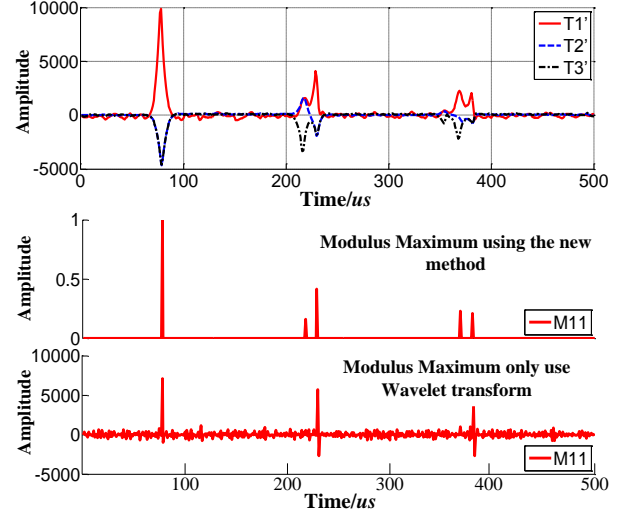


Fig.3 principle components of multiple lines and MM results comparison

## III. CONCLUSION

Accurately identification can be achieved under the situation that:  $C=5nF\sim 30nF$ ;  $SNR=35\sim 50dB$ . Thus, a more effective wave-head selection and success STWFL can be done.

# Study of Wind Power Curtailment Considering Transient Stability

Takato Otani, Toshiki Takayama, and Shinichi Iwamoto

Power Systems Laboratory, Department of Electrical Engineering and Bioscience, Waseda University, Tokyo, 169-8555, Japan  
 Email:iwamoto.lab.pwrs@gmail.com

**Abstract--** Recently, some renewable energy sources such as wind power generation have been investigated extensively because of environmental problems associated with greenhouse gas emissions. Moreover, the suspension of nuclear power and feed-in tariff (FIT) systems accelerate the penetration of renewable energy, particularly wind power. In addition, there is more frequency deviation because of the fluctuation in the wind power output. Therefore, the importance of curtailment is growing. In this paper, we propose two methods regarding curtailment. One is an optimal curtailment order of the wind powers to maximize the transient stability by using transient stability sensitivity. The other is to maximize the voltage stability by using voltage stability sensitivity. Then, we compare these two methods with random curtailment methods by carrying out numerical simulations using a 9 machine 20 bus system.

**Index Terms—**Wind Power, Curtailment, Load Frequency Control, Transient Stability, Voltage Stability

## I. KEY EQUATIONS

$$\frac{d\delta_i}{dt} = \omega_i - 2\pi f_0, \dots \dots \dots (1)$$

$$\frac{d\omega_i}{dt} = \frac{\pi f}{H_i} (P_{mi} - P_{ei}), \dots \dots \dots (2)$$

## II. KEY FIGURES

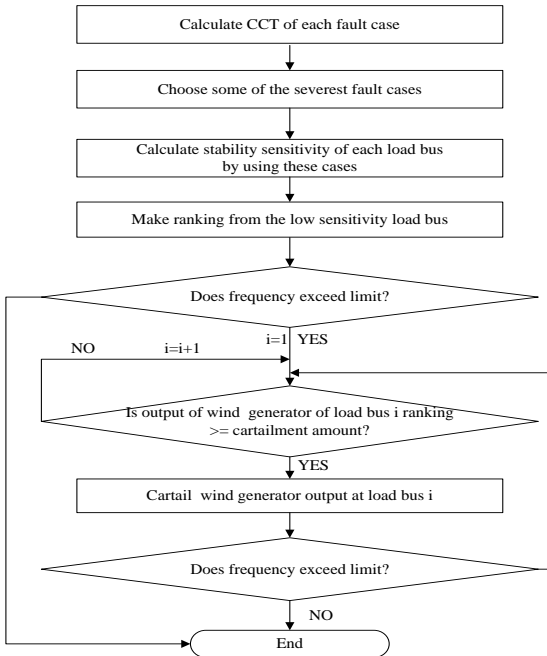


Fig. 1. Flowchart of the Stability method

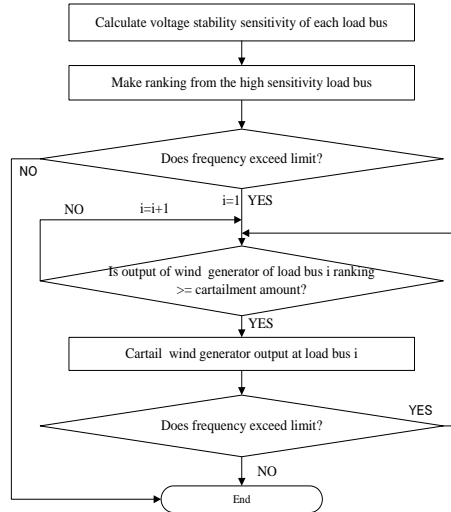


Fig. 2. Flowchart of Voltage method

## III. KEY RESULTS

Table 1. The results regarding curtailment (curtailing 15% at a time)

Number of curtailment	Stability Method	Voltage method	Simple method	Random method
1	W1	W3	W1,W2,W3	W1
2	W1	W3	W1,W2,W3	W2
3	W1	W3	W1,W2,W3	W1
4	W1	W3	W1,W2,W3	W3
5	W1	W3	W1,W2,W3	W2
6	W1	W3	W1,W2,W3	W1
7	W2	W1	W1,W2,W3	W1

Table 2. Voltage characteristic comparison

	$Q_{Lossmax}$	The rate of $Q_{Lossmax}$ deviation [%]	The sum of voltage deviation $g$	The rate of $f$ deviation [%]
Voltage method	0.148	-	26.2	-
Stability method	0.150	1.35	26.5	1.15
Simple method	0.150	1.35	26.4	0.763
Random method	0.150	1.35	26.5	1.15

$$g = \sum_{i=1}^l \sum_{j=1}^n |V_{ij} - V_{ref}| \cdot \Delta t \dots \dots \dots (3)$$

l: Number of lines n: Number of steps  $V_{ij}$ : Bus voltage on line j  
 $V_{ref}$ : Reference Voltage  $\Delta t$ : Step time

# Dynamic Modeling of Electric Vehicle Movable Loads based on Driving Pattern Analysis

Difei Tang, *Student Member, IEEE*, Peng Wang, *Member, IEEE*

School of Electrical and Electronic Engineering

Nanyang Technological University

Singapore

dtang002@e.ntu.edu.sg

**Abstract**—With the electrification of transportation, a growing number of electric vehicles (EVs) will emerge as new loads in power system. Comparing to traditional stationary loads, EV charging loads can be regarded as movable loads connecting among buses of a power system. The random moving and charging process of EVs is inherited from the stochastic driving pattern of EV drivers. Moreover, EVs closely link power system and transportation system. An effective traffic management will alleviate the impact of massive EV charging loads on power system. This paper propose a technique to model the stochastic moving feature of EV charging loads based on driving pattern analysis. Graph theory is used to bridge the transportation and transmission network. The spatial and temporal distributions of expected nodal EV charging loads are determined by Monte Carlo simulation (MCS). The system studies show that number of daily trips plays a key role in EV charging loads modeling.

## I. KEY ALGORITHMS AND RESULTS

As shown in Fig. 1, the movement of EVs is modeled from trip chain level to trip level. The trip chain level generates the daily trip chain of an individual EV driver, while the trip level produces the destination, path and distance for each trip.

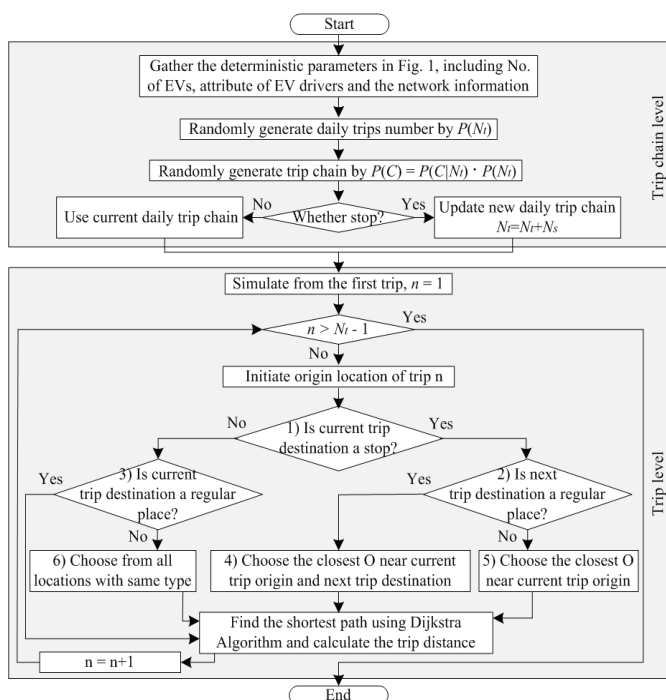


Fig. 1. Flowchart of spatial modeling of EV movement.

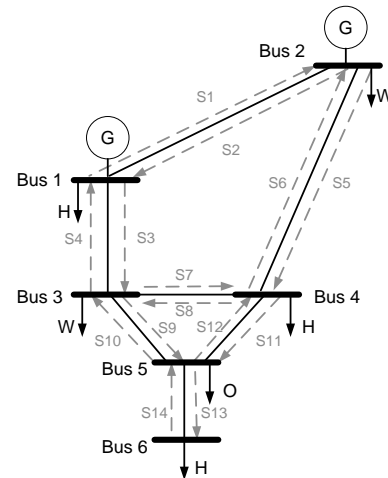


Fig. 2. The combination of transportation network and the RBTS system.

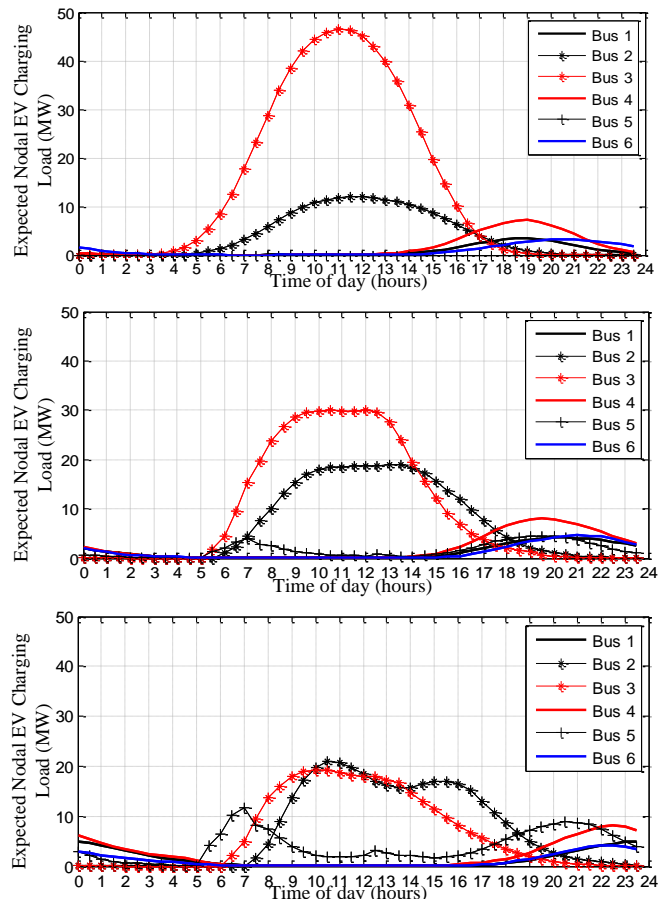


Fig. 3. Expected nodal EV charging load (2, random and 6 daily trips).

# Combinatorial Weighting Method for Lightning Transformation Effect Evaluation of 500kV Transmission Lines

R.C. Duan, F.H. Wang, Y.D. Liu, *Member*, IEEE

Department of Electrical Engineering  
Shanghai Jiaotong University  
Shanghai, China  
superdrc@126.com

H. Huang

Electric Power Research Institute  
Shanghai Power Grid Co. Ltd.  
Shanghai, China  
13631561618@139.com

**Abstract**—As the effective lightning protection measures can improve the lightning protection performance of transmission line and reduce line shielding failure rate, an assessment method based on combinatorial weighting method is proposed to formulate lightning protection measures in accordance with the evaluation process of screen-selection-optimization. Economic and technical analysis of several commonly used lightning transformations is performed first to verify their effectiveness. Then the combinatorial weighting method is applied to calculate the weight value of these measures relative to the target according to the relationship between objectives and guidelines, furthermore the theoretical optimal lightning protection measure is selected. The application of this method is illustrated with a typical 500 kV transmission line under complex terrain, and the expected evaluation result shows the lightning protection performance can meet the transformation requirements. Thus this method can be suitably used as reference in practical engineering.

## I. KEY METHODS

When using CW method to analyze problems, we should methodize and stratify the factors by setting the structure of evaluation including 7 basic measures and 5 criteria.

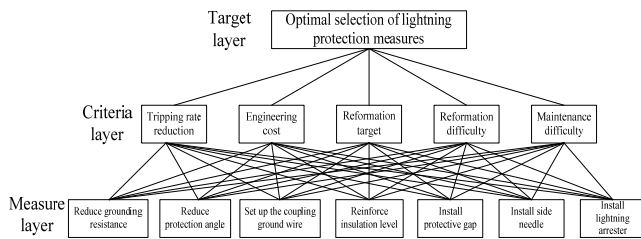


Figure 1. Evaluation model of lightning protection

## II. KEY RESULTS

The evaluation results of lighting protection measures and the optimal choice are shown in Tab.1 and Tab.2.

TABLE I. EVALUATION RESULTS (PROTECTION EFFECT)

Tower	reduce ground resistance	erect coupled ground wire	increase insulation level	add side needle	assemble line arrester
72	0.1448	0.1757	0.2358	0.4438	
74	0.1758	0.2457	0.2548		0.3238
75	0.2500		0.1689	0.5810	
76	0.1275	0.1432	0.1671	0.1115	0.4507
78	0.1570	0.1471	0.1132	0.1615	0.4275
79	0.1448	0.1757	0.2358	0.4438	
80	0.2438	0.4358	0.1457	0.1748	

TABLE II. OPTIMAL PROTECTION MEASURES

Tower	Protection Measure by CW	Shielding Rate Before Transformation (times/100km·a)	Shielding Rate After Transformation (times/100km·a)	Optimal Measure After Examination
72	add side needle	0.24	0.0705	add side needle
74	erect coupled ground wire	0.2	0	erect coupled ground wire
75	add side needle	0.15	0.041	add side needle
76	assemble line arrester	0.49	0.1724	assemble line arrester
78	assemble line arrester	0.26	0.1266	assemble line arrester
79	add side needle	0.25	0.181	add side needle
80	erect coupled ground wire	0.48	0.2765	erect coupled ground wire



# A Hybrid MILP Approach to Unit Commitment

Yury Dvorkin, *Student Member, IEEE*, and Daniel Kirschen, *Fellow, IEEE*

**Abstract**—This poster presents a new transmission-constrained unit commitment method that combines the cost-efficient but computationally demanding stochastic optimization and the expensive but tractable interval optimization techniques to manage uncertainty on the expected net load. The performance of this hybrid formulation is compared to the stochastic, and interval formulations using Monte Carlo simulations on a modified 24-bus IEEE Reliability Test System. The results demonstrate that the proposed unit commitment formulation results in the least expensive day-ahead schedule among all formulations and can be solved faster than the stochastic unit commitment.

**Index Terms**—unit commitment, stochastic optimization, interval optimization, uncertainty.

## I. CONCEPT

THE concept of the Hybrid Unit Commitment (HUC) formulation is shown in Fig. ?? . The Stochastic Unit Commitment (SUC) formulation is applied to the first ( $t^{sw} - 1$ ) hours of the optimization horizon, which have relatively accurate scenarios of renewable generation. The remaining hours, which are characterized by less accurate scenarios, are solved using the Interval Unit Commitment (IUC) formulation. The switching time  $t^{sw}$  is optimized in such a way that the expected day-ahead cost is minimum.

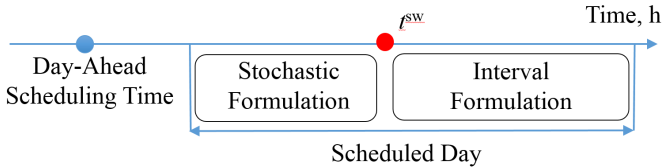


Fig. 1. Schematic representation of the Hybrid Unit Commitment.

## II. RESULTS

The HUC formulations has been solved in two implementations: i) the parallel computing implementation solves the HUC model for each operating hour simultaneously and ii) the single processor implementation iteratively solves the HUC model using the three-point grid search method. However, the

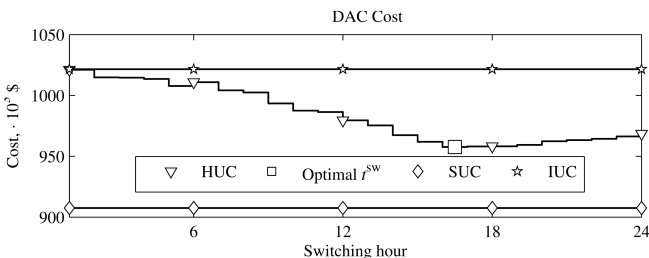


Fig. 2. Comparison of the total day-ahead costs (DAC) of the IUC, SUC, and HUC formulations. The optimal switching time is highlighted with a square.

execution time varies for both implementations, they result in the same schedule and operating cost.

Fig. ?? illustrates the day-ahead cost of the HUC as a function of the switching time, bounded by the day-ahead cost of the SUC and IUC formulations. Fig. ?? compares the hourly committed capacity for different UC approaches. Fig. ?? and Table ?? demonstrate that the HUC model results in the least expensive operating cost in Monte Carlo simulations for different wind penetration levels. Additionally, the HUC results in lower load shedding, as compared to the SUC model, and more efficient accommodation of wind generation, as compared to the HUC model.

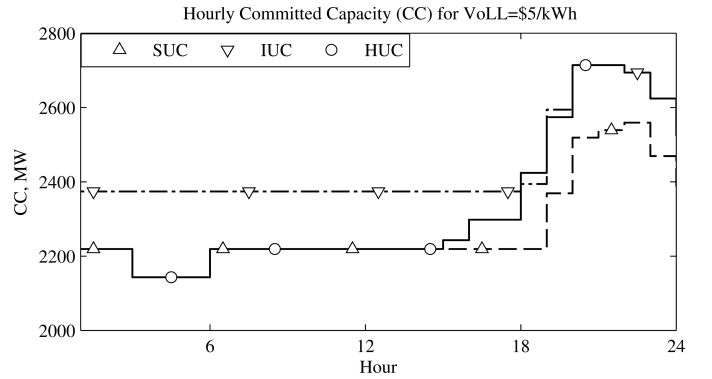


Fig. 3. Comparison of the hourly committed capacity for the day-ahead schedules of IUC (dash-dot), SUC (dash-dash), and HUC (solid) formulations.

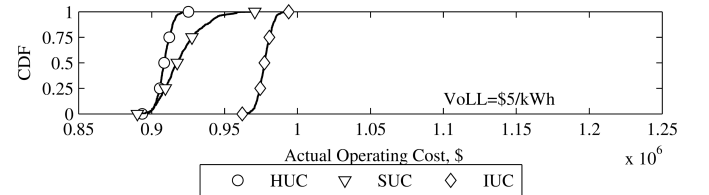


Fig. 4. Cumulative distribution function (CDF) of the actual operating cost (AOC) obtained with Monte Carlo simulations.

TABLE I  
STATISTICS OF MONTE CARLO SIMULATIONS FOR DIFFERENT WIND PENETRATION (COSTS ARE IN  $10^3$ , \$)

Wind Penetration	Parameter	HUC	SUC	IUC
10 %	$E(C)$	908.7	919.6	977.4
	$EEENS$ , MWh	0.019	0.34	0
	$WS$ , MWh	33.4	18.5	24.3
20 %	$E(C)$	712.4	727.8	800.1
	$EEENS$ , MWh	0.023	0.59	0
	$WS$ , MWh	99.6	108.1	214.3
30 %	$E(C)$	654.1	679.7	709.4
	$EEENS$ , MWh	0.024	0.59	<0.001
	$WS$ , MWh	151.4	152.0	331.2

# A MIP Based Optimization Framework for Unit Commitment and Energy Pricing

Yu Xia and Joe H. Chow  
Rensselaer Polytechnic Institute  
Troy, NY, USA  
[xiay4@rpi.edu](mailto:xiay4@rpi.edu), [chowj@rpi.edu](mailto:chowj@rpi.edu)

**Abstract**— A Power system unit commitment (UC) problem involves selecting a subset of the total generating units and a sub-problem of computing how much power should be generated by each committed unit, both in an economic manner. The subproblem known as economic dispatch (ED) is polynomially solvable. An efficient simultaneous perturbation approach has recently been proposed in [1] for solving ED problems with inter-temporal constraints. The UC problem as a whole, however, is a NP-complete problem. Solution methods for the UC problem have been explored, which include dynamic programming, priority listing and Lagrangian relaxation. Mixed integer programming (MIP) methods have gained interests recently because of the drastic improvement in numerical solution times of commercial MIP solvers. MIP improves not only the solution but also the modeling capability. Most of the ISOs are leaning towards MIP to solve the UC problem in their day-head markets.

In the traditional Lagrangian relaxation approach, the Lagrange multiplier  $\lambda$  is often referred to as a “pseudo price” [1]. In the original MIP approach, however, we cannot readily obtain these price signals because the dual variables are not available from the mixed integer optimizers. Even though there are duality theorems in MIP to some extent, they are not well developed and are not implemented in any standard solvers.

In this poster, we present a MIP based framework which can obtain the UC solution as well as the price signals. The proposed framework contains a MIP master problem and a nonlinear convex programming subproblem with integrity constraints relaxed. The upper bound and lower bound of those relaxed integer variables are set to the optimal solution from the master problem. Because the resulting subproblem is polynomially solvable, it can be readily solved by the simplex or barrier algorithm with both primal and dual solutions. The dual value associated with the power balance constraint refers to the market clearing price.

**Key Words**—Lagrange relaxation, MIP, unit commitment, energy pricing, economic dispatch, nonlinear programming.

[1] Y. Xia, S. Ghiocel, D. Dotta, D. Shawhan, A. Kindle and J. H. Chow, “A simultaneous perturbation approach for solving economic dispatch problems with emission, storage, and network constraints,” IEEE Transactions on Smart Grid, vol. 4, no. 4, Dec. 2013.

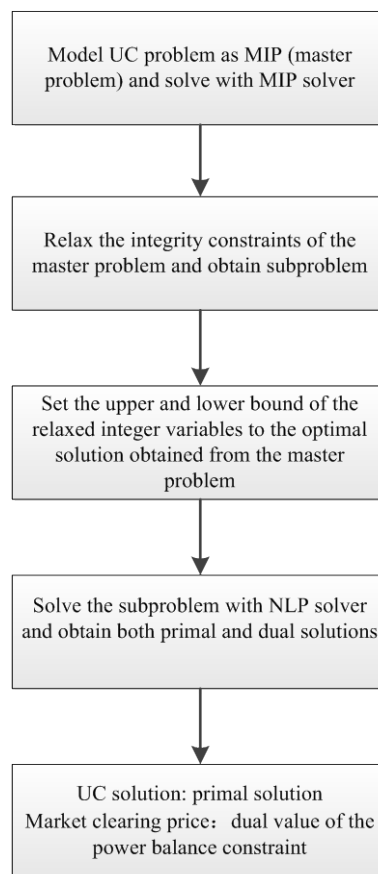


Figure 1. Flow chart for the MIP based framework

# Impact of Wind Variations on Power System Sub-Synchronous Oscillation

Meng Wu and Le Xie

Department of Electrical and Computer Engineering, Texas A&M University, College Station, Texas 77840

Email: marie126@tamu.edu, lxie@ece.tamu.edu

**Abstract**—In recent years, sub-synchronous oscillations (SSO) have been observed in many wind-integrated power systems. This paper aims at analyzing the impact of wind speed variations on system SSO. Nonlinearly-coupled electrical and mechanical subsystem models are proposed. Cross-excitation condition between subsystems is studied, and autoparametric resonance induced by wind speed variation is discovered. Numerical simulations are performed on a modified IEEE first benchmark system for verification.

## I. KEY FORMULATIONS

The electrical subsystem model for 1-generator-infinite -bus system can be expressed as:

$$\dot{x} = \begin{bmatrix} A_g(\omega_r(t)) & 0 \\ 0 & A_n \end{bmatrix} x + \begin{bmatrix} B_g & 0 \\ 0 & B_n \end{bmatrix} u \quad (1)$$

where  $x = [i_{qs}, i_{ds}, i_{qr}, i_{dr}, i_{ql}, i_{dl}, v_{qc}, v_{dc}]^T$ ,  $u = [v_{qs}, v_{ds}, v_{qr}, v_{dr}, v_{qs} - v_{qinf}, v_{ds} - v_{dinf}, 0, 0]^T$ .  $A_g(\omega_r(t))$  and  $B_g$  are the state and input matrices of doubly-fed induction generator (DFIG) model under synchronous d-q transformation, respectively;  $A_n$  and  $B_n$  are the state and input matrices of series-compensated network model under synchronous d-q transformation, respectively;  $i_{qs}, i_{ds}, i_{qr}, i_{dr}$  are DFIG stator and rotor currents on q and d axes, respectively;  $i_{ql}, i_{dl}, v_{qc}, v_{dc}$  are network inductor current and capacitor voltage on q and d axes, respectively;  $v_{qinf}$  and  $v_{dinf}$  are infinite bus voltage on q and d axes, respectively.

The 2-mass mechanical subsystem model can be expressed as:

$$[J] \begin{bmatrix} \ddot{\delta}_w \\ \ddot{\delta}_g \end{bmatrix} + [D] \begin{bmatrix} \dot{\delta}_w \\ \dot{\delta}_g \end{bmatrix} + [K] \begin{bmatrix} \delta_w \\ \delta_g \end{bmatrix} = \begin{bmatrix} \tau_w \\ \tau_g \end{bmatrix} \quad (2)$$

where  $[J]$ ,  $[K]$  and  $[D]$  are inertia, stiffness and damping matrices for the subsystem, respectively;  $\delta_w$  and  $\delta_g$  are the mechanical rotor angle of wind turbine and DFIG, respectively;  $\tau_w$  and  $\tau_g$  are torques of wind turbine and DFIG, respectively.

## II. KEY INSIGHTS

It can be observed from (1) the electrical subsystem is parametrically excited by the vibration of  $\omega_r$ , which is state variable of mechanical subsystem in (2). It is also obvious the state matrix of electrical subsystem varies as steady-state value of  $\omega_r$  changes. For type-3 wind generator with variable-speed-variable-pitch control, typical relationship of wind speed and steady-state  $\omega_r$  is shown in Fig. 1. Therefore,

as wind speed changes, the natural frequencies of electrical subsystem, which can be calculated through eigenvalues of its state matrix, change accordingly. However, natural frequencies of mechanical subsystem remain the same under different wind speed conditions. Thereby, if the vibrating frequency of parametric excitation  $\omega_r$ , reflecting the natural frequency of mechanical subsystem, coincides with natural frequency of electrical subsystem at certain wind speed, autoparametric resonance can be expected.

## III. KEY FIGURES

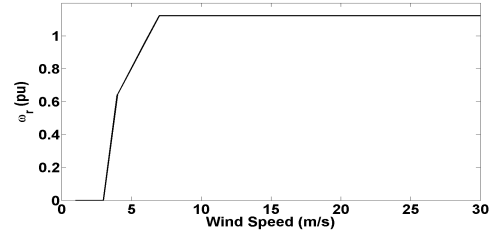


Fig. 1. Relationship between wind speed and generator rotor speed

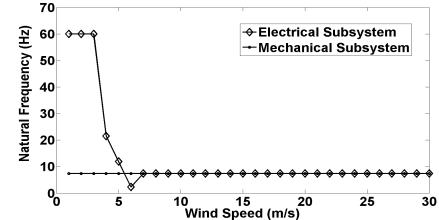


Fig. 2. Wind speed impact on one of the electrical subsystem natural frequencies (when wind speed =14 m/s, both electrical and mechanical subsystem have natural frequency of 7.35 Hz)

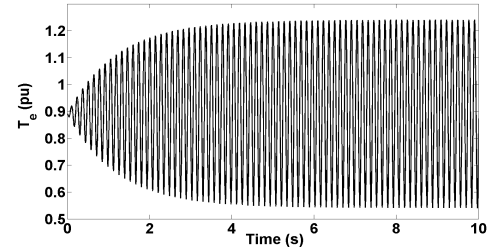


Fig. 3. Sub-synchronous oscillation of generator electrical torque when wind speed = 14 m/s (oscillation frequency = 7.35 Hz)

# Constraint relaxation based on risk-based security constrained economic dispatch

Xian Guo, Qin Wang and James McCalley  
 Dept. of Electrical and Computer Engineering  
 Iowa State University  
 Ames, IA, USA  
 xianguo@iastate.edu and jdm@iastate.edu

**Abstract**—Security-constrained economic dispatch (SCED) is widely used in ISOs. However, due to generation re-dispatch, complex network structure and market software limits, the SCED model maybe infeasible. Thus, how to address infeasible operating conditions is of interest. The constraint relaxation method based on risk-based security constrained economic dispatch (RB-SCED) is proposed to deal with this situation. Compared with the traditional penalty price method, this model relaxes circuit constraints while still ensuring system-level security, by imposing a constraint representing the overall system risk. Selection of proper control parameters  $K_C$  and  $K_R$ , not only ensures the security and economy are enhanced, but also less volatile LMPs are obtained. The corresponding theory is verified on a typical six-bus system and IEEE 30 bus system.

**Index Terms**—risk, SCED, constraint relaxation, penalty price

## I. KEY EQUATIONS

### A. System overall risk

$$Risk(\underline{g}_1(P_0), \dots, \underline{g}_{NC}(P_0)) = \sum_{k=1}^{NC} (Pr_k Sev(\underline{g}_k(P_0))) \quad (1)$$

### B. RB-SCED model

$$\text{Min} \sum_{i=1}^{NG} c_i \times P_i \quad (2)$$

Subject to:

$$\sum_{i=1}^{NG} P_i - \sum_{i=1}^{NG} D_i - Loss = 0, \quad (3)$$

$$\sum_{i=1}^{NG} GSF_{l-i}^0 (P_i - D_i) \leq Limit_l^0, \text{ for } l \in \{\text{all lines}\}, \quad (4)$$

$$P_i^{\min} \leq P_i \leq P_i^{\max}, \quad (5)$$

$$h_i^k = \sum_{i=1}^{NG} GSF_{l-i}^k (P_i - D_i), \quad (6)$$

for  $l \in \{\text{all lines}\}, k \in \{\text{all contingencies}\},$

$$h_i^k \leq K_C \times Limit_i^k, \quad (7)$$

for  $l \in \{\text{all lines}\}, k \in \{\text{all contingencies}\},$

$$Sev_i^k \geq 0, \quad (8)$$

$$Sev_i^k \geq a_{li} h_i^k - 9, \quad (9)$$

$$Sev_i^k \geq a_{2l} h_i^k - a_{3l}, \quad (10)$$

$$Sev_i^k \geq a_{4l} h_i^k - a_{5l}, \quad (11)$$

$$\sum_{k=1}^{NC} Pr_k \sum_{l=1}^{NL} Sev_l^k \leq K_R \times Risk_{max} \quad (12)$$

## II. KEY RESULTS

Table 1: Results of typical six-bus system

Bus Name	SCED <sup>1</sup>	RB-SCED ( $K_C=1.034; K_R=0.4$ )			
	LMP (\$)	RLMP (\$)	Energy (\$)	Congestion (\$)	Risk (\$)
A	13.53	13.53	13.53	0	0
B	200	15.57	13.53	0	2.03
C	200	20.03	13.53	0	6.50
D	200	14.13	13.53	0	0.60
E	200	9.58	13.53	0	3.95
F	13.36	16.92	13.53	0	3.38

1. with penalty price set as \$200.

Table 2: Results of IEEE 30 bus system

		Risk( $10^{-2}$ )	Cost( $10^4$ \$/hr)
SCED	/	11.5	11.62
RB-SCED	$K_C=1;$ $K_R=0.5$	5.75	12.59
	$K_C=1.05;$ $K_R=0.5$	5.75	10.34
	$K_C=1.2;$ $K_R=0.5$	5.75	10.21

## III. KEY CONCLUSION

RB-SCED model could handle the constraints violations, by relaxing the circuit security requirements, while satisfying the system overall risk level. It could enhance security and economy at the same time. Furthermore, the RB-LMPs across buses were more tightly distributed than the LMPs, suggesting that utilization of RB-LMPs may decrease volatility through time.

(This research is supported by PSEER program)

# An Optimal Framework for Residential Load Aggregators

Qinran Hu, Fangxing Li

The Department of Electrical Engineering and Computer Science, the University of Tennessee, Knoxville, TN 37996, USA,  
Email: {qhu2, fli6}@utk.edu

**Abstract**— With the development of intelligent demand-side management with automatic control, distributed populations of large residential loads, such as air conditioners (ACs), have the opportunity to provide effective demand-side ancillary services while reducing the network operating costs. This work presents an optimal framework for residential load aggregators. Under this framework, the load aggregators are able to: 1) have an optimal control strategies over ACs and electrical water heaters (EWHs); 2) quickly and automatically response to the request from load serving entities. To residents, the framework is designed with probabilistic model of comfortableness, which ensures the residents' daily life will not be affected. Also, the framework fairly and strategically rewards residents who participated in the demand response program, which may stimulate the potential capability of loads optimized and controlled by the load aggregator. In addition, the proposed framework will be validated on several numerical case studies.

## I. MOTIVATION

The development of communication and sensor technologies provide the platform for consumers and suppliers to interact with each other. This creates an opportunity for load aggregators to play an increasingly vital role in demand response by applying optimal control strategies over loads. According to Monthly Energy Review April 2012 made by U.S. Energy Information Administration, the residential electricity use in US in 2011 is 1,423,700 million kWh consisting 38% of the total electricity use. Therefore, it is reasonable to consider designing an optimal framework for residential load aggregators to provide effective demand-side ancillary service by strategically controlling the residential loads and rewarding the residents.

Based on several pilot trial runs by utilities, ACs and EWHs are especially critical here, because they are increasingly predominant and can provide fast responses with minimal impact to residents in a short time period. Moreover, in most of the countries, ACs and EWHs typically account for one half of the total peak demand in residential aspects. Therefore, this work considers the aggregate demand of populations of ACs and EHWs.

## II. INTRODUCTION AND PRE-STUDY

There are several assumptions for the proposed framework, 1) ACs and EWHs have two-way communication with load aggregators; 2) Users provide a temperature range in which they feel comfortable with; and 3) Users decide whether they are willing to compromise about the temperature range. Following the above assumptions, the load aggregator is able to use the proposed framework to dispatch the loads need to be reduced without affecting residents daily life, while sending out the rewards to residents according to the contributions they made.

Fig.1 is the brief schematic figure of the control and rewards mechanism. Based on the proposed framework, some preliminary studies have been carried out. For example, here Fig.2 and TABLE I show the preliminary results of a 10-user case study regarding the residents' satisfaction as well as the reward distribution.

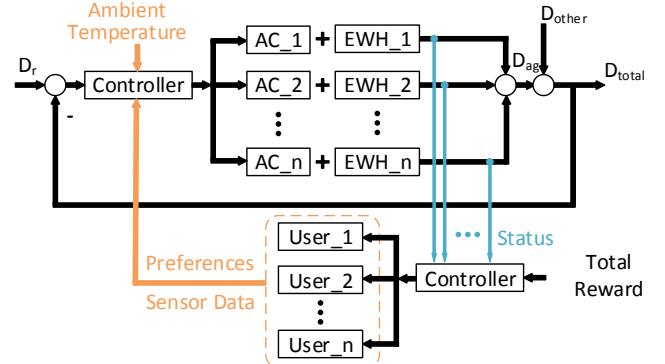


Fig.1 Schematics of the control and rewards mechanism

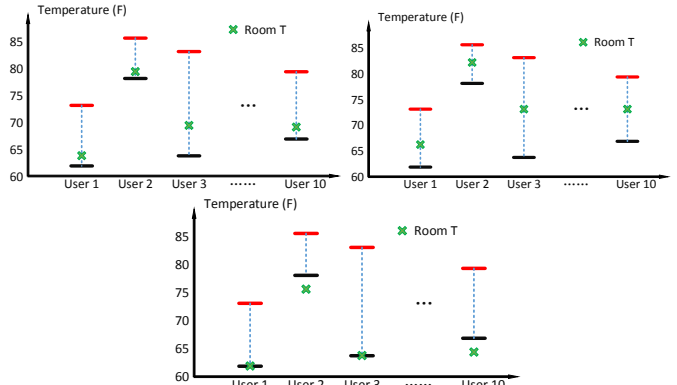


Fig.2. The operating points of ACs under some typical scenarios

TABLE I. PRELIMINARY RESULT (LENGTH: ONE WEEK)

User	Temperature (F)	Compromise	Satisfaction (%)	Rewards (\$)
1	62-73	No	100	3.2
2	78-85	Yes	84	3.0
3	64-82	No	100	4.5
10	67-80	Yes	96	3.7

## III. CONTENT TO INCLUDE IN THE WORK

With the above motivation, introduction and pre-study, this work proposes an optimal structure for residential load aggregators with both effective demand-side ancillary service and strategic rewarding mechanism. Also, the detailed of the framework design, including optimization problem formulation, probabilistic comfortableness model, and the rewarding mechanism will be detailed in the work. In addition, the proposed framework will be validated on numerical case studies.

# Investigation of the Communication Delay and Its Impact on Wide-area Monitoring, Protection and Control Systems

Can Huang and Fangxing Li

EECS Department, University of Tennessee, Knoxville, TN 37996

Email: [chuang16@utk.edu](mailto:chuang16@utk.edu)

**Abstract**—In modern electrical power system, PMU-based wide-area measurement system (WAMS) promises to provide more accurate and timely data on the state of the power system. In this project, a statistics of communication delays in WAMS is shown. Instead of simulations in previous research works, experimental latencies in FNET (Frequency monitoring Network) are measured and analyzed in a statistical point of view. In addition, impacts of latencies on wide-area monitoring, protection and control systems are explored.

## I. DEFINITION OF THE COMMUNICATION DELAY

Generally, the communication delay may be represented as:

$$T = T_s + T_b + T_p + T_r = P_s / D_r + T_b + l/v + T_r$$

where  $T_s$  is the serial delay,  $T_b$  is the between packet delay,  $T_p$  is the propagation delay,  $T_r$  is the routing delay,  $P_s$  is the size of the packet (bits/packet),  $D_r$  is the data rate of the network,  $l$  is the length of the communication medium, and  $v$  is the velocity at which the data are sent though the communications medium (e.g., 0.6 to , where is the speed of light).

## II. REAL-TIME REQUIREMENTS OF WIDE-AREA MONITORING, PROTECTION AND CONTROL SYSTEMS

Table I PMU based protection and control applications

Application	Latency	Data	Protocols
Short-term stability control (e.g. transient stability)	~ 100 ms	Phasor	IEEE 1344, IEEE C37.118
Long-term stability control (e.g. wide area frequency, voltage stability)	1-5 seconds	Phasor	IEEE 1344, IEEE C37.118
FACTS feedback control, Smart switch-able networks	1-5 seconds	Phasor, SCADA	IEEE C37.118

## III. RESULTS AND DISCUSSION

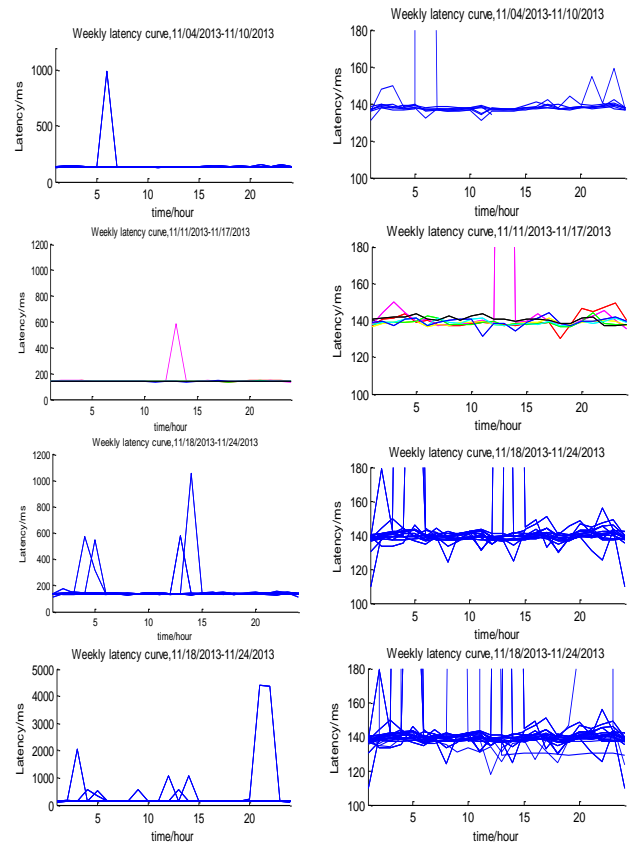


Fig. 1. Daily latency curve, unit 601, Richmond, November, 2013.

In this project, a practical statistics of communication delays in a wide area power system is presented. It is found that the latencies between station center and different measurements points show Normal distribution. Plus, it is observed that losses of sampled data have certain impacts on data delay through statistical result. Their relationship is worthy of further study. Moreover, with the known expectation of the distribution, various forecasting and estimation methods could be used to predict and calculate the real latency. Further work may include the study of impacts of different latencies on various PMU applications.



# Singular Value Sensitivity Based Optimal Control of Embedded VSC Based HVDC for Enhancing System Voltage Stability

Omar A. Urquidez\*, *Student Member, IEEE*, Le Xie\*, *Member, IEEE*

**Abstract**— In this paper [1], we propose a novel control algorithm for improving quasi-static voltage stability by use of an embedded Voltage Source Converter (VSC) based High Voltage Direct Current (HVDC) system. By embedding HVDC we refer to a meshed AC system with one or more HVDC terminals connected within the AC grid. The objective of the Singular Value Sensitivity (SVS) based algorithm is to produce a control order for the embedded VSC based HVDC system that maintains a quasi-static voltage stability margin for the meshed AC system. A voltage correction scheme is proposed for the VSC to jointly satisfy the system-wide voltage stability margin as well as the local voltage magnitude requirements. A contour-based mapping of the VSC capability space is introduced to illustrate how the SVS control achieves both the local and global control goals. The efficacy of the proposed algorithm is shown via numerical examples on a 6 bus and 118 bus system with and without static VAR compensation.

## I. KEY EQUATIONS

$$J = \begin{bmatrix} J_{P\theta} & J_{PV} \\ J_{Q\theta} & J_{QV} \end{bmatrix} \quad (1)$$

$$\sigma_c = \min \{ \bar{\sigma}_{J_R} \} \quad (2)$$

$$\min \sum P_{sr,k+1}^2 + Q_{s,k+1}^2 + Q_{r,k+1}^2 \quad (3)$$

st.

$$a_{1a} \Delta P_{sr,k} + a_{1b} \Delta Q_{s,k} + a_{1c} \Delta Q_{r,k} = \Lambda_\sigma \quad (4)$$

where,

$$a_{1a} = \frac{\sigma_c(P_k + \bar{\delta}_{P_{sr}}, Q_k) - \sigma_c(P_k, Q_k)}{\delta_{P_{sr}}} \quad (5)$$

$$a_{1b} = \frac{\sigma_c(P_k, Q_k + \bar{\delta}_{Q_s}) - \sigma_c(P_k, Q_k)}{\delta_{Q_s}}$$

$$a_{1c} = \frac{\sigma_c(P_k, Q_k + \bar{\delta}_{Q_r}) - \sigma_c(P_k, Q_k)}{\delta_{Q_r}} \quad (6)$$

## II. KEY FIGURES

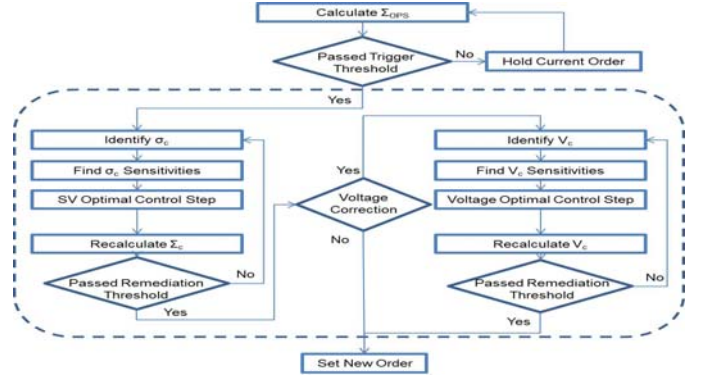


Figure 1. SVS based Optimal Control Flow Diagram.

## III. KEY RESULTS

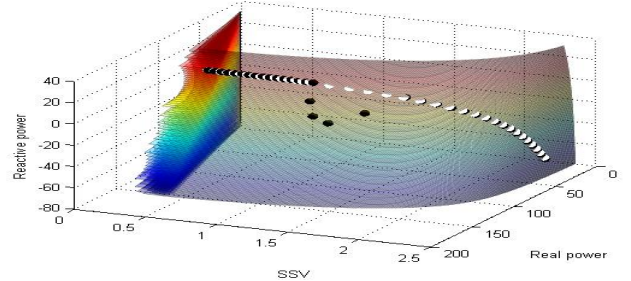


Figure 2. SVS Results for IEEE 118 Bus System in the Singular Value Capability Space.

## IV. CONCLUSION

Singular Value Sensitivity based optimal control utilizes the capabilities of a VSC based embedded HVDC system for the prevention of Quasi-Static Voltage Instability.

The algorithm performs an iterative process to step the system to a more secure operating point using sensitivities of the critical singular value of the reduced load flow Jacobian to the independent control variables of the VSC based embedded HVDC system via an optimal control step.

The singular value capability space is introduced as a visualization aid that builds vital intuition into the new paradigm introduced by the incorporation of a VSC based embedded HVDC system.

## V. REFERENCES

- [1] O. Urquidez, and L. Xie, "Singular Value Sensitivity Based Optimal Control of Embedded VSC based HVDC for Enhancing System Voltage Stability", *Working Paper, TAMU-ECE-2014-Apr-01*.

\*Department of Electrical and Computer Engineering, Texas A&M University, College Station, TX USA. Email: Lxie@ece.tamu.edu, omar.urquidez@tamu.edu

# Available Transfer Capability of Photovoltaic Generation Incorporated System

Xin Fang, Fangxing (Fran) Li  
Dept. of EECS  
The University of Tennessee  
Knoxville, TN, USA  
[fli6@utk.edu](mailto:fli6@utk.edu)

Ningchao Gao  
Qingpu Power Supply Company  
SMEPC  
Shanghai, China

Qiang Guo  
Dept. of Power System  
China EPRI  
Beijing, China

**Abstract**—Available transfer capability (ATC) has been broadly used to measure further reliable power transfer capability between two areas in a power system. With the rapid development of photovoltaic (PV) generation, the research concerning impacts of high PV penetration on ATC has received increasing interests due to PV's characteristic of uncertainty and intermittence. This paper presented a method to evaluate this impact. Firstly, an annual random PV generation fluctuation model is established with random weather conditions. The model considers the probability, the maximum solar radiation, the radiation fluctuation due to clouds mask, and the temperature variation under various weather conditions. Secondly, an ATC computation method based on the sequential Monte Carlo simulation (MCS) and the sensitivity analysis of the direct current (DC) power flow is proposed. Expectation, variance and corresponding annual indices are used to evaluate the impacts of PV on ATC. Finally, the proposed model and algorithm are validated by an analysis performed on the IEEE Reliability Test System (RTS).

**Index Terms**--Available Transfer Capability (ATC); Photovoltaic (PV) generation; sensitivity analysis; sequential Monte Carlo simulation.

## I. INTRODUCTION

With the energy crisis and the increasing environmental concern, the utilization of renewable energy has received increasing attention. The solar energy has great potentials as one of the main renewable energy sources [1]. In the last decade, a sustained and rapid development has been carried out in the photovoltaic (PV) generation such that the grid-connected PV generation is becoming one of the main means to utilize the solar energy. Due to the uncertainty and intermittence of PV, the system planners need to pay more attention on its impact when the PV penetration increases in future power systems [2].

Available transfer capability (ATC) is required to be posted on Open Access Same-time Information System (OASIS) to maintain a competitive and effective environment in the power market operation. According to NERC definition [3], ATC is a measure of the remaining transfer capability in the physical transmission network for future commercial activity over and above already committed uses.

There are some existing research works in the literatures. For instance, in [4], researchers have presented some methods to calculate ATC in the deterministic sense. In [5], the transmission lines contingencies and load uncertainty are considered for ATC calculation. In [8], the probabilistic distribution of load is considered using interval arithmetic method, which can provide some probabilistic information. The Monte Carlo simulation is utilized in [7] to consider all equipment unavailability and load uncertainty, which can provide the probabilistic information of ATC. The probabilistic models and algorithms of ATC is presented in [8] with a fast calculation speed using a model of two nodes as a simplification of two areas. Motivated by these previous works, this paper aims to address the ATC calculation in the probabilistic sense with high penetration PV generation considered.

In this paper, an annual chronological random PV power output model is established based on solar radiation and meteorological data. The model considers the probability, the maximum solar radiation, the radiation fluctuation due to clouds mask, and the temperature variation of different weather conditions. Then, an ATC calculation method based on sequential Monte Carlo simulation (MCS) and sensitivity analysis of DC power flow is presented. In this method, Monte Carlo simulation is employed to incorporate the system random contingencies and load uncertainty. The ATC calculation method between the source area and the sink area is derived from the DC power flow sensitivity analysis to evaluate the PV impact on ATC in a probabilistic sense. Finally, the presented method is validated through the simulation in the standard IEEE Reliability Test System.

# Cost Allocation in Stochastic Market Clearing

Ting Qiu

Department of Electrical Engineering  
University of Washington  
Seattle, USA  
[tqiu@uw.edu](mailto:tqiu@uw.edu)

Tobias Haring

Power Systems Laboratory  
ETH Zurich  
Zurich, Switzerland  
[tharing@eeh.ee.ethz.ch](mailto:tharing@eeh.ee.ethz.ch)

Daniel Kirschen

Department of Electrical Engineering  
University of Washington  
Seattle, USA  
[kirschen@uw.edu](mailto:kirschen@uw.edu)

**Abstract**— Electricity market designs have to cope with a growing share of renewable in-feed. Payments to generators have to ensure revenue sufficiency and adequate pricing of rising flexibility requirements. We investigate in this paper the welfare effects of (a) the introduction of cheap storage and (b) market redesign which allows the use of short-term information. In a rolling horizon setting and the inclusion of highly flexible devices like storage, generators may suffer from significant losses due to additional commitment costs. Thus, long-term reliability of the system may be jeopardized. The contributions of this paper are twofold: First, we assess the welfare impact of uncertainty. Second, we propose a pricing method which guarantees a profitable operation of all scheduled generators while maximizing the consumer surplus and compare it with existing cost-recovery methods. Simulation results show that the investigated market design changes have diverse effects on generators and a reduction of the commitment horizon may conflicts the profitability of storage. Further, the proposed pricing method outperforms the benchmark methods in terms of efficiency.

## I. INTRODUCTION

Current day ahead electricity market design have to be re-designed due to fluctuating in-feed in large scale. In this paper we focus on the re-design of centrally organized markets since it is shown that a centrally organized commitment is more cost efficient than a self-scheduling process. Centrally managed markets have to deal with two issues:

1. Higher commitment costs due to fluctuating in-feed in large scale may amplify or alleviate inter-hour and intra-hour flexibility and reserve requirements.
2. The trade-off between cost efficiency and coverage of non-convex costs. Thus, the establishment of a pricing framework that is capable of dealing with binary start-up and shut-down decisions.

Uncertainty and increased flexibility resources may be addressed in day ahead scheduling by introducing stochastic optimization, or the reduction of the commitment horizon. Cost recovery may be achieved through complex bidding where start-up costs are separately stated by generators with proper pricing mechanisms which balance the objectives of cost and revenue sufficiency, or the inclusion of energy storage devices in order to avoid financial burden through additional commitment costs. In this paper we assess market frameworks which combine the proposed measures of a short-term rolling horizon optimization, cost recovery, and the inclusion of highly flexible storage.

## II. METHODOLOGY

The approach is split in two consecutive steps: In the auction stage and a pricing stage. Fig. 1 shows a flow chart of the considered rolling horizon unit commitment for a rolling period of 12 hours. Solid bars indicate events which take place in the same time period. Arrow shows the direction of data flows. The left side arrow shows the time line. In the right side, each row indicates one rolling interval which contains three parts: wind forecast, look-ahead unit commitment using interval optimization and data recording.

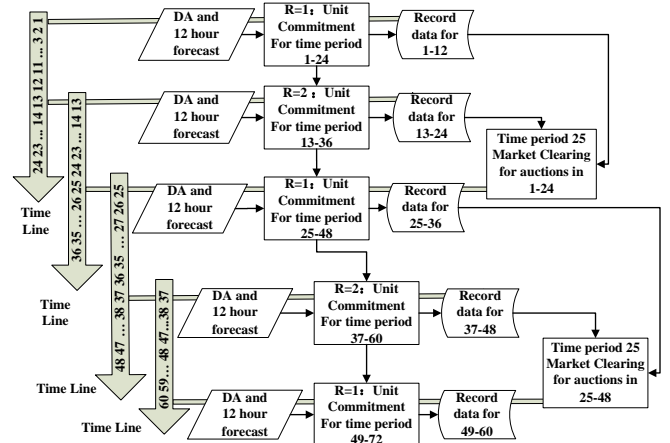


Fig. 1 Flow chart of rolling horizon unit commitment. The left side arrow shows the time line. In the right side, each row indicates one rolling interval.

### A. Auction Stage

We apply a rolling horizon commitment combined with interval optimization. We consider rolling periods of 4h, 6h and 12h. The forecasted wind data used in the unit commitment are updated accordingly.

### B. Pricing Stage

Pricing is done on a 24 hours basis. We test three different pricing methods with the aim of commitment cost recovery and compare them to a benchmark approach which comprises Locational Marginal Pricing (LMP) and no cost recovery.

# Multi-objective Robust Optimization Model for Microgrids Considering Tie-line Power Constraints and Wind Uncertainty

Linquan Bai, Fangxing Li, Tao Ding, Hongbin Sun

## Extended Abstract:

As an important clean energy source, wind power develops very fast in recent years, including microgrids. The wind power prediction techniques have been significantly studied. However, it is very difficult to accurately predict the wind power due to the intermittent nature of wind, which brings negative effects on the utilization of wind power.

When the microgrids operate at grid-connected mode, the tie-line power is always scheduled within a certain range to ensure the grid's security and stability in case of a contingency event.

The objectives of the energy management in microgrids may include maximizing the lifetime of energy storage (ES) and minimizing the utilization of power produced by the thermal units from the grid.

To address the above challenges, this paper proposes a multi-objective robust optimization model for microgrids with the consideration of tie-line constraints and wind uncertainty. The proposed method can effectively identify the optimal scheduling of ES and thermal power from the grid under the worst wind power forecast scenarios.

The objective function is given by:

$$f = \max_{P_w^{\min} \leq P_w^{(s)} \leq P_w^{\max}} \begin{cases} \min_{P_g} \sum C_1(P_g) \\ \max_E \sum C_2(E) \end{cases} \quad (1)$$

where  $P_g$  is the power produced by thermal units from the grid;  $E$  is the energy in the ES;  $P_w^{\max}$  and  $P_w^{\min}$  denote the upper and lower bound of wind power output with the consideration of the wind power forecast errors; and  $P_w^{(s)}$  is the wind power in a specific scenario.

In order to solve the multi-objective problem, the Pareto frontier is employed by transforming the multi-objective into a single one via the dualistic factor contrast method.

The constraints of the model can be expressed as (2)-(7).

### (i) Tie-line power constraint:

$$P_{line}^{\min}(t) \leq \sum_{i=1}^{N_g} P_{g,i}(t) + \sum_{k=1}^{N_w} P_{w,k}^f(t) + \sum_{j=1}^{N_e} P_{E,j}(t) - \sum_{r=1}^{N_d} P_{d,r}(t) \leq P_{line}^{\max}(t) \quad (2)$$

where  $P_{g,i}(t)$  is the power supplied by the  $i$ th thermal unit to

the microgrid;  $P_{w,k}^f(t)$  is the forecasted wind power;  $P_{E,j}(t)$  is the ES output; and  $P_{d,r}(t)$  is the load in the microgrid.

It should be noted that (2) is different from the energy balance constraints of traditional economic dispatch model, since the microgrid could exchange energy with the grid within a scheduled range  $[P_{line}^{\min}, P_{line}^{\max}]$ .

### (ii) Ramping constraint:

$$DR_i \leq P_{g,i}(t) - P_{g,i}(t-1) \leq UR_i \quad (3)$$

where  $UR_i$  and  $DR_i$  are the upper and lower ramping power, respectively, for a thermal unit.

### (iii) Transmission line constraint:

$$|P_{l-ij}(t)| \leq P_{l-ij}^{\max} \quad (4)$$

where  $P_{l-ij}(t)$  is the power flow on the transmission line and  $P_{l-ij}^{\max}$  indicates the capacity for each transmission line.

### (iv) Energy storage constraints:

In this work, the power output of ES is positive when it discharges and negative when it is charged.

$$-E_e \cdot \beta_C \leq E(t) - E(t-1)(1-\sigma) \leq E_e \cdot \beta_D \quad (5)$$

$$SOC_{\min} \leq E(t) / E_e \leq SOC_{\max} \quad (6)$$

where  $\beta_C$  is the maximum charge rate,  $\beta_D$  is the maximum discharge rate,  $\sigma$  is the self-discharge rate of ES;  $E_e$  is the rated capacity of ES;  $SOC_{\max}$  is the upper limit of SOC; and  $SOC_{\min}$  is the lower limit.

The equations with superscript (s) indicate all possible scenarios within the given wind power output range.

$$\begin{cases} P_{line}^{\min}(t) \leq \sum_{i=1}^{N_g} P_{g,i}^{(s)}(t) + \sum_{k=1}^{N_w} P_{w,k}^{(s)}(t) + \sum_{j=1}^{N_e} P_{E,j}^{(s)}(t) - \sum_{r=1}^{N_d} P_{d,r}(t) \leq P_{line}^{\max}(t) \\ DR_i \leq P_{g,i}^{(s)}(t) - P_{g,i}(t-1) \leq UR_i \\ |P_{l-ij}^{(s)}(t)| \leq P_{l-ij}^{\max} \\ SOC_{\min} \leq E^{(s)}(t) / E_e \leq SOC_{\max} \\ -E_e \cdot \beta_C \leq E^{(s)}(t) - E(t-1)(1-\sigma) \leq E_e \cdot \beta_D \end{cases} \quad (7)$$

where the second and the fifth sub-equations in (7) are the ramping constraints to deal with the uncertain wind power next time period.

To solve the above optimization problem, robust optimization method is very suitable to be introduced to find the optimal solutions of scheduling ES and thermal power in the worst scenario.

L. Bai and F. Li are with the EECS Department, The University of Tennessee at Knoxville (UTK), TN, USA.

T. Ding is with the Department of Electrical Engineering, Tsinghua University, Beijing, China and the EECS Department at UTK, TN, USA.

H. Sun is with the Department of Electrical Engineering, Tsinghua University, Beijing, China.

Contact: F. Li, [fli6@utk.edu](mailto:fli6@utk.edu).

# Power Flow Analysis with GPU-based Chebyshev Preconditioner and Conjugate Gradient Method

Xue Li, Fangxing Li

The Department of Electrical Engineering and Computer Science, the University of Tennessee, Knoxville, TN 37996, USA,  
Email: {xli44, fli6}@utk.edu

**Abstract**— Traditionally, linear equations in power system applications are solved by direct methods based on LU decomposition. With the development of advanced power systems controls, the industrial and research community is more interested in simulating larger, interconnected power grids. Iterative methods such as the conjugate gradient method have been applied to power system applications in the literature for its parallelism potential with larger systems. Preconditioner, used for preconditioning the linear system for a better convergence rate in iterative computations, is an indispensable part of iterative solving process. This work implemented a polynomial preconditioner Chebyshev preconditioner with graphic processing unit (GPU), and integrated a GPU-based conjugate gradient solver. Results show that GPU-based Chebyshev preconditioner can reach around 27x speedup for the largest test system, and conjugate gradient can gain more than 5x speedup. This demonstrates great potentials for GPU application in power system simulation.

## I. KEY EQUATIONS

```

Initialization:
 $\beta = \max(\text{eig}(A));$ 
 $\alpha = \beta/\text{ratio};$ 
 $Z = \frac{2}{\beta - \alpha}A - \frac{\beta + \alpha}{\beta - \alpha}I;$ 
 $q = (1 - \sqrt{(\alpha/\beta)})/(1 + \sqrt{(\alpha/\beta)});$ 
 $c_0 = (-q)^0/\sqrt{\alpha\beta}; c_1 = (-q)^1/\sqrt{\alpha\beta};$ 
 $T_{p0} = I; T_{p1} = Z;$ 
 $G = \frac{c_0 I}{2} + c_1 T_{p1}$ 
for i = 2:r
     $T = 2ZT_{p1} - T_{p0};$ 
     $c = (-q)^i/\sqrt{\alpha\beta};$ 
     $G = G + cT;$ 
     $T_{p0} = T_{p1}; T_{p1} = T;$ 
endfor
    
```

Fig. 1. Algorithm of the conjugate gradient method

## II. KEY RESULTS

TABLE I. CHEBYSHEV PRECONDITIONER PERFORMANCE COMPARISON BETWEEN MATLAB AND GPU IMPLEMENTATION OF VARIOUS SYSTEMS

System	Size	CPU(ms)	GPU(ms)	Speedup
IEEE30	29 by 29	0.780	2.190	0.36
IEEE57	56 by 56	0.891	2.185	0.41
IEEE118	117 by 117	1.517	2.292	0.66
IEEE300	299 by 299	4.162	5.043	0.83
494-bus	494 by 494	8.642	5.187	1.67
662-bus	662 by 662	15.176	5.293	2.87
685-bus	685 by 685	17.411	5.187	3.36
1138-bus	1138 by 1138	47.850	5.876	8.14
UCTE	1253 by 1253	58.209	5.579	10.43
Case2383wp	2382 by 2382	159.580	6.927	23.04
Case2736sp	2735 by 2735	206.658	7.526	27.46

TABLE II. CONJUGATE GRADIENT PERFORMANCE COMPARISON BETWEEN MATLAB AND GPU IMPLEMENTATION OF VARIOUS SYSTEMS

System	Size	CPU(ms)	GPU(ms)	Speedup
IEEE30	29 by 29	1.173	1.587	0.74
IEEE57	56 by 56	1.969	2.636	0.75
IEEE118	117 by 117	5.516	6.743	0.82
IEEE300	299 by 299	13.232	13.585	0.97
494-bus	494 by 494	61.598	62.821	0.98
662-bus	662 by 662	38.957	25.984	1.50
685-bus	685 by 685	41.752	26.555	1.57
1138-bus	1138 by 1138	142.718	71.262	2.00
UCTE	1253 by 1253	15.095	6.513	2.32
Case2383wp	2382 by 2382	236.725	68.058	3.48
Case2736sp	2735 by 2735	244.193	46.737	5.22

# Unified Stochastic and Robust Unit Commitment

Chaoyue Zhao and Yongpei Guan

Department of Industrial and Systems Engineering, University of Florida  
cherryzhao09@ufl.edu, guan@ise.ufl.edu

**Abstract**—Due to increasing penetration of intermittent renewable energy and introduction of demand response programs, uncertainties occur in both supply and demand sides in real time for the current power grid system. To address these uncertainties, most ISOs/RTOs perform reliability unit commitment runs after the day-ahead financial market to ensure sufficient generation capacity available in real time to accommodate uncertainties. Two-stage stochastic unit commitment and robust unit commitment formulations have been introduced and studied recently to provide day-ahead unit commitment decisions. However, both approaches have limitations: 1) computational challenges due to the large scenario size for the stochastic optimization approach and 2) conservativeness for the robust optimization approach. In this paper, we propose a novel unified stochastic and robust unit commitment model that takes advantage of both stochastic and robust optimization approaches. That is, this innovative model can achieve a low expected total cost while ensuring the system robustness. By introducing weights for the components for the stochastic and robust parts in the objective function, system operators can adjust the weights based on their preferences. Finally, a Benders' decomposition algorithm is developed to solve the model efficiently. The computational results indicate that this approach provides a more robust and computationally trackable framework as compared to the stochastic optimization approach and a more cost-effective unit commitment decision as compared to the robust optimization approach.

## I. KEY CONTRIBUTIONS

- (1) Our proposed approach takes the advantages of both the stochastic and robust optimization approaches. Our approach can provide a day-ahead unit commitment decision that can lead to a minimum expected total cost while ensuring the system robustness.
- (2) Our proposed approach can generate a less conservative solution as compared to the two-stage robust optimization approach, and a more robust solution as compared to the two-stage stochastic optimization approach.
- (3) Our proposed approach can be implemented in a single Benders' decomposition framework. The computational time can be controlled by the system operators. Meanwhile, the system operators can also adjust the weights in the objective function, based on their preferences on stochastic and/or robust optimization approaches.

## II. KEY EQUATIONS

The uncertainty set of the load:

$$\mathcal{D} := \left\{ d \in \mathcal{R}^{|B| \times |T|} : D_t^{b-} \leq d_t^b \leq D_t^{b+}, \forall t, \forall b \right. \\ \left. \sum_{b \in B} \pi_b^t d_b^t \leq \bar{\pi}^t, \sum_{t=1}^T \sum_{b \in B} \pi_b^t d_b^t \leq \bar{\pi} \right\}.$$

The master problem:

$$\min_{y, u, v \in \{0,1\}} (\mathbf{a}^T u + \mathbf{b}^T v) + \alpha \frac{1}{N} \sum_{n=1}^N \theta^n + (1 - \alpha) \bar{\theta} \\ s.t. \quad \mathbf{A}y + \mathbf{B}u + \mathbf{C}v \geq \mathbf{r}, \\ \text{Feasibility cuts, Optimality cuts.}$$

## III. KEY RESULTS

TABLE I  
RESULTS UNDER DIFFERENT RATIO% AND BUDGET % SETTINGS

Ratio%		Budget%		
		5%	15%	25%
5%	Obj. Val.(\$)	737,134	737,134	737,134
	# of Start-ups	10	10	10
	Time(sec)	48	48	48
15%	Obj. Val.(\$)	737,439	738,372	738,272
	# of Start-ups	10	11	11
	Time(sec)	61	163	163
25%	Obj. Val.(\$)	738,561	739,374	740,175
	# of Start-ups	12	12	13
	Time(sec)	106	392	1193

TABLE II  
COMPARISON BETWEEN SO AND SR APPROACHES

Budget%	Model	T.C.(\$)	UC.C.(\$)	# of Start-ups	Time(sec)
3%	SO	737,799	49,500	10	62
	SR	737,799	49,500	10	50
5%	SO	738,112	49,500	10	59
	SR	738,112	49,500	10	47
10%	SO	740,878	49,500	10	62
	SR	739,911	52,500	11	126
15%	SO	752,575	49,500	10	63
	SR	741,170	51,000	11	167
20%	SO	782,361	49,500	10	63
	SR	742,866	54,000	12	222

TABLE III  
COMPARISON BETWEEN RO AND SR APPROACHES

Budget%	Model	T.C.(\$)	UC.C.(\$)	# of Start-ups	Time (sec)
3%	RO	737,294	49,500	10	375
	SR	737,275	49,500	10	49
5%	RO	738,514	51,000	11	292
	SR	737,275	49,500	10	48
10%	RO	739,515	54,000	12	375
	SR	738,190	52,500	11	127
15%	RO	739,868	54,000	12	339
	SR	738,506	51,000	11	168
20%	RO	749,064	63,300	15	303
	SR	739,320	54,000	12	223



# Stochastic Optimization Formulations for Reliability Unit Commitment Runs

Kai Pan, *Student Member, IEEE*, Yang Lu, Yongpei Guan, *Senior Member, IEEE*, and Jean-Paul Watson, *Member, IEEE*

**Abstract**—To address the uncertainties caused by the penetration of intermittent renewable energy, most ISOs/RTOs perform day-ahead and look-ahead reliability unit commitment (RUC) runs, ensuring sufficient generation capacity available in real time to accommodate the uncertainties. Two-stage stochastic optimization models have been studied extensively to strengthen the RUC runs, while multi-stage stochastic optimization models were barely studied. In this paper, we investigate the unit commitment and economic dispatch decision differences generated by these two approaches considering the load uncertainties in the system. The stochasticity is represented by a set of scenarios for the two-stage model and a scenario tree for the multi-stage case.

**Index Terms**—Unit commitment, mixed-integer linear programming, two-stage stochastic optimization, multi-stage stochastic optimization

## I. KEY FORMULATIONS

### A. Two-Stage Stochastic Unit Commitment (TSUC)

$$\min \sum_{t=1}^T \sum_{i \in \mathcal{G}} (\text{SU}_i u_t^i + \text{SD}_i v_t^i) + \frac{1}{N} \sum_{n=1}^N \mathcal{Q}(y, u, v, \xi^n) \quad (1)$$

$$\text{s.t.} \quad -y_{t-1}^i + y_t^i - y_k^i \leq 0, \quad \forall k : 1 \leq k - (t-1) \leq \text{MU}_i, \quad \forall i \in \mathcal{G}, \forall t \quad (2)$$

$$y_{t-1}^i - y_t^i + y_k^i \leq 1, \quad \forall k : 1 \leq k - (t-1) \leq \text{MD}_i, \quad \forall i \in \mathcal{G}, \forall t \quad (3)$$

$$y_t^i - y_{t-1}^i \leq u_t^i, \quad \forall i \in \mathcal{G}, \forall t \quad (4)$$

$$v_t^i = y_{t-1}^i - y_t^i + u_t^i, \quad \forall i \in \mathcal{G}, \forall t \quad (5)$$

$$y_t^i, u_t^i, v_t^i \in \{0, 1\}, \quad \forall i \in \mathcal{G}, \forall t, \quad (6)$$

where for each  $m$ ,  $\mathcal{Q}(y, u, v, \xi^m)$  is equal to

$$\min \sum_{t=1}^T \sum_{i \in \mathcal{G}} F_i(q_t^i(\xi^m)) + \sum_{t=1}^T (\alpha_t z_t(\xi^m) + \beta_t w_t(\xi^m)) \quad (7)$$

$$\text{s.t.} \quad L_i y_t^i \leq x_t^i(\xi^m) \leq U_i y_t^i, \quad \forall i \in \mathcal{G}, \forall t \quad (8)$$

$$x_t^i(\xi^m) - x_{t-1}^i(\xi^m) \leq (2 - y_{t-1}^i - y_t^i) \overline{\text{UR}}_i + (1 + y_{t-1}^i - y_t^i) \text{UR}_i, \quad \forall i \in \mathcal{G}, \forall t \quad (9)$$

$$x_{t-1}^i(\xi^m) - x_t^i(\xi^m) \leq (2 - y_{t-1}^i - y_t^i) \overline{\text{DR}}_i + (1 - y_{t-1}^i + y_t^i) \text{DR}_i, \quad \forall i \in \mathcal{G}, \forall t \quad (10)$$

$$\sum_{i \in \mathcal{G}} x_t^i(\xi^m) + w_t(\xi^m) - z_t(\xi^m) = \sum_{b \in \mathcal{B}} d_t^b(\xi^m), \quad \forall t. \quad (11)$$

$$x_t^i(\xi^m) \geq 0, w_t(\xi^m), z_t(\xi^m) \geq 0, \quad \forall i \in \mathcal{G}, \forall t. \quad (12)$$

### B. Multi-Stage Stochastic Unit Commitment (MSUC)

$$\min \sum_{n \in \mathcal{V}} p_n \left( \sum_{i \in \mathcal{G}} (\text{SU}_i r_n^i + \text{SD}_i s_n^i + F_i(q_n^i) + \alpha_n \lambda_n + \beta_n \mu_n) \right) \quad (13)$$

$$\text{s.t.} \quad o_n^i - o_{n-}^i \leq o_k^i, \quad \forall n \in \mathcal{V}, \forall i \in \mathcal{G}, \forall k \in \mathcal{H}_{\text{MU}_i}(n), \quad (14)$$

$$o_{n-}^i - o_n^i \leq 1 - o_k^i, \quad \forall n \in \mathcal{V}, \forall i \in \mathcal{G}, \forall k \in \mathcal{H}_{\text{MD}_i}(n), \quad (15)$$

$$o_n^i - o_{n-}^i \leq r_n^i, \quad \forall n \in \mathcal{V}, \forall i \in \mathcal{G}, \quad (16)$$

$$s_n^i = o_{n-}^i - o_n^i + r_n^i, \quad \forall n \in \mathcal{V}, \forall i \in \mathcal{G}, \quad (17)$$

$$L_i o_n^i \leq q_n^i \leq U_i o_n^i, \quad \forall n \in \mathcal{V}, \forall i \in \mathcal{G}, \quad (18)$$

$$\sum_{i \in \mathcal{G}} q_n^i + \mu_n - \lambda_n = \sum_{b \in \mathcal{B}} d_n^b, \quad \forall n \in \mathcal{V}, \quad (19)$$

$$q_n^i - q_{n-}^i \leq (2 - o_n^i - o_{n-}^i) \overline{\text{UR}}_i + (1 + o_{n-}^i - o_n^i) \text{UR}_i, \quad \forall n \in \mathcal{V}, \forall i \in \mathcal{G}, \quad (20)$$

$$q_{n-}^i - q_n^i \leq (2 - o_n^i - o_{n-}^i) \overline{\text{DR}}_i + (1 - o_{n-}^i + o_n^i) \text{DR}_i, \quad \forall n \in \mathcal{V}, \forall i \in \mathcal{G}, \quad (21)$$

$$o_n^i, r_n^i, s_n^i \in \{0, 1\}, q_n^i \geq 0, \quad \forall n \in \mathcal{V}, \forall i \in \mathcal{G}. \quad (22)$$

## II. KEY RESULTS

TABLE I: Results for IEEE Six-bus System

T	Load at Root Node (MW)	Model	Obj. (\$)	Percentage (%)	CPU times (sec)
5	[460,630]	TSUC	18389.6	2.91	1.31
		MSUC	17853.7		45.94
5	[500,670]	TSUC	19755.8	2.53	1.19
		MSUC	19255.1		4.41
6	[460,610]	TSUC	21685.4	1.56	79.17
		MSUC	21346.8		735.47
6	[480,580]	TSUC	22283.5	1.50	74.73
		MSUC	21949		96.34

TABLE II: Results for IEEE 118-bus System

T	Load at Root Node (MW)	Model	Obj. (\$)	Percentage (%)	CPU times (sec)
6	[2500,4500]	TSUC	313340	7.04	45.41
		MSUC	291268		185.80
6	[2550,4450]	TSUC	308256	4.14	43.23
		MSUC	295495		118.81
6	[2450,4550]	TSUC	329569	8.30	85.94
		MSUC	302170		120.44
6	[2400,4600]	TSUC	342778	10.40	33.61
		MSUC	307187		124.36

# Dynamic Adjustment of OLTC Parameters using Voltage Sensitivity while utilizing DG for Volt/VAR Support

D. Ranamuka, *Student Member, IEEE*, A. P. Agalgaonkar, *Senior Member, IEEE*, and K. M. Muttaqi, *Senior Member, IEEE* - Australian Power Quality and Reliability Centre, University of Wollongong, Australia

**Abstract**--A novel methodology is proposed in this paper to assess the impact of voltage support DG on voltage correction and update the substation OLTC parameters dynamically. As an assessment tool, first order sensitivity of the regulating point voltage,  $V_{LC}$  to the change in reactive power support provided by voltage support DG,  $Q_{DG}$  is derived. The estimated value of voltage change by means of VAR support by DG at the load centre, obtained using proposed sensitivity analysis, is used to assess the impact of voltage support DG on the operation of line drop compensation (LDC). Based on such information, a strategy is proposed to dynamically update the OLTC parameters for effective voltage control in the presence of voltage support DG. The simulation results show the accuracy of the mathematical model used for analysis and its successful implementation.

## I. PROPOSED VOLTAGE SENSITIVITY - KEY EQUATIONS

From the equation for  $V_{LC}$ , it can be seen that the  $V_{LC}$  is a function of  $V_{OLTC}$ ,  $\alpha_{OLTC}$ ,  $I$ ,  $\theta$ , and  $R_L$ ,  $X_L$  (LDC settings).

$$\begin{aligned} \Delta V_{LC} &= \left( \frac{\partial V_{LC}}{\partial V_{OLTC}} \right) \Delta V_{OLTC} + \left( \frac{\partial V_{LC}}{\partial \alpha_{OLTC}} \right) \Delta \alpha_{OLTC} + \left( \frac{\partial V_{LC}}{\partial I} \right) \Delta I + \\ &+ \left( \frac{\partial V_{LC}}{\partial \theta} \right) \Delta \theta \\ \Delta V_{LC} &= (LC1) \Delta V_{OLTC} + (LC2) \Delta \alpha_{OLTC} + (LC3) \Delta I + (LC4) \Delta \theta \end{aligned}$$

From the phasor diagram and system Jacobian matrix :

$$\begin{aligned} \frac{\Delta I}{\Delta Q_{DG}} &= (I1) \times (M_{VQ})_{oltc,k} + (I2) \times (M_{VQ})_{(oltc+1),k} + (I3) \times \\ &\times \left( (M_{\alpha Q})_{oltc,k} - (M_{\alpha Q})_{(oltc+1),k} \right) \end{aligned}$$

$$\begin{aligned} \frac{\Delta \theta}{\Delta Q_{DG}} &= \left( \frac{1 - \theta 1.12}{\theta 3} \right) \times (M_{VQ})_{(oltc+1),k} - \left( \frac{\theta 2 + \theta 1.11}{\theta 3} \right) \times \\ &\times (M_{VQ})_{oltc,k} - \left( \frac{\theta 4 + \theta 1.13}{\theta 3} \right) \times \left( (M_{\alpha Q})_{oltc,k} - (M_{\alpha Q})_{(oltc+1),k} \right) \end{aligned}$$

Proposed voltage sensitivity y :

$$\begin{aligned} \frac{\Delta V_{LC}}{\Delta Q_{DG}} &= (LC1) \times (M_{VQ})_{oltc,k} + (LC2) \times (M_{\alpha Q})_{oltc,k} + \\ &+ (LC3) \times \left( \frac{\Delta I}{\Delta Q_{DG}} \right) + (LC4) \times \left( \frac{\Delta \theta}{\Delta Q_{DG}} \right) \end{aligned} \quad (A)$$

## II. DYNAMIC ADJUSTMENT OF OLTC PARAMETERS

The severity of DG impact on operation of LDC is based on how much the voltage change by DG at load centre contributes to violate dead-band limit or supports to minimize the voltage error for OLTC control. On that basis, the proposed strategy for dynamically updating the LDC settings in presence of voltage support DG is developed. It is proposed to practically

implement this strategy using a substation centered DMS for on-line voltage control. The diagrammatic representation of proposed system design is shown in Fig. 1.

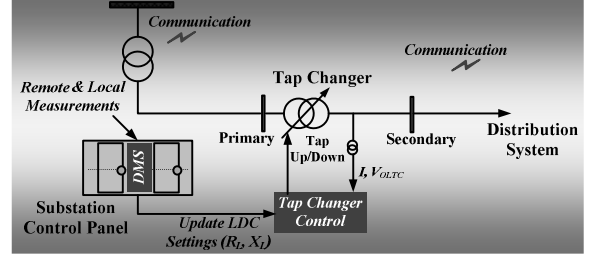


Fig. 1. Topology of system design for proposed dynamic operation of OLTC.

## III. KEY RESULTS

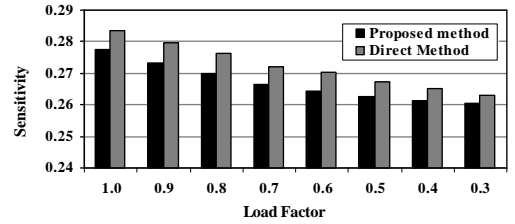


Fig. 2. Sensitivity values derived using proposed and direct methods

TABLE I

ESTIMATED VOLTAGE CHANGE BY QDG USING PROPOSED SENSITIVITY			
Load Factor	Proposed method/(pu)	Multiple Power Flow/(pu)	Mismatch /(pu)
1.000	0.0183	0.0182	0.0001
0.900	0.0181	0.0179	0.0002
0.800	0.0178	0.0177	0.0001
0.700	0.0176	0.0174	0.0002
0.500	0.0173	0.0171	0.0002
0.400	0.0172	0.0170	0.0002

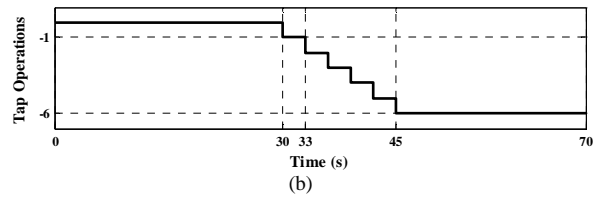
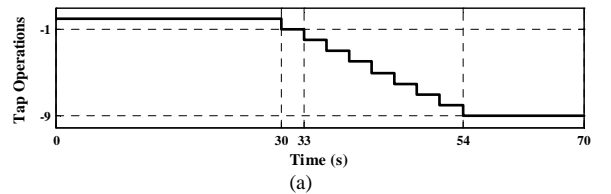


Fig. 3. Tap operations of substation OLTC (a) under conventionally derived LDC settings and (b) under proposed LDC settings, where load factor is 0.8.

# Adaptive frequency control application for a real autonomous islanded grid

Yiannis Tofis

Yiasoumis Yiasemi

Elias Kyriakides

Department of Electrical and Computer Engineering

KIOS Research Center for Intelligent Systems

and Networks

University of Cyprus

Nicosia, Cyprus

{ytofis01, yiasemi.yiasoumis, elias}@ucy.ac.cy

Klaus Kansala

VTT Technical Research Centre of Finland

Oulu, Finland

klaus.kansala@vtt.fi

**Abstract**—This poster presents an adaptive frequency remote control of an islanded autonomous grid equipped with a 5.5 kW wind generator, 7.2 kW solar panels, and 58 kWh energy storage. The islanded grid is located at VTT premises in Finland. The grid was controlled remotely from Cyprus using a communication protocol. The ultimate aim of the work described in this paper is to control and balance the generation and demand in the islanded grid through direct load management based on a single point measurement of the electric frequency.

**Index Terms**—Adaptive frequency control, frequency response, direct load management, islanded grid.

## I. INTRODUCTION

In this paper an adaptive frequency control scheme is applied to a real islanded grid (see Fig. 1). Even though the system is small, the concept can be extended to larger systems as well. The pilot grid under consideration has two modes of operation: the utility grid-connected operation and the islanded operation mode. The loads were the appliances of a smart home and an Electric Vehicle (EV). The controllable appliances in the smart home were the electric sauna (4.5 kW), the kitchen oven (5.0 kW) and the floor heating (0.5 kW). The islanded grid is supplied by a 3-phase inverter with a total output capacity of 15 kW (3 x 5 kW).

Because of the variable nature of renewables integrated to the island, sudden power imbalances occur. These imbalances are reflected on the frequency characteristic of the system resulting in frequency fluctuations. This paper studies the effect of the application of an adaptive frequency control scheme applied on a real islanded grid in order to mitigate these frequency fluctuations and minimize the frequency variation from its nominal value of 50 Hz. This is achieved via a direct load management that maintains the instantaneous

balance between generation and demand.

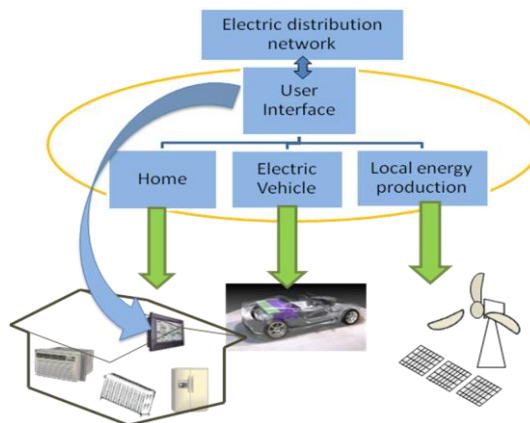


Figure 1. Local energy production test site

## II. METHODOLOGY AND IMPLEMENTATION

The proposed method is based on the online, approximation based feedback linearization of the swing equation of the system under consideration.

The whole control scheme is running on a MATLAB session in Cyprus on a personal computer. The control server at VTT premises was remotely accessed via Secure Shell (SSH) protocol while the communication between the MATLAB session and the frequency meter on site was achieved through the TCP Modbus protocol, an open Master/Slave application protocol used on top of Ethernet-TCP/IP. Next, the communication between the MATLAB session (master) and the manageable devices was achieved through the Unitronics PCOM protocol.

Finally, the charging of the EV is employed in order to represent an accountable load disturbance since it absorbs 32A of current in fast charging mode on a 400 V line to line.

# Emission-based Optimal Dispatch Framework with DR and Volatile Wind Power

Hantao Cui, *Student Member, IEEE*, Fangxing Li, *Senior Member, IEEE*

**Abstract**—The increasing penetration of wind power aims at reducing fuel consumption and the consequent emissions. On the contrary, volatility of wind power, especially the prediction error, increases the number of unintended startups or shutdowns of the prevailing thermal units thus elevates the emission level. This paper presents a framework for ISO and LSE to handle emission-based security-constrained optimal dispatch that accommodates demand response (DR) and volatility of wind power (WP) output. Expected results for the established model would demonstrate the effectiveness of minimizing emissions.

## I. FRAMEWORK DESCRIPTION

In the proposed framework, for day-ahead market, ISO commits the units according to emissions bids from generators, predicted WP output and informed load level by load side entity (LSE). ISO also checks network security of each commitment result to rule out violations. LSE, as an aggregator of demand side, performs voluntary DR programs internally and reviews load interrupting requests outside from ISO. LSE can be viewed as the sole demand side participant, on behalf of all loads, in the market operated by ISO.

Two types of incentive-based DR programs are included: voluntary and mandatory. Voluntary programs are managed by LSE with the forecasted electricity price. Mandatory programs are called for by ISO during network security check and verified by LSE. Volatility of WP is also incorporated into the framework, derived from the prediction error described by Beta distribution [1].

This framework adopts the flexibility at demand side, takes into account the impact of volatile WP and aims at minimizing emissions. Through nodal prices, balance of demand side and generation is achieved. It also clarifies the duties and steps for ISO and LSE, which is amenable for day-ahead optimal dispatch. Scheme of the framework is given in Fig. 1.

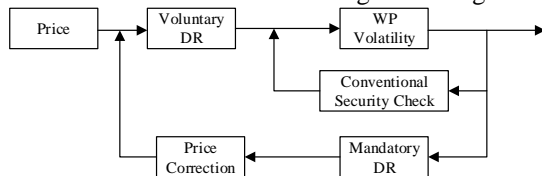


Fig. 1. Scheme of the presented framework

## II. MODELING FORMULATION

An input-based model is used to capture the emission characteristics of units. With a non-parametric Nadaraya-Watson kernel estimator of  $SO_x$  and  $NO_x$  emissions level[2], an estimate function that specifies the pollution level of pollutant  $p$  as a function of generator  $g$ 's burned fuel  $f$  is given as (1), where  $\phi_{g,p}$  and  $f_g^n$  are the observed actual emission level and

the actual fuel consumed, respectively.  $K(\cdot)$  is the kernel of smoothing function and  $h$  the bandwidth by which weight is exercised on neighboring observations.

$$\phi_{g,p}(f) = \frac{\sum_{n \in N} K\left(\frac{f - f_g^n}{h}\right) \phi_{g,p}^n}{\sum_{n \in N} K\left(\frac{f - f_g^n}{h}\right)} \quad (1)$$

Voluntary DR are modeled with fixed price elasticity and determined at early stage of the iterative scheduling process. Elasticity is given as

$$\varepsilon_k = \frac{\partial D_k / D_k}{\partial PR_k / PR_k} \quad (2)$$

Mandatory DR supplied by generators with high marginal emissions rate would be demanded curtailment by ISO, rather than those located within high LMP zones. However, ISO faces the dilemma that each location differs in the sensitivity of price and emission. To identify the nodes where curtailment of DR is both economically and environmentally beneficial, emissions price (in \$/ton  $SO_x$  and  $NO_x$ ) is defined to convert emissions reduction to value in dollar. Overall value of DR at bus  $j$  composes of LMP reduction and emissions reduction value, is given as

$$\beta_j = f(\lambda_j) + g(\kappa_j) \quad (3)$$

where  $\lambda_j$  and  $\kappa_j$  are the LMP and marginal emissions rate at bus  $j$ , respectively[3].

Finally, with Bender's decomposition, UC with SC for ISO is decomposed into two iterative problems. Master problem solves unit commitment and eliminates Bender's cut from sub problem, while sub problem checks network security and generates Bender's cuts. The whole framework is modeled as mixed-integer programming problem and solved by CPLEX.

## III. EXPEDTED RESULTS

To illustrate the validity and effectiveness of the presented framework and model, case study will be performed on ISO New England 39-bus system with 10 generators. Volatility of wind power will be identified with fixed Beta distribution parameters, followed with Monte-Carlo sampling and Cholesky decomposition. Voluntary DR resources will also follow a fixed elasticity.

Design of cases will focus on the configuration of Mandatory DR resources, i.e. locations, maximum curtailment power and duration. Successful solving the iterative model will show the validity of the model. A more promising result would be that under certain circumstances DR will be dispatched for emissions reduction purpose at the cost of higher LMP, although it could be used to reduce the latter. Meanwhile, time consumption to solve the model needs concern as an evaluation of its practical use.

# Valuation of the Deterministic and Stochastic Uncertainty Models in Unit Commitment Applications

Yishen Wang, Yury Dvorkin, and Daniel. S. Kirschen  
 Department of Electrical Engineering  
 University of Washington Seattle, USA.  
 E-mail: ywang11@uw.edu

**Abstract**— Intensive integration of renewable generation encourages system operators to revise their day-ahead decision-making procedures to mitigate the impact of the stochastic nature of these resources on power system’s ex-post operating cost and reliability. This challenge suggests the usage of stochastic models of the net load uncertainty, such as a set or a range of scenarios, instead of the deterministic models, which may miscalculate vagaries of renewable generation.

A number of scenario reduction techniques has been proposed to facilitate the practical implementation of a various stochastic unit commitment formulations. This paper compares these different scenario reduction techniques, Fast Forward Selection (FFS), Simultaneous Backward Reduction (SBR), K-means and Importance Sampling (IS) in terms of the resulting operating cost, obtained using Monte Carlo simulations, and the computational time of the stochastic UC.

## I. MOTIVATION

Power systems re-assess their flexibility requirements as additional quantities of renewable generation are installed. In the deterministic UC framework, this results in additional capacity, ramp rate, and ramping duration requirements [1], which ensure the ability of system operators to balance supply and demand, if these are to deviate from the central forecast. In the stochastic UC formulations, flexibility requirements are assessed using stochastic scenarios, Fig. 1, derived as explained in [2]. The deterministic and stochastic uncertainty models result in different costs and computational performance, which is discussed by the authors in this work.

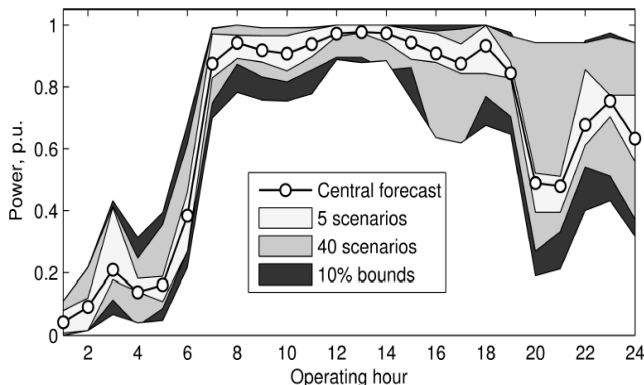


Figure 1. Comparison of the range of uncertainty obtained for different number of scenarios and 10% bounds

## II. KEY RESULTS

TABLE I. DAY-AHEAD COST (IN  $10^3\$$ ) / COMPUTATIONAL TIME (s)

Positively Correlated Wind				
Scenarios	FFS	SBR	K-means	IS
5	566.7*/53.8	568.8/54.1	567.0/58.9	567.7/59.0
10	570.6/168	571.2/156	570.5*/291	575.2/271
40	576.0*/2208	576.6/3516	578.1/4097	578.2/4801
Negatively Correlated Wind				
Scenarios	FFS	SBR	K-means	IS
5	657.1*/45.5	657.6/42.7	656.7/52.8	652.4/55.8
10	657.1/108.0	659.1/115.7	656.9*/101.9	660.3/111.9
40	660.6*/2635	662.6/1645	663.5/3797	663.2/7890

TABLE II. EXPECTED EX-POST COST (IN  $10^3\$$ ) OF THE SCENARIO-BASED SCHEDULE

Positive Correlated Wind				
Scenarios	FFS	SBR	K-means	IS
5	593.0*	593.1	593.1	596.2
10	590.4*	591.0	590.8	592.2
40	593.3*	593.5	594.2	596.7
Negative Correlated Wind				
Scenarios	FFS	SBR	K-means	IS
5	666.6*	669.0	668.4	667.6
10	667.4*	669.1	668.7	668.1
40	669.1*	671.9	671.7	671.0

## III. CONCLUSION

The authors conclude that the FFS scenario-reduction technique outperforms other stochastic and deterministic uncertainty models.

## REFERENCES

- [1] Y. Dvorkin, M. A. Ortega-Vazquez, D. S. Kirschen, “Assessing Flexibility in Power Systems,” accepted for publication in *IET on Generation, Transmission, and Distribution*, 2014.
- [2] Y. Dvorkin, Y. Wang, H. Pandzic, D. S. Kirschen, “Comparison of Scenario Reduction Techniques for the Stochastic Unit Commitment,” in Proc. of *2014 IEEE Power and Energy Society General Meeting*, Washington DC, 2014.

# Determination of Design Parameters for Direct-Drive Wind Turbines

Yichuan Niu

Student Member, IEEE

Department of Electrical & Computer Engineering  
The University of Texas at Austin  
yichuan.niu@utexas.edu

Surya Santoso

Senior Member, IEEE

Department of Electrical & Computer Engineering  
The University of Texas at Austin  
ssantoso@mail.utexas.edu

**Abstract**—Starting with rotor blade performance and permanent magnet synchronous machine data, a series of equations for determining preliminary aerodynamic and electrical design parameters of a direct-drive wind turbine with a given converter topology is presented in this paper. Serving as a case study, these equations, derived based on aerodynamic, circuit analysis and electric machine theories, can determine blade radius, expected cut-in, rated, and cut-out wind speeds, sizes of inline inductors on machine and grid sides and the DC capacitor, and controller limits accurately. The efficacy of the method is demonstrated by modeling and simulating a complete Type 4 wind turbine based on the derived design parameters. It is shown that performance and response of the simulated wind turbine model meet the design criteria.

**Index Terms**-- Full converter, parameter design, Type 4, wind power generation.

## I. INTRODUCTION

The objective of this paper is to develop a series of equations as a case study to determine design parameters of a direct-drive wind turbine (Type 4) with the assumptions that the converter topology along with turbine rotor performance  $C_p$  and electric machine data are given. These equations are derived using aerodynamic, circuit analysis and electric machine theories. It will be demonstrated that these equations can be used to conveniently determine aerodynamic and electrical parameters such as blade radius, expected cut-in, rated, and cut-out wind speeds, sizes of inline inductors on machine and grid sides and the DC capacitor, and controller limits accurately. Researchers and practicing engineers who want to develop a wind turbine system will find this paper useful as a benchmark and a basis for initial design.

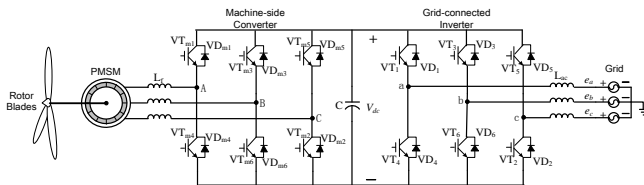


Figure 1. Equivalent circuit of a Type 4 direct-drive wind turbine

## II. KEY FIGURES

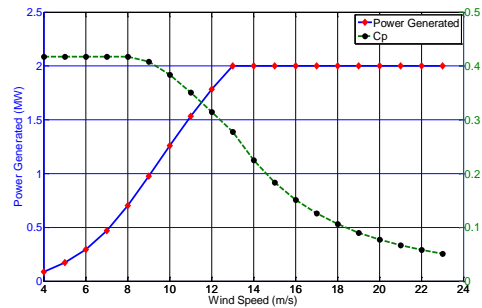


Figure 4. Power curve and blade performance of the wind turbine

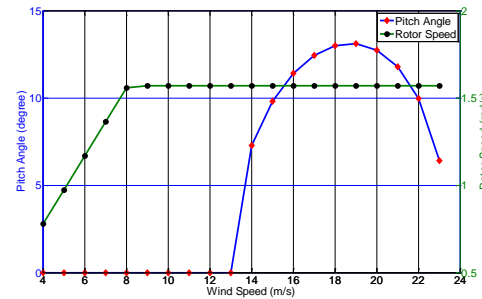


Figure 5. Pitch angle and rotor speed

TABLE I. DESIGN REQUIREMENTS AND SYSTEM ACTUAL RESPONSE

Items	Designed Values	Simulation Results
Active power generated ( $P_{gen}$ )	2.0 MW (0.8921 pu)	2.0010 MW (0.8925 pu)
Rated angular speed ( $\omega_m$ )	15 rpm (1 pu)	15.0005 rpm (1 pu)
DC-link voltage ( $V_{dc}$ )	1220 V (3.06 pu)	1220.4 V (3.064 pu)
Maximum DC voltage ripple ( $\Delta V_{dc,ref}$ )	24.4 V (2%)	9.959 V (0.8 %)
Voltage ascending time ( $t_r$ )	0.005 s	0.0009 s
Maximum grid current harmonic at switching frequency ( $\Delta i_{r,ref}$ )	300 A (0.113 pu)	377.85 A (0.142 pu)
Maximum machine current harmonic at switching frequency ( $\Delta i_{s,ref}$ )	100 A (0.0377 pu)	119.38 A (0.045 pu)



# Assessing the Influence of Climatic Variables on Electricity Demand

Dao H. Vu, *Student member, IEEE*, Kashem M. Muttaqi, *Senior Member, IEEE*, and Ashish. P. Agalgaonkar, *Senior Member, IEEE*

Australian Power Quality and Reliability Center, SECTE, University of Wollongong, Wollongong, NSW, Australia  
Email: dhv972@uowmail.edu.au; kashem@uow.edu.au; ashish@uow.edu.au

**Abstract** — The electricity demand is significantly dependent on the weather information. Such weather information is comprised of different climatic variables such as temperature, humidity, wind speed, evaporation, rain fall and solar exposure which constantly change. Therefore, analysing the impacts of these variables on demand is necessary for predicting the future change in demand. In this paper, the cooling and heating degree days are utilised to capture the relationship between the per capita demand to temperature, one of the key climatic variables. In addition, Pearson correlation analysis has been employed to investigate the interdependency between different climatic variables and electricity demand. Finally, back-ward elimination based multiple regression is used to exclude non-significant climatic variables and evaluate the sensitivity of significant variables to the electricity demand. A case study has been reported in this paper by acquiring the data from the state of New South Wales, Australia. The results reveal that the climatic variables such as heating degree days, humidity, evaporation, and wind speed predominantly affect the electricity demand of the state of New South Wales.

where:  $c_i$  are coefficients, (*Hum*) is humidity, (*Rai*) is rainfall, (*Eva*) is evaporation, (*Win*) is wind speed, (*Sol*) is solar exposure. and  $\varepsilon$  is error term.

## I. KEY EQUATIONS

Cooling degree days (*CDD*) and heating degree days (*HDD*) represent the requirement of cooling and heating due to temperature being higher or lower than the balance point temperature respectively.

$$CDD = \sum_{i=1}^N CDD_i, \quad CDD_i = \begin{cases} (T_i - T_b) & \text{if } (T_i > T_b) \\ 0 & \text{if } (T_i < T_b) \end{cases} \quad (1)$$

$$HDD = \sum_{i=1}^N HDD_i, \quad HDD_i = \begin{cases} (T_b - T_i) & \text{if } (T_i < T_b) \\ 0 & \text{if } (T_i > T_b) \end{cases} \quad (2)$$

where,  $N$  is the number of days in a year,  $T_i$  is the average temperature of day  $i$ ,  $T_b$  is the balance point temperature,  $CDD_i$  and  $HDD_i$  are the cooling and heating degree in day  $i$  respectively.

Relationship between demand and weather variables:

$$D = c_0 + c_1 CDD + c_2 HDD + c_3 Hum + c_4 Rai + c_5 Eva + c_6 Win + c_7 Sol + \varepsilon \quad (3)$$

## II. KEY FIGURES

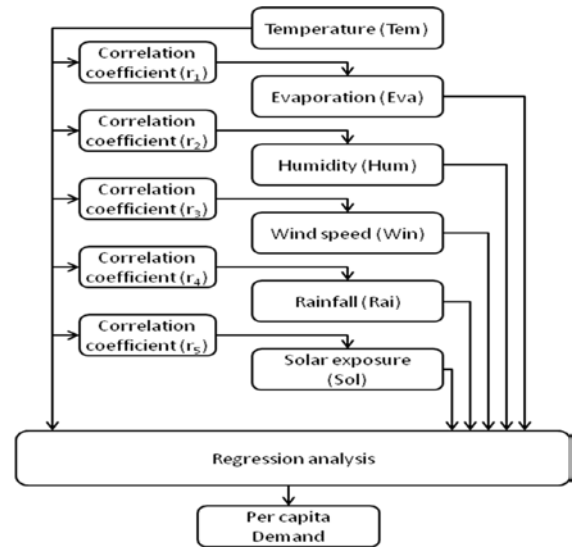


Figure 1. Conceptual framework to derive electricity demand using regression analysis.

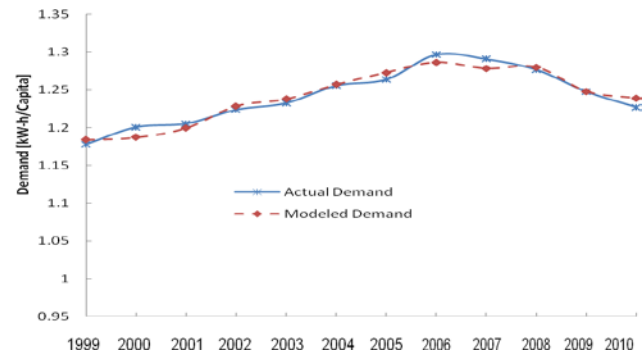


Figure 2. Actual and modeled demand

TABLE I. BACK-WARD ELIMINATION REGRESSION ANALYSIS

Model no.	Model summary			Significance level of predictors							
	R	R <sup>2</sup>	Adjusted R <sup>2</sup>	Constant	Hum	Eva	Win	HDD	Sol	Rai	CDD
1	0.981	0.962	0.894	0.028	0.085	0.030	0.004	0.112	0.391	0.466	0.597
2	0.979	0.958	0.909	0.010	0.040	0.012	0.002	0.059	0.414	0.461	Removed
3	0.976	0.953	0.914	0.001	0.004	0.004	0.001	0.026	0.409	Removed	Removed
4	0.973	0.947	0.917	0.001	0.002	0.002	0.000	0.020	Removed	Removed	Removed

# Application of Multifractal Spectrum to the Vibration Analyses of Power Transformer under DC Bias

P. Gao, F. H. Wang, *Member, IEEE*  
 Department of Electrical Engineering  
 Shanghai Jiaotong University  
 Shanghai, China

L. Su  
 Condition Evaluation Center  
 Electric Power Research Institute  
 Shanghai, China

**Abstract**—This paper deals with the vibration features of power transformer under DC bias with the method of multifractal spectrum. First, vibration mechanisms of power transformer are analyzed. Then the typical parameters of multifractal spectrum including the width of multifractal spectrum and the absolute value of density difference are calculated to describe the vibration signals of power transformer based on the DC bias experiment of a 10kV power transformer. The experimental results have shown that the width of multifractal spectrum and the absolute value of density difference could fully describe the fluctuation degree and intensity of vibration signals in power transformer. Moreover, the relationship between multifractal spectrum parameters and influence degree of DC bias on power transformer is obtained, which is beneficial for evaluating the ability of the power transformer to endure the DC bias.

## I. KEY EQUATIONS

When there is no DC bias, the vibration characteristics of power transformer is shown in (1).

$$\varepsilon_{vib} = \frac{\lambda_s - \lambda_0(\sigma)}{M_{ws}^2} M^2 \quad (1)$$

When DC current is injected from the neutral point of power transformer, the vibration characteristics of power transformer is shown in (2).

$$\varepsilon_{vib}' = \frac{\lambda_s - \lambda_0(\sigma)'}{M_{ws}} M + \frac{\lambda_s - \lambda_0(\sigma)}{M_{ws}^2} M^2 + \frac{\lambda_s - \lambda_0(\sigma)''}{M_{ws}^3} M^3 + \dots \quad (2)$$

The multifractal spectrum characteristics are listed as follows

$$\begin{cases} \alpha = d\tau(q)/dq \\ f(\alpha) = q\alpha(q) - \tau(q) \end{cases} \quad (3)$$

The width of the multifractal spectrum  $\Delta\alpha = \alpha_{\max} - \alpha_{\min}$  could describe the fluctuation degree of vibration signal. The corresponding density difference  $\Delta f = f(\alpha_{\max}) - f(\alpha_{\min})$  could describe the fluctuation degree of vibration signal.

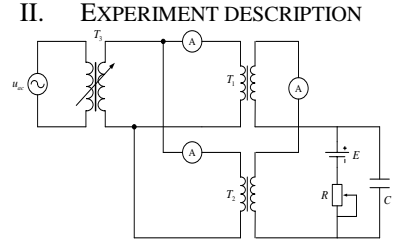


Fig. 1 Schematic diagram of the DC bias experiment of test transformers

## III. KEY RESULTS

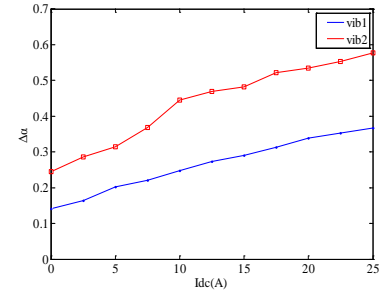


Fig. 2 Relationship between  $\Delta\alpha$  and  $I_{dc}$  for vib1 and vib2

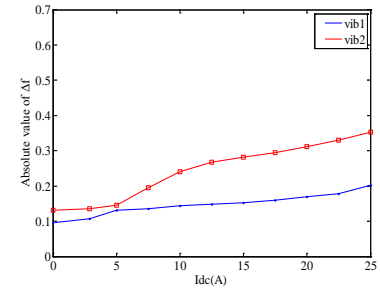


Fig. 3 Relationship between absolute value of  $\Delta f$  and  $I_{dc}$  for vib1 and vib2

The width of multifractal spectrum and the absolute value of density difference increase with the increasing of bias DC  $I_{dc}$ . It describes the relationship between the vibration levels and influence degree of DC bias to power transformer exactly.

# High performance FPGA-based digital real-time controller for electric power conversion applications

Tomasz Dziwiński<sup>‡</sup>, *Graduate Student Member, IEEE* and Krzysztof Chmielowiec<sup>§</sup>, *Graduate Student Member, IEEE*

<sup>‡</sup>AGH University of Science and Technology, Department of Automatics and Biomedical Engineering,  
Al. Mickiewicza 30, 30-059 Kraków  
Email: tdz@agh.edu.pl

<sup>§</sup>AGH University of Science and Technology, Department of Power Electronics and Energy Control Systems,  
Al. Mickiewicza 30, 30-059 Kraków  
Email: kchmielo@agh.edu.pl

**Abstract**—The goal of this paper is to describe the structure, principal use, features and limitations of the FPGA-based digital real-time controller. The presented hardware platform, based on reconfigurable devices, is dedicated to drive power semiconductor devices, usually Insulated Gate Bipolar Transistors (IGBT) and Metal-Oxide Semiconductor Field-Effect Transistor (MOS-FET) in switching applications. The flexibility of the discussed controller allows to work with various power converter topologies.

## I. THE CONTROLLER ARCHITECTURE

The high performance FPGA-based digital real-time controller consists of modular analog-to-digital (A/D) and digital-to-analog (D/A) converter boards, direct fiber-optic digital output module, main signal-processing module and power supply module. Each A/D board has four 16-bits, 1 MSPS converters allow for accurate capture of voltage and current waveforms at very high sampling rate. The direct digital output module allows to control semiconductors with the PWM signal at a carrier frequency of up to 100 kHz. Fiber optics provide adequate electrical isolation between the control system and the power electronic circuit. Main signal processing module contains FPGA integrated circuit and dual core floating point DSP processor. Fig. 1 shows the front view of the unit with all components described above.

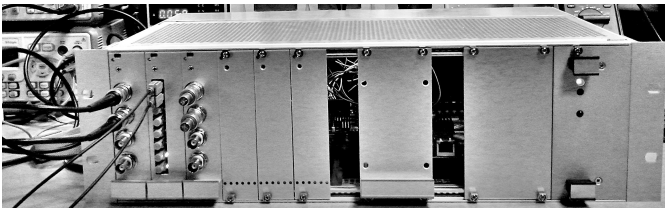


Fig. 1. The front view of industrial-ready FPGA-based real-time controller

## II. EXAMPLE APPLICATION

In this example, controller is configured to operate with a high-current single-phase buck converter. Power converter is fed from 325 V DC line and supply a linear load.

The controller drives MOS-FET transistor over a fiber optic link using 4 kHz PWM signal. A schematic diagram of the converter is shown in Fig. 2. Both, the input ( $u_{in}$ ) and output ( $u_{out}$ ) voltages and currents ( $i_{in}$ ,  $i_{out}$ ), are measured by appropriate transducers. The control algorithm is based on PID adopted for hardware implementation and optimized for robustness (phase and gain margins). The step response of the buck converter is presented in Fig. 3.

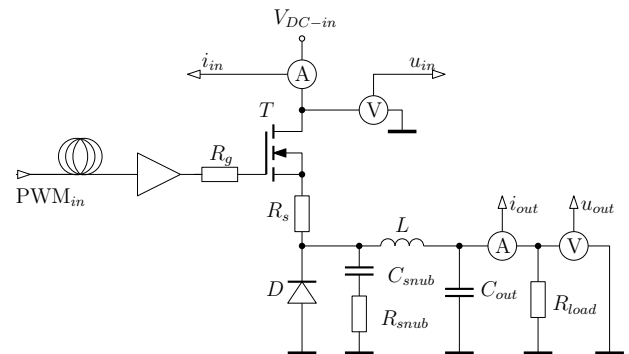


Fig. 2. Buck converter circuit

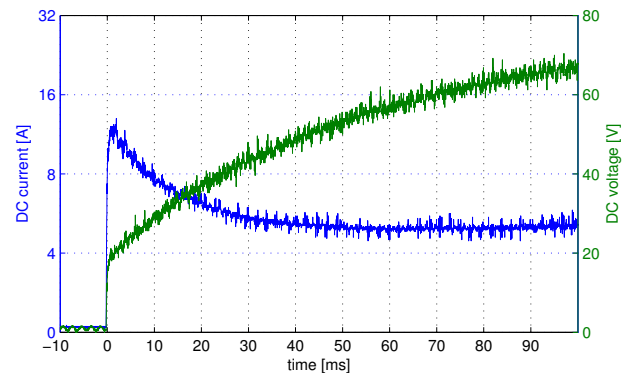


Fig. 3. Step response of the system

Work realized in the scope of project titled “ProInterface” Project has been co-funded by KIC InnoEnergy supported by the European Institute of Innovation and Technology.

# Identification of power system stressed conditions

Anagnostou, Georgios

Department of Electrical and Electronic Engineering  
Imperial College London  
London, United Kingdom  
[georgios.anagnostou11@imperial.ac.uk](mailto:georgios.anagnostou11@imperial.ac.uk)

Pal, Prof. Bikash C.

Department of Electrical and Electronic Engineering  
Imperial College London  
London, United Kingdom  
[b.pal@imperial.ac.uk](mailto:b.pal@imperial.ac.uk)

**Abstract**—The electric power industry is undergoing significant changes: Power systems have become deregulated with many partners been involved in their operation, contributing to their complexity in terms of structure, data sharing and controllability; the growing impact of electricity market on economic dispatch leads to complex and uncertain dispatch; a shift is on track from centralized generation units based on synchronous machines to distributed inverter interfaced inertia-less generation, characterized by stochasticity, such as wind power and photovoltaics; new forms of generation and energy storage devices, such as fuel cell generators and batteries are coupled with advanced control systems and special protection components, which increase system's dependency on them and lead to unpredictable behavior of nonlinear nature; aged system components and limited investments, especially in the transmission level, lead to system operation closer to its limits. In the context of dynamic security assessment, transient stability analysis remains a challenging issue. This has its roots in the modern system structure, which is associated with a complicated system behavior with various operating points corresponding to different system conditions and configurations. Accurate system margin estimation and critical clearing time (CCT) quantification greatly rely on high system model accuracy. The operation of a power system under stressed conditions can have a dramatic impact on system margin, whose estimation requires the identification of whether the system is stressed or not. This poster aims to study the identification of system stresses and their impact on power system stability limit estimation. Here, a representative 16-machine, 68-bus, 5-area power system model is used, in order to assess the impact of stressed system operation on transient stability margin. Compared to traditional power system models used for transient stability studies, in this study the power network is modelled in a more detailed way, including the models of limiting and switching devices. MATLAB/Simulink is used for the modeling and simulation of the model network. The synchronous machines are modelled based on transient dynamics, whereas the loads are modelled as constant impedance loads. The study presented in this poster is intended to set the context of power system's stressed condition identification and transient stability margin estimation under these conditions.

**Index Terms**—Power system control, power system simulation, power system stability, smart grids.

## I. KEY FIGURES

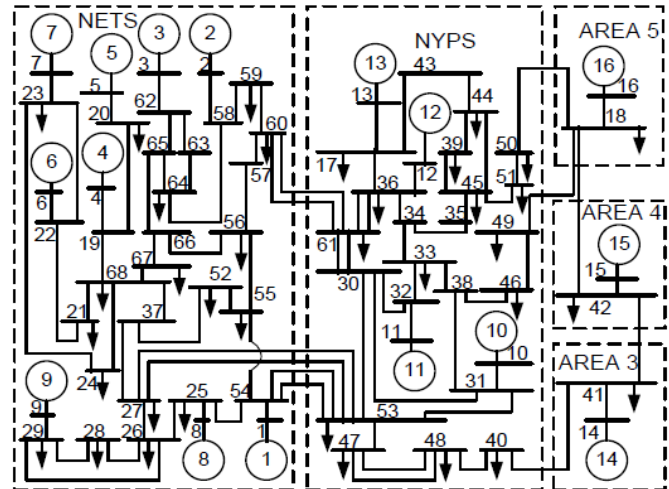


Figure 1. IEEE 5-area 16-machine system

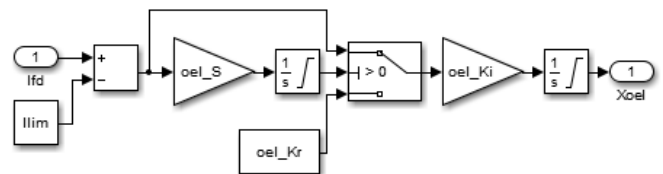


Figure 2. Overexcitation limiter model (summed type)

## II. KEY REFERENCES

- K. Morison, L. Wang, and P. Kundur, "Power System Security Assessment," *Power and Energy Magazine, IEEE*, vol.2, no.5, pp.30,39, Sept.-Oct. 2004
- P. Panciatici, G. Bareux, and L. Wehenkel, "Operating in the Fog: Security Management Under Uncertainty," *Power and Energy Magazine, IEEE*, vol.10, no.5, pp.40,49, Sept. 2012
- T. Van Cutsem, and C. Vournas, *Voltage Stability of Electric Power Systems*. Norwell, MA: Kluwer, 1998.

# Smart Grid Distributed Energy Management under Packet Loss Environment

Yuan Zhang, *Student Member, IEEE*, and Mo-Yuen Chow, *Fellow, IEEE*

Department of Electrical and Computer Engineering, North Carolina State University, Raleigh, NC 27695, USA  
Email: yzhang50, chow@ncsu.edu

**Abstract**—With the development of smart grid technology, the future power system will become a complex cyber-physical system. The existing system control and management infrastructure will facing new challenges such as scalability in its computational and communications effort, and robustness to single point of failure. Decentralized cooperative control algorithms such as consensus algorithm are promising to control and manage such a system in a more efficient and robust way. Because of the sensitivity to communications imperfections, the performance of the consensus based algorithms degrade when the communication packet loss happens in practical applications. Different from other consensus based algorithms, the Hybrid Incremental Cost Consensus algorithm is robust against communications imperfections by integrating gossip algorithm and consensus algorithm together. Several case studies are presented to illustrate the performance of the proposed Hybrid ICC algorithm and demonstrate the scalability and robustness under packet loss scenarios.

## I. HYBRID INCREMENTAL COST CONSENSUS ALGORITHM

$$C_{gen,i}(P_{gen,i}) = a_i + b_i P_{gen,i} + c_i P_{gen,i}^2 \quad (1)$$

$$\Delta P(k) = P_a(k) - \frac{\lambda(k) - \mathbf{b}}{2\mathbf{c}} \quad (2)$$

$$\Delta \hat{P}(k+1) = \mathbf{W}' \Delta \hat{P}(k) + \Delta P(k+1) - \Delta P(k). \quad (3)$$

$$\lambda(k+1) = \mathbf{W}\lambda(k) + \alpha \Delta \hat{P}(k), \quad (4)$$

## II. KEY RESULTS

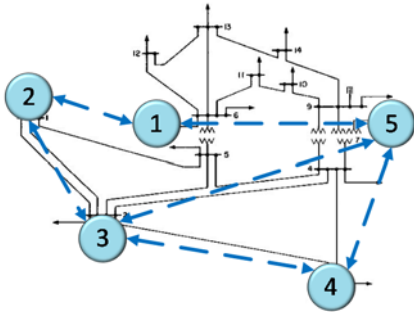


Figure 1. IEEE 14 Bus system with communications network

TABLE I. PARAMETERS OF THE FIVE- UNIT-SYSTEM.

Unit	$a_i$	$b_i$	$c_i$	Local Demand (MW)
1	561	7.92	0.001562	200
2	310	7.85	0.00194	200
3	78	7.97	0.00482	200
4	561	7.92	0.001562	200
5	78	7.97	0.00482	200

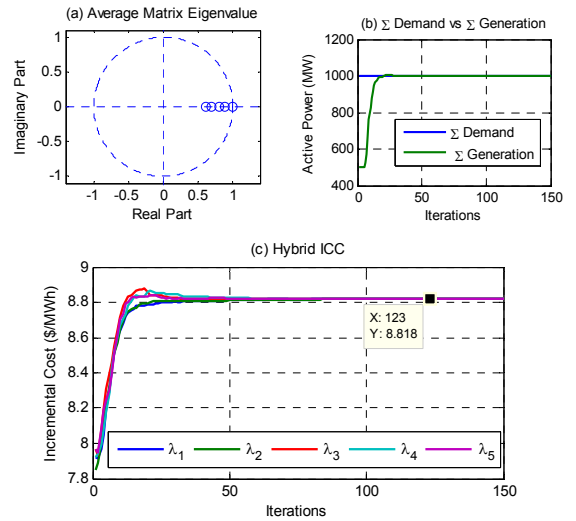


Figure 2. Hybrid ICC algorithm simulation: (a) average updating matrix eigenvalue, (b) power mismatch, and (c) IC of each generation unit.

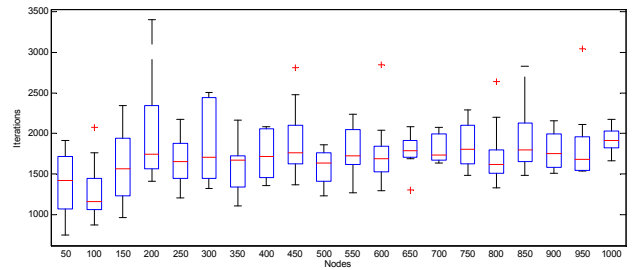


Figure 3. Large scale Hybrid ICC algorithm simulation



# Unbalanced Distribution System Three-Phase State Estimation

Majumdar, Ankur

Department of Electrical and Electronic Engineering  
Imperial College London  
London, United Kingdom  
[ankur.majumdar@imperial.ac.uk](mailto:ankur.majumdar@imperial.ac.uk)

Pal, Dr. Bikash C.

Department of Electrical and Electronic Engineering  
Imperial College London  
London, United Kingdom  
[b.pal@imperial.ac.uk](mailto:b.pal@imperial.ac.uk)

**Abstract**—The modern distribution is transforming from a passive to a smart active distribution system, where it can improve the performance and flexibility of operation. It can improve and maintain the quality of service, reduce costs and increase the capacity of grid to host distributed connected resources. The conventional measurement infrastructure is also getting replaced by smart meters. To enable these smart functionalities of the network the states of the unbalanced distribution system need to be observed properly. The distribution management systems (DMS) will play a crucial role in control and operation of the smart distribution systems. Central to every DMS are two functional blocks: the state estimator and the control scheduling block. Hence, the development of the distribution system state estimation (DSSE) plays a major role in the distribution network operation. The distribution system is more prone to unbalances due to the presence of both 1-ph and 3-ph loads and also due to the presence of 1-ph, 2-ph and 3-ph laterals. The distribution system is also different from the transmission system due to its typical nature. Due to high R/X ratio, the distribution system suffers more losses than the transmission system. This poster aims to study the modelling of overhead lines and underground cables, three-phase transformers and loads. It then aims to study the three-phase unbalanced distribution system state estimation (DSSE). The measurement data collected from remote terminal units (RTU) have inherent errors associated with them. To this end, we have used a modified version of IEEE-13 bus unbalanced system with a 4.16-kV feeder. The weighted least squares (WLS) estimation has been used assuming that the errors are independently and identically distributed and follow normal distribution. Due to its vastness and radial nature, the distribution system cannot afford to have enough real measurements. Therefore, the loads are modeled as pseudo measurements from daily or annual load curve data. The zero injection measurements are considered as equality constraints to help avoid the ill-conditioning of the Gain matrix and thus the Gain matrix has been found to be numerically more stable than the conventional one. MATLAB is used for the modeling and simulation of the system. The feeders are modeled by modified Carson's equations; the measurements are modeled as real measurements while the loads, considered as pseudo measurements, are modeled as ZIP loads; the transformers are modeled as the combination of three single-phase transformers. The study and results presented in this poster are intended to form a foundation for a further and more detailed analysis of the security aspects of the system.

**Keywords**—Distribution System State Estimation (DSSE); Distribution Management Systems (DMS); smart meters

## I. KEY FIGURES

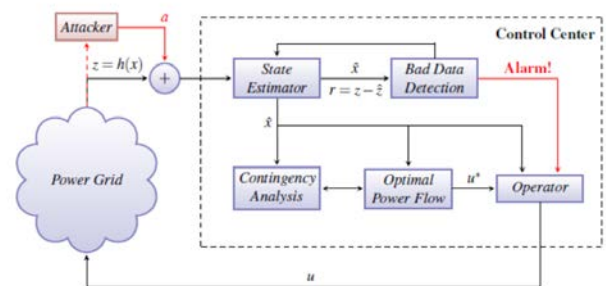


Figure 1: Schematic of DMS architecture

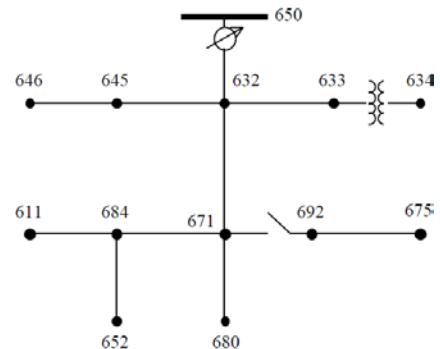


Figure 2: One-Line diagram of IEEE-13 bus distribution system

## KEY REFERENCES

- [1] A. Abur and A. G. Exposito, "Power System State Estimation, Theory and Implementation," CRC Press
- [2] W. H. Kersting, *Distribution system modelling and analysis*. CRC Press, 2012
- [3] Y. F. Huang, S. Werner, J. Huang, N. Kashyap and V. Gupta, "State Estimation in Electric Power Grids" *IEEE Signal Processing Magazine*, Page 33-43, September 2012



# Decision Tree Based Novel Control Techniques for Microgrid Stability Enhancement

Riyasat Azim<sup>1</sup>, Hira Saleem<sup>1</sup>, Yongli Zhu<sup>1</sup>, Kai Sun<sup>1</sup>, Di Shi<sup>2</sup>, Ratnesh Sharma<sup>2</sup>, Fangxing Li<sup>1</sup>

<sup>1</sup>Dept. of Electrical Engineering and Computer Science, University of Tennessee, Knoxville, TN 37996

<sup>2</sup>NEC Laboratories America, Cupertino, CA 95014

*Abstract*— This poster proposes a decision tree (DT) based systematic approach for microgrid islanding and control. This approach adopts a new methodology that trains two contingency oriented DTs by databases generated from contingency simulations in both the main grid as well as in the islanded microgrid. The DTs are employed for microgrid islanding decision support and preventive control decision support during the islanded operation of microgrid respectively. The performance of the approach is demonstrated on a microgrid implemented with IEEE 13 feeder distribution system with three distributed generation units which include photovoltaic (PV) generation, diesel generator and a battery.

# Real-Time Tuning of Power System Stabilizer

Arunagirinathan Paranietharan, Student Member, IEEE and G.Kumar Venayagamoorthy, Senior Member, IEEE  
Real-Time Power and Intelligent Systems Lab.

Holcombe Department of Electrical and Computer Engineering, Clemson University, SC 29634, USA

*Abstract—It is imperative to have the devices and techniques in power system be gradually updated as transformation of power system into smart grid. As such, power system stabilizer (PSS) with real-time tuning using particle swarm optimization method (PSO) and phasor measurement unit (PMU) makes the conventional PSSs control gradually suitable for the smart grid era. The function of PSS is to add to the generator's automatic voltage regulator (AVR) an auxiliary signal that improves the damping of power system oscillations. The PSSs parameters are tuned in the continuous time using the real-time digital simulators (RTDS), which has the ability to simulate large scale power systems in real-time and also enables the simulated power system to connect actual physical devices. A MATLAB-based PSO algorithm is used and interfaced with the RTDS system using transmission control protocol (TCP). RTDS script is achieved for the real-time tuning of the PSSs parameters. The two-area power system is simulated and the best PSSs parameters are obtained in the real-time. The supervisory control and data acquisition system (SCADA) verifies the tuned PSSs parameters with the generators' speed signals obtained from the PMU.*

**Index Terms** – Power System Stabilizer, Particle Swarm Optimization method, real-time Tuning, RTDS, Phasor Measurement Unit

## I. INTRODUCTION

Transformation of power system into smart grid is not easy to implement as an intense action. The focus is to achieve the updating of the devices and techniques in power system gradually. One of the power system conventional oscillation damping devices is the power system stabilizer (PSS). The function of PSS is to add to the generator's automatic voltage regulator (AVR) an auxiliary signal that improves the damping of power system oscillations. Practically, it is better and more accepted to make the conventional PSSs control gradually adaptive which is suitable for the smart grid era than to have a fixed set of parameters. Particle Swarm Optimization (PSO) is a robust

optimization technique for large scale power systems with high nonlinearity. In this work, a Real-time digital simulation (RTDS) is used for testing new methods such online PSO for tuning PSSs remotely using PMU data.

## II. FOCUS OF THE WORK

The power system (Fig. 1) is the two area four machine system [3] which is simulated on the RTDS. PMUs are connected to the RTDS and speed signals of the generators are obtained at the control center that performs simultaneous tuning of four PSSs.

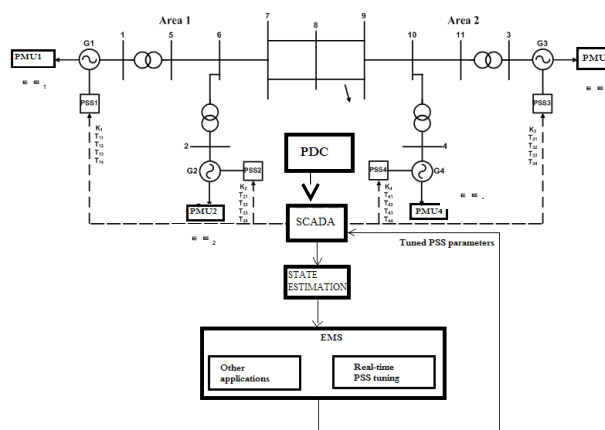


Figure.1

## III. REFERENCES

- [1] P. Kundur, Power System Stability and Control, McGraw-Hill, New York, USA, 1994.
- [2] J. Kennedy and R. Eberhart, "Particle swarm optimization," in Proc. IEEE Int. Conf. Neural Networks, pp. 1942-1948, Perth, WA, USA, Nov/Dec 1995.
- [3] T. K. Das, G. K. Venayagamoorthy, U. O. Aliyu, "Bio-inspired Algorithms for the Design of Multiple Optimal Power System Stabilizers: SPPSO and BFA", IEEE Transactions on Industry Applications, Vol. 44, Issue 5, pp. 1445-1457, September/October 2008.
- [4] RTDS, Real Time Digital Simulator for the Power Industry, RSCAD Version 4.0 User Manual, 2012.

# Decentralized Communication and Control Systems for Power System Operation

Yannan Wang, Pradeep Yemula, Anjan Bose

School of Electrical Engineering and Computer Science, Washington State University, Pullman, WA, USA

emails: [yannan.wang@email.wsu.edu](mailto:yannan.wang@email.wsu.edu), [yemula.pradeep@gmail.com](mailto:yemula.pradeep@gmail.com), [bose@wsu.edu](mailto:bose@wsu.edu)

**Abstract**—Due to the rapid deployment of phasor measurement units (PMUs), a new class of monitoring and control applications is made possible. To meet the stringent latency requirements of such application the communication and power infrastructures have to collaborate strongly. In this paper, a process for design and simulation of both communication network and power network has been proposed with the objective of damping inter-area oscillations. A method is also developed to determine the optimal location of data routing hubs so as to minimize the volume of communications. The IEEE 118 bus system is used and the performance of wide area damping control system on both centralized and decentralized topologies is studied. One of the conclusions we draw is that, the decentralized communication architectures, involving data routing hubs, are better suited for control applications requiring fast control actions.

## I. PROBLEM STATEMENT

SINCE in centralized communication scheme, the control center which receives all PMU measurements and sends control signals might be far away from substations. It is not suitable to provide information for applications that have latency requirements less than one second. To achieve faster data delivery, it is necessary to develop a procedure to design and simulate a communication network for power grids in a decentralized way, in which a new level of communication node acting like data routing hubs are involved. Each area in the power system is assumed to have one hub acting as distributed data base and route required information according to off-line configurations.

To find the optimal locations for these hubs in a communication network overlaid transmission lines, a metric namely Mega-bit-hop is defined in Equation (1) to quantify the amount of traffic volume related to different hub locations.

$$Mbh_c = \sum_{i=1}^N (h_i * p_i) \quad (1)$$

where,  $c$  is the location of hub,  $i$  represents the flow ID,  $N$  is the total number of flows,  $h_i$  is the number of hops taken by the packets on  $i^{\text{th}}$  flow and  $p_i$  is the packet size of  $i^{\text{th}}$  flow in Megabits.

## II. KEY FIGURES

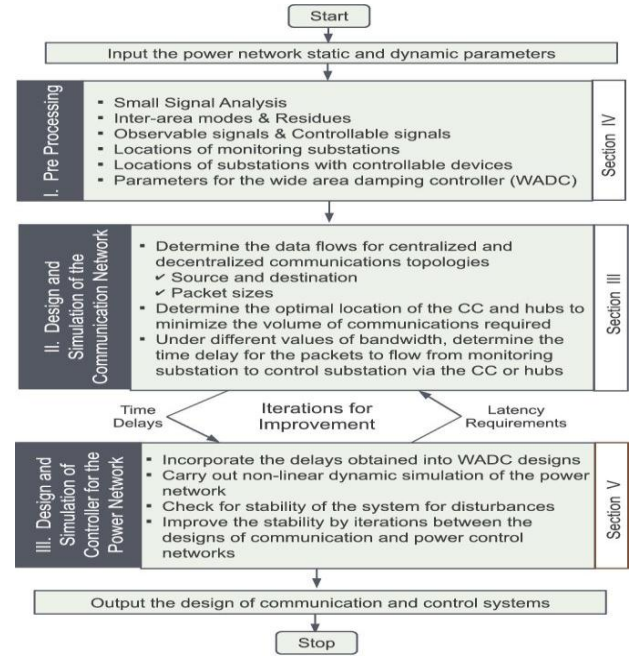


Fig. 1. Process for design of communication architecture.

## III. PROBLEM STATEMENT

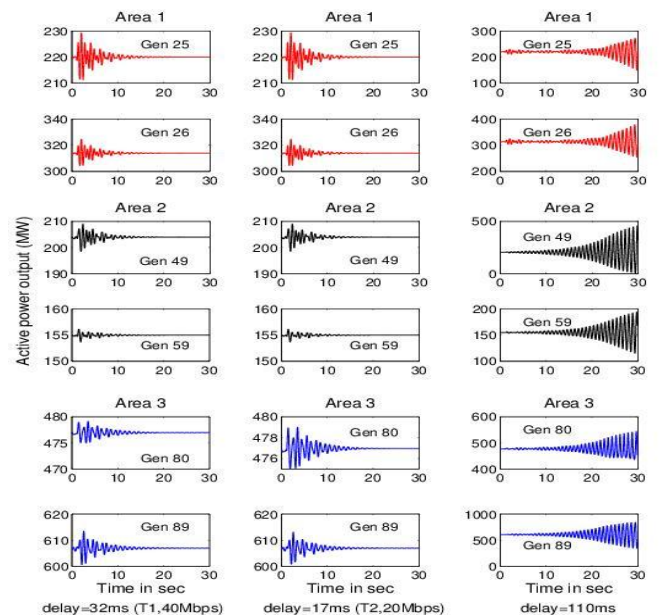


Fig. 2. System dynamic performance under different delay.



# Generalized Sequence Impedances and Fault Types for Polyphase Power Systems

Brian J. Pierre, Student Member, IEEE

G. T. Heydt, Life Fellow, IEEE

**Abstract**— This paper addresses polyphase electric power systems. The subject is potentially important due to the high power density capability of high phase order AC transmission systems. The generalization of symmetrical components is used for high phase order, and methods to calculate the generalized sequence impedances of a polyphase transmission system are presented. The first method utilizes properties of circulant Toeplitz matrices and the discrete Fourier transform. The second method uses a new formulation based on geometric parameters. These two methods are compared with Fortescue's approach. A novel method to design the sequence impedances to specifications is presented. The decoupled impedance model of a polyphase system is suggested for fault analysis. The calculation of the number of fault types and number of *significant* fault types for any phase order system is shown.

## I. KEY POINTS AND EQUATIONS

The line impedance matrix ( $Z_{ph}$ ) of an  $n$ -phase system is a circulant matrix for circularly configured or transposed transmission lines. The eigenvectors of a circulant matrix are given by,

$$v_q = \frac{1}{\sqrt{n}} \left[ e^0, e^{\frac{j2\pi q}{n}}, \dots, e^{-\frac{j2\pi q(n-1)}{n}} \right]^t \quad (1)$$

for  $q = 0, 1, 2, \dots, n-1$ . Following Fortescue's approach, in matrix notation, the eigenvectors are arranged in columns to form an  $n \times n$  modal matrix,  $T$ ,

$$\frac{1}{\sqrt{n}} \begin{bmatrix} a^{-0*0} & a^{-0*1} & \dots & a^{-0*(n-1)} \\ a^{-1*0} & a^{-1*1} & \dots & a^{-1*(n-1)} \\ \vdots & \vdots & \ddots & \vdots \\ a^{-(n-1)*0} & a^{-(n-1)*1} & \dots & a^{-(n-1)*(n-1)} \end{bmatrix} \quad (2)$$

where  $a$  is  $e^{j2\pi/n}$ . Sequence impedances are found from the diagonal entries of  $Z_{seq}$

$$Z_{seq} = T^{-1} Z_{ph} T. \quad (3)$$

The eigenvalues of the circulant line impedance matrix can be found directly,

$$Z_q = \sum_{p=1}^n Z_{ph,1,p} e^{-j2\pi q(p-1)/n}. \quad (4)$$

for  $q = 0, 1, 2, \dots, n-1$ . When  $q = 0$  the zero sequence is obtained;  $q = 1$  corresponds to positive sequence; and  $q = n-1$  refers to negative sequence. The range  $1 < q < n-1$  correspond to sequences that do not exist for three phase circuits.

An integrated approach to finding the sequence impedances utilizes the distances between the conductors directly. This is similar to the approach using the geometric mean distance (GMD) to calculate the positive sequence reactance of a three phase line,

$$X_{3ph}^1 = 0.12134 \ln \left( \frac{GMD}{GMR} \right) \frac{Ohm}{mi} \quad (5)$$

where GMR is the geometric mean radius of the conductors. However, when there are more than three phases, the sequence reactances are found by extending (5) by the replacing the distance parameter GMD by an equivalent,

$$D_{Xq} = \prod_{p=1}^{n-1} \left[ \prod_{m=1}^n d_{m,(m+p)} \right]^{\frac{1}{n} \cos \frac{2\pi p(q)}{n}} \quad (6)$$

where  $d_{m,k}$  is the distance between conductor  $m$  and  $k$ ,  $n$  is the phase order, and  $D_{Xq}$  is the sequence reactance distance parameter. Note that

$$d_{m,k} = d_{m,k-n} \text{ while } k > n.$$

The corresponding sequence impedance is calculated from,

$$Z_q = R + jX_q, \quad (7)$$

where  $R$  is the resistance of the conductor and  $X_q$  is the sequence reactance,

$$X_q = 0.12134 \ln \left( \frac{D_{Xq}}{GMR} \right) \quad q \neq 0, \quad (8)$$

$$X_0 = 0.12134 \left[ \ln \left( \frac{D_{X0}}{GMR} \right) + 7.93402n \right], \quad (9)$$

(as derived from Carson's equations). Eqs. (8-9) are in ohms/mi. Note that simplifications can be made to the general form in (6) for zero sequence or for specific conductor arrangements, such as circular configuration.

The calculation of the sequence impedances can be used in an innovative idea to design the sequence impedances of high phase order transmission lines to specifications: given specified sequence impedances, determine the conductor arrangement and phase spacing that minimizes the constrained least square difference between the given and actual specifications.

The most important application for generalized sequence components and sequence impedances is the analysis of polyphase transmission systems, and fault analysis of these systems. The number of fault types for an  $n$ -phase system is,

$$2^{n+1} - 2 - n. \quad (10)$$

Fault types can be grouped together: the number of *significant* (i.e., distinct) fault types is,

$$K - 3 + \sum_{d|n} \varphi(d) \frac{2^{\frac{n}{d}}}{n} \quad (11)$$

$$\text{where } K = \begin{cases} \text{for odd } n: & 2^{\frac{n-1}{2}+1} \\ \text{for even } n: & 2^{\frac{n}{2}} + 2^{\frac{n}{2}-1} \end{cases}$$

where  $\varphi$  is 'Euler's totient function', and the summation is over all integer values of  $d$  such that  $d|n$  is an integer.

# Generalized Sequence Impedances and Fault Types for Polyphase Power Systems

Brian J. Pierre, Student Member, IEEE

G. T. Heydt, Life Fellow, IEEE

**Abstract**— This paper addresses polyphase electric power systems. The subject is potentially important due to the high power density capability of high phase order AC transmission systems. The generalization of symmetrical components is used for high phase order, and methods to calculate the generalized sequence impedances of a polyphase transmission system are presented. The first method utilizes properties of circulant Toeplitz matrices and the discrete Fourier transform. The second method uses a new formulation based on geometric parameters. These two methods are compared with Fortescue's approach. A novel method to design the sequence impedances to specifications is presented. The decoupled impedance model of a polyphase system is suggested for fault analysis. The calculation of the number of fault types and number of *significant* fault types for any phase order system is shown.

## I. KEY POINTS AND EQUATIONS

The line impedance matrix ( $Z_{ph}$ ) of an  $n$ -phase system is a circulant matrix for circularly configured or transposed transmission lines. The eigenvectors of a circulant matrix are given by,

$$v_q = \frac{1}{\sqrt{n}} \left[ e^0, e^{\frac{j2\pi q}{n}}, \dots, e^{-\frac{j2\pi q(n-1)}{n}} \right]^t \quad (1)$$

for  $q = 0, 1, 2, \dots, n-1$ . Following Fortescue's approach, in matrix notation, the eigenvectors are arranged in columns to form an  $n \times n$  modal matrix,  $T$ ,

$$\frac{1}{\sqrt{n}} \begin{bmatrix} a^{-0*0} & a^{-0*1} & \dots & a^{-0*(n-1)} \\ a^{-1*0} & a^{-1*1} & \dots & a^{-1*(n-1)} \\ \vdots & \vdots & \ddots & \vdots \\ a^{-(n-1)*0} & a^{-(n-1)*1} & \dots & a^{-(n-1)*(n-1)} \end{bmatrix} \quad (2)$$

where  $a$  is  $e^{j2\pi/n}$ . Sequence impedances are found from the diagonal entries of  $Z_{seq}$

$$Z_{seq} = T^{-1} Z_{ph} T. \quad (3)$$

The eigenvalues of the circulant line impedance matrix can be found directly,

$$Z_q = \sum_{p=1}^n Z_{ph,1,p} e^{-j2\pi q(p-1)/n}. \quad (4)$$

for  $q = 0, 1, 2, \dots, n-1$ . When  $q = 0$  the zero sequence is obtained;  $q = 1$  corresponds to positive sequence; and  $q = n-1$  refers to negative sequence. The range  $1 < q < n-1$  correspond to sequences that do not exist for three phase circuits.

An integrated approach to finding the sequence impedances utilizes the distances between the conductors directly. This is similar to the approach using the geometric mean distance (GMD) to calculate the positive sequence reactance of a three phase line,

$$X_{3ph}^1 = 0.12134 \ln \left( \frac{GMD}{GMR} \right) \frac{Ohm}{mi} \quad (5)$$

where GMR is the geometric mean radius of the conductors. However, when there are more than three phases, the sequence reactances are found by extending (5) by the replacing the distance parameter GMD by an equivalent,

$$D_{Xq} = \prod_{p=1}^{n-1} \left[ \prod_{m=1}^n d_{m,(m+p)} \right]^{\frac{1}{n} \cos \frac{2\pi p(q)}{n}} \quad (6)$$

where  $d_{m,k}$  is the distance between conductor  $m$  and  $k$ ,  $n$  is the phase order, and  $D_{Xq}$  is the sequence reactance distance parameter. Note that

$$d_{m,k} = d_{m,k-n} \text{ while } k > n.$$

The corresponding sequence impedance is calculated from,

$$Z_q = R + jX_q, \quad (7)$$

where  $R$  is the resistance of the conductor and  $X_q$  is the sequence reactance,

$$X_q = 0.12134 \ln \left( \frac{D_{Xq}}{GMR} \right) \quad q \neq 0, \quad (8)$$

$$X_0 = 0.12134 \left[ \ln \left( \frac{D_{X0}}{GMR} \right) + 7.93402n \right], \quad (9)$$

(as derived from Carson's equations). Eqs. (8-9) are in ohms/mi. Note that simplifications can be made to the general form in (6) for zero sequence or for specific conductor arrangements, such as circular configuration.

The calculation of the sequence impedances can be used in an innovative idea to design the sequence impedances of high phase order transmission lines to specifications: given specified sequence impedances, determine the conductor arrangement and phase spacing that minimizes the constrained least square difference between the given and actual specifications.

The most important application for generalized sequence components and sequence impedances is the analysis of polyphase transmission systems, and fault analysis of these systems. The number of fault types for an  $n$ -phase system is,

$$2^{n+1} - 2 - n. \quad (10)$$

Fault types can be grouped together: the number of *significant* (i.e., distinct) fault types is,

$$K - 3 + \sum_{d|n} \varphi(d) \frac{2^{\frac{n}{d}}}{n} \quad (11)$$

$$\text{where } K = \begin{cases} \text{for odd } n: & 2^{\frac{n-1}{2}+1} \\ \text{for even } n: & 2^{\frac{n}{2}} + 2^{\frac{n}{2}-1} \end{cases}$$

where  $\varphi$  is 'Euler's totient function', and the summation is over all integer values of  $d$  such that  $d|n$  is an integer.



# Application of Game-theoretic approaches for Cyber-Physical Security of Smart Grid

Aditya Ashok, Manimaran Govindarasu  
Department of Electrical and Computer Engineering  
Iowa State University  
Ames, Iowa.  
Email: [aashok@iastate.edu](mailto:aashok@iastate.edu)

**Abstract**—Recent findings, documented in government reports and literature, indicate the growing threat of cyber-based attacks in numbers and sophistication on nation’s electric grid and other critical infrastructure systems. Increasing adoption of smart grid technologies will significantly expand the grid’s dependencies on sensing, monitoring, and control, therefore, making it more vulnerable to cyber attack. The state-of-the-art research in cyber risk modeling and mitigation is inadequate to capture the cyber-physical coupling of the infrastructure systems, and the dynamic and uncertain nature of the Advanced Persistent Threats (APTs). The poster presents a framework to explore and develop game-theoretic models and analytical tools to defend the power grid against such coordinated cyber attacks to design attack-resilient smart grid of the future.

## I. KEY QUESTIONS

The poster intends to address several key questions that are pertinent to cyber-physical security of the smart grid:

- 1) How to model all three aspects of Risk, namely Threats, Vulnerabilities and Impacts explicitly?
- 2) How to model cyber attacks and their physical impacts in terms of costs across cyber and physical layers?
- 3) How to develop optimal counter measures for attacks such that the impacts can be minimized?
- 4) How to develop real-time operational planning strategies using appropriate game-theoretic formulations to deal with multiple contingencies?

In summary, the game-theoretic framework proposed in the poster would help to develop ‘attack-resilient’ algorithms for enhancing the cyber-physical security, addressing a broad class of problems ranging from risk assessment, impact analysis to attack-aware operational planning strategies in wide-area monitoring, control and protection of the smart grid.

## II. KEY FIGURES

The proposed game-theoretic framework for cyber-physical security of smart grid is presented in Figure 1.

## III. ATTACK-AWARE OPERATIONAL PLANNING STRATEGIES

Traditionally, the contingency set is populated based on the plausibility and likelihood of the multiple elements failing together. However, such a contingency set is inadequate under the context of coordinated cyber attacks. The poster will present how the proposed game-theoretic framework will help

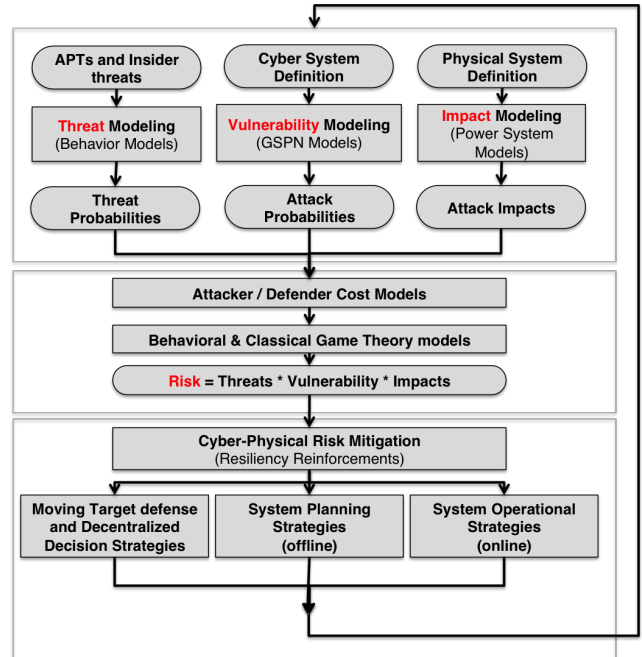


Fig. 1. Cyber-physical Framework

to develop planning approaches which are capable of handling (N-k) contingencies in the presence of coordinated attacks. In essence, game-theoretic models can be applied to develop a *dynamic contingency set* based on the equilibrium strategies for a specified attacker behavior.

### A. Game-theoretic model

The strategic interaction between the attacker and the defender can be modeled in this case as a two player *non-zero-sum game* where the attacker aims to choose a set of components from his available attack surface and cause power system impacts in terms of load loss, line flow violations, indirectly affecting the net cost of generation. The defender’s action is to choose a strategy which tries to minimize the impact of the attack caused by the attacker’s actions. The defender achieves this by selecting a contingency set for which he runs a security constrained economic dispatch, which minimizes the impacts of the attacker’s strategy.

# Validation, Testing and Implementation of the Linear State Estimator in a Real Power System

Lin Zhang and Anjan Bose

School of Electrical Engineering and Computer Science  
Washington State University  
Pullman, WA, USA  
lin.zhang@wsu.edu

**Abstract**—As more and more Phasor Measurement Units (PMUs) are coming on-line, a linear state estimator (LSE) utilizing only PMU data becomes possible. In the Pacific and Gas Energy (PG&E) linear state estimator project, an actual LSE application has been designed and developed to run in a real power system. LSE core algorithm and data flow for EMS have been presented and implemented. The LSE application has been tested on steady state data, simulated RTDS data. In case study, it shows the great performance of LSE. LSE can run as fast as 30 frames per second and it is much faster than traditional state estimator. It enables us to have the ability to see the transient system states. The inherent bad data detection algorithm is able to filter out bad data from raw PMU measurements. The validation of PMU data could be very important since any PMU related applications are put on line from day one. The output of LSE could be used for other applications in EMS.

## I. KEY IDEAS

If enough voltage and current phasors are measured to make the network observable, state estimation could become linear. The measurements are voltage phasor and current phasor, and states are voltage phasor. The relationship between measurement and state is linear on the condition when the phasors are in the form of rectangular coordinate. The measurement vector  $Z$  is given by

$$Z = \begin{bmatrix} V \\ I \end{bmatrix} + \begin{bmatrix} \sigma_V \\ \sigma_I \end{bmatrix}$$

Where  $V$  and  $I$  are the vectors of true values of bus voltage and branch current measurements while  $\sigma_V$  and  $\sigma_I$  are the measurement error vectors. The covariance matrix  $W$  can be expressed by

$$W = \begin{bmatrix} W_V & 0 \\ 0 & W_I \end{bmatrix}$$

The relationship between  $V$  and  $I$  can be shown as

$$I = Y * V$$

Where  $Y$  can be obtained through network admittance matrix and note that  $I$  in equation (4) is identity matrix, so

$$Z = \begin{bmatrix} I \\ Y \end{bmatrix} V + \begin{bmatrix} \sigma_V \\ \sigma_I \end{bmatrix}$$

$$Z = HV + \sigma$$

The weighted least squares of estimate for the state vector  $V$  can be easily calculated,

$$V = (H^TWH)^{-1}H^TWZ$$

Where the Gain matrix is shown

$$G = H^TWH$$

## II. KEY FIGURES

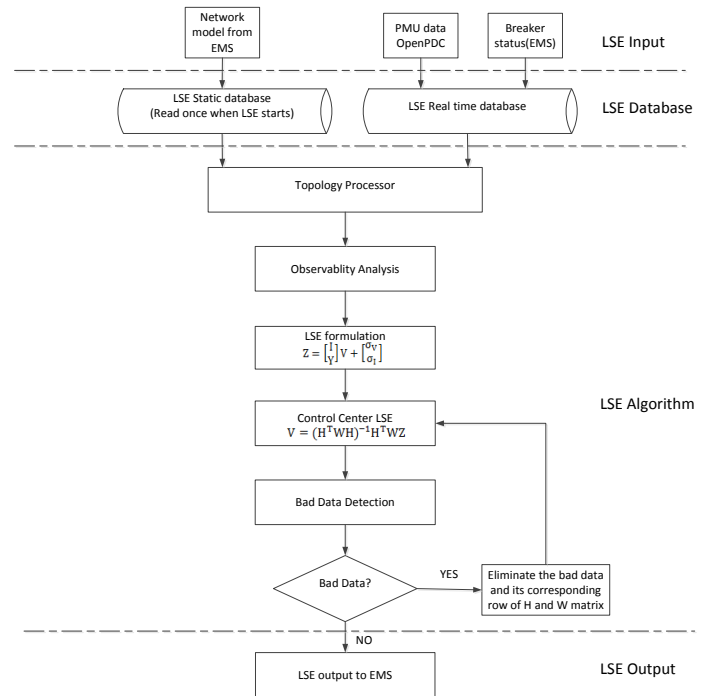


Figure 1. LSE algorithm and data flow at control center

## III. KEY RESULTS

Not yet established, will be completed before July 20, 2014

# Distributed Automatic Generation Control

Siqi Wang

Dept. of Electrical Engineering and Computer Science  
The University of Tennessee  
Knoxville, TN, USA  
swang31@utk.edu

Kevin Tomsovic

Dept. of Electrical Engineering and Computer Science  
The University of Tennessee  
Knoxville, TN, USA  
tomsovic@utk.edu

**Abstract**— To allow for high penetration of distributed generation and alternative energy units, it is critical to minimize the complexity of generator controls and the need for close coordination across regions. We propose a distributed implementation based on wide area monitoring with PMUs. We demonstrate the concept on a modified NPCC system with high penetration of wind.

**Index Terms**—AGC; distributed control; frequency response; wind generation;

## I. INTRODUCTION

Renewable energy resources, such as wind generation, are playing a greater role in large power systems. However, the variation in these resources can cause continuous generation change across local and interconnected areas. In order to reduce unnecessary generator ramping, modified automatic generation control strategies are needed [1]. This work demonstrates a distributed frequency control scheme on a modified NPCC system with a high level of wind generation.

## II. NPCC SYSTEM DESCRIPTION

The equivalent NPCC system can be simply divided into five interconnected areas: NYISO, MSIO, IESO, PJM and ISO-NE, connected by sixteen tie-lines shown in Figure 1. The system configuration data are represented in Table I. In order to obtain the area frequency-response characteristic (1/R+D) and use it to calculate the system bias factors, the 700 MW unit generation trip is conducted at bus 120 in area MISO. The estimated generation change, responding load change and the system bias factors are shown in Table II.

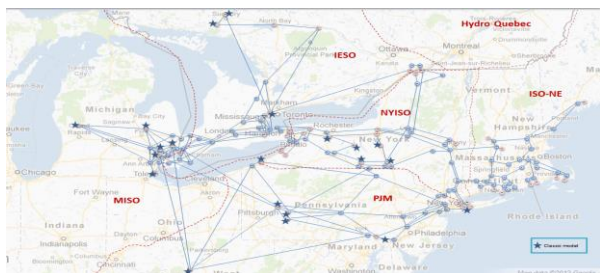


Figure 1 Equivalent NPCC System

TABLE I. SYSTEM CONFIGURATION DATA

Element	MSIO	NYISO	IESO	PJM	ISO-NE
Total Generation (MW)	2577	6707	5415	5585	4939
Total Load (MW)	2539	6759	5322	5020	5680

TABLE II. FREQUENCY-RESPONSE AND BIAS FACTORS

Element	MSIO	NYISO	IESO	PJM	ISO-NE
Generation Change (MW)	-19.37	206.1	77.53	115.9	99.97
Load Change (MW)	-158.36	-3.43	-38.79	25.34	-32.66
$\Delta f$ (HZ)	-0.032	-0.032	-0.032	-0.032	-0.032
B=1/R+D (MW/HZ)	4343	6548	3635	2830	4145

## III. CASE STUDY

In this study, AGC is assigned to one generator in each area. At 20s, generator 120 is tripped and AGC works to operate total generation in all the five areas. The frequency response and net power change are shown in Figure 2. After 600 seconds, the system frequency and the total net power are back to the nominal value. The poster will demonstrate this response with ACE replaced by tracking PMU trajectories.

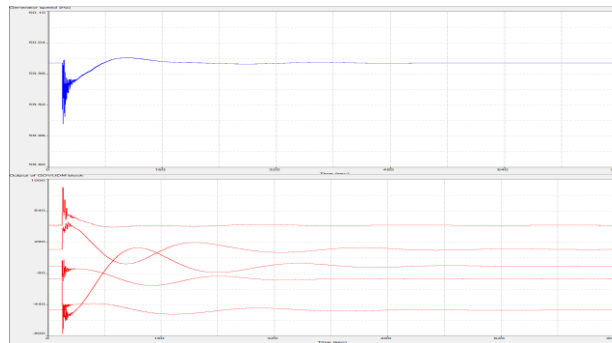


Figure.2 Frequency-response and Total Net Power Change

## IV. CONCLUSIONS AND FUTURE WORK

The implemented AGC strategy has the ability to coordinate frequency control across wide areas. In the future work, the speed-variable wind model will be added to replace conventional generators in certain places. With wind penetration, the control effect on conventional AGC and a distributed flatness-based AGC will be tested [1].

## REFERENCES

- [1] M.H. Variani and K. Tomsovic, "Distributed automation generation control using flatness-based approach for high penetration of wind generation", *IEEE Trans. on Power System*, vol. 28, no. 3, August 2013, pp. 3002-3009.

# Optimal Power Flow with Primary and Secondary Frequency Constraint

Guangyuan Zhang, *Student Member, IEEE*, James McCalley, *Fellow, IEEE*  
 Dept. of Electrical and Computer Engineering  
 Iowa State University  
 Ames, IA, USA  
 gzhang1@iastate.edu, jdm@iastate.edu

**Abstract**—The large integration of renewable energy such as wind and solar has significantly influenced the power system frequency performance. Firstly, the inertial response and primary response from conventional generators have been declining since they are not provided from the renewable energy naturally. Secondly, the high variability and uncertainty of the renewable energy impose the extra burden on the conventional generators to balance the generation and load. Under such background, we would expect a more restrictive requirement for the Primary Frequency Response (PFR) and Secondary Frequency Response (SFR). We propose a Frequency Constrained Optimal Power Flow (FC-OPF) model to include the PFR and SFR adequacy requirement so that satisfactory frequency performance after the large generation contingency can be ensured. A 5 area system is simulated to test the proposed model.

**Index Terms**— Primary Frequency Response, Secondary Frequency Response, Frequency Nadir, Optimal Power Flow

## I. FREQUENCY CONSTRAINED OPF MODEL

$$\min \sum_i C_i(g_i) + \sum_i C_i(y_i) + \sum_i C_i(r_i) \quad (1.1)$$

Subject to:

$$\sum_i g_i + \sum_i w_i = d \quad (1.2)$$

$$\sum_i SF_{fi}(g_i + w_i - d_i) \leq f_i \quad (1.3)$$

$$w_i \leq wf_i \quad (1.4)$$

$$g_i + y_i + r_i \leq \bar{g}_i \quad (1.5)$$

$$g_i - r_i \geq \underline{g}_i \quad (1.6)$$

$$y_i \leq rr_i \cdot t_{\text{nadir}} \quad (1.7)$$

$$\sum_i y_i \geq P_{\text{loss}} \quad (1.8)$$

$$\sum_i SF_{fi}(g_i + y_i + w_i - d_i) \leq Kc_i \cdot f_i \quad (1.9)$$

$$r_i \leq 10RR_i \quad (1.10)$$

$$\sum_i r_i \geq ACE_{\text{tot}} \quad (1.11)$$

$$\sum_i SF_{fi}(g_i + r_i + w_i - \Delta w_i - d_i - \Delta d_i) \leq f_i \quad (1.12)$$

## II. TEST SYSTEM AND SIMULATION RESULT

Table 1: Results of PJM five-area system

FC-OPF						
Area	Energy	PFR	SFR	LMP	PFR MCP	SFR MCP
A	106.96	3.04	0	16.28	20	4
B	417.27	1.52	10.00	24.75	20	4
C	96.96	3.04	0	28.00	20	4
D	291.51	7.60	0	36.95	20	4
E	50.00	14.79	32.00	10.00	20	4

Fig 1: Frequency Performance between OPF and FC-OPF

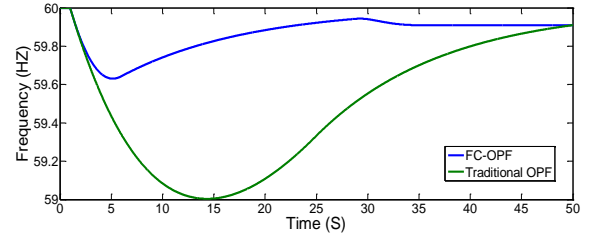


Table 3: Key Frequency Performance Metrics

	OPF	FC-OPF
Nadir Frequency	59.628 HZ	59.010 HZ
Nadir Time	~5s	~15s
Nadir Based Frequency Response	806.45 MW/0.1HZ	303.03 MW/0.1HZ
Settle Frequency	59.91 HZ	59.91 HZs
Settle Time	35 s	>50 s

## III. CONCLUSION AND FUTURE WORK

With the comparison between traditional OPF and FC-OPF, we found the FC-OPF gives a better frequency performance from multiple frequency metrics such as nadir frequency, nadir time, nadir based frequency response, settling time and settling frequency. In the future, we will test the applicability of the proposed approach within a large power system model; we will also explore the possibility of incentivizing renewables, storage and demand response to provide the fast frequency response.

# Stability Improvement with Series compensation on Transmission networks with Asynchronous Generation

Prem K Naik, Akshya Swain and Nirmal-Kumar C Nair

Department of Electrical and Computer Engineering

University of Auckland, New Zealand

[prem.k@ieee.org](mailto:prem.k@ieee.org); [a.swain@auckland.ac.nz](mailto:a.swain@auckland.ac.nz); [n.nair@auckland.ac.nz](mailto:n.nair@auckland.ac.nz)

**Abstract**—Recently, attention is increasing on Transient stability assessment and secure mode of operation of power system with asynchronous generation. This is due to asynchronous mode of generation like wind farms increasing in capacity and promising to displace existing high inertia synchronous generation. Participation of wind farms (which are primarily inertia decoupled) during power system transient disturbance will become necessary. This poster will present an approach for assessing and the assumptions made thereof to obtain transient stability limit using Potential Energy Boundary Surface Method. We also demonstrate use of FACT devices for generator series compensation to improve transient stability margin lost due to reduced inertia at a generation bus. The outputs are optimal compensation value and the generator bus location that can help maintain transient stability limit during credible contingencies.

**Index Terms**—Energy Function method, TCSC, Inertia-less generation.

## I. KEY EQUATIONS

Energy function of a Multi-machine system in center of angle formulation

$$V(\theta, \tilde{\omega}) = \frac{1}{2} \sum_{i=1}^n M_i \tilde{\omega}_i^2 - \sum_{i=1}^n P_i (\theta_i - \theta_i^s) - \sum_{i=1}^{n-1} \sum_{j=i+1}^n \left[ C_{ij} (\cos \theta_{ij} - \cos \theta_{ij}^s) - \int_{\theta_i^s + \theta_j^s}^{\theta_i + \theta_j} D_{ij} \cos \theta_{ij} d(\theta_i + \theta_j) \right] \quad (1)$$

$$= V_{KE}(\tilde{\omega}) + V_{PE}(\theta)$$

PEBS method has been used to obtain critical clearing time and energy on a three machine system for several fault conditions.  $X_{c2}$  and  $X_{c3}$  are the series compensation provided to Machine 2 and Machine 3 with series  $X_d$  of 0.1198 and 0.1813 respectively. Machine 2 Inertia is dropped from 6.4 to 5.0(s). TCSC is provided at each machine for twelve contingencies so that clearing time kept same for both values of inertia (6.4 and 5.0).

## II. KEY FIGURES

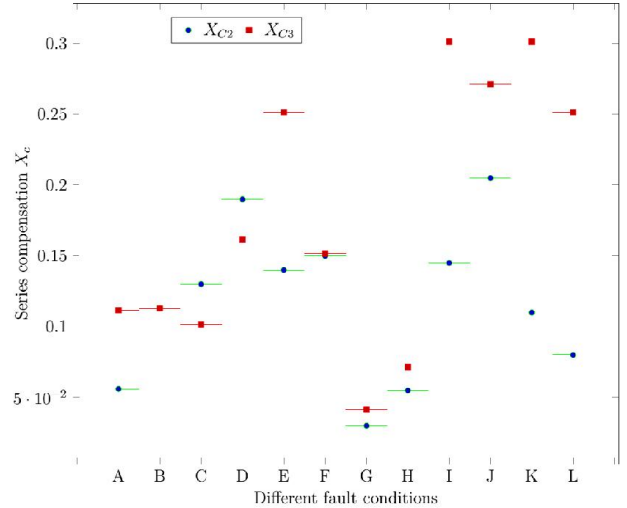


Fig. 1. Series compensation at Machine 2 and 3 for different fault conditions

## III. KEY RESULTS

TABLE I  
CRITICAL CLEARING TIME AND COMPENSATION

FAULT BUS	LINE REMOVED	EXISTING SYSTEM H=6.4		COMPENSATION FOR H=5.0			
		CRITICAL CLEARING TIME	CRITICAL ENERGY	Xc2 0.1198-XG2	VCR	XG3 0.1873-XG3	VCR
7	7-5	0.1800	1.2478	0.0558	1.8492	0.1113	1.6966
7	8-7	0.2000	1.8480	0.1128	3.1110	0.1128	3.1100
5	7-5	0.3150	1.0276	0.1298	1.7604	0.1013	1.4557
5	5-4	0.4050	2.3819	0.1898	5.9046	0.1613	3.7985
4	4-6	0.3100	2.4734	0.1398	4.7341	0.2513	4.0424
4	5-4	0.3100	2.4705	0.1498	4.2125	0.1513	3.7963
9	6-9	0.2400	2.1020	0.0298	2.1625	0.0413	2.2154
9	9-8	0.2400	2.7247	0.0548	3.3909	0.0713	3.4856
8	9-8	0.3200	2.9796	0.1448	5.8028	0.3013	5.0689
8	8-7	0.3150	2.8198	0.2048	5.6115	0.2713	5.4707
6	4-6	0.4450	2.4317	0.1098	3.9282	0.3013	5.0861
6	6-9	0.3850	1.3426	0.0798	2.0007	0.2513	2.1967

Critical clearing time and Energy obtained for several faults. Inertia of Generator 2 is reduced from 6.4 to 5.0, necessary compensation at Generator 2 and 3 to maintain clearing time



# Automatically Gain Tuning Control Method for Automatic Generation Control with Effects of Wind Resources

Yao Xu, Fangxing Li, Maryam Hassani Variani and Zhiqiang Jin

The Department of Electrical Engineering and Computer Science, the University of Tennessee (UT), Knoxville, TN 37996, USA,

Email: [yxu25@utk.edu](mailto:yxu25@utk.edu), [fli6@utk.edu](mailto:fli6@utk.edu)

**Abstract**—Variable and uncertain wind power output introduces lots of new challenges to power system frequency stability. Automatic generation control (AGC) is very important to maintain power system frequency stability. Various control methods have been discussed in order to design control gains and obtain a good frequency response performance. However, the existing methods are either time consuming or are affected by the designer’s experience. Moreover, the control gains usually are fixed and designed for specific scenarios in the studied power system. The desired response may not be obtained when high penetration of wind power is integrated in power system. To address these challenges, an automatically gain tuning control (AGTC) for AGC is proposed in this paper. Wind power model is built on the partial load area. By the proposed control method, control gains can be dynamically self-adjusted to reach the desired performance. The proposed method is tested in an IEEE 39 bus system with wind resources and compared with the conventional control with well-tuned and fixed gains in the simulation. The simulation results show that the proposed control provides better AGC response with less deviation of system frequency and tie line flow.

**Index Terms**- Area control error (ACE), automatic generation control (AGC), proportional-integral (PI) control, automatically gain tuning control (AGTC), frequency stability.

## I. KEY FIGURES

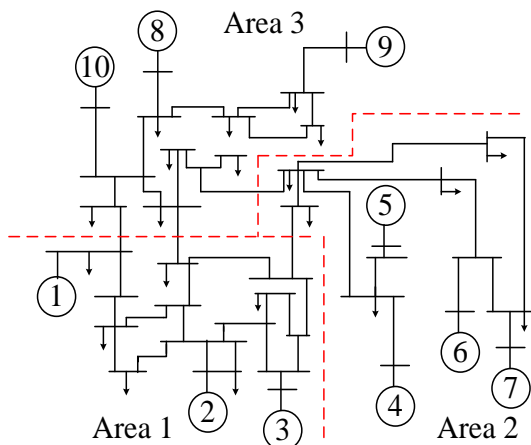


Fig. 1. The studied system

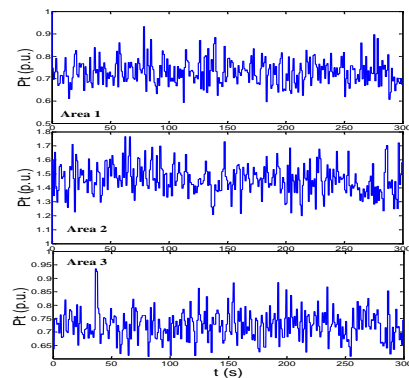


Fig.2 Wind Power Profile

## II. KEY RESULTS

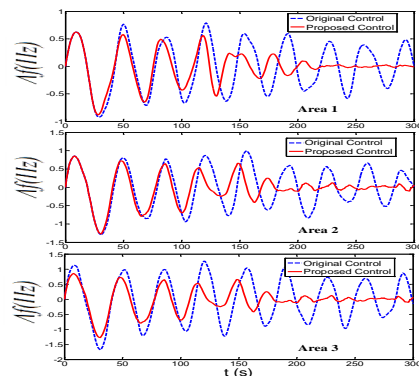


Fig. 3. Results of frequency deviation

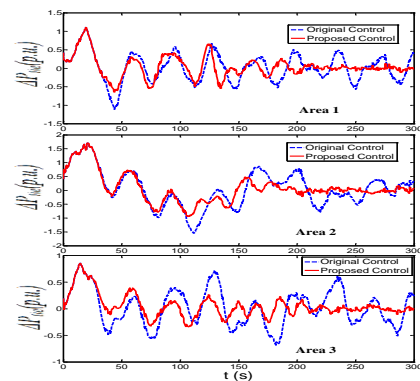


Fig. 4. Results of tie power deviation



# Minimizing Wind Power Spillage Using an OPF With FACTS Devices

Amin Nasri  
and Mehrdad Ghandhari  
Electric Power System Department  
KTH Royal Institute of Technology  
Stockholm SE 100-44, Sweden

Antonio J. Conejo  
Department of Electrical  
& Computer Engineering  
The Ohio State University  
Columbus, OH 43210-1271

S. Jalal Kazempour  
Department of Mechanical  
Engineering  
Johns Hopkins University  
Baltimore, MD 21218-2682

**Abstract**—This paper proposes an Optimal Power Flow (OPF) model with Flexible AC Transmission System (FACTS) devices to minimize wind power spillage. The uncertain wind power production is modeled through a set of scenarios. Once the balancing market is cleared, and the final values of active power productions and consumptions are assigned, the proposed model is used by the system operator to determine optimal reactive power outputs of generating units, voltage magnitude and angles of buses, deployed reserves, and optimal setting of FACTS devices. This system operator tool is formulated as a two-stage stochastic programming model, whose first-stage describes decisions prior to uncertainty realization, and whose second-stage represents the operating conditions involving wind scenarios. Numerical results from a case study based on the IEEE RTS demonstrate the usefulness of the proposed tool.

## I. DECISION FRAMEWORK

The framework considered is depicted in Fig. 1. After clearing the balancing market, the proposed OPF model is used by the system operator to minimize wind power spillage. It is important to note that the OPF proposed does not represent the market stages, i.e., the system operator runs such an OPF after closing the last market, i.e., the balancing or real-time market. Thus, the time frame of this OPF spans from the closing of the balancing market to power delivery. In most real-world electricity markets this time period is smaller than one hour. This model is cast as a two-stage stochastic programming problem in which the first-stage refers to the decisions “prior to uncertainty realization”, while the second-stage represents the “operating conditions involving wind scenarios”. In the first-stage, the market operator makes “scheduling decisions” appropriate for any plausible wind production scenario, while in the second-stage, “operating decisions” corresponding to each individual scenario are made.

## II. KEY EQUATIONS

The objective function of the proposed two-stage OPF problem is formulated below:

$$\begin{aligned} \text{Minimize}_{\underline{\mathbf{x}}} \quad & \sum_s \rho_s \left[ \sum_{k \in \mathcal{K}} \alpha_k^{\text{SP}} W_{ks}^{\text{SP}} + \sum_{d \in \mathcal{D}} \alpha_d^{\text{SH}} L_{ds}^{\text{SH}} \right. \\ & \left. + \sum_{n(m \in \Omega_n)} \alpha_{nm}^{\text{L}} P_{nms}^{\text{L}}(\mathbf{v}, \boldsymbol{\theta}, \mathbf{x}^{\text{tcsc}}) \right] \end{aligned} \quad (1)$$

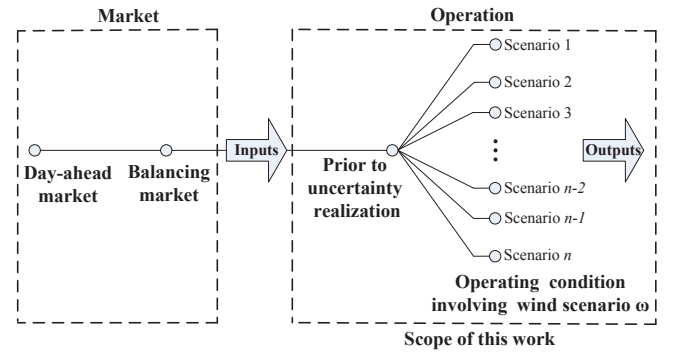


Fig. 1. Decision framework of the proposed model.

The main goal of objective function (1) is to minimize wind power spillage, while the second priority is to minimize active power losses in the network. In addition, load shedding is also considered in (1) to avoid load curtailment. Weighting factors  $\alpha_k^{\text{SP}}$ ,  $\alpha_d^{\text{SH}}$  and  $\alpha_{nm}^{\text{L}}$  specify the degree of importance of their corresponding terms. The objective function (1) is subject to a set of constraints, e.g., active and reactive power balance at each node and voltage magnitudes and angles of each node.

## III. KEY RESULTS

In this study three different cases are analyzed: (A) No FACTS device is installed, (B) An installed single fixed series capacitor (FSC) and (C) An installed single Thyristor Controlled Series Capacitor (TCSC). The numerical results for the three cases considered are given in Table I. Additionally, Table II illustrates the optimal reactance setting of the TCSC for each wind scenario.

TABLE I  
NUMERICAL RESULTS FOR CASES CONSIDERED

	The value of objective function (1) [p.u.]	Expected value of wind power spillage percentage ( $\tilde{W}^{\text{SP}}$ ) [%]	CPU time [second]
Case A	146.5	16.4	29.4
Case B	117.6	13.2	28.9
Case C	101.8	11.4	65.5

TABLE II  
OPTIMAL REACTANCE SETTING OF TCSC PER SCENARIO (CASE C)

$s$	$x_{nms}^{\text{tcsc}}$ [p.u.]	$s$	$x_{nms}^{\text{tcsc}}$ [p.u.]	$s$	$x_{nms}^{\text{tcsc}}$ [p.u.]	$s$	$x_{nms}^{\text{tcsc}}$ [p.u.]	$s$	$x_{nms}^{\text{tcsc}}$ [p.u.]
s1	0.261	s6	0.261	s11	0.261	s16	0.256	s21	0.248
s2	0.261	s7	0.261	s12	0.261	s17	0.256	s22	0.248
s3	0.261	s8	0.261	s13	0.261	s18	0.256	s23	0.248
s4	0.131	s9	0.131	s14	0.131	s19	0.185	s24	0.198
s5	-0.200	s10	-0.200	s15	-0.003	s20	0.096	s25	0.119

# A Study of Hardware Requirements on Implementations of Phasor Measurement Algorithms

Samarth Deo, Nithin Somasundaran, Kun Zhu, Hans Bjorklund, and Lars Nordström

**Abstract**—Over the last decades, Phasor Measurement Unit (PMU) has been recognized as a main enabler to the smart grid at transmission level. There have been a plethora of algorithms proposed to calculate synchrophasors, however, due to a lack of requirements and standardization efforts, particularly from in industry, many of these algorithms have not been tested on off-the-shelf hardware platforms even their feasibility to be implemented has not been well discussed. As a response, this paper intends to capture the general hardware requirements of three well-cited synchrophasor calculation algorithms from literature.

**Keywords:** PMU, NASPI, WECC, C37.118 Standard.

## I. INTRODUCTION

Phasor Measurement Units (PMU)s deliver precise time-tagged data at high sampling rates. These sampling rates could be as high as 1024 samples/window for measurement applications where high accuracy is required in the calculation of the intended quantities. In [2], the authors proposed a recursive discrete fourier-based algorithm to accurately measure the phasor. Further, there are multiple literature that discusses robust algorithms in presence of input harmonics, off-nominal frequencies and low-frequency oscillations in power systems, e.g., [3], [4] and [5] among others.

Both North American Synchrophasor Initiative (NASPI) and Western Electricity Coordinating Council (WECC) have laid down requirements of PMU's under dynamic test conditions (a brief summary is provided in Section II-A). As real power flow in a power line is directly proportional to the sine of the angle difference between voltages at the two terminals of the line; accurate phasor measurement have become a topic of wide importance across the globe. As an example, PMU frequency plots provide a good indication of the generation loss a frequency drop of 0.1 Hz is almost equivalent to 800 MW generation loss in WECC [6]. Multiple algorithms have been developed around the world to accurately measure the phasor magnitude, angle, frequency and Rate Of Change Of Frequency (ROCOF). It is therefore necessary that the hardware required to implement these algorithms are able to support the calculations and reporting. This paper focuses

S. Deo and L. Nordström are with the Industrial Information & Control Systems, KTH - the Royal Institute of Technology, Stockholm, Sweden. E-mail: [samarth.deo@ics.kth.se](mailto:samarth.deo@ics.kth.se), [larsn@ics.kth.se](mailto:larsn@ics.kth.se).

K. Zhu is with Ventyx, an ABB company, Västerås, Sweden. E-mail: [kun.zhu@ventyx.abb.com](mailto:kun.zhu@ventyx.abb.com).

N. Somasundaran is with Amrita University, Coimbatore, India. E-mail: [nithin1664@gmail.com](mailto:nithin1664@gmail.com).

Hans Bjorklund is with ABB AB, HVDC, Ludvika, Sweden. E-mail: [hans.bjorklund@se.abb.com](mailto:hans.bjorklund@se.abb.com).

on the hardware requirements and limitations required by an industry compliant PMU.

### A. Purpose

This article discusses the various hardware requirements for a PMU complying with the NASPI/WECC requirements presented later. Specifically, in this paper, three highly accurate phasor measurement algorithms have been implemented and tested on different hardware's and their efficiency have been discussed. Moreover, this study also suggests the bottlenecks of the algorithm in question with respect to the two PMU accuracy class, i.e., P-class and M-class [7]. The P-Class PMU requires the device to have a faster response time but less accurate; whereas, the M-Class PMU requires the measurements to be much accurate with slower response time. P-class has no explicit requirements for filtering. The letter "P" refers to the protection applications which require fast response. The letter "M" refers to the measurement class of devices since measurements require better precision are flexible on the minimal reporting delay. M-class PMUs can be affected by the aliased signals. In general, the PMU vendors do provide the option to choose from one of the PMU class required but a PMU with both the classes in one box would be a more appreciated option. However, the corresponding hardware solutions are typically sophisticated, as it shall meet precision and performance requirements simultaneously. This is also discussed in this paper.

### B. Outline

The remainder of this paper is structured as follows. Section II presents a generalized architecture of a PMU in simple blocks and discusses the bottlenecks. Section III discusses the algorithms used for this discussion. Section IV discusses implementation of the algorithms and the hardware implemented on. Finally, section V concludes the paper.

## II. REQUIREMENTS ON PMU RESPONSE AND GENERIC ARCHITECTURE OF A PMU

This section provides a brief summary of the requirements on the PMU dynamic performance from NASPI, which is later endorsed by WECC, and a generic architecture of a PMU.

### A. NASPI/WECC Requirements

In [8], the authors have summarized the frequency response of a NASPI/WECC PMU as follows

- Is -3 dB or greater at 5 Hz;
- Does not exceed -40 dB at frequencies above the Nyquist frequency (a limit of -60 dB is preferred);

# Optimal Coordination of Q(P) Characteristics among PV Systems in Distribution Grids for Minimizing Reactive Power Consumption

Afshin Samadi and Lennart Söder

Electric Power System Department, KTH Royal Institute of Technology, Stockholm SE 100-44, Sweden  
[afshin.samadi@ee.kth.se](mailto:afshin.samadi@ee.kth.se), [lennart.soder@ee.kth.se](mailto:lennart.soder@ee.kth.se)

**Abstract**— Accommodating more and more photovoltaic (PV) systems within load pockets in distribution grids due to encouraging feed-in-tariffs has raised new technical challenges such as voltage rise. Different remedies have been proposed to deal with the voltage violation. The most common remedy is supporting the voltage profile via reactive power contribution of PV systems. The recent German Grid Codes (GGC) also requires reactive power contribution of PV systems. The GGC also proposes an active power dependent (APD) power factor standard characteristic  $\cos\phi(P)$ . However, the standard characteristic lacks a systematic approach to set the  $\cos\phi(P)$  parameters according to the location of PV systems within the grid. A systematic APD voltage regulation  $Q(P)$  with four design variants has been proposed in the literature to coordinate the  $Q(P)$  characteristics among PV systems. This paper also proposes a systematic APD voltage regulation  $Q(P)$  to optimally coordinate  $Q(P)$  parameters among PV systems without the aid of any communication systems. The contribution of the proposed APD method, in contrast to its predecessor, is being an optimization-based procedure; thus,  $Q(P)$  characteristics are optimally designed and coordinated among PV systems. In other words, the main objective of this study is to deploy the voltage sensitivity matrix to optimally coordinate the  $Q(P)$  parameters among PV systems within the grid. The performance of the proposed optimal APD is compared with its predecessor; the results show that the proposed method can considerably reduce the total reactive power consumption and the corresponding losses in comparison with the predecessor APD method.

## I. KEY EQUATION, FIGURES AND RESULTS

The objective of the proposed method is to design the slope and the threshold of PV systems that can minimize the sum of the individual PV reactive power consumption over its corresponding production profile, which is the hatched area in the Fig. 1. Hence, the following objective function is

$$\min_{(P_{th,i}, \Delta Q_i)} \left( \sum_{i=1}^n (P_{\max, pv,i} - P_{th,i}) \Delta Q_{\max,i} \right)$$

The performance of the proposed method is investigated in a test utility grid in Fig. 2. Fig. 3 shows the superiority of the proposed optimal APD in reducing reactive power consumption and losses.

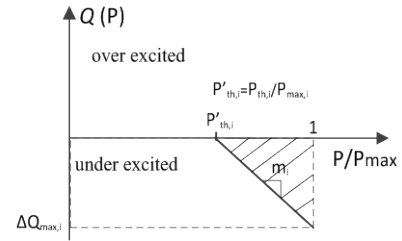


Figure 1. Block diagram of the voltage control in the PV model.

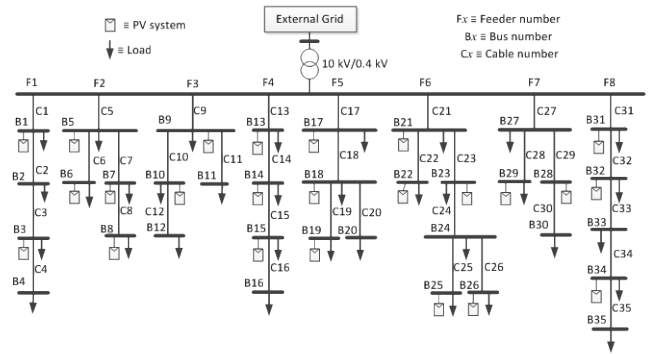


Figure 2. Test utility distribution grid

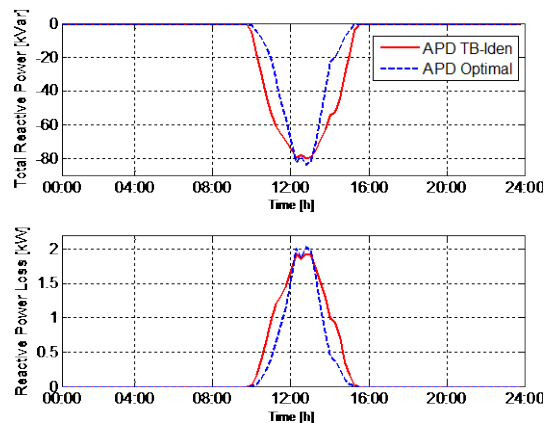


Figure 3. Daily total reactive power consumptions by PV systems and their associated losses in the presence of the APD optimal and APD TB-Iden.

# Methodology for droop control dynamic analysis of multi-terminal VSC-HVDC grids for offshore wind farms

E. Prieto-Araujo<sup>1</sup>, Student Member, F. D. Bianchi<sup>2</sup>, A. Junyent-Ferré<sup>3</sup>, Member IEEE and O. Gomis-Bellmunt<sup>3</sup>, Member IEEE

<sup>1</sup>CITCEA-UPC, Av. Diagonal, 647, Planta 2, 08028, Barcelona (Spain), eduardo.prieto-araujo@citcea.upc.edu

<sup>2</sup>C&P Imperial College, Exhibition Road, London, SW7 2AZ

<sup>3</sup>IREC, Jardins de les Dones de Negre 1, pl. 2, 08930 Sant Adrià de Besòs, (Spain)

**Abstract** — This paper addresses the control of multiterminal voltage-source converters at high-voltage direct current in the context of offshore wind farms. Droop control is commonly used to regulate the dc voltage in this kind of grid, and droop parameters are selected on the basis of steady-state analyses. Here, a control design methodology is proposed based on the frequency-response analysis. This methodology provides a criterion to select the droop gains, taking into account the performance specifications [i.e., the desired voltage errors and the maximum control inputs (currents)]. The application of the methodology is illustrated with a four-terminal grid.

## I. INTRODUCTION

The following study is based on the design of the droop controller parameters used in the HVDC multiterminal voltage regulation under two different operation modes, the normal and the grid fault operation mode [1].

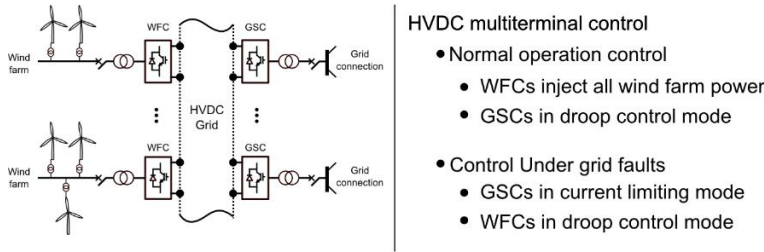


Fig. 1 Magnetization as a function of applied field.

## II GRID MODELLING

The grid model is obtained combining the average model of the VSC converters and the  $\pi$ -equivalent model of the cables. Defining the controlled and non-controlled inputs, the controlled and non-controlled outputs and the state variables, the state-space model and the system transfer functions can be obtained. Analyzing these transfer functions, the droop controller constants can be selected.

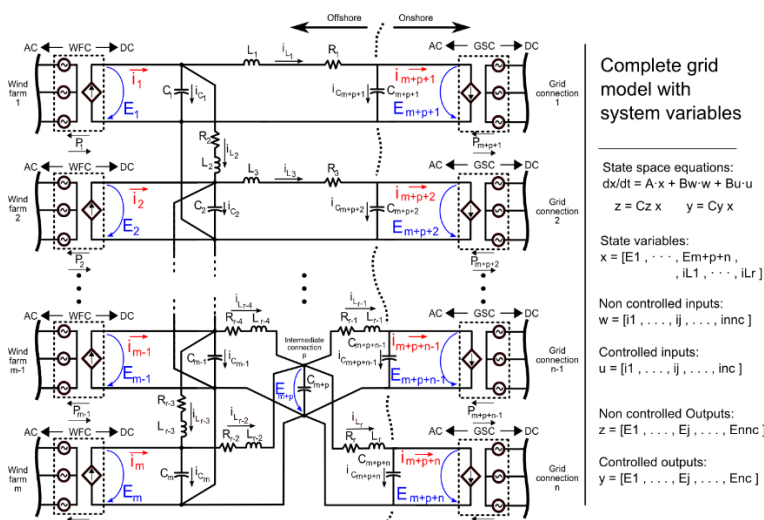


Fig. 2 VSC current loop performing droop control

## III. FOUR TERMINAL GRID ANALYSIS [NORMAL OPERATION]

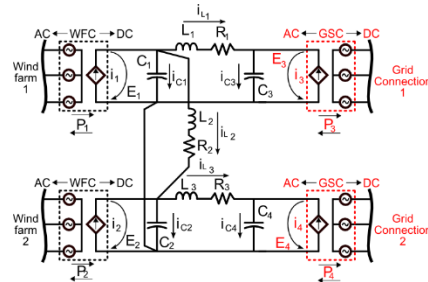


Fig. 3 Four terminal grid node

- Two Wind farms and Two Grid connections.
- System variables definition  
 $z = [E1 \ E2] \ y = [E3 \ E4]$   
 $w = [i1 \ i2] \ u = [i3 \ i4]$   
 $Eo = [Eo3 \ Eo4]$
- Droop controller parametrization:  

$$K = K_G \begin{bmatrix} 1 & 0 \\ 0 & 1 \end{bmatrix}$$

## A. Controller performance specifications

- Voltages must be maintained within certain limits
- Currents flowing through the grid should be limited
- The control action should not exceed the bandwidth of the converter.

These control requirements are imposed as gain limitations of the grid transfer functions frequency response. Figure 4 show the suitable controllers that accomplish the control requirements (shadowed part).

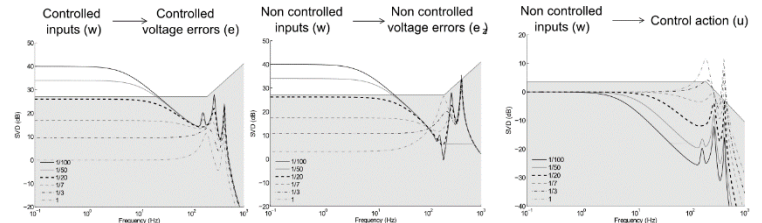


Fig. 4 Multivariable frequency analysis. Suitable controllers – shadowed lines

## B. Simulation Results

Step change of incoming power from the wind farms [100 MW].

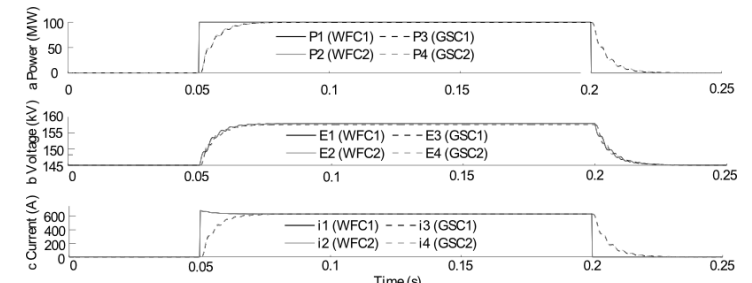


Fig. 1 Simulation results

## REFERENCES

- [1] J. Liang, O. Gomis-Bellmunt, J. Ekanayake, and N. Jenkins, "Control of multi-terminal VSC-HVDC transmission for offshore wind power," in Proc. 13th Eur. Conf. Power Electron. Appl., 2009, pp. 1–10. H. Simpson, *Dumb Robots*, 3<sup>rd</sup> ed., Springfield: UOS Press, 2004, pp.6-9.
- [2] L. Xu, L. Yao, and M. Bazargan, "DC grid management of a multiterminal HVDC transmission system for large offshore wind farms," in Proc. Int. Conf. Sustainable Power Generation and Supply, 2009, pp. 1–7.
- [3] S. Skogestad and I. Postlethwaite, *Multivariable Feedback Control, Analysis and Design*. Hoboken, NJ: Wiley, 2007.

# Challenges for Balancing Area Coordination Considering High Wind Penetration

Robin Broder Hytowitz<sup>1,2</sup>, *Student Member, IEEE*, and Benjamin Hobbs<sup>1</sup>, *Fellow, IEEE*

<sup>1</sup>Department of Geography and Environmental Engineering, Johns Hopkins University, Baltimore, MD 21218, USA

<sup>2</sup>Center for Electric Power and Energy, Technical University of Denmark, Lyngby, Denmark

Email: hytowitz@jhu.edu and bhobbs@jhu.edu

**Abstract**— Renewable energy adds variability and uncertainty to the operation of electric power grids. Accommodating these issues can be difficult and there have been many proposals for changes to operations, including enlargement of balancing areas. Because of load and renewable production diversity, larger areas will see less variability compared to small balancing areas, making it advantageous to optimize over one large area. The trend toward making larger balancing areas will facilitate more efficient utilization of resources (e.g., reserve, unit scheduling, etc.), decrease peak generation requirements, and increase minimum load levels. These are, for example, major rationales for the California ISO’s proposal for an Energy Imbalance Market in the Western US, which at this writing is planned to encompass the CAISO and PacifiCorp.

However, there are tradeoffs that are made when network size increases. A larger system size creates larger models with more nodes and variables, which makes incorporating additional complexities into system operations difficult. Furthermore, as system size increases, it becomes more of a challenge to solve scheduling models to optimality (larger duality gaps, etc., become necessary because of the model size), so the putative efficiency improvements of enlarging balancing areas might not be realized.

Combining balancing areas will increase the number of variable resources and the geographic area where the resources are located. While this might reduce the impact of output variability, it does not directly impact the effects of forecast uncertainty. Day-ahead forecasts of renewable energy are uncertain, and this uncertainty will increase as the penetration of renewables grows.

In order to assess the impacts of balancing area interactions in the presence of a high penetration of renewable energy, different models for day-ahead scheduling, including some that consider both variability and uncertainty, are created and compared. The interactions between two different systems will be analyzed using unit commitment (UC) models, including deterministic, stochastic, and trading models. These models will be used to simulate day-ahead schedules and estimated costs. Once simulation results for these models are obtained, the efficiency of the day-ahead schedules and accuracy of cost estimates from each model type can be evaluated using a real-time balancing model that evaluates how the system performs under the actually realized load

and variable generation. This comparison will reveal the drawbacks, both economic and reliability-related, of each model type so that we can better evaluate the benefits and costs of enlarging balancing areas.

## I. KEY EQUATIONS

The equations show the objective functions for a deterministic unit commitment model (1), stochastic unit commitment model (2), and a real-time model (3).

$$\min \sum_{\forall t} \sum_{\forall g} (c_g P_{g,t} + c_g^{SU} v_{g,t} + c_g^{NL} u_{g,t}) \quad (1)$$

$$\min \sum_{\forall c} \pi_c \sum_{\forall t} \sum_{\forall g} (c_g P_{g,t,c} + c_g^{SU} v_{g,t,c} + c_g^{NL} u_{g,t,c}) \quad (2)$$

$$\min \sum_{\forall t} \sum_{\forall g} c_g P_{g,t} + c_g^{NL} u_{g,t} \quad (3)$$

## II. INITIAL RESULTS

The Reliability Test System 1996 (RTS) was used in simulations. Benchmark results are shown for the three-zone model for both stochastic and deterministic day-ahead unit commitment. Further results divide the RTS grid into two adjacent balancing areas to compare results from trading. These initial results indicate no-load cost savings of 1.3% by using the stochastic model.

TABLE I: DAY-AHEAD AND REAL-TIME MODELING RESULTS

	Day-Ahead				Real-Time	
	Deterministic	Stochastic			Deterministic	Stochastic
	Middle Forecast	High Forecast	Middle Forecast	Low Forecast	Actualized Wind Generation	
Linear (\$)	1,948,591	1,952,139	1,944,830	1,907,353	1,889,514	1,887,644
No Load (\$)	225,612	222,735	222,735	221,596	225,612	222,735
Total Cost (\$)	2,250,770	2,236,210 (expected)			2,191,693	2,186,870

## REFERENCES

- [1] J. C. Smith, M. R. Milligan, E. A. DeMeo, and B. Parsons, “Utility wind integration and operating impact state of the art,” *IEEE Trans. Power Syst.*, vol. 22, no. 3, pp. 900–908, 2007.
- [2] WECC Variable Generation Subcommittee Marketing Workgroup, “Electricity markets and variable generation integration whitepaper,” 2011.
- [3] A. H. van der Weijde and B. Hobbs, “Locational-based coupling of electricity markets: benefits from coordinating unit commitment and balancing markets,” *J. of Regul. Econ.*, vol. 39, no. 3, pp 223-251, 2011.
- [4] B. A. Corcoran, N. Jenkins, and M. Z. Jacobson, “Effects of aggregating electric load in the United States,” *Energy Policy*, vol. 46, pp. 399–416, Jul. 2012.
- [5] J. King, B. Kirby, M. Milligan, and S. Beuning, “Flexibility reserve reductions from an energy imbalance market with high levels of wind energy in the western interconnection,” NREL Technical Report TP-5500-52330, Golden, CO, 2011.



# Distributed Excitation Control for Future Power Systems

Meimanat Mahmoudi, Kevin Tomsovic, Seddik Djouadi and Husheng Li  
 Department of Electrical Engineering and Computer Science  
 University of Tennessee, Knoxville, 37996

**Abstract**--Integration of cyber technologies capable of monitoring, communicating, and controlling the electric power system, renders the smart grid one of the most complex cyber physical systems. For the smart grid to be resilient to disturbances, wide-area monitoring and control is a necessity. While local controllers are blind to the widespread effects of disturbances and centralized controllers are challenging to implement, distributed controllers can achieve a trade-off between performance and associated cost. In this work, the design and performance of two distributed excitation control schemes are presented. We show that distributed control can help prevent disturbances from propagating in large power networks. Moreover, we demonstrate the effectiveness of distributed control in damping inter-area oscillations. In order to highlight the advantages of the proposed controllers, results are compared with local and centralized control schemes.

**Index Terms**--Cyber-physical systems, distributed control, smart grid, and wide-area control.

## I. INTRODUCTION

THE next generation of electricity grid, also known as the “Smart Grid”, is one of the most complex cyber physical systems (CPS) due to its extreme dimension, geographic reach and high reliability requirements. For the smart grid to be resilient, wide-area monitoring and control is a necessity. The interconnected structure of the power grid poses a great risk of system-wide failures in the network. A local disturbance can influence the system over a wide area and lead to cascading failures and blackouts. Prior to the introduction of real-time phasor measurement units (PMUs) power system control was primarily local. Except for the very slowest of controllers and a few specialized schemes, engineers have designed systems largely through local decisions based on local measurements. Due to the lack of observability in local measurements of certain inter-area modes, existing control schemes may fail to deliver the expected performance and reliability. Therefore, using wide-area measurements becomes a key element in designing control.

The purpose of this research is twofold. First, we show that distributed control can help prevent disturbances from propagating in large power networks. In doing so, we used the continuum model test systems. Second, we demonstrate the effectiveness of distributed control in damping inter-area oscillations and compare the results with the performance of local and centralized control schemes. For this, we use a two-

area four machine test system which has been widely used for analysis of inter-area modes. Due to the distributed nature of the design, communication between local controllers helps to improve the damping of inter-area modes, which are not readily apparent for the local controller. Moreover, there is no need to model a large-scale system as a whole and deal with the complexities arising in a centralized scheme.

## II. DISTRIBUTED EXCITATION CONTROL FOR POWER NETWORKS

### A. Distributed LQR Control Design: Regular Network

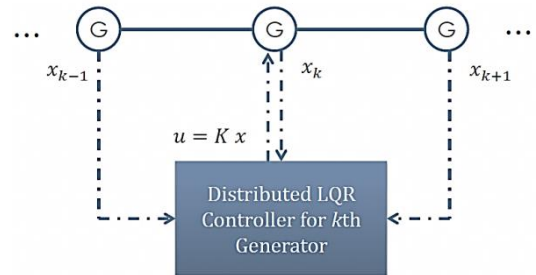


Fig. 1. Distributed LQR control agent and information exchanges for part of a radial structure.

### B. Distributed LQR Control Design: Known and Limited Communication

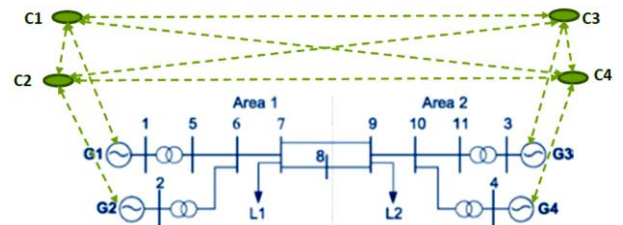


Fig. 2. Physical layer (in blue) and cyber layer (in green) for Two-area four machine test system.

## ACKNOWLEDGMENT

The authors gratefully acknowledge the support of the National Science Foundation through grant CNS-1239366 and support by the Engineering Research Center Program of the National Science Foundation and the Department of Energy under NSF Award Number EEC-1041877 and the CURENT Industry Partnership Program.



# MDP Methods for Valuation of Multi-Purpose Battery Energy Storage under Uncertainty

Jonathan Donadee, *Student Member, IEEE*, Jianhui Wang, *Senior Member, IEEE*,  
and Marija D. Ilić, *Fellow, IEEE*

*Abstract*—This poster proposes using the modeling and computational techniques of the Markov decision problem (MDP) framework to estimate the net present value (NPV) of a grid-scale battery energy storage system (BESS) operating in a liberalized market setting. First, we propose an MDP to optimize hourly operational decisions under uncertainty and while considering battery capacity degradation. The profits earned by an ESR will depend on how it is operated. ESR operations should consider multiple sources of revenue simultaneously to maximize profits. In this problem, The BESS earns profit by arbitraging the daily cycle of energy prices and also by providing regulation service. The solution of this MDP is then used to estimate the rate at which the BESS earns profits and the rate at which the maximum energy storage capacity of the BESS degrades. Finally, we utilize the methods developed in this paper to estimate a BESS's NPV.

## A. Key Equation

The infinite horizon average reward MDP for the BESS that we have described is shown in (1). (1) can be solved for  $z^*(s)$ , the maximum per-period average expected reward over an infinite horizon when starting in state  $s$ , for each state  $s$ .  $z^*(s)$  is composed of an optimal bias for starting in some initial state,  $\gamma^*(s)$ , and the optimal gain or stationary reward,  $z^*$ , as shown in (2).

$$z^*(s) = \max_{\pi \in \Pi} \lim_{N \rightarrow \infty} \frac{1}{N} \mathbb{E}_s^\pi \left[ \sum_{t=1}^N r_t(s, a) \right], \forall s \in S \quad (1)$$

$$z^*(s) = \gamma^*(s) + z^*, \forall s \quad (2)$$

A stationary Markov operating policy  $\pi$  takes the form of a look-up table such that  $a(s) = \pi(s)$ .  $\pi$  lists the action to take given the current state of the system, regardless of the decision epoch. An operating policy  $\pi$  must be in the set of feasible decision making policies  $\Pi$ , ensuring  $\pi(s) \in A_e$  for all  $s$ .

Solving (15) yields the optimal gain,  $z^*$ , and biases,  $\gamma^*(s)$ , as well as the optimal stationary Markov operating policy  $\pi^*$ , where the optimal action is given for each state by  $a^*(s) = \pi^*(s)$ . The BESS MDP presented in this section can be solved using the policy iteration algorithm.

## B. Key Figures

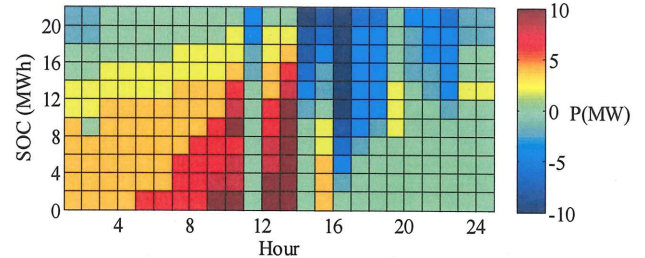


Figure 1. Optimal baseline charge rate policy when considering battery degradation

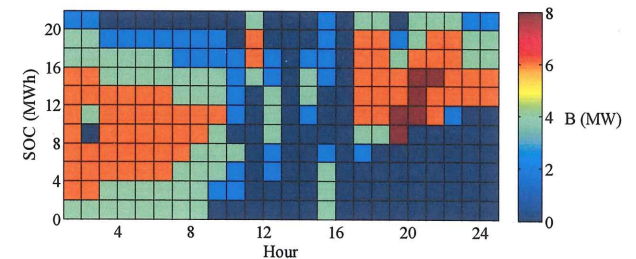


Figure 2. Optimal regulation capacity policy when considering battery degradation

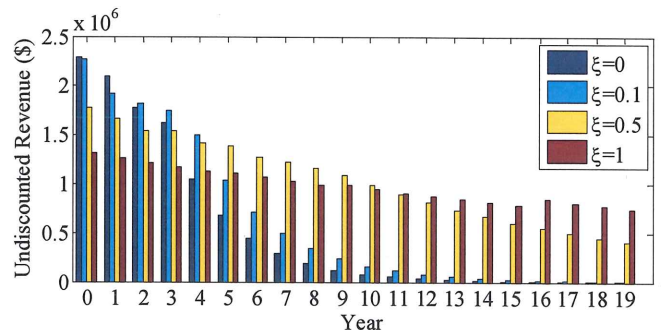


Figure 3. Annual undiscounted revenues with various degradation penalty scaling factor values

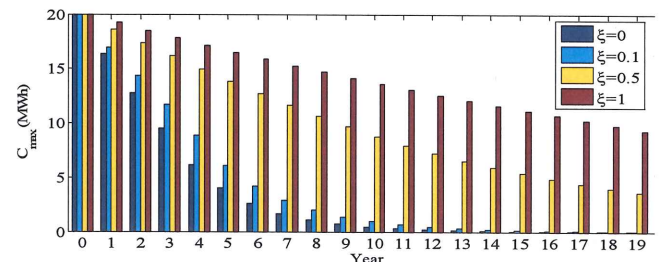


Figure 4. Maximum energy storage capacity,  $C_{max}$ , over the planning horizon with various degradation penalty scaling factor values

TABLE I  
ESTIMATED NPV FOR ALL TEST CASES

Case	$\xi=0$	$\xi=0.1$	$\xi=0.5$	$\xi=1$
NPV (\$MM)	8.575	9.644	12.659	11.101

# Optimal Bidding Strategy of a Strategic Wind Power Producer in the Short-Term Market

Ting Dai, *Student Member, IEEE*, and Wei Qiao, *Senior Member, IEEE*

Department of Electrical Engineering, University of Nebraska-Lincoln, Lincoln, NE 68588, USA

Email: ting.dai@huskers.unl.edu and wqiao@engr.unl.edu

**Abstract**—Wind energy is a clean and renewable energy source which is rapidly growing globally. As the penetration level of wind power grows, the system operators need to consider wind power producers as strategic producers whose bidding behavior will have an impact on the locational marginal prices. This paper proposes a bilevel stochastic optimization model to obtain the optimal bidding strategy for a strategic wind power producer in the short-term electricity market. The upper-level problem of the model represents the profit maximization of the wind power producer while the lower-level problem represents the market clearing processes of both day-ahead and real-time markets. The uncertainties in the demand and wind power production are considered in the model. By using the duality theory and Karush-Kuhn-Tucker condition, the bilevel model is transferred into a mixed-integer linear problem. Case studies are performed to show the effectiveness of the proposed model.

## I. KEY EQUATION

The problem to determine the optimal bidding strategy for a strategic wind power producer is formulated as a bilevel stochastic optimization model. The upper level problem (1) maximize the total profit of wind power producer in both day-ahead and real-time market. The lower-level problem (2) and (3) represent the market clearing process of the day-ahead and real-time market respectively.

### A. The upper level problem

$$\min_{\xi} \sum_{wt\omega} \pi_{\omega} \left[ \sum_b (-\lambda_{(m:w \in \Psi_m^W)_t}^{DA} p_{bwt}^{WD}) + \lambda_{(m:w \in \Psi_m^W)_{t\omega}}^{RT} P_{wt\omega}^{WR} \right] - \beta \left( \zeta - \frac{1}{1-\alpha} \sum_{\omega} \pi_{\omega} \eta_{\omega} \right) \quad (1a)$$

Subject to:

$$0 \leq \lambda_{(b-1)_{wt}}^{WD} \leq \lambda_{bwt}^{WD} \leq \lambda^{CapD}, \quad \forall w, b \geq 2, t \quad (1b)$$

$$0 \leq \lambda_{wt\omega}^{WR} \leq \lambda^{CapR}, \quad \forall w, t, \omega \quad (1c)$$

$$\eta_{\omega} \geq 0, \quad \forall \omega \quad (1d)$$

$$\zeta - \eta_{\omega} \leq \sum_{wt} \left[ \sum_b (-\lambda_{(m:w \in \Psi_m^W)_t}^{DA} p_{bwt}^{WD}) + \lambda_{(m:w \in \Psi_m^W)_{t\omega}}^{RT} P_{wt\omega}^{WR} \right], \quad \forall \omega \quad (1e)$$

### B. The lower level problem

$$\min_{\xi} \sum_{bi} \lambda_{bit}^{CD} p_{bit}^{CD} + \sum_{bw} \lambda_{bwt}^{WD} p_{bwt}^{WD} - \sum_{ld} \lambda_{ldt}^{LD} p_{ldt}^{LD} \quad (2a)$$

Subject to day-ahead market clearing constraints

$$\min_{\xi} \sum_i (\lambda_{it}^{CR+} p_{it\omega}^{CR+} - \lambda_{it}^{CR-} p_{it\omega}^{CR-}) + \sum_w \lambda_{wt\omega}^{WR} P_{wt\omega}^{WR} + \sum_i (\lambda_{it}^{RU} r_{it\omega}^U + \lambda_{it}^{RU} r_{it\omega}^L) - \sum_d \lambda_{dt\omega}^{LR} P_{dt\omega}^{LR} \quad (3a)$$

Subject to real-time market clearing constraints

### C. Problem reformulation

To facilitate the solution process, the bilevel programming problem (1)-(3) is transferred into an equivalent single-level

mathematical problem with equilibrium constraint (MPEC) problem through the KKT conditions of the lower-level problems (2) and (3). The whole problem is converted into a mixed-integer linear problem (MILP).

## II. KEY RESULTS

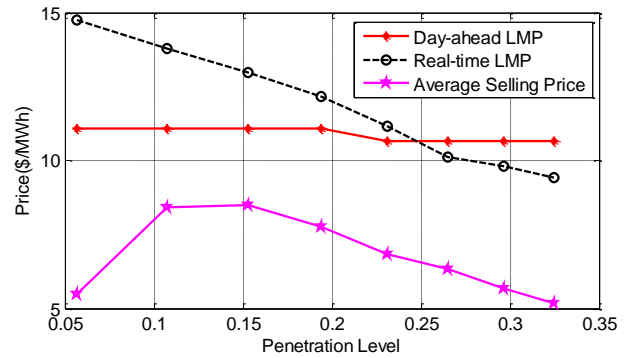


Fig. 1. Day-ahead LMP, average real-time LMP at bus 8, and average selling price of the wind power producer for different penetration levels of wind power.

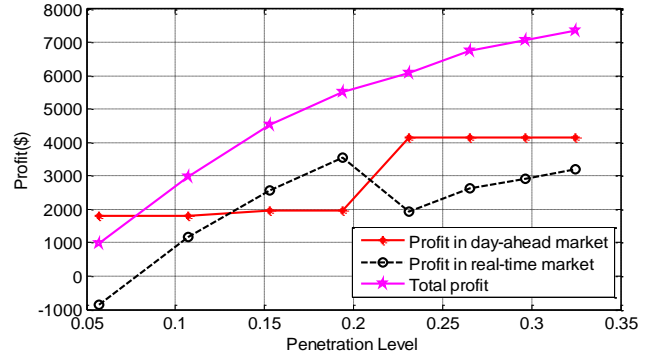


Fig. 2. Day-ahead, real-time, and total profits of the wind power producer for different penetration levels of wind power.

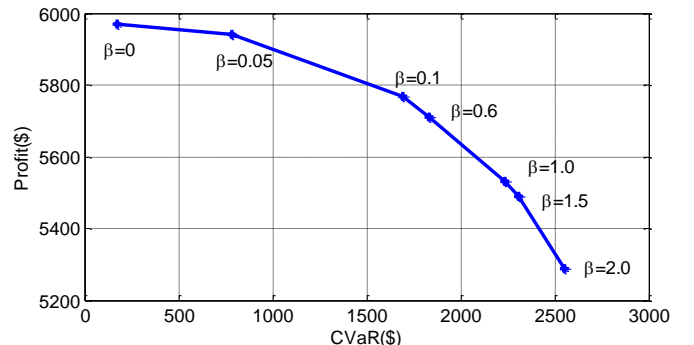


Fig. 4. The expected total profit and CVaR of the wind power producer for different values of  $\beta$ .

# Frequency-Based Load Control Schemes Through Voltage Reduction for Power Systems with Wind Penetration

Felipe Wilches-Bernal, *Student Member, IEEE*, and Joe H. Chow, *Fellow, IEEE*  
 Department of Electrical and Computer and Systems Engineering  
 Rensselaer Polytechnic Institute  
 110 8th street, Troy, NY 12180, USA.

**Abstract**—Regulating frequency is a key component of power system operation and control, a task traditionally achieved by continuously controlling the power output of the generators according to load changes. In a power system with a considerable amount of wind generation, controlling frequency becomes a more challenging undertaking as wind generation is not controllable and lacks inertia response.

In this research we investigate an alternative approach to frequency regulation by controlling the load side, an idea already proposed in works as [1], for power systems with wind generation. We present an assessment of three different frequency-based load control schemes through voltage reduction. The first reduces the load by controlling the reactance that connects it to the transmission/distribution system (similar to the method in [2] for aluminum smelting loads). The second controls the voltage through a shunt reactance in parallel to the load. The third is simply a frequency controlled tap changing transformer. Here we present the results for the three load control schemes evaluated in the two area system [3], [4] with wind penetration. The study was performed in PST using the newly implemented WTG models [5]. Results show that controlling load with any of the analyzed methods improves the frequency response of the system.

**Index Terms**—Frequency control, wind power, demand side.

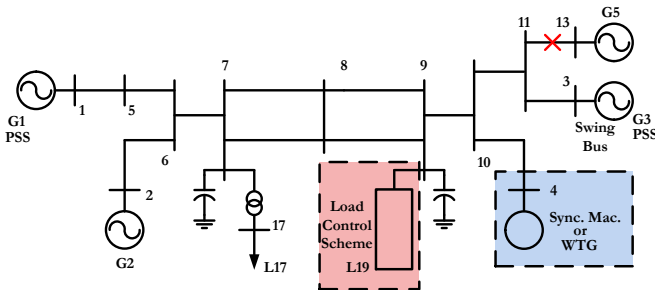


Fig. 1. Power System under consideration the KRK 2-area system. WTG displaces conventional generation at Bus 4 in Area 2. Load schemes are attached to load 19.

## REFERENCES

[1] D. Trudnowski, M. Donnelly, and E. Lightner, “Power-system frequency and stability control using decentralized intelligent loads,” in *Transmission and Distribution Conference and Exhibition, 2005/2006 IEEE PES*. IEEE, 2006, pp. 1453–1459.  
 [2] H. Jiang, J. Lin, Y. Song, W. Gao, Y. Xu, B. Shu, X. Li, and J. Dong, “Demand side frequency control scheme in an isolated wind power system for industrial aluminum smelting production,” *Power Systems, IEEE Transactions on*, vol. 29, no. 2, pp. 844–853, 2014.

Load Control Schemes

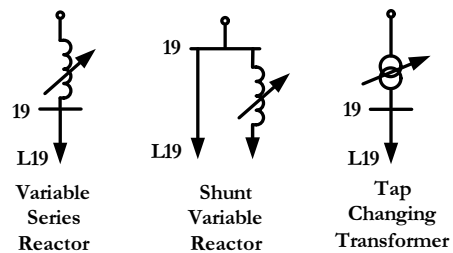


Fig. 2. Load reduction schemes implemented at Bus 19.

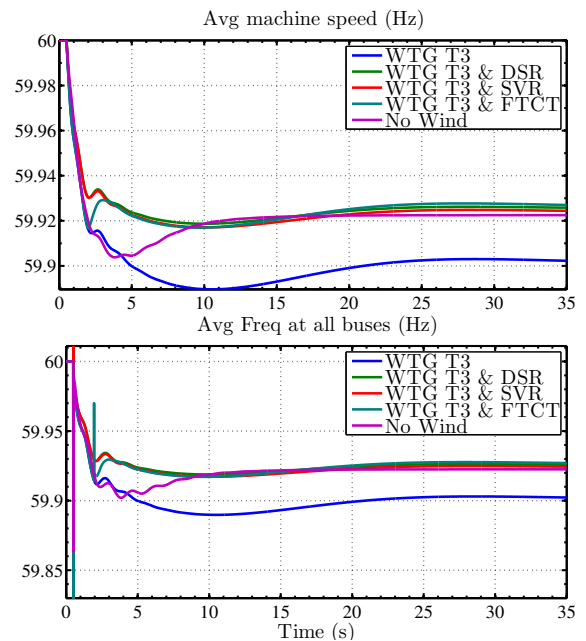


Fig. 3. Frequency response of the system.

[3] M. Klein, G. Rogers, P. Kundur *et al.*, “A fundamental study of inter-area oscillations in power systems,” *IEEE Transactions on Power Systems*, vol. 6, no. 3, pp. 914–921, 1991.  
 [4] P. Kundur, N. J. Balu, and M. G. Lauby, *Power system stability and control*. McGraw-hill New York, 1994, vol. 7.  
 [5] F. Wilches-Bernal, J-J. Sanchez-Gasca and J. Chow, “Implementation of wind turbine generator models in the power system toolbox,” in *Power and Energy Conference at Illinois (PECI), 2014 IEEE*. IEEE, 2014, pp. 1–5.

# Load Modeling in a Reduced WECC Model for Studying Voltage Controls

Yidan Lu

Dept. of Electrical Engineering and Computer Science  
The University of Tennessee  
Knoxville, TN, USA  
ylu16@utk.edu

Kevin Tomsovic

Dept. of Electrical Engineering and Computer Science  
The University of Tennessee  
Knoxville, TN, USA  
tomsovic@utk.edu

**Abstract**— The construction of a reduced WECC system with different levels of wind penetration was verified by conducting an transfer limit analysis and transient simulation following a generation trip. The system model is extended to reflect observed fault induced delayed voltage recovery due to air-conditioner stalling. A composite load model which includes modeling of induction machine and single phase compressor is developed and considered in the stability analysis. The application of composite load model enables the simplified system to have similar delayed voltage recovery following a 230kV transmission fault. Simulations show a significant impact on the transfer limit and therefore useful for analyzing new wide area voltage controls.

**Keywords**— composite load model; frequency response; transfer limits; wind generation.

## I. INTRODUCTION

The modern power grid is undergoing a dramatic change in its generation mix. Conventional energy sources are being replaced by renewable energy sources. The rapid change in generation as well as transmission indicates the need for new system models to represent large grids of the future.

## II. DYNAMIC RESPONSE VERIFICATION

The frequency response of the reduced WECC system is verified by frequency response following a 1400 MW Montana generation trip. The curve recorded by FNET units is used as benchmark for frequency response verification. The frequency responses comparison is displayed in Table I. The transfer limit over the California-Oregon Intertie (COI) is calculated according to accepted WECC operating criteria. The CAISO 2012 OSS report is used as reference during the calculation of COI transfer limit [1]. Only single element outages are considered in the calculation and WECC-NERC standards are followed. The transfer limits of system with different renewable penetrations are shown in Table II.

TABLE I. FREQUENCY RESONSE COMPARISON

Element	FNET	Case I	Case II	Case III
Wind Generation	-----	0GW	7.37GW	13.54GW
Max Freq. Drop	164mhz	180mhz	168mhz	156mhz
Recovery Time	15S	15S	15S	12S
Final Deviation	85.20mhz	90mhz	90mhz	90mhz

TABLE II. TRANSFER LIMIT COMPARISON

System\Event	Transfer Limit	Limiting Factor	Contingency
Detailed Case	4800MW	VAR Limit	DC outage
Case I	4605MW	Volt. Drop in Malin	DC outage
Case II	4593MW	Volt. Drop in Malin	DC outage
Case III	4520MW	Volt. Drop in Malin	DC outage

## III. APPLICATION OF COMPOSITE LOAD MODEL

A composite load model has been developed in PSLF by WECC task force to present delayed voltage recovery from transmission faults. As in [2], different load compositions are assigned for different WECC climate zones. For simplicity, the reduced WECC system model only has a composite load model applied in southern California and ignores load-side transformer tap change. Table III displays the detail of load composition for the developed model. Simulation results under this load constitution match well the recorded events presented in [2].

TABLE III. LOAD CONSTITUTION OF WECC SYSTEM

Load Type	Percentage		U/V relay		Thermal Relay	
	SC	PARDEE	Pick-up V	Portion	Heating T	Portion
Const. Power	34	80	None	0%	None	0%
Elec-tronic	14	0	None	0%	None	0%
3-p motor	42	0	0.65	20%	None	0%
1-p motor	10	20	0.50	10%	20S	100%

## IV. CONCLUSION AND FUTURE WORK

Motor loads tend to decrease the allowable transfer limit of the COI intertie due to the delayed voltage recovery. With developed load model, the transfer limit decreases by about 1GW due to inadequate reactive support during stalling period. Strategies dealing with motor stalling need to be developed for voltage control in this situation.

## REFERENCES

- [1] R. Chakkapalli and P. Poonpun, " SYSTEM OPERATING LIMIT STUDY REPORT," CAISO, folsom, CA January 31, 2012 2012.
- [2] D. Kosterev, A. Meklin, J. Undrill, B. Lesieutre, W. Price, D. Chassin, et al., "Load modeling in power system studies: WECC progress update," in *Power and Energy Society General Meeting-Conversion and Delivery of Electrical Energy in the 21st Century, 2008 IEEE*, 2008, pp. 1-8.



# Optimal branch numbering for UPFC benefit study

Niannian Cai, Student Member, IEEE, Joydeep Mitra, Senior Member, IEEE  
 Electrical & Computer Engineering, Michigan State University  
 East Lansing, MI 48824, USA  
 cainiann@msu.edu, mitraj@msu.edu

**Abstract**—In smart grid, Unified Power Flow Controller (UPFC) will be widely used to achieve flexible electricity transportation. Most of traditional UPFC benefit study does not realize the importance of the numbering of branches; therefore when using intelligent methods to search for the optimal location, it is usually very inefficient and time-consuming. In this poster, it will study the methods of numbering of branches and present how it affects the searching speed of intelligent methods.

## I. INTRODUCTION

UPFC is one of the most widely used Flexible Alternating Current Transmission Systems (FACTS) devices that can control real and reactive power flow through a transmission line and regulate bus voltage simultaneously and independently. Utilization of UPFC can increase the transfer capability of existing transmission lines and potentially reduce the demand for new transmission facilities.

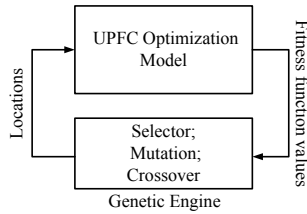


Fig. 1. Equivalent model of UPFC

Fig. 1 presents the computational diagram for UPFC benefit study using genetic algorithm. The effect of UPFC is equivalent to two injected sources at bus  $i$  and bus  $j$  respectively, expressed as (1)–(4) [1].

$$P_i = -V_s^2 G_{ij} - 2V_i V_s G_{ij} \cos(\varphi_s - \delta_{ij}) + V_j V_s (G_{ij} \cos \varphi_s + B_{ij} \sin \varphi_s) \quad (1)$$

$$Q_i = V_i I_q + V_i V_s [G_{ij} \sin(\varphi_s - \delta_{ij}) + B_{ij} \cos(\varphi_s - \delta_{ij})] \quad (2)$$

$$P_j = V_j V_s (G_{ij} \cos \varphi_s - B_{ij} \sin \varphi_s) \quad (3)$$

$$Q_j = -V_j V_s (G_{ij} \sin \varphi_s + B_{ij} \cos \varphi_s) \quad (4)$$

## II. OPTIMAL BRANCH NUMBERING

The objective function, operating cost, has area characteristics. In some areas where the power transmissions are highly congested, the objective function can be greatly improved by installing transformer-less UPFC. However, in some other

areas where transmission systems are not congested, installing transformer-less UPFC may not provide any benefit.

Coding locations based on the area can provide better efficiency for the genetic algorithm. It helps good solution candidates share a few common genes. Hence good genes can survive and reproduce while bad genes die out. Fig. 4 below gives three examples of coding scenarios. Black area is the total solution space; purple area is the collection of good solution with smaller fitness function values; Red dot is the optimal solution with the smallest fitness function value. In the first one, Fig. 2 (a), locations are coded randomly. Good solutions and the optimal solution are distributed evenly in the solution space. In this case, the good solutions and optimal solution do not share the common genes. The population will be very difficult to converge to the optimal solution. Hence, it is very inefficiency for the GA to find the optimal solution. Fig. 2 (b) codes the optimal solution outside the region of good solutions. It is very likely that the final result will converge to a sub-optimal solution in the purple area. Fig. 2 (c) is a good coding strategy. Initially, the population is evenly distributed over the solution space, but after a certain generations, the population will converge to the purple good solution area and finally find the optimal one inside the purple area.

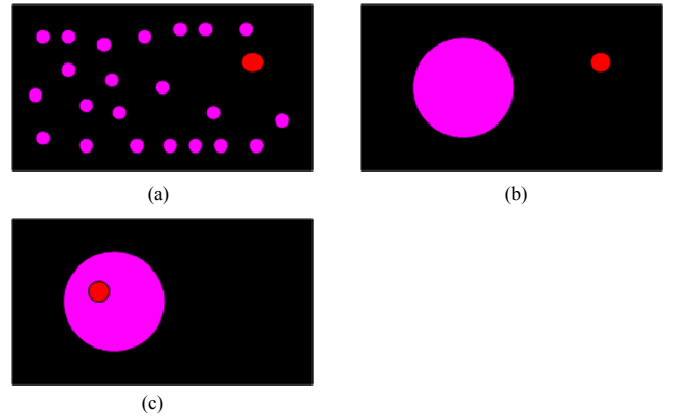


Fig. 2. (a) Bad solution space; (b) bad solution space; (c) good solution space

## REFERENCES

- [1] Shaoyun Ge, "Optimal power system operation and control incorporating FACTS Devices," Ph.D. Dissertation, The Hong Kong Polytechnic University, Aug. 1998.

# Value of Wind Diversity for Increased Integration of Wind Power into the Grid

Josh Novacheck, *Student Member*, IEEE, Jeremiah Johnson

Department of Mechanical Engineering and School of Natural Resources and Environment,  
University of Michigan  
Ann Arbor, MI  
jnova@umich.edu

**Abstract**— One of the largest challenges in integrating large quantities of wind power into the grid is the variability in its power output. The fast ramping up or down of its power output can have negative consequences for grid operations, including increased costs, inefficient operation of conventional generators, and the need for additional ancillary services. One method to deal with the wind variability is to diversify the wind power portfolio. To optimize diversified wind, a modified version of the multi-objective optimization method called Mean-Variance Portfolio optimization is used. Ten-minute interval wind power data from NREL’s Eastern Wind Dataset is used in the optimization. To measure the benefits of diversified wind power, wind portfolios of different ramp rate variabilities are assessed in an economic dispatch model of the U.S. Eastern Interconnection. Diverse wind is found to mitigate negative system level impacts of wind variability with small increases in installed wind power capacity.

## Index Terms--

### I. KEY EQUATIONS

The two objectives of the design problem are:

1. Minimize the installed capacity of wind power,

$$\text{Min } \sum_{i=1}^n x_i, \quad (1)$$

- and, 2. Minimize the ramp rate variance from time step to time step,

$$\text{Min } x^T \Pi x, \quad (2)$$

while delivering a minimum amount of wind energy,  $E_{min}$ , to the system,

$$\text{s.t., } (8766 \text{ hours/year}) * \sum x_i CF_i \geq E_{min}, \quad (3)$$

$$0 \leq x_i \leq x_{i,max} \quad (4)$$

where,  $x_i$  is the installed capacity at site  $i$ ,  $x$  is a vector of all  $x_i$ ,  $CF_i$  is the capacity factor at site  $i$ ,  $x_{i,max}$  is the maximum capacity at site  $i$ , and  $\Pi$  is the ramp rate covariance matrix, which holds the ramp rate covariance between all wind sites.

### II. KEY FIGURES

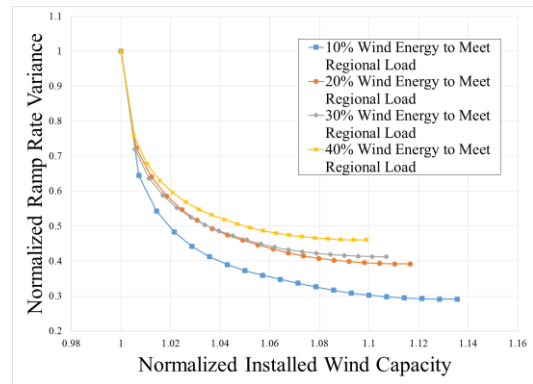


Figure 1. Pareto frontiers with varying minimum wind energy constraints normalized to the portfolio with the minimum installed wind power capacity.

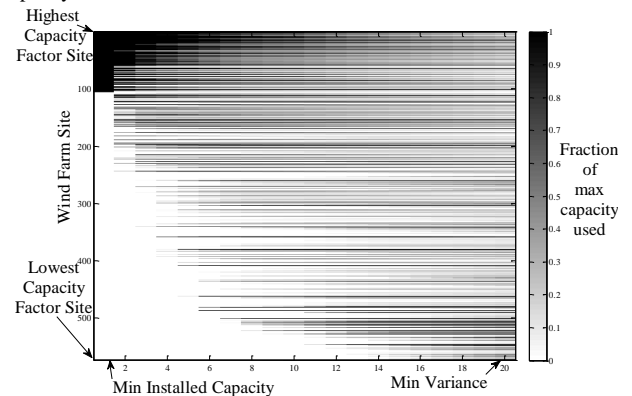


Figure 2. The fraction of the wind farm size capacity used at each site changes along the Pareto frontier. Initially, only sites with highest capacity factors are used. As more weight is given to minimizing variability, the resource is spread out to more, lower quality wind sites.

### III. KEY RESULTS

	90th Percentile Absolute Ramp Rate (MW/10Min)			
	10% Wind	20% Wind	30% Wind	40% Wind
Min Installed Capacity	233	416	615	784
Min Ramp Rate Variance	127	261	395	531



# Stability Design Criteria for Distribution Systems with Solid State Transformers

D. G. Shah, *Student Member, IEEE* and M. L. Crow, *IEEE Fellow*

Department of Electrical and Computer Engineering  
Missouri University of Science and Technology, Rolla, MO 65401

**Abstract**—Due to recent advancements in semiconductor technology, power electronic converters for high voltage, high power, and high frequency applications will soon be commercially available. The theoretical concept of a distribution solid state transformer (SST) is not recent, but with the use of advanced electronic switches and control strategies, the SST may soon become a practical reality. Conventional single phase distribution transformers are replaced by solid state transformers in a distribution test system to investigate their interactive dynamics. Under certain circumstances, instabilities due to harmonic resonance are observed.

Distribution transformers are an integral component in the delivery of electrical power to the end customer. The distribution transformer provides voltage transformation by stepping down the voltage from the distribution circuit to the voltage level used by the customer. Conventional distribution transformers are passive components and without additional capabilities cannot provide voltage regulation, reactive power support, or power quality improvement. Solid state transformers (SST) have been proposed as a powerful, highly flexible alternative to conventional transformers [1]-[4]. SSTs are insensitive to harmonics or user-side faults, can perform power factor correction and voltage regulation, and do not use potentially toxic coolant oils.

A solid state transformer consists of three stages: an active rectifier, and bi-directional dc-to-dc dual active bridge converter, and an inverter. These three stages together provide the key attractive features of the SST. The solid state transformer can provide active compensation to the point of grid coupling; therefore it can draw unity power factor or provide reactive compensation for voltage regulation. Additionally, it can provide active filtering to the load side such that the load is isolated from momentary sags, swells, and harmonics on the ac grid. Furthermore, the low voltage dc link can provide a dc bus to which photovoltaic panels, energy storage devices, or electric vehicle chargers can be connected. These additional features and flexibility provide a platform with which to build the future smart grid infrastructure.

The inclusion of a high number of power electronic converters in a traditionally ac grid introduces a number of technical issues in control and stability that have not previously been encountered. One area of concern is the potential for instability caused by SST interactions. This instability may take the form of a harmonic resonance induced by the interaction of the input impedance and the source output impedance [5]. Regardless of the load composition on the customer side, the active front end of the SST (the high-voltage rectifier) will appear to the ac grid as a constant power load [6]. Constant impedance loads are generally considered to be self-correcting loads in that as the voltage decreases, the power consumption will also decrease. Constant power loads however, draw the same power and are sometimes referred to as “negative impedances” and can destabilize dc networks if not properly designed [7]. This type of instability is not frequently experienced in ac distribution systems, but may become increasingly prevalent with the advent of SSTs. It is anticipated that SSTs will replace many, if not

all, conventional transformers and the ability to “plug-and-play” without additional design considerations is desirable. In this poster, we present the circumstances that may lead to SST interaction and instability and present a design approach to avoid this problematic behavior.

## REFERENCES

- [1] E. R. Ronan, S. D. Sudhoff, S. F. Glover, and D. L. Galloway, “A power electronic-based distribution transformer,” *IEEE Transactions on Power Delivery*, vol. 17, no. 2, pp. 537–547, April 2002.
- [2] X. She, A. Q. Huang, and R. Burgos, “Review of the solid state transformer technologies and its application in power distribution system,” *IEEE Journal of Emerging and Selected Topics in Power Electronics*, early access, 2013.
- [3] H. Qin and J. W. Kimball, “Solid-state transformer architecture using ac-ac dual-active-bridge converter,” *IEEE Transactions on Industrial Electronics*, vol. 60, no. 9, pp. 3720–3730, 2013.
- [4] X. She, A. Q. Huang, S. Kukic, and M. E. Baran, “On integration of solid-state transformer with zonal dc microgrid,” *IEEE Transactions on Smart Grid*, vol. 3, no. 2, pp. 975–985, 2012.
- [5] J. Sun, M. Chen, and K. J. Karimi, “Analysis and mitigation of system interactions involving single-phase PFC converters,” *IEEE Transactions on Aerospace and Electronic Systems*, vol. 44, no. 1, pp. 217–226, 2008.
- [6] N. Bottrell, M. Prodanovic, and T. C. Green, “Dynamic stability of a microgrid with an active load,” *IEEE Transactions on Power Electronics*, vol. 28, no. 11, pp. 5107–5119, November 2013.
- [7] A. Kwasinski and C. Onwuchekwa, “Dynamic behavior and stabilization of dc microgrids with instantaneous constant-power loads,” *IEEE Transactions on Power Electronics*, vol. 26, no. 3, pp. 822–834, March 2011.

# Near Optimal Fuel Scheduling for Enhanced Real Time Dispatch (RTD) with Diverse Generation Technologies

Nipun Popli *Student Member, IEEE* and Marija D.Ilić *Fellow, IEEE*

**Abstract**—A formal mathematical framework for enhanced economic dispatch is proposed as a novel alternative to the static real-time dispatch (RTD) being currently implemented by the power industry. The proposed approach may be seen as a load-following function to schedule diverse generation technologies for following intra-hour variations. Our proposed approach involves pre-scheduling system-wide fuel-input in response to large intra-hour variations in load and wind forecasts.

**Index Terms**—Real Time Dispatch (RTD), Load Following, Ramp-Rates, Tertiary Control

## I. ENHANCED REAL-TIME ENERGY DISPATCH

Prior to deregulation, load was followed using governor-based reserves. For near perfect load forecasts, the expenditure for governor-based reserves is low. But maintaining higher reserve margins to follow large variations in wind or solar power output is constrained by economic factors, particularly fuel-cost. To avoid increased reserve expenses, a formal-mathematical framework is proposed for efficient pre-scheduling of fuel input, and its real-time<sup>1</sup> updates, in anticipation of forecasted load or wind variations. A generator's response rate is primarily determined by non-linear energy conversion dynamics of its fuel sub-system. A simplified industry definition is the maximum possible change in power output of a generator over the dispatch interval  $T_{RTD}$ , once the generator is online  $R = \frac{|\Delta P_{G,max}|}{T_{RTD}}$ . This scalar averaged ramp rate is known as generator's ramp rate. The interval  $T_{RTD}$  is determined by the duration of real-time markets, i.e., economic dispatch. For all generation technologies, fast or slow, large or small, the ramp rates are defined over market's time interval  $T_{RTD}$ . The proposed framework, based on the energy-conversion dynamics of different generation technologies, is illustrated on 5-bus system in Fig. 1. A near-optimal real-time dispatch schedule (Fig. 3) for hydro  $H_1$ , coal  $C_2$  and gas  $G_3$  in anticipation of forecasted load variations (Fig. 2) is obtained. For all generators, sequences of steady-state schedules are defined for 12 dispatch intervals, as depicted in Fig. 3. The proposed approach results in a smooth RTD schedules (Fig. 3) as compared to conventional economic dispatch (Fig. (4)) by taking into account their energy-conversion dynamics. Proposed RTD results in smoother schedule for the generators

Nipun Popli is with Carnegie Mellon University, Pittsburgh, PA, USA (email: npopli@andrew.cmu.edu).

Marija D. Ilić is with Carnegie Mellon University, Pittsburgh, PA, USA, and Delft University of Technology, Delft, The Netherlands (email: milic@ece.cmu.edu).

<sup>1</sup>Real-time updates in a sense of economic dispatch, i.e., 5-10 minutes.

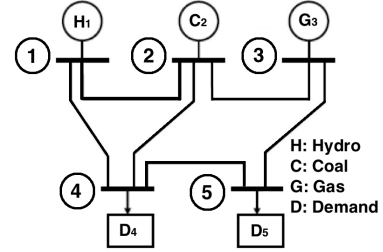


Fig. 1. 5-bus system

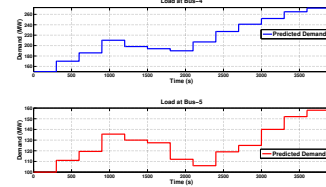


Fig. 2. Predicted Load for 5-minute Discrete Time Interval

to follow, resulting in less wear and tear. The ramping effort is distributed among all the participating generators, instead of just the cheapest or the most expensive generator. Lower chance of encountering physical limits of generators as compared to static economic dispatch approach where only one generator is rescheduled at a time.

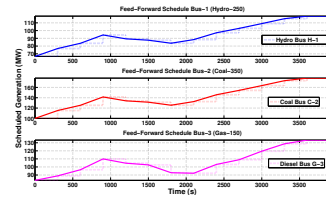


Fig. 3. Generation Schedule under Enhanced RTD

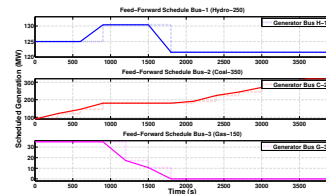


Fig. 4. Generation Schedule under Static RTD

# Incentive Based Demand Response to Reduce Costs and Minimize Price Volatility

Ailin Asadinejad Kevin Tomsovic

Department of Electrical Engineering and Computer Science  
University of Tennessee  
Knoxville, Tennessee  
aasadine@utk.edu  
tomsovic@utk.edu

**Abstract**— An incentive based demand response (DR) program is proposed. The required load reduction and adequate incentive payment assume a Load Serving Entity (LSE) designs the tariff. The tariff is designed to be simple to implement for both customer and LSE while achieving considerable saving. To equitably share the benefits of DR, the LSE can decrease the wholesale price for all customers, including those who do not participate in the DR program.

Different thresholds above market variable price are considered as trigger for demand response. We compare a constant threshold and an optimal threshold based on analysis of historical load and generation. In this optimization, savings for the LSE and the customer are maximized but consumer inconvenience is limited by constraining the number of interruptions per day and season. Results show a constant threshold has a greater impact on average LMP and price volatility in the summer (peak summer load system) while a greater value of DR can be realized throughout the year by optimizing the threshold. Data and parameters required for numerical test are derived from a WECC 240 bus reduced model. The load profiles of each device in residential and commercial sector sectors are used to find reducible part of load at each hour.

## I. KEY FORMULA

The objective function of each LSE can be written as:

$$\max : \sum_{i=1}^M (D_i - \Delta D_i) P_{FR} - (D_i - \Delta D_i) P_{RT-i} - \Delta D_i \cdot P_{inc-i} \quad (1)$$

$$\Delta D_i = \sum_{j=1}^3 \Delta D_j \quad (2)$$

$$lb_j \leq \Delta D_j \leq ub_j \quad (3)$$

$$\Delta D_j = \varepsilon_j (P_{inc-i}) \quad (4)$$

where

$P_{FR}$  is flat rate tariff for retail customer;

$P_{RT-i}$  is wholesale market price at time  $i$ ;

$D_i$  is demand at time  $i$ ;

$M$  is total number of hour that DR implement;

$\Delta D_i$  is total load reduction at time  $i$ ;

$\Delta D_j$  is total load reduction at sector  $j$  of load type

$P_{inc-i}$  is incentive payment at time  $i$ ;

$\varepsilon_j$  is the inherent demand elasticity of consumer.

## II. KEY RESULT

Table 1: Customer benefit in different regions

Region	Without DR (\$)	After DR (\$)	Benefit (\$)
Southwest	176,211,262	174,417,219	1,794,043
LADWP	31,511,902	27,114,504	4,397,398
Bay area	16,989,929	14,460,552	2,529,376
PGE other	56,140,460	48,112,042	8,028,418
Rocky MT	38,661,052	34,333,941	4,327,111
Nevada	12,475,355	11,285,744	1,189,611
SCE other	96,451,751	86,885,274	9,566,478

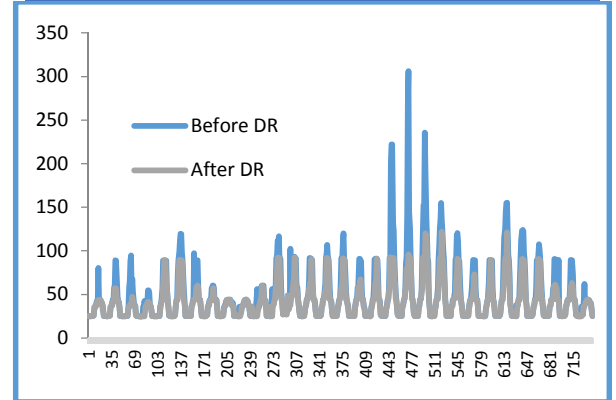


Figure 1: LMP variation in July in PGE other region

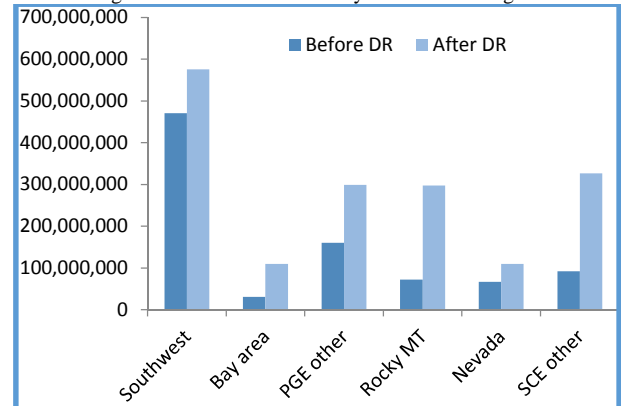


Figure 2: LSE benefit in different regions

# Modeling and Monte Carlo Simulation of Markovian Switching in Power Grid

Yichen Zhang

Dept. of Electrical Engineering and Computer Science  
The University of Tennessee  
Knoxville, TN, USA  
yzhan124@utk.edu

Kevin Tomsovic

Dept. of Electrical Engineering and Computer Science  
The University of Tennessee  
Knoxville, TN, USA  
tomsovic@utk.edu

**Abstract**— In this work, a general approach to model the stochasticity of  $N-1$  contingency by a Markovian switching process is proposed. The general framework is derived on a one node model and applied into ring and grid systems. A Monte Carlo method is used to obtain numerical solutions of the developed model.

**Keywords**—  $N-1$  contingency; Markovian switching; Monte Carlo method;

## I. INTRODUCTION

In general, classical modeling approaches for the power grid have been based on a set of Differential Algebraic Equations (DAE) of the power system dynamics and flows, coupled by the real power. However, nowadays the bulk power network becomes wider range and gains complexity because of penetration of renewable energy systems as well as communication technology applied in the system, which can be regarded as a cyber-physical system. For such a wide-area and complicated system, one cannot guarantee no unstable or insecurity cases happen after fault or perturbation. So to model uncertainty can give new analysis approaches for system stability under switching and contingency as well as remedial action schemes. Moreover, new issues and answers may be found.

## II. MARKOVIAN SWITCHING MODELING AND MONTE CARLO SIMULATION

Fig. 1 is a general one node model [1] that can be expanded into a variety of connections. The dynamics of the generator in each node is governed by the swing equation. The real power output can be calculated through:

$$P_i^e = \sum_{x=x(\alpha)} \frac{V^2 R_{ix}}{|Z_{ix}|^2} - \sum_{x=x(\alpha)} \frac{V^2 R_{ix} \cos(\delta_i - \delta_x)}{|Z_{ix}|^2} - \sum_{x=x(\alpha)} \frac{V^2 X_{ix} \sin(\delta_i - \delta_x)}{|Z_{ix}|^2} + V^2 \operatorname{Re}[Y_i] \quad (1)$$

The parameter  $x$  indicates the connection of other nodes with node  $N$ , and is controlled by the Markovian switching described below [2]:

$$P\{\alpha(t+\Delta) = j \mid \alpha(t) = i\} = \begin{cases} p_{ij}\Delta + o(\Delta) & i \neq j \\ 1 + p_{ii}\Delta + o(\Delta) & \text{otherwise} \end{cases} \quad (2)$$

where  $p_{ii} = -\sum_{j=1, j \neq i}^N p_{ij}$ . The full system model is obtained as:

$$\begin{bmatrix} \dot{\delta}_i \\ \dot{f}_i \end{bmatrix} = \begin{bmatrix} 0 & 1 \\ 0 & -\frac{D_i}{M_i} \end{bmatrix} \begin{bmatrix} \delta_i \\ f_i \end{bmatrix} + \begin{bmatrix} 0 \\ P_i^m \end{bmatrix} - \begin{bmatrix} 0 \\ P_i^e(\alpha) \end{bmatrix} \quad (3)$$

$$P_e = \operatorname{Re}[\mathbf{V} \cdot \bar{\mathbf{I}}] = \operatorname{Re}[\mathbf{V} \cdot \overline{(\mathbf{Y}(\alpha) \cdot \mathbf{V})}] \quad (4)$$

$P_i^e(\alpha)$  is a matrix and can be calculated from (4). So the switching characteristic is described by the  $\mathbf{Y}$  matrix.

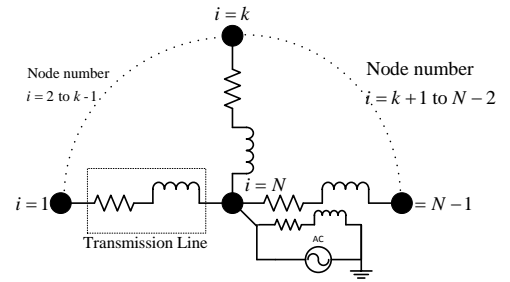


Fig. 1 The one node model

The general approach is employed on a  $3 \times 3$  squared grid system. By using Monte Carlo method, the angle oscillation after loss of one line is shown in Fig. 2.

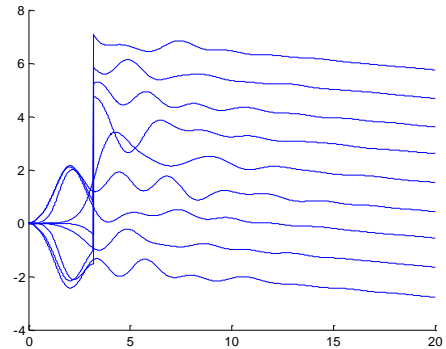


Fig. 2 Angle oscillation after loss of one line

## REFERENCES

- [1] L. Husheng, *et al.*, "Flocking generators: A PdE framework for stability of smart grids with communications," in *Smart Grid Communications (SmartGridComm), 2012 IEEE Third International Conference on*, 2012, pp. 540-545.
- [2] X. Junlin, *et al.*, "Local Mode Dependent Decentralized Stabilization of Uncertain Markovian Jump Large-Scale Systems," *Automatic Control, IEEE Transactions on*, vol. 54, pp. 2632-2637, 2009.

# Modeling Flexibility and Optionality in Grid Planning using Multistage Stochastic Programming: The Benefits of Additional Decision Stages

S. Kasina, *Student Member, IEEE*, B.F. Hobbs, *Fellow, IEEE*, and P. Donohoo, *Member, IEEE*

Department of Geography and Environmental Engineering, Johns Hopkins University, Baltimore, MD 21218, USA

**Abstract**—Investments in transmission networks have not kept pace with changing load patterns and generation investments. There is an urgent need for models that accurately capture market forces, incentives and planning time-lines while giving planners the maximum flexibility possible. We present a multistage stochastic mixed-integer program that evaluates investments in transmission, assuming that generators make their investment decisions competitively in response to locational marginal prices. Scenarios depict future uncertainty while multiple-decision stages allow grid owners to delay decisions and adapt the network to changing conditions. We analyze how the number of times the operator is allowed to delay or modify investment decisions or exercise options i.e., the number of decision stages affect the timing and location of generation and transmission decisions, and expected system cost. Finer-grained representation of investment timing increases the flexibility and the value of real options for expanding and modifying the grid.

## I. INTRODUCTION

Traditionally, transmission investments followed generation investments. Now, after deregulation, transmission planning is decoupled from generation planning. Transmission planners need to invest in transmission anticipating generator investments [1]. They have to do this such that the resulting set of investments ensure that the electricity grid meets reliability and renewable energy targets at minimum possible cost. We present a multistage stochastic investment and operations model that assumes a central planner plans for transmission investments in the face of future uncertainty (modeled as scenarios), and simultaneously, generators invest in generation competitively over multiple stages (time-periods). We then analyze the improvement in strategies that result from considering additional decision stages in order to more fully capture the flexibility of those strategies.

## II. MODEL OVERVIEW

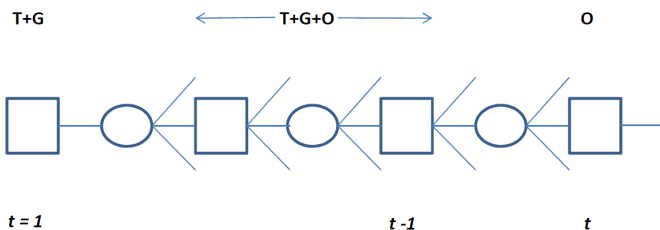


Fig. 1: Multistage Stochastic Planning

The squares in Figure 1 represent decision-nodes and circles represent uncertainty nodes. After each uncertainty node, one of several possible scenarios is realized. In decision nodes, the grid owner decides which transmission lines to invest in. Generators will

simultaneously invest in generation at each stage. In the first stage, only transmission and generation investments are decided ( $T$  and  $G$ ), the last stage consists only of operating the already built lines and plants ( $O$ ), and in stages in between, there is both investment and operation ( $T$ ,  $G$  and  $O$ ).

The model's objective function and most relevant constraints are:

$$\text{Min} \quad \sum_i CX_1^i x_1^i + \sum_l CL_1^l z_1^l + \sum_{t,s} \{p_{t,s} (\sum_i CX_{t,s}^i x_{t,s}^i + \sum_l CL_{t,s}^l z_{t,s}^l + \sum_{i,h} CY_{t,s}^i y_{t,s}^{i,h})\}$$

s.t.

$$y_{t,s}^{i,h} \leq \sum_{\substack{\tau \leq \\ t-L(i,t)}} x_{\tau,s}^i \quad \forall t, s, i, h \quad (1)$$

$$\sum_{\substack{\tau \leq \\ t-L(l,t)}} -F_{\tau,s}^l \leq f_{t,s}^{l,h} \leq \sum_{\substack{\tau \leq \\ t-L(l,t)}} F_{\tau,s}^l \quad \forall t, s, l, h \quad (2)$$

Here,  $CX_{t,s}^i$ ,  $CL_{t,s}^l$ , and  $CY_{t,s}^i$  are vectors of capital costs of investing in generation, transmission, and the cost of operating the generator respectively in scenario  $s$  and stage  $t$ .  $CX_1^i$ ,  $CL_1^l$ , and  $CY_1^i$  are the corresponding investment costs in the first stage (See Figure 1).  $x_{t,s}^i$ ,  $z_{t,s}^l$  are vectors of continuous and binary variables that represent generation investment (in  $MW$ ) and transmission investment respectively.  $y_{t,s}^{i,h}$  is the scalar energy output from generator  $i$  in hour  $h$ . The objective is to minimize the expected cost of investments in generation, transmission, and of operating these plants over all possible scenarios and stages. We assume new capacity takes time to be built and will not come online until a later stage determined by the lag factor,  $L_{i,t}$ . Hence, the constraint (1) states that the maximum energy produced from any generator, in stage  $t$ , cannot exceed the total corresponding capacity that is built upto  $t - L_{i,t}$ . Similarly, a transmission line can only be operated within corresponding limits (2). Additional constraints this model is subject to are the Kirchhoff voltage and current laws, demand, spinning reserves requirement, and scenario-specific assumptions such as renewable targets [2]. Furthermore, constraints specific to a particular scenario are also present.

We use this model to explore the effect of the number of decision-stages on the resulting generation and transmission investments while considering the trade-off this has on the computation time.

## REFERENCES

- [1] A. L. Liu et al, "White paper: Co-optimization of transmission and other supply resources," *Online: <http://communities.nrri.org/documents/68668/ed420212-f582-4dbc-a247-77db11d5692>*, Sep 2013.
- [2] F. Munoz, B. Hobbs, J. Ho, and S. Kasina, "An engineering-economic approach to transmission planning under market and regulatory uncertainties: Case study," *IEEE TPRWS* 29(1) 2013 307-314.

# Economic Assessment of Demand Side Response in the Future GB Electricity System

F Teng, M Aunedi, G Strbac, Imperial College London

**Abstract**— The demand for ancillary service is expected to increase significantly in the future GB system. In particular, the need for frequency regulation services, required to deal with sudden frequency drops following a loss of large generating plant, will increase due to the limited inertia capability of renewable generation. This paper focuses on quantifying the requirements for primary frequency response and the value of Demand Side Response (DSR) in future GB system.

## I. METHODOLOGY

A multi-stage stochastic unit commitment model is developed to optimize the system operation by simultaneously scheduling the energy production, standing/spinning reserves and the inertia dependent dynamic frequency regulation services in the light of uncertainties associated with renewable production and generation outages. The scenario tree is used to replace exogenous ancillary service requirements in deterministic scheduling. The scenarios are weighted according to their probability so that the model can choose how much and what kind of generation capacity to schedule in each scenario, given the cost to provide that capacity and the VOLL. A simplified model of system dynamics is adopted to guarantee the system security by satisfying the National Grid post-fault frequency requirements, namely RoCoF, minimum frequency and steady state frequency. A represented example of primary frequency response requirement is shown in Figure 1. Assumptions on generation and demand background for future GB system have been based on the balanced EMR scenario analyzed by the Department of Energy and Climate Change

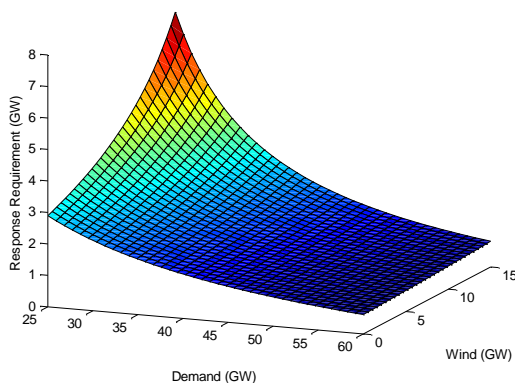


Figure 1 Primary frequency response requirement under different system conditions

## II. RESULTS

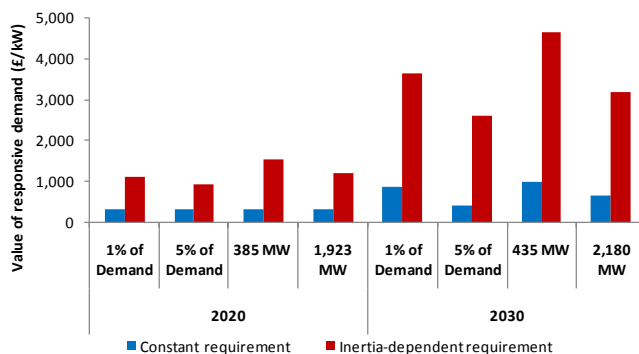


Figure 2 Value of DSR in the future GB system

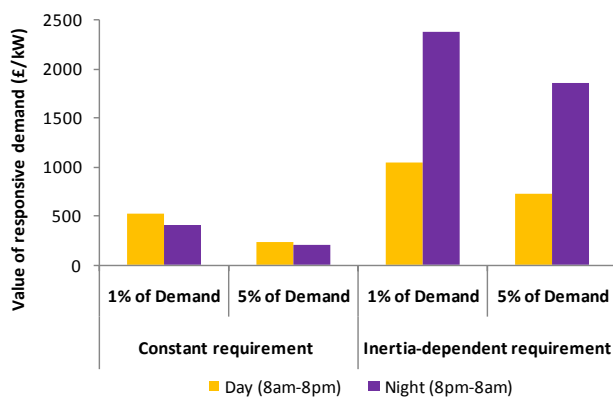


Figure 3 Value of DSR across times of day

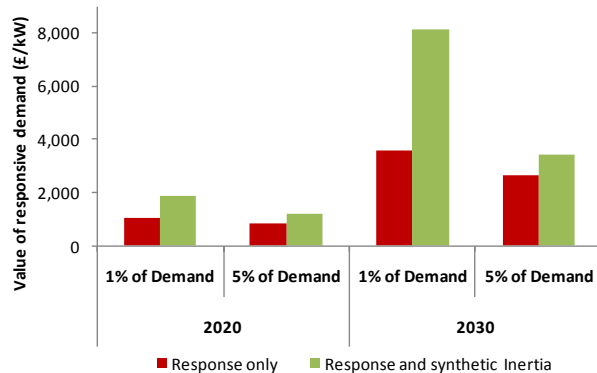


Figure 4 Value of simultaneous provision of frequency response and synthetic inertia by DSR



# Aggregator based Economic Model for Residential Distribution Systems with DR and V2H

Long Zhao *Student Member, IEEE* and Visvakumar Aravinthan *Member IEEE*

Department of Electrical Engineering and Computer Science  
Wichita State University  
Wichita, KS, USA  
lxzhao2@wichita.edu

**Abstract**—Forecasting the residential demand accurately and participating in the market with minimum uncertainty is a biggest challenge for the distribution utilities. Even with the most sophisticated forecasting techniques, still there will be a difference between forecasted load and real time load. Risk decreases if the utility purchases exactly the same amount of energy which customers will consume during that specific time interval. If the real time power consumption exceeds the contracted power they bought from energy market, utility companies will have to buy energy from spot market with extremely fluctuating prices. Additionally, because of increasing penetration of plug-in electric vehicles (EVs) in the auto market, charging of these vehicles need to be considered into future power grids. Many studies have showed that uncontrollable EV charging could cause overloading and speed up the degradation of distribution assets at the distribution level. Demand response (DR) is considered as a load control mechanism and currently it is considered as a most popular peak shaving strategy. However, DR users have to face their comfort and convenience losses more or less during the DR application. Vehicle to Grid power supply (V2G) is an alternative approach to manage the distribution level demand in a smart grid scenario. V2G is developed as a power storage option which could be considered as a part of distribution generators and ancillary service tool, nevertheless, battery degradation and high financial cost significantly affect the V2G's feasibility. A new economic model is developed in this paper, in order to help distribution utilities to reduce the market risks and also to help customers interface with energy wholesale market so that both their benefits could be maximized. In order to effectively control the demand side, aggregator is implemented between utilities and customers. DR and V2H are applied as a load modifying tool to compensate each other's disadvantage under an aggregator.

## I. INTRODUCTION AND KEY EQUATIONS

Oscillation factor ( $OF$ ) is defined as a parameter to describe difference between real time demand and forecasted demand. The objective of this work is to minimize the  $OF$ .

$$\min_{P_i(t)} OF = \left( \frac{\sum_{i=1}^N P_i(t) - DL_A(t)}{DL_A(t)} \right)^2 \quad (1)$$

Where,  $P_i(t)$  is the real time demand of residential household  $i$  at time  $t$ ,  $N$  is the total number of residential households connected with the particular aggregator, and  $DL_A(t)$  is the forecasted demand limit for the aggregator at time  $t$ .

Power demand of each household at a given time  $DL_i(t)$  depends on several factors such as their daily routine, size of

the house, and number of individuals living in the household etc. The household flexibility ratio is given by,

$$R_i(t) = \frac{P_i(t)}{DL_i(t)} \quad (2)$$

A control factor  $CF$  for each household at time  $t$  is defined as their willingness to participate in the demand response scheme. This information would be collected by the aggregator.

## II. KEY FIGURES

Based on the demand response model developed in [1], if  $P_A(t) > DL_A(t)$ , aggregator will find the maximum  $R_i(t)$  and apply V2H and/or DR to reduce their power consumption until the value  $OF$  is acceptable. If  $P_A(t) < DL_A(t)$ , then the aggregator would activate G2V and/or find the maximum  $CF$  and to run appropriate controllable loads at time  $t$  until  $OF$  is acceptable.

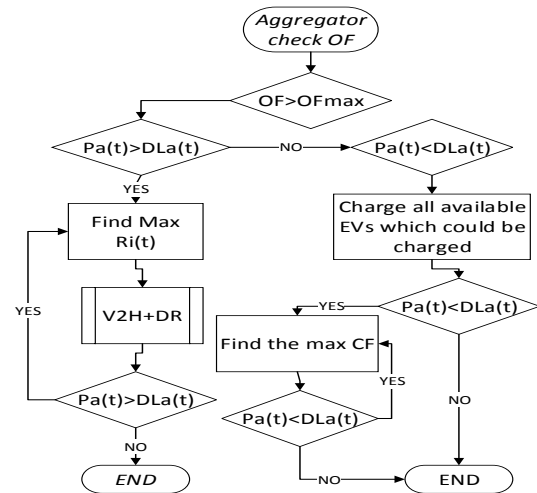


Fig. 1. Flow chart of aggregator process

## III. KEY RESULT

Key results will be presented in the conference.

## REFERENCES

- [1] L. Zhao and V. Aravinthan. "Strategies of residential peak shaving with integration of demand response and V2H," *In Proc. 5th IEEE PES Asia pacific power and energy Conf.* Hong Kong, 2013.

# Comprehensive and Smarter Load Shedding Scheme

Kaium Uz Zaman Mollah , Momen Bahadornejad, Nirmal K.C. Nair

Department of Electrical and Computer Engineering  
University of Auckland, Auckland, New Zealand

E-mail: [kmol006@aucklanduni.ac.nz](mailto:kmol006@aucklanduni.ac.nz), [m.bahadornejad@auckland.ac.nz](mailto:m.bahadornejad@auckland.ac.nz), [n.nair@auckland.ac.nz](mailto:n.nair@auckland.ac.nz)

**Abstract**—Load shedding is the last action that is applied to avoid wide area system collapse when all other possibilities are exhausted. Most of the existing load shedding schemes are well established in transmission/sub-transmission level and are implemented by controlling the feeder load. In recent years traditional networks are shifting towards smart grid framework where devices are equipped with smart technologies and follow the new standards communication protocols. The controlling mechanisms are also shifting from distribution to end users. This paper develops and presents a smart scheme that uses a combination of demand response and load shedding to recover the frequency in an islanded active distribution system. The proposed scheme is illustrated by simulations on a modified 15 bus test network.

## I. KEY EQUATIONS

The control layer calculates the actual amount of load deficit in each islanded distribution system (DS) and it can be obtained as following (if governor action is ignored)

$$P_D = P_L - P_{DG} = \frac{2H_d * S_{GN}}{f_0} \frac{df}{dt} \quad (1)$$

Where,  $P_D$  is the imbalance load for each DS,  $P_L$  is the total load in the island,  $P_{DG}$  is the total distributed generation (DG) in the DS if any,  $H_d$  is the equivalent inertia constant of the DGs,  $S_{GN}$  is the DG rating.

The economic layer calculates the available demand response (DR) load in each DS. If the DS has  $N_d$  DR participant nodes, then the DR load for that DS can be calculated as follows.

$$P_{DR} = \sum_{i=1}^{N_d} P_{DR_i} \quad (2)$$

The DR aggregators have to make pre-agreements with customers and they offer the incentive benefit based on the agreements.

The post disturbance imbalance load that needs to be shed can be obtained as

$$\Delta x = P_D - P_{DR} \quad (3)$$

A supervised ROCOF relay is used to identify the system standalone condition in the system. If  $|df/dt| \leq 2.5$  then the system is considered in standalone mode. The first frequency threshold (49.2 Hz) is set for the DR load and LS scheme thresholds are set to 48.8Hz, 48.6 Hz and 48.2 Hz, respectively with the constant time delay of 20 cycles. The DR

load controller triggers DR loads if the frequency goes down to 49.2 Hz with a time delay of 15 cycles. The three stages LS is designed to balance the load and generation. If the system frequency goes down to 47.5 Hz, then a supervised ROCOF relay is used to trigger the imbalance ( $\Delta x$ ) load.

## II. KEY FIGURES

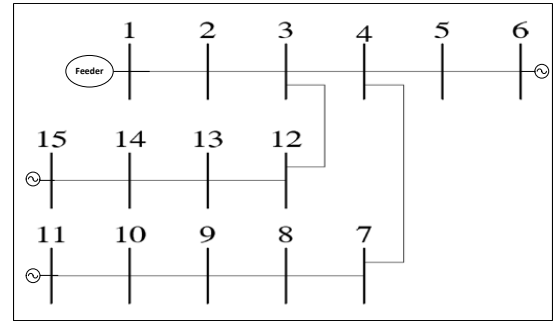


Fig.1. Single line diagram of a modified 15 bus radial system

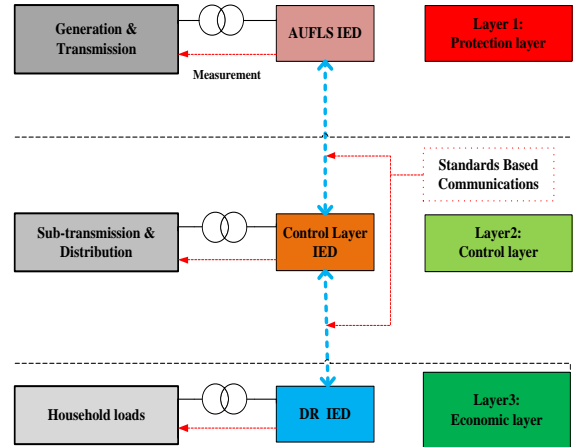


Fig. 2. Proposed scheme architecture

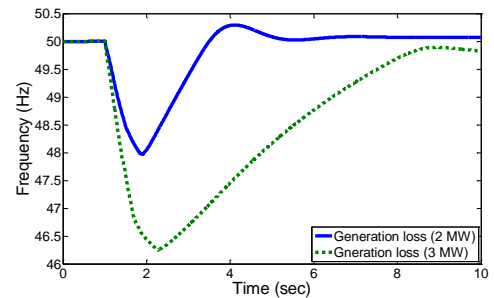


Fig.3. Frequency response of standalone system with generation loss

# A Lyapunov Function Based Remedial Action Screening Tool Using Real-Time Data

Mohammed Benidris, *Student Member, IEEE* and Joydeep Mitra, *Senior Member, IEEE*

**Abstract**—This work introduces a fast transient stability screening tool to classify a designated set of contingencies into stable and unstable subsets using direct methods. The proposed method is based on the conservativeness of the transient stability direct methods. The classification processes of the contingencies are performed along the solution trajectory towards the Controlling Unstable Equilibrium Point, controlling UEP. The proposed screening tool is intended to reliably capture the unstable contingencies and efficiently reduce the number of contingencies that need further analyses. If a numerical problem is encountered during the computation, the proposed scheme applies homotopy-based approaches to find the desired solution. If the numerical problem can not be solved using homotopy-based methods, the contingency is sent to a time-domain simulator for further analysis. The method is applied to the Western System Coordinating Council (WSCC) test system and results are presented.

**Keywords**—*Transient stability, screening, Lyapunov function, homotopy.*

## I. INTRODUCTION

As a result of market forces, increased renewable generation, and recent advances in power flow control technologies, power systems are increasingly being operated closer to their stability limits. On-line transient stability assessment, TSA, has become one of the important features for systems that operate in such stressed environment. Attempts to reach on-line transient stability assessment have been facing high computation burden and low calculation speed. Most of the current strategies drop off the non-severe contingencies using screening tools and perform detailed simulations on the severe contingencies. The most important factors of any screening tool are the absolute capture of the unstable events and the efficiency of capturing the stable events.

The existing on-line transient stability analysis tools based on transient stability direct methods have introduced several system dependent thresholds for classifications. These thresholds are used to classify a set of contingencies to stable, unstable or undecided subsets. The undecided contingencies are the contingencies that have numerical convergence problems such as failure to calculate the controlling unstable equilibrium point, controlling UEP. In order for these thresholds not to fail in classifying the contingencies, off-line transient stability analyses are required. Also, for the unstable or undecided contingencies, detailed time-domain simulations are performed. Therefore, we can see that these methods need off-

line transient stability assessments and may excessively use time-domain simulations.

## II. FOCUS OF THIS WORK

In this work, we propose a fast screening tool to classify a designated set of contingencies into stable and unstable subsets using transient stability direct methods. The proposed method utilizes the advantages of the conservativeness of the direct methods to initially classify the designated set of contingencies into stable, “potentially” unstable and undecided subsets. The potentially unstable subset is further divided into stable, potentially unstable and undecided subsets along the solution trajectory towards the controlling UEP. The undecided subset which has numerical problem is checked again using homotopy-based approaches.

The effective scheme utilized in this work is to check the stability of different points by transient stability direct methods to screen out a large number of stable contingencies, and then apply time-domain simulation to check those potentially unstable contingencies. The excessive use of time-domain simulations is considerably reduced by applying homotopy-based approaches in the case iterative methods fail to find a solution.

Depending on the speed of the computation and the extent of conservatism, this procedure checks stability by sequentially checking energy margin at exit point, minimum gradient point and controlling UEP. If numerical problems, such as convergence issues, are encountered during the computation, the studied contingency is sent to time-domain simulation for stability check. However, before sending the contingency for the time domain simulator, if the numerical problem is related to the calculation of the post-fault stable equilibrium point, SEP, the minimum gradient point or the controlling UEP, we use homotopy-based approaches to find the controlling UEP. On the other hand, if the numerical problem is related to the exit point or the homotopy-based approaches fail to find the desired solution, the contingency is sent to the time-domain simulator for further analysis. The homotopy-based approaches are utilized in this work to increase the efficiency of the screening tool and to reduce the number of contingencies that need further analyses using time-domain simulations. The strategy of using direct method to filter out a large number of contingencies first and conducting further analysis on a much smaller number of contingencies makes the on-line transient stability screening feasible.

---

The authors are with the Department of Electrical and Computer Engineering, Michigan State University, East Lansing, MI, 48823 USA e-mail: (benidris@msu.edu andmitraj@msu.edu).

# A Comparative Study of Optimal PMU Placement Algorithms for Cost Minimization

Anthony S. Deese, Tim Nugent, and Stephen Coppi  
Department of Electrical and Computer Engineering  
The College of New Jersey (TCNJ)  
Ewing, NJ USA  
deesea@tcnj.edu

**Abstract** – Optimal placement of phasor measurement units (PMU's) within a power system is essential to maximize network observability while minimizing implementation cost. As such, it is a popular topic with academic as well as industry researchers. The authors of this work review several innovative optimal PMU placement algorithms published in the IEEE Transactions as well as conference proceedings. From their published results, they compare and contrast the performance of several popular optimal PMU placement algorithms. The authors' objective is to provide power engineers with interest in optimal PMU placement a reference or starting point for further study of this topic.

**Index Terms** – power system analysis, optimization, phasor measurement unit (PMU)

## I. INTRODUCTION

In recent decades, power grids have become increasingly stressed due to lack of proper transmission network expansion. Electricity prices have steadily risen due to changes in fuel supply and demand. As such, it is important that the power engineering community develop new techniques and technologies to improve network efficiency and reliability. One part of this solution is the use of phasor measurement units (PMU) to perform effective, real-time power system monitoring. The measurements they provide facilitate better state estimation and awareness of problematic events like faults.

The first large-scale implementations of real-time power system monitoring emerged in late 1980's, utilizing a device known as the *power* measurement unit. Unlike modern *phasor* measurement units (PMU) that yield both the magnitude and phase of AC waveforms, a basic power measurement unit indicated only whether a bus was electrified or not [1]. The first phasor measurement unit was developed in 1988 by Dr. Arun G. Phadke and Dr. James S. Thorp at Virginia Tech University [3]. A commercial PMU was released by Macrodyne in 1992 [3]. PMU technology continued to develop throughout the 1990's, largely due to advancements in digital control and wireless communication hardware.

The 2003 East Coast Blackout highlighted the need for improved power system reliability and served as a driving force for further development of PMU technology. By 2008, grids throughout the world (including Brazil, China, India, Russia, as well as much of North America and Europe) were embedded with some advanced monitoring technology. And, although PMU penetration is still limited by economic and security concerns, the need for this technology and the role it plays in many "smart grid" initiatives is undeniable. The results of academic as well as industry research promise to motivate greater commercial adoption of PMU's in coming years [11]. One prime example is the Frequency Monitoring Network (FNET) project directed by researchers at Virginia Tech University and University of Tennessee, Knoxville [3]. A low-cost alternative to the PMU is the smart meter (SM). Although it lacks the precision and phase measurement capability that PMU's provide, the SM may be effectively used to supplement PMU measurement data and facilitate better state estimation-based analyses, especially in the short-term.

Optimal placement of both PMU and SM devices is essential to achieve maximum observability with minimal cost. As such, this topic is popular in both academic and industry research. Several recent IEEE publications on optimal PMU placement serve as the basis for this work [6, 7, 8, 10, 12, 13, 14, 15, 16]. In this paper, the authors examine a number of optimal PMU placement algorithms. From previously published results, they attempt to compare and contrast the performance of popular optimal placement algorithms. This work is funded by the National Science Foundation's (NSF) Transforming Undergraduate Education in STEM (TUES) Program. It represents the work of faculty and undergraduate students / research assistants participating in TCNJ's Mentored Undergraduate Summer Experience (MUSE) Program during the summer of 2013.

# Unlocking Energy from Stable Limit Cycles

Aaron Rosenthal, *Student Member, IEEE*, and Dr. Ram Prasad, *Faculty Advisor*  
Klipsch School of Electrical and Computer Engineering, New Mexico State University

**Abstract**—Stable limit cycles exist in several classes of biological systems that harvest and scavenge energy from the ambient and utilize a portion of this energy as work done. In this poster, we demonstrate how electrical circuits may be driven into stable limit cycles using semiconductor devices that exhibit differential negative resistance (DNR) regions in their voltage-current characteristics. By harvesting ambient energy such as light, pressure, and sound, the proposed electrical circuits have the potential to yield energy on the order of nanowatts to kilowatts for prolonged periods of time. The result is a self-sustaining, revolutionary power source that has applications to biotechnology, information technology, and space exploration.

## I. INTRODUCTION

**E**LECTRICAL circuit configurations, such as the Van der Pol oscillator proposed in the 1920s and the FitzHugh-Nagumo model proposed in the 1960s, have long been known to exhibit stable limit cycle behaviors. However, the utilization of limit cycles to realize a self-sustaining energy source has not yet been fully explored. By driving electrical circuits into stable limit cycles, we may provide an uninterrupted means to charge battery and capacitor-based energy storage systems. Such electrical circuits, proposed as a modification to the FitzHugh-Nagumo model, have the potential to overcome operational limitations due to the discharge duration of energy storage devices. This is made possible through the use of semiconductor devices such as tunnel diodes, which exhibit regions of DNR.

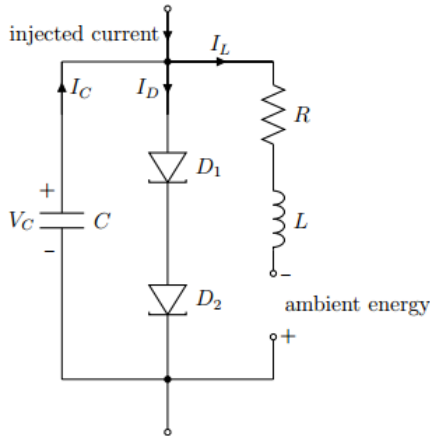


Fig. 1. Modified FitzHugh-Nagumo model

## II. THEORETICAL OPERATION

By biasing tunnel diodes in their DNR regions, we may achieve a bistable mode of operation that emulates the effect

of excitation-relaxation patterns seen in certain biological systems. It is this bistable mode of operation that results in high-speed switching necessary to continuously transfer power between reactive devices. By combining  $n$  tunnel diodes in series, it is possible to obtain  $2^n$  states of bistable operation over a wider voltage range than a single tunnel diode. This allows the circuit to be driven into limit cycles whose size are proportional to the amount of energy inherent in the ambient.

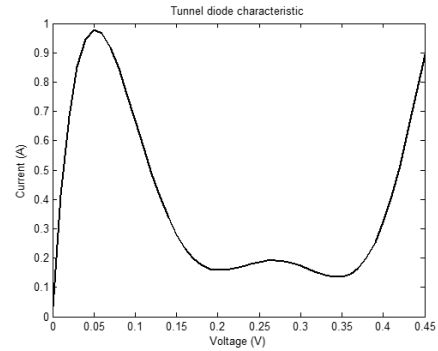


Fig. 2. Tunnel diode voltage-current characteristic

When viewed in the phase space, the resulting effect is an emerging stable limit cycle. Because points on this limit cycle constitute instantaneous voltage and current readings, the maximum energy potential of this limit cycle can be approximated as the area contained within the limit cycle.

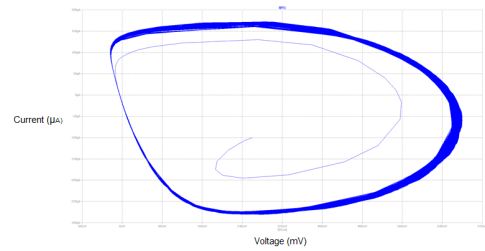


Fig. 3. SPICE simulation of stable limit cycle

## III. CONCLUSION

Stimulating electrical circuits into stable limit cycle behaviors is a key step in developing small-power, sustainable energy sources. Such devices have direct applications to information technology companies such as Amazon and Google, as well as space exploration needs expressed by NASA.



# Secure Distributed Energy Management in the Presence of Misbehaving Generation Units

Wente Zeng, *Student Member, IEEE*, Ziang Zhang, *Member, IEEE* and Mo-Yuen Chow, *Fellow, IEEE*  
 Department of Electrical and Computer Engineering, North Carolina State University, Raleigh, NC, USA  
 Email: [wzeng3@ncsu.edu](mailto:wzeng3@ncsu.edu), [zzhang15@ncsu.edu](mailto:zzhang15@ncsu.edu) and [chow@ncsu.edu](mailto:chow@ncsu.edu)

**Abstract**—A variety of distributed control algorithms are being applied for smart grid energy management because of their flexibility, robustness, and local communication and computation features. These algorithms, however, increase the vulnerability of smart grid to adversaries. Thus, there is an urgent need to protect the distributed energy management algorithms from malicious cyber attacks. A reputation-based secure distributed energy management framework is proposed to guarantee an accurate control computation in distributed energy management algorithms to solve the economic dispatch problem in the presence of misbehaving generation units. The proposed method is capable of performing a secure distributed control without a central coordinator and allows all the well-behaving generation units reach the correct state asymptotically.

## I. KEY EQUATIONS

The Incremental Cost Consensus (ICC) algorithm is used as an example of distributed energy management algorithm. The block diagram of the secure distributed energy management algorithm for each generation unit is shown in Fig. 1. A neighborhood monitor and a local reputation manager have been embedded into the ICC algorithm and achieve attack-resilience in a distributed fashion. The update rule for the distributed energy management block, the neighborhood monitor block and the local reputation manager block are described by equation (1), (2) and (3) respectively.

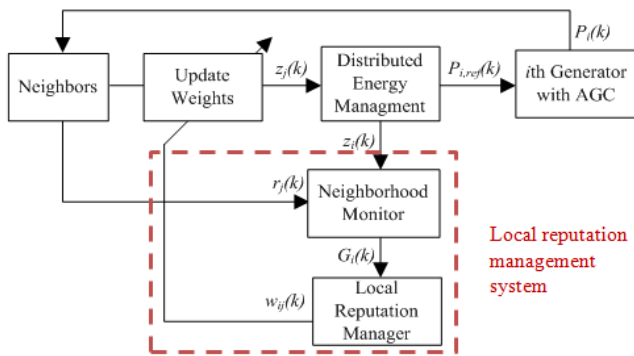


Fig. 1. The secure distributed energy management algorithm for the  $i$ th generation unit

$$z_i[k+1] = \sum_{j=1}^n w_{ij}[k] z_j[k], i = 1, \dots, n. \quad (1)$$

where  $z_i$  is the incremental cost for the  $i$ th generation unit,  $w_{ij}$  is the update weight between the  $i$ th unit and the  $j$ th unit.

$$G_{ij}[k] = \begin{cases} G_{ij}[k-1] + 1, & r_j[k-1] - z_j[k] = 0 \\ G_{ij}[k-1], & r_j[k-1] - z_j[k] \neq 0 \end{cases} \quad (2)$$

where  $r_j$  is the reference incremental cost of the  $j$ th unit,  $G_{ij}$  is the total number of correct states of the neighbor unit  $j$ .

$$\begin{cases} rep_{ij}[k] = \frac{G_{ij}[k] + 1}{k + 2}, \\ w_{ij}[k] = rep_{ij}[k] / \sum_{j=1}^n rep_{ij}[k]. \end{cases} \quad (3)$$

where  $rep_{ij}$  is the reputation value of neighbor unit  $j$  up to time-step  $k$  in unit  $i$ 's local reputation manager.

## II. KEY FIGURES

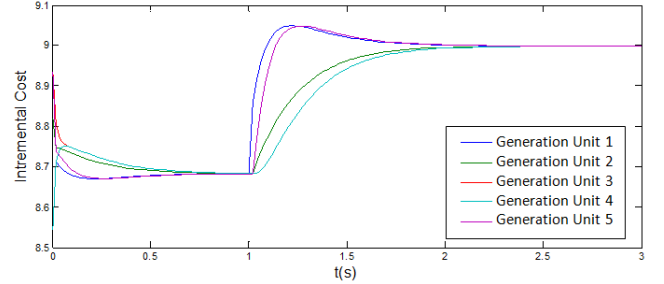


Fig. 2. Using a 5-unit system as an example. The incremental costs of five generation units reach consensus under normal conditions (assume no unit reaches generation limits and behaves abnormally).

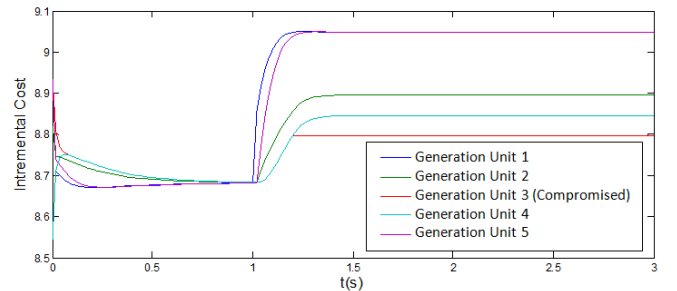


Fig. 3. The consensus network fails when the 3<sup>rd</sup> unit has been compromised, the system operates at a non-optimal condition.

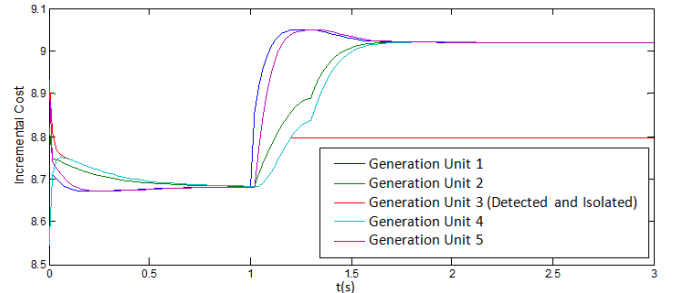


Fig. 4. By isolating the misbehaving unit, the rest of the well-behaving generation units reach the correct consensus state and operate at the optimal point again.



# Grid-Adaptive Equivalencing of Power System for Generator Tripping

Daham Min, *Student Member, IEEE* and Kyeon Hur, *Senior Member, IEEE*  
 School of Electrical and Electronic Engineering, Yonsei University, Seoul, South Korea,  
 Email: gokachu@gmail.com

**Abstract**—This poster presents a practical yet accurate method for equivalencing power system for an online transient stability assessment. The proposed vector composition method effectively aggregates the multi-generation and multi-transmission lines, and then develops grid-adaptive equivalent system for which well-established equal area criterion can be applied to assess the power system stability and finally activate control action, i.e., the generator tripping to stabilize the system as desired. The parameters of the equivalent circuit can be refined using the synchronized measurement data, and the transient stability margin can be recalculated. The efficacy and accuracy have been validated for a multi-machine infinite bus system, and the Korea electric power system.

## I. KEY EQUATIONS

The total power delivered from bus 1 is  $P_{total} = P_{1-2} + P_{1-3}$  and can be represented as an equivalent power angle equation:

$$P_{total} = \frac{V_1 V_2 \sin(\theta_1 - \theta_2)}{x_e || x'_e} + \frac{V_1 V_3 \sin(\theta_1 - \theta_3)}{x''_e} = \frac{V_1 V_4 \sin(\theta_1 - \theta_4)}{x'''_e} \quad (1)$$

The equivalent vector sum can be calculated using vector composition as:

$$\left( \frac{V_1 V_4}{x'''_e} \right)^2 = \left( \frac{V_1 V_2}{x_e || x'_e} \right)^2 + \left( \frac{V_1 V_3}{x''_e} \right)^2 + 2 \frac{V_1 V_2}{x_e || x'_e} \frac{V_1 V_3}{x''_e} \cos(\theta_2 - \theta_3) \quad (2)$$

## II. KEY FIGURES

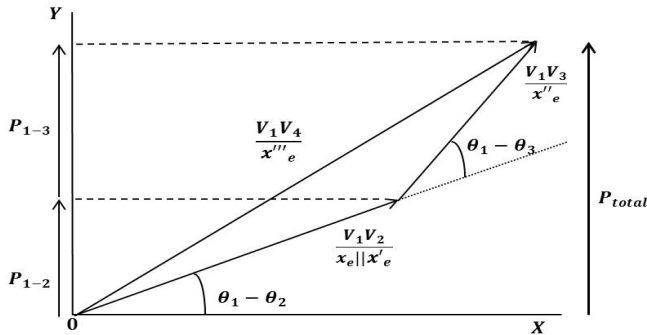


Fig. 1. Vector composition.

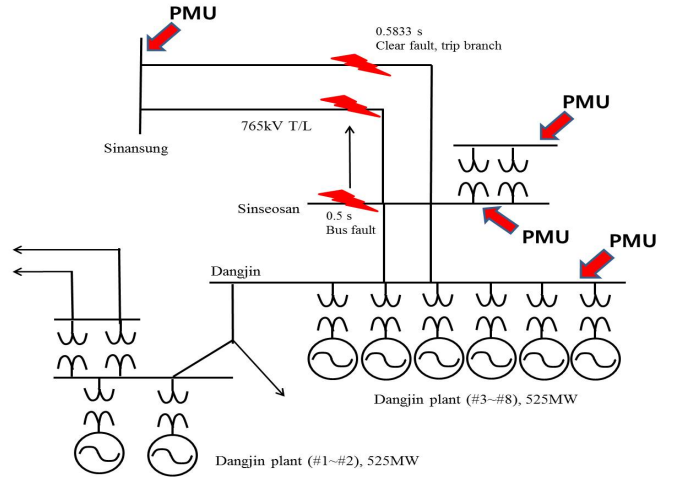


Fig. 2. The Korea electric power system (near Dangjin plant).

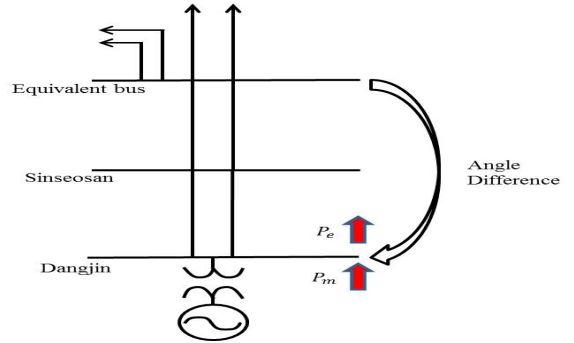


Fig. 3. Equivalent model.

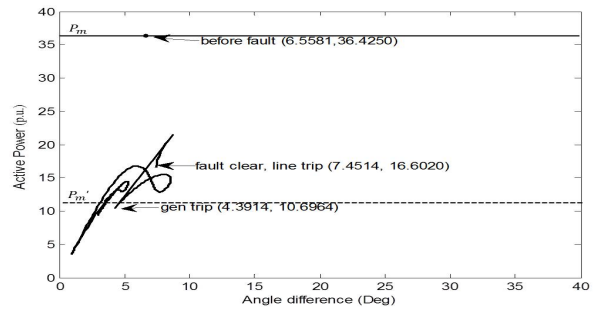


Fig. 4. Power-angle curve of Dangjin plant.

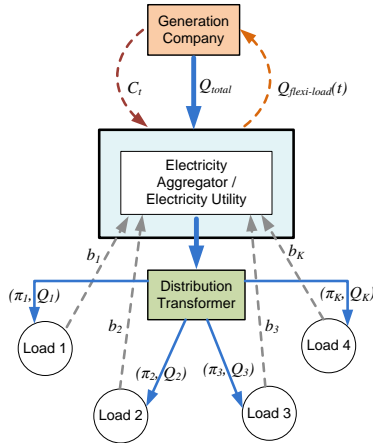
# Scheduling of Flexi-load through Extended Second Price Auctions in Smart Distribution Grids

Saptarshi Bhattacharya<sup>1</sup>, Koushik Kar<sup>1</sup>, Joe H. Chow<sup>1</sup> and Aparna Gupta<sup>2</sup>

<sup>1</sup>Department of Electrical, Computer and Systems Engineering, <sup>2</sup>Lally School of Management and Technology, Rensselaer Polytechnic Institute, Troy, NY - 12180, USA.

**Abstract**—Efficient scheduling of flexi-load in the distribution grid through coordinated control mechanisms has been a crucial area of research over the last few years. Recent advances in communication technologies allow system operators to involve end user feedback as a means of shaping the overall grid load. In this work, we study two mechanisms based on second price auctions - (a) the *Multi-stage Second Price (MSP) auctions*: one-shot auction mechanism where users declare valuation of pre-determined energy levels and (b) the *Progressive Second Price (PSP) auctions*: iterative auction mechanism where users make two dimensional bids to improve their utility. These processes are shown to intelligently cater to the flexi-load by maximizing the value of the energy, by reducing grid congestion, by ensuring the “truthfulness” of the user feedback to a significant degree and by providing end users with competitive prices for electricity usage.

## I. KEY EQUATIONS AND FIGURES



- **Step 1(a)**:  $b_k$  – Bid vector and usage preferences of agent  $k$  reported to aggregator.
- **Step 1(b)**:  $C_t$  - Generator prices floated by generation company.
- **Step 2**: Computation and requesting dispatch of optimal flexi-load  $Q_{flexi-load}(t)$ .
- **Step 3(a)**:  $\pi_k$  - Total cost to be paid by agent  $k$  communicated to agent  $k$ .
- **Step 3(b)**:  $Q_k$  - Dispatched energy allocation vector for agent  $k$ .

Fig. 1. Generalized schematic diagram of the proposed algorithm.

A self explanatory diagram that describes the algorithm of the studied methodologies has been shown in Figure 1. Assuming generation cost functions  $f_t(\cdot)$  which are convex in the net grid load and concave utility functions for individual end users  $\theta_k(\cdot)$ , the system objective (from the aggregator’s viewpoint) can be represented by the following equation, subject to some appropriate constraints.

$$\arg \max \sum_{k \in \mathcal{K}} \theta_k \left( \sum_{t \in T_k} Q_k^t \right) - \sum_{t \in \mathcal{T}} f_t \left( \sum_{k \in \mathcal{K}} Q_k^t \right). \quad (1)$$

Set  $T_k$  enumerates the “time of usage” preferences for any user  $k$ . The allocation rule for the MSP process is enumerated as below,

$$\arg \max \sum_{k \in \mathcal{K}} \bar{\theta}_k \left( \sum_{t \in T_k} Q_k^t \right) - \sum_{t \in \mathcal{T}} f_t \left( \sum_{k \in \mathcal{K}} Q_k^t \right). \quad (2)$$

Here,  $\bar{\theta}_k(\cdot)$  represents the discretized  $n$ -level valuation function for user  $k$ ;  $n$  being specified by the aggregator. For the PSP mechanism, the allocation rule is given as,

$$\arg \max \sum_{k \in \mathcal{K}} p_k \left( \sum_{t \in T_k} Q_k^t \right) - \sum_{t \in \mathcal{T}} f_t \left( \sum_{k \in \mathcal{K}} Q_k^t \right). \quad (3)$$

Here the two dimensional bid of each user is  $(q_k, p_k)$  and allocation rule in equation (3) ensures that  $\sum_{t \in T_k} Q_k^t \leq q_k$ .

The payment rule ( $\pi_k$  being the payment for user  $k$ ) for the two processes can be described by the generic equation as given below,

$$\pi_k = (Oppcost_k) + (Gencost_k), \quad (4)$$

where  $Oppcost_k$  is the opportunity cost of user  $k$  and  $Gencost_k$  is the additional generator cost imposed by user  $k$ .

## II. KEY RESULTS

The salient results as obtained are • The MSP process is approximately efficient; the efficiency increases with increasing bid-complexity. • The PSP process also has an approximately socially efficient  $\epsilon$ -Nash equilibrium (NE) ( $\epsilon$  being the cost of bid). • Both MSP and PSP processes are approximately *incentive compatible*.

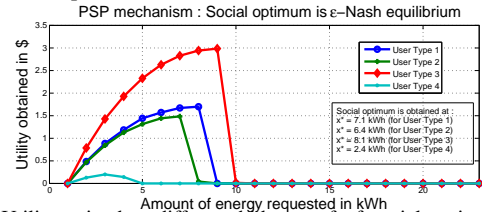


Fig. 2. Utility gained at different bids; proof of social optimum being an  $\epsilon$ -NE.

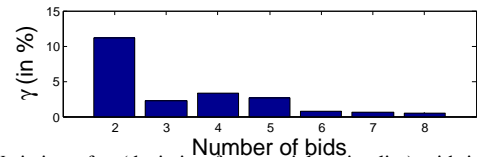


Fig. 3. Variation of  $\gamma$  (deviation from social optimality) with increasing bid complexity.

# Consumption Shifting Methodology and Optimization Approach for Demand Response Programs

Pedro Faria, Zita Vale

GECAD - Knowledge Engineering and Decision Support Research Center  
 IPP - Polytechnic Institute of Porto  
 Porto, Portugal  
[pnfar@isep.ipp.pt](mailto:pnfar@isep.ipp.pt), [zav@isep.ipp.pt](mailto:zav@isep.ipp.pt)

**Abstract**— The introduction of distributed generation and Electric Vehicles (EVs), both connected to distribution networks, bring several huge challenges in the operation and planning tasks. This new paradigm requires improved energy resources management approaches in order to accomplish not only the generation, but also the consumption management through demand response programs, energy storage units, EVs and other players in a liberalized electricity markets environment. The work here presented includes a methodology to be used by Virtual Power Players (VPPs), concerning the consumption shifting in smart grids, minimizing the VPP operation costs. The case study considers a 33-bus distribution network with 218 consumers of 5 types with consumption shifting capability. The obtained results concerns three scenarios taking into account the consumption reduction need due to generation unavailability in 2 distinct periods of the day. The number of periods before or after the shifting origin period is a parameter. The period for which the consumption is shifted is optimally scheduled. Several constraints are considered.

**Index Terms**— Demand response, distributed generation, wind generation, remuneration tariffs.

## I. KEY EQUATIONS

Minimize

$$VPPOC = \sum_{t=to-BT}^{t \leq T+FT} \left[ P_{Supply(t)} \times C_{Supply(t)} + \sum_{i \leq t+FI} \sum_{t-BI \leq i} \sum_{ct=1}^{CtN} \left( P_{DR(t,i,ct)} \times C_{DR(t,i,ct)} + P_{Load}^{NSP}(t,ct) \times C_{Load}^{NSP}(t,ct) \right) \right] \quad (1)$$

$$\sum_{ct=1}^{CtN} \left( P_{Load}^{Base}(t,ct) - P_{Load}^{NSP}(t,ct) + \sum_{t-BI \leq i}^{i \leq t+FI} [P_{DR(i,t,ct)} - P_{DR(t,i,ct)}] \right) = P_{Supply}(t) \quad (2)$$

$$P_{DR(t,i,ct)} \leq P_{Max}^{t \rightarrow i}{}_{DR(t,i,ct)}; \quad \forall t - BI \leq t \leq T + FI \quad (3)$$

## II. KEY FIGURE

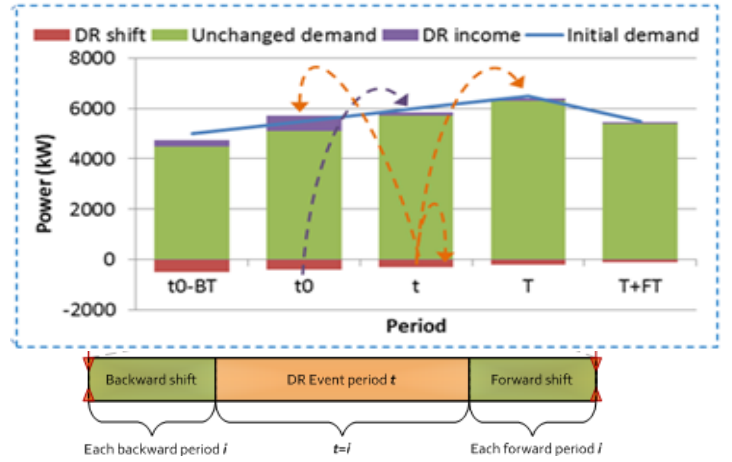


Figure 1. ERM proposed methodology.

## III. KEY RESULTS

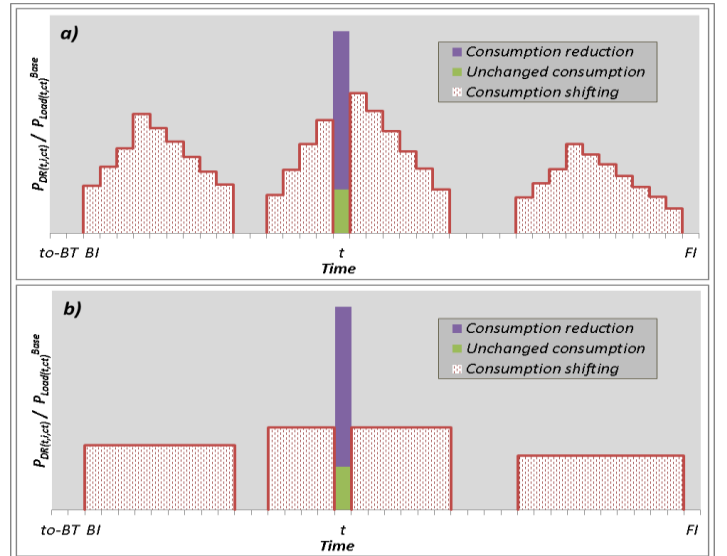


Figure 2. Day-ahead load demand forecast and EVs charge scheduling.

This work is supported by FEDER Funds through COMPETE program and by National Funds through FCT under the projects FCOMP-01-0124-FEDER: PEst-OE/EEI/UI0760/2011, PTDC/SEN-ENR/122174/2010 and SFRH/BD/80183/2011 (P. Faria PhD).

# Appearance of multiple stable load flow solutions under power flow reversal conditions

Hung D. Nguyen  
 School of Mechanical Engineering  
 Massachusetts Institute of Technology  
 Cambridge, MA 02139  
 Email: hunghtd@mit.edu

Konstantin S. Turitsyn  
 School of Mechanical Engineering  
 Massachusetts Institute of Technology  
 Cambridge, MA 02139  
 Email: turitsyn@mit.edu

**Abstract**—In complex power systems, nonlinear load flow equations have multiple solutions. Under typical load conditions only one solution is stable and corresponds to a normal operating point, whereas the second solution is not stable and is never realized in practice. However, in future distribution grids with high penetration of distributed generators more stable solutions may appear because of active or reactive power reversal. The systems can operate at different states, and additional control measures may be required to ensure that it remains at the appropriate point. This paper focuses on the analysis of several cases where multiple solution phenomena is observed. A non-iterative approach for solving load flow equations based on the Gröbner basis is introduced to overcome the convergence and computational efficiency associated with standard iterative approaches. All the solutions of load flow problems with their existence boundaries are analyzed for a simple 3-bus model. Furthermore, the stability of the solutions is analyzed using a derived aggregated load dynamics model, and suggestions for preventive control are proposed and discussed. The failure of naïve voltage stability criteria is demonstrated and new voltage stability criteria is proposed. Some of the new solutions of load flow equations are proved to be stable.

**Index Terms**—Distributed generator, Gröbner basis, load flow problem, solution boundaries, voltage stability.

## I. KEY EQUATIONS

Application of Buchberger’s algorithm transforms the power flow equations in a new “triangular” form:

$$\begin{aligned} \sum_{k=0}^{2^{n-1}} a_k V_n^k I_m &= 0 \\ \sum_{k=0}^{2^{n-1}} b_k V_n^k I_m + A_n V_n Re &= 0 \\ \sum_{k=0}^{2^{n-1}} c_k V_n^k I_m + B_{n-1} V_{n-1} I_m &= 0 \\ \sum_{k=0}^{2^{n-1}} d_k V_n^k I_m + A_{n-1} V_{n-1} Re &= 0 \end{aligned} \quad (1)$$

The proposed universal model for the load dynamics:

$$|\dot{y}| = -f(|V|^2)(p - P^0) \quad (2)$$

$$\mathbf{J} = -\mathbf{U}_y \text{diag}(f(U)) \mathbf{p}_U \quad (3)$$

## II. KEY FIGURES

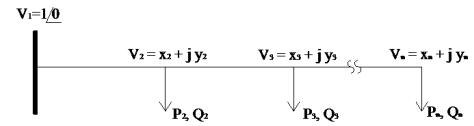


Figure 1: A radial network

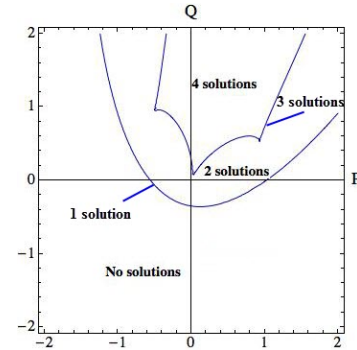


Figure 2: A 3-bus network’s solution boundaries

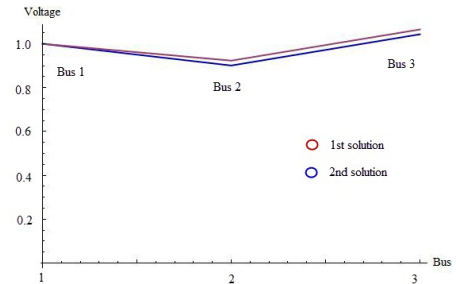


Figure 3: Multiple high voltage solutions

# Impact of Induction Motor Load Dynamics on Droop Controlled Inverter based Microgrid

Puspal Hazra<sup>1</sup>, Ramtin Hadidi<sup>1</sup>, Elham Makram<sup>1</sup>, Sukumar Mishra<sup>2</sup>

<sup>1</sup>Clemson University, Clemson, South Carolina, USA

Email: [phazra@clemson.edu](mailto:phazra@clemson.edu)

<sup>2</sup>Indian Institute of Technology, Delhi, New Delhi, India

**Abstract**— Impact of Induction Motor load dynamics on microgrid stability has been analyzed in this paper. Dynamic model of a droop controlled inverter based distributed generator based medium voltage microgrid has been developed. Supplementary frequency control has been augmented with primary frequency control. Small signal stability analysis shows that there exists lightly damped low frequency oscillatory mode in the presence of induction motor loads. Participation factors of state variables of microgrid dynamic model on the low frequency mode has been calculated. It has been observed from participation factors that electromechanical dynamics of the induction motor causes a low frequency lightly damped oscillation in microgrid. Eigenvalues shows that small signal stability of the microgrid also depends on share of induction motor load in the system.

## I. KEY RESULTS

Droop Coefficients $m_1 = 0.005 pu$ , $m_2 = 0.008 pu$ , $n_1 = 0.01 pu$ , $n_2 = 0.01 pu$			
Modes	Eigen Values	Modes	Eigen Values
1	-738.294	16	-0.288 + j1.167
2	-393.640 + j370.083	17	-0.288 - j1.167
3	-393.640 - j370.083	18	-0.086 + j1.218
4	-519.963	19	-0.086 - j0.999
5	-455.822	20	-1.863
6	-296.775	21	-1.987
7	-278.750	22	-2.001
8	-257.541 + j1.189	23	-2.000
9	-257.541 - j1.189	24	-0.461
10	-88.355 + j1.303	25	-0.195
11	-88.355 - j1.303	26	-0.069
12	-0.118 + j7.763	27	-0.167
13	-0.118 - j7.763	28	-0.167
14	-4.812	29	-0.167
15	-2.935		

## I. KEY FIGURES

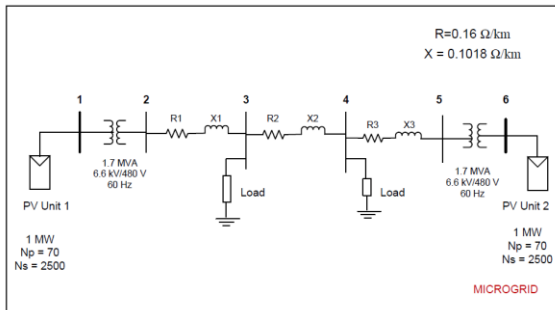


Fig. 1. Microgrid Schematic

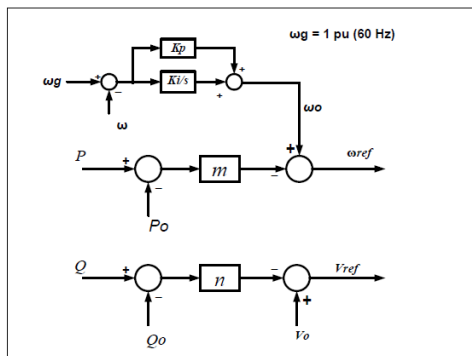


Fig. 2. Droop Control Scheme

## I. KEY FEATURES OF MICROGRID MODEL

A 6.6 kV, 60 Hz microgrid model has been used. Total static load of the microgrid is 1 MW. A 200 HP induction motor has been connected to bus 4 (Fig. 1). Decoupled Voltage and Current controllers have been used for control of DERs. Differential and algebraic equations of microgrid dynamic model has been solved using MATLAB® ODE15s solver.

Fig. 3. Small Signal Stability of the microgrid

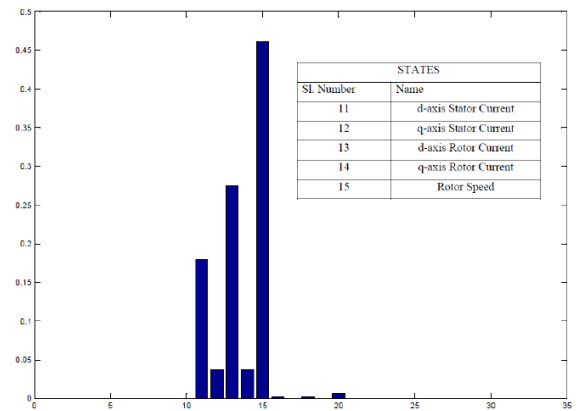


Fig. 4. Participation of Induction Motor states on Mode 12 & 13

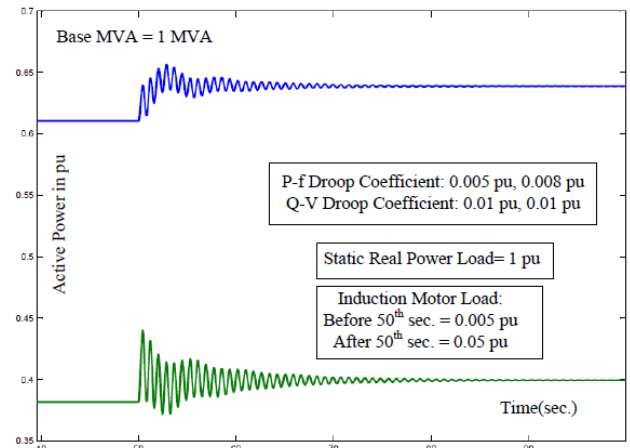


Fig. 5. Active Power Sharing with change in induction motor load

# A Multi-agent Simulation Platform for Incentive-based Demand Response in Smart Distribution Grid

Xinbo Geng

Department of Electrical and Computer Engineering  
Texas A&M University  
College Station, USA  
gengxbtamu@neo.tamu.edu

Le Xie

Department of Electrical and Computer Engineering  
Texas A&M University  
College Station, USA  
lxie@ece.tamu.edu

**Abstract**—Incentive-based demand response (IDR) is designed to induce electricity usage reduction at times of high wholesale market prices or when power system reliability is jeopardized [1]. By eliciting voluntary response from end users, the operation of power systems could be more reliable and the load serving entities (LSEs) could reduce their loss at times of high prices. However, it is challenging to model and analyze the outcome of human behavior in uncertain environment. The LSE cannot know how each end user will respond and it is impossible for the LSE to use a centralized method to solve the problem. Multi-agent system (MAS) theory, which decomposes a complicated system into several autonomous simple systems (agents), is an ideal candidate for building the simulation platform to assess the impact of IDR programs. Considering the huge expenditure and difficulty of large-scale experiments in the real life, we can model the most significant factors and do large-scale simulation using the platform. In this poster, we first propose a general structure for IDR programs based on MAS theory, and then utilize the general structure to implement a simulation platform for a novel type of demand response – coupon-incentive demand response (CIDR). An example is provided to illustrate the effectiveness of the simulation platform. With given end user behavior model, we could compare different demand response programs using this platform.

**Index Terms**—multi-agent system, incentive-based demand response, customer behavior

## I. PROBLEM FORMULATION

In contrast with most price-based demand response mechanisms, coupon incentive-based demand response (CIDR) offers a voluntary award-based mechanism to extract end-users' flexibility whenever needed [2]. Built upon the theoretical and empirical work that this team has been doing on CIDR, this poster proposes a multi-agent simulation platform for critical assessment in CIDR in smart distribution grids. We model two major participants, namely the LSE and end users, as two categories of intelligent agent. The LSE agent tries to avoid loss by delivering price signals (coupons, in the CIDR case) when there will be price spikes in the real-time market. Each end user agent controls several appliances and makes decisions using different strategies. This approach

builds models close to reality and provides flexibility and extensibility to examine different user models and IDR schemes.

## II. KEY FIGURES

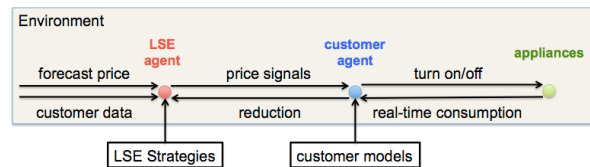


Figure 1. General Structure of the Simulation Platform

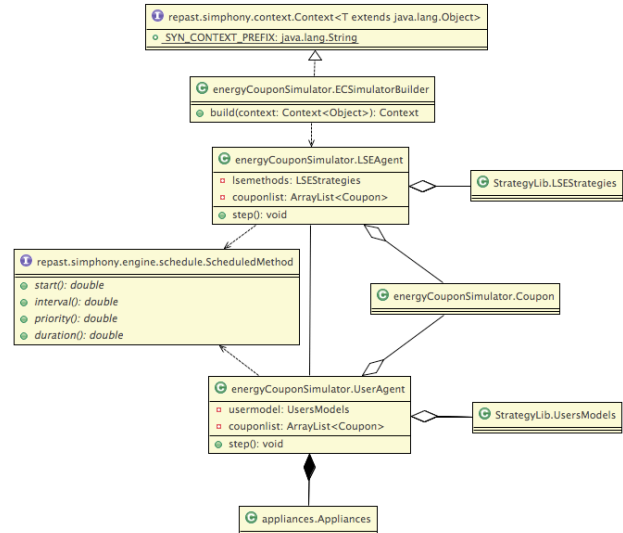


Figure 2. UML Diagram of the CIDR Simulation Platform.

## REFERENCES

- [1] M.Albad and E.El-Saadany, "A Summary of Demand Response in Electricity Markets," *Electric Power Systems Research*, vol. 78, pp. 1989-1996, Nov. 2008.
- [2] H.Zhong, L.Xie, and Q.Xia, "Coupon Incentive-Based Demand Response: Theory and Case Study," *IEEE Trans. Power Systems*, vol. 28, pp. 1266-1276, May. 2013.



# A Two-Stage Hybrid State Estimator for Dynamic Monitoring of Power Systems

Markos Asprou and Elias Kyriakides

Department of Electrical and Computer Engineering  
KIOS Research Center for Intelligent Systems and Networks  
University of Cyprus  
Nicosia, Cyprus  
asprou.markos@ucy.ac.cy, elias@ucy.ac.cy

Saikat Chakrabarti

Department of Electrical Engineering  
Indian Institute of Technology Kanpur  
Kanpur, India  
saikatc@iitk.ac.in

**Abstract**— When a fault is not detected and suppressed timely, it can affect the operating condition of the power system. Although fault recorders can track the transients in the power system states (i.e., bus voltage magnitude and angle) during a fault, they cannot provide a wide area picture of the power system operating condition. The provision to track the transients is of great interest for the power system operators. In this work, a two-stage state estimator based on both conventional and PMU measurements is presented. The estimator is able to track the dynamics of the power system states during a fault. The advantage of the proposed state estimator is that it does not require full power system observability by the PMU measurements. The two-stage state estimator was successfully tested on the IEEE 14 and 118 bus systems.

**Index Terms**-- Fault, phasor measurement unit, real time monitoring, state estimator.

## I. INTRODUCTION

Modern power systems are being operated under heavily stressed conditions due to the ever-increasing demand for electricity, environmental constraints, and competitive energy markets. The large scale integration of renewable energy sources that inherently have high uncertainty in the energy production is making the secure and reliable operation of power systems even more challenging. Real time monitoring of power systems has therefore become very important. The timely detection of contingencies has also become important in order to allow the undertaking of remedial actions to avoid any potentially dangerous situation. In this sense, a state estimator that could provide the power system states in sub-second time intervals would be a very useful tool for monitoring the power system in near real time, and take necessary remedial actions quickly. Although the contemporary state estimator provides the steady state operating condition of the power systems, the use of PMU measurements in the state estimator facilitates the execution of the state estimator in quasi real time. In this work, a two-stage state estimator that provides the power system states in high rate is developed enabling the dynamic monitoring of the power system condition.

## II. TWO-STAGE STATE ESTIMATOR

The two-stage state estimator is based on the fast reporting rate of the PMU measurements in order to track the transients of the power system states in case of faults. The proposed state estimator does not require complete observability of the system by PMUs. The use of the two-stage SE in a partially observable power system by PMUs in the case of a fault is based on the creation of pseudomeasurements for the unobservable buses. A hybrid state estimator is executed as the conventional measurements are updated, while a linear state estimator is executed as the PMU measurements are updated. The pseudomeasurements are created for rendering the power system observable when the linear state estimator is executed. In the proposed state estimator, the current phasors of the previous time instant are used as pseudomeasurements. The sequence of operation of the two-stage state estimator is illustrated in Fig. 1.

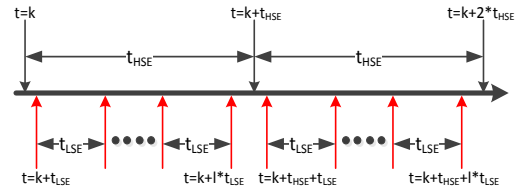


Fig. 1. Time diagram of the two-stage state estimator

The performance of the two stage state estimator in the case of fault is examined using the IEEE 14 and 118 bus systems. The average voltage magnitude and angle estimation errors for the PMU unobservable buses of the IEEE 14 bus system are shown in Table I.

TABLE I  
AVERAGE VOLTAGE MAGNITUDE AND ANGLE ESTIMATION ERROR

Bus number	Average voltage magnitude error (p.u.)	Average voltage angle error (degrees)
10	$2.4 \times 10^{-3}$	0.31
11	$2.8 \times 10^{-3}$	0.35
12	$2.7 \times 10^{-3}$	0.40
13	$2.8 \times 10^{-3}$	0.42
14	$6 \times 10^{-3}$	0.49



# Addressing illiquidity for intra-day and real-time markets for short-term hydropower planning

## Abstract:

To develop a stochastic planning model for price-taker hydropower producer in sequential markets is a challenging, meanwhile an important task. The model is a stochastic Quadratic Program (QP), which considers not only expected profit but also profit variance. To consider the market prices continuously clearing nature rolling planning is applied, which allows re-forecasting and re-dispatching according to the arrival of new information. The simulated results have shown that intra-day and real-time markets are illiquid. However addressing the issue deeper we have found a link between wind power diurnal variation and level of liquidity in intra-day and real-time markets.

## Objective:

To develop multi-stage stochastic QP bidding strategy for three sequential markets for a profit maximizer hydropower producer.

## Key figure:

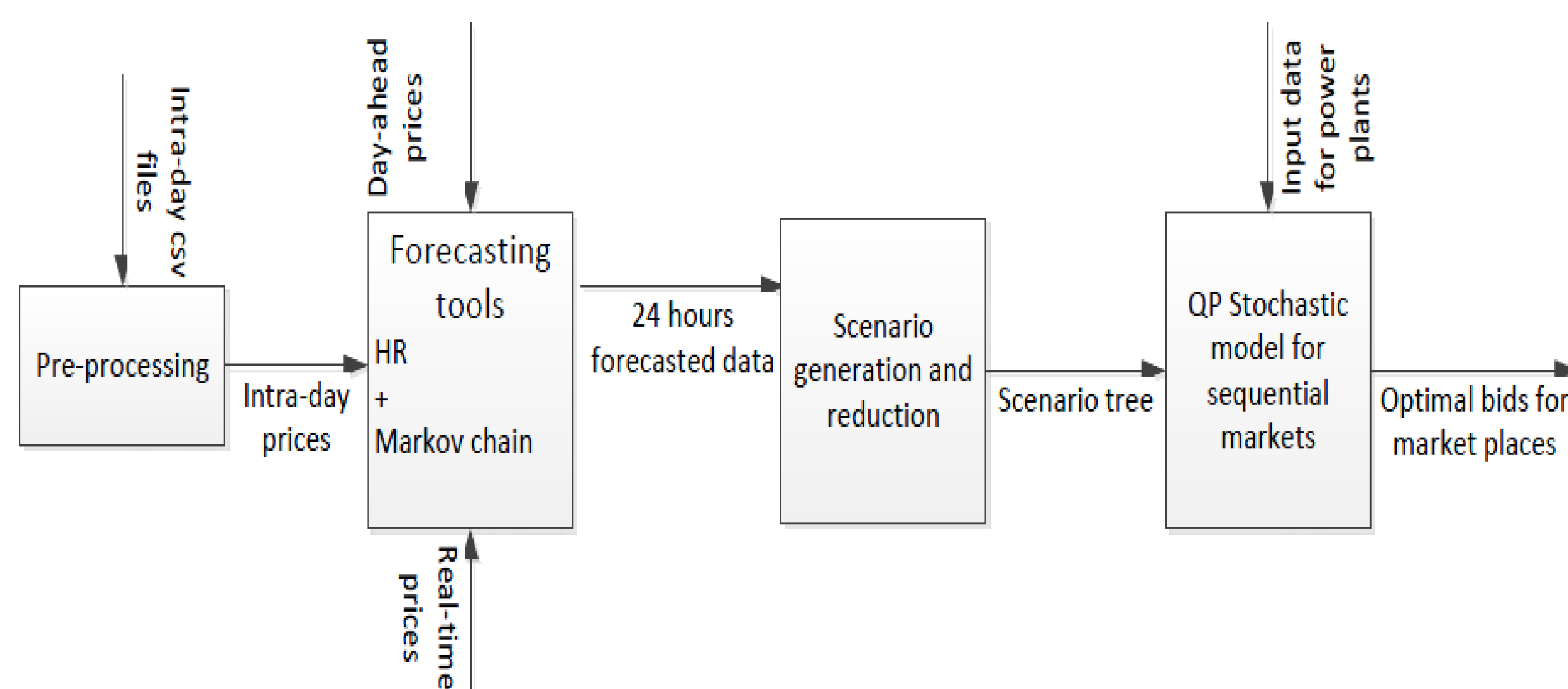


Figure 1: Summary of the work

## Key equations: QP formulation

$$\text{Min} \quad \bar{c}^T x + \gamma x^T \Sigma x$$

$$\text{S.t.} \quad Gx \leq h$$

$$Ax = b$$

where  $\bar{c}^T x = Ec^T x$

$$x^T \Sigma x = E(c^T x - Ec^T x)^2 = \text{Var}(c^T x)$$

$\gamma \geq 0$ , called **risk-aversion** parameter

## Case study:

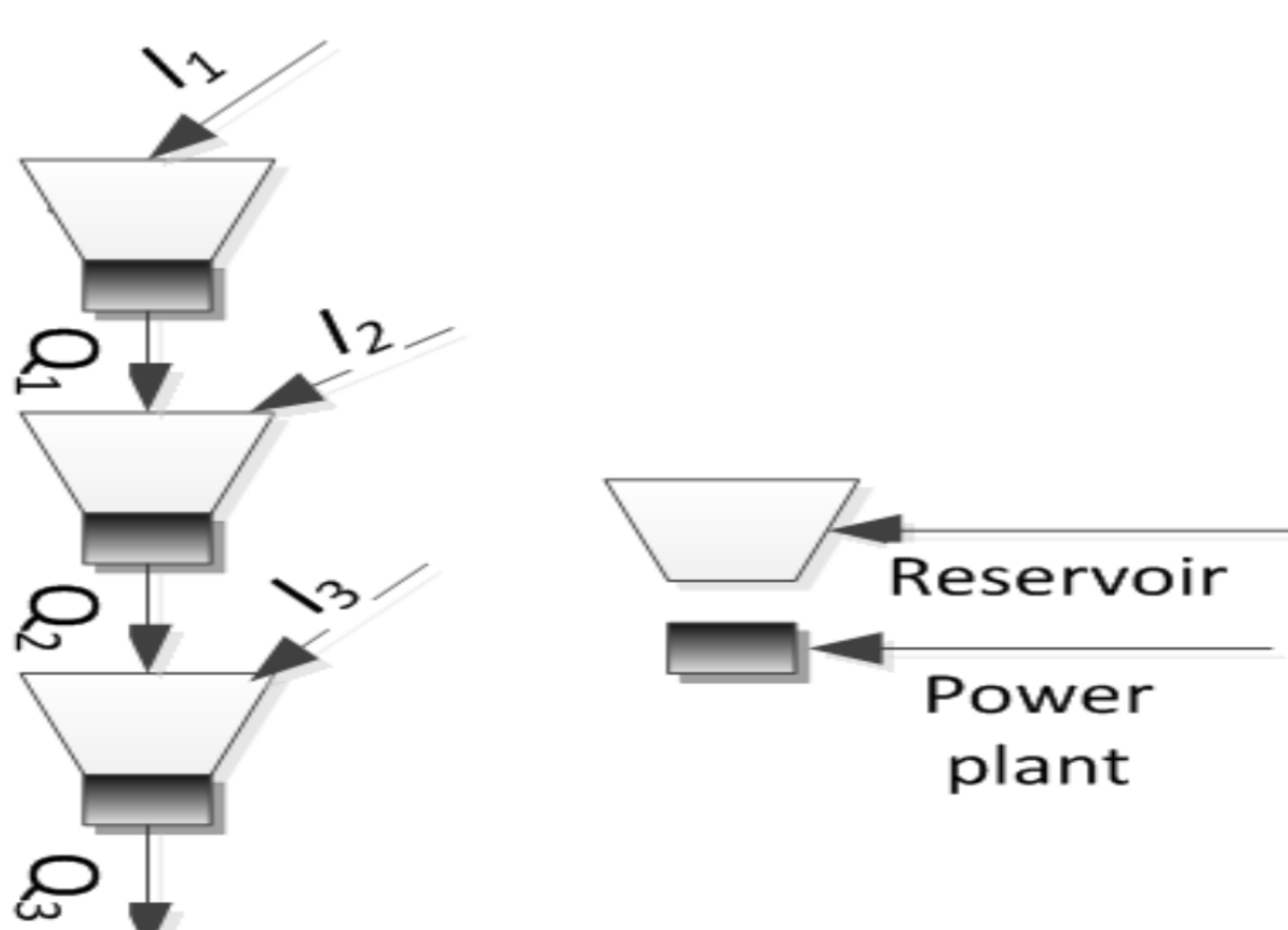


Figure 2: The hydropower system used to test the model

## Key results:

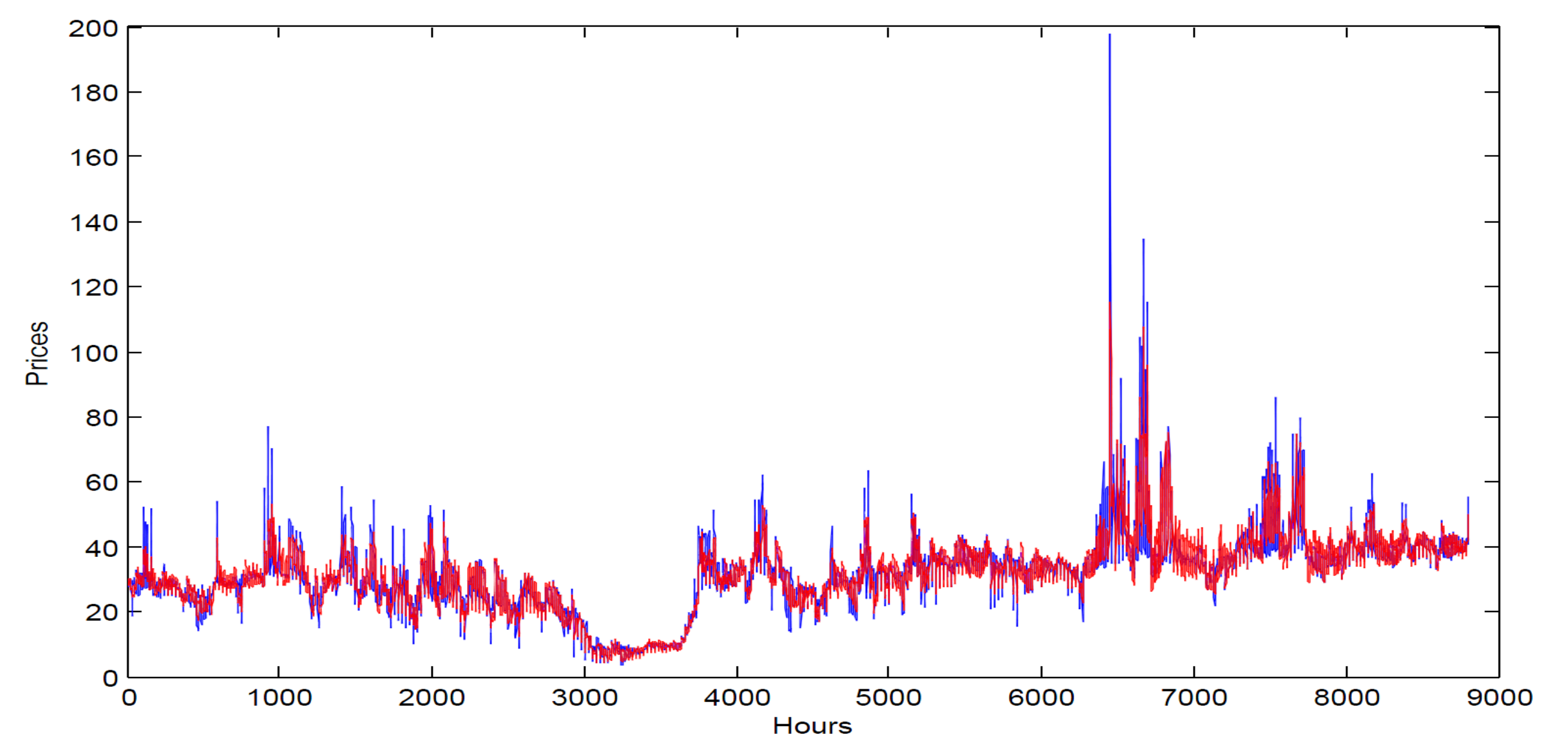


Figure 3: Simulated fit for day-ahead market prices using HW method; blue-real data and red-simulated data

Table 1: Expected profit through all iterations

	It. I	It. II	It. III	It. IV
Total Expected value	206930	206690	206520	206520
Expected day-ahead profit	29148	29185	29300	29300
Expected intra-day profit	3953	5805	5054	5054
Expected real-time profit	582	436	561	561
Profit variance	841	1146	1138	1138

Table 2: Electricity trading in day-ahead, intra-day and real-time markets for six different days

	Jan.11	Mar.11	May11	Aug.11	Oct.11	Dec.11
Expected profit	233770	206523	178073	145929	212138	210905
Day-ahead trading	79824	29300	15545	7015	78481	64085
Intra-day trad. (sell.)	358	5486	1654	1978	2680	3368
Intra-day trad. (buy.)	256	404	79	42	3010	0
Real-time trad. (up)	2597	2190	1874	1375	1738	1731
Real-time trad. (down)	1348	1463	41	268	1842	1934
Total trading	84383	38843	19193	10678	77751	71118
Day-ahead trad.(%)	94	75	81	65	88	90
Adjustment trad.(%)	6	25	19	35	12	10

## Conclusion

According to the results, trading on intra-day and real-time markets are much less compared that of on day-ahead market. However, the results has shown that the need for adjustment market increases when wind power diurnal variation increases. Hence, the continuous increase in wind power share in the power system brings continuous increase in trading on intra-day and real-time markets. To sum up, it is significantly important to model intra-day and real-time markets for short-term hydro power production, since wind power share together with diurnal variation will increase continuously corresponding to the wind power targets in 2020, 2030 and 2050.



# A Voltage Sag Severity Index Considering the Power System and Consumer Equipment

X. Zhou, *Student Member, IEEE* and F. H. Wang, *Member, IEEE*

Department of Electrical Engineering, Shanghai Jiaotong University, Shanghai, China

Email:zhouxianghello@yeah.net and fhwang7723@sjtu.edu.cn

**Abstract**—Voltage sag indices are essential for the evaluation of voltage sag effects on the power system and electric utilities, and for the improvement of power quality. In the paper, a comprehensive index is presented to describe the voltage sag severity considering the supply and consumer side simultaneously. First, the IEC 61000-2-8 table is applied to derive the statistical index of power system with the improved analytic hierarchy process. Then the utility outage probability is obtained based on a modified equipment outage model. Finally, the comprehensive index is extracted from the preceding two indices via the vector normalization method. The voltage sags are analyzed based on the power quality monitoring system installed in some city in China. Calculated results have shown that the proposed index could represent the voltage sag severity of given monitoring sites more explicitly, which is beneficial for the improvement of power quality and supply reliability.

**Index Terms**-- analytic hierarchy process, comprehensive index, vector normalization, voltage sag, utility outage probability.

## I. KEY EQUATIONS

$Q_1$  and  $Q_2$  of power system and consumer equipment can be obtained respectively based on AHP method and utility outage estimation proposed in [1][2] as :

$$b_{ij} = \begin{cases} \frac{r_i - r_j}{R} \times \left( \frac{r_{\max}}{r_{\min}} - 1 \right) + 1 & .r_i \geq r_j \\ \left( \frac{r_i - r_j}{R} \times \left( \frac{r_{\max}}{r_{\min}} - 1 \right) + 1 \right)^{-1} & .r_i \leq r_j \end{cases} \quad (1)$$

$$\bar{W} = \frac{1}{n} \sum_{j=1}^n \frac{10^{\frac{1}{n} \sum_{k=1}^n (c_{jk} - c_{jk})}}{10^{\frac{1}{n} \sum_{k=1}^n (c_{jk} - c_{jk})}} \quad (2)$$

$$Q_1 = \sum (i \times \bar{w}_j) \quad (3)$$

$$P_k = \sum_{i=1}^{N_E} P_{ki} \quad (4)$$

$$Q_2 = \sum_k P_k \times \alpha_k \quad (5)$$

The comprehensive index  $Q$  can be calculated as:

$$Q = \sqrt{2} \times \sqrt{(Q_1^*)^2 + (Q_2^*)^2} \quad (6)$$

## II. KEY RESULTS

The proposed method is applied to analyze practical data from 110 kV substations. The voltage sag complaint record is set as the objective criterion of severity in comparison with the proposed index and other single index of supply or consumer side. The result shows the proposed comprehensive index is related more closely to the objective voltage sag severity.

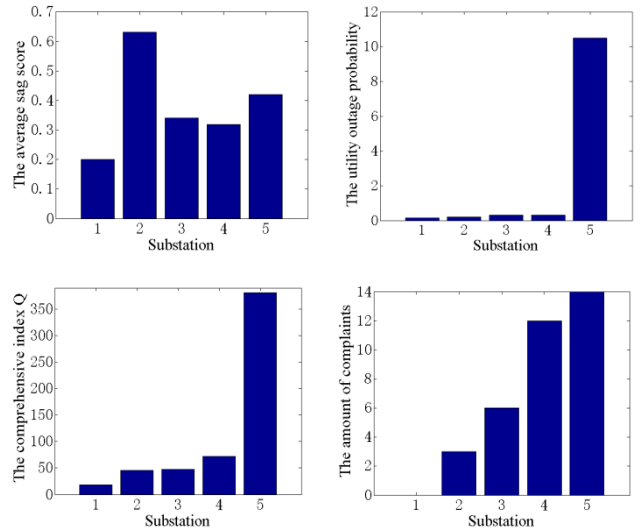


Figure 1. Voltage sag indices and the amount of complaints

## REFERENCES

- [1] Albano, A. M., Muench, J., Schwartz, C., Mees, A. I., & Rapp, P. E. "Singular-value decomposition and the Grassberger-Procaccia algorithm." *Physical Review A* 38.6 (1988): 3017.
- [2] Rosenstein, Michael T., James J. Collins, and Carlo J. De Luca. "A practical method for calculating largest Lyapunov exponents from small data sets." *Physica D: Nonlinear Phenomena* 65.1 (1993): 117-134.

# Experimental Research of Vibration Characteristics of Shunt Reactor

S. Chen, F. H. Wang  
 Department of Electrical Engineering  
 Shanghai Jiaotong University  
 Shanghai, China  
[csongsk@126.com](mailto:csongsk@126.com)

L. Su  
 Condition Evaluation Center  
 Shanghai Electric Power Research Institute  
 Shanghai, China  
[dsy\\_sul@ec.sgcc.com.cn](mailto:dsy_sul@ec.sgcc.com.cn)

**Abstract**—The widely developed and used HVDC transmission systems will cause DC bias phenomenon occurred in some electromagnetic facilities of power grids with the results of several negative effects on the secure and reliable operation, including vibrations and noises. However, there has been few studies regarding the influence DC bias has on shunt reactors. To fully explore the vibration characteristic of a shunt reactor and then reduce its vibration, this paper discusses the experimental results of a shunt reactor under different voltages, currents and additional DC currents. Through the experiment and following analysis, we found that the vibration intensity rises with the increase of voltage, current and additional DC current and the frequency spectrum of vibration changes as well. Then a characteristic quantity of the vibration frequency is introduced to reflect the working condition of a shunt reactor. This experimental analysis is helpful for developing on-line monitoring system for shunt reactors.

## I. KEY EQUATIONS

When a shunt reactor is running in a power grid, magnetostriction and magnetic force act on the iron, the differential equation of a vibration system is represented as follow:

$$[M]\{\ddot{X}\} + [K]\{X\} = \{F\} \quad (1)$$

where  $\{F\} = [P\cos(4\pi ft + \varphi), 0, \dots, 0]^T$ ,  $f$  is the current frequency of 50Hz,  $P$  is the amplitude of the force. The particular solution of this equation is represented as follow:

$$\{X\} = [X_1 \cos(4\pi ft + \varphi_1), X_2 \cos(4\pi ft + \varphi_2), \dots, X_N \cos(4\pi ft + \varphi_N)]^T \quad (2)$$

This particular solution indicates that when a reactor is under the influence of magnetostriction and magnetic force, the vibration frequency of any point in the reactor is identical to the frequency of magnetostriction and magnetic force, which is 100Hz in this case.

## II. KEY RESULTS

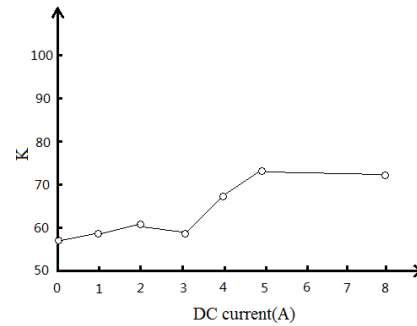


Fig.1 Relationship between K and DC current

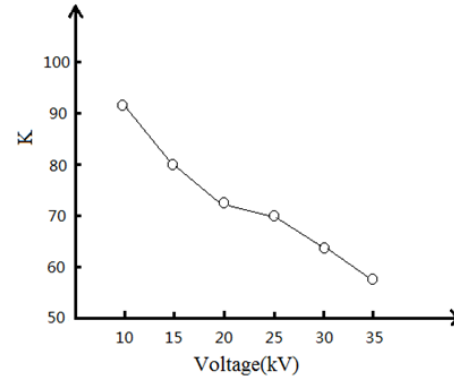


Fig.2 Relationship between K and voltage

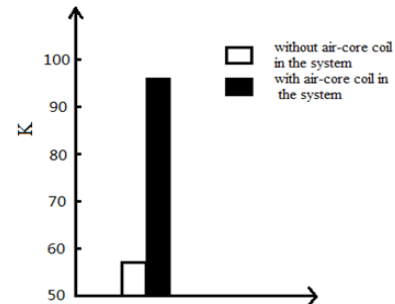


Fig.3 Relationship between K and current

# Analysis of Time-varying Harmonics of Wind Power Plants using Wavelet Transform

Choongman Lee, *Student Member, IEEE* and Kyeon Hur, *Senior Member, IEEE*,  
 School of Electrical and Electronic Engineering, Yonsei University, Seoul, Korea  
 Email: [your2cm@yonsei.ac.kr](mailto:your2cm@yonsei.ac.kr), [khur@yonsei.ac.kr](mailto:khur@yonsei.ac.kr)

**Abstract**—Compared with traditional power plants, wind power plants (WPP) have some concerns about power quality (PQ) because of their characteristics derived from variable wind speeds. In order to integration of wind power plant with power grids, fast switching elements, like converters, are necessary to provide stable power and voltage since wind power plants have variability on the their own generation source. However, harmonic problems may take place on the voltages and currents because of not only variable wind speeds, but converters and other elements of grid. In addition, these harmonics can be changed depending on conditions of grid. To detect these problems, time-frequency analysis is conducted in this research. This study focuses on monitoring PQ with Wavelet Transform that enables time-frequency domain analysis. From the simulation results, time-varying frequency characteristic of system is shown and harmonic problems can be detected.

**Index Terms**—Wind Power Plants (WPP), Wavelet Transform, PQ, Harmonics.

## I. KEY FIGURES

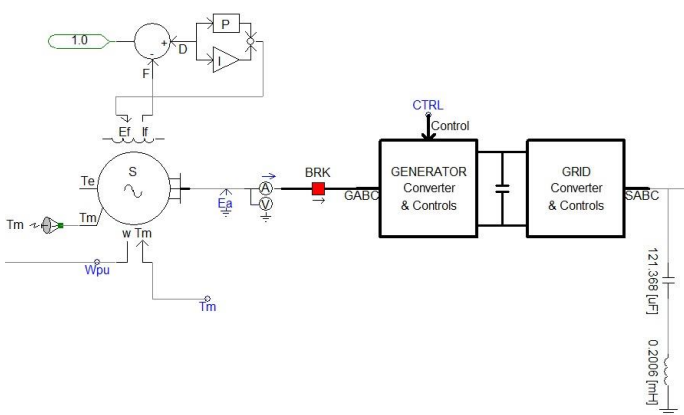


Fig. 1. Schematic of wind power plant system

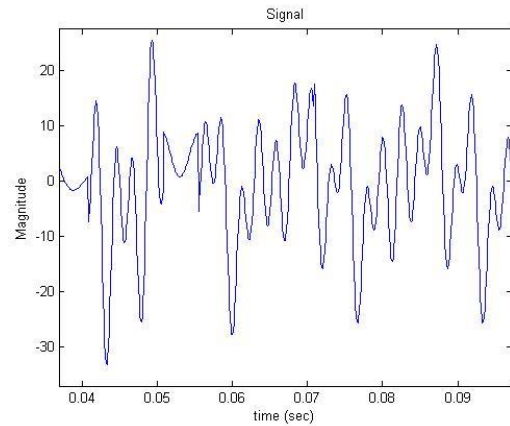


Fig. 2. Voltage data sample for simulation

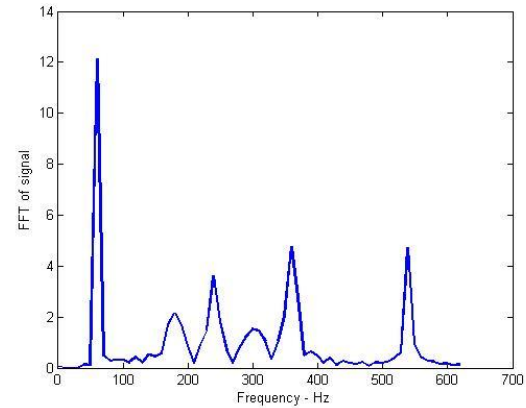


Fig. 3. Frequency response of voltage data sample

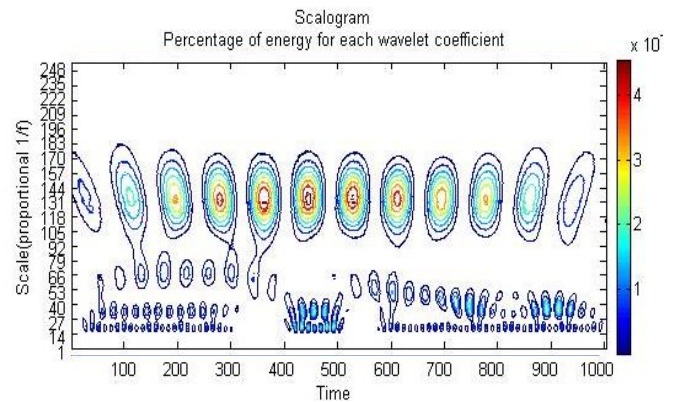


Fig. 4. Time-frequency response of voltage data sample using Wavelet Transform.

# Control of DC voltage in Multi-Terminal VSC-HVDC System using H-infinity method

Mohammad Nazari and Mehrdad Ghandhari  
 Electric Power Systems, School of Electrical Engineering  
 KTH Royal Institute of Technology  
 Stockholm, Sweden  
 Email: nazarim@kth.se, mehrdad@kth.se

**Abstract**—Multi-terminal High-Voltage Direct-Current transmission system (MTDC) is finding its way to the power system. Voltage Source Converters may be an attractive solution for building VSC-based MTDC systems. Controlling the DC voltage in these systems, which have very fast dynamic, is one of the important challenges. In the power system literature, different DC voltage control methods have been proposed. Among them, Voltage Margin Method and Voltage Droop Method are the most well-known methods. In voltage droop method each controller uses a proportional controller to control the its DC voltage. In this study, an H-infinity controller, based on Linear Matrix Inequality, is proposed, which uses a proportional controller like voltage doop method and controls the MTDC system such that the deviations of DC voltages from their initial values will be minimized, and limits the injected power of each terminal. Meanwhile, the injected currents of converters are weighted according to the difference between their injected power and their maximum allowed injected current. Also the currents of DC cables are limited in the acceptable range. The simulations are done in MATLAB/Simulink.

## I. KEY EQUATIONS AND FIGURES OF THE SYSTEM

Fig.1 shows a 4-terminal MTDC system, which connects 4 different AC systems together.

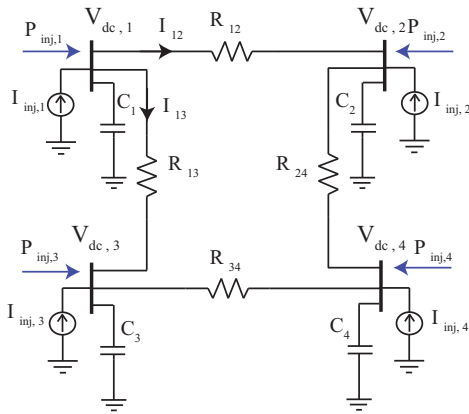


Fig. 1. A 4-terminal HVDC grid. Converters are modeled as current sources and the DC cables are modeled with resistances.

The dynamic of the system is given by:

$$C_{dc,i} \frac{dV_{dc,i}}{dt} = I_{inj,i} - \sum_{j \in N_i} \frac{V_{dc,i} - V_{dc,j}}{R_{ij}}, \quad (1)$$

where  $V_{dc,i}$  and  $P_{inj,i}$  are the DC voltage and injected active power of terminal  $i$ , respectively and  $N_i$  is the set of terminals which are connected to terminal  $i$ .

## II. THE CONTROL STRATEGY

The H-infinity controller uses LMI and controls the system such that

$$\begin{aligned} & \text{Minimize } |V_{dc,i}^{ref} - V_{dc,i}|, \quad i \in N_p \\ & \text{subject to } \begin{cases} I_{inj,i}^{max} < I_{inj,i} < I_{inj,i}^{max} \\ |I_{ij}| < I_{ij}^{max} \\ I_{inj,i} \propto H.R.I_i \end{cases}, \end{aligned} \quad (2)$$

$$H.R.I_i = \frac{H.R.i}{\sum_{i \in N_p} H.R.i}, \quad (3)$$

where  $N_p$  is the set of all terminals participating in DC voltage control,  $H.R.i$  is the available headroom of converter  $i$  and  $H.R.I_i$  is defined as Head-Room Index.

## III. KEY RESULTS

Fig.2 shows a case study of the system. At  $t = 0.5(s)$ , terminal 2 (which was operating as inverter) is disconnected from the MTDC system.

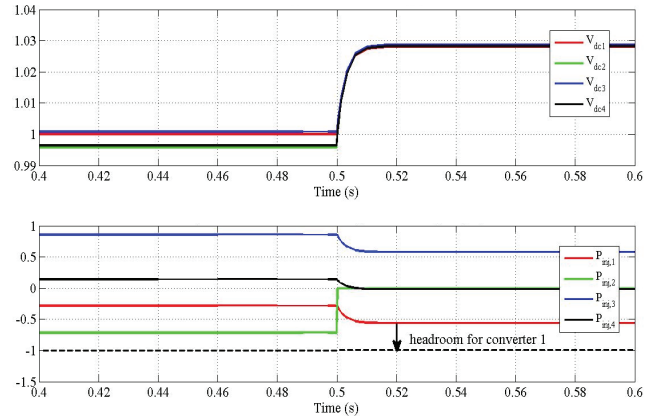


Fig. 2. The DC voltages and Injected active powers of the terminals.



# A Study of Hardware Requirements on Implementations of Phasor Measurement Algorithms

Samarth Deo, Nithin Somasundaran, Kun Zhu, Hans Bjorklund, and Lars Nordström

**Abstract**—Over the last decades, Phasor Measurement Unit (PMU) has been recognized as a main enabler to the smart grid at transmission level. There have been a plethora of algorithms proposed to calculate synchrophasors, however, due to a lack of requirements and standardization efforts, particularly from in industry, many of these algorithms have not been tested on off-the-shelf hardware platforms even their feasibility to be implemented has not been well discussed. As a response, this paper intends to capture the general hardware requirements of three well-cited synchrophasor calculation algorithms from literature.

**Keywords:** PMU, NASPI, WECC, C37.118 Standard.

## I. INTRODUCTION

Phasor Measurement Units (PMU)s deliver precise time-tagged data at high sampling rates. These sampling rates could be as high as 1024 samples/window for measurement applications where high accuracy is required in the calculation of the intended quantities. In [2], the authors proposed a recursive discrete fourier-based algorithm to accurately measure the phasor. Further, there are multiple literature that discusses robust algorithms in presence of input harmonics, off-nominal frequencies and low-frequency oscillations in power systems, e.g., [3], [4] and [5] among others.

Both North American Synchrophasor Initiative (NASPI) and Western Electricity Coordinating Council (WECC) have laid down requirements of PMU's under dynamic test conditions (a brief summary is provided in Section II-A). As real power flow in a power line is directly proportional to the sine of the angle difference between voltages at the two terminals of the line; accurate phasor measurement have become a topic of wide importance across the globe. As an example, PMU frequency plots provide a good indication of the generation loss a frequency drop of 0.1 Hz is almost equivalent to 800 MW generation loss in WECC [6]. Multiple algorithms have been developed around the world to accurately measure the phasor magnitude, angle, frequency and Rate Of Change Of Frequency (ROCOF). It is therefore necessary that the hardware required to implement these algorithms are able to support the calculations and reporting. This paper focuses

on the hardware requirements and limitations required by an industry compliant PMU.

### A. Purpose

This article discusses the various hardware requirements for a PMU complying with the NASPI/WECC requirements presented later. Specifically, in this paper, three highly accurate phasor measurement algorithms have been implemented and tested on different hardware's and their efficiency have been discussed. Moreover, this study also suggests the bottlenecks of the algorithm in question with respect to the two PMU accuracy class, i.e., P-class and M-class [7]. The P-Class PMU requires the device to have a faster response time but less accurate; whereas, the M-Class PMU requires the measurements to be much accurate with slower response time. P-class has no explicit requirements for filtering. The letter "P" refers to the protection applications which require fast response. The letter "M" refers to the measurement class of devices since measurements require better precision are flexible on the minimal reporting delay. M-class PMUs can be affected by the aliased signals. In general, the PMU vendors do provide the option to choose from one of the PMU class required but a PMU with both the classes in one box would be a more appreciated option. However, the corresponding hardware solutions are typically sophisticated, as it shall meet precision and performance requirements simultaneously. This is also discussed in this paper.

### B. Outline

The remainder of this paper is structured as follows. Section II presents a generalized architecture of a PMU in simple blocks and discusses the bottlenecks. Section III discusses the algorithms used for this discussion. Section IV discusses implementation of the algorithms and the hardware implemented on. Finally, section V concludes the paper.

## II. REQUIREMENTS ON PMU RESPONSE AND GENERIC ARCHITECTURE OF A PMU

This section provides a brief summary of the requirements on the PMU dynamic performance from NASPI, which is later endorsed by WECC, and a generic architecture of a PMU.

### A. NASPI/WECC Requirements

In [8], the authors have summarized the frequency response of a NASPI/WECC PMU as follows

- Is -3 dB or greater at 5 Hz;
- Does not exceed -40 dB at frequencies above the Nyquist frequency (a limit of -60 dB is preferred);

S. Deo and L. Nordström are with the Industrial Information & Control Systems, KTH - the Royal Institute of Technology, Stockholm, Sweden. E-mail: [samarth.deo@ics.kth.se](mailto:samarth.deo@ics.kth.se), [larsn@ics.kth.se](mailto:larsn@ics.kth.se).

K. Zhu is with Ventyx, an ABB company, Västerås, Sweden. E-mail: [kun.zhu@ventyx.abb.com](mailto:kun.zhu@ventyx.abb.com).

N. Somasundaran is with Amrita University, Coimbatore, India. E-mail: [nithin1664@gmail.com](mailto:nithin1664@gmail.com).

Hans Bjorklund is with ABB AB, HVDC, Ludvika, Sweden. E-mail: [hans.bjorklund@se.abb.com](mailto:hans.bjorklund@se.abb.com).

# Expediting the Optimization Process of Measurement-based Load Modeling by Parameter Sensitivities

Jae-Kyeong Kim, *Student Member, IEEE*, and Kyeon Hur, *Senior Member, IEEE*  
 School of Electrical and Electronic Engineering, Yonsei University, Seoul, Korea  
 Email: JK.Kim@yonsei.ac.kr, khur@yonsei.ac.kr

**Abstract**—This paper proposes an effective parameter optimization for measurement-based load modeling with a composite load structure using the correlation of parameter sensitivity. When the model parameters are adjusted in the optimization procedure to fit real load dynamics, some parameters are modified with comparable tendencies in every iterative process. These parameters, which have similar sensitivity to the output of the composite load model, will be identified by analyzing the partial derivatives with respect to all of the model parameters. Based on this result, the number of the load model parameters needed to be identified in the estimation process will be reduced, but the structure and order of the defined model will remain unmodified. This approach facilitates more efficient parameter estimation of measurement-based load modeling by reducing the dimension of the composite load parameter in the optimization process. Case studies demonstrate the computational efficiency and performance of the proposed method with reference to cases where all parameters of the composite load model are estimated simultaneously.

**Index Terms**—Load modeling, composite load model, optimization, parameter sensitivity, power system stability

## I. KEY EQUATIONS

The objective of the load modeling is minimizing difference between actual load and modeled output.

$$\min \sum (\mathbf{y} - \mathbf{f}_{\text{comp}})^2 \quad (1)$$

The sensitivities of model parameter are calculated by using partial derivatives:

$$\frac{\partial f}{\partial x} \approx \frac{f(x+h, \mathbf{p}) - f(x-h, \mathbf{p})}{2h} \quad (2)$$

The similarity of partial derivative is compared from Root Mean Square Error(RMSE) and correlation.

## II. KEY FIGURES

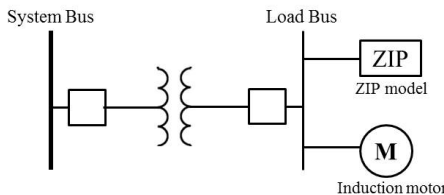


Fig. 1. One line diagram of power system with composite load structure.

The composite load model has twelve parameters to be identified. In this study, three parameters are reduced from analysis of parameter sensitivity.

## III. KEY RESULTS

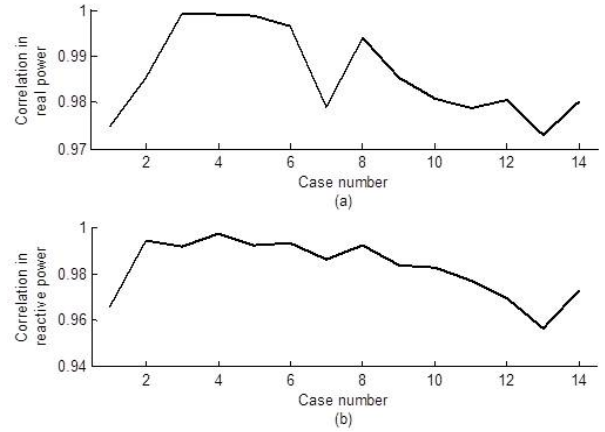


Fig. 2. Correlations of partial derivative between  $X_r$  and  $X_s$  for fourteen parameter sets in (a) real power. (b) reactive power.

TABLE I  
 AVERAGES OF MODEL ERROR FOR TEN FIELD MEASUREMENTS

Estimation Method	Real Power	Reactive Power
12-parameter estimation	0.01561	0.00957
9-parameter estimation	0.01562	0.00968

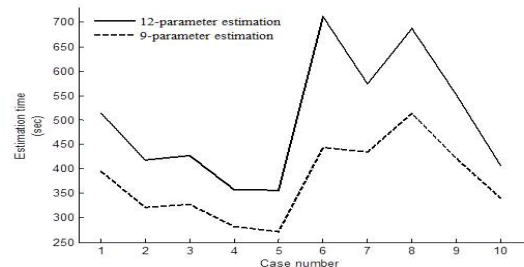


Fig. 3. Computational time for the two methods with ten actual measurements.

# Aggregation of Induction Motor Load Models using Coherency-Based Technique

<sup>1</sup>Kyungsung An, *Student Member, IEEE*, and <sup>1</sup>Kyeon Hur, *Senior Member, IEEE*

<sup>1</sup>School of Electrical and Electronic Engineering, Yonsei University, Seoul, South Korea,

Email: [anks86@yonsei.ac.kr](mailto:anks86@yonsei.ac.kr), [khur@yonsei.ac.kr](mailto:khur@yonsei.ac.kr)

**Abstract**— Recently, load modeling techniques with considering induction motors have widely studied to reflect dynamic responses in power system stability analysis. Nevertheless, a large number of induction motors can cause computational problem on dynamic simulation. In order to improve computational efficiency, it is necessary to aggregate induction motors for dynamic load modeling to an extent where it captures the important dynamic characteristics of real load but computationally feasible. Motivated by existing research efforts in generator model reduction, this research presents a dynamic equivalencing method for numerous induction motors using inertial coherency aggregation technique. In our technique, induction motors are grouped by rotor dynamics under disturbance condition. Then, multiple induction motors in each coherent group are represented with a single induction motor. Time-domain simulation case study demonstrates computational efficiency and accuracy of the reduced model.

## I. KEY FIGURES

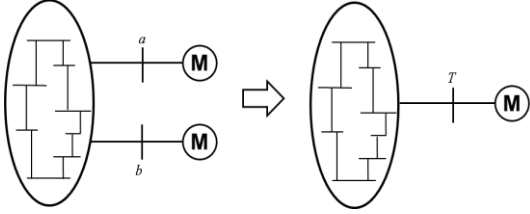


Fig. 1. Aggregation of coherent induction motors

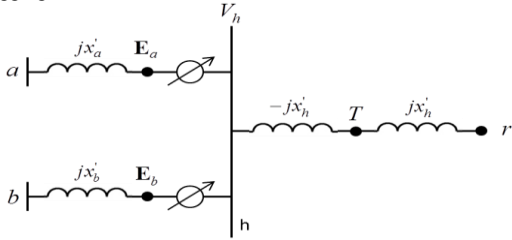


Fig. 2. Inertial aggregation technique

## II. KEY ALGORITHM

- Step 1. Compute the internal node voltages of induction motor loads
- Step 2. Create the hypothetical bus "h"
- Step 3. Add new branches from bus "a" and "b" to bus "h"
- Step 4. Aggregate induction motors
- Step 5. Create a new terminal bus "T" and new internal bus "r"
- Step 6. Adjust load on buses "a", "b", and "T"

## III. KEY EQUATIONS

The criterion to identify coherent group is:

$$\Delta\theta_a(t) - \Delta\theta_b(t) < \varepsilon \quad (1)$$

where  $\Delta\theta_a(t)$  and  $\Delta\theta_b(t)$  are the rotor angle deviation of induction motor "a" and "b", respectively, and  $\varepsilon$  is the tolerance degrees.

The voltage of hypothetical bus "h" is given by

$$\mathbf{E}_h = (H_a \mathbf{E}_a + H_b \mathbf{E}_b) / (H_a + H_b) \quad (2)$$

where  $H_a$  and  $H_b$  are the inertia constant, and  $\mathbf{E}_a$  and  $\mathbf{E}_b$  are the internal voltage phasor of induction motors. The voltage ratio of transformer from internal voltage  $\mathbf{E}_a$  and  $\mathbf{E}_b$  to hypothetical bus voltage  $\mathbf{V}_h$  is given by

$$\alpha_i = \mathbf{E}_i / \mathbf{V}_h \quad i = a, b \quad (3)$$

The inertia constant of induction motors is obtained by

$$H_T = H_a + H_b. \quad (4)$$

$$x'_h = \frac{1}{(1/x'_a + 1/x'_b)} \quad (5)$$

## IV. KEY RESULTS

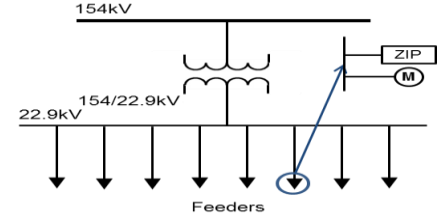


Fig. 3. Distribution system for simulation with eight feeders containing composite load model

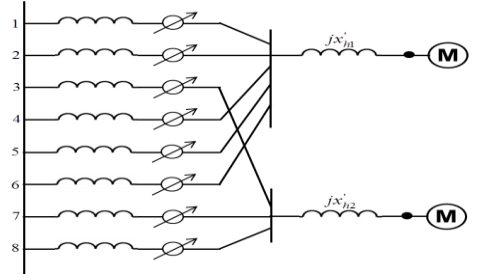


Fig. 4. Aggregated induction motors

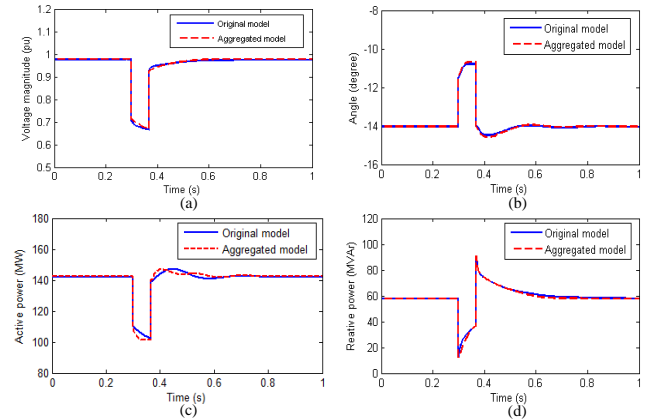


Fig. 5. Comparison of original model with aggregated model (a) bus voltage response (b) bus angle response (c) active power response (d) reactive power response

# Behavior of Power Cable Resonant Frequencies Under Fault Conditions

Youngdeug Kim and Keith E. Holbert  
 School of Electrical, Computer and Energy Engineering  
 Arizona State University, Tempe, AZ 85287-5706  
 ykim187@asu.edu

**Abstract**—This paper studies the behavior of resonant frequencies of power cables based on the transfer function derived from an equivalent pi model. The resonant frequencies are determined for variable load conditions and for variable fault condition and positions using PSCAD.

**Index Terms**—Power transmission, transmission lines, electrical fault detection.

## I. INTRODUCTION

Recently, researchers have focused on the frequency domain signal analysis methods for fault detection and location, because these approaches are believed to yield high accuracy without additional measurement devices and without disconnection to the power grid, e.g., fault location based on the travelling wave natural frequency analysis method [1] [2].

## II. BEHAVIOR OF RESONANT FREQUENCIES

The approximate resonant peak frequencies of the exact transmission line model can be expressed as [3]

$$\omega_{(n+1)/2} \cong \frac{n\pi}{2l\sqrt{LC}}, \quad n = 1, 3, 5, \dots \quad (1)$$

where  $l$  is the cable length. The behavior of the resonant frequencies was simulated using PSCAD. The reference resonance frequency peaks obtained from simulation for a 154 kV, 1200 mm<sup>2</sup>, 10.5 km transmission underground power cable are 3,392 Hz and 10,240 Hz for a 270 MVA load with a power factor of  $\cos(15^\circ)$ . Load changes are not found to have a significant effect on the resonant frequencies. The resonant frequency peaks decrease with descending load change as -32 Hz for 10% load of 270 MVA with a power factor angle of  $15^\circ$ . We found that cable faults make new resonant frequency peaks as shown in Fig. 1. These new resonant frequencies are plotted against fault location in Fig. 2.

## III. CONCLUSION

We recognize several characteristics of the resonant frequencies. 1) The resonant frequencies are inversely proportional to the cable length. 2) A load connection does not significantly change the peak frequencies. 3) Introduction of a fault into the transmission system creates multiple new resonant frequency peaks are found along with fault location.

These peaks are pronounced for small fault resistance and increase with fault locations far from the source.

Additional study should be undertaken to develop effective frequency analysis methods for extraction of actual resonant frequencies and a reasonable algorithm to calculate the location of the problematic point in the system from real data.

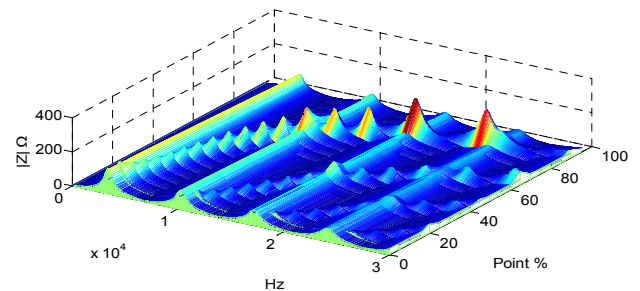


Fig. 1. Behavior of resonant frequencies as a function of cable fault location.

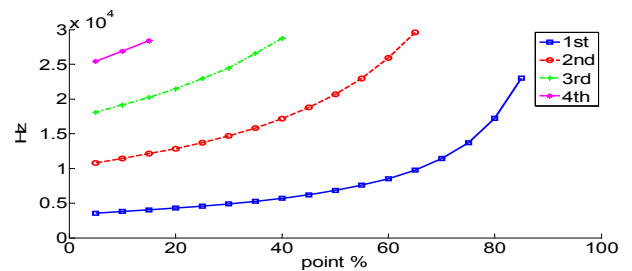


Fig. 2. New peak resonant frequencies as a function of fault position.

## REFERENCES

- [1] L.-Y. Wu, Z.-Y. He and Q.-Q. Qian, "A new single ended fault location technique using travelling wave natural frequencies," in *Power and Energy Engineering Conference, APPEEC*, 2009.
- [2] Z. Haifeng, Q. Yulin and J. Huibin, "Medium voltage distribution network traveling wave fault location method based on wavelet packet energy spectrum," vol. 3, pp. 1650- 1655, 2011.
- [3] K. Lin and K. E. Holbert, "Applying the equivalent pi circuit to the modeling of hydraulic pressurized lines," *Mathematics and Computers in Simulation*, vol. 79, no. 7, pp. 2064-2075, March 2009.

# Latency Monitoring of PMU Packets for Detecting Packet-Drop Attacks

Seemita Pal, Biplab Sikdar and Joe Chow  
 Department of Electrical, Computer and Systems Engineering  
 Rensselaer Polytechnic Institute, Troy, NY, 12180

**Abstract**—Phasor Measurement Units (PMU) are powerful tools in power systems and the data they generate enables the real-time health monitoring of the grid, thereby allowing timely control actions. Due to its high importance, this PMU data is vulnerable to different kinds of cyber attacks, one of them being packet-drop attack. This paper shows that the one-way latency of the data packets sent from the PMU to the Phasor Data Concentrator (PDC) is strongly correlated to the packet-drops caused by congestion but has low correlation to the packets dropped by attacker. Thus, monitoring this latency can give an indication of the network state and this data can be further utilized to reliably detect any packet-drop attack without adding any overhead to the network.

## I. INTRODUCTION

PMU data packet drops can easily lead to the loss of observability of the system and render useless a number of power systems control and protection applications that heavily rely on the reliable delivery of PMU data. The objective of this paper is to develop features that can be used to detect packet-drop attacks. The main challenge in detecting packet-drop attacks is differentiating malicious packet drops from drops due to network congestion.

## II. KEY EQUATIONS AND RESULTS

In this paper, three metrics adapted from [1] have been applied to data simulated using the Network Simulator (ns2) tool [2] for quantifying the correlation between the packet losses due to congestion and the one-way latencies observed at the PDC.

The first metric is the Correlation Indication Metric (CIM) which counts the number of times the short-term average  $x_m(i)$  of one-way latencies of  $m$  packets preceding the  $i_{th}$  packet are greater than the sum of the long-term average  $x_n(i)$  and standard deviation  $sdev_n(i)$  of preceding  $n$  packets with  $n > m$ . In other words, CIM is the number of occurrences when

$$\frac{x_m(i)}{x_n(i) + sdev_n(i)} \geq 1$$

is true before a packet gets dropped by congestion or attacker.

The second metric or the Loss Conditioned Delay Correlation (LDCD) metric calculates the average and standard deviation of the one-way latencies of the PMU packets whose  $j^{th}$  preceding ( $j$  is negative) or following ( $j$  is positive) packet is dropped.

The third metric is the loss conditioned delay cumulative distribution function (CDF) metric. It is a visual metric in

This work was supported primarily by the ERC Program of the National Science Foundation and the Department of Energy under NSF Award Number EEC-1041877 and the CURENT Industry Partnership Program.

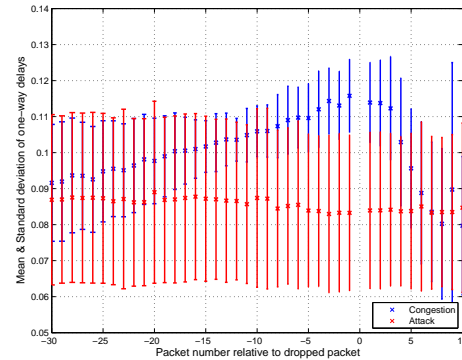


Fig. 1. Figure showing metric 2 results.

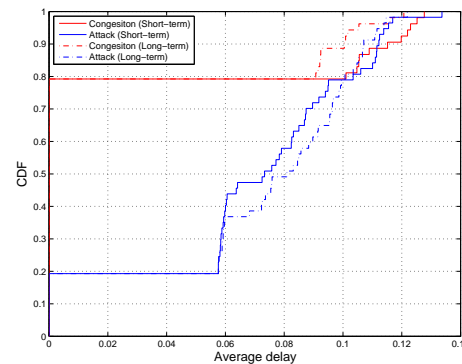


Fig. 2. Figure showing metric 3 results

which plot of the CDF of the short-term average latency is superposed on the CDF plot of the long-term average latency separately for packets dropped by congestion and those dropped by attacker.

The three metrics have been computed for data simulated using different topologies and it has been verified that there is a strong correlation between the one-way latencies of the PMU packets and the packets dropped due to congestion. For the first metric, it was observed that the  $CIM > \alpha$  for congestion drops and  $CIM < \alpha$  for attack drops. Graphs showing the results for the second and third metrics for one of the configurations are shown in Figures 1 and 2. Thus, the packet latency can reveal information regarding the security state of the network without adding any overhead at all. This latency information can be further utilized to detect and identify packets dropped by any attacker.

## REFERENCES

- [1] J. Martin, A. Nilsson and I. Rhee, "Delay-Based Congestion Avoidance in TCP," *IEEE/ACM Transactions on Networking*, vol.11, no.3, pp.356-369, June 2003.
- [2] The Network Simulator. Univ. California, Berkeley, CA. [Online]. Available: <http://www-mash.cs.Berkeley.EDU/ns/>



# Sequential Quadratic Programming Based Optimal Power Flow Incorporated with Magnetic Amplifier

Xiaohu Zhang<sup>1</sup>, Kevin Tomsovic<sup>1</sup> and Aleksandar Dimitrovski<sup>2</sup>

<sup>1</sup>Dept. of Electrical Engineering and Computer Science, University of Tennessee, Knoxville, Tennessee, USA

<sup>2</sup>Oak Ridge National Laboratory, Oak Ridge, Tennessee, USA

Email: xzhang46@utk.edu

**Abstract**—A Magnetic amplifier (MA) is a series reactor with continuous reactance regulation. It has been recently proposed to control power flow in the power system. Since it is controlled by a simple power electronics circuit, the cost of MA is far less than the cost of a similarly rated FACTS device. In this paper, a planning method which is based on Sequential Quadratic Programming (SQP) [1] is investigated to select the proper locations and settings of MA. The objective of the optimization problem is to maximize the system loadability. IEEE 9-, 30-, 39-, 118-bus systems are simulated to validate the proposed method.

## I. KEY FIGURE

The ideal model of MA is shown in Figure 1.

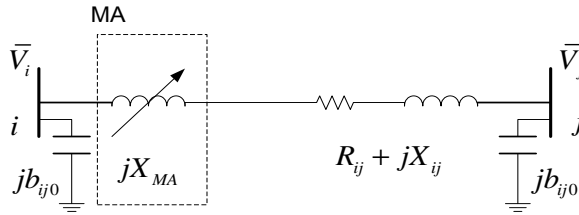


Fig. 1: Static Model of MA.

## II. KEY EQUATIONS

The optimization variables can be expressed as

$$\mathbf{w} = [\boldsymbol{\theta} \ \mathbf{V} \ \mathbf{P}_g \ \mathbf{Q}_g \ \mathbf{X}_{MA} \ \xi]^T \quad (1)$$

where:

- $\boldsymbol{\theta}$  is the vector for bus voltage angle.
- $\mathbf{V}$  is the vector for bus voltage magnitude.
- $\mathbf{P}_g$  is the vector for generator active power generation.
- $\mathbf{Q}_g$  is the vector for generator reactive power generation.
- $\mathbf{X}_{MA}$  is the vector of MA output reactance for each transmission line.
- $\xi$  is the loadability factor.

*Inequality constraints*

$$P_{ij}^2 + Q_{ij}^2 \leq \overline{S_{ij}}^2, \quad (i, j) \in l(i, j) \quad (2)$$

$$\sum X_{MA} \leq k_f \sum X_{ij}, \quad (i, j) \in l_{ntr}(i, j) \quad (3)$$

$$\underline{\mathbf{w}} \leq \mathbf{w} \leq \overline{\mathbf{w}} \quad (4)$$

*Equality constraints*

$$P_{gi} - \xi \cdot P_{di} = \sum_{j=1, j \neq i}^{nbus} P_{ij}, \quad i = 1, 2, \dots, n \quad (5)$$

$$Q_{gi} - \xi \cdot Q_{di} = \sum_{j=1, j \neq i}^{nbus} Q_{ij}, \quad i = 1, 2, \dots, n \quad (6)$$

*Objective Function*

$$\max \ \xi \quad (7)$$

## III. KEY RESULTS

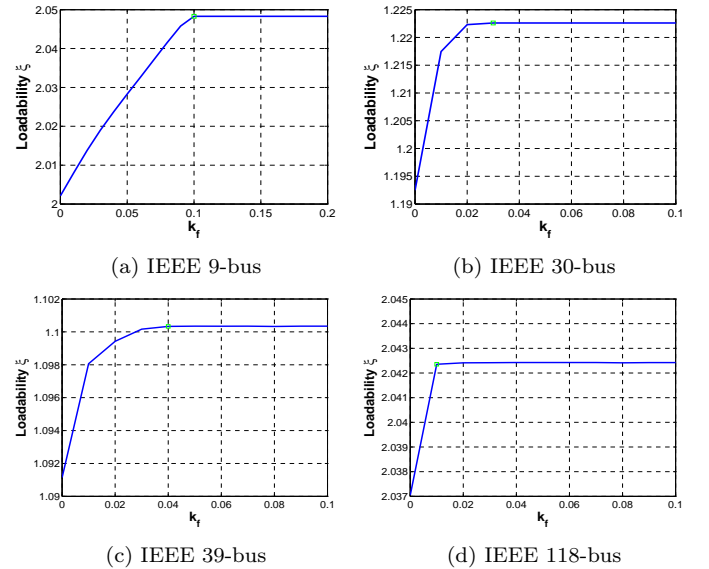


Fig. 2: System loadability enhancement versus limit number  $k_f$

## REFERENCES

- [1] J. Nocedal and S. Wright, *Numerical Optimization*. New York: Springer, 2006.



# Lyapunov Function Based Remedial Action Schemes

Mohammad Ehsan Raoufat, Kevin Tomsovic, Seddik Djouadi  
Department of Electrical Engineering and Computer Science  
University of Tennessee, Knoxville, 37996

**Abstract**—System protection schemes (SPS) or remedial action schemes (RAS) are corrective actions designed to mitigate the disturbance during extreme contingencies in power system. RAS can increase overall system reliability and performance by implementing actions, such as generator tripping, remote load shedding, turbine fast valving, dynamic breaking resistor, and so on. In general, RAS are designed and evaluated using extensive off-line studies. However, these schemes should be able to operate properly in wide range of system operating conditions, disturbances and uncertainties. The present study is devoted to develop Lyapunov function based RAS for different faults and improve their robustness against uncertainties in power system and detecting signals.

**Keywords**— Remedial Action Scheme, Lyapunov Function, Transient Energy Method.

## I. INTRODUCTION

Electric power is becoming more and more important in the modern world. Reliability and continuity of service to loads are main designing criteria in power system. As a result remedial actions have to be taken to increasing power system stability toward extreme contingencies. A RAS is designed to detect abnormal system conditions and utilizes a set of automatic corrective actions to preserve system integrity and provide acceptable system performance [1]. In general, RAS are pre-set according to a large number of off-line simulations to cover all possible operational conditions and events.

There are several different ways to classify RAS. According to their input variables, RAS can be classified into the following categories [2]:

- I. Event-based:** The event-based schemes directly detect the outage or fault in the system and initiate pre-planned target actions to mitigate the problem. These types of RAS are used when the phenomena are fast and easy to identify. Still, reliability is a big concern and to ensure their reliability, numerous off-line simulations with high computation burden are needed.
- II. Response-based:** These types of remedial actions are generally slower and they need to wait for the system response such as frequency or voltage drop.

As shown in Fig.1, RAS are designed to detect particular system condition that caused the disturbance and take some kind of predetermined corrective actions to counteract the disturbance in a controlled manner. These schemes should be able to operate properly in wide range of operating conditions and disturbances. This has led to need for newer and more robust RAS. This work is exploring the possibility of adapting Lyapunov function theory [3] to RAS design to improve the overall robustness of the target system during extreme faults in power system.

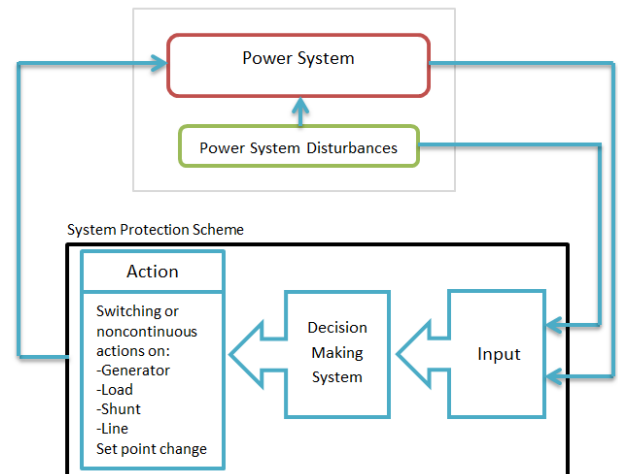


Figure 1. General SPS or RAS structure [2].

## REFERENCES

- [1] *System Protection Schemes in Power Networks*, CIGRE Task Force 38.02.19., Jun 2001.
- [2] Y. Zhang and K. Tomsovic, "Adaptive Remedial Action Scheme based on Transient Energy Analysis," *Proceedings of the 2004 Power Systems Conference & Exposition (PSCE)*, Oct. 2004, New York.
- [3] H. K. Khalil, *Nonlinear systems* (3rd ed.). Upper Saddle River, NJ, Prentice Hall, 2002.

# Flatness-Based Control of Doubly Fed Induction Generator

Maryam H Variani and Kevin Tomsovic

Dept. of Electrical Engineering and Computer Science  
University of Tennessee, Knoxville, TN 37996, USA,  
Email: [mhassani@utk.edu](mailto:mhassani@utk.edu) and [tomsovic@utk.edu](mailto:tomsovic@utk.edu)

**Abstract**— New generator control designs with minimum complexity are of prime importance to cope with the challenges associated with integrating rapidly increasing renewables into the power grid. We suggest existing controls can be replaced by a two-tier structure of local control operating within a global context of situational awareness that supports overall operation. Flatness-based approach is well adopted to control systems in such a structure where the tasks of planning, trajectory generation, and tracking the desired trajectories can be easily separated. In this study, implementation of flatness-based control on Doubly Fed Induction Generator (DFIG) is investigated. The system is decoupled into two trivial linear systems. While in vector control the trajectories are found using PI controllers, in the proposed control structure the trajectories are computed directly, through algebraic equations. Desired active and reactive powers are used to develop the set points for trajectory generation. Tracking of the desired trajectories is guaranteed through feedback linearization. The two level control structure enables active power control and the opportunity for wind plants to contribute in frequency regulation. The proposed control shows promising results in tracking the desired reactive power and the active power across a variety of scenarios and in providing ancillary service to support the frequency regulation of the grid.

**Index Terms**— Doubly Fed Induction Generator (DFIG), Flat Differential Systems, Trajectory Tracking, Trajectory Generation, Wind Power, Frequency Regulation, Secondary Control.

## I. KEY EQUATIONS

The main objective in the present study is to track the active and reactive power delivered to the grid. In a DFIG, the stator dynamics are very slow and stator fluxes are usually considered constant in modeling. In fact, stator transients are usually neglected in power system stability studies which results in a 3<sup>rd</sup> order DFIG model. On the other hand, since rotor speed is not controlled directly in generator control, it is considered as a parameter in system equations. We select the rotor flux argument,  $\theta$  and electrical torque,  $T_e$ , as flat outputs of the reduced order system. The system control inputs,  $v_{dr}$  and  $v_{qr}$ , can be expressed in terms of flat outputs and their derivatives, by transforming the system state variables to flat outputs:

$$v_{dr} = f_{v_{dr}}(\theta, \dot{\theta}, T_e, \dot{T}_e, \omega_r) \quad (1)$$

$$v_{qr} = f_{v_{qr}}(\theta, \dot{\theta}, T_e, \dot{T}_e, \omega_r) \quad (2)$$

where  $\dot{\theta}$  and  $\dot{T}_e$  are found through comparing flat outputs with reference values and applying appropriate proportional gains. The reference values for flat outputs,  $\theta^{ref}$  and  $T_e^{ref}$ , are derived from (3) and (4), where  $P_g^{ref}$  and  $Q_g^{ref}$  are desired active and reactive powers.

$$P_g^{ref} = f_{P_g}(\theta^{ref}, T_e^{ref}, \omega_r) \quad (3)$$

$$Q_g^{ref} = f_{Q_g}(\theta^{ref}, T_e^{ref}, \omega_r) \quad (4)$$

## II. KEY RESULTS

The proposed approach is implemented on a wind farm in a 4-bus system and different scenarios are studied. Figure 1 shows the active power control for maximum power point tracking (MPPT) for flatness-based method and traditional vector control. Delta control, providing a constant reserve to contribute in frequency regulation, is shown in Figure 2. For the dashed line results, the wind machine is maintained at optimal tip speed ratio to ensure that the system will return to the MPPT operating point instantaneously when the pitch angle is returned to normal.

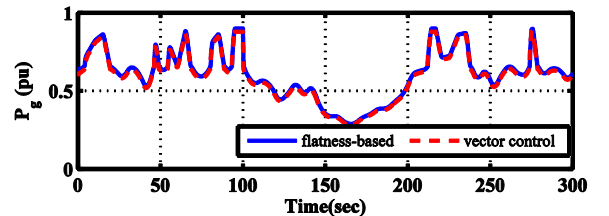


Figure 1. Active power for MPPT control.

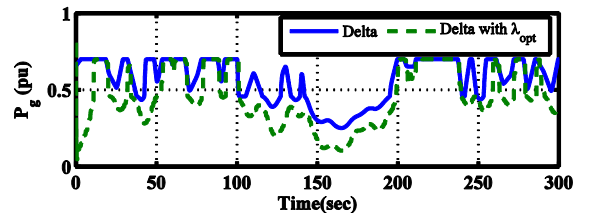


Figure 2. Active power for delta control

# PV Interconnection Risk Analysis through Distribution System Impact Signatures and Feeder Zones

Matthew J. Reno, Kyle Coogan, Santiago Grijalva  
Georgia Institute of Technology  
Atlanta, Georgia USA

Robert J. Broderick, Jimmy E. Quiroz  
Sandia National Laboratories  
Albuquerque, NM, USA

**Abstract** — High penetrations of PV on the distribution system can impact the operation of the grid and may require interconnection studies to prevent reliability problems. In order to improve the interconnection study process, the use of feeder zones and PV impact signatures are proposed to group feeders by allowable PV size as well as by their limiting factors for the interconnection. The feeder signature separates feeders into different impact regions with varying levels of PV interconnection risk, accounting for impact mitigation strategies and associated costs. This locational information improves the speed and accuracy of the interconnection screening process. The interconnection risk analysis methodology is based on the feeder and interconnection parameters such as: feeder type, feeder characteristics, and location and size of a PV system. PV impact signatures, hosting capacity, and feeder risk zones are demonstrated for four realistic distribution systems.

## I. METHODOLOGY

Several distribution systems are analyzed for the impacts caused by PV plants interconnected at various locations around the feeder. The three-phase distribution system analysis is performed in OpenDSS to solve the power flow for each case. The analysis iterates through possible interconnection locations, sweeping through a range of PV sizes up to 10MW at each location, and checks for any violations on the feeder. The fundamental procedure of the PV analysis has been discussed in previous papers, and the focus here is the analysis of the results to characterize differences between feeders and regions of the feeder.

## II. RESULTS

After performing the analysis of hundreds of thousands of PV scenarios for each feeder, the results in Figure 2 classify how often a given PV size is permissible at different locations and whether the violation is a voltage or thermal issue. For a given PV size and interconnection location, if the scenario can possibly create a voltage or thermal issue at any daytime feeder load level or PV ramp rate, the scenario is classified as a violation. The feeder signature shows the differences between feeders in the defining factors for their areas of risk.

Region A and Region B contain allowed interconnection locations that have no violations. Region A includes the PV sizes below which a system could be interconnected anywhere on the feeder without further investigation. The other regions refer to system sizes that require consideration before determining the feasibility of a PV system. Region B contains interconnections that are ultimately allowed but must use some locational details such as PCC distance to the substation and/or conductor type before making this assessment. Regions C, D, and E all include interconnections that have at least one violation and therefore cannot be connected given the current state of the feeder without some mitigation. The legend for the regions is shown in Figure 1.

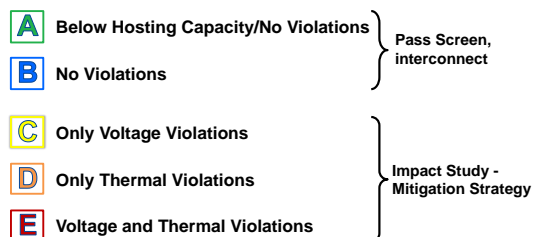


Figure 1. Feeder regions legend.

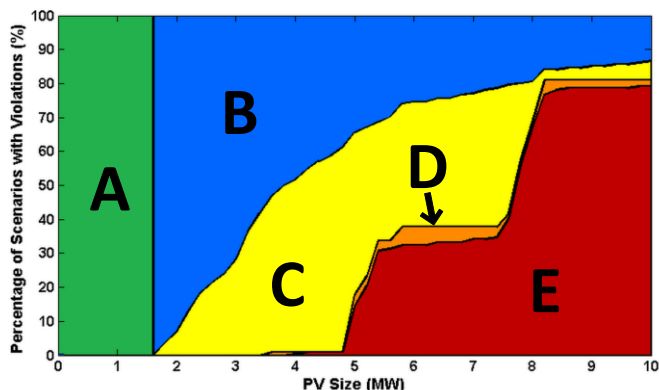


Figure 2. Example PV interconnection feeder signature for Ckt5.

The purpose of performing the large number of PV scenario simulations is to analyze the patterns that exist due to feeder characteristics, and which can then be translated into levels of feeder risk for PV interconnection impacts. Simple parameters such as distance to the substation and conductor type can allow a distribution feeder to be classified into interconnection zones. For example, the hosting capacity of Ckt5 is 1.6 MW, but Figure 3 shows the feeder interconnection zone map for Ckt5 where 25% of the buses are capable of handling a 6 MW interconnection.

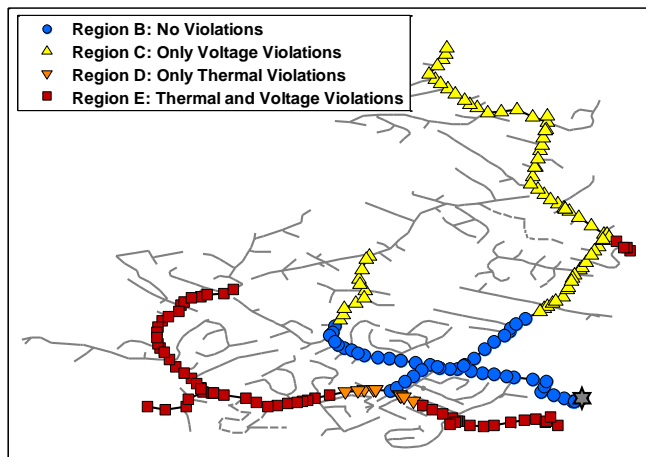


Figure 3. Example feeder interconnection zone map of 3-phase line section for a 6 MW PV plant on Ckt5.

# Performance Evaluation of Relays and Auto-Reclosing Operations

Min Lwin and Surya Santoso  
 Department of Electrical and Computer Engineering  
 The University of Texas at Austin

**Abstract**—This paper presents a specific application of using data captured by intelligent electronic devices (IEDs) during a fault to evaluate relay performance and auto-reclosing operations. A simple approach is presented to assess recloser performance based on IED waveform data. Furthermore, the data requirement to conduct the analysis and its limitations are also presented. Given the voltage and current waveforms recorded by IEDs, one can determine whether protective relays operated as intended and whether the operations are within the set time limits. A viable concept of relay performance evaluation is first presented and specifies under what conditions this evaluation approach applies. Next, a step by step procedure is presented to determine the performance of a relay given the voltage and current waveforms. Finally, the approach is applied to two short-circuit faults where data is available from the relay event recorders. A discussion of the results and data requirements is presented in the conclusion.

**Index Terms**—Power system protection, relays

## I. RECLOSER PERFORMANCE EVALUATION APPROACH

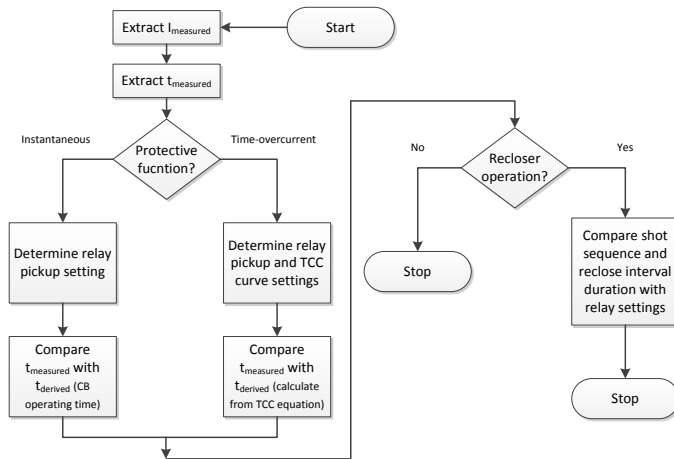


Figure 1. Flow diagram for recloser performance evaluation.

## II. APPLICATION TO FAULT AND RELAY DATA

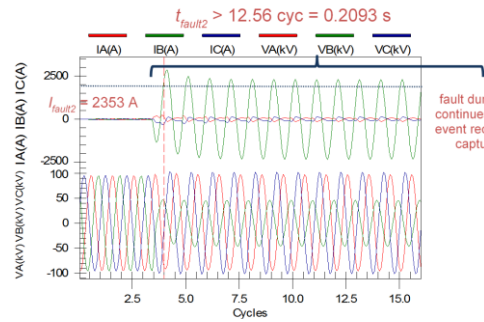


Figure 2. Event 2 shows a partial capture of the second recloser shot for the same single line-to-ground fault on phase B.

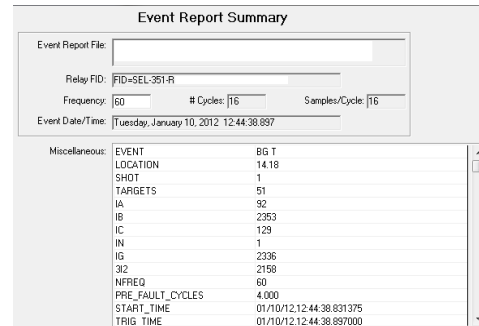


Figure 3. Relay event report summary for Event 2.

Equation for relay's inverse time-overcurrent curve for Event 2:

$$t(I) = TD \left( \frac{3.88}{M^2 - 1} + 0.0963 \right) \quad (1)$$

TABLE I. CALCULATION OF RELAY OPERATION FOR EVENT 2 ON U3 VERY INVERSE CURVE

Operation	$I_{\text{fault}}$ (A)	Pickup	$M$	$TD$	$t$ (s)	$t$ (cycles)
Shot 2	2336	288	8.1	1.48	0.2312	13.87

# Neighborhood Electric Vehicle Charging Scheduling Using Particle Swarm Optimization

Jouni Peppanen, Santiago Grijalva  
 School of Electrical and Computer Engineering  
 Georgia Institute of Technology  
 Atlanta, USA

**Abstract**—Chargeable electric vehicles are projected to gain increasing market share becoming a significant load in distribution systems. An un-controlled charging of a large number of electric vehicles can potentially lead to problems in distribution circuits including low voltage levels and component overloads. These problems can be avoided by implementing a vehicle charging control scheme. This poster and the related paper propose a particle-swarm optimization-based method to centrally control vehicle charging on a neighborhood level. Vehicle charging is scheduled day-ahead for a given distribution system area while minimizing the total charging cost subject to grid and vehicle constraints. The proposed algorithm reduces the charging cost while enforcing voltage or line flow limits applying linear sensitivities. We demonstrate the method in a model of a real meshed 121-bus, 57-vehicle European low voltage distribution system.

## I. FRAMEWORK

A centralized EV charging scheme is assumed with the information flows shown in Figure 1.

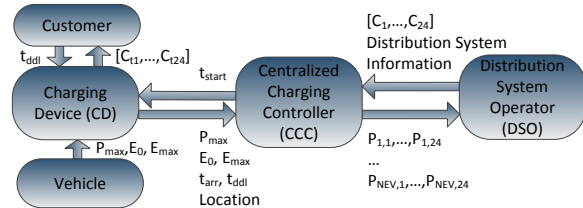


Figure 1. Information flows for centralized scheduling of EV charging

## I. OPTIMIZATION PROBLEM

A modified particle swarm optimization algorithm was used to minimize the sum of the total 24-hour charging cost of EVs in given grid area and the line flow violations:

$$J_i(k) = J_{i,1}(k) + \gamma J_{i,2}(k)$$

$$J_{i,1}(k) = \sum_{n=1}^{N_{EV}} \left( \sum_{h=1}^{24} C_h P_{i,n,h}(k) \right)$$

$$J_{i,2}(k) = \sum_{l=1}^{N_l} \left( \sum_{h=1}^{24} |\min(0, P_{Free,l,h} - P_{EV,l,h,i}(k))| \right)$$

$$P_{EV,l,h,i}(k) = PTDF_l \times P_{EV,h,i}(k).$$

EV availability and technical constraints were implicitly considered. Distribution systems line flow limits were enforced with PTDF sensitivities:

$$P_{j,h} = \begin{cases} P_{max,j}, & \text{for } t \in \{t_{start,j}, \dots, t_{start,j} + T_j - 1\} \\ 0, & \text{otherwise} \end{cases}$$

$$T_j = \text{ceil}((E_{max} - E_0)/P_{max})$$

$$t_{start,j} \in \{t_{arr}, \dots, t_{ddl} - T_j\}.$$

## II. CASE STUDY AND RESULTS

The implemented charging optimization algorithm was tested in a model of a real 3-phase 400 V<sub>L-L</sub> balanced European meshed urban residential low voltage grid for four different charging principle alternatives. With 200 iterations and 114 particles, the PSO optimization took approximately 14 seconds to solve.

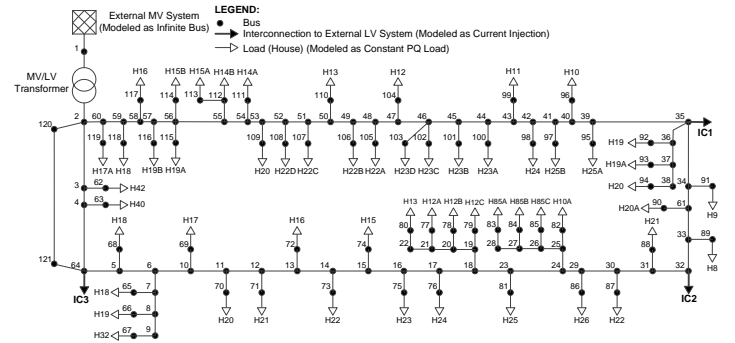


Figure 2. Case study distribution system model

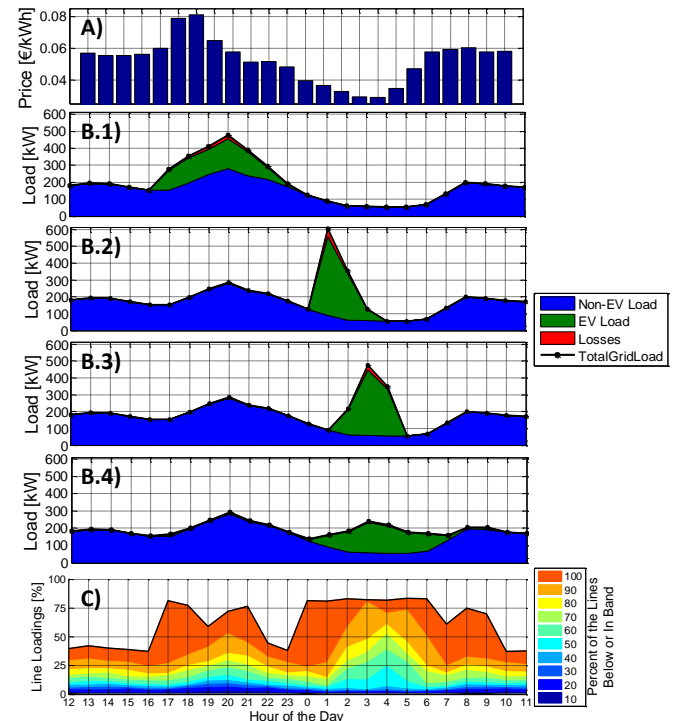


Figure 3. A) Average of hourly electricity spot prices in European Energy Exchange in November 22-28, 2013; B.1-B.4) Distribution system loads, EV charging loads, and losses for Cases 1-4; C) Case 4 distribution of relative line loadings



# Increasing Distribution System Model Accuracy with Extensive Deployment of Smart Meters

Jouni Peppanen, Jose Grimaldo,  
Matthew J. Reno, Santiago Grijalva  
School of Electrical and Computer Engineering  
Georgia Institute of Technology  
Atlanta, USA

Ronald G. Harley  
School of Electrical and Computer Engineering  
Georgia Institute of Technology  
Atlanta, USA  
University of KwaZulu-Natal  
Durban, South Africa

**Abstract**—The advent of smart metering infrastructure has paved the way to enhance the accuracy of conventional distribution system models. However, the size and complexity of the smart meter data and information systems present new issues, including the cumbersome process of extracting and analyzing data from various data sources. The focus of this poster and the related paper is to create a highly accurate distribution system model using Big Data from smart meters. It presents details on how traditional modeling can be improved by smart meter data as well as practical methods to make the data functional for analysis.

## I. GEORGIA TECH DISTRIBUTION SYSTEM

The Georgia Tech distribution system consists of 15 distribution feeders, all fed from 230 kV/19.8 kV utility-owned substation, which serve more than 200 buildings. The 19.8 kV dominantly underground distribution feeders are configured as either open-loop feeders or isolated spot network feeders. The substation is monitored by a SCADA system and the campus buildings are equipped with approximately 400 revenue grade smart meters. A measurement database is kept with 15-minute granularity.

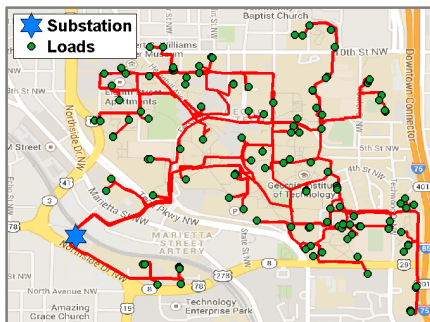


Figure 1. Georgia Tech distribution system.

## II. MODEL VALIDATION WITH SMART METER DATA

An accurate campus distribution system model is developed in OpenDSS. The model is verified using smart meter data that had to be pre-processed before use. The model validation steps are:

1) Identify and remove measurement problems independent of other measurements. Found issues include: wrongly set CT parameters, improper time synchronization, inconsistent units, false values, configuration/setup errors.

2) Compare the sum of all meters readings on a feeder to feeder total metered values over a time period. Large Mean absolute percentage errors:  $(MAPE = \frac{1}{n} \sum_{i=1}^n \frac{|V_{sim} - V_{meas}|}{V_{meas}})$  potentially indicate that a portion of the load on that feeder is

not being measured or that multiple meters are not operating properly.

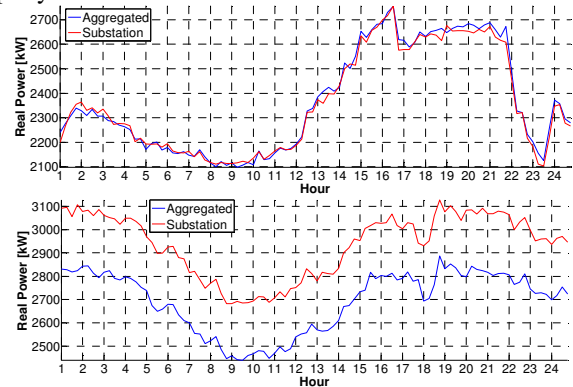


Figure 2. Example of aggregated load comparison of feeders with and without data related issues (top MAPE=0.66 %, bottom MAPE=8.25 %)

3) Verify the model accuracy by running power flow analyses over a time period by comparing the simulated voltages to the measured voltages at the meters. Positive mean bias errors  $(MBE = \frac{1}{n} \sum_{i=1}^n \frac{V_{sim} - V_{meas}}{V_{meas}})$  values indicate too low voltage drops in the circuit likely caused by too low circuit impedances.

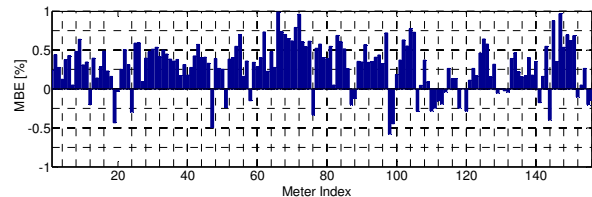


Figure 3. Mean bias error (MBE) of simulated load voltages compared to measured load voltages for one day

The general accuracy of any point can be given as the standard deviation of the individual error measurements for that meter. These standard deviations can be interpreted as error bars for the simulation results.

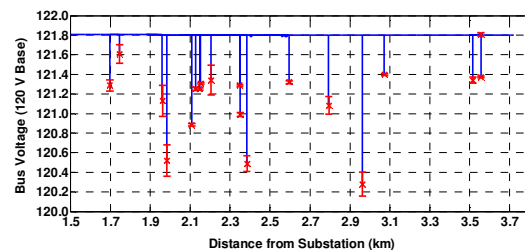


Figure 4. A Feeder voltage profile with standard deviations of the simulation errors for the day shown in red error bars



# Application of Computational Intelligence in Reliability Improvement of Active Distribution Systems Through Feeder Reconfiguration

Salem Elsaiah, *Student Member, IEEE*, and Joydeep Mitra, *Senior Member, IEEE*  
Department of Electrical and Computer Engineering  
Michigan State University  
East Lansing, Michigan 48824, USA  
(elsaihs@msu.edu)

**Abstract**—This paper describes a method for reliability improvement of power distribution system via feeder reconfiguration. The work presented here is developed based on a linearized network model in the form of DC power flow and linear programming model in which current carrying capacities of distribution feeders and real power constraints have been considered. The optimal open/close status of the sectionalizing and tie-switches are identified using an intelligent binary particle swarm optimization based search method. The probabilistic reliability assessment is conducted using a method based on high probability order approximation. A micro-power optimization model based on Homer software is used to account for the uncertainty in the output power of the intermittent renewable energy sources. Several case studies are carried out on a 33 bus radial distribution system, which is extensively used as an example in solving the distribution system reconfiguration problem. The effect of distributed generators has been considered in one several scenario. The obtained results are reported, discussed, and thoroughly analyzed.

**Index Terms**—Distribution system reconfiguration, reliability, particle swarm optimization, intermittent energy sources.

## I. BACKGROUND

Distribution systems have long been operated in a vertical manner for best control and coordination of their protective devices. Distribution systems are equipped with two types of switches; sectionalizing and tie-switches. The sectionalizing switches are normally closed and are used to connect various distribution line segments. The tie-switches, on the other hand, are normally opened and can be used to transfer loads from one feeder to another during abnormal and emergency conditions. Feeder reconfiguration is among the several operational tasks that are performed frequently on distribution systems. Basically, it denotes to the process of changing the topological structure of the distribution network by altering the open/close status of sectionalizing and tie-switches to achieve certain objectives. Of these objectives, loss minimization, voltage profile improvement, and reliability and security enhancement are of most concern.

Due to numerous environmental, political, and economical concerns, the structure of the distribution systems has been changed in recent years. A crucial part of this change has come through the installation of small sources of energy, constantly denoted as distributed generators, on several distribu-

tion systems. Examples of these energy sources include wind turbine induction generators and solar generators. Despite their numerous advantages, the inclusion of these intermittent renewable energy sources in the steady-state analysis of power distribution system such as feeder reconfiguration for loss reduction or reliability enhancement, for instance, has also brought up a number of technological and operational issues that need to be addressed.

## II. KEY RESULTS

TABLE I: Parameters of the BPSO

Parameter	Value
Number of particles	50
Social constant ( $c_1$ )	2
Social constant ( $c_2$ )	2
Max. number of iterations	1500

TABLE II: 33-Bus System Results—Case Study I

Network Status	Set of Opened Switches	EDNS kW/year
Initial Configuration	S33, S34, S35, S36, S37	10.08
Final Configuration	S6, S10, S13, S27, S32	8.49

TABLE III: 33-Bus System Results—Case Study II

Network Status	Set of Opened Switches	EDNS kW/year
Initial Configuration	S33, S34, S35, S36, S37	14.17
Final Configuration	S6, S10, S12, S27, S36	11.89

TABLE IV: 33-Bus System Results—Case Study III

Network Status	Set of Opened Switches	EDNS kW/year
Initial Configuration	S33, S34, S35, S36, S37	9.86
Final Configuration	S6, S10, S13, S26, S36	7.71

# Production Scheduling Considering Energy Consumption

Mostafa Ghafoorivarzaneh      Rupy Sawhney      John E. Kobza  
 Department of Industrial and System Engineering  
 University of Tennessee  
 Knoxville, Tennessee  
 mghafoor@utk.edu  
 sawhney@utk.edu  
 jkobza@utk.edu

**Abstract**— Production planning and scheduling allocates resources and time to production activities in order to meet the demand in a specific time period. Planning and scheduling problems are optimization problems aiming to meet the demand with highest profit or lowest cost. A considerable part in production cost is energy cost, but in most of production scheduling optimizations this part has been disregarded. With recent development in power market, rising awareness of CO<sub>2</sub> emissions and opportunity to save money by applying different strategies in demand response programs, the need for reconsideration of production scheduling models arises. The electricity consumption cannot be neglected in mathematical modeling anymore.

In this study a single machine and 3 type of products are considered. In addition to traditional scheduling terms, the following energy parts have been added to the model:

- Energy consumption for producing each item for each type,
- Energy consumption for startup,
- Energy consumption when the line is idle,
- Energy consumption for changing setup between production types

## I. KEY FORMULA

The objective function can be written as:

$$\begin{aligned}
 & \min \sum_{t=1}^T \sum_{i=1}^I (cp_i p_{it} + cq_i q_{it}) + \sum_{t=1}^T v_t * StC \quad (1) \\
 & + \sum_{t=1}^T \sum_{i=1}^I (psu_{it} * sc_i - nsu_{it} * sc_i) + \\
 & iE * \sum_{t=1}^T \left( PerTime * x_t - v_t * StT - \sum_{i=1}^I psu_{it} * st_i - tp_i p_{it} \right) \\
 & + \sum_{t=1}^T v_t * StE + \sum_{t=1}^T \sum_{i=1}^I (psu_{it} * se_i - nsu_{it} * se_i)
 \end{aligned}$$

where

$cp_i, ep_i, tp_i$  are production cost, energy and time for each item  $i$   
 $StC, StE, StT$  are startup cost, energy and time for each item  
 $iE$  is energy consumption in idle mode  
 $sc_i, se_i, st_i$  are setup cost, energy and time for each item  $i$

In this report, traditional and trivial constraints like available time, demand equality etc. are not reported and only new constraints are presented:

- Necessary Setups

$$\begin{cases}
 p_{it} \leq M(1 - z_{it}) & (2) \\
 -psu_{it} \leq -1 + Mz_{it} & (3) \\
 -p_{it} \leq -\varepsilon + Mz_{it} & (4) \\
 psu_{it} \leq M(1 - z_{it}) & (5)
 \end{cases}$$

- Setup orders:

$$inisetup_{it} \leq psu_{it} \quad (6)$$

$$finsetup_{it} \leq psu_{it} \quad (7)$$

$$\sum_{i=1}^I inisetup_{it} + dummy1 = 1 \quad (8)$$

$$\sum_{i=1}^I finsetup_{it} + dummy2 = 1, \forall t \quad (9)$$

$$\begin{cases} finsetup_{i,t-1} + inisetup_{it} - nsu_{it} \leq 1 & (10) \\ -finsetup_{i,t-1} - inisetup_{it} + 2nsu_{it} \leq 0 & (11) \end{cases}$$

- Startup constraints:

$$\sum_{i=1}^I P_{it} \leq 0 + M(1 - w_t) \quad (12)$$

$$-Y_t \leq -1 + M * w_t \quad (13)$$

$$Y_t - x_{t-1} \leq v_t \quad (14)$$

## II. KEY RESULT

The proposed model, not only considers production line constraints, but also modulates the planning based on energy consumption and provides scheduling with setup orders and optimal time for idle run.

Hour 1			Hour 2			Hour 3			Hour 4		
Type 1	Type 2	Type 3	Type 3	Type 2	Type 1	Idle			Type 1	Type 3	Type 2

Hour 1			Hour 2			Hour 3			Hour 4		
Type 1	Type 2	Type 3	off			off			Type 1	Type 3	Type 2

Figure 1: 8 Hourly production scheduling result for two different demands

# Cyber Risk Modeling of Hidden Failures in Smart Grid Protection System

Pengyuan Wang, Aditya Ashok, Manimaran Govindarasu

Department of Electrical and Computer Engineering

Iowa State University, Ames, IA, USA

Email: pywang@iastate.edu

**Abstract**—Hidden failures (HF) in protection system of the smart grid would amplify the severity of faults under certain operating conditions, and even lead to a cascading outage. A lot of efforts have been spent on the HF mode analysis and impact evaluation. However, little work has been done about the HFs resulting from cyber-attacks. From an attack-defense perspective, this poster analyzes the cyber actions which could lead to protection HFs. Different cyber-physical attack vectors aiming at common system protection schemes (SPS) are designed, and then, potential risk is calculated in terms of load loss based on stochastic Petri Net model and power system simulation. Possible mitigation strategies are also proposed and included in the risk modeling. A case study is conducted with the IEEE 39-bus model to exhibit the risk due to protection HFs and how the mitigations could alleviate the risk.

## I. PROBLEM STATEMENT

The number of cyber-attacks on smart grid has been increasing rapidly these days as well as the attack intelligence and complexity. It is critical to reconsider the operation of various power system applications such as protection from a new perspective. Figure 1 depicts the interaction among power grid, protection system, plausible attacks and mitigation strategies. From cyber security standpoint, an attack might involve compromising a protection scheme in order to interrupt power grid operation. To prevent such attacks, mitigation strategies could be implemented as a standalone function, which on the other hand might also become a target of attackers. Besides, physical-attacks could be launched to aid the cyber-attacks.

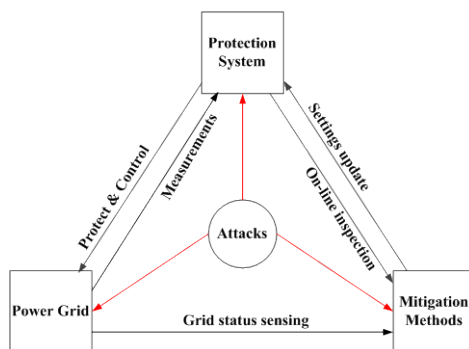


Figure 1. Interaction among power grid, protection, attack and mitigation

Similar to power system contingency analysis, it is necessary to take cyber risk analysis beforehand for protection system with a model which accurately describes the cyber-physical interaction. Protection HF is a kind of failure remains undetected until being triggered by another event. Therefore, compared with direct attacks that open breakers or shut down a power plant, HF attacks are less noticeable, and may cause much greater impacts due to the complex interdependency between protection schemes and power grid operation. HF attacks also have several unique characteristics which make them harder to be analyzed: 1) More targets, substations or plants, will be involved; 2) HF impacts on the power grid are not explicitly clear; 3) During the latent period, mitigation strategies like periodic online inspection & settings update might be carried out to eliminate the HFs in time.

Considering the above statement, this poster mainly focuses on three issues:

- Petri Net based wide-area HF attack modeling;
- HF risk assessment through real-time simulation;
- Mitigation validation and effectiveness testing.

## II. METHODOLOGY

Figure 2 shows the main procedures of the proposed methodology. Dotted lines in the figure represent HF mitigations that could be possibly adopted into the modeling.

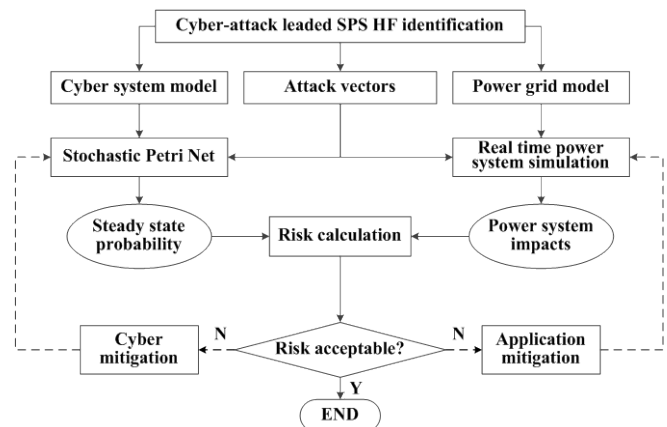


Figure 2. HF modeling & risk assessment procedures

# Agent Arbitration Approach for Coordinated Control in Active Power Network Management System

Ayodeji Owonipa, Student Member IEEE

Institute of Energy and Environment, University of Strathclyde, Glasgow, UK  
Email: ayodeji.owonipa@strath.ac.uk

***Abstract-*** Future Distribution Management Systems will comprise many heterogeneous cooperating intelligent agents, each with disparate network management and control functionality. The objective of this research is to develop an agent to arbitrate between the goals of the different heterogeneous cooperating agents. It involves agent-based modelling of an 'intelligent' network management system; enhanced to leverage the knowledge of a *corroboration agent* within a meta-level reasoning layer. The arbitration agent will have oversight of the community's knowledge, local plans and actions; capture in real-time knowledge of Distribution Network Operator's priorities and represent the acquired knowledge symbolically to provide an appropriate level of transparency for arbitration decisions. Its explicit goal is to be able to detect conflict and ultimately coordinate actions of network control and management agents on a Medium Voltage distribution network.

The arbitration agent pursues a set of goals autonomously and responds to the challenges and opportunities of the dynamic and uncertain power network environment. The research involves investigating the area of coordination in multi-agent systems which have multiple, conflicting goals (e.g. voltage control; power flow management; restoration; and minimization of losses) and mutually exclusive means of achieving those goals. The subsequent implementation of an agent incorporating the arbitration algorithm will be valuable for maximally exploiting the capabilities of individual agents and minimizing conflicts between them.

***Index terms:*** active network management, decentralised control, multi-agent systems, smart grids.

# A Partially Observable Markov Decision Process Approach to Customer Home Energy Management Systems

Timothy Hansen, *Graduate student member, IEEE*

Colorado State University  
Department of Electrical and Computer Engineering, Fort Collins, CO 80523, USA  
Email: timothy.hansen@colostate.edu

*Abstract*— A key assumption in demand response programs, such as real-time pricing (RTP) mechanisms, is customer participation and response. If customer assets (e.g., household loads, electric vehicles) are managed intelligently in an RTP market, the customer has the opportunity to benefit from a reduced cost of electricity. A greedy approach is to use assets at the cheapest forecast RTP value. This greedy approach may not be optimal as (a) the RTP is only forecast for 24-hours in advance and (b) if everyone acts in the greedy manner, the market will respond accordingly which may result in higher RTP and cost. Instead, if there is flexibility in the use of some assets (e.g., run a load of laundry in the next three days), it might be beneficial to delay the use of said assets. We propose a partially observable Markov decision process (POMDP) approach to customer asset control. Using our POMDP formulation, we design a non-myopic receding horizon control method (a general approach that is applied to many approximate dynamic programming problems) that trades short-term gains for long-term performance. The control decisions, or actions, that must be determined for each customer asset is whether to use the asset now, or wait until a later time to maximize customer electricity cost savings. To predict the RTP, generalized autoregressive conditional heteroskedastic (GARCH) models will be used in conjunction with particle filtering and parallel-rollout-like policies. We will compare the customer savings using a POMDP home energy management system to a greedy solution and one that uses time-of-use pricing.

## I. KEY EQUATIONS

The customer can take an action,  $a_i$ , for each of their assets  $i$  from the set of possible actions  $A$  (i.e.,  $a_i \in A$ ). Let  $\hat{a}$  be the vector of actions a customer will take (one entry for each asset). An example action is choosing the time to run a household load. The customer should choose  $\hat{a}$  to maximize their reward (e.g., maximize savings for using assets). We use Bellman's principle [1], given in (1), to determine  $\hat{a}$  to maximize customer reward. The objective function, called the Q-value and given in (2), is comprised of two components: the immediate reward and the expected reward-to-go. A greedy decision would only consider the immediate reward, but our non-myopic approach also considers future reward.

Let  $x$  be the current state,  $x'$  be the next state,  $R(x, \hat{a})$  be the immediate reward for taking action  $\hat{a}$  in state  $x$ ,  $V^*(x)$  be the optimal reward value given an initial state  $x$ ,  $Q(x, \hat{a})$  be the Q-value of taking action  $\hat{a}$  in state  $x$ , and  $\pi^*(x)$  be

the optimal action at state  $x$ . The customer should take actions  $\hat{a} = \pi^*(x)$  at each state  $x$ , described in (1) and (2).

$$\pi^*(x) = \operatorname{argmax}_{\hat{a}} Q(x, \hat{a}) \quad (1)$$

$$Q(x, \hat{a}) = R(x, \hat{a}) + E[V^*(x')|x, \hat{a}] \quad (2)$$

## II. KEY FIGURES

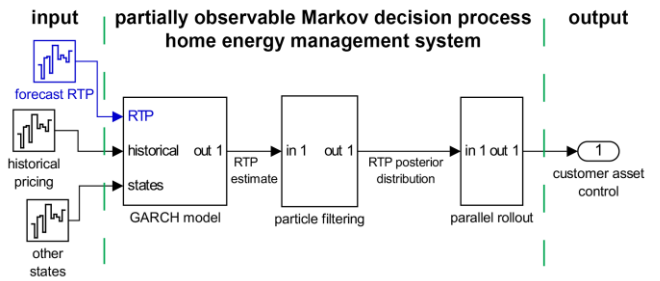


Figure 1. Partially observable Markov decision process based control system for a customer home energy management system.

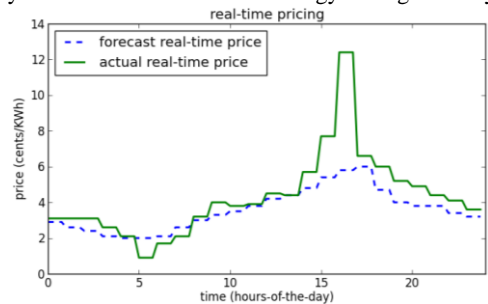


Figure 2. Example RTP data from ComEd. The blue line represents the forecast and the green line is the actual RTP. If the customer home energy management system could predict the large price spike, greater savings could be achieved.

## III. KEY RESULTS

Initial results will be presented in the accompanying poster.

## REFERENCE

- [1] R. E. Bellman, *Dynamic Programming*, Princeton University Press, Princeton, NJ, 1957.

# Load Forecasting Methods for Demand Resource Planning

Jonathan Berardino and Chika Nwankpa,

Center for Electric Power Engineering, Electrical and Computer Engineering Department, Drexel University, Philadelphia, PA 19104, USA,

Email: [jnb38@drexel.edu](mailto:jnb38@drexel.edu), [con22@drexel.edu](mailto:con22@drexel.edu),

**Abstract**— This poster presents an examination of several load forecasting methods for the purposes of predicting a building’s electrical load for demand resource planning. Load forecasting is used extensively by electric utilities for system planning and operation. The goal of this work is to introduce a similar focus when considering the participation of a controllable load in the energy market. Accurate building level demand forecasts will act as a tool for the manager of a controllable building load to assess his or her risk and capabilities when participating in the energy market. It is also important to ensure that aspects of building load behavior that can be leveraged to enhance a load forecast model are captured in order to support a facility’s overall energy optimization strategy.

Using building data collected from the Drexel University building management system, building-specific load behavior can be characterized based on actual measurements. This allows the temporal dependencies intrinsic to building electrical demand and correlation between demand and building-specific parameters are demonstrated and explained. To demonstrate the benefits of including these measurements in a load forecasting approach, several conventional forecasting methods are trained on this data. A series of day ahead forecasts are performed, showing consistency and improved accuracy compared to when only traditional factors are included.

## I. BACKGROUND AND MOTIVATION

Historically the outputs of a load forecast (particularly short term load forecasts) have been a critical factor in solving the unit commitment problem and ensuring dispatchers schedule adequate capacity in the most economical way possible. The goal of this work is to introduce a similar focus when considering the participation of a controllable load in the energy market, where the controllable load is considered to be the electrical demand of a building. It is therefore desirable to consider a forecasting method that incorporates effects of variants that specifically influence the electrical demand in a building. This will provide the end-user with a decision making tool to optimally plan demand resources, highlighting specifically the benefits of including building-specific measurements.

## II. KEY FIGURES

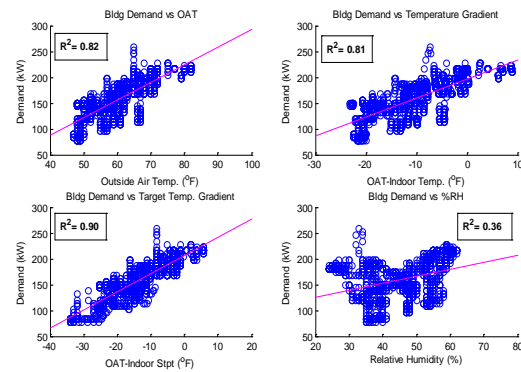


Figure 1. Linear correlation between demand and several variables: OAT (top left), OAT-Temp (top right), OAT-Stpt (bottom left), %RH (bottom right)

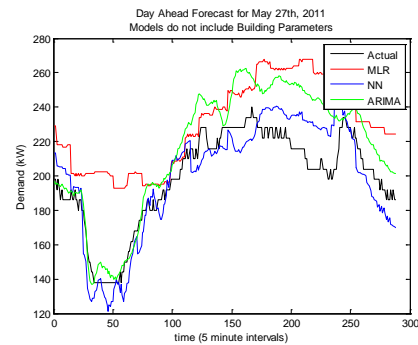


Figure 2. Day ahead forecast (all methods) plotted against actual demand. Forecast models do not include building-specific parameters

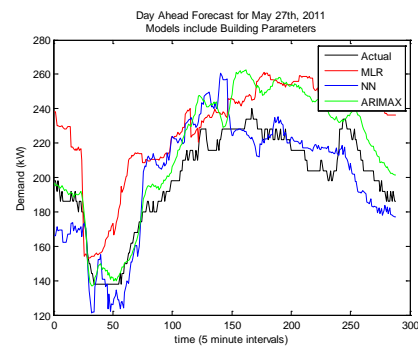


Figure 3. Day ahead forecast (all methods) plotted against actual demand. Forecast models include building-specific parameters



# Reliability Evaluation of Distribution System using Modified Sequential Monte Carlo Simulation.

Avinash S.Banajiger, *Student Member, IEEE*, Mohammad Heidari, *Student Member, IEEE*,  
and Visvakumar Aravinthan, *Member, IEEE*  
Dept. of Electrical Engineering and Computer Science,  
Wichita State University,  
Wichita, Kansas.

**Abstract**—Analytical techniques have pervasively used in distribution system reliability evaluation. These techniques are used to evaluate the mean reliability indices of a system to an acceptable accuracy. However, reliability evaluation of a sufficiently detailed system requires simulation based techniques. Techniques such as Time Sequential Monte Carlo (TSMC) evaluate the reliability indices by a series of stochastic processes. Stochastic processes simulate the basic behavioral patterns of elements in a chronological order. This paper presents an ameliorated method to TSMC technique for the evaluation of customer based reliability indices. The proposed method has been tested on one of the feeder (F1) in BUS 2 of Roy Billinton Test System (RBTS) and the results are compared with the analytical and Time Sequential Monte Carlo Technique.

**Keywords**— Reliability, load point indices, reliability indices, Sequential Monte Carlo Simulation.

## I. INTRODUCTION

The power system today is constantly evolving, to encompass the random nature of the system and to evaluate the reliability is pivotal. Several analytical techniques have been used to evaluate the load point and reliability indices, however, there are many underlying assumptions when these techniques are applied to large systems and the analysis thus resulting may lose its significance. To respond to the stochastic nature of the system many simulation techniques have been excogitated weighing all the aspects and contingencies inherent in the power system. Time Sequential Monte Carlo Simulation [1] is one such technique that simulates the operating life of each component in a system over a long period of time and provides important information on the effect of failure of components although infrequently occurring on the whole system. [3]

One of the limitations of the TSMC is that it considers the failure an element even when the system is down. This work considers the drawback and proposes a method to address the issue. The methodology has been tested on one of the feeders of RBTS and simulated in MATLAB.

## II. KEY EQUATIONS.

The failure rates and repair times can have different probability distributions, but exponential distribution is used to simulate the operating (TTF) and restoration times (TTR) of the elements [2]. Therefore the failure distribution is given by:

$$f(x) = \begin{cases} \lambda e^{-\lambda t} & 0 < t < \infty \\ 0 & \text{otherwise} \end{cases} \quad (1.1)$$

where,  $\lambda$  is the failure rate of the element.

This work considers the effect of failed element on all the other elements up and downstream to it. Equation 1.2 Thus,

solving the problem of element failure again, when the system is down.

$$TTF_{\text{affected element}} = TTF_{\text{old}} + TTR_{\text{failed element}} \quad (1.2)$$

## III. KEY FIGURES

Test Feeder 1 from the RTBS test system is used to evaluate convergence time of the modified TSMC. Fig.1 shows the simple feeder section that was used in this work.

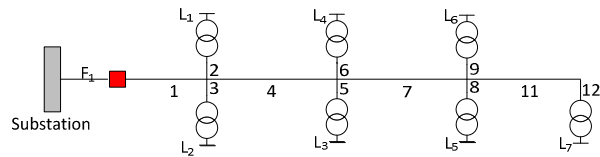


Figure 1: Distribution Test Feeder F1 of RBTS Bus 2

Using the failure rate and repair times given in [2] the comparison between the computed values of both TSMC and the proposed method is given in Fig.2

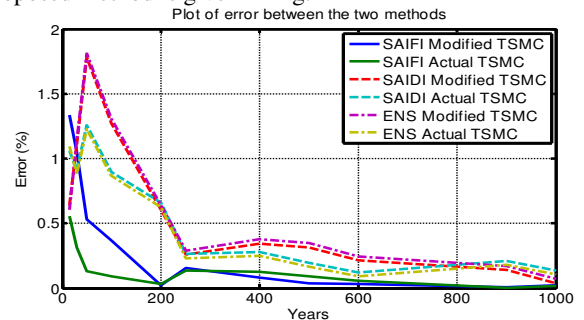


Figure 2: Comparison of results from the two methods.

## IV. CONCLUSION

The limitation discussed above has been addressed and the results of modified TSMC are consistent over different time intervals and convergence time is faster than the TSMC as depicted in Fig.2.

## V. REFERENCES CONCLUSION

- [1] Billinton R. and P. Wang, "Teaching distribution system reliability evaluation using Monte Carlo Simulation", IEEE Trans. on power Systems, vol.14(2), pp.397-403, May 1999
- [2] R.N. Allan, R. Billinton, I. Sjarrief, L.Goel, and K.S. So, "A reliability Test System for Educational Purpose-Basic Distribution System Data and results", IEEE Trans. on Power Systems, vol.6, No 2, May 1991
- [3] Billinton R. and Allan R.N. "Reliability evaluation of power system", 2<sup>nd</sup> edition, Plenum Press, New York, 1996

# Modeless Reconstruction of Missing Synchrophasor Measurements

Pengzhi Gao, Meng Wang, Scott G. Ghiocel, Joe H. Chow,  
 Department of Electrical, Computer, and Systems Engineering  
 Rensselaer Polytechnic Institute, Troy, NY, 12180, USA  
 Email: {wangm7,gaop, ghiocs2, chowj}@rpi.edu

**Abstract**—This paper presents a new framework of reconstructing missing synchrophasor measurements (erasures) without the modeling of power system dynamics. Leveraging the approximate low-rank property of phasor measurement unit (PMU) data, we connect the problem of reconstructing PMU data erasures with the recent advance in *low-rank matrix completion* methods. Erasures can be reconstructed through existing computationally-efficient algorithms such as singular value thresholding (SVT) and information cascading matrix completion (ICMC). Numerical experiments on actual PMU data are conducted to verify the effectiveness of the proposed method. Since existing analysis for matrix completion methods assumes an independent-erasure model that does not capture the correlation among PMU data erasures, we propose two models to characterize temporal correlation and channel correlation in PMU data erasures. We provide theoretical guarantees of the ICMC algorithm in reconstructing correlated erasures in both models.

**Index Terms**—low rank, matrix completion, missing data, phasor measurement unit.

## I. KEY THEOREMS

**Theorem 1.** For every positive  $\gamma$ , there exists a positive constant  $c(\gamma)$  such that if

$$p \geq \left( \frac{c(\gamma)\tau r \log n}{n} \right)^{\frac{1}{\tau(\tau+1)}} \quad (1)$$

holds, then ICMC correctly reconstructs  $M$  with probability at least  $1 - n^{-\gamma}$ .

**Theorem 2.** For every  $\gamma > 0$ , there exists a constant  $c(\gamma)$  such that if both

$$p_{i1}q_i \geq \left( \frac{c(\gamma)d_{\max}r \log n}{n} \right)^{\frac{1}{\tau+1}}, \quad \forall i, \quad (2)$$

and

$$p_{ij}q_i \geq \frac{c(\gamma)r \log n}{n}, \quad \forall i, j, \quad (3)$$

hold, then ICMC correctly reconstructs  $M$  with probability at least  $1 - n^{-\gamma}$ .

## II. KEY RESULTS

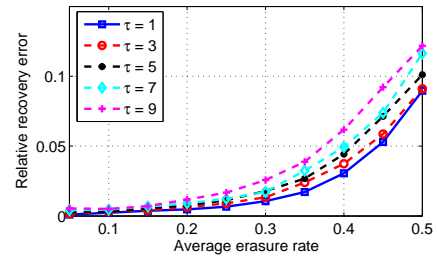


Fig. 1. Relative recovery error of the SVT algorithm

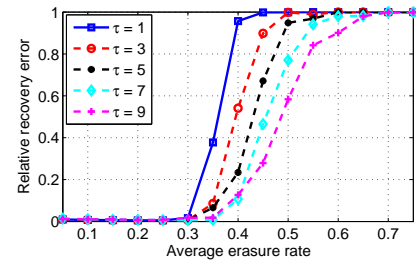


Fig. 2. Relative recovery error of the ICMC algorithm

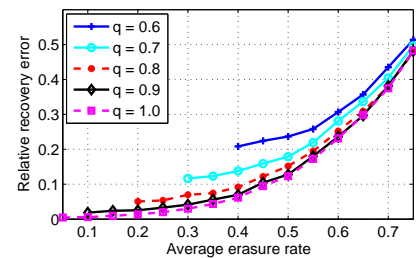


Fig. 3. Relative recovery error of the SVT algorithm

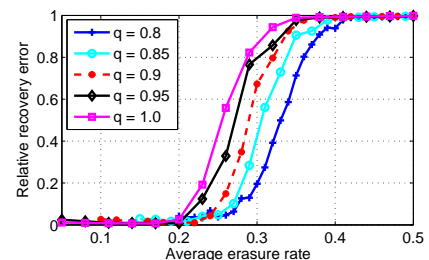


Fig. 4. Relative recovery error of the ICMC algorithm

# Conceptual Architecture of Building Energy Management Open Source Software (BEMOSS)

A. Saha, W. Khamphanchai, K. Rathinavel, M. Kuzlu, M. Pipattanasomporn, and S. Rahman  
Virginia Tech – Advanced Research Institute, Arlington, VA

Email: avijit@vt.edu, kwarodom@vt.edu, kruthika@vt.edu, mkuzlu@vt.edu, mpipatta@vt.edu, srahman@vt.edu

**Abstract**— The objective of this poster is to present the conceptual architecture of a Building Energy Management Open Source Software (BEMOSS) platform. The proposed BEMOSS platform is expected to improve sensing and control of equipment in small- and medium-sized buildings, reduce energy consumption and help implement demand response (DR). It aims to offer: scalability, robustness, plug-and-play, open protocol, interoperability, cost-effectiveness, as well as local and remote monitoring. BEMOSS has an open architecture to allow seamless integration with device controllers from various manufacturers, as well as offers an application gateway feature to provide interoperability among different standards. In this poster, the concept of BEMOSS and its software architecture are presented. A laboratory test bed is being designed at the Advanced Research Institute of Virginia Tech (VT-ARI) with simulated building loads to demonstrate the functionality of BEMOSS.

**Index Terms**— Building energy management, open source, and demand response.

## I. BEMOSS CONCEPT

### A. Key Features

**Application:** Open architecture to make it easy for developers to contribute to BEMOSS.

**Usability:** Interoperability among various standards and protocols, plug & play of devices and scalability.

**Advanced Monitoring:** Real-time monitoring of building energy consumption and device status through web and mobile interfaces.

**Advanced Control:** Advanced algorithms for sensing and control of equipment.

**Cost-effectiveness:** Cost-effective implementation with open-source platform and low-cost embedded systems.

### B. Target Buildings and supported types of devices

BEMOSS mainly targets small- (<5,000 sqft) and medium-sized (between 5,000 and 50,000 sqft) commercial buildings. BEMOSS controls HVAC, lighting and selected plug loads. It supports load control devices, like: smart thermostats, VAV controllers, lighting controllers, and smart plugs. It also supports power/energy meters and sensors (e.g., light, temperature and humidity).

### C. Supported Communication Technologies and Protocols

Currently, BEMOSS supports prevalent communication technologies, like Ethernet (IEEE 802.3), Serial (RS-485), ZigBee (IEEE 802.15.4) and Wi-Fi (IEEE 802.11), and popular data exchange protocols, like BACnet, Modbus, Web, OpenADR and Smart Energy Profile (SEP).

## II. BEMOSS ARCHITECTURE

Fig. 1 illustrates BEMOSS software architecture, which comprises the following four layers:

- *User Interface (UI) Layer:* manages web and mobile interfaces for user interaction with BEMOSS.
- *Application and Data Management Layer:* supports applications that allow monitoring and intelligent control of devices and data management using databases.
- *Operating System and Framework Layer:* deploys distributed agent technology to implement distributed control decisions and data analysis.
- *Connectivity Layer:* takes care of communications between the upper layers and physical hardware devices.

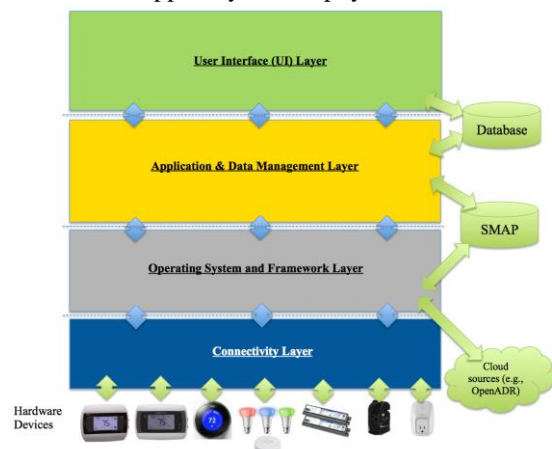


Fig. 1. BEMOSS software architecture.

A part of the laboratory setup at VT-ARI is shown in Fig. 2.



Fig 2. BEMOSS lab setup at VT-ARI.

This work was supported in part by the U.S. Department of Energy under Grant# DE-EE-0006352.0000.

# Intelligent Power Conditioning and Monitoring Interface for Smart Grids Prosumers (Prosumer Interface)

Krzysztof Chmielowiec<sup>1</sup>, *Graduate Student Member, IEEE*, Tomasz Dziwinski<sup>2</sup>, *Graduate Student Member, IEEE*

<sup>1</sup>AGH University of Science and Technology, Department of Power Electronics and Energy Control Systems  
Al. Mickiewicza 30, 30-059 Krakow, Poland  
Email: kchmielo@agh.edu.pl

<sup>2</sup>AGH University of Science and Technology, Department of Automatics and Biomedical Engineering  
Al. Mickiewicza 30, 30-059 Krakow, Poland  
Email: tdz@agh.edu.pl

**Abstract**— Prosumer Interface solves problem of integration of prosumers (consumers, dispersed energy sources, and possible energy storage technologies) with a low voltage electric power grid for, so as to ensure effective two-direction power flowing. With the ability to operate with energy storage units, Prosumer Interface can be designed to optimize energy cost, in order to maximize financial profits of its holder. It also aims at improving the quality of electric power supplying a consumer through the grid and ensuring fulfilment of power quality requirements.

**Index Terms**—Power Electronic Converter, Prosumer, Smart Grid.

## I. INTRODUCTION

Currently the electrical energy market offers individual solutions capable to solve problems and needs of energy prosumers. Uninterruptible Power Supplies (UPS) are used to maintain the power supply of susceptible load during voltage sags and interruptions. Active and passive filters and dynamic voltage restorers are used for keeping voltage parameters on the appropriate level. Reactive power control is provided by static var compensators. Smart meters and power quality analyzers are used to monitor energy consumption and voltage parameters. However in practice, there is no device at the market that would carry out all these tasks comprehensively.

The list of problems affected energy consumers is long and include: Problem 1: Additional energy costs due to the absence of energy production and consumption optimization), Problem 2: Cost of downtime and lower efficiency of industrial processes due to power quality disturbances affecting susceptible loads, Problem 3: Increased energy costs due to ineffective reactive power compensation, Problem 4: Power quality claims from

energy distributor (or other parties on the energy market) for emission of power quality disturbances (harmonics, flicker, etc.) caused by non-linear and disturbing loads.

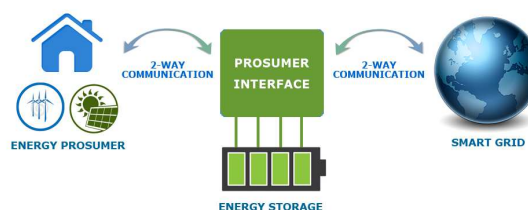


Fig. 1 The concept of Prosumer Interface

According to Strategic Business Plan of IEC/PC [1], in the next years, there will be observed a high focus placed on technology named *Smart Grid User Interface* which links directly to the proposed concept - Prosumer Interface.

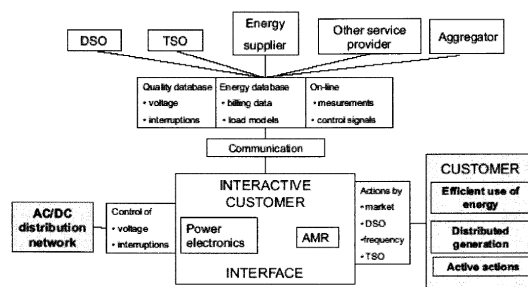


Fig. 2 The concept of Smart Grid User Interface [1]

## REFERENCE

- [1] IEC PC 118 "Strategic Business Plan" SMB/4823/R
- [2] [http://www.derlab.net/downloads/derlab\\_d2.8\\_whitebook\\_static\\_converters\\_rev0-0.pdf](http://www.derlab.net/downloads/derlab_d2.8_whitebook_static_converters_rev0-0.pdf)

# Power System Severe Contingency Screening Considering Renewable Energy

Yazhou Jiang, Guanqun Wang, Sandip Roy, Chen-Ching Liu  
 Washington State University, Pullman, WA, USA  
 Email: {yjiang1, gwang, sroy, liu}@eecs.wsu.edu

**Abstract** - The integration of intermittent-renewable resources into the power system is having a significant impact on system operations, because these resources introduce uncertainty as well as variability in operations. As the penetration of intermittent renewables increases, day-ahead unit scheduling and hourly economic dispatch conducted by the independent system operator will seek to fully use such clean energy, to reduce the fuel cost associated with conventional units; indeed, many efforts are underway to achieve effective unit commitment and economic dispatch for high renewables-penetration scenarios. In comparison with traditional operations, these new operational paradigms will involve more extensive redistribution of the power flow, and will be subject to greater uncertainty in the power-flow solution at the decision-making horizon. An important consequence is that profiles of transmission congestion will be more variable compared to the current grid, and further may have significant uncertainty at the operational horizon. This increased variability and uncertainty in congestion patterns will complicate contingency analysis and management: new vulnerabilities may be introduced, severe contingencies will be more difficult to forecast, and the classical N-1 security paradigm may be subject to revision. Thus, there is a need for new tools in the control room, which provide operators with situational awareness about congestion profiles and severe contingencies. In this work, we take an initial step toward developing contingency-management tools for the renewables-rich grid, by developing a strategy for detecting severe contingencies under changing renewable-generation profiles.

## I. KEY EQUATIONS

A graph-partitioning approach is used to detect severe contingencies for a particular renewable-generation future. Specifically, the most congested cut (the one with smallest remaining margin line transmission) is found. This requires solving the following optimization:

$$\min \sum_{(i,j) \in \text{Cut}} \left(1 - \frac{\theta_i - \theta_j}{(\theta_i - \theta_j)_{\text{limit}}}\right).$$

A spectral-partitioning approach is used to solve the optimization. This involves constructing a Laplacian matrix  $M$  with off-diagonal entries:

$$[M]_{ij} = \begin{cases} -\left(1 - \frac{\theta_i - \theta_j}{(\theta_i - \theta_j)_{\text{limit}}}\right) & (i, j) \in \text{Line} \\ 0 & \text{otherwise} \end{cases}$$

and diagonal entries chosen to achieve zero row sums. The subdominant eigenvector of  $M$  is used for partitioning.

## II. KEY FIGURES

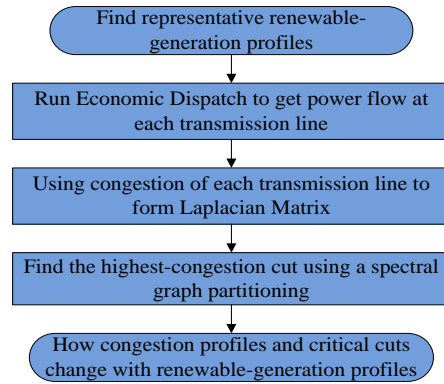


Fig.1 Flowchart for detecting the severe contingency

## III. KEY RESULT

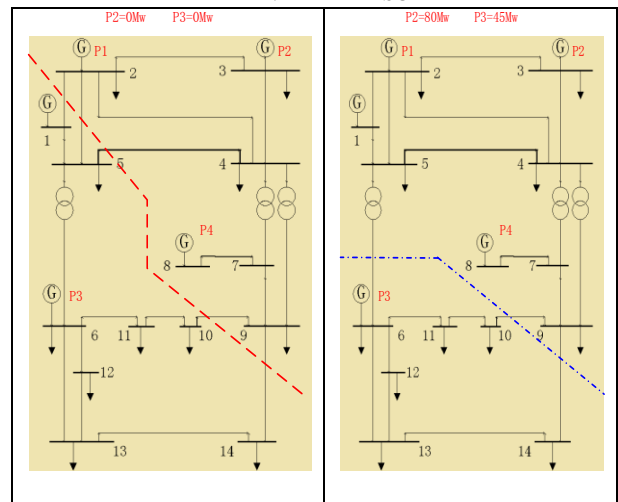


Fig. 2 Severe contingency cuts under changing renewable-generation profiles



# Operating Regions of Modular Multilevel Converter under Various Cell Capacitances

Hee Jin Kim

School of Electronic and Electrical Engineering, Yonsei University  
Seoul, South Korea

E-mail: [jimmykim07@yonsei.ac.kr](mailto:jimmykim07@yonsei.ac.kr)

**Abstract**—The poster presents operating regions of (P-Q capability) Modular Multilevel Converter (MMC) in different energy storages. The required stored energy, which is directly related with cell capacitance and average voltage, determines energy variation in the arms of MMC. The amount of energy variation in each arm is different from power factors of the converter. Because the maximum excess energy of each arm is fixed by rated voltage of the cell, the apparent power of the converter is limited by power factors, which means that as the reactive power increases, the rated apparent power decreases. This characteristic of energy and power factor determines operating regions of MMC. The poster presents the basic principle and methodology for seeking the energy requirement of MMC. The maximum excess energy storage capability of MMC is derived with the equations. The operating regions of two different energy storages are analyzed. The simulation result with detailed equivalent model in PSCAD/EMTDC is presented.

**Index Terms**—MMC, Cell capacitance,.

## I. KEY EQUATIONS

$$v_{cell}(t) \leq k_{max} \cdot V_{cell,avg} = V_{cell,rated} \quad (1)$$

$$e_{arm}(t) = \frac{N}{2} \cdot C_{cell} v_{cell}^2(t) \quad (2)$$

$$E_{arm,avg} = \frac{N}{2} \cdot C_{cell} V_{cell,avg}^2 \quad (3)$$

$$E_{arm,rated} = \frac{N}{2} C_{cell} V_{cell,rated}^2 = \frac{N}{2} C_{cell} k_{max}^2 V_{cell,avg}^2 = k_{max}^2 E_{arm,avg} \quad (4)$$

$$\Delta E_{max} = E_{arm,rated} - E_{arm,avg} \quad (5)$$

$$\Delta E_{max} = (k_{max}^2 - 1) E_{arm,avg} = \frac{k_{max}^2 - 1}{k_{max}^2} E_{arm,rated} \quad (6)$$

$$\Delta E_{max} = \max(e_u(t)) = \max(e_l(t)) \quad (7)$$

$$v_u(t) = \frac{1}{2} V_{dc} (1 - m \cos(\omega t)) \quad (8)$$

$$i_u(t) = \frac{1}{2} \hat{i}_{ac} \left( \frac{1}{2} m \cos(\varphi) + \cos(\omega t + \varphi) \right) \quad (9)$$

$$p_u(t) = \frac{1}{3} P_s \left( \frac{1}{m} \cos(\omega t + \varphi) - \frac{1}{2} m \cos(\varphi) \cos(\omega t) - \frac{1}{2} \cos(2\omega t + \varphi) \right) \quad (10)$$

$$e_u(t) = \frac{P_s}{3\omega} \left( \frac{1}{m} \sin(\omega t + \varphi) - \frac{1}{2} m \cos(\varphi) \sin(\omega t) - \frac{1}{4} \sin(2\omega t + \varphi) \right) \quad (11)$$

## II. KEY TABLE

TABLE I. SPECIFICATION OF TEST SYSTEM

	Case 1	Case 2
$\Delta E_{max}$	413.7 J	375.7 J
Average Energy	1970 J	1789 J
Rated Apparent Power	440 MVA	400 MVA
Cell Capacitance	5 mF	4.5 mF
Average Cell Voltage	2 kV	
Number of Cells	200 per arm	
DC Voltage	$\pm 200$ kV	
AC Voltage	150 kV	
Modulation Index	0.75	

## III. KEY FIGURES

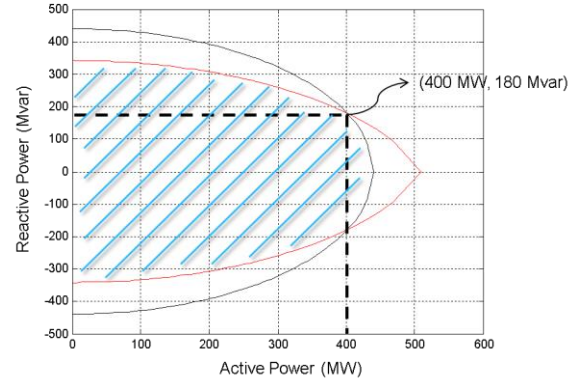


Fig. 1. Operating Region of MMC where cell capacitance is 5 mF (Case1)

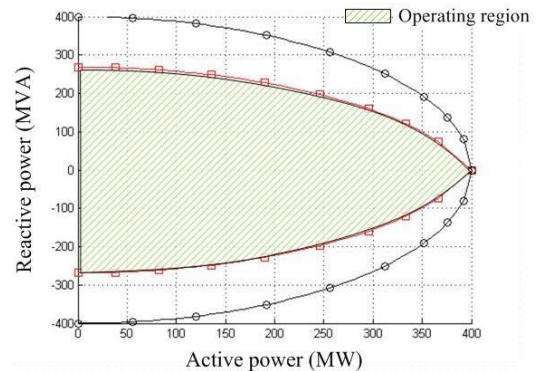


Fig. 2. Operating Region of MMC where cell capacitance is 4.5 mF (Case2)



# Distributed Flywheel Energy Storage Systems for Mitigating the Effects of Pulsed Loads

Ahmed T. Elsayed, *Student Member, IEEE*, and Osama A. Mohammed, *Fellow, IEEE*

**Abstract**— This paper presents a distributed Flywheel Energy Storage System (FESS) for mitigating the effects of pulsed loads such as those exist in Shipboard Power Systems (SPS). A comparison between distributed and centralized allocation of FESS was provided with and without the utilization of ultra-capacitors on the DC side. A model for hybrid AC/DC SPS with zonal distribution architecture was built in a simulation software. In order to accurately evaluate the performance of the system, three different case studies are presented with and without the FESS. The results of each case are analyzed and discussed. It can be shown that the distributed allocation of FESS can reduce the overloading on the generators and frequency fluctuations.

**Index Terms**—Flywheel energy storage system (FESS), PMSM, pulsed load, shipboard power system.

## I. KEY FIGURES

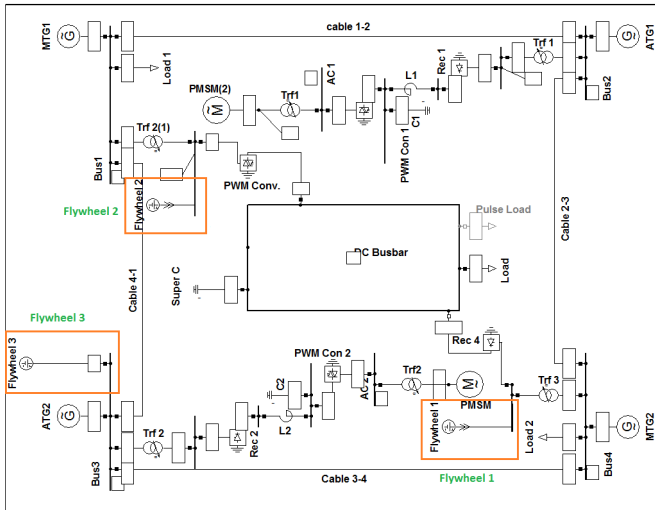


Fig. 1. Configuration of system under study.

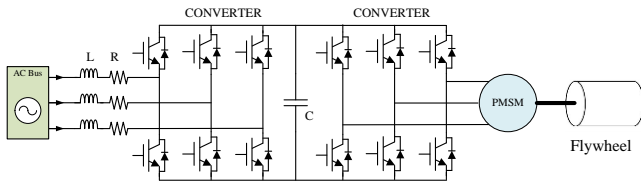


Fig. 2. Integration of flywheel through back to back six step converter.

Different simulation cases using DlgSILENT powerfactory software are run with flywheels installed at three different locations. The 3 locations of the 3 flywheels are selected as follows:

1. Flywheel 1: is installed on the low voltage side of the transformer connected to the main generator 2.

2. Flywheel 2: is installed on the low voltage side of the transformer connected to the main generator 1. Flywheels 1, 2 are responsible for supporting the power flow for the pulsed load on the DC bus.
3. Flywheel 3: is installed on intermediate location between generators 1 and 2, which is the bus of the auxiliary generator 2.

## II. KEY RESULTS

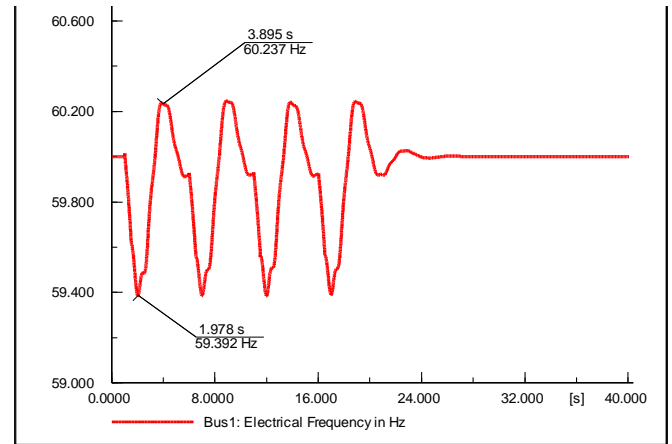


Fig. 3. System frequency without FESS.

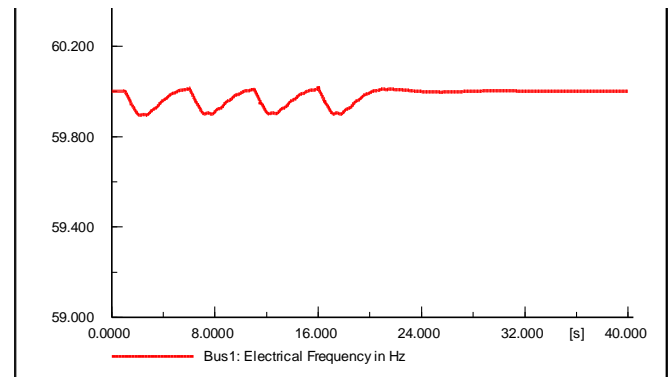


Fig. 4. System frequency with FESS.

## III. CONCLUSION

This work presents a study on the distributed FESS for mitigating the effects pulsed load. Three different cases are presented, the results of each case is analyzed and discussed. It is shown that flywheels can play an effective role in maintaining the system's stability and reduce the frequency oscillations. Furthermore, a comparison between the distributed and centralized FESS was conducted. It was shown that three small flywheels can provide better results than one large flywheel.

# Holonic Architecture for Loss Minimization in Distribution Systems with High Rooftop PV Penetration

A. R. Malekpour, *Graduate Student Member, IEEE*, A. Pahwa, *Fellow, IEEE*, and B. Natarajan, *Senior Member, IEEE*

Department of Electrical and Computer Engineering, Kansas State University, Manhattan, KS 66506, USA,

Email: [malekpour@ksu.edu](mailto:malekpour@ksu.edu), [pahwa@ksu.edu](mailto:pahwa@ksu.edu), [bala@ksu.edu](mailto:bala@ksu.edu)

**Abstract--** Over the next few decades, the number of customers installing rooftop solar generation will increase dramatically. Hence, there may be significant potential to reduce electric losses and take advantage of inverter-based PV units to manage Power distribution systems (PDS) more efficiently. Moreover, deploying smart devices will add further complexity to the PDS which is, by nature, highly distributed and hierarchical in structure. Basically, PDS is composed of unbalanced three phase and single phase feeders and laterals serving customers through unbalanced line configurations with different phase loading levels. Therefore, house level PVs with active/reactive power injection capability in an unbalanced network may result in voltage violation for a phase or three phase voltage imbalance at a bus. Hence, the reactive power injection capability of smart inverters for loss reduction and voltage control in PDS with large penetration of PV generation is becoming an emerging research area.

To capture the energy saving benefits associated with house level PVs and based on the hierarchical nature of PDS, this paper proposes a holonic architecture to minimize the power losses in a decentralized scheme. Thanks to the concept of holarchies, a three-level Holonic optimization is suggested to minimize the power losses by optimizing the utilization of renewable resources. In particular, the optimization problem determines the optimal reactive power injection/absorption from house level inverter-based PV units.

## I. MODEL EQUATIONS

### A. Problem formulation

- Minimize power losses

$$f = \sum_{i=1}^{Nbr} R_i \times |I_i|^2$$

### B. Constraints

- Distribution power flow equations

$$P_i = \sum_{j=1}^{N_{bus}} V_i V_j Y_{ij} \cos(\theta_{ij} - \delta_i + \delta_j)$$

$$Q_i = \sum_{j=1}^{N_{bus}} V_i V_j Y_{ij} \sin(\theta_{ij} - \delta_i + \delta_j)$$

- Bus voltage limits

$$V_i^{\min} \leq V_i^t \leq V_i^{\max}$$

- Distribution line limits

$$|P_{ij}^{Line}| < P_{ij,max}^{Line}$$

- Reactive power limit of PV generators

$$|Q_{PV}| \leq Q_{PV}^{max}$$

## II. KEY FIGURES & RESULTS

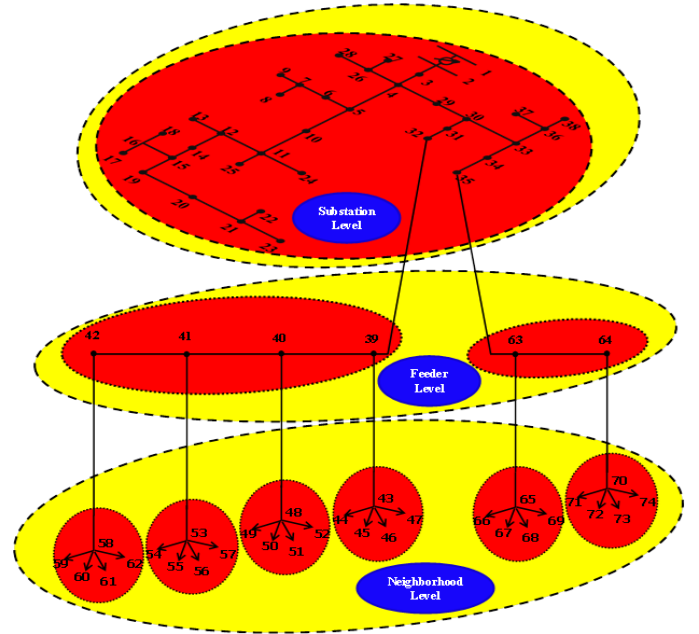


Fig 1: Representation of PDS as three-level holarchy

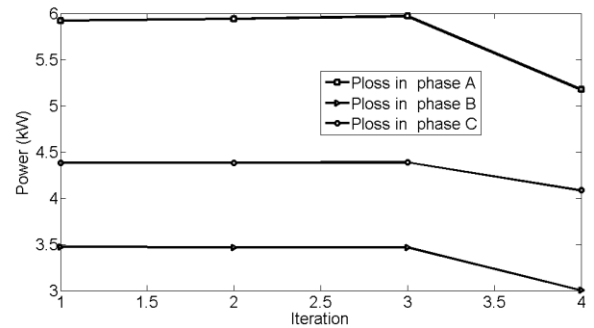


Fig. 2: Total three-phase power losses

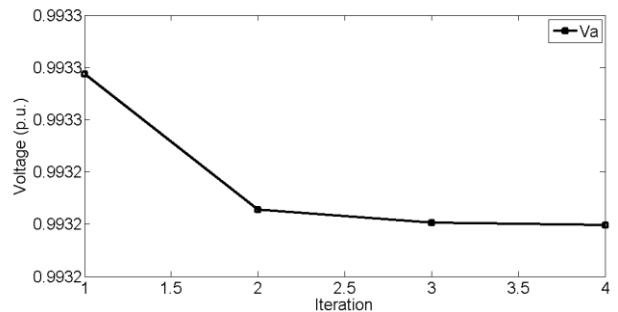


Fig. 2: Voltage in Phase A at node 32

# Multi-Agent-Based Information Collection Algorithm for Isolated Power Systems

Guanqun Wang<sup>1</sup>, Chen-Ching Liu<sup>1</sup> and Feng Liu<sup>2</sup>

1. School of Electrical Engineering and Computer Science, Washington State University, Pullman, WA, 99163, USA
  2. Department of Electrical Engineering, Tsinghua University, Beijing 100084, China
- Email: [gwang@eecs.wsu.edu](mailto:gwang@eecs.wsu.edu), [liu@eecs.wsu.edu](mailto:liu@eecs.wsu.edu) and [lfeng@mail.tsinghua.edu.cn](mailto:lfeng@mail.tsinghua.edu.cn)

**Abstract**—The power system used on shipboards, airplanes or space stations, for example, are classified as isolated power systems (IPS). Compared with traditional centralized structure of IPS, the multi-agent-based decentralized structure can serve as a better structure for its avoiding single-point-of-failure and improving the survivability of IPS in extreme conditions. In multi-agent system, agent can only communicate with its neighboring agents, thus raises the problem that how can one agent get global information through information exchange between its immediate neighbors. Based on decentralizing of the Adjacent Matrix Algorithm, a distributed information collection algorithm is proposed in this work. Agents can get the global state information of all loads, generators and switches through coordination and iteration of local information, and then obtain global topology of the entire system. Compared with existing methods, this algorithm has a better calculating efficiency and can recognize complicated fault scenarios in system like the communicating fault or loss of agents. Based on this algorithm, further application can be made in multi-agent system such as load shedding and system reconfiguration.

## I. KEY EQUATIONS

For a  $n$ -agent system,  $A = (a_{ij})$  is the adjacent matrix. Assuming  $x_i \in \mathbb{R}^n$  is the state vector of agent  $i$ , the iteration process is carried out as

$$x_i^{k+1} = \sum_{j=1}^n a_{ij} x_j^k$$

By iteration for at most  $n$  time, the global states of the system can be obtained by agent  $i$ .

## II. KEY FIGURES

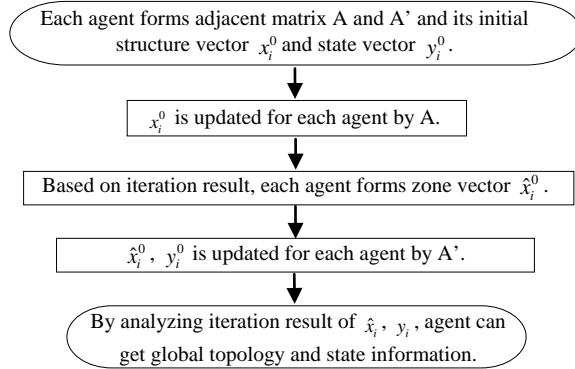


Figure 1. Flowchart of decentralized information collection algorithm

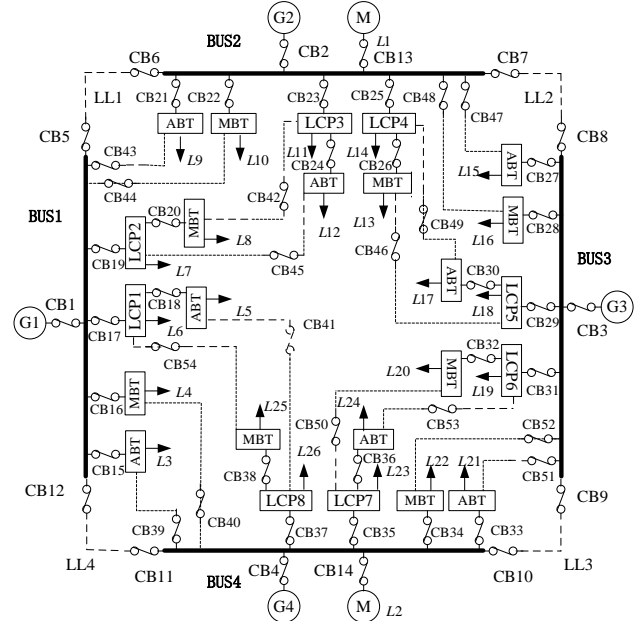


Figure 2. Simplified figure of a typical IPS

## III. KEY RESULTS

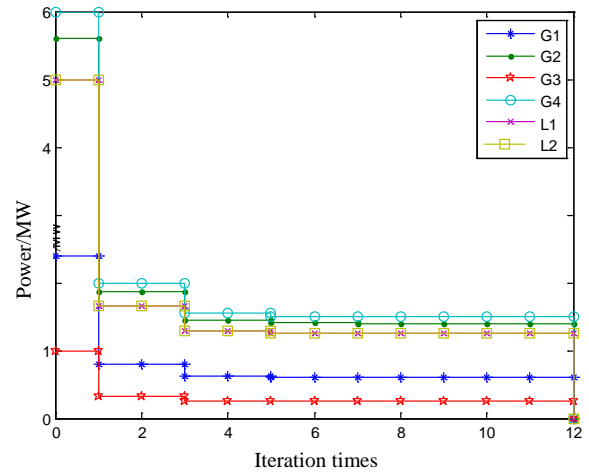


Figure 3. Iteration process of information collection algorithm

# Transmission Expansion Planning Under Uncertainty: the Stochastic Transmission Expansion Planning (STEP) Model

Pearl Donohoo<sup>1</sup>, *Member, IEEE*, Mort Webster<sup>2</sup>, *Member, IEEE* and Ignacio Pérez-Arriaga<sup>3</sup>, *Fellow, IEEE*

**Abstract--** The proposed integration of electricity markets and high penetrations of location-constrained renewable generation across wide-areas creates a major challenge to electric transmission network expansion planning (TNEP). To integrate location-constrained generation and energy markets areas the size of continental Europe or the Eastern Interconnect in the United States, hundreds to thousands of transmission nodes and investments must be considered. This change of scale compared to traditional planning produces two major problems: dimensionality and a change of scope from system reinforcement to system design.

The STEP model is a new approach to solving wide-area transmission network expansion planning. As a multi-stage stochastic method, the STEP model is able to capture trade-offs between economies of scale in new transmission lines and flexibility and adaptability required when planning under significant uncertainty. The STEP model optimizes patterns of transmission investment rather than individual transmission investments. This pattern-based approach has two major advantages. Overcomes the curses of dimensionality and allows for the optimization of more realistically-sized wide-area networks. Identifying optimal patterns of investment also provides two distinct sets of information to the system planner: a core set of transmission lines which form the network architecture and can be prioritized and a set of high value/low cost plans which can be built around this set of common core lines.

**Index Terms**—Transmission Expansion Network Planning, Power System Planning, Decision Making Under Uncertainty

## I. KEY FIGURES

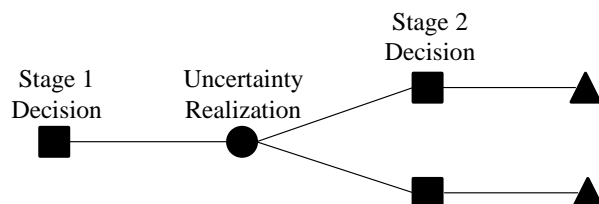


Figure 1: Illustration of Multi-Stage Stochastic Transmission Planning

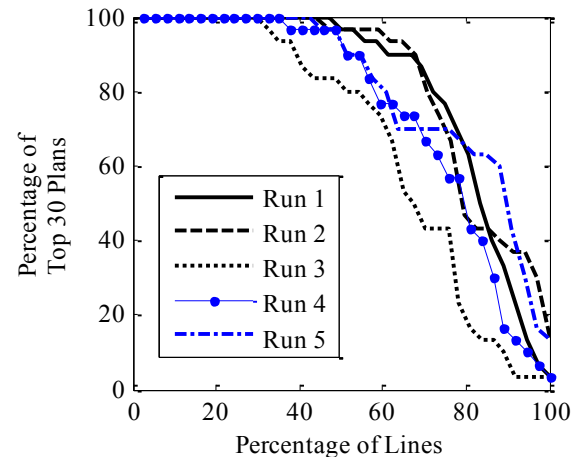


Figure 2: Frequency of Development for Transmission Lines Across Top 30 Plans for Each Model Run

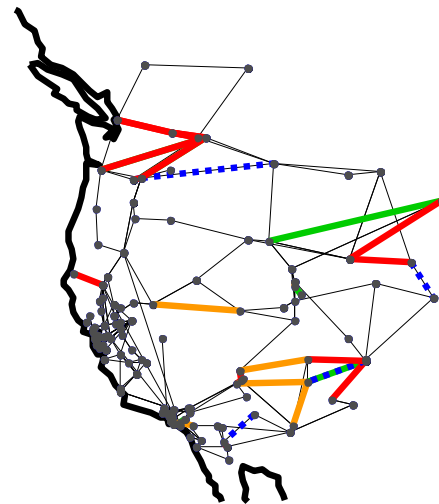


Figure 3: Transmission Lines Constructed 100% of Top Solutions (Red), >90% of Top Solutions (Orange), >50% Top Solutions (Green) and <50% Top Solutions (Blue-Dash)

This work was supported by the U.S. National Science Foundation grant number 835414, the U.S. Department of Energy, Grant No. DE-SC0005171 and from the National Science Foundation Graduate Research Fellowship.

<sup>1</sup> Pearl Donohoo is a post-doctoral researcher at Johns Hopkins University (email: pdv@jhu.edu)

<sup>2</sup> Mort Webster is an Associate Professor of Energy and Mineral Engineering at Pennsylvania State University (email: mdw18@psu.edu)

<sup>3</sup> Ignacio Pérez-Arriaga is a Professor and Director of the BP Chair on Sustainable Development at IIT, the Pontifical Comillas University (email: Ignacio.Perez@iit.upcomillas.es)

# An Investigation of Capacitor Control and Demand Response Actions for Voltage Spread Reduction in Distribution Systems

Nicole Segal and Karen Miu

Center for Electric Power Engineering, Department of Electrical and Computer Engineering  
Drexel University, Philadelphia, Pennsylvania, U.S.A.  
nus23@drexel.edu, karen@coe.drexel.edu

**Abstract**— This work investigates practical constraint determined control sequences of capacitors and demand response loads (DRL) for the voltage spread reduction objective during peak loading conditions. In particular, the purpose of the work is to examine the interaction between demand response and capacitor control. This is important because there is a continued effort to reduce peak load as a means to improve energy efficiency [1]. As more demand response participants emerge a re-evaluation of capacitor control schemes which were previously based on time of day algorithms or voltage set points is warranted.

Reduction of peak load can be facilitated by performing voltage spread reduction with feeder capacitor banks supplying voltage support [2]. Voltage spread reduction aims to minimize the voltage differential along all feeders in the network, thereby allowing system operators to reduce substation voltages. Therefore, the problem is initially studied as the capacitor control problem and is formulated to address voltage spread reduction in distribution networks.

Another technique utilities employ to reduce peak load conditions is demand response. The utility provides financial compensation for residential customers to decrease or delay their electric load for a given period of time in response to a price signal or network reliability concern. The locations of DRL are not controlled with respect to a system viewpoint.

Following [3], the problem is studied using an in-service distribution circuit. The location and size of capacitors are provided. Additionally, the peak and minimum load profile as well as the average load profile have been given. Subsequently, control sequences were determined and the number and order of control actions were evaluated.

## I. KEY EQUATIONS

$$\min_{u_k \in U} \max_{\substack{p \in \{a,b,c\} \\ i,j \in N}} \left\| |V_i^p(u_k)| - |V_j^p(u_k)| \right\| \quad (1)$$

*Subject To :*

$\exists$  a control sequence:

$$u_{cs} = [u_1, \dots, u_{k-1}, u_k, u_{k+1}, \dots, u_{N_{LL}}] \quad (2)$$

where, alphabetically:

$N$  : set of all buses

$N_{LL}$  : number of load levels

$p$  : present phase ( $a, b, c$ ) at a bus  $i$

$U$  : search space of capacitor placement and control schemes

$u_k$  : a binary vector of nodal capacitor and demand response settings at a load level  $k$

$u_1, u_{N_{LL}}$  : a binary vector of capacitor and demand response settings at the initial and final load setting, respectively

$u_{cs}$  : a feasible set of binary control actions that transitions from  $u_1$  to  $u_{N_{LL}}$

$V_k$  : vector of complex node (bus and phase) voltages at  $k$ th load setting,

$V_i^p, V_j^p$  : voltage magnitude at bus  $i$  and bus  $j$ , for a phase  $p$

The objective in (1) also is subject to electrical constraints, such as, a multi-phase unbalanced power flow with detailed network components. The system is also subject to operating constraints, such as, the maximum number of switch operations, voltage restrictions, reactive power considerations and thermal limitations.

## REFERENCES

- [1] Pennsylvania Act 129, October, 2008, Pennsylvania Public Utility Commission (PUC), <http://www.puc.state.pa.us/>, 2008. August 25, 2011  
<[http://www.puc.pa.gov/filing\\_resources/issues\\_laws\\_regulations/act\\_129\\_information.aspx](http://www.puc.pa.gov/filing_resources/issues_laws_regulations/act_129_information.aspx)>.
- [2] N. Segal, M. Kleinberg, A. Madonna, K. Miu, H. Lehmann, T. Figura, "Analytically Driven Capacitor Control for Voltage Spread Reduction," *IEEE Power Engineering Society Transmission and Distribution Conference and Exposition 2012*, pp.1-4, May 7-10, 2012.
- [3] N. Segal, A. Madonna, M. Kleinberg, K. Miu, H. Lehmann, T. Figura, "Realizable Constraint Driven Capacitor Placement and Control Sequences in Distribution Systems" submitted to *IEEE Trans. on Power System*.

# Modeling of Water Tree Capacitance in Underground Cables

Qi Chen, Klaehn Burkes, Elham Makram, Ramtin Hadidi

Clemson University, Clemson, South Carolina, USA

Email: [qic@clemson.edu](mailto:qic@clemson.edu)

**Abstract:** Water tree is corrosion phenomenon which can potentially lead to faults in underground cables. It is difficult to detect due to its high impedance and difficult to model due to its random nature. In this paper, a mathematical model is developed for the capacitance of a vented water tree originated from insulation surface. The model uses a section of linearly changing permittivity to represent water tree branches and finite element analysis to calculate the capacitance associated with water tree.

**Keyword:** water tree, vented tree, modeling, capacitance

## I. KEY FIGURE

Finite Element Analysis of Water Tree Afflict Region

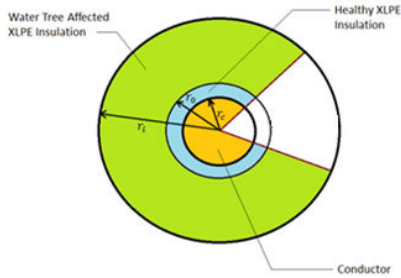


**Figure 1: Finite Element Analysis Cable Model**

The white pie shaped section in Figure 1 can be broken down into smaller piece as shown in Figure 2.

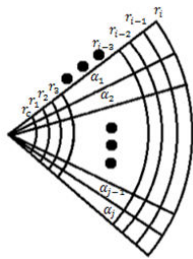


**Figure 2: Finite Element Analysis of the Ellipsoid Shape**

The cable insulation is separated into layers. Each layer is a concentric ring centered at the conductor. With sufficient number of layers, ellipsoid region becomes a component which occupies  $\frac{\alpha_i}{2\pi}$  portion of the concentric ring.

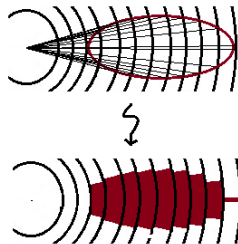


**Figure 3: FEM Breakdown of Ellipsoid Shape**

## II. KEY EQUATION

The cable capacitance can be calculated using the cylindrical capacitor with multiple dielectrics model.

$$C_{total} = \frac{2\pi L}{\frac{\ln(r_0/r_c)}{\epsilon_2} + \frac{\ln(r_i/r_0)}{\epsilon_1 * \frac{\alpha}{2\pi} + \epsilon_2 * (1 - \frac{\alpha}{2\pi})}}$$

So the capacitance equation expands to:

$$C_{total} = \frac{q}{V_{total}} = \frac{2\pi L}{\frac{\ln(r_0/r_c)}{\epsilon_2} + \frac{\ln(r_i/r_0)}{\epsilon_1 * \frac{\alpha}{2\pi} + \epsilon_2 * (1 - \frac{\alpha}{2\pi})}}$$

## III. KEY RESULT

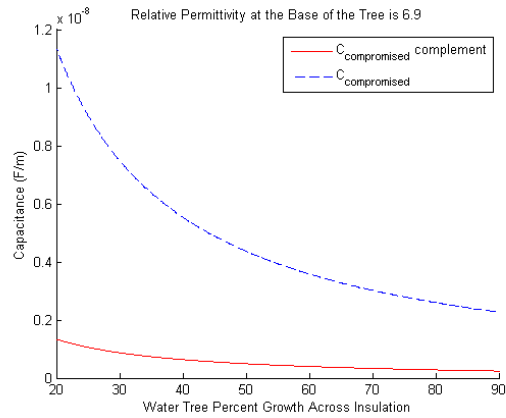


**Figure 4: Capacitance of Water Affected Area**

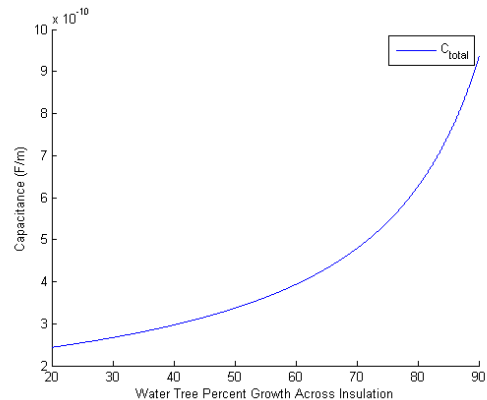


**Figure 5: Overall Capacitance**



# Outages on the GB Transmission Network due to Adverse or Extreme Weather

Kirsty Murray and Keith R.W. Bell

Department of Electronic and Electrical Engineering, University of Strathclyde, Glasgow, UK

[kirsty.murray@strath.ac.uk](mailto:kirsty.murray@strath.ac.uk), [keith.bell@eee.strath.ac.uk](mailto:keith.bell@eee.strath.ac.uk)

**Abstract**— There are current worries surrounding climate change and with some of the effects already being seen, such as a rise in coastal temperatures and more extreme weather, greater research into how society will be affected is required. With the possibility of increased frequency and intensity of adverse or extreme weather there is a concern that this will affect the reliability of the electricity transmission network in GB which currently suffers from regular faults with a significant percentage of them caused by adverse or extreme weather.

There have been many examples of how extreme weather can affect power grids all over the world. Wind storms Lothar and Martin hit France in December 1999 when nearly 3.4 million homes were left without power for up to 17 days and repairs cost almost €1.5 billion. Snow and ice can also cause complete and utter destruction of power systems as seen during the Canadian ice storm of 1998 where around 3 million people were left without power, some for up to a month during one of the worst winters seen and cost the operator billions of dollars to rebuild its electricity transmission network. The UK is also starting to experience similar difficulties with the severe wind storms hitting the UK in December 2011 and January 2012. Although less devastating than the previous examples, they still cause significant power outages for many people across the UK.

This research has investigated the current effects of weather on the transmission system using data supplied by the three transmission companies that own and operate the GB network: Scottish Power Ltd., National Grid plc. and SSE plc. It has been found that on average 50% of faults that occur on the transmission network are caused by weather with, generally, the three main weather causes being ‘Lightning’, ‘Snow, Sleet, Blizzard and Ice’, and ‘Wind and Gales’. The research discussed in this poster will focus on extreme and adverse weather and its effects on the GB transmission network. It also presents the beginnings of a relationship between the top three weather types.

## I. KEY EQUATIONS

Using Bayes’ theorem to calculate the probability of a fault occurring if a certain weather type occurs is an important feature as it will allow changes to the weather type occurrences to be made and see what the effects will be on the fault numbers and in turn the overall fault rate and security of the network. Where  $P(A|B)$  is the probability of a weather related fault occurring based on a weather type within the bin occurring.  $P(B)$  is the probability of a weather type in each bin occurring based on historical records.

$P(B|A)$  is the total number of faults occurrences in each bin divided by the total number of occurrences over all bins and  $P(A)$  is the fault rate for weather related faults.

$$P(A|B) = \frac{P(B|A) \times P(A)}{P(B)} \quad (1)$$

## II. KEY RESULTS

There are three types of weather that have caused 85% of weather related faults: ‘Lightning’, ‘Snow, Sleet, Blizzard & Ice’ and ‘Wind, Gales and Windborne Objects’. Overhead line faults were further analysed to determine the fault rate on a *per year per 100 km* basis for each company, to allow for comparison.

TABLE I. OHL WEATHER FAULT RATES PER YEAR PER 100 KM

Category	Mean per year per 100km			Median per year per 100km		
Company	A	B	C	A	B	C
Lightning	0.43	0.27	0.29	0.36	0.20	0.30
SSB & Ice	0.47	0.41	0.03	0.18	0.06	0.00
Wind & Gales	0.38	0.55	0.12	0.20	0.14	0.05
Total	1.34	1.33	0.55	1.19	0.67	0.55

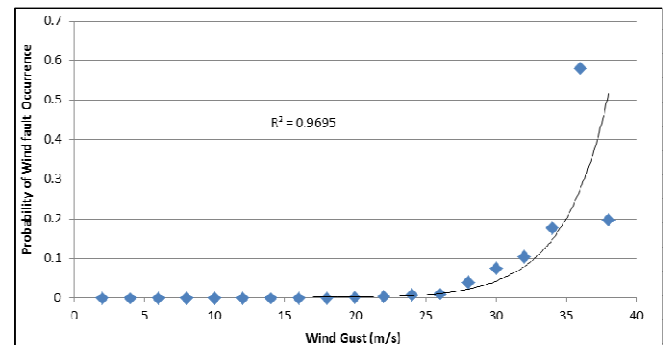


Fig. 1. Probability of a Fault Occurring for each 10meter Wind Gust

Fig. 1 shows that there is a logarithmic trend to the probabilities i.e. as the wind gusts increase as does the probability of a fault occurring. It also shows the coefficient of the determination ( $R^2$ ) for this logarithmic fit. This value means that 97% of the variation of the probability of a wind fault occurrence is caused by the magnitude of the 10 m wind gusts.

# Applications of Direct Matrix Converters for Type-4 Wind Turbines

Tuan Ngo and Surya Santoso

Department of Electrical and Computer Engineering, The University of Texas at Austin.

**Abstract**— A Type-4 wind turbine with a matrix converter has been modeled in the time-domain and simulated. A Type-4 wind turbine is typically comprised of a generator and a back-to-back PWM converter to transfer power. The matrix convert is superior to the voltage source back-to-back converter in Type-4 wind turbine application since it delivers power directly to the grid using only one power conversion stage and without using any storage components. The output frequency in the matrix converter is converted from the input frequency by switching devices and is stabilized while the input frequency fluctuates. In addition, the active and reactive power in the matrix converter can be independently controlled. The converter can also provide enough reactive power for the generator to start up. In this paper, the frequency response and the possibility to decouple power controllers of the matrix converter are verified by simulation results..

## I. KEY EQUATIONS

The output voltage and input voltage relation of the matrix converter (Mx $C$ ) is given by:

$$\begin{bmatrix} v_A(t) \\ v_B(t) \\ v_C(t) \end{bmatrix} = \begin{bmatrix} m_{11} & m_{12} & m_{13} \\ m_{21} & m_{22} & m_{23} \\ m_{31} & m_{32} & m_{33} \end{bmatrix} \begin{bmatrix} v_a(t) \\ v_b(t) \\ v_c(t) \end{bmatrix}$$

With the modulation index is modeled as

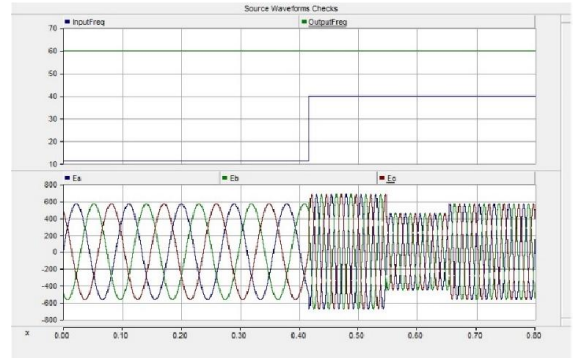
$$\begin{aligned} m_{11} &= \Delta + M_a + (k_m + k_A)\sin(\omega_i t - \varphi) \\ m_{12} &= \Delta + M_b + (k_m + k_A)\sin(\omega_i t - \varphi - 2\pi/3) \\ m_{13} &= \Delta + M_c + (k_m + k_A)\sin(\omega_i t - \varphi - 4\pi/3) \\ m_{31} &= \Delta + M_a + (k_m + k_C)\sin(\omega_i t - \varphi) \\ m_{32} &= \Delta + M_b + (k_m + k_C)\sin(\omega_i t - \varphi - 2\pi/3) \\ m_{33} &= \Delta + M_c + (k_m + k_C)\sin(\omega_i t - \varphi - 4\pi/3) \\ m_{21} &= \Delta + M_a + (k_m + k_B)\sin(\omega_i t - \varphi) \\ m_{22} &= \Delta + M_b + (k_m + k_B)\sin(\omega_i t - \varphi - 2\pi/3) \\ m_{23} &= \Delta + M_c + (k_m + k_B)\sin(\omega_i t - \varphi - 4\pi/3) \end{aligned}$$

where

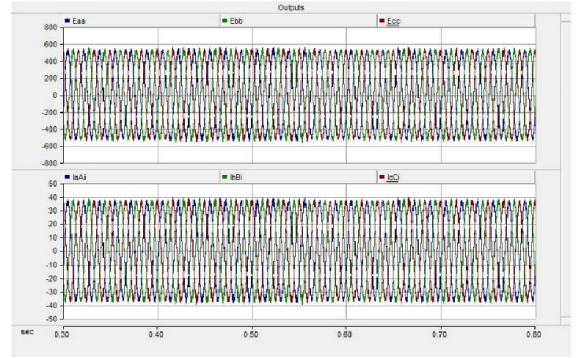
$$\begin{aligned} M_a &= |0.5 \sin(\omega_i t - \varphi)| \\ M_b &= |0.5 \sin(\omega_i t - \varphi - 2\pi/3)| \\ M_c &= |0.5 \sin(\omega_i t - \varphi - 4\pi/3)| \\ \Delta &= (1 - M_a - M_b - M_c)/3 \\ k_A &= k \sin(\omega_o t) \\ k_B &= k \sin(\omega_o t - 2\pi/3) \\ k_C &= k \sin(\omega_o t - 4\pi/3) \\ k_m &= -0.5(\text{MAX}(k_A, k_B, k_C) + \text{MIN}(k_A, k_B, k_C)) \end{aligned}$$

## II. KEY RESULTS

The simulation results for changing input voltage frequency and magnitude are presented. In addition, the decoupling real and reactive power ability is indicated by phase angle difference between input voltage and current waveforms.



(a)



(b)

Fig. 1. (a)The input voltage and frequency changes, (b) The output voltage and current waveforms.

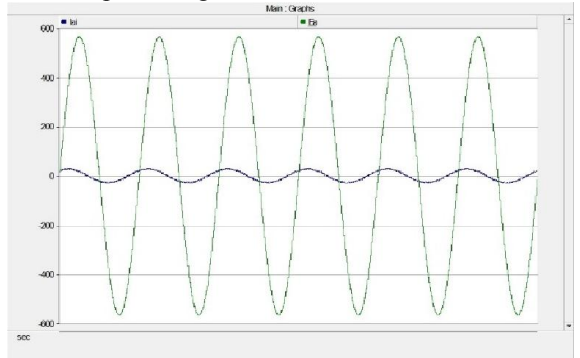


Fig. 2. The input current and voltage phase difference for decoupling power control.

# Improving Performance of Single-Phase SOGI-FLL under DC-Offset Voltage Condition

Tuan Ngo and Surya Santoso

Department of Electrical and Computer Engineering, The University of Texas at Austin.

**Abstract**— The second-order-generalized-integrator frequency-locked loop (SOGI-FLL) is typically employed to synchronize with the grid in the single-phase grid-connected converter. The SOGI creates two orthogonal signals from an input grid voltage, and estimates the magnitude while the frequency locked-loop identifies the grid frequency. If there is a DC component in the grid voltage due to the measurement process, it degrades the accuracy of SOGI-FLL estimates. The SOGI-FLL, therefore, cannot identify accurate information of the grid voltage. This paper introduces an improved control method for the SOGI-FLL when the grid contains a DC component. The value of the DC component voltage is estimated online and totally removed from the frequency control loop. The controller, thus, responds faster and more precisely detects both the magnitude and frequency of the input voltage. Simulation results are presented to verify the theoretical analyses.

## I. KEY EQUATIONS

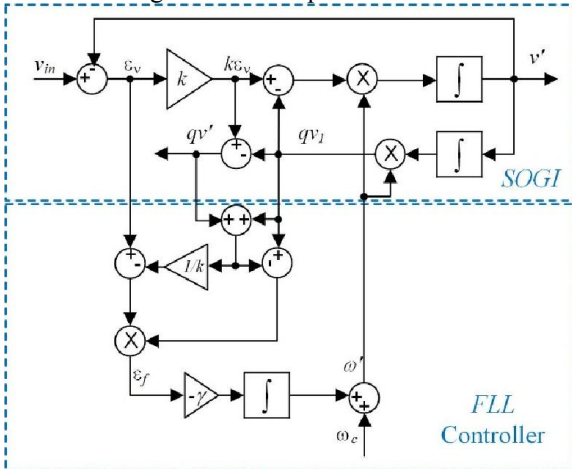
The two orthogonal output signal of the improved SOGI-FLL is given by:

$$v'(t) = V \sin(\omega't) + \frac{(kA - V)}{\sqrt{1 - (k/2)^2}} e^{-\frac{k}{2}\omega't} \sin(\omega' \sqrt{1 - (k/2)^2} t)$$

$$qv'(t) = V \cos(\omega't) - \frac{(kA - V)}{\sqrt{1 - (k/2)^2}} e^{-\frac{k}{2}\omega't} \sin(\omega' \sqrt{1 - (k/2)^2} t + \cos^{-1}(k/2))$$

## II. KEY FIGURE

The block diagram of the improved SOGI-FLL method is:



## III. KEY RESULTS

The simulation results for a DC offset in the input voltage are presented. The output signals are perfectly orthogonal. In addition, the grid frequency is detected correctly.

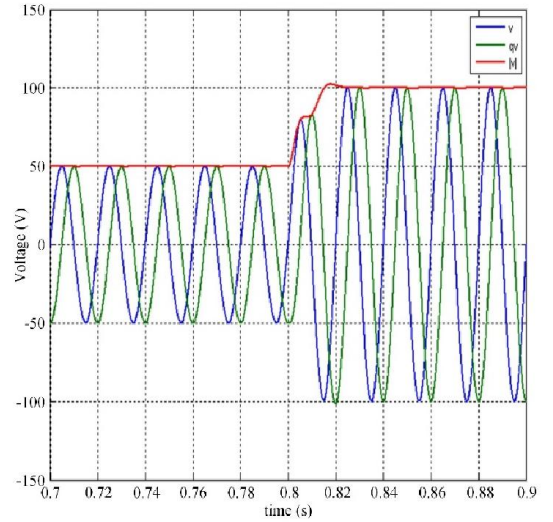


Fig. 1. The output voltages of the improved method.

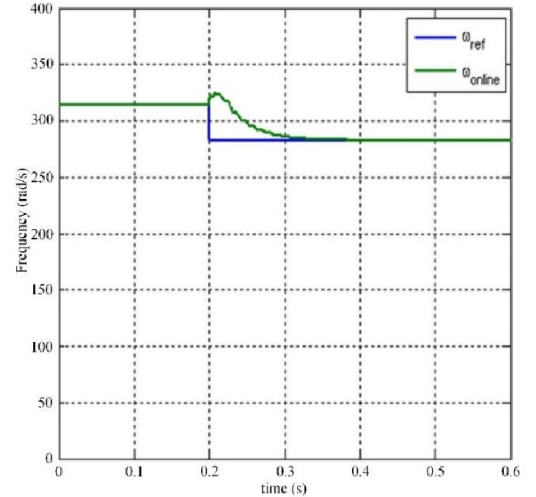


Fig. 2. The frequency control response.

# Implications of Cyber Attacks on Distributed Power System Operations

Jiazi Zhang, Lalitha Sankar, Kory Hedman  
 Dept. of Electrical, Computer, and Energy Engineering,  
 Arizona State University, Tempe, AZ 85287.  
 Email: {jzhan188,lalithasankar,kory.hedman}@asu.edu

**Abstract**—While the electric grid is managed in a distributed fashion, it requires data sharing and information exchange between operators managing inter-connected areas for reliable functioning. A class of cyber-attacks that limit real-time topology information sharing is introduced and the consequences of such attacks are studied in this paper. It is shown that local outages that percolate through the network as a result of limited data sharing can be mimicked by this class of cyber-attacks. Countermeasures for such attacks are also presented.

**Index Terms**—Cyber-attack, Topology, Information Sharing

## I. INTRODUCTION

In this paper, we focus on a class of cyber-attacks that limit information sharing between two inter-connected areas. The aim of our proposed class of attacks is to limit information sharing between adjacent areas particularly when one area is experiencing topology changes (e.g., line outages either due to natural or malicious causes) in an effort to quantify both the consequences of limited data sharing and the countermeasures. While wide-area monitoring and information sharing has been proposed by the Federal Energy Regulatory Commission, real-time data sharing in the grid is still done in an ad hoc manner between connected areas. For example, in the Northeast blackout of 2003, a line out in one area (Ohio) was not conveyed for a sufficient period of time to the Midwest Operator leading to failure of convergence of the state estimator and other cascading problems. We introduce a class of distributed communication attacks wherein an attack on the Energy Management System (EMSs) of one area causes it to share the same static topology information with the other area (in automated systems where topology may be shared real-time or frequently, this can be achieved via software-based duplication attacks). To understand the broader consequences of (unobservable) attacks on measurements or shared data, we focus on a distributed two-area (managed by two control centers) network. We focus on attacks that create or exploit outages in one area and limit information sharing via a communication attack thereby affecting the power flow solutions and dispatch in a connected area that has incorrect topology information. Our results demonstrate that such an attack in a distributed power network leads to a range of possibilities from relatively benign oscillations in the power flow solutions between the two areas that eventually fix themselves (infrequent) to more complex situations (more likely) over time including voltage instability, progressively

severe lack of convergence of OPF in both areas, and actual physical line overflows that are not observable from the cyber measurements that can eventually cause line overheating and cascading outages.

## II. KEY FIGURE

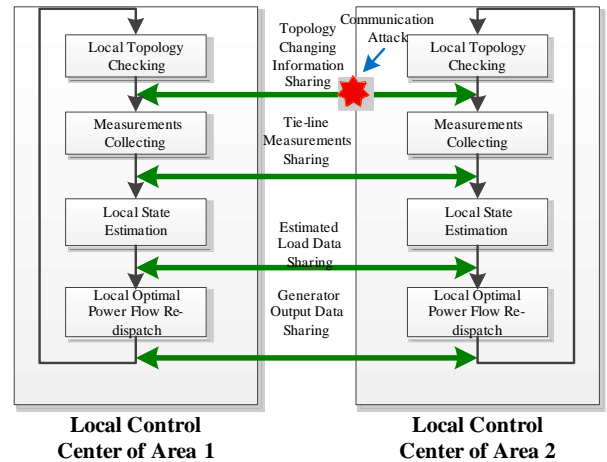


Figure 1. Computational units and data interactions between the two areas of the network

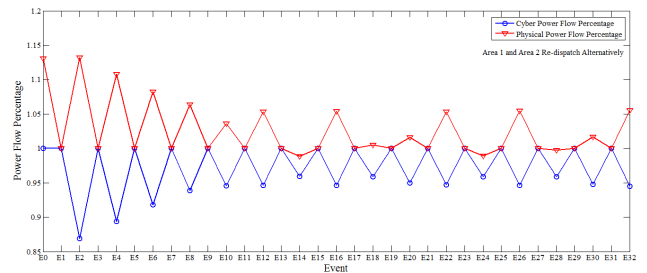


Figure 2. Typical Attack Results - Power Flow Overload Oscillating Case

# Modeling Six-level MMC with PQ Control in Simulink

Yin Li, Student Member, IEEE, Yan Ma, Student Member, IEEE

**Abstract**—In this project, a six-level Modular Multilevel Converter (MMC) is designed with a modified phase-shift pulse-width-modulation (PS-PWM) in Simulink. The converter's output is connected to a three-phase grid and it is controlled by output real and reactive power. This project also employs a circulating current suppressing controller (CCSC) in the MMC. The purpose of the CCSC is to reduce the ripple generated by the multilevel switches. To control the effect of the double and quadruple-frequency components of the circulating current, the corresponding PR controller is designed for each phase. The results of this project are produced by the Simulink of Matlab.

**Index Terms**—Circulating current, Modular multilevel converter (MMC), PS-PWM, Double and quadruple frequency.

## I. SYSTEM CONFIGURATION

The topology of this project is shown in Fig.1. It consists of a 60kV DC voltage source, a six-level modular multilevel converter, and a three-phase grid with 20kV voltage rating. The advantage of MMC is to avoid series connection of power-electronic switches and to reduce the stresses on devices. The six-level MMC has 6 sub-models in each arm, each sub-model is a single phase buck converter shown in Fig.2. For a three-phase MMC, inner difference current,  $I_{diff,j}$ , will be generated in each phase. The inner difference current contains DC component, double and quadruple-frequency components. To reduce the effect (or amplitude) of the AC components of  $I_{diff,j}$ , the circulating current suppressing controller (CCSC) is designed with PR controller. The output of the CCSC are the inner unbalance voltage,  $u_{diff,j}$ . The PS-PWM signal will be generated based on  $u_{diff,j}$  and the desired EMF of the converter which the output the power control loop. Fig.4 shows the effect of CCSC, after one second the CCSC is activated, the circulating current is limited in tens amperes.

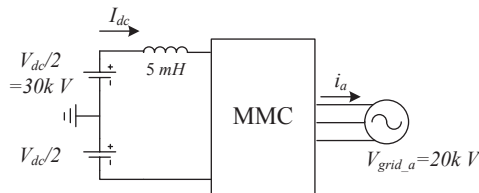


Fig. 1. The topology of the project (5mH inductor is to reduce the ripple of the DC input current when the CCSC starts to work)

## II. KEY RESULTS IN SIMULINK

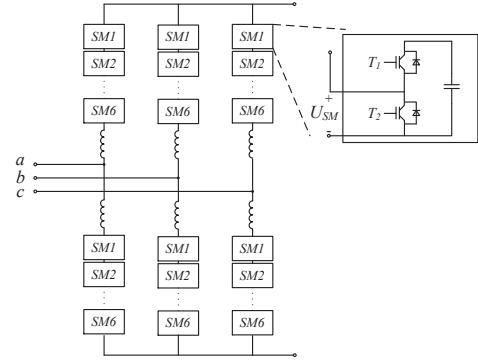


Fig. 2. It is the three-phase six-level MMC and the right upper figure displays the sub-module.

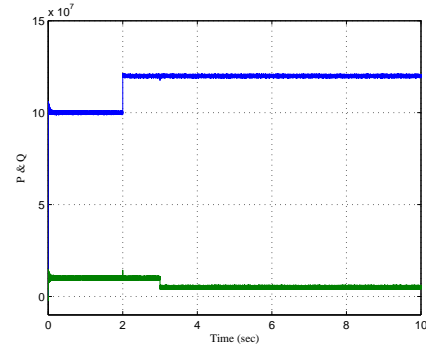


Fig. 3. The initial value: P(real power)=100MW, Q(reactive power)=10MVA; P increases to 120MW at 2s; Q increases to 5MVA at 3s.

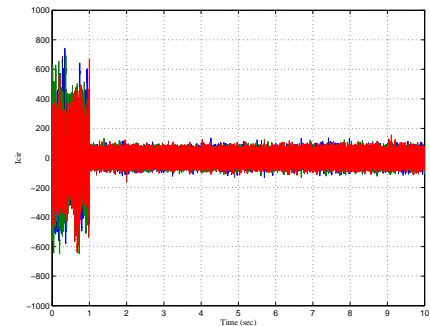


Fig. 4. From 1s, CCSC starts to work and the ripple of the circulating current,  $I_{cir}$ , is reduced to 40A from 500A.



# Improved Method for Locating Faults Upstream from Distributed Generation

Kyung Woo Min, Surya Santoso  
The University of Texas at Austin

**Abstract**—Impedance-based fault locating methods use voltage and current measurements to estimate the distance to fault locations. This paper discusses the effect of distributed generation (DG) on fault location estimates when a fault occurs upstream from the DG. By using the estimated measurements at the point of interconnection (POI), the errors in fault location estimates are reduced to at most 1.33% for all simulation cases.

**Index Terms**—Fault location, distributed power generation, power quality, power system reliability

## I. FAULT LOCATING APPROACH IN DISTRIBUTION SYSTEMS WITH DISTRIBUTED GENERATION

Consider a distribution system shown in Fig. 1. The substation and a local synchronous generator are connected at the POI. Using the pre-fault measurements from the substation and DG, the synchronization operator  $e^{j\theta}$  can be derived as in (2).

$$V_G - I_G \times dZ_{line} = V_{DG}e^{j\theta} - I_{DG}e^{j\theta} \times Z_{line,DG} \quad (1)$$

$$e^{j\theta} = \frac{V_G - I_G \times dZ_{line}}{V_{DG} - I_{DG} \times Z_{line,DG}} \quad (2)$$

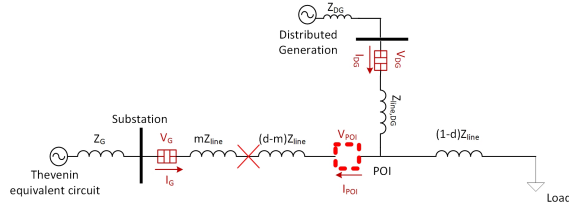


Fig. 1. Fault is located upstream from DG.

An improved method is described as follows. A virtual monitor is assumed to be present in the POI facing the substation as shown in Fig. 1. Then pre-fault (subscripted *pre*) and during-fault measurements (subscripted *flt*) captured at this monitor can be estimated using the measurements taken at the substation and the DG.

$$V_{pre,POI} = V_{pre,DG} - I_{pre,DG} \times Z_{line,DG} \quad (3)$$

$$V_{flt,POI} = V_{flt,DG} - I_{flt,DG} \times Z_{line,DG} \quad (4)$$

$$I_{pre,POI} = -I_{pre,G} \quad (5)$$

$$I_{flt,POI} = I_{flt,DG} - \frac{V_{flt,POI}}{(1-d)Z_{line} + Z_{load}} \quad (6)$$

$$Z_{load} = \frac{V_{pre,G} - I_{pre,G} \times dZ_{line}}{I_{pre,G} + I_{pre,DG}} - (1-d)Z_{line} \quad (7)$$

The measurements from this virtual monitor can be used in the application of the two-ended method and can provide the remote source impedance for the Eriksson method.

## II. APPLICATION OF PROPOSED FAULT LOCATING APPROACH ON SIMULATED FAULT DATA

The fault location estimated using the POI measurements and without using the POI measurements are compared in this section. Single line-to-ground faults are considered for each simulated fault.

TABLE I  
FAULT LOCATION ESTIMATES FROM THE SUBSTATION WITH  $R_f = 5\Omega$   
(A) LUMPED LOAD (B) DISTRIBUTED LOAD

		(a)			
		Actual Location (1 mi.)		Actual Location (2 mi.)	
$R_f = 5$		Estimate (mi.)	Error (%)	Estimate (mi.)	Error (%)
Eriksson (Substation + DG)		1.23	3.83	2.45	7.50
Neg.-sequence (Substation + DG)		0.93	-1.17	1.94	-1.00
Eriksson (Substation + POI)		0.98	-0.33	2.00	0.00
Neg.-sequence (Substation + POI)		1.00	0.00	2.00	0.00
		(b)			
		Actual Location (1 mi.)		Actual Location (2 mi.)	
$R_f = 5$		Estimate (mi.)	Error (%)	Estimate (mi.)	Error (%)
Eriksson (Substation + DG)		1.30	5.00	2.52	8.67
Neg.-sequence (Substation + DG)		0.94	-1.00	1.96	-0.67
Eriksson (Substation + POI)		1.05	0.83	2.08	1.33
Neg.-sequence (Substation + POI)		1.01	0.17	2.02	0.33



# Optimal transformer rating in the presence of probabilistic electric vehicle charging

Sachin Argade and Visvakumar Aravinthan

Department of Electrical Engineering and Computer Science

Wichita State University

{sgargade, visvakumar.aravinthan}@wichita.edu

**Abstract**— Electric Vehicle (EV) charging has impact on distribution transformer loss of life. To accommodate increasing EV penetration on distribution system it is vital to get optimal rating for secondary distribution transformer. In this work size of a distribution transformer with no-load losses and capital cost is minimized while limiting the acceleration of the transformer loss of life and by taking in to consideration probabilistic EV charging. Charging patterns are developed using a probabilistic model for vehicle arrival time and charge left at arrival. These charging patterns are used for transformer loading on top of the base loading of the transformer.

**Index Terms**—Transformer sizing, probabilistic EV charging, transformer loss of life, reliability, distribution Transformer

## I. OBJECTIVE FUNCTION TO MINIMIZE NO LOAD LOSSES AND CAPITAL COST

Impact of electric vehicle charging to the grid is of vital concern for distribution systems. Based on the stochastic nature of the EV charging load, controlled charging strategies are investigated by the authors [1]. These strategies are used in this work to model the optimal sizing of secondary distribution transformer. Based on Fig.1 generalized relationship between a transformer no-load loss and a transformer rating ( $P_R$ ) is

$$P_{Loss} = bP_R + c \quad (1)$$

Where,  $b = 1.4191$   $c = 22.494$

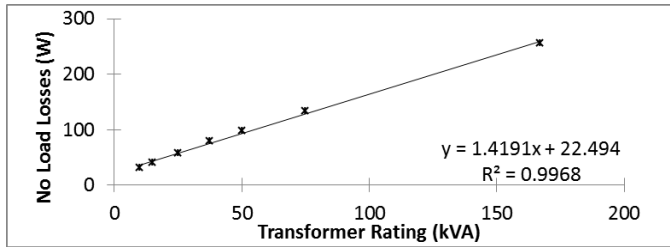


Fig. 1: Linearized Transformer Loss Curve for Single-Phase Transformer

Relationship between transformer rating and capital cost of transformer is given as [2]

$$Cost = K_1 P_R + K_0 \quad (2)$$

Cost of loss for a year is given as

$$Cost = P_{Loss} \times \underbrace{24 \times 365 \times \$}_{\alpha} \quad (3)$$

Objective of the work is to minimize no load losses as well as capital cost of the transformer hence objective function is

$$\min(\alpha P_{Loss} + Cost) \quad (4)$$

$$\min \left( \underbrace{\alpha b + K_1}_{\hat{b}} P_R + \underbrace{\alpha c + K_0}_{\hat{c}} \right) \quad (5)$$

$$\min(\hat{b} P_R + \hat{c}) \quad (6)$$

## II. CONSTRAINTS

**Transformer aging:** Based on IEEE std. C57.91–2011, transformer hot-spot temperature rise due to the electric vehicle charging for a day (annual average) is modified as,

$$\Theta P_R^2 - \sum \left[ \underbrace{\frac{\Delta \theta_{TO,R}}{(R+1)^{0.8}}}_{\psi} \left( P_R^2 + 0.8 \underbrace{(L_t)^2}_{\phi_t} R \right) + \underbrace{\Delta \theta_{H,R}}_{\beta_t} (L_{t-1}) P_R \right] \geq 0 \quad (2)$$

**Transformer loading:** In addition to limiting transformer loss of life due to EV charging, it is important to limit the maximum loading. Relation is given as

$$P_R \geq \eta L_{\max} \quad (3)$$

where  $L_{\max} = \max_{t=1, \dots, N} \{L_t\}$ , and  $\eta$  is maximum load limit factor.

## III. OPTIMAL SOLUTION

Lagrangian for the above problem could be developed as

$$L(P_R, \lambda_1, \lambda_2) = (\hat{b} P_R + \hat{c}) - \lambda_2 (P_R - \eta D_{MAX}) - \lambda_1 (\Theta - N\psi) P_R^2 - \left( \sum (\mathcal{G}_t) P_R - \sum (\beta_t) \right) \quad (4)$$

Where,  $\lambda_1$  and  $\lambda_2$  are slack variables. Since this is a convex problem, the Karush-Kuhn-Tucker (KKT) condition is used.

**The General Solution:**

$$P_R^* = \begin{cases} \frac{(\sum (\mathcal{G}_t)) \pm \sqrt{(\sum (\mathcal{G}_t))^2 + 4(\Theta - N\psi)(\sum (\beta_t))}}{2(\Theta - N\psi)} & \text{if } f \geq 1 \\ \eta L_{\max} & \text{if } f \leq 1 \end{cases} \quad (5)$$

$$f = \frac{(\sum (\mathcal{G}_t)) + \sqrt{((\sum (\mathcal{G}_t)))^2 + 4(\Theta - N\psi)(\sum (\beta_t))}}{2(\Theta - N\psi)\eta L_{\max}} \quad (6)$$

## IV. REFERENCE

- [1] S. Argade, V. Aravinthan, and W. Jewell, "Probabilistic modeling of EV charging and Its Impact on Distribution Transformer Loss of Life," in *Proc. 1<sup>st</sup> IEEE Int. Electric Vehicle Conference*, March 2012
- [2] J.J. Wakileh and A. Pahwa, 1996, "Distribution System Design Optimization for Cold Load Pickup", *IEEE Trans. on Power Systems*, vol. 11, no. 4, pp. 1879-1884

# Battery Energy Management System

Sherif Abdelrazek & Sukumar Kamalasan

This poster aims to present a summary of a complete electrochemical energy storage management scheme to maximize potential value that can be brought forth to medium voltage feeders. In general, the potential performance benefits produced by possible energy storage applications include improved system reliability, dynamic stability, enhanced power quality, transmission capacity enhancement and area protection. Here we propose a unique control algorithm that enhances coordination of ancillary services applications mainly voltage support along with renewables capacity firming. Optimization of control parameters and set points are considered for management between the mentioned applications. The design is tested on an EMTP simulation platform which provided valuable results.

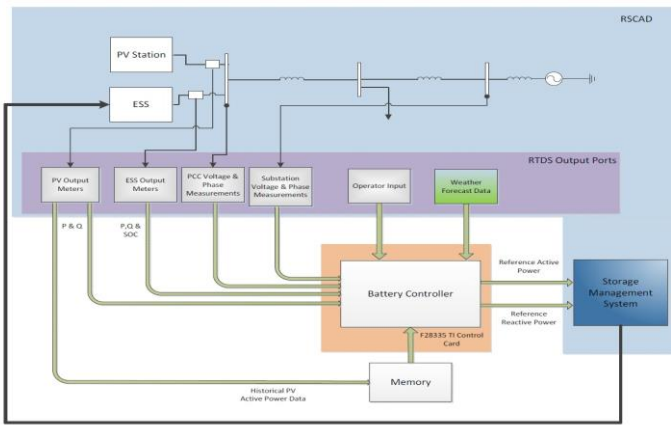


Fig 1: Data Acquisition Topology

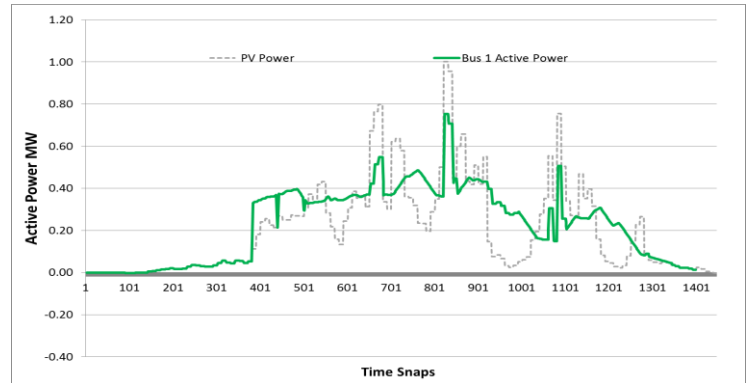


Fig 2: Sample Results for PV Smoothing

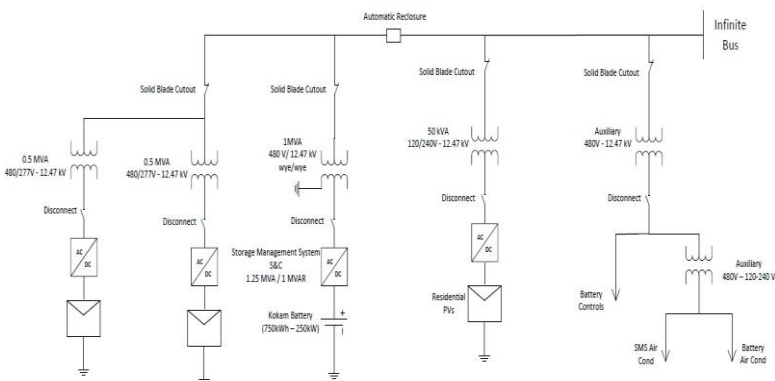


Fig 3: Test System Topology

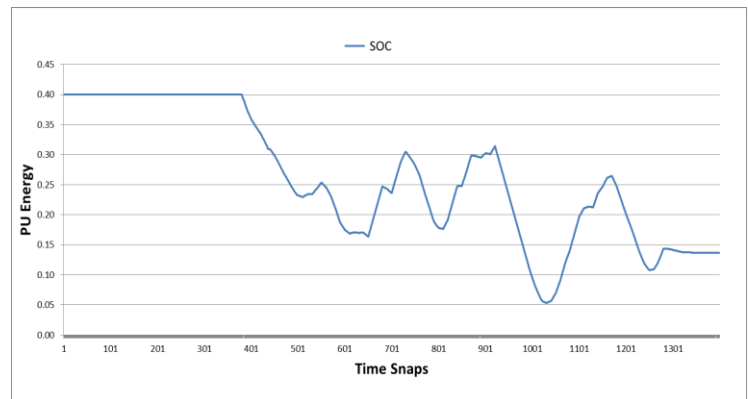


Fig 4: Battery SoC for shown sample day

# Wide Area Control of Multi-machine Power Systems using Online Coherency Analysis

Ke Tang, *Student Member, IEEE*, Ganesh K. Venayagamoorthy, *Senior Member, IEEE*  
 Real-Time Power and Intelligent Systems (RTPIS) Laboratory  
 The Holcombe Dept. of Electrical and Computer Engineering  
 Clemson University, SC 29634, USA  
 Emails: [ktang@clemson.edu](mailto:ktang@clemson.edu), [gkumar@ieee.org](mailto:gkumar@ieee.org)

**Abstract** – In multi-machine power systems, generators tend to oscillate in coherency groups. Study of generator coherency casts light on the inter-area mode of oscillation that can be damped by Wide Area Controller (WAC). In this study, a coherency-based controller that is adaptive to system operating condition is applied to realize WAC and maintain power system stability.

**Index Terms:** Generator coherency; multi-machine power system; damping; adaptive control

## INTRODUCTION

Low-frequency oscillation that includes both intra-area and inter-area modes is often observed in multi-machine power systems. Wide Area Controller (WAC) signals are employed to damp out inter-area modes by injecting a supplementary control signal that is based on global information into the Automatic Voltage Regulators (AVR). In most cases, since generators in power systems tend to be clustered in coherent groups that oscillate against each other in lower frequency range, the study of generator coherency can be a guideline for implementation of WAC.

Previous studies applied various control techniques such as H-infinity control in WAC; yet in most cases, generator coherency was not considered and the controllers were non-

adaptive. The notion of Virtual Generator (VG) was suggested in [1], and neural network based adaptive controller is employed. Yet the VG's are obtained by offline clustering, which is in contradiction to the fact that generator coherency may change in the real time.

An adaptive control scheme is applied in this study as indicated in Fig 1. VG's are formed by a real-time clustering algorithm; the virtual speed of each VG goes through a predesigned Wide Area Controller; later on, these several channels of Wide Area Controller are calibrated and assigned to each generator as supplementary by matrix switches. Prony analysis is applied to examine the benefit of this approach.

## REFERENCES

- [1] D. Molina, G. K. Venayagamoorthy, J. Liang and R. G. Harley, "Intelligent local area signals based damping of power system oscillations using virtual generators and approximate dynamic programming," *IEEE Transactions on Smart Grid*, vol. 4, pp. 498 – 508, January 2013.
- [2] M. Jonsson, M. Begovic and J. Daalder, "A new method suitable for real-time generator coherency determination," *IEEE Transactions on Power Systems*, vol. 19, pp. 1437–1482, 2004.
- [3] B. P. Padhy, S. C. Srivastava, K.N. Verma, "A Coherency-Based Approach for Signal Selection for Wide Area Stabilizing Control in Power Systems", *IEEE System journal*, vol. 7, pp. 807-815, 2013

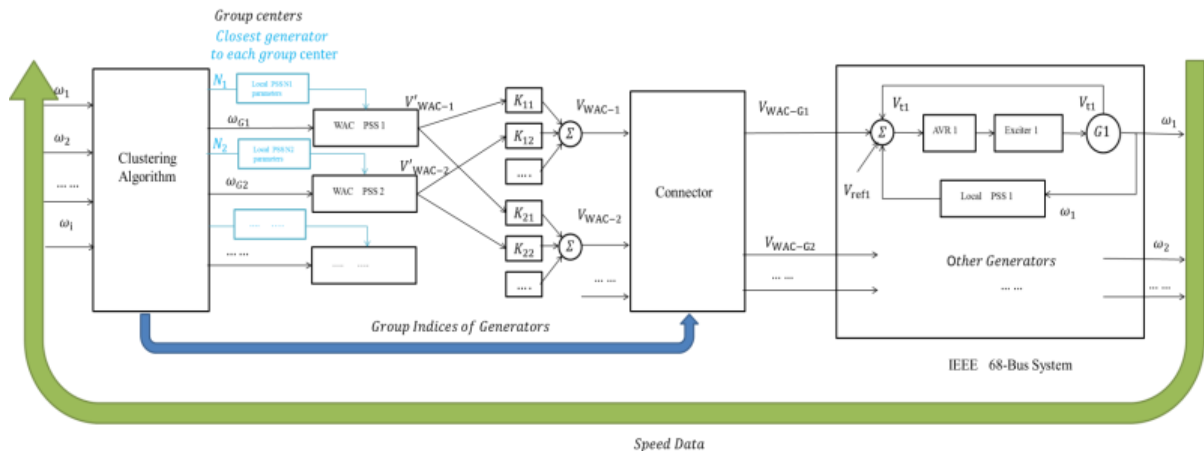


Fig 1. The diagram of control scheme

# A Power Factor-Based Estimator of Load Capability for Smart Distribution Systems

Nicholas S. Coleman, *Student Member, IEEE*, Karen N. Miu, *Member, IEEE*

**Abstract**—The availability of measurement devices in distribution grids makes short-term or real-time assessment of load capability possible at the distribution level. This paper defines a load capability estimator based on current and power factor metrics; specifically, a modified current-based estimator is presented and a power factor-based estimator is introduced. Cases are simulated on a 2055-bus distribution circuit to test an accompanying solution algorithm. Results demonstrate that the model and algorithm are effective, and justify monitoring load capability with respect to power factor in practical distribution systems that are subject to multi-phase, non-uniform load variations. The presented algorithm can replace repetitive power flow methods that utilize trial-and-error or expert systems. Computing load capability with respect to power factor constraints did not require an iterative process, and can be appended to existing techniques without increasing computational complexity. Future work can apply the model presented here to daily or weekly load forecasts to identify critical times when control actions are necessary.

**Index Terms**—load capability, power distribution, power factor, smart grids

## I. KEY EQUATIONS AND FIGURE

Current magnitude-limited load capability, originally presented in [2] and modified for this work is:

$$\lambda_I = \sum_{m=1}^M \left( \min_i \min_p \frac{I_{i,M}^{p,(m)}}{\sum_{j \in C_i} (\hat{S}_j^p / V_j^{p,(m)})^*} \right) \quad (1)$$

The power factor-based estimator is the primary contribution of this work. Power factor (PF)-limited load capability is:

$$\lambda_{h,PF} = \begin{cases} \infty, & \text{Conditions I, IV} \\ \frac{Q_{h,init}^p - \beta_{h,L}^p P_{h,init}^p}{\beta_{h,L}^p \hat{P}_h^p - \hat{Q}_h^p}, & \text{Condition II} \\ \frac{Q_{h,init}^p - \beta_{h,U}^p P_{h,init}^p}{\beta_{h,U}^p \hat{P}_h^p - \hat{Q}_h^p}, & \text{Condition III} \end{cases} \quad (2)$$

$$\lambda_{PF} = \min_h \min_p \lambda_{h,PF} \quad (3)$$

where load buses  $h \in D_{PF}$  have power factor constraints,  $\beta_{h,L,U}^p = \tan \phi_{h,L,U}^p = \tan(\text{acos}(PF_{h,L,U}^p))$  are power ratios corresponding to lower/upper limits on the PF angles  $\phi_{h,L,U}^p$ ,

$P_{h,init}^p, Q_{h,init}^p$  are initial injection conditions,  $\hat{P}_h^p, \hat{Q}_h^p$  are forecasted injection variations, and the conditions on each node are defined as:

- I: PF tending towards an acceptable value.
- II: PF tending towards a value that violates the lower limit.
- III: PF tending toward a value that violates the upper limit.
- IV: PF constant, but the complex load is decreasing.

The active condition on a node can be determined graphically using Fig. 1. Overall load capability is:

$$\lambda = \min\{\lambda_I, \lambda_{PF}\} \quad (4)$$

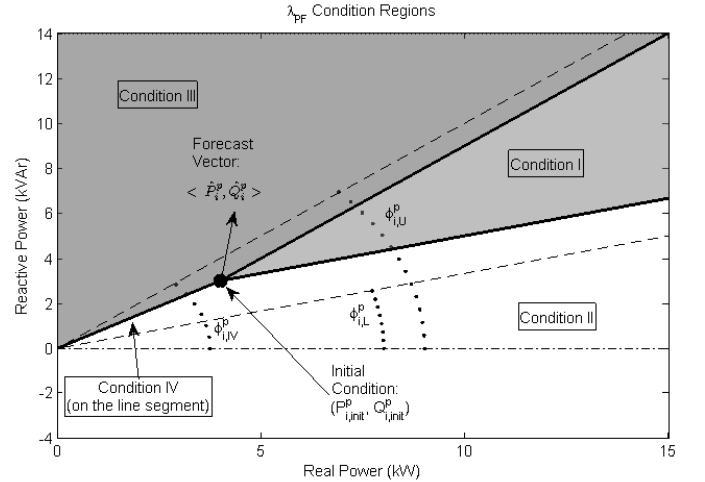


Fig 1. The region between the two dashed lines (inclusive) contains operating points with acceptable power factors. When a forecast vector falls into either the Condition II or Condition III region, the operating point will eventually cross a dashed line, thus resulting in unacceptable power factor. In this example, the forecast vector lies in the Condition III region; load capability is limited by the upper power factor constraint on this phase.

## II. KEY REFERENCES

- [1] P. W. Sauer, R. J. Evans Jr. and M. A. Pai, "Maximum unconstrained loadability of power systems," in *Circuits and Systems, 1990., IEEE International Symposium on*, New Orleans, 1990.
- [2] K. N. Miu and H.-D. Chiang, "Electric distribution system load capability: problem formulation, solution algorithm, and numerical results," *Power Delivery, IEEE Transactions on*, vol. 15, no. 1, pp. 436-422, Jan. 2000.
- [3] J.W. Bialek, P. Varaiya, F. Wu, J. Zhong, "Risk-limiting dispatch of smart grid," in *Power and Energy Society General Meeting, 2010 IEEE*, pp.1,2, 25-29 July 2010.
- [4] N. S. Coleman, "Load Capability for Smart Distribution Systems," M.S. thesis. Dept. of Electrical and Computer Engineering, Drexel Univ., Philadelphia, PA, 2013.

# Modeling Six-level MMC with PQ Control in Simulink

Yin Li, Student Member, IEEE, Yan Ma, Student Member, IEEE

**Abstract**—In this project, a six-level Modular Multilevel Converter (MMC) is designed with a modified phase-shift pulse-width-modulation (PS-PWM) in Simulink. The converter's output is connected to a three-phase grid and it is controlled by output real and reactive power. This project also employs a circulating current suppressing controller (CCSC) in the MMC. The purpose of the CCSC is to reduce the ripple generated by the multilevel switches. To control the effect of the double and quadruple-frequency components of the circulating current, the corresponding PR controller is designed for each phase. The results of this project are produced by the Simulink of Matlab.

**Index Terms**—Circulating current, Modular multilevel converter (MMC), PS-PWM, Double and quadruple frequency.

## I. SYSTEM CONFIGURATION

The topology of this project is shown in Fig.1. It consists of a 60kV DC voltage source, a six-level modular multilevel converter, and a three-phase grid with 20kV voltage rating. The advantage of MMC is to avoid series connection of power-electronic switches and to reduce the stresses on devices. The six-level MMC has 6 sub-models in each arm, each sub-model is a single phase buck converter shown in Fig.2. For a three-phase MMC, inner difference current,  $I_{diff,j}$ , will be generated in each phase. The inner difference current contains DC component, double and quadruple-frequency components. To reduce the effect (or amplitude) of the AC components of  $I_{diff,j}$ , the circulating current suppressing controller (CCSC) is designed with PR controller. The output of the CCSC are the inner unbalance voltage,  $u_{diff,j}$ . The PS-PWM signal will be generated based on  $u_{diff,j}$  and the desired EMF of the converter which the output the power control loop. Fig.4 shows the effect of CCSC, after one second the CCSC is activated, the circulating current is limited in tens amperes.

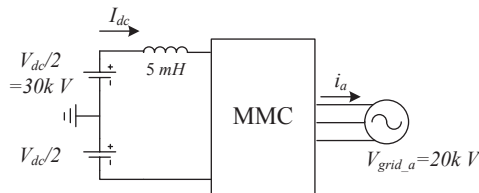


Fig. 1. The topology of the project (5mH inductor is to reduce the ripple of the DC input current when the CCSC starts to work)

## II. KEY RESULTS IN SIMULINK

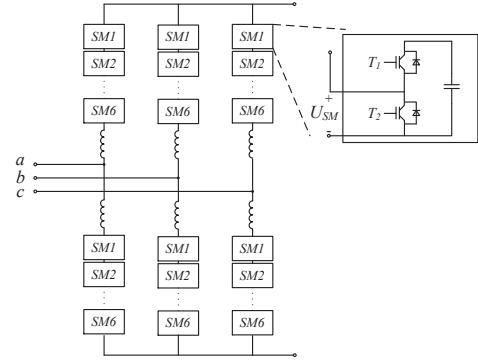


Fig. 2. It is the three-phase six-level MMC and the right upper figure displays the sub-module.

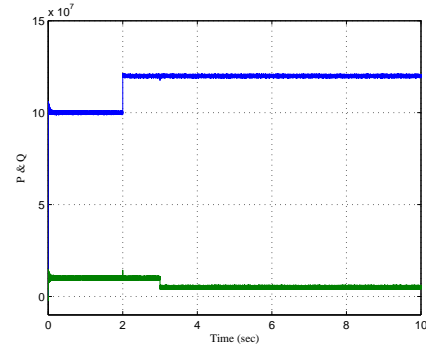


Fig. 3. The initial value: P(real power)=100MW, Q(reactive power)=10MVA; P increases to 120MW at 2s; Q increases to 5MVA at 3s.

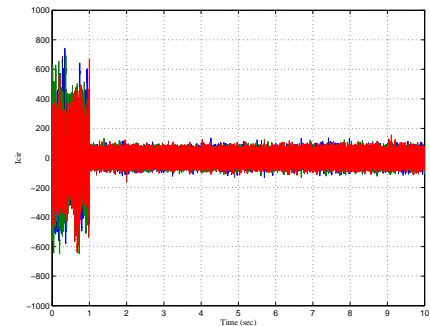


Fig. 4. From 1s, CCSC starts to work and the ripple of the circulating current,  $I_{cir}$ , is reduced to 40A from 500A.

# Medium Frequency Soft Switching DC/DC Converter Based HVDC Transmission System

Tao Li, *Student Member*, Leila Parsa, *Senior Member, IEEE*  
 Department of Electrical, Computer and Systems Engineering  
 Rensselaer Polytechnic Institute  
 Troy, NY 12180-3590, USA  
 E-mail: [lit4@rpi.edu](mailto:lit4@rpi.edu), [parsa@ecse.rpi.edu](mailto:parsa@ecse.rpi.edu)

**Abstract**—A HVDC transmission system based on isolated medium frequency zero voltage zero current switching (ZVZCS) DC/DC converter is proposed. Soft switching is achieved over the entire load range, via resonance between transformer leakage inductance and capacitance across primary switches. Since transformer leakage inductance is utilized in the resonant circuit, its design procedure is elaborated as well. Finite element simulation aided iterative design ensures transformer has leakage inductance close enough to desire value. Controller design is completed and the closed-loop system is simulated in PLECS®. Converters series connected at the output are also simulated to show scalability.

**Index Terms**-- DC-DC power converters, HVDC transmission, Zero current switching, Zero voltage switching

## I. KEY FIGURES

The proposed DC/DC topology is shown in Fig. 1. The converter has six active switches. All primary side switches are turned off with zero voltage and all secondary switches are turned on with zero current. The phase shift between S2S3 and S5 is the control input. The output current is regulated that soft switching can be achieved over entire load range. Compared to previous results in [1], this paper presents an easier modeling process. Also, transformer magnetizing inductance is no longer a factor in soft switching. The ZCS and ZVS can be observed in the simulation results in Fig. 3. Series-connected modules have also been simulated.

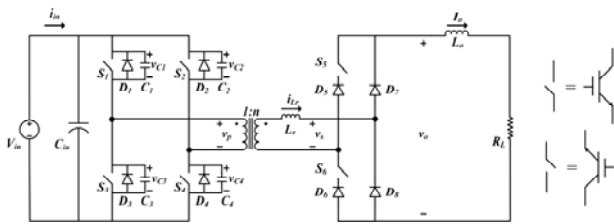


Figure 1. Converter topology

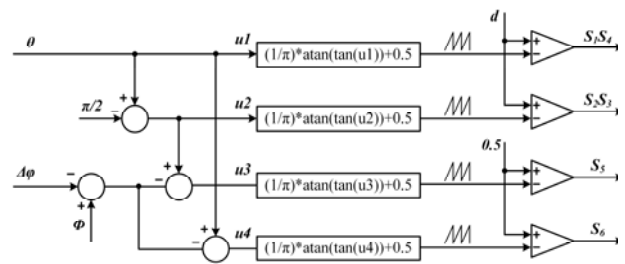


Figure 2. Modulation system

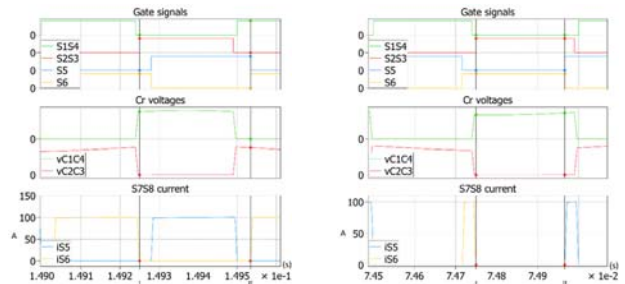


Figure 3. Soft switching at full load (left) and 10% load (right)

## REFERENCES

- [1] K. Akamatsu, T. Mishima, and M. Nakaoka, "A zero voltage and zero current soft-switching PWM DC-DC converter with synchronous phase shifting hybrid rectifier," in *28th Annu. IEEE Applied Power Electron. Conf. and Expo.*, Long Beach, CA, 2013, pp. 1–8.
- [2] T. Li, "Medium frequency soft switching DC/DC converter based HVDC transmission system for offshore wind farms," M.S. thesis, Dept. Elect., Comput. and systems Eng., Rensselaer Polytechnic Inst., Troy, NY, 2014.



# Nash Equilibria with Energy Trading in PV-Equipped Microgrids

M. Nazif Faqiry<sup>1</sup>

Rupam Kundu<sup>2</sup>

Sanjoy Das<sup>4</sup>

Rohan Mukherjee<sup>3</sup>

Anil Pahwa<sup>5</sup>

<sup>1,4,5</sup>Department of Electronics & Communications  
Jadavpur University  
Kolkata, WB, India.

<sup>1,4,5</sup>Department of Electrical & Computer Engineering  
Kansas State University  
Manhattan, KS, USA.

**Abstract**—During fault incidents, electricity generation is limited to renewable resources, such as photovoltaic (PV) panels in islanded grids or microgrids. This paper models electricity consumption and trading patterns among various nodes of such a grid, including those with PV-generation capabilities, within a multi-agent system framework. Energy consumption and trade among producer/consumer nodes that are modeled as agents, during Nash equilibrium, are determined using genetic algorithms. Cases with and without energy trade, as well as with and without batteries for storing electrical energy, have been considered. A second genetic algorithm is used to determine optimal pricing policies under such scenarios, to maximize the overall user benefit. Simulation results from this research can be of great significance in the design of the smart grid, as well as in decision-making.

**Keywords**—component; formatting; style; styling; insert (key words)

## I. MODEL EQUATIONS

### Agent Objective

Maximize w.r.t.  $\alpha_i(t), t \in \{1, 2, \dots, T\}; \tau_{i,k}, k \in \{1, 2, \dots, K\}$ :

$$V_i^{NE} = \max_{\alpha_i(t), \tau_{i,k}} \left\{ \sum_{t=1}^T TR(P_i(t)) + \sum_{t=1}^T LF_i q(\alpha_i) + \sum_{k=1}^K d_{i,k}(\tau_{i,k}) \right\}.$$

Such that for all  $t \in \{1, 2, \dots, T\}$ :

$$P_i(t) = PV_i(t) - \alpha_i(t)LF_i(t) - \sum_{k=1}^K LS_{i,k} \delta(t, \tau_{i,k}).$$

### Global Objective

$$\Lambda = \sum_{i=1}^N \left\{ \sum_{t=1}^T TR(P_i(t)) + \sum_{t=1}^T LF_i q(\alpha_i) + \sum_{k=1}^K d_{i,k}(\tau_{i,k}) \right\}.$$

### Power Balance Constraint (No Battery)

For all  $t \in \{1, 2, \dots, T\}$ :

$$\sum_{i=1}^N P_i(t) = 0.$$

## II. KEY FIGURES

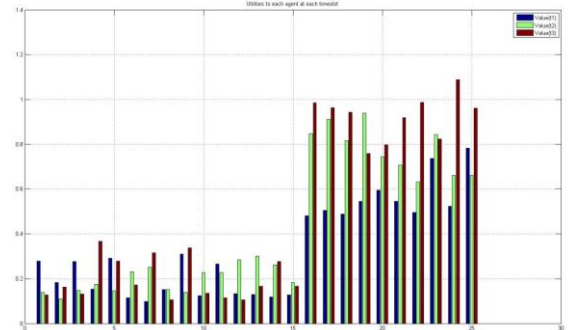


Fig. 1. Agent utilities under fixed pricing scheme ( $N=25, T=3$ ).

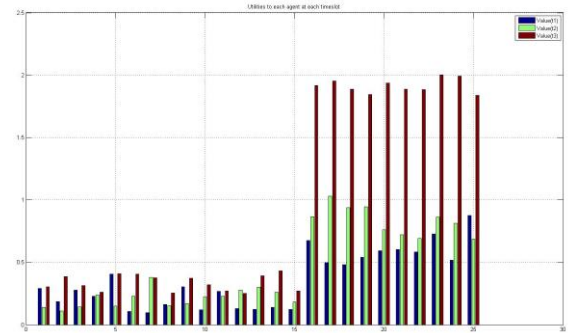


Fig. 1. Agent utilities under variable pricing scheme ( $N=25, T=3$ ).

# Large Scale Energy Storage Sizing to Mitigate Challenges in High Wind Penetration Scenarios

Hamideh Bitaraf, *Student Member, IEEE*, Manisa Pipattanasomporn, *SM, IEEE*, and Saifur Rahman, *Fellow, IEEE*  
Bradley Department of Electrical and Computer Engineering and Advanced Research Institute

Virginia Tech

Arlington, Virginia, USA

Email: [hamideh@vt.edu](mailto:hamideh@vt.edu), [mpipatta@vt.edu](mailto:mpipatta@vt.edu) and [srahman@vt.edu](mailto:srahman@vt.edu)

**Abstract**—High wind penetration can cause challenges to electric power systems due to its variability and uncertainty. The objective of this paper is to present a novel method to determine capacity and energy ratings of large scale energy storage systems, which can be a combination of Pumped Hydro Energy Storage (PHES) or Compressed Air Energy Storage (CAES), and large scale batteries, like NaS battery. The balancing signal is used for storage sizing. This balancing signal can be derived from wind power forecast errors and/or Fluctuation Mitigation Requirements (FMR) that limit ramp rates of wind power. The proposed methodology decomposes the Discrete Fourier Transform (DFT) of the balancing signal into slow cycling, intra-day and intra-hour components. A small system frequency deviation is allowed to decrease the required energy storage size. To showcase the proposed approach, this poster presents a simulation case study based on a real-world 5-minute interval data from Bonneville Power Administration (BPA) in 2013.

**Index Terms**—wind forecast error, wind fluctuation mitigation requirement, Discrete Fourier Transform (DFT), large scale energy storage sizing, frequency bias constant.

## I. INTRODUCTION

IN an electric power system with high wind penetration, uncertainty and variability of wind power output has brought about many challenges in power system operation and control. Energy storage can be sized and scheduled to compensate wind forecast errors and wind power fluctuation.

To compensate for wind forecast errors, a balancing signal is derived from the difference between a real-world 5-minute wind power output data from BPA and its hour-ahead forecasts. To compensate for wind power fluctuation, a balancing signal is derived to limit the ramp rate of wind power output within 4% of the rated wind power capacity in any 10-minute evaluation window. This is also known as Fluctuation Mitigation Requirements (FMR).

To size a combination of large-scale energy storage technologies, the Discrete Fourier Transform (DFT) of a balancing signal is decomposed into three components,

including slow cycling, intra-day and intra-hour.

- A low-pass filter is used to obtain the slow cycling component with more than 4-hour cycling characteristics. This component can be compensated by conventional generators.
- The band-pass filter is used to determine the intra-day component having 1-4 hour cycling characteristics. Large-scale storage units, like CAES and PHES, can follow the intra-day component due to their slow response time characteristics and mechanical limits.
- Lastly, the high-pass filter is used to find the intra-hour component, which is defined to have less than 1-hour charging/discharging period. This is appropriate for large-scale batteries, like NaS, that has fast response time and can tolerate high frequency cycling.

A small frequency deviation of 0.1Hz from the power system operating frequency of 60Hz is also allowed by considering a frequency bias constant ( $\beta$ ) to decrease the required energy storage size.

## II. CASE STUDY AND RESULT DISCUSSION

Using the proposed methodology, recommended energy storage sizes (both capacity and energy ratings) for different balancing signals are presented in Table 1.

TABLE I. RECOMMENDED ENERGY STORAGE SIZES TO MITIGATE WIND POWER FORECAST ERRORS AND FLUCTUATIONS

Balancing signal used	Component	Power (GW)	Energy (GWh)
Forecast error	Intra hour	1.04	0.61
	Intra day	0.85	35
FMR @ 4%	Intra hour	1.10	0.18
	Intra day	0.13	0.55
Forecast error and FMR @ 4%	Intra hour	1.83	0.68
	Intra day	0.88	35.55
Forecast error, FMR @ 4% and $\beta$ @ 400MW/0.1Hz	Intra hour	1.74	0.31
	Intra day	0.45	7.39

# Grid Connected Building Load Operation

Mohammed Muthalib, Chika Nwankpa  
 Department of Electrical and Computer Engineering  
 Drexel University  
 Philadelphia, PA USA  
[mkm46@drexel.edu](mailto:mkm46@drexel.edu), [con22@drexel.edu](mailto:con22@drexel.edu)

**Abstract**— Increased interest in demand response programs stemming from technological advancements as well as changes in energy regulatory structure have prompted more buildings to actively participate in the energy market. With this increased participation, a need has risen to further investigate the behavior of grid connected buildings. Under demand response and demand dispatch operations, buildings are primarily controlled through thermostatic temperature setpoint variations. These electro-thermal load variations are subject to load-temperature operating limits determined by the HVAC equipment capacities as well as electric grid operating limits. Load variations in multiple buildings are coupled thermally to ambient temperature variations while also being coupled electrically through the interconnected network. This brings about a temperature-voltage coupling that imposes operating limits on the local network. Operating without regard for such behavior could bring about inefficiencies and even have potentially detrimental effects on the power system. This work presents appropriate models capable of describing the building electro-thermal coupling as well as the building-grid coupling. The goal is to facilitate an improved understanding of grid connected building operation.

## I. METHODOLOGY

An adequate representation of the load bus at which a building connects to the grid is essential for demand response purposes. Any action taken on the building side is reflected to the grid through this junction. This work adopts an Energy Hub representation (1) of the transfer point that includes a thermostatically controlled load portion as well as an uncontrolled load portion. The uncontrolled load is modeled as a ZIP load (2) that includes the bus voltage dependence. The thermostatically controlled building load is modeled through an equivalent circuit analysis and is sensitive to both thermostatic setpoint variations as well as ambient temperature variations (3). An equivalent electrical-thermal energy conversion efficiency is included that captures the load dependent performance of the HVAC equipment.

$$P_m^{elec} = P_{UC}^{elec} + \frac{1}{\eta^{eq}} P_B^{th} \quad (1)$$

$P_{UC}^{elec}$  – Building uncontrollable electric load  
 $P_B^{th}$  – Net controllable thermal building load  
 $\eta^{eq}$  – Equivalent efficiency of conversion

$$P_{UC}^{elec} = P_0 \left[ Z_p \left( \frac{|V|}{|V_0|} \right)^2 + I_p \left( \frac{|V|}{|V_0|} \right) + P_p \right] \quad (2)$$

$$0 = -(R^{th} + R_a) \Psi + R_a u + R^{th} \Psi_a \quad (3a)$$

$$P_B^{th} = P_n^{th} \left( \frac{\Psi}{\Psi_n} \right)^\alpha + \frac{\Psi_a - \Psi}{R_a} \quad (3b)$$

$Z_p, I_p, P_p$  – ZIP coefficients  
 $P_0$  – Nominal uncontrollable electrical load (kW)  
 $V_0$  – Nominal bus voltage (p.u.)  
 $0$  –  $-(R^{th} + R_a) \Psi + R_a u + R^{th} \Psi_a$   
 $P_B^{th}$  –  $P_n^{th} \left( \frac{\Psi}{\Psi_n} \right)^\alpha + \frac{\Psi_a - \Psi}{R_a}$   
 $\Psi$  – Building internal zone temperature (°F)  
 $\Psi_a$  – Ambient temperature (°F)  
 $\Psi_{set}$  – Zonal temperature setpoint (°F)  
 $R^{th}$  – Building internal thermal resistance (°F/kW)  
 $C^{th}$  – Building thermal capacitance (kWh/°F)  
 $R_a$  – Building envelope thermal resistance (°F/kW)  
 $P_B^{th}$  – Building equivalent thermal load (kW)  
 $P_n^{th}$  – Nominal controllable thermal load (kW)  
 $\Psi_n$  – Building nominal internal temperature (°F)  
 $\alpha$  – Building thermal load sensitivity

## II. RESULTS

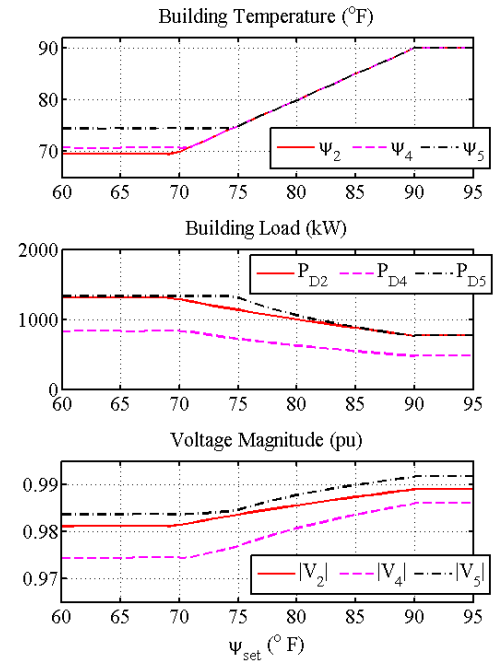


Figure 1: Results of temperature setpoint variation ( $60^\circ\text{F} \leq \Psi_{set} \leq 95^\circ\text{F}$ ) with ambient temperature  $\Psi_a = 90^\circ\text{F}$ .

# Frequency Dependent Network Equivalent Model for Simultaneous Electromechanical and Electromagnetic Transient Analysis

Xu Zhang, *Student Member, IEEE*, and Alexander J. Flueck, *Senior Member, IEEE*

**Abstract**—An electromechanical-electromagnetic transient simulator is the combination of a transient stability (TS) simulator and an electromagnetic transient (EMT) simulator, which is capable of fulfilling the modeling requirements of a large network by providing a fast as well as a detailed simulation. In previous work, the fundamental frequency equivalent is used as the network equivalent of the external system. While simple, this fundamental frequency equivalent is only accurate for a single frequency, the fundamental frequency. This may lead to an inaccurate equivalent of the transient stability network. This paper extends previous work by using FDNE derived from the vector fitting technique. The FDNE is able to resolve the transient over a wider frequency spectrum leading to a more accurate representation of the TS network. Results demonstrating the accuracy of the proposed scheme are presented on the IEEE 118 bus system.

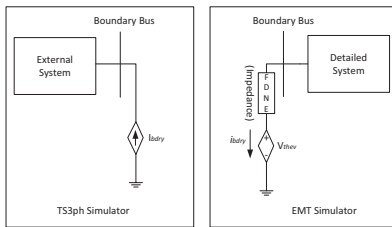
**Index Terms**—Frequency dependent network equivalent, transient stability, electromagnetic transient.

## I. HYBRID SIMULATOR (TS3PH-EMT SIMULATOR)

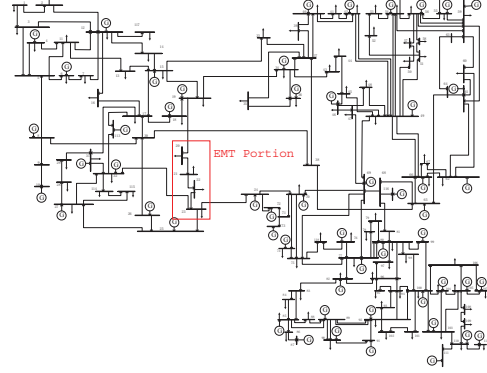
Hybrid simulator is the combination of electromechanical transient simulator and electromagnetic transient simulator and the main idea of hybrid simulator is to split the power system into two portions: External system (the large portion) and detailed system (the small portion).

External system is running on TS3ph simulator (a three phase transient stability simulator) and detailed system is running on EMT simulator. Two simulator communicate with each other through the equivalents of each portion and the fundamental frequency equivalent is used as the network equivalent of the external system.

## II. HYBRID SIMULATOR WITH FREQUENCY DEPENDENT NETWORK EQUIVALENT (TS3PH-EMT + FDNE)



- The equivalent of EMT portion in TS3ph simulator is a current source  $I_{bdry}$ ; Fourier transform is used to extract fundamental frequency component ( $I_{bdry}$ ) from the instantaneous boundary current ( $i_{bdry}$ ) data over one cycle (1/60s) from EMT simulation.
- The equivalent of TS3ph portion in EMT simulator is in the form of Thevenin equivalent:  $v_{thev}$  in series with FDNE impedance.  $v_{thev}$  is generated by a fundamental frequency sine wave generator (the generated waveform signal is dependent on the voltage magnitude and angle of  $V_{bdry}$ ). FDNE impedance is derived from vector fitting, which is an accurate representation of the network in TS3ph portion under various frequencies.

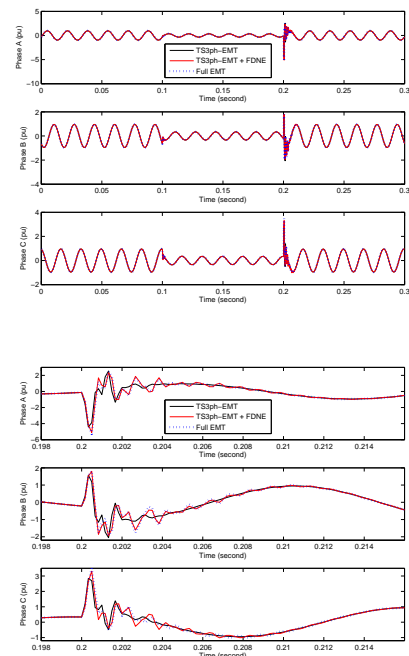


## III. CASE STUDY

- TS3ph portion: Bus 1-20, Bus 23-118
- EMT portion: Bus 20-23
- Boundary Bus: Bus 20, Bus 23
- Generator Model: GENROU
- Exciter Model: IEEE1
- Load Model: Constant Impedance

The disturbance scenario is a three-phase to ground fault with fault impedance 0.001 pu at bus 21 (initiated at  $t=0.1$  second and cleared at  $t=0.2$  second).

The voltage waveforms on boundary bus 20 are shown below:



# Stochastic Process Based Harmonic Current Regeneration for Harmonic Assessment in Wind Power Plant

<sup>1</sup>Youngho Cho, *Student Member, IEEE*, <sup>1</sup>Choongman Lee, *Student Member, IEEE*,  
and <sup>1</sup>Kyeon Hur, *Senior Member, IEEE*

<sup>1</sup>School of Electrical and Electronic Engineering, Yonsei University, Seoul, Korea  
Email: [sglab@yonsei.ac.kr](mailto:sglab@yonsei.ac.kr), [your2cm@yonsei.ac.kr](mailto:your2cm@yonsei.ac.kr), [khur@yonsei.ac.kr](mailto:khur@yonsei.ac.kr)

**Abstract**—As wind power generation has been largely increasing, the impact of harmonic emissions from wind power plant should be carefully investigated in planning studies. However, conventional harmonic research based on FFT analysis during certain period is hard to reflect the uncertainty of harmonic generation. In this research, stochastic process in harmonic study is proposed in consideration of random characteristics of harmonics generated by wind turbine. Using this data, parameter estimation is performed and best-fitted distribution is selected. Random variables that follow the selected distribution will be used for regeneration of current wave including stochastic characteristics of harmonics. This makes it possible to handle not only the uncertainty of harmonics in wind power plants but also the effect of harmonic uncertainty on grid parallel resonance.

**Index Terms**— Harmonics, Random variables, Stochastic approach, Wind power plant, Planning studies.

## I. KEY RESULTS

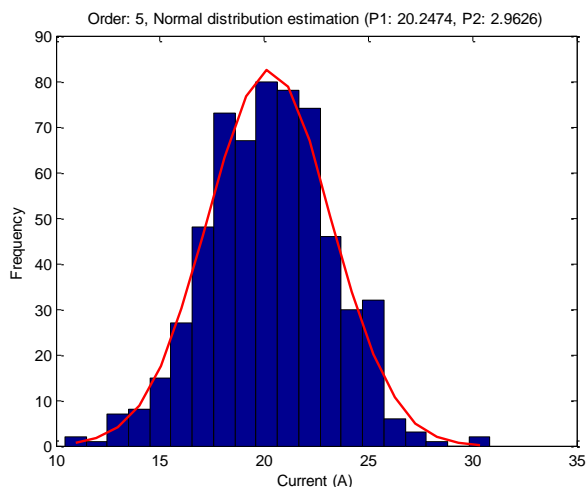


Fig. 1. Parameter estimation of 5<sup>th</sup> harmonic distribution following normal distribution. P1: mean value, P2: variance

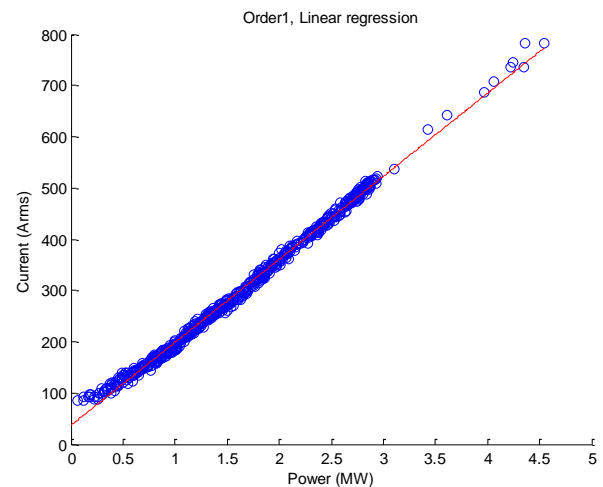


Fig. 2. Linear regression of currents in fundamental frequency. It is assumed that current is proportional to power generation.

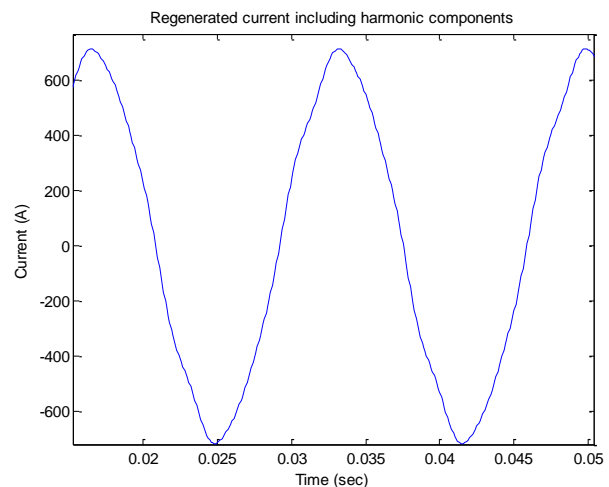


Fig. 3. Regenerated current wave including random characteristics of selected harmonics.



# Circulating Current Control for Reducing Energy Storage Requirement in Modular Multilevel Converter

<sup>1</sup>Sang Min Kim, <sup>1</sup>Hee Jin Kim, *Student Member, IEEE*, and  
<sup>1</sup>Kyeon Hur, *Senior Member, IEEE*

<sup>1</sup>School of Electrical and Electronic Engineering, Yonsei University, Seoul, Korea  
 Email: [sang\\_kim@yonsei.ac.kr](mailto:sang_kim@yonsei.ac.kr), [jimmykim07@yonsei.ac.kr](mailto:jimmykim07@yonsei.ac.kr), [khur@yonsei.ac.kr](mailto:khur@yonsei.ac.kr)

**Abstract**—Modular Multilevel Converter (MMC) has been grown as the most promising topology for voltage sourced converter high-voltage direct current (VSC-HVDC) power transmission providing technical advantages such as the reactive power control ability and the less or no filtering requirement. The MMC has its unique component called Sub-Module(SM) which consists of the transistor (IGBT), diode, and capacitor as the energy storage unit. The large size of capacitor can reduce the capacitor voltage ripple, though it requires high cost. The amount of voltage ripple determines the required capacity of the energy storage unit. The injection of the second-order harmonic circulating current can diminish the capacitor voltage ripple resulting in reduction of the required energy storage capacity. However it can increase the amount of loss due to the increased rms current value of the circulating current. In addition, controlling the harmonic of circulating current can affect the polarity of current through the SM, which can produce adverse effect on the operation of the MMC. 201-level MMC system is simulated in order to examine the effect of the injection of second-harmonic current on operation of MMC and the variability of the polarity of the current.

**Index Terms**— Modular Multilevel Converter (MMC), Capacitor, Second-order harmonic circulating current.

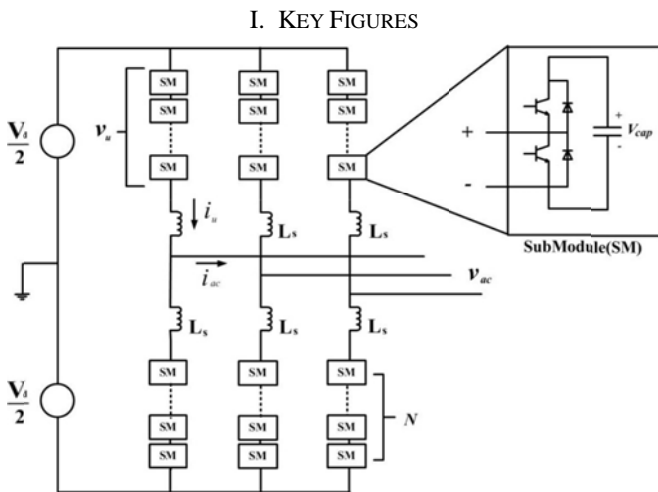


Fig. 1. The structure of the MMC and SM

## II. KEY RESULTS

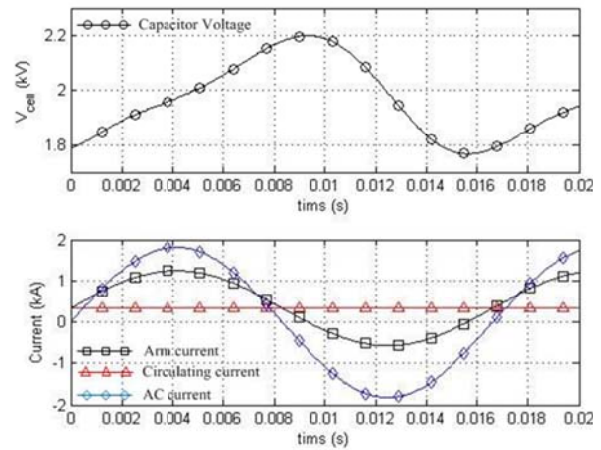


Fig. 2. Cell voltage (circle), AC current (diamond), arm current (square), and circulating current (triangle) without the second-order harmonic current.

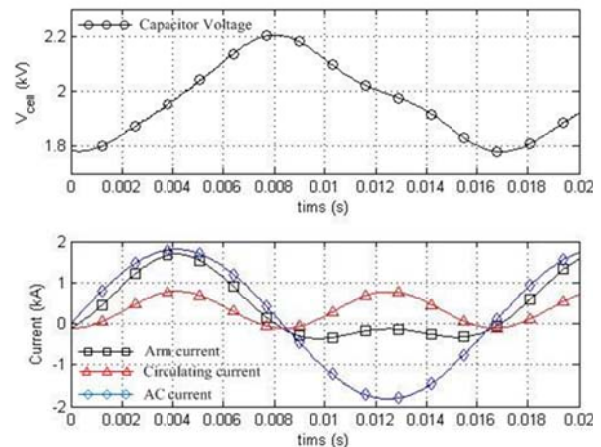


Fig. 3. Cell voltage (circle), AC current (diamond), arm current (square), and circulating current (triangle) with the second-order harmonic current.



# Case Study on Korea-China Grid Interconnection from Perspective of South Korea

Hyun-Jae Lee, *Student Member, IEEE*, and Kyeon hur, *Senior Member, IEEE*  
 School of Electrical and Electronic Engineering, Yonsei University, Seoul, South Korea,  
 Email: newbee123@nate.com

**Abstract**—As South Korean Power Grid suffers from lack of available reserve power and expensive generation cost, interests in Grid interconnection has arisen. Network security must be analysed before commencing the project as injection or outflow of power can harm reliability of power grid.

## I. INTRODUCTION

Korea - China Grid Interconnection project has its advantage on peak-sharing and generator expansion. Both countries do not share peak-load time which can lead to transaction of power for peak-load sharing and contingency resilience. Several scenarios will be analysed through Powerworld and PSS/E.

## II. PROCESS FLOW CHART

A flow chart of the assessment procedure is present on Fig.1. This analysis will be conducted for each connection point candidates.

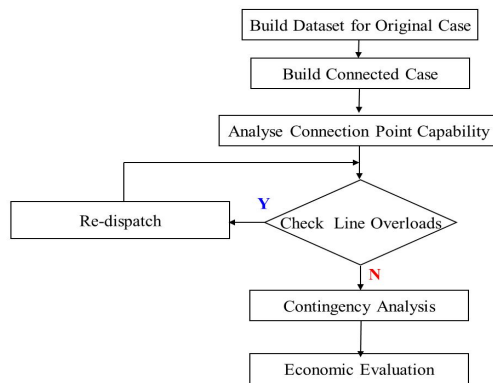


Fig. 1. Flow chart of feasibility assessment

The flow of assessment is listed below.

1. South Korean Power Grid data will be built for base-case.
2. A generator or load will be connected to one of the candidate connection points as equivalence of china grid according to the interconnection scenario.
3. Power transfer capability of connection point will be analysed through PV analysis.
4. Thermal line capacity overloading will be monitored. If violation occurs, generation re-dispatch will be conducted for better system reliability.

5. Transient stability of connected case will be analysed for potential contingencies.

6. Economic effect of the interconnection will be evaluated by OPF.

## III. KEY RESULT

TABLE I  
 LINE LOADING DATA OF MOST ENDANGERED TRANSMISSION LINE

	Base Case	Peak-Sharing Case
Line Limit	611.1 A	611.1 A
Power Flow	629.9 A	779.9 A
% Usage	101.79 %	127.6 %

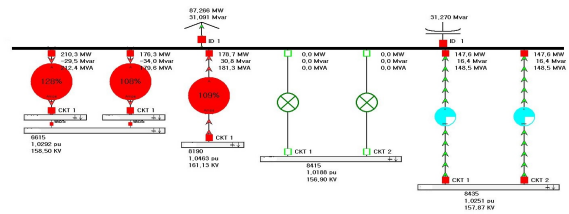


Fig. 2. One-line diagram of thermal limit violating bus.

For power injection scenario, thermal line limit has been violated. Generator is re-dispatched to relieve violation as seen in Table 2 and Fig.3.

TABLE II  
 LINE LOADING HAS BEEN RELIEVED THROUGH GENERATION RE-DISPATCH

	Peak-Sharing Case	Relieved Case
Line Limit	611.1 A	611.1 A
Power Flow	629.9 A	593.0 A
% Usage	101.79 %	97 %

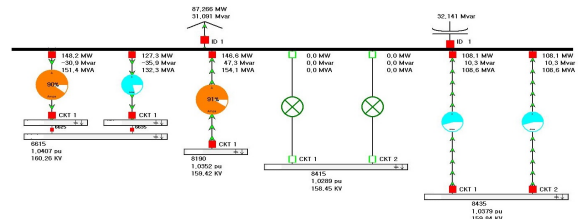


Fig. 3. One-line diagram of relieved network.

# Estimation of Stator Resistance in Direct Torque Control Synchronous Motor Drives

Younes Sangsefidi and Ali Mehrizi-Sani

School of Electrical Engineering and Computer Science, Washington State University, Pullman, WA, USA

Email: younes.sangsefidi@email.wsu.edu; mehrizi@eecs.wsu.edu

**Abstract**—Direct torque control (DTC) is a high performance sensorless method that provides effective control of stator flux modulus and electromagnetic torque of electric motors. However, an error in estimation of stator resistance significantly degrades the performance of DTC drive system, especially for a synchronous motor. A method to distinguish and track stator resistance variations is proposed. The method is based on finding a reference value for the angle between the stator flux and the stator current vectors and tracking this reference value by changing the estimated stator resistance. The proposed stator resistance estimator is validated using experimental case studies.

## I. PROBLEM STATEMENT

Desirable features such as fast dynamic response, no need to mechanical sensors, simple structure, and less dependence on motor parameters have made DTC drive systems an attractive option for the industry. DTC provides effective control of stator flux modulus and electromagnetic torque in a synchronous motor. However, one of its main limitations is that *a priori* knowledge of the stator resistance is required to estimate the stator flux vector and electromagnetic torque. Due to variations in temperature and frequency, stator resistance can vary considerably. A basic DTC synchronous drive is unable to track these variations, and consequently its performance may degrade.

## II. KEY EQUATIONS

The reference value of the angle between stator flux and current vectors is found by

$$T_e^* = \frac{mP|\lambda_s|^* \lambda_f}{2L_d} \sin \delta^* + \frac{mP|\lambda_s|^*{}^2}{4} \left( \frac{1}{L_q} - \frac{1}{L_d} \right) \sin 2\delta^* \quad (1)$$

and

$$\tan(\varphi_{i\lambda}^*) = \frac{T_e^*}{\frac{mP|\lambda_s|^*{}^2}{2L_d} \cos^2 \delta^* + \frac{mP|\lambda_s|^*{}^2}{2L_q} \sin^2 \delta^* - \frac{mP|\lambda_s|^* \lambda_f}{2L_d} \cos \delta^*} \quad (2)$$

The estimated angle between stator flux and current vectors is found by

$$\tilde{\varphi}_{i\lambda} = \tan^{-1} \left( \frac{i_{\tilde{y}s}}{i_{\tilde{x}s}} \right) = \tan^{-1} \left( \frac{\tilde{\lambda}_{Ds} i_{Qs} - \tilde{\lambda}_{Qs} i_{Ds}}{\tilde{\lambda}_{Ds} i_{Ds} + \tilde{\lambda}_{Qs} i_{Qs}} \right). \quad (3)$$

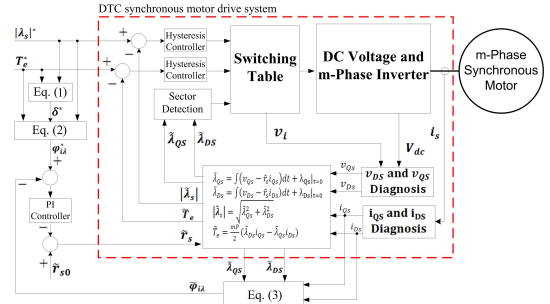


Fig. 1. The modified DTC synchronous motor drive system with stator resistance estimation.

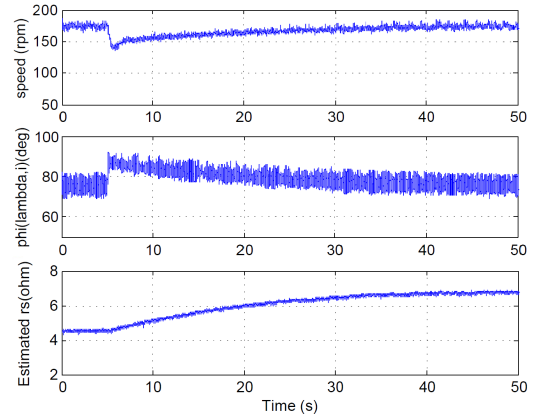


Fig. 2. The modified DTC synchronous motor drive system with the proposed stator resistance estimator.

To estimate the stator resistance, a PI controller can be designed as

$$\tilde{r}_{s0} - \tilde{r}_s = K_p(\varphi_{i\lambda}^* - \tilde{\varphi}_{i\lambda}) + K_i \int (\varphi_{i\lambda}^* - \tilde{\varphi}_{i\lambda}) dt, \quad (4)$$

The block diagram of the proposed stator resistance estimator is shown in Fig. 1.

## III. KEY EXPERIMENTAL RESULTS

The drive system starts working with correct value of stator resistance. At  $t = 5$  s,  $2.35 \Omega$  resistors are added in series with each phase of the motor. Experimental results are presented in Fig. 2. It can be observed that the proposed method successfully tracks the variations of the stator resistance.

# Resilience of Power Grids against Random Failures

Deepjyoti Deka and Sriram Vishwanath

Department of Electrical & Computer Engineering University of Texas at Austin

Email: deepjyotideka@utexas.edu, sriram@ece.utexas.edu

**Abstract**—Random failures in power grids can propagate geographically and potentially fragment the network. The propagation of such failures in power grid graphs differs significantly from that of random networks. This paper presents a framework to study cascading failures based on the adjacency matrix of a power grid graph. Improved bounds on the size of the surviving network following random failures are analyzed and presented through simulations.

## I. INTRODUCTION

It is well-known that structure of the power grid network affects the extent of damage caused by cascading failures of its transmission lines and buses [1]. In the past, failure propagation have been studied for complex networks using ideas from percolation theory and random graph theory [2]. However, the structure of an actual power grids differs significantly from random graphs. Hence, insights from failure analysis of random graphs do not extend directly to real grids. In this work, we use the known structure of a power grid graph to determine bounds on its vulnerability to cascading node failures. Design strategies aimed at improving these bounds can the grid more resilient to random failures.

## II. ANALYSIS OF FAILURE PROPAGATION

**System Model:** The grid is represented as a graph  $G = (V, E)$ , where sets  $V$  and  $E$  denote the nodes (buses) and the undirected edges (transmission lines) respectively. Let  $A_G$  be the known adjacency matrix of the graph  $G$ . We initialize the cascade process by assuming that each node in the graph fails independently with probability  $p$ . Additionally, nodes that get disconnected from the rest of the network due to removal of all their graph neighbors are also considered as failed nodes.

We now analyze the propagation of failures in discrete time steps. Let  $\lambda_t^V$  denote the vector of survival probabilities of nodes in  $V$  at time  $t$ . Consider a node  $i$  in  $G$ . We have  $\lambda_0^V(i) = 1 - p$ . According to the failure propagation model, node  $i$  survives at time  $t$  if it did not fail at time  $t = 0$  and at least one of its neighbors did not fail by time  $t - 1$ . Mathematically,

$$\begin{aligned} \lambda_t^V(i) &= (1 - p)\mathbb{P}\left[\bigcup_{j:(ij)\in E} \{\text{node } j \text{ survives at } t - 1\}\right] \\ \Rightarrow \lambda_t^V &\leq (1 - p)A_G\lambda_{t-1}^V \quad (\text{By Union Bound}) \end{aligned} \quad (1)$$

Let  $\beta_A$  be the largest eigenvalue of adjacency matrix  $A_G$ . Using relation (1), it is clear that if  $(1 - p)\beta_G < 1$ ,  $\lambda_\infty^V \rightarrow 0$ . This provides a **lower bound** (not a sharp threshold) on the probability of random failures ( $p$ ) at which the grid fragments. Unlike random network analysis, failures in neighboring nodes are not considered as independent in our analysis. Notice

that each surviving node connects to the remaining surviving network through an edge. Consider two neighboring nodes  $i$  and  $j$ . Let  $B_t^E(ij)$  be the event that node  $i$  is connected to the surviving nodes through node  $j$ . Let  $\lambda_t^E(ij) = \mathbb{P}[B_t^E(ij)]$ . We have  $\lambda_t^V(i) = (1 - p)\mathbb{P}[\bigcup_{j:(ij)\in E} [B_t^E(ij)]]$ . Similarly, we can define  $B_t^E(ji)$  and  $\lambda_t^E(ji)$  for node  $j$  surviving due to edge with node  $i$ . Thus, every edge gives rise to two sets of probabilities. Note that the evolution of  $\lambda_t^E(ij)$  in turn depends on  $\lambda_{t-1}^E(jk)$  where  $k \neq i$  is another neighbor of  $j$ . Mathematically, we can write

$$\begin{aligned} \lambda_t^E(ij) &= (1 - p)\mathbb{P}\left[\bigcup_{k:(kj)\in E, k\neq i} B_{t-1}^E(jk)\right] \\ \Rightarrow \lambda_t^E(ij) &\leq (1 - p) \sum_{k:(kj)\in E, k\neq i} \lambda_{t-1}^E(jk) \end{aligned} \quad (2)$$

Following (1), we can write relation (2) in terms of a **modified adjacency** matrix  $L_G$  where every edge direction is a node (eg.  $\lambda_t^E(ij)$ ,  $\lambda_t^E(ji)$ ) and two edge directions are neighbors if one's end is another's origin (eg.  $\lambda_t^E(ij)$ ,  $\lambda_t^E(jk)$ ). Following similarly, we get that  $\beta_L$ , the largest eigenvalue of  $L_G$ , can define a bound on resilience of the network that is tighter than  $\beta_A$ . Using this matrix  $L_G$ , one can also get upper bounds on the expected number of failures in the grid following an initial set of random failures. We show one such simulation in Fig. 1 for IEEE 300-bus system.

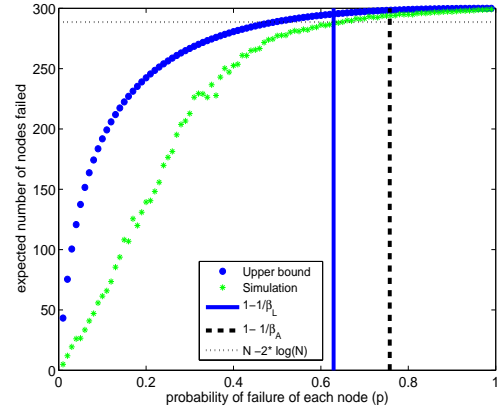


Fig. 1. Upper bounds for number of failed nodes and Lower bound on  $p$  in IEEE 300 bus system

## REFERENCES

- [1] R. Albert, H. Jeong, and A.-L. Barabasi, "Error and attack tolerance of complex networks", *Nature*, vol. 406, 2000.
- [2] S.V. Buldyrev, R. Parshani, G. Paul, H.E. Stanley, and S. Havlin, "Catastrophic cascade of failures in interdependent networks", *Nature*, vol. 464, 2010.

# A Novel Renewable Energy Technology - Energy Harvesting from Distilled and Stationary Water

Chien-Chang K. Kung  
Electrical Engineering  
University of Washington  
Seattle, USA  
ckung@uw.edu

Gerald H. Pollack  
Bioengineering  
University of Washington  
Seattle, USA  
ghp@uw.edu

**Abstract**—This research introduces a novel renewable energy technology that uses water as a medium to convert light, especially infrared light, into electricity.

**Keywords**—renewable energy; water; energy harvesting

## INTRODUCTION

Renewable energy technology is one of the most important topics in applied engineering with a high level of potential societal impact. While renewable energy sources vary widely, solar energy is the most popular and ubiquitous. The photovoltaic cell is one of the common technologies that allow us to utilize the energy from sun; however, it does not work without direct sunlight exposure. Here we propose a novel energy source using light, but not necessarily direct sunlight to generate electricity. The photovoltaic medium is water.

Recent studies show that adjacent to many hydrophilic surfaces, water forms a unique crystalline structure[1], [2]. This crystalline structure causes charge separation between interfacial water and bulk water [3]. Therefore, the practical outcome from the charge separation is the production of electrical energy. From our previous works, we have learned that weak infrared light can increase the size of structured interfacial water dramatically [4]. Our preliminary experiments also indicate infrared light is the major contributor to the charge separation in water. In other words, water can be use as a medium to convert the infrared light into electricity.

In order to understand how much power we can harvest from interfacial water, we placed the probing micropipette electrode right next to the hydrophilic material, such as Nafion, in water, and placed reference electrode remotely in the bulk water region. As a result, we were able to obtain 1 nano-watts over a 1 micron- square micropipette electrode (Fig. 1). All the measurements are done under room temperature and regular laboratory environment without any external energy or light source, so it means the ubiquitous infrared emission from the normal environment is sufficient to rebuild the structure in the interfacial water and causes charge separation. Therefore, we are able to harvest the electricity from water day and night.

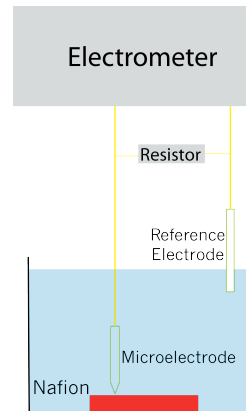


Fig. 1. Single pair of micropipette electrode measurement set-up.

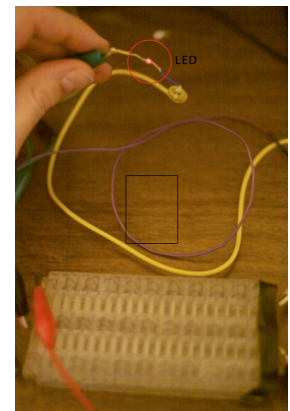


Fig. 2. 500 microwatts single LED is powered by water.

We anticipate turning the nano-watts power we are now able to harvest from water into the scale of milli-watts in the near future. We are working on a planar microelectrode array design. Basically, we are using microfabrication technology to make an array of electrodes on a silicon wafer and we are also trying 3D printing technology for rapid prototyping. If we think of each electrode as a single battery, then this array of electrodes can mimic many batteries that are electrically connected in parallel. When we replace the single micropipette electrode with the microelectrode array, we should be able to scale up the power to a usable level.

## REFERENCES

- [1] J. E. M. McGeoch and M. M. W, "Entrapment of water by subunit c of ATP synthase," pp. 1-31, Jun. 2007.
- [2] N. F. Bunkin, P. S. Ignatiev, V. A. Kozlov, A. V. Shkirin, and S. D. Zakharov, "STUDY OF PHASE STATES OF WATER CLOSE TO NAFION INTERFACE," pp. 1-28, Oct. 2012.
- [3] J.-M. Zheng, W.-C. Chin, E. Khijniak, E. Khijniak Jr., and G. H. Pollack, "Surfaces and interfacial water: Evidence that hydrophilic surfaces have long-range impact," *Advances in Colloid and Interface Science*, vol. 127, no. 1, pp. 19-27, Nov. 2006.
- [4] B. Chai, H. Yoo, and G. H. Pollack, "Effect of Radiant Energy on Near-Surface Water," *J. Phys. Chem. B*, vol. 113, no. 42, pp. 13953-13958, Oct. 2009.

# A Diffusion-Driven Model for Investigating Moisture Effects on Dielectric Response Measurement of Transformer Insulation

Yi Cui, Hui Ma, Tapan Saha, Chandima Ekanayake

School of Information Technology and Electrical Engineering  
The University of Queensland, Brisbane, QLD, 4072, Australia

Email: [y.cui3@uq.edu.au](mailto:y.cui3@uq.edu.au), [huima@itee.uq.edu.au](mailto:huima@itee.uq.edu.au), [saha@itee.uq.edu.au](mailto:saha@itee.uq.edu.au), [chandima@itee.uq.edu.au](mailto:chandima@itee.uq.edu.au)

**Abstract**— This paper proposes a diffusion-driven dielectric response model, which aims to reveal the effect of moisture diffusion on the dielectric response measurement of transformer insulation. In the proposed diffusion-driven model, the oil-impregnated pressboards are modeled as multiple layers and it is assumed moisture diffuses from one side of the pressboard. Then the dependency between the moisture concentration and dielectric losses and permittivity of the pressboard is studied. Subsequently, the dielectric response of the pressboard is calculated to model the dielectric relaxation behavior driven by the moisture migration between oil and pressboard. The proposed model is verified by laboratory experimental results.

## I. KEY EQUATIONS

During diffusion process, the moisture distribution inside the pressboard is calculated by solving the Fick's second law.

$$\frac{\partial C(x,t)}{\partial t} = \frac{\partial}{\partial x} \left( D \frac{\partial C(x,t)}{\partial x} \right) \quad (1)$$

The impedance  $Z(\omega)$  of the pressboard in frequency domain can be written as (2)

$$Z^*(\omega) = \frac{1}{S} \left[ \int_0^l \frac{\sigma_x}{\sigma_x^2 + (\omega \varepsilon_0 \varepsilon'_x)^2} dx - j \int_0^l \frac{\omega \varepsilon_0 \varepsilon'_x}{\sigma_x^2 + (\omega \varepsilon_0 \varepsilon'_x)^2} dx \right] \quad (2)$$

Admittance and capacitance can be written as (3) and (4)

$$G_i^*(\omega) = (\sigma_i + j\omega \varepsilon_0 \varepsilon'_i) \frac{S}{\Delta x} \quad (3)$$

$$C_i^*(\omega) = \varepsilon_i^*(\omega) C_0 = \varepsilon_0 \frac{S}{\Delta x} (\varepsilon'_i + j\varepsilon''_i) \quad (4)$$

Complex capacitance (4) can be expressed as (5)

$$C_i^*(\omega) = \frac{G_i^*(\omega)}{j\omega} = (\varepsilon_0 \varepsilon'_i - j \frac{\sigma_i}{\omega}) \frac{S}{\Delta x} \quad (5)$$

By comparing (4) and (5), it can be obtained

$$\varepsilon'_x = \varepsilon'_i, \quad \sigma_x = \sigma_i = \varepsilon_0 \omega \varepsilon''_i \quad (6)$$

## II. KEY FIGURES

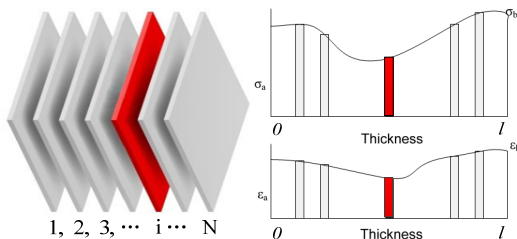


Fig. 1. Diffusion-driven model of pressboard in transformer

## III. KEY RESULTS

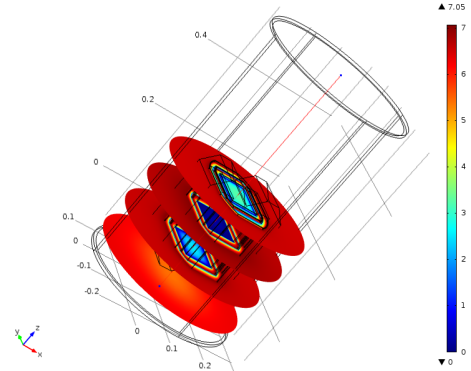


Fig. 2. FEM modelled moisture distribution in transformer during diffusion process

An exponential function is used for describing the dependency between the loss and the position before uniform moisture distribution has reached

$$\sigma = e^{\alpha + \beta \cdot x} \quad (7)$$

TABLE I. FITTING PARAMETERS FOR DIELECTRIC LOSS WITH RESPECT TO DIFFUSION POSITION (AFTER 18 HOURS DIFFUSION)

Freq	$\alpha$	$\beta$	Mse.	Freq	$\alpha$	$\beta$	Mse.
1000	-20.58	0.04	$5.20 \times 10^{-13}$	$4.6 \times 10^{-2}$	-24.94	-0.80	$7.86 \times 10^{-14}$
10	-23.31	-1.03	$4.53 \times 10^{-13}$	$2.2 \times 10^{-2}$	-25.31	-0.64	$4.76 \times 10^{-14}$
1	-23.77	-1.36	$3.21 \times 10^{-13}$	$10^{-2}$	-25.80	-0.89	$3.52 \times 10^{-14}$
0.46	-23.97	-1.30	$2.61 \times 10^{-13}$	$4.6 \times 10^{-3}$	-25.92	-0.36	$1.76 \times 10^{-14}$
0.22	-24.23	-1.14	$1.90 \times 10^{-13}$	$2.2 \times 10^{-3}$	-26.09	-0.23	$1.02 \times 10^{-14}$
$10^{-1}$	-24.57	-0.97	$1.25 \times 10^{-13}$	$10^{-3}$	-26.20	-0.15	$6.31 \times 10^{-15}$

Freq: frequency in Hz. MSE: mean square error.

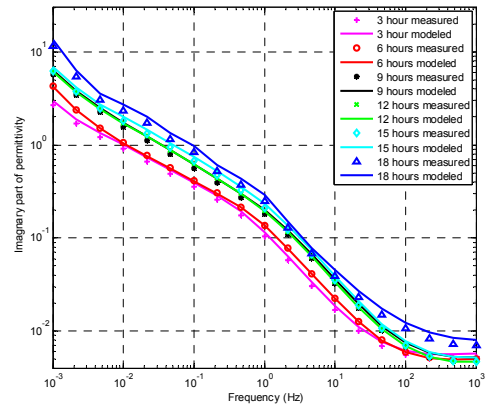


Fig. 3. Comparison between measured and modelled imaginary part (dielectric dissipation) of complex permittivity



# Secure Distributed Energy Management in the Presence of Misbehaving Generation Units

Wente Zeng, *Student Member, IEEE*, Ziang Zhang, *Member, IEEE* and Mo-Yuen Chow, *Fellow, IEEE*  
 Department of Electrical and Computer Engineering, North Carolina State University, Raleigh, NC, USA  
 Email: [wzeng3@ncsu.edu](mailto:wzeng3@ncsu.edu), [zzhang15@ncsu.edu](mailto:zzhang15@ncsu.edu) and [chow@ncsu.edu](mailto:chow@ncsu.edu)

**Abstract**—A variety of distributed control algorithms are being applied for smart grid energy management because of their flexibility, robustness, and local communication and computation features. These algorithms, however, increase the vulnerability of smart grid to adversaries. Thus, there is an urgent need to protect the distributed energy management algorithms from malicious cyber attacks. A reputation-based secure distributed energy management framework is proposed to guarantee an accurate control computation in distributed energy management algorithms to solve the economic dispatch problem in the presence of misbehaving generation units. The proposed method is capable of performing a secure distributed control without a central coordinator and allows all the well-behaving generation units reach the correct state asymptotically.

## I. KEY EQUATIONS

The Incremental Cost Consensus (ICC) algorithm is used as an example of distributed energy management algorithm. The block diagram of the secure distributed energy management algorithm for each generation unit is shown in Fig. 1. A neighborhood monitor and a local reputation manager have been embedded into the ICC algorithm and achieve attack-resilience in a distributed fashion. The update rule for the distributed energy management block, the neighborhood monitor block and the local reputation manager block are described by equation (1), (2) and (3) respectively.

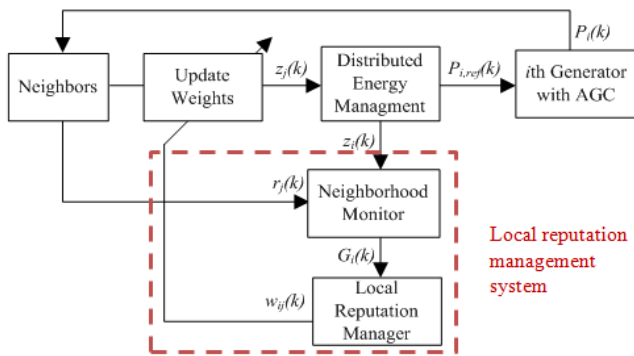


Fig. 1. The secure distributed energy management algorithm for the  $i$ th generation unit

$$z_i[k+1] = \sum_{j=1}^n w_{ij}[k] z_j[k], i = 1, \dots, n. \quad (1)$$

where  $z_i$  is the incremental cost for the  $i$ th generation unit,  $w_{ij}$  is the update weight between the  $i$ th unit and the  $j$ th unit.

$$G_{ij}[k] = \begin{cases} G_{ij}[k-1]+1, & r_j[k-1] - z_j[k] = 0 \\ G_{ij}[k-1], & r_j[k-1] - z_j[k] \neq 0 \end{cases} \quad (2)$$

where  $r_j$  is the reference incremental cost of the  $j$ th unit,  $G_{ij}$  is the total number of correct states of the neighbor unit  $j$ .

$$\begin{cases} rep_{ij}[k] = \frac{G_{ij}[k]+1}{k+2}, \\ w_{ij}[k] = rep_{ij}[k] / \sum_{j=1}^n rep_{ij}[k]. \end{cases} \quad (3)$$

where  $rep_{ij}$  is the reputation value of neighbor unit  $j$  up to time-step  $k$  in unit  $i$ 's local reputation manager.

## II. KEY FIGURES

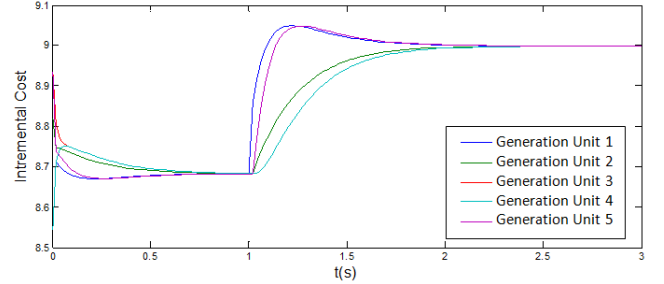


Fig. 2. Using a 5-unit system as an example. The incremental costs of five generation units reach consensus under normal conditions (assume no unit reaches generation limits and behaves abnormally).

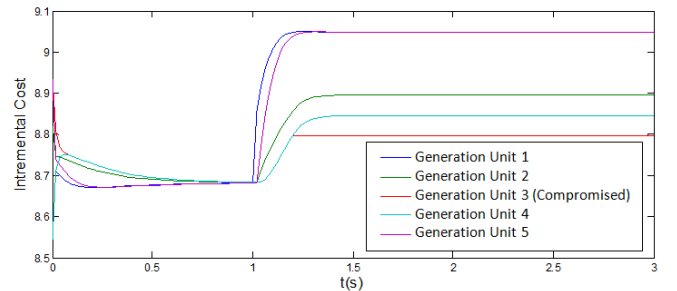


Fig. 3. The consensus network fails when the 3<sup>rd</sup> unit has been compromised, the system operates at a non-optimal condition.

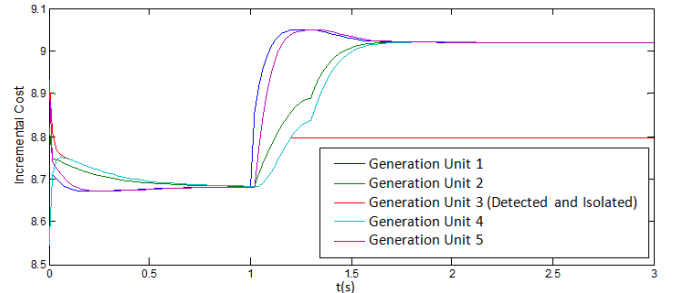


Fig. 4. By isolating the misbehaving unit, the rest of the well-behaving generation units reach the correct consensus state and operate at the optimal point again.



# Estimation of Stator Resistance in Direct Torque Control Synchronous Motor Drives

Younes Sangsefidi and Ali Mehrizi-Sani

School of Electrical Engineering and Computer Science, Washington State University, Pullman, WA, USA

Email: younes.sangsefidi@email.wsu.edu; mehrizi@eecs.wsu.edu

**Abstract**—Direct torque control (DTC) is a high performance sensorless method that provides effective control of stator flux modulus and electromagnetic torque of electric motors. However, an error in estimation of stator resistance significantly degrades the performance of DTC drive system, especially for a synchronous motor. A method to distinguish and track stator resistance variations is proposed. The method is based on finding a reference value for the angle between the stator flux and the stator current vectors and tracking this reference value by changing the estimated stator resistance. The proposed stator resistance estimator is validated using experimental case studies.

## I. PROBLEM STATEMENT

Desirable features such as fast dynamic response, no need to mechanical sensors, simple structure, and less dependence on motor parameters have made DTC drive systems an attractive option for the industry. DTC provides effective control of stator flux modulus and electromagnetic torque in a synchronous motor. However, one of its main limitations is that *a priori* knowledge of the stator resistance is required to estimate the stator flux vector and electromagnetic torque. Due to variations in temperature and frequency, stator resistance can vary considerably. A basic DTC synchronous drive is unable to track these variations, and consequently its performance may degrade.

## II. KEY EQUATIONS

The reference value of the angle between stator flux and current vectors is found by

$$T_e^* = \frac{mP|\lambda_s|^* \lambda_f}{2L_d} \sin \delta^* + \frac{mP|\lambda_s|^*{}^2}{4} \left( \frac{1}{L_q} - \frac{1}{L_d} \right) \sin 2\delta^* \quad (1)$$

and

$$\tan(\varphi_{i\lambda}^*) = \frac{T_e^*}{\frac{mP|\lambda_s|^*{}^2}{2L_d} \cos^2 \delta^* + \frac{mP|\lambda_s|^*{}^2}{2L_q} \sin^2 \delta^* - \frac{mP|\lambda_s|^* \lambda_f}{2L_d} \cos \delta^*} \quad (2)$$

The estimated angle between stator flux and current vectors is found by

$$\tilde{\varphi}_{i\lambda} = \tan^{-1} \left( \frac{i_{\tilde{y}s}}{i_{\tilde{x}s}} \right) = \tan^{-1} \left( \frac{\tilde{\lambda}_{D_s} i_{Q_s} - \tilde{\lambda}_{Q_s} i_{D_s}}{\tilde{\lambda}_{D_s} i_{D_s} + \tilde{\lambda}_{Q_s} i_{Q_s}} \right). \quad (3)$$

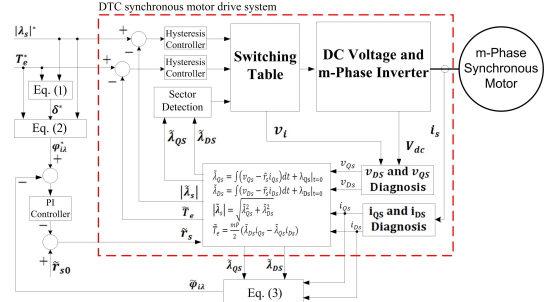


Fig. 1. The modified DTC synchronous motor drive system with stator resistance estimation.

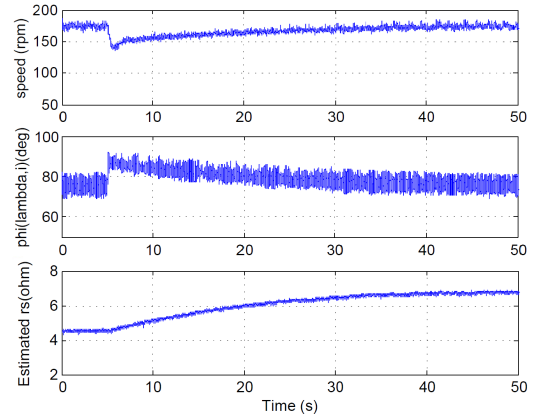


Fig. 2. The modified DTC synchronous motor drive system with the proposed stator resistance estimator.

To estimate the stator resistance, a PI controller can be designed as

$$\tilde{r}_{s0} - \tilde{r}_s = K_p(\varphi_{i\lambda}^* - \tilde{\varphi}_{i\lambda}) + K_i \int (\varphi_{i\lambda}^* - \tilde{\varphi}_{i\lambda}) dt, \quad (4)$$

The block diagram of the proposed stator resistance estimator is shown in Fig. 1.

## III. KEY EXPERIMENTAL RESULTS

The drive system starts working with correct value of stator resistance. At  $t = 5$  s,  $2.35 \Omega$  resistors are added in series with each phase of the motor. Experimental results are presented in Fig. 2. It can be observed that the proposed method successfully tracks the variations of the stator resistance.

# Induction Motor Control Based on Approximate Stator Flux

Saleh Ziaeinejad and Ali Mehrizi-Sani

School of Electrical Engineering and Computer Science, Washington State University, Pullman, WA, USA  
 Email: saleh.ziaeinejad@email.wsu.edu; mehrizi@eecs.wsu.edu

**Abstract**—A novel sensorless method for the induction motor control is proposed. In this method, magnitude and rotational speed of approximate stator flux vector are controlled. In the proposed approximate stator flux control (ASFC) method, utilization of the mechanical sensors and current transducers is not required. Therefore, implementation cost of ASFC is comparable with that of conventional scalar control method. Using experimental case studies, ASFC method is compared with the scalar method in terms of motor behavior in starting and steady state operation.

## I. PROBLEM STATEMENT

Among different strategies proposed for control of induction motors, scalar method is widely used in low-cost applications. One deficiency of scalar control method is its inherent poor dynamic behavior: Pulsating electromagnetic torque can lead to torsional vibrations and fatigue of the mechanical parts and premature of them. There is the need to a low cost drive system which does not suffer from this deficiency of scalar control system.

## II. THE PROPOSED METHOD

The proposed ASFC method is based on finding approximate stator flux vector and controlling amplitude and rotating speed of this vector. In order to find the approximate stator flux vector, a simplified voltage-based stator flux estimator is utilized. In a wide speed range, the error introduced by the simplified flux estimator is negligible and thus the performance of ASFC method is satisfactory. ASFC method is based on dynamic model of the induction motor. Therefore, it provides good dynamic behavior of the motor. Two different control approaches are proposed for motor control in linear and overmodulation ranges. As shown in Fig. 1, in the linear modulation range, a PWM-based approach is used and in the overmodulation range, a simple switching-table-based control approach is utilized.

## III. KEY EXPERIMENTAL RESULTS

ASFC drive system is implemented in laboratory settings and its performance is compared with the performance of the scalar drive system. Figs. 2 and 3 show comparison of ASFC and scalar control methods in linear and overmodulation ranges, respectively. It can be observed that in both cases, ASFC presents better dynamic behavior of the motor and smooth variation of the motor speed.

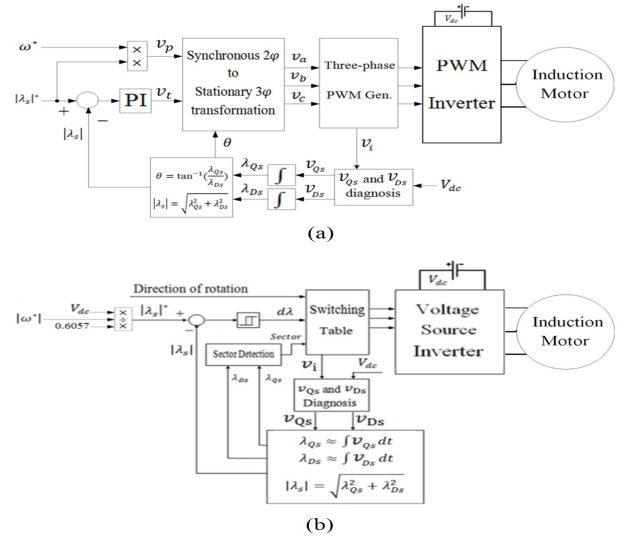


Fig. 1. ASFC drive system in (a) linear and (b) overmodulation ranges.

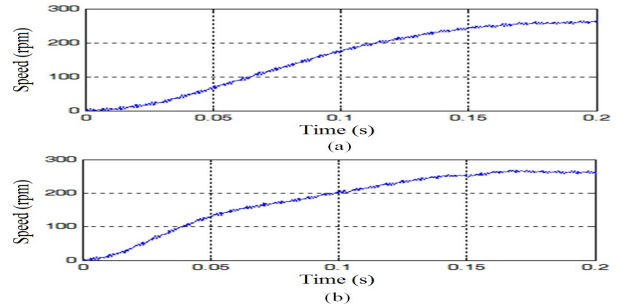


Fig. 2. Experimental results of motor speed in (a) ASFC and (b) scalar control methods in the linear modulation range with  $\omega = 125.0 \frac{rad}{s}$ .

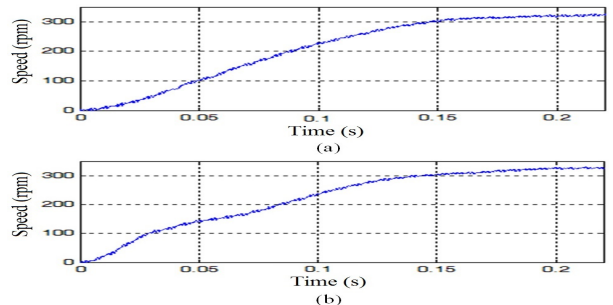


Fig. 3. Experimental results of motor speed in (a) ASFC and (b) scalar control methods in the overmodulation range with  $\omega = 151.4 \frac{rad}{s}$ .

# Application of a Resistive Superconducting Fault Current Limiter for Shunt Capacitor Bank Switching

Elizaveta O. Egorova, *Student Member, IEEE*

Department of Electrical and Computer Engineering,  
Michigan Technological University, Houghton, MI, USA

**Abstract**—This work has an objective of studying transients due to capacitor bank switching in a single phase 115-kV system with two capacitor banks in parallel. To limit high currents and dangerous values of  $I_p \times f$  product in the system, two options have been studied: current limiting reactor (CLR) in series with each capacitor bank and resistive superconducting fault current limiter (SFCL) in series with each capacitor bank. These two options were compared with the case where no limiting device was installed and the results showed that for the system recovery the most beneficial option is with SFCL in series with each capacitor bank due to introducing a considerable damping effect on the transients. However, amount of investments into SFCL device versus cheap and simple CLR makes the former the least appealing. Thus, more time is needed for industry to develop cheaper SFCL devices.

**Index Terms**— Alternative Transient Program (ATP-EMTP), shunt capacitor bank, capacitor bank energization, inrush current, outrush current, superconducting fault current limiter, transient recovery voltage.

## I. INTRODUCTION

OPERATION of capacitor banks in a power system can produce transients that can be damaging for the equipment. High frequency and high magnitude currents due to energization inrush or outrush due to a fault produce conditions which can damage contacts of a circuit breaker. The indicator of such a condition is a  $I_p \times f$  factor and in order to reduce it, utilities install current limiting reactors (CLRs) in series with each capacitor bank. This work explored the effect of installation of a resistive superconducting fault current limiter (SFCL) in series with each capacitor bank. The shunting branch of an SFCL has a CLR.

## II. KEY EQUATIONS

The simulations were performed in Alternative Transient Program (ATP-EMTP). The superconducting elements were modeled as nonlinear resistance elements and resistance evolution is governed by three equations:

$$R_1 = \frac{dV}{dI} = \frac{nV_c I^{n-1}}{I_c^n} \quad (1)$$

$$R_2 = R_{\max} e^{-t/\tau} \quad (2)$$

$$R_3 = R_{\text{crit}} - \frac{R_{\text{crit}}}{\text{slope}} (t_c - t_{\text{crit}}) \quad (3)$$

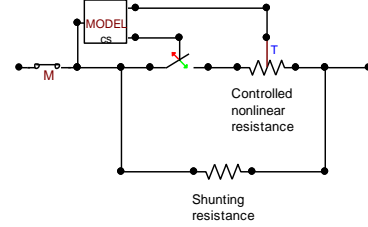


Fig. 1. Simplified control of nonlinear resistance. Four elements are connected in parallel in the implemented model.

## III. KEY RESULTS

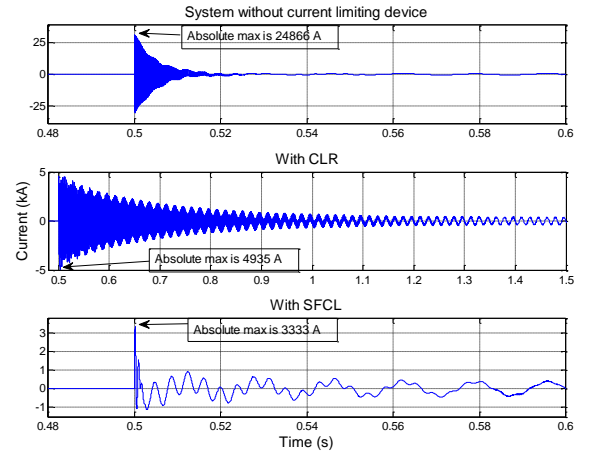


Fig. 2. Mitigation of inrush for back-to-back switching of capacitor banks.

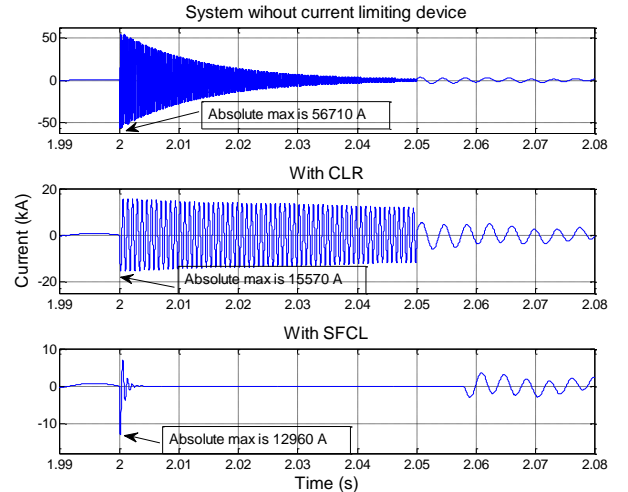


Fig. 3. Outrush current from both capacitor banks for a nearby bus fault.

# Dynamic Adjustment of OLTC Parameters using Voltage Sensitivity while utilizing DG for Volt/VAR Support

D. Ranamuka, *Student Member, IEEE*, A. P. Agalgaonkar, *Senior Member, IEEE*, and K. M. Muttaqi, *Senior Member, IEEE* - Australian Power Quality and Reliability Centre, University of Wollongong, Australia

**Abstract**--A novel methodology is proposed in this paper to assess the impact of voltage support DG on voltage correction and update the substation OLTC parameters dynamically. As an assessment tool, first order sensitivity of the regulating point voltage,  $V_{LC}$  to the change in reactive power support provided by voltage support DG,  $Q_{DG}$  is derived. The estimated value of voltage change by means of VAR support by DG at the load centre, obtained using proposed sensitivity analysis, is used to assess the impact of voltage support DG on the operation of line drop compensation (LDC). Based on such information, a strategy is proposed to dynamically update the OLTC parameters for effective voltage control in the presence of voltage support DG. The simulation results show the accuracy of the mathematical model used for analysis and its successful implementation.

## I. PROPOSED VOLTAGE SENSITIVITY - KEY EQUATIONS

From the equation for  $V_{LC}$ , it can be seen that the  $V_{LC}$  is a function of  $V_{OLTC}$ ,  $\alpha_{OLTC}$ ,  $I$ ,  $\theta$ , and  $R_L$ ,  $X_L$  (LDC settings).

$$\begin{aligned} \Delta V_{LC} &= \left( \frac{\partial V_{LC}}{\partial V_{OLTC}} \right) \Delta V_{OLTC} + \left( \frac{\partial V_{LC}}{\partial \alpha_{OLTC}} \right) \Delta \alpha_{OLTC} + \left( \frac{\partial V_{LC}}{\partial I} \right) \Delta I + \\ &+ \left( \frac{\partial V_{LC}}{\partial \theta} \right) \Delta \theta \\ \Delta V_{LC} &= (LC1) \Delta V_{OLTC} + (LC2) \Delta \alpha_{OLTC} + (LC3) \Delta I + (LC4) \Delta \theta \end{aligned}$$

From the phasor diagram and system Jacobian matrix :

$$\begin{aligned} \frac{\Delta I}{\Delta Q_{DG}} &= (I1) \times (M_{VQ})_{oltc,k} + (I2) \times (M_{VQ})_{(oltc+1),k} + (I3) \times \\ &\times \left( (M_{\alpha Q})_{oltc,k} - (M_{\alpha Q})_{(oltc+1),k} \right) \end{aligned}$$

$$\begin{aligned} \frac{\Delta \theta}{\Delta Q_{DG}} &= \left( \frac{1 - \theta 1.12}{\theta 3} \right) \times (M_{VQ})_{(oltc+1),k} - \left( \frac{\theta 2 + \theta 1.11}{\theta 3} \right) \times \\ &\times (M_{VQ})_{oltc,k} - \left( \frac{\theta 4 + \theta 1.13}{\theta 3} \right) \times \left( (M_{\alpha Q})_{oltc,k} - (M_{\alpha Q})_{(oltc+1),k} \right) \end{aligned}$$

Proposed voltage sensitivity y :

$$\begin{aligned} \frac{\Delta V_{LC}}{\Delta Q_{DG}} &= (LC1) \times (M_{VQ})_{oltc,k} + (LC2) \times (M_{\alpha Q})_{oltc,k} + \\ &+ (LC3) \times \left( \frac{\Delta I}{\Delta Q_{DG}} \right) + (LC4) \times \left( \frac{\Delta \theta}{\Delta Q_{DG}} \right) \end{aligned} \quad (A)$$

## II. DYNAMIC ADJUSTMENT OF OLTC PARAMETERS

The severity of DG impact on operation of LDC is based on how much the voltage change by DG at load centre contributes to violate dead-band limit or supports to minimize the voltage error for OLTC control. On that basis, the proposed strategy for dynamically updating the LDC settings in presence of voltage support DG is developed. It is proposed to practically

implement this strategy using a substation centered DMS for on-line voltage control. The diagrammatic representation of proposed system design is shown in Fig. 1.

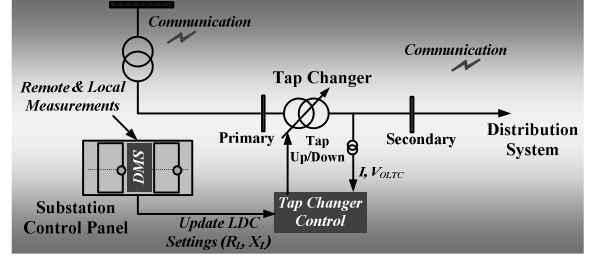


Fig. 1. Topology of system design for proposed dynamic operation of OLTC.

## III. KEY RESULTS

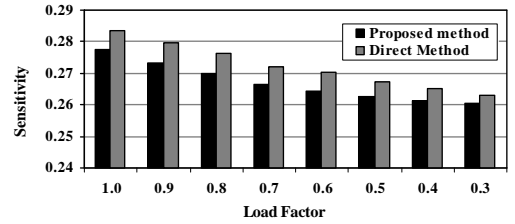


Fig. 2. Sensitivity values derived using proposed and direct methods

TABLE I

ESTIMATED VOLTAGE CHANGE BY QDG USING PROPOSED SENSITIVITY			
Load Factor	Proposed method/(pu)	Multiple Power Flow/(pu)	Mismatch /(pu)
1.000	0.0183	0.0182	0.0001
0.900	0.0181	0.0179	0.0002
0.800	0.0178	0.0177	0.0001
0.700	0.0176	0.0174	0.0002
0.500	0.0173	0.0171	0.0002
0.400	0.0172	0.0170	0.0002

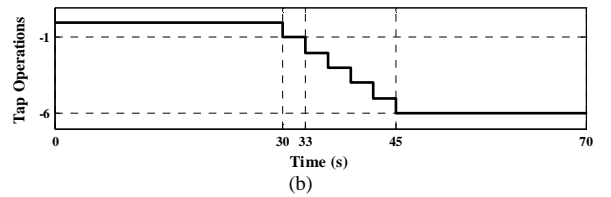
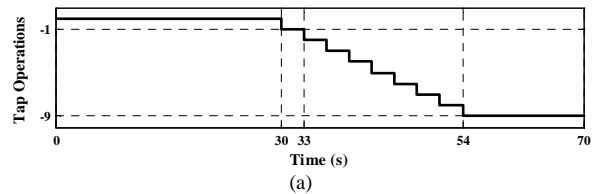


Fig. 3. Tap operations of substation OLTC (a) under conventionally derived LDC settings and (b) under proposed LDC settings, where load factor is 0.8.

# Tie-Line Bias Control of a Power System with Variable Renewable Energy Generation

Iroshani Jayawardene, *Student Member, IEEE*, Ganesh K. Venayagamoorthy, *Senior Member, IEEE*  
 Real-Time Power and Intelligent Systems (RTPIS) Laboratory  
 The Holcombe Dept. of Electrical and Computer Engineering  
 Clemson University, SC 29634, USA  
 Emails: [ijayawardene@gmail.com](mailto:ijayawardene@gmail.com), [gkumar@ieee.org](mailto:gkumar@ieee.org)

**Abstract** - In this study, a two-area power system with large MW PV plants was considered, in which Area 1 provided power interchange to Area 2. To minimize power fluctuations and maintain the desired system frequency while concurrently maximizing the penetration of PV power into Area 2, automatic generation control (AGC) with tie-line bias control was implemented. The objective was to increase/decrease generations in Area 1, thus varying the tie-line power flow to balance out the PV power variability. Furthermore, the output power of the PV plant used in Area 1 AGC control was predicted based measurements obtained from a phasor measurement unit at the PV plant bus. Typical results are shown for the steady state, variable PV generation and large tie-line disturbance conditions.

**Index Terms**—Large PV plants, neural networks, phasor measurement units, predictions, tie-line bias control, tie-line power flow and frequency control

## I. INTRODUCTION

The increasing penetration of uncertain and variable renewable energy into the transmission grid introduces challenges in real-time power system operation. A large photovoltaic (PV) system or a wind farm’s power output fluctuation due to weather conditions (irradiance, temperature, wind speed and direction) causes the system’s frequency to fluctuate. The power and frequency fluctuations in systems with large MW variable generation raise dynamic and transient stability concerns. In this study, a 200 MW PV plant was connected to a two-area, four-machine system, as shown in Fig 1.

In order to maintain the system’s frequency and tie-line flows, a secondary control, AGC, was implemented such that each area had its own regulator. The block diagrams of the AGCs in Areas 1 are shown in Fig 2. Fig. 3 shows the tie-line power variations without predictions of the variable generation used in the Area 1 AGC. The control can be improved by predicting the PV plant generation using a neural network, and replacing the real-time PV plant generation value with the predicted value in the tie-line bias control. The predictions intervals studied are 30 to 90 seconds. Optimal prediction step size has to be determined for the best control.

## II. KEY FIGURES

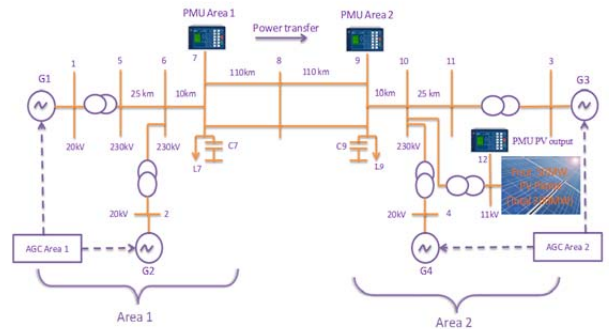


Fig 1. 200 MW PV plant integrated into a two-area power system.

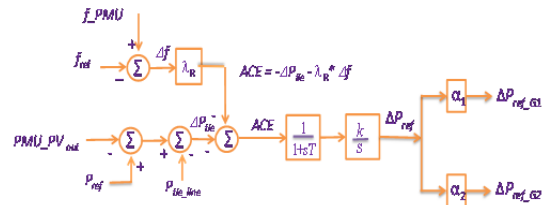


Fig 2. Area 1 AGC functional diagram for the power system shown in Fig 1.

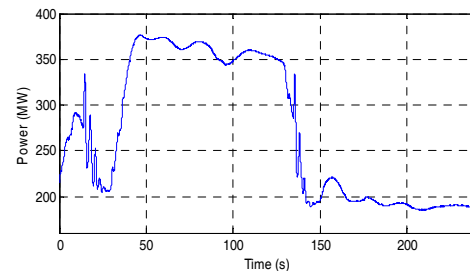


Fig. 3. The tie-line power variations.

## REFERENCES

- [1] S. Eftekharijrad, V. Vittal, G. T. Heydt, B. Keel, and J. Loehr, "Impact of increased penetration of photovoltaic generation on power systems," *IEEE Transactions on Power Systems*, vol. 28, no. 2, May 2013, pp. 893- 901.
- [2] G. K. Venayagamoorthy, "Tie-Line Bias Control of a Power System with Large PV Plants Using PMU Information", *XIII Symposium of Specialists in Electric Operational and Expansion Planning*, May 18-21, 2014, Foz do Iguaçu (PR), Brazil.



# Impact of Demand Side Management on the Tap Operation of Primary Distribution Transformers

Suvagata Chakraborty, *Student Member, IEEE* and Visvakumar Aravinthan, *Member, IEEE*

Department of Electrical Engineering and Computer Science  
Wichita State University  
Kansas, USA

{sxchakraborty, visvakumar.aravinthan}@wichita.edu

**Abstract**—Demand Side Management (DSM) refers to the action taken on the customer’s premises that are actively encouraged or carried out by the utility to modify energy use patterns for the reduction of electricity cost. The initial analysis of this work is to determine the impact on tap changes without demand response (DR) and effect on accuracy of the information obtained at different rates of control intervals. This work also focuses on the analysis of the impact of controlled and uncontrolled demand response on the tap changing operation for the primary distribution transformer for different months and different rates of control intervals. The controlled demand response is done using peak shaving and valley filling, whereas the uncontrolled demand response is done using proprietary data load shape. The analysis was performed on IEEE Test Case 13 Node Circuit modeled in OPENDSS.

## I. INTRODUCTION

Demand response (DR) schemes will change the way the system operates and has the potential to affect the system reliability [1]. In addition to affecting the traditional reliability indices such as energy not served, DR has the potential to affect the distribution assets. In this work information accuracy at different control interval is analyzed. The interval rates used are 1min, 15min, 30min and 60min. Number of tap changes of the primary distribution transformer for different months and different control intervals were monitored. It is assumed that DR will adjust the total load to a certain threshold value. As the control interval increases there is an irregularity in the total number of expected tap changes for a month as system loading is averaged and hence affects the accuracy of the sampled information from the real time information. 15min and 30min sample rate tend to overshoot the number of tap changes in respect to 1min sample rate data, whereas 60min undershoot the value. The results for month of January are shown in Table I.

TABLE 1:

TOTAL NUMBER OF TAP CHANGES AT DIFFERENT AVERAGE LOAD RATES

	Reg.Ph.A	Reg.Ph.B	Reg.Ph.C	Total
1min	373	215	468	1056
15min	446	245	489	1180
30min	429	242	471	1142
60min	380	202	387	969

## II. IMPACT OF DEMAND RESPONSE ON OLTC

This part of the work analyzed the impact on tap changes due to different demand response schemes. Controlled demand response is obtained using peak shaving and valley filling, where the aggregator can manage energy usage of consumer at a specific time interval[1]. Three different percentages 5%,

10%, 20% for peak reduction is used and that load is shifted to fill the valley. As the percentage of reduction increases the number of tap changes decreases. Results for a month are shown in Table II.

TABLE 2:  
NUMBER OF TAP CHANGES FOR PEAK SHAVING

	Reg.Ph.A	Reg.Ph.B	Reg.Ph.C
0%	446	245	489
5%	392	217	443
10%	354	187	405
20%	272	133	349

The uncontrolled demand response is done using proprietary data where consumers are expected to reduce their consumption during a certain time of the day. Results for a month are shown in Table III.

TABLE 3:  
NUMBER OF TAP CHANGES FOR DEMAND RESPONSE

	Reg.Ph.A	Reg.Ph.B	Reg.Ph.C	Total
No DR	380	202	387	969
DR	408	234	465	1107

## III. KEY FIGURE

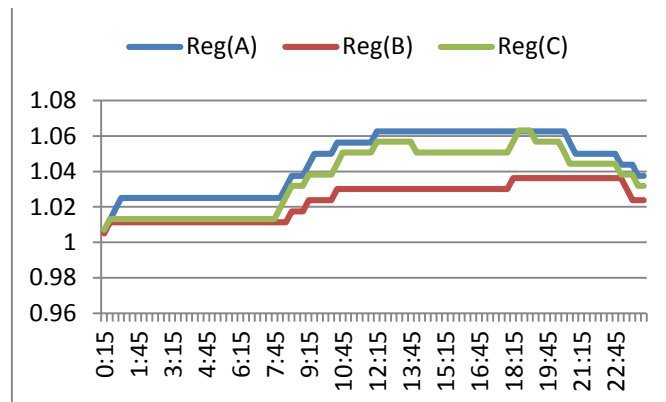


Fig1. Tap Change for 1day at 20% peak shaving (15min interval)

The other figures will be displayed at the poster presentation.

## REFERENCE

- [1] S.Mohagheghi, F. Yang, and B. Falahati, “Impact of Demand Response on DistributionSystem Reliability” In Proc. IEEE PES General Meeting, July 2011



# Bi-level Linear Programming Based Interval Optimization for SCED in the Presence of Wind Power Uncertainty

Tao Ding, *Student Member, IEEE*, Hongbin Sun, *Senior Member, IEEE*, Forrest Harley, *Student Member, IEEE*, Fangxing Li, *Senior Member, IEEE*, Rui Bo, *Senior Member, IEEE*

Security constrained economic dispatch (SCED) is widely used in recent day-ahead market, especially when there is a large penetration of wind power in the power grid. In this work the wind generation uncertainty is modeled as an interval number, which leads to an interval optimal objective value (fuel costs) of the original SCED, as well as its interval optimal solution (each unit's generation). In order to obtain the true upper and lower bound of the interval optimal objective value and solution, a bi-level programming model is initialized so that the combinatorial nature of bi-level programming can be observed through the study of the single-level reformulation obtained in replacing the inner level problem with its KKT condition.

$$\text{(SCED-I)} \quad Z^\pm = \min \quad \mathbf{c}^T \mathbf{x} \quad (1-a)$$

$$s.t. \quad \mathbf{Ax} = [\mathbf{b}^-, \mathbf{b}^+] \quad (1-b)$$

$$\mathbf{Bx} \leq [\mathbf{d}^-, \mathbf{d}^+] \quad (1-c)$$

$$\mathbf{Dx} \leq \mathbf{e} \quad (1-d)$$

$$\mathbf{x}^{\min} \leq \mathbf{x} \leq \mathbf{x}^{\max} \quad (1-e)$$

It is obvious that model (1) is an interval optimization model, and if the interval uncertainties are combined using the basic interval operations defined in the last sub-section, the (SCED-I) can be formulated as (2) without loss of generality, where the interval of uncertainty is located only on the right hand side.

$$Z^\pm = \min \quad \mathbf{c}^T \mathbf{x} \quad (2-a)$$

$$s.t. \quad \mathbf{Ax} = [\mathbf{b}^-, \mathbf{b}^+], \quad \mathbf{Vx} \leq [\mathbf{v}^-, \mathbf{v}^+] \quad (2-b)$$

The objective value and the optimal solution of the general interval optimization model (2) are both intervals ranging from the lower bound (objective value is  $Z^-$  and optimal solution is  $\mathbf{x}^-$ ) to the upper bound (objective value is  $Z^+$  and optimal solution is  $\mathbf{x}^+$ ). At first, the interval objective value can be obtained by solving two respective sub-optimization models.

(Lower Bound)

(Upper Bound)

$$Z^- = \min_x \quad \mathbf{c}^T \mathbf{x} \quad Z^+ = \max_{b^- \leq \eta \leq b^+} \min_x \quad \mathbf{c}^T \mathbf{x}$$

$$s.t. \quad \mathbf{b}^- \leq \mathbf{Ax} \leq \mathbf{b}^+ \quad (4) \quad s.t. \quad \mathbf{Ax} = \boldsymbol{\eta} \quad (3)$$

$$\mathbf{Vx} \leq \mathbf{v}^+$$

$$\mathbf{Bx} \leq \mathbf{v}^-$$

As is apparent, the lower bound model is a simple linear programming (LP) model that can be easily solved using the Simplex method, whereas the upper bound model is an NP-hard problem that is difficult to address due to combinatorial interval equality constraints, which can be transformed into single-level reformulation obtained by

$$x_i^\pm = \max_x / \min_x \quad x_i$$

$$s.t. \quad x_i^{\min} \leq x_i \leq x_i^{\max}$$

$$\mathbf{b}^- \leq \boldsymbol{\eta} \leq \mathbf{b}^+$$

$$\mathbf{v}^- \leq \mathbf{v} \leq \mathbf{v}^+$$

$$\mathbf{Ax} = \boldsymbol{\eta} \quad i = 1, \dots, N_g \quad (4)$$

$$\mathbf{c} + \mathbf{A}^T \boldsymbol{\mu} + \mathbf{V}^T \boldsymbol{\lambda} = \mathbf{0}$$

$$-M(1-z) \leq \mathbf{Vx} - \mathbf{v} \leq \mathbf{0}$$

$$Mz \geq \boldsymbol{\lambda} \geq \mathbf{0}, \quad z \in \{0, 1\}$$

The IEEE 118-bus test system with 24 time periods is studied to investigate the effectiveness of proposed interval SCED model using bi-level programming. The detailed parameter information of the network and generators can be found in MATPOWER, where the 19 units are in-service for a SCED model with 6 wind farms. The maximum capacity of each wind farm is 100MW. The total load demand and wind generation forecast is shown in Fig.1 where the shapes are similar to the real operating conditions of the northern Chinese province of Jilin. The IEEE 118-bus test system with 24 time periods is studied to investigate the effectiveness of proposed interval SCED model using bi-level programming. It can be observed that the interval optimal generation of each unit is computed by (4). The results, with two scenarios under  $\alpha=0.1$ , are shown in Fig.1, where: (1-a) and (1-b) depict the generation of all units during 11:00~12:00 a.m.; (1-c) and (1-d) depict the generation of unit 5 over 24 hours.

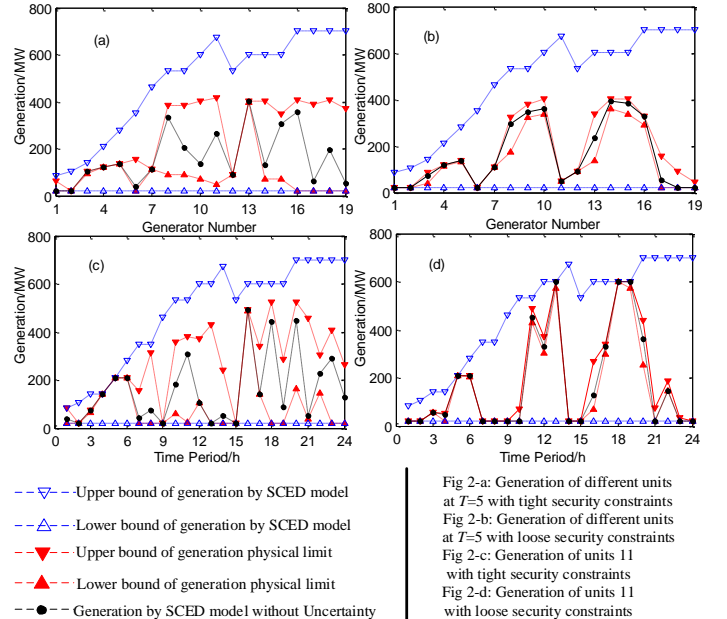


Fig.1 Comparison of upper and lower bound of generation with tight and loose security constraints

# Application of Computational Intelligence in Reliability Improvement of Active Distribution Systems Through Feeder Reconfiguration

Salem Elsaiah, *Student Member, IEEE*, and Joydeep Mitra, *Senior Member, IEEE*  
 Department of Electrical and Computer Engineering  
 Michigan State University  
 East Lansing, Michigan 48824, USA  
 (elsaihs@msu.edu)

**Abstract**—This paper describes a method for reliability improvement of power distribution system via feeder reconfiguration. The work presented here is developed based on a linearized network model in the form of DC power flow and linear programming model in which current carrying capacities of distribution feeders and real power constraints have been considered. The optimal open/close status of the sectionalizing and tie-switches are identified using an intelligent binary particle swarm optimization based search method. The probabilistic reliability assessment is conducted using a method based on high probability order approximation. A micro-power optimization model based on Homer software is used to account for the uncertainty in the output power of the intermittent renewable energy sources. Several case studies are carried out on a 33 bus radial distribution system, which is extensively used as an example in solving the distribution system reconfiguration problem. The effect of distributed generators has been considered in one several scenario. The obtained results are reported, discussed, and thoroughly analyzed.

**Index Terms**—Distribution system reconfiguration, reliability, particle swarm optimization, intermittent energy sources.

## I. BACKGROUND

Distribution systems have long been operated in a vertical manner for best control and coordination of their protective devices. Distribution systems are equipped with two types of switches; sectionalizing and tie-switches. The sectionalizing switches are normally closed and are used to connect various distribution line segments. The tie-switches, on the other hand, are normally opened and can be used to transfer loads from one feeder to another during abnormal and emergency conditions. Feeder reconfiguration is among the several operational tasks that are performed frequently on distribution systems. Basically, it denotes to the process of changing the topological structure of the distribution network by altering the open/close status of sectionalizing and tie-switches to achieve certain objectives. Of these objectives, loss minimization, voltage profile improvement, and reliability and security enhancement are of most concern.

Due to numerous environmental, political, and economical concerns, the structure of the distribution systems has been changed in recent years. A crucial part of this change has come through the installation of small sources of energy, constantly denoted as distributed generators, on several distribu-

tion systems. Examples of these energy sources include wind turbine induction generators and solar generators. Despite their numerous advantages, the inclusion of these intermittent renewable energy sources in the steady-state analysis of power distribution system such as feeder reconfiguration for loss reduction or reliability enhancement, for instance, has also brought up a number of technological and operational issues that need to be addressed.

## II. KEY RESULTS

TABLE I: Parameters of the BPSO

Parameter	Value
Number of particles	50
Social constant ( $c_1$ )	2
Social constant ( $c_2$ )	2
Max. number of iterations	1500

TABLE II: 33-Bus System Results—Case Study I

Network Status	Set of Opened Switches	EDNS kW/year
Initial Configuration	S33, S34, S35, S36, S37	10.08
Final Configuration	S6, S10, S13, S27, S32	8.49

TABLE III: 33-Bus System Results—Case Study II

Network Status	Set of Opened Switches	EDNS kW/year
Initial Configuration	S33, S34, S35, S36, S37	14.17
Final Configuration	S6, S10, S12, S27, S36	11.89

TABLE IV: 33-Bus System Results—Case Study III

Network Status	Set of Opened Switches	EDNS kW/year
Initial Configuration	S33, S34, S35, S36, S37	9.86
Final Configuration	S6, S10, S13, S26, S36	7.71

# Distributed Security-Constrained Unit Commitment for Large-Scale Power Systems

Amin Kargarian, *Student Member, IEEE*, Yong Fu, *Senior Member, IEEE*, and Zuyi Li, *Senior Member, IEEE*

**Abstract**— The independent system operators (ISOs) of restructured power markets solve the security-constrained unit commitment (SCUC) problem to plan a secure and economic generation schedule. However, as the size of the power system increases, the current centralized SCUC algorithms could face critical challenges ranging from modeling accuracy to calculation complexity. This paper presents an efficient and fast distributed SCUC (D-SCUC) algorithm for large-scale power systems. In this algorithm, the power system is decomposed into several scalable zones which are connected together through the tie lines. Each zone has its own SCUC problem. A parallel calculation method is proposed to coordinate these D-SCUC problems. In the paper, the modified IEEE 48-bus, IEEE 118-bus, and the 4672-bus power systems are studied to show the effectiveness of the proposed algorithm.

## I. KEY EQUATIONS

1. Objective function of the D-SCUC of area  $j$  which is connected to actual area  $k$  through the physical tie-line:

$$\begin{aligned} \text{Min } f_j(\tilde{\mathbf{x}}_j) & \\ & + \sum_{t=1}^{NT} \sum_{b,b'=1}^{NSC} \{ a_{bjkt} (\delta_{bjkt}^* - \delta_{bjkt}) + \left\| \beta_{bjkt} \circ (\delta_{bjkt}^* - \delta_{bjkt}) \right\|_2^2 \\ & + a_{b'jkt} (\delta_{b'jkt}^* - \delta_{b'jkt}) + \left\| \beta_{b'jkt} \circ (\delta_{b'jkt}^* - \delta_{b'jkt}) \right\|_2^2 \} \end{aligned}$$

2. Objective function of the optimization problem of area  $j$  which is connected to the virtual area  $m$  (master problem):

$$\begin{aligned} \text{Min } f_j(\tilde{\mathbf{x}}_j) & \\ & + \sum_{t=1}^{NT} \sum_{b,b'=1}^{NSC} \{ a_{bjmt} (\hat{\delta}_{bjmt}^* - \delta_{bjmt}) + \left\| \beta_{bjmt} \circ (\hat{\delta}_{bjmt}^* - \delta_{bjmt}) \right\|_2^2 \\ & + a_{b'jmt} (\hat{\delta}_{b'jmt}^* - \delta_{b'jmt}) + \left\| \beta_{b'jmt} \circ (\hat{\delta}_{b'jmt}^* - \delta_{b'jmt}) \right\|_2^2 \} \end{aligned}$$

3. Objective function of the optimization of master problem:

$$\begin{aligned} \text{Min } \sum_{t=1}^{NT} \sum_{J=1}^{NZ} \sum_{b,b'=1}^{NSC} \{ a_{bJmt} (\hat{\delta}_{bJmt}^* - \delta_{bJmt}^*) + \left\| \beta_{bJmt} \circ (\hat{\delta}_{bJmt}^* - \delta_{bJmt}^*) \right\|_2^2 \\ + a_{b'Jmt} (\hat{\delta}_{b'Jmt}^* - \delta_{b'Jmt}^*) + \left\| \beta_{b'Jmt} \circ (\hat{\delta}_{b'Jmt}^* - \delta_{b'Jmt}^*) \right\|_2^2 \} \end{aligned}$$

4. Constraints of the optimization of master problem:

$$\begin{aligned} \hat{\delta}_{bmjt} &= \hat{\delta}_{b'mkt} & \forall t \\ \hat{\delta}_{b'mjt} &= \hat{\delta}_{b'mkt} & \forall t \end{aligned}$$

A. Kargarian and Y. Fu are with the Department of Electrical and Computer Engineering, Mississippi State University, Mississippi State, MS 39762 USA (e-mail: ak836@msstate.edu, fu@ece.msstate.edu).

Z. Li is with the Department of Electrical and Computer Engineering, Illinois Institute of Technology, Chicago, IL 60616 USA (e-mail: lizuyi@iit.edu).

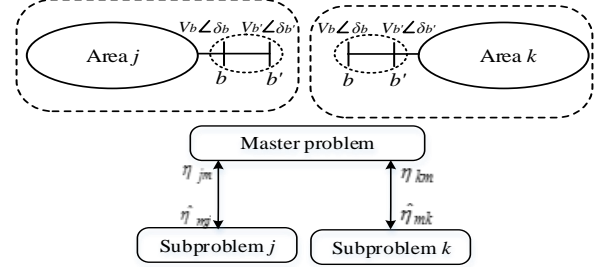


Fig. 1. Modeling shared variables between zones  $j$  and  $k$ , and using virtual zone to disconnect the actual zones and parallelize the D-SCUC algorithm.

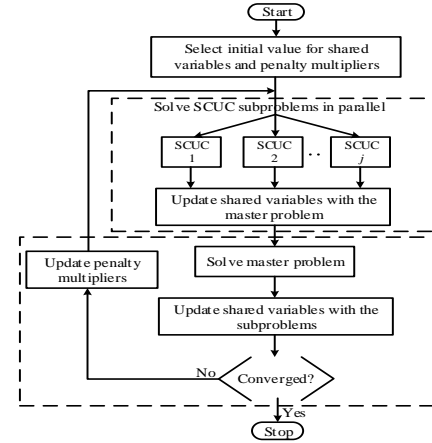


Fig. 2 Solution algorithm.

## II. KEY RESULTS

TABLE I  
COMPARISON OF C-SCUC AND D-SCUC WITH FOUR ZONES

Items	C-SCUC	D-SCUC
Total operating cost (\$)	1,339,000	1,34400
Total calculation time (sec.)	69	22

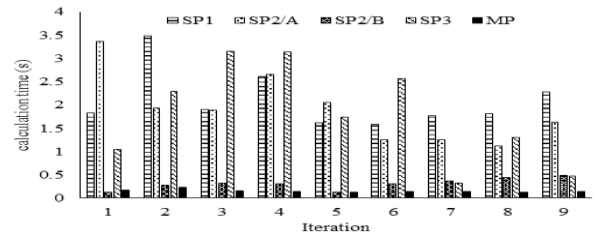


Fig. 3. Detail of calculation time for D-SCUC.

TABLE II  
COMPARISON OF C-SCUC AND D-SCUC FOR THE 4762-BUS SYSTEM

Items	C-SCUC	D-SCUC
Total operating cost (\$)	8,217,023	8,233,437
Total calculation time (min.)	27	8

# Security Constrained Unit Commitment Considering Voltage Stability

Mojtaba Khanabadi, *Student Member, IEEE*, Yong Fu, *Senior Member, IEEE*

**Abstract**— Security constrained unit commitment problem is executed every day to find the hourly schedule for next 24 hours. However, the solution of this problem might jeopardize the system security in real operation of power system due to lack of AC constraints and voltage stability consideration. This study introduces an approach to solve the SCUC problem and find the minimum operation cost while the voltage stability is respected. The proposed method takes advantage of augmented Lagrangian Relaxation (LR) method to decompose and solve SCUC problem iteratively. Using this concept, the original problem is decomposed to multiple sub-problems after introducing the duplication of units generation variables in each iteration and each sub-problem can be solved in parallel to decrease the execution time and complexity of the model. In the next iteration, the Lagrangian multipliers will be updated and the problem will be solved again. This iterative process will continue until the convergence criterion being satisfied. The effectiveness of proposed model is tested on 6-Bus test system.

## I. KEY EQUATIONS AND CONCEPTS

1. With introducing the duplicated variables, the objective function of the decomposed problem can be formulated as follow:

$$L(P, P^\Delta, I, \lambda) = \sum_{i=1}^{NG} \sum_{t=1}^{NT} L_1 + \sum_{i=1}^{NG} \sum_{t=1}^{NT} L_2 + \sum_{i=1}^{NG} \sum_{t=1}^{NT} L_3,$$

where

$$L_1(P, I, \lambda) = \sum_{i=1}^{NG} \sum_{t=1}^{NT} StCost_{it} + SdCost_{it} + (C_p + \alpha_i)(P_{G_{it}}^k)^2 + \left[ \beta_i - \lambda_{it}^k - C_p (P_{G_{it}}^{\Delta k-1} - P_{G_{it}}^{k-1}) \right] P_{G_{it}}^k$$

$$L_2(P, \lambda) = \sum_{i=1}^{NG} \sum_{t=1}^{NT} C_p (P_{G_{it}}^{\Delta k})^2 + \left[ \lambda_{it}^k - C_p (P_{G_{it}}^{\Delta k-1} - P_{G_{it}}^{k-1}) \right] P_{G_{it}}^k$$

$$L_3 = \sum_{i=1}^{NG} \sum_{t=1}^{NT} C_p \left[ (P_{G_{it}}^{\Delta k-1})^2 - (P_{G_{it}}^{k-1})^2 \right]$$

2. The second part of objective function can be solved for each hour independently. It means that we would be able to find the  $L_2$  results for each hour without any correlation with other hours. Therefore, we can express the second part as:

$$L_2(P, \lambda) = \sum_{t=1}^{NT} L'_2(t)$$

$$L'_2(t) = \sum_{i=1}^{NI} C_p (P_{G_i}^{\Delta k})^2 + \left[ \lambda_i^k - C_p (P_{G_i}^{\Delta k-1} - P_{G_i}^{k-1}) \right] P_{G_i}^k$$

3. The third part of the objective function is related to the previous iteration so this part does not need to be optimized.

4. Lagrangian multipliers are updating in each iteration in order to modify the feasible solution as follows.

$$\lambda_{it}^k = \lambda_{it}^{k-1} + C_p (P_{G_{it}}^{\Delta k-1} - P_{G_{it}}^{k-1})$$

5. Constraints of the optimization for the first and second sub-problem are categorized as:

- General SCUC constraints for  $L_1$
- AC and voltage stability constraints associated with penalty function for  $L_2$

6. Solution algorithm is shown using the following flowchart:

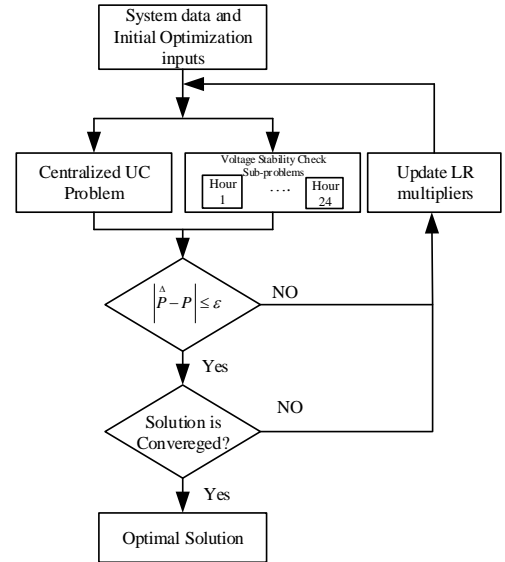


Figure 1: Solution Flowchart

## II. KEY RESULTS

TABLE II  
UNIT COMMITMENT RESULTS FOR THE CONVENTIONAL SCUC FOR 6-BUS TEST SYSTEM

U	Hours (1-24) - Daily Cost (\$97573.5)																	
1	1	1	1	1	1	1	1	1	1	1	1	1	1	1	1	1	1	1
2	0	0	0	0	0	0	0	0	0	0	0	0	0	0	0	0	0	0
3	0	0	0	0	0	0	0	0	1	1	1	1	1	1	1	1	1	1

TABLE III  
UNIT COMMITMENT RESULTS FOR SCUC PROBLEM USING THE PROPOSED METHOD CONSIDERING VOLTAGE STABILITY FOR 6-BUS TEST SYSTEM

U	Hours (1-24) - Daily Cost (\$106425.5)																	
1	1	1	1	1	1	1	1	1	1	1	1	1	1	1	1	1	1	1
2	1	1	0	0	0	0	0	0	1	1	1	1	1	1	1	1	1	1
3	1	1	1	1	1	1	1	1	1	1	1	1	1	1	1	1	1	1

# Stochastic Security Constrained Unit Commitment in Parallel Structure

Chunheng Wang, *Student Member, IEEE*, and Yong Fu, *Senior Member, IEEE*

**Abstract**—This paper presents a parallel stochastic security constrained unit commitment (SCUC) model for large-scale power systems with wind and load uncertainties. In the proposed parallel stochastic SCUC model, augmented Lagrangian relaxation (ALR) combined with variable duplication technique and auxiliary problem principle (APP) are adopted to decompose the original problem into individual unit commitment (UC) problems and hourly network security (NS) problems. In addition, trust region technique is employed to ensure the accuracy of approximation of APP method, which improves the convergence performance of the proposed parallel stochastic SCUC model. Numerical case studies on the modified IEEE 118-bus system demonstrate the effectiveness and efficiency of the proposed parallel stochastic SCUC model for the secure and economic operation with various uncertainties.

**Index Terms**—augmented Lagrangian relaxation, parallel algorithm, stochastic SCUC

## I. KEY EQUATION AND FIGURES

With the increasing of renewable energy integration and size of modern large-scale power system, the impact of uncertain factors to power system security and economic grows significantly. In this paper, the objective is to minimize the operating cost of stochastic SCUC problem with consideration of uncertainties.

$$\begin{aligned} \min \quad & F(x, y) \\ \text{s.t.} \quad & Ax + by \geq d \\ & Ey \geq h \end{aligned} \quad (1)$$

With the help of variable duplication technique and augmented Lagrangian relaxation method, (1) can be rewritten as

$$\begin{aligned} \min \quad & F(x, y) + \lambda(\hat{y} - y) + \frac{c}{2}(\hat{y} - y)^2 \\ & Ax + by \geq d \\ & E\hat{y} \geq h \end{aligned} \quad (2)$$

In proposed paper, auxiliary problem principle is adopted to make approximation of coupled term in second order penalty function, in order to decompose (2) into two subproblems, which can be solved simultaneously. In addition, trust region technique is adopted in proposed stochastic SCUC model to ensure the accuracy of approximation. The flowchart is shown in Fig. 1.

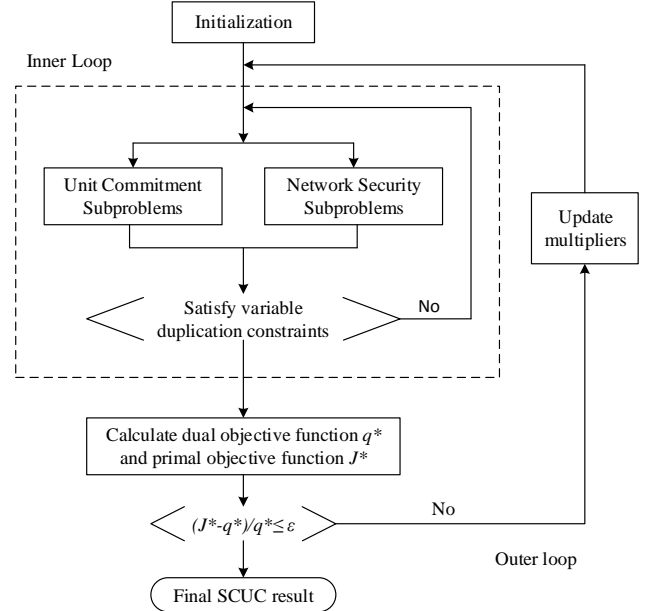


Fig. 1. Flowchart of the proposed parallel SCUC algorithm.

## II. KEY RESULT

We applied the proposed approach to a modified IEEE118-bus power system. The computational CPU time and cost difference are shown in Table I and II, respectively. The solution results in this study indicate that the proposed parallel stochastic SCUC model would obtain an acceptable optimal solution in much less CPU time, which is applicable to the day-ahead SCUC calculation of large-scale power system.

TABLE I  
COMPUTATIONAL CPU TIME

# of Scenarios	0	3	5
Centralized	8.12s	160.06s	185.59s
Parallel	7.36s	24.84s	37.5s

TABLE II  
COST DIFFERENCE

# of Scenarios	0	3	5
Centralized	\$1,646,187.76	\$1,646,299.99	\$1,646,350.05
Parallel	\$1,646,550,532	\$1,646,664.88	\$1,646,566.78
Difference	0.022%	0.022%	0.013%

## III. CONCLUSIONS

This proposed stochastic SCUC approach minimizes the operation cost of system by possibility expectation of each scenarios, which can adaptively and robustly adjust unit commitment and dispatch in response to constraints in different scenarios. Computational performance of numerical results shows that the proposed SCUC approach is a suitable alternative for solving the day-ahead scheduling problem with uncertainty in real-world power systems.

# Do-not-exceed Limits for Renewable Resources with Robust Corrective Topology Control

Akshay S. Korad and Kory W. Hedman

School of Electrical, Computer, and Energy Engineering, Arizona State University, Tempe, AZ 85287, USA  
Email: [korad@asu.edu](mailto:korad@asu.edu) and [Kory.Hedman@asu.edu](mailto:Kory.Hedman@asu.edu)

**Abstract**— In recent years, the penetration of renewable resources, such as wind and solar generation, in electrical power systems has increased. These renewable resources add more complexities to power system operations, due to their intermittent and unpredictable nature. As a result, operators must acquire additional reserves in order to maintain a balanced system. However, one persistent challenge is determining the optimal location of the reserves and this challenge is exacerbated by the inability to predict key transmission bottlenecks due to this added uncertainty. The presented research utilizes robust corrective topology control as a congestion management tool to manage power flows and the associated renewable uncertainty. The proposed day-ahead method determines the maximum amount of uncertainty in renewable resources in terms of do-not-exceed (DNE) limits combined with corrective topology control actions. The day-ahead topology control formulation is based on the direct current optimal power flow; therefore, switching solutions obtained from these algorithms are tested for AC feasibility and system stability. The numerical results presented are based on the IEEE-118 bus test case with 20% wind penetration.

## I. KEY EQUATIONS

The robust corrective topology control algorithm to determine DNE limits is a three stage optimization problem; however, it can be reduced to a two stage optimization problem. The generic form of two stage robust topology control formulation is given in (1)-(3).

$$\min_{x \in X} (c^T x + \max_{w \in W} b^T y(w)) \quad (1)$$

$$\text{s.t.} \quad Fx \leq f, Hy(w) \leq h, Ax + By(w) \leq g, \quad (2)$$

$$Ey(w) = d, x \in \{0,1\}. \quad (3)$$

## II. KEY FIGURES

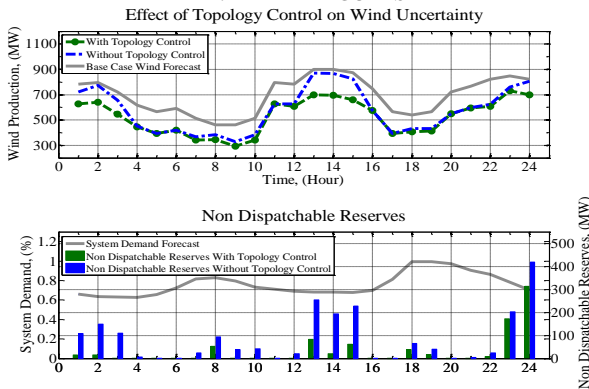


Figure 1. Lower bound of do-not-exceed limits with and without topology control actions.

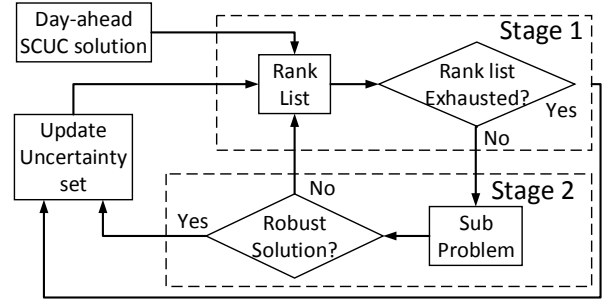


Figure 2. Solution method for robust corrective topology control.

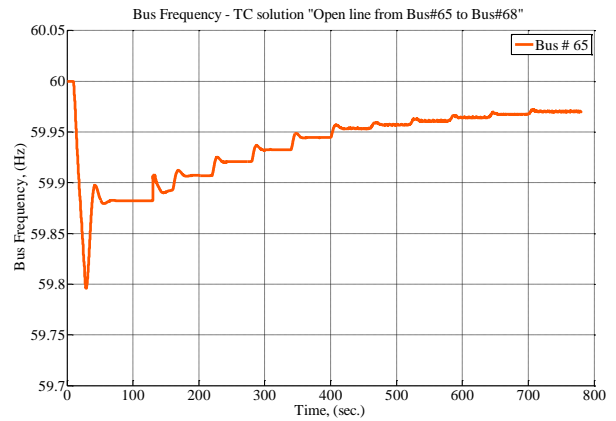


Figure 3. Effect of sudden drop of wind and associated corrective topology control action on system frequency.

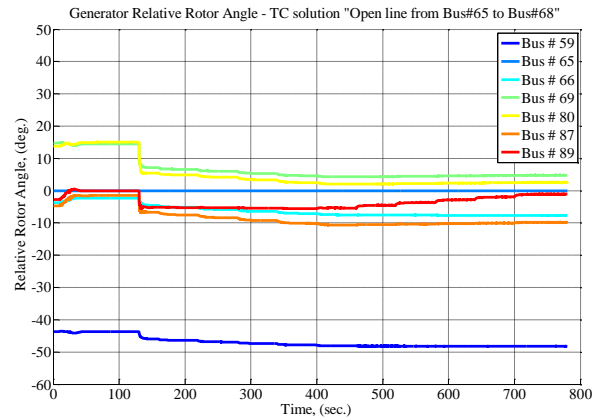


Figure 4. Effect of sudden drop of wind and associated corrective topology control action on generator relative rotor angles.



# Local Cyber Attacks in Power Systems and Protection Strategy

Xuan Liu, *Member, IEEE*, Zuyi Li, *Senior Member, IEEE*

**Abstract**—Recent studies have shown that an attacker can inject pre-determined false data into smart meters such that it can pass the residue test of conventional state estimator. However, the calculation of the false data vector relies on the network (topology and parameter) information of the entire grid. In practice, it is impossible for an attacker to obtain all network information of a power grid. Unfortunately, this does not make power systems immune to false data injection attacks. In this paper, we propose a local load redistribution attacking model based on incomplete network information and show that an attacker only needs to obtain the network information of the local attacking region to inject false data into smart meters in the local region without being detected by the state estimator.

**Index Terms**—false data injection attacks, incomplete information, local load redistribution, power systems.

## I. LOCAL ATTACKING MODEL

We propose local cyber attacks based on incomplete network information. We assume that the attacker aims to attack region  $A$  as shown in Fig. 1.

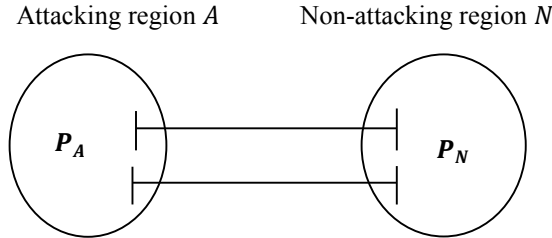


Fig. 1 Illustrative diagram for attacking region and non-attacking region

**Local attacking Scheme:** Suppose a connected power grid is decomposed into two connected regions  $A$  and  $N$  by a set of lines (tie lines). If an additional injected power  $\Delta P_A$  into region  $A$  makes the phase angles of all its boundary buses increase or decrease the same, then there will no power flow in or out of the attacking region.

Thus, the attacker does need to know the full network information of the attacking region, instead of that of the entire power grid.

**Feasibility Theorem:** Suppose a connected power grid is decomposed into an attacking region  $A$  and a non-attacking region  $N$  by a set of lines (tie lines). Suppose the attacking region  $A$  consists of  $\rho$  non-boundary buses and  $\sigma$  boundary buses. The  $\sigma$  boundary buses in  $A$  are connected to  $n$  non-attacking islands. If there are at most  $q = \rho + n - 2$  non-attackable bus injection measurements in region  $A$ , then there exists a feasible non-zero attacking vector.

TABLE 1: AVERAGE NUMBER OF LINES IN THE OPTIMAL ATTACKING REGION

System	Percentage			
	$\gamma_b = 0.1$	$\gamma_b = 0.05$	$\gamma_b = 0.025$	$\gamma_b > 0$
IEEE 30	10.60 (25.9%)	7.70 (18.8%)	5.80 (14.2%)	3.60 (8.8%)
IEEE 39	8.52 (18.5%)	6.38 (15.6%)	5.71 (12.4%)	3.86 (8.4%)
IEEE 57	8.40 (10.5%)	5.79 (7.2%)	5.31 (6.6%)	3.29 (4.1%)
IEEE 118	9.09 (4.9%)	6.39 (3.4%)	4.34 (2.3%)	3.00 (1.6%)
Polish 2383	9.98 (0.34%)	6.80 (0.23%)	5.18 (0.18%)	2.56 (0.09%)

## II. PROTECTION STRATEGY

The protection strategy is composed of primary protection and secondary protection.

**Primary Protection:** Suppose that a connected attacking region of bus  $b$  has  $\rho$  non-boundary buses and  $q$  non-load buses, and all its boundary buses are set to be the same incremental phase angle. Then there are at least  $\max\{0, \rho - q\}$  measurements at load buses to be protected if we are to make the attacking region infeasible.

$$\min \sum_{d \in \Omega_{1_{b_1}} \cup \Omega_{1_{b_2}} \dots \cup \Omega_{1_{b_m}}} \beta_d + \sum_{l \in \Omega_{2_{b_1}} \cup \Omega_{2_{b_2}} \dots \cup \Omega_{2_{b_m}}} \beta_l \quad (1)$$

Subject to

$$\sum_{d \in \Omega_{1_{b_1}}} \beta_d + \sum_{l \in \Omega_{2_{b_1}}} \beta_l \geq \rho_{b_1} - q_{b_1} \quad (2.1)$$

$$\sum_{d \in \Omega_{1_{b_2}}} \beta_d + \sum_{l \in \Omega_{2_{b_2}}} \beta_l \geq \rho_{b_2} - q_{b_2} \quad (2.2)$$

$\vdots$

$$\sum_{d \in \Omega_{1_{b_m}}} \beta_d + \sum_{l \in \Omega_{2_{b_m}}} \beta_l \geq \rho_{b_m} - q_{b_m} \quad (2.m)$$

**Secondary Protection:** After the primary protection, there may still exist a set of feasible attacking regions for each bus. We then optimally determine the remaining measurements to be protected.

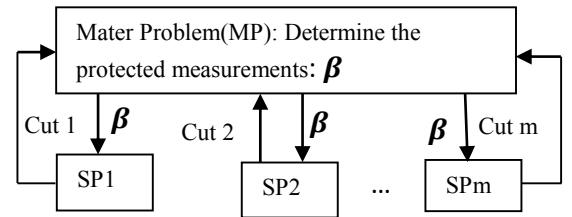


Fig. 2 Secondary protection strategy

TABLE 2 SIMULATION RESULT FOR IEEE-39 BUS

M	$np_1$	$t_1(s)$	$np_2$	$t_2(s)$
10	6	10.82	6	9.94
20	13	59.28	12	46.44
30	15	81.65	16	66.25
40	18	110.98	16	24.25
50	19	111.58	19	11.85